JGR B

Journal of Geophysical Research

VOLUME 65 APRIL 1960 NUMBER 4

THE SCIENTIFIC PUBLICATION

OF THE AMERICAN GEOPHYSICAL UNION

Journal of Geophysical Research

An International Scientific Publication

OFFICERS OF THE UNION

LLOYD V. BERKNER, *President*
F. W. REICHELDERFER, *Vice President*
A. NELSON SAYRE, *General Secretary*
WALDO E. SMITH, *Executive Secretary*

OFFICERS OF THE SECTIONS

Geodesy
CHARLES PIERCE, *President*
FLOYD W. HOUGH, *Vice President*
BUFORD K. MEADE, *Secretary*

Seismology
LEONARD M. MURPHY, *President*
JAMES A. PEOPLES, JR., *Vice President*
BENJAMIN F. HOWELL, JR., *Secretary*

Meteorology
THOMAS F. MALONE, *President*
GORDON E. DUNN, *Vice President*
WOODROW C. JACOBS, *Secretary*

Geomagnetism and Aeronomy
L. R. ALLDREDGE, *President*
C. T. ELVEY, *Vice President*
J. HUGH NELSON, *Secretary*

Oceanography
WALTER H. MUNK, *President*
DONALD W. PRITCHARD, *Vice President*
EUGENE C. LAFOND, *Secretary*

Volcanology, Geochemistry, and Petrology
ALFRED O. C. NIER, *President*
FRANCIS J. TURNER, *Vice President*
IRVING FRIEDMAN, *Secretary*

Hydrology
WALTER B. LANGBEIN, *President*
WILLIAM C. ACKERMANN, *Vice President*
CHARLES C. MCDONALD, *Secretary*

Tectonophysics
PATRICK M. HURLEY, *President*
LOUIS B. SLICHTER, *Vice President*
H. RICHARD GAULT, *Secretary*

BOARD OF EDITORS

Editors: PHILIP H. ABELSON and J. A. PEOPLES, JR.

ASSOCIATE EDITORS

1960

HENRY G. BOOKER — WALTER B. LANGBEIN
E. C. BULLARD — ERWIN SCHMID
JULE CHARNEY — HENRY STOMMEL
GEORGE T. FAUST — J. TH. THIJSSE
DAVID G. KNAPP — A. H. WAYNICK
J. TUZO WILSON

1960-1961

HENRI BADER — T. NAGATA
K. E. BULLEN — FRANK PRESS
CONRAD P. MOOK — A. NELSON SAYRE
WALTER H. MUNK — MERLE A. TUVE
JAMES A. VAN ALLEN

1960-1962

JULIUS BARTELS — TOR J. NORDENSON
E. G. BOWEN — E. N. PARKER
JOHN E. CHAPPELEAR — GEORGE P. RIGSBY
G. D. GARLAND — WALTER O. ROBERTS
GORDON J. F. MACDONALD — C. N. TOUART
L. A. MANNING — JAMES R. WAIT

This Journal welcomes original scientific contrib
tions on the physics of the earth and its environmer

Manuscripts should be transmitted to J. A. People
Jr., Geology Department, University of Kansa
Lawrence, Kansas. Authors' institutions, if in t
United States or Canada, are requested to pay a pu
lication charge of $25 per page, which, if honored, e
titles them to 100 free reprints.

Subscriptions to the *Journal of Geophysical R*
search and *Transactions, AGU* are included in mer
bership dues.

Non-member subscriptions, *Journal of Geophysic*
Research. . $30 for back Volume of 1959, $4 f
this issue; $20 for the calendar year 1960.

Non-member subscriptions, *Transactions, AGU*. . .
. . . . . $4 per calendar year, $1.25 per cop

Subscriptions, renewals, and orders for back numbe
should be addressed to American Geophysical Unio
1515 Massachusetts Ave., Northwest, Washington
D. C. Suggestions to authors are available on reque

Advertising Representative: Howland and Howlan
Inc., 230 Park Ave., New York 17, N. Y.

Beginning with the January 1959 issue (Vol. 64, No. 1) the *Journal of Geophysical Research* is publish
monthly by the American Geophysical Union, the U. S. National Committee of the International Uni
of Geodesy and Geophysics organized under the National Academy of Sciences-National Research Coun
as the U. S. national adhering body. Publication of this journal is supported by the National Science Fou
dation and the Carnegie Institution of Washington. The new monthly combines the type of scienti
material formerly published in the bi-monthly *Transactions, American Geophysical Union*, and the quarter
Journal of Geophysical Research. The *Transactions, American Geophysical Union* will continue as a quarter
publication for Union business and items of interest to members of the Union.

Published monthly by the American Geophysical Union from 1407 Sherwood Avenue, Richmond, Virgin
Second class postage paid at Richmond, Virginia.

YSTEMS
GINEERING

with standard components

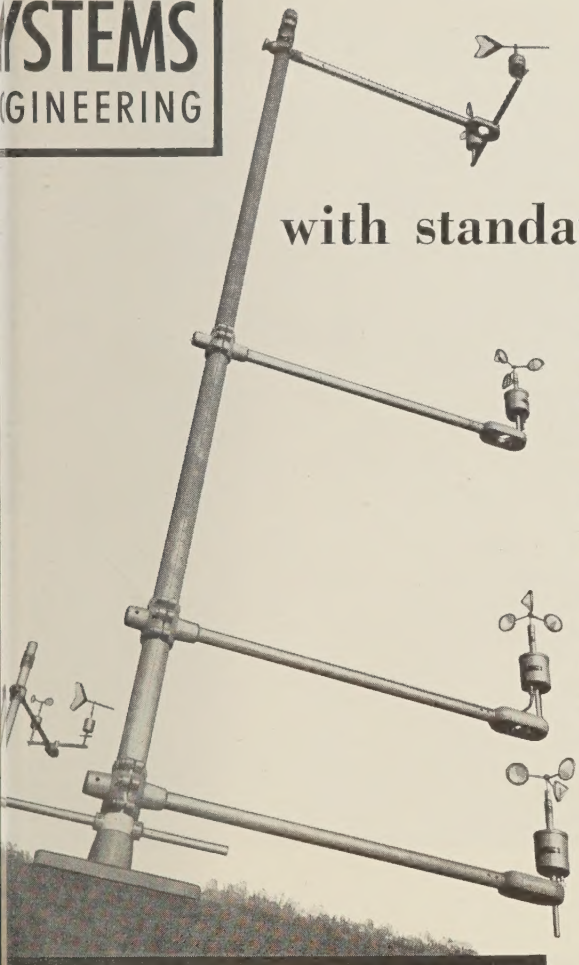

Where a complete meteorological system is required, Beckman & Whitley offers everything you need: 1. Time-tried and proved anemometers, wind-direction units, thermal radiometers, soil heat-flow transducers, etc, of the highest quality and performance, and 2. A knowledgeable and experienced engineering and meteorological group prepared to develop these elements into a complete met system to meet your particular needs.

EXAMPLE: Illustrated here is a complete automatic wind-profile system created for IGY glacier studies. The logarithmic pickup array is composed of standard transmitters mounted on a standard meteorological mast and telemetered to standard translator units driving a special photographic recording unit.

Shown below, this device automatically records the readings from digital counters representing the four wind-speed pickups, together with the indication from a clock face, operating on an interval basis which can be anything from seconds to hours. Wind direction is written on a standard strip-chart recorder.

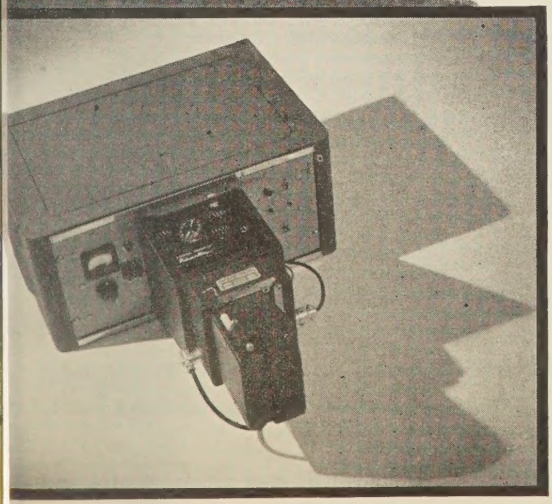

There are many other examples ranging from small portable weather stations to rocket-motor test-tower instrumentation running into dozens of pickup points on numerous towers, and data presentation on punch cards, typewriters, calculator tapes, and the like.

Check with us on your particular problems.

Beckman & Whitley INC.

SAN CARLOS 15, CALIFORNIA

Another achievement in gravity measurement from LaCoste & Romberg

Now for the first time, gravity surveys of inaccessible areas can be made from the air, using a LaCoste & Romberg airborne gravity meter. This new meter requires no gyroscopic stabilization platform. Its accuracy is better than 10 milligals.

Commercial airborne surveys are now available from Fairchild LaCoste Gravity Surveys, Inc.

LaCoste & Romberg 6606 NO. LAMAR AUSTIN, TEXAS

Manufacturers of airborne, submarine, shipborne and surface gravity meters for both exploration and geodetic surveys

Please mention JOURNAL OF GEOPHYSICAL RESEARCH, when writing to advertisers

Expanding the Frontiers of Space Technology in

SPACE PHYSICS

Lockheed Missiles and Space Division is broadening its studies in space physics to keep pace with this rapidly growing field of fundamental research.

Positions are available for physicists with advanced degrees, at our Palo Alto facilities in the Stanford Industrial Park, for work in basic research on the physics of the earth's upper atmosphere and beyond.

Typical research projects include: measurement of atmospheric composition and density at satellite altitudes; laboratory experiments on upper atmospheric atomic and molecular reactions; hydromagnetic interactions with the earth's magnetic fields; simulation and study of meteor impacts; and particle radiation.

The successful solution to problems such as these calls for advancement of the state of the art to unknown environments and the maximum of scientific effort.

Engineers and Scientists—We invite you to join us in this challenging effort and to share in the future of a company that has an outstanding record of achievement.

Write: Research and Development Staff, Dept. D-59, 962 W. El Camino Real, Sunnyvale, California. U.S. citizenship or existing Department of Defense clearance required.

Lockheed / **MISSILES AND SPACE DIVISION**

Systems Manager for the Navy POLARIS FBM; the Air Force AGENA Satellite in the DISCOVERER Program and the MIDAS and SAMOS Satellites; Air Force X-7; and Army KINGFISHER

SUNNYVALE, PALO ALTO, VAN NUYS, SANTA CRUZ, SANTA MARIA, CALIFORNIA
CAPE CANAVERAL, FLORIDA • ALAMOGORDO, NEW MEXICO • HAWAII

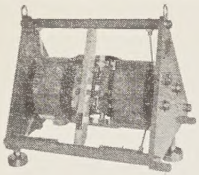

BENIOFF
SEISMOMETERS
HORIZONTAL
and
VERTICAL

- **SENSITIVE**—can detect 1 millimicron of earth motion at 1 cps; 8 separate coils; 1 mv output per coil per micron of motion at 1 cps.
- **DUAL PURPOSE**—can drive long and short-period galvanometers simultaneously.
- **POWERFUL**—magnification of 300,000 at 1 cps; can drive galvanometers remoted 10 miles without amplification.
- **CALIBRATION**—locally, or remote with Remote Calibration Kits 5227 or 5528.
- **RUGGED**—push-pull variable-reluctance transducer; large air gaps; readily adjusted; weather resistant plating; designed for years of trouble-free operation.

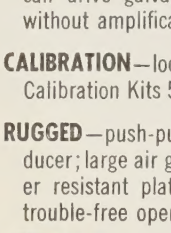

AMPLIFIER
MODEL 4300

- **VOLTAGE GAIN**—½ million at 2 cps.
- **NOISE LEVEL**—1 x 10^{-8} volts, p-p referred to input; employs .01 cps high-pass filter for long-term drift elimination; 70 db dynamic range.
- **DRIFT**—.1 microvolts in 8 hours; can operate unattended for months; separate power supply.
- **RUGGED**—heavy cast-aluminum construction; can be shipped anywhere.
- **PRINCIPAL**—twin photocells and a rugged Geotech Galvanometer. Series 4100, whose sensitivity is 2 x 10^{-8} amps/mm at 1 meter at 2 cps.
- **DELIVERY 30 DAYS**—write for information to:

GEOTECH

THE GEOTECHNICAL CORP.

3401 Shiloh Road
Garland, Texas

P. O. Box 28277
Dallas 28, Texas

Ready shortly

DYNAMICS OF CLIMATE

Edited by Richard L. Pfeffer

The proceedings of a Conference on the Application Numerical Integration Techniques to the Problem of General Circulation, sponsored jointly by the Institu for Advanced Study and the U. S. Air Force Geophys Research Directorate.

$6.

Available

RECENT ADVANCES IN ATMOSPHERIC ELECTRICIT

Edited by L. G. Smith

Proceedings of the Second Conference on Atmosphe Electricity sponsored by Aerophysics Laboratory, U. Air Force Geophysics Research Directorate. This b describes current experimental and theoretical inve gations into the many natural electrical phenomena the atmosphere. The papers are by leading internatio specialists in this field, and the discussions that follo them are summarized. It will be of great value a supplementary text in advanced courses in meteorol and geophysics, and in certain branches of electrical communication engineering, as well as serving a stimulus to further work in this field. In three pa

I. FAIR WEATHER ELECTRICITY. E. T. PIERCE
II. THUNDERSTORM ELECTRICITY. D. R. FITZGERA and H. R. BYERS
III. THE LIGHTNING DISCHARGE. D. ATLAS

$17

PHYSICS AND CHEMISTRY OF THE EARTH

Edited by Professor L. M. Ahrens, Cape Town, Professor Frank Press, Pasadena, California, and Professor W. K. Runcorn, Newcastle-on-Tyne.

This series of volumes, to be published annually, cover, in the course of several years, all the more portant developments in the physics and chemistry of earth. Each section will be written by an expert in field, and topics treated will include such diverse jects as geochemistry and geophysics, geology, phys oceanography and volcanology, etc.

Vol. 2, $10.00; Vol. 3, $15.00; Vol. 4 in prep.

ARTIFICIAL STIMULATION OF RAIN

Edited by Helmut Weickmann, Chairman, Committee on Cloud Physics, American Geophys Union, and Waldo Smith, A.G.U.

The subject of cloud physics has been increasing in portance in the last few years, and within this field branch relating to cloud and precipitation particles been a very active field of research. This volume tains the papers presented at a conference of c physics and precipitation particles held at Woods Oceanographic Institution in Massachusetts, spons by the Geophysics Research Directorate, Air F Cambridge Research Center, Massachusetts, and physics Branch, Office of Naval Research.

$1

Write for
1960 Catalog GEOLOGY & GEOPHYSI

PERGAMON PRESS, I
122 East 55th Street, New York 22, N

FOUR IMPORTANT NEW BOOKS FROM McGRAW-HILL

IGNEOUS AND METAMORPHIC PETROLOGY, *New Second Edition*

By Francis J. Turner and John Verhoogen, *both of the University of California, Berkeley.* 694 pages, $12.00

As before, the book represents a unified general impression of origin and evolution of rocks that have crystallized, or have been profoundly modified, at high temperatures. It is correlated with modern conceptions as to the nature and prevailing physical conditions of the earth's crust and of the outer part of the underlying mantle. Igneous and metamorphic phenomena have been treated, in a single volume, as partially dependent on each other, and as being controlled by the same general physico-chemical principles.

INTRODUCTION TO GEOPHYSICAL PROSPECTING, *New Second Edition*

By Milton B. Dobrin, *Triad Oil Company, Ltd. Calgary, Alberta, Canada.* 446 pages, $9.50.

A thorough revision of a highly successful text. It is designed to present the principles of current techniques of geophysical prospecting for oil and minerals to students and technical personnel employed in the fields of petroleum and mineral exploration. The book covers all the major methods of geophysical prospecting. For each method it discusses fundamental physical principles, instruments, field techniques, reduction of data, interpretation, and examples showing results of actual surveys.

GEOLOGY: Principles and Processes, *New Fifth Edition*

By William H. Emmons. Ira S. Allison, *Oregon State College;* George A. Thiel, *University of Minnesota;* and Clinton R. Stauffer, *California Institute of Technology.* Ready in April.

A textbook for a beginning one-semester course in Physical Geology. It has been a standard and leading text for this field for over 27 years. This new fifth edition has been the most extensive of all its revisions. It is receiving special editing treatment and the result will be a completely rewritten text, with entirely new art work done by a professional scientific illustrator, and a skilled use of two colors throughout. The text is suitable for both terminal cultural courses, or for introductory courses for majors in the subject.

PRINCIPLES OF PETROLEUM GEOLOGY, *New Second Edition*

By William L. Russell, *Agricultural and Mechanical College of Texas.* In Press.

This new edition of one of the most important books in this area has been carefully revised; much new material has been added, and all other information has been brought fully up to date. The first 17 chapters deal with principles; the remaining 12 chapters cover the specialized methods or techniques used by petroleum geologists. The book will be of value, therefore, not only to students, but also to those involved in the oil industry.

Send for Copies on Approval

McGRAW-HILL BOOK COMPANY, INC.

330 West 42nd Street **New York 36, N. Y.**

Please mention JOURNAL OF GEOPHYSICAL RESEARCH, when writing to advertisers

PORTABLE, ACCURATE, EASY TO OPERATE
Sprengnether's Blast and Vibration Seismograph

Ideal for recording all types of vibrations caused by blasting, pile driving, heavy industrial machinery and other sources of strong motion vibrations.

Portability (38 lbs. — 25 x 10 x 8 in.) Unit is self contained and free from external power source.

Extremely Accurate To guard against error, each instrument is tested and calibration data furnished. Frequency response, 3 to 200 cycles per second. Timing lines are across record at intervals of 0.02 seconds with accuracy of 0.1%.

Easy to Operate: All controls are easily accessible. Instrument can be set up, leveled and made ready to operate within minutes.

Seismometer System: A mechanical, optical seismometer employing three independent pendulum systems with magnetic damping. System is contained within unit, hence, no need for external geophones.

Recording System: Photographic recording of all three components appearing on 2¾ inch wide paper. Cartridge type cameras are replaceable and can be pre-loaded to facilitate in the field camera replacement.

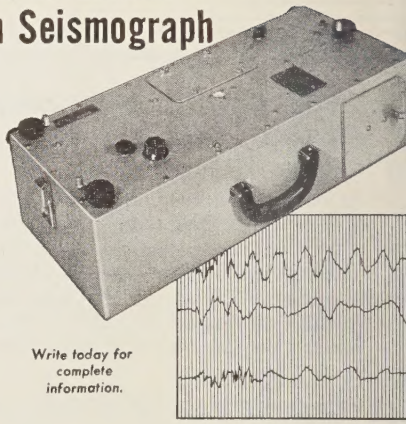

Write today for complete information.

OTHER SPECIFICATIONS

Natural Period (All Components)..... 0.75 se
Damping (Fraction of Critical)..... .55
Static Magnification..... *
*May be specified by purchaser from 50 to 200. Two ranges in one instrument available.

Internationally Known Mfrs. of Seismological, Geophysical Instruments.

W.F. SPRENGNETHER INSTRUMENT CO., INC
4567 SWAN AVENUE • ST. LOUIS 10, MO.

Back issues available . . .

Journal of Geophysical Research • 1959 • Volume 64

Complete set of 12 (2488 pp.)—$30.00

January (132 pp.) $2.00	May (98 pp.) $2.00	September (230 pp.) $3.00
February (138 pp.) $2.00	June (110 pp.) $2.00	October (284 pp.) $4.00
March (112 pp.) $2.00	July (168 pp.) $2.00	November (390 pp.) $5.00
April (106 pp.) $2.00	August (268 pp.) $4.00	December (452 pp.) $6.00

Scientific Effects of Artificially Introduced Radiations at High Altitudes (74-page Symposium reprinted from the August issue) $1.50

International Symposium on Fluid Mechanics in the Ionosphere (202-page Symposium reprinted from the December issue) $4.50

Subscriptions to Journal of Geophysical Research, Calendar Year 1960..... $20.00

AMERICAN GEOPHYSICAL UNION

1515 Massachusetts Avenue, N.W. • Washington 5, D. C.

Note: The former publisher of the *Journal of Geophysical Research* has turned over the stock of back numbers, 1958 and earlier, to Walter J. Johnson, Inc., 111 Fifth Avenue, New York 3, New York.

FIGURES OF EQUILIBRIUM OF CELESTIAL BODIES

With Emphasis on Problems of Motion of Artificial Satellites

by Zdeněk Kopal

An exhaustive self-contained account of the hydrostatic theory of self-gravitating celestial bodies such as the earth, other planets, and the stars. Studied in detail is the interpretation of the proximity phenomena in close binary systems, and the motion of the earth's artificial satellites.

$3.00

THE UNIVERSITY OF WISCONSIN PRESS

430 Sterling Court — Madison 6, Wisconsin

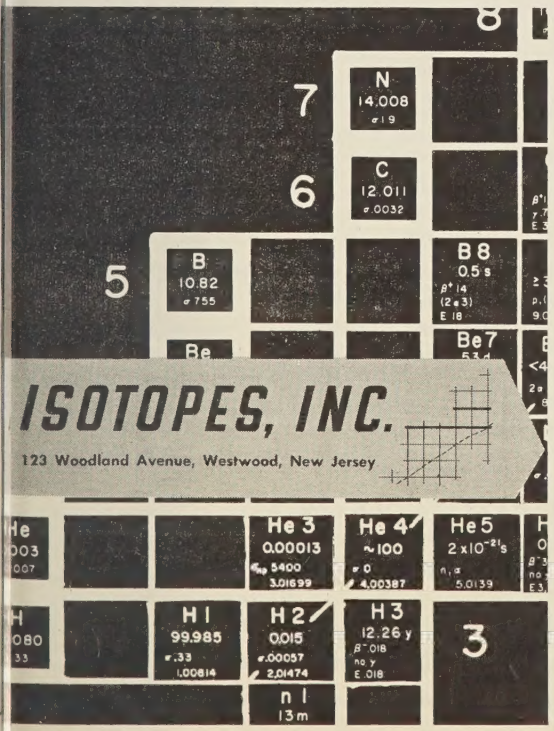

ISOTOPES, INC.

123 Woodland Avenue, Westwood, New Jersey

MEASUREMENT OF TRITIUM

in natural waters

This New Service Enables

- **METEOROLOGISTS** to study mixing, transport and diffusion of water vapor in the atmosphere.
- **OCEANOGRAPHERS** to study rates of movement and mixing of surface ocean water.
- **HYDROLOGISTS** to study surface runoff, mixing in lakes and reservoirs, infiltration rates and ground water circulation.

Write for further information.

Other services include low level C^{14} measurements and radium determinations by the emanation method.

An important new series published in cooperation with the American Geophysical Union . . .

SOVIET RESEARCH IN GEOPHYSICS

(TRANSACTIONS OF THE GEOPHYSICAL INSTITUTE OF THE USSR ACADEMY OF SCIENCES)

IN ENGLISH TRANSLATION

Volume 1 A COLLECTION OF ARTICLES ON DYNAMIC METEOROLOGY

edited by I. A. Kibel'

The seven papers presented are the results of original investigations, including a newly proposed theory for the calculation of soil temperature at various depths from a given air temperature; a solution to the problem of the distribution with depth of a steady current in a baroclinic ocean layer; a new method of calculating the advective heat influx, and other reports on recently accumulated data in the field.

cloth 228 pages $8.00

Volume 2 ISOSTASY AND ISOSTATIC HYPOTHESES

by E. N. Lyustikh

The classic theories of Airy, Pratt, Dutton, and others are discussed, criticized, and amplified in the light of new data. The methods of gathering this information, the means of analysis, and the applications of original Soviet research are expounded fully both in the text and on related maps. Present theories related to isostatic rebound, compensation and overcompensation, gravitational anomalies showing concentrations of density, etc., are illustrated with accompanying pertinent data. Designed to produce a clearer and more up-to-date picture of the isostatic status of the earth.

cloth 150 pages $6.50

Volume 3 THE MICROSTRUCTURE AND MACROSTRUCTURE OF ELASTIC WAVES IN ONE-DIMENSIONAL CONTINUOUS NONHOMOGENEOUS MEDIA

by B. N. Ivakin

This book discusses the problems of the structure of waves propagating in continuous nonhomogeneous and generally absorbing media, with a single spatial coordinate, over intervals infinitesimally small or comparable with a wavelength (microstructure) and over intervals larger or appreciably larger than a wavelength (macrostructure). The solutions of the wave problems posed are presented in operator notation, making it possible to study nonsteady-state oscillations, although detailed calculations and graphs are given for steady-state sinusoidal oscillations as well.

cloth 120 pages $6.00

Volume 4 INVESTIGATION OF THE MECHANISM OF EARTHQUAKES

by O. D. Gotsadze

The results of work conducted by the Geophysics Institute of the Academy of Sciences, USSR, since 1948 on the investigation of fault plane displacements are documented in this volume. During this period a method was evolved which makes it possible to determine the mechanical type of fractures at the focus, the dip and strike of the fault plane, and the direction of the displacement and order of the relative intensity of the first shock. Many of the methodological conclusions and results of interpretations are being published for the first time.

cloth 208 pages $7.50

TABLE OF CONTENTS UPON REQUEST

You may order on approval from

CONSULTANTS BUREAU ENTERPRISES, INC.

227 West 17th St. • New York 11, N. Y.

Journal of
GEOPHYSICAL RESEARCH

LUME 65 APRIL 1960 No. 4

The Velocity of Compressional Waves in Rocks to 10 Kilobars, Part 1[1]

FRANCIS BIRCH[2]

Harvard University
Cambridge, Massachusetts

Abstract. The velocity of compressional waves has been determined by measurement of travel time of pulses in specimens of rock at pressures to 10 kilobars and room temperature. Most of the samples, mainly igneous and metamorphic rocks, furnished three specimens oriented at right angles to one another. The present paper gives experimental details, modal analyses, and numerical tables of velocity as function of direction of propagation, initial density, and pressure. Discussion of various aspects of the measurements is reserved for part 2.

ntroduction. Laboratory measurements of tic constants or of the velocities of elastic es in rocks are needed for the interpretation eismic velocities in terms of materials. The useful measurements were of compressibil- extended to 10 or 12 kilobars by Adams and collaborators and by Bridgman, they have led inferences about crust and substratum , by extrapolation, still deeper levels. In r investigations [*Birch and Bancroft,* 1938,)], the velocity V_s of shear waves was meas- l to 4 and then 10 kilobars, with tempera- s reaching about 600°C [*Birch,* 1943, 1955]. s velocity may be found with good precision n the resonant frequency of vibration in the ional mode of cylindrical bars. Attempts to sure elastic constants entering in the fre- ncy equation of other modes of vibration ensional, flexural) encountered difficulties associated with the reaction of the pressure medium upon the motion of the specimen. An effort to determine velocity by observation of the travel times of pulses, made in the late 1930's with the aid of Dr. Dennison Bancroft, was hampered by the inadequacy of the oscilloscopes and other electronic devices of that period; a primitive time-measuring device was constructed, however [*Bancroft,* 1940], which showed a degree of promise. This situation was transformed by the wartime development of pulse circuitry, fast-writing oscilloscopes, and many other useful components; it then became relatively easy to accomplish what had previously seemed virtually impossible.

Responding to these new possibilities, a number of investigators have published measurements of wave velocities in rocks, as well as in many other materials. Among those especially interesting for geophysical problems are the papers by Hughes and others, showing effects of both pressure and temperature [*Hughes and Jones,* 1950, 1951; *Hughes and Cross,* 1951; *Hughes and Kelly,* 1952; *Hughes and Maurette,* 1956, 1957*a*, 1957*b*]; by *Wyllie, Gregory, and Gardner* [1956, 1958]; and by *Volarovich and Balashov* [1957].

[1] Published under the auspices of the Committee on Experimental Geology and Geophysics and the Division of Geological Sciences at Harvard University.

[2] *Editors' note:* Professor Birch is to be the recipient of the Twenty-Second Award of the Wilbur Bowie Medal during the 1960 Annual Meeting of the American Geophysical Union.

To add to this already considerable quantity of data may seem superfluous. Aside from the desirability of independent confirmation, however, there is a need for more systematic and comprehensive sampling of the accessible parts of the earth and for the development of a rational correlation of velocity with mineralogical and chemical composition. The diversity of rocks is such that, once started on such a program, one finds it difficult to stop. The measurements recorded below seem to afford a basis for a number of generalizations, to be discussed in part 2.

The directional dependence of velocity has been examined with some thoroughness; with few exceptions, each sample of rock has furnished three specimens oriented at right angles to one another. Inclusion of all these measurements greatly swells the tables of data, but there seems to be no other method of indicating adequately the degree and variations of anisotropy.

Sedimentary rocks have received much attention from the writers cited above, and are represented by no more than a few samples in the present study. Most of the samples are igneous and metamorphic silicate rocks, ranging from serpentine and granite to iron-rich dunite and eclogite.

The present paper, part 1, contains details of the experimental arrangements and procedures, condensed descriptions of the samples, and tables of numerical data showing the velocity of compressional waves (V_P) as a function of pressure. A few results have appeared in earlier publications [*Tocher*, 1957; *Balakrishna*, 1958*a*, 1958*b*; *Birch*, 1958; *Verma*, 1960].

Theoretical considerations. Investigations of great generality [*Love*, 1927, p. 303] show that, in an isotropic elastic medium, the first motion resulting from an arbitrary disturbance is propagated with the velocity V_P of compressional waves in an unbounded medium; in terms of elastic constants, this velocity may be written as $[(\lambda + 2\mu)/\rho]^{1/2}$ or $[(K + 4/3\ \mu)/\rho]^{1/2}$ or equivalent forms. Experimentally, the problem is to recognize the 'first motion,' which may be obscured by noise, and which, even when strong, is found to arrive gradually, rather than suddenly, when examined with high amplification. In this respect, laboratory 'seismology' faces problems exactly comparable to those of ordinary seismology, on a different scale of time an dimensions. The laboratory has the advantag however, that the disturbance at the source, th noise level, and the receiving transducers are a subject to control, as well as the proportions an size of the medium.

For many practical reasons, the most co venient shape for specimens is a circular cyli der. For the observation of the velocity V_P, th ratio of length to diameter should not exceed or 5; for greater values, less energy arrives wi the velocity V_P, as more is converted by boun ary reflection to disturbances arriving later tha the first motion. Eventually, for long, thin ba the disturbance that travels with velocity fades into the noise level, while a strong sign is found to travel with the 'bar velocity,' whi approaches $(E/\rho)^{1/2}$ for wavelengths long wi respect to the bar diameter. A large number papers have been devoted to the discussion wave propagation in cylindrical bars, but the seems to be no complete theoretical solution f the propagation of pulses in short bars. (For recent review, see, for example, *Mason*, 195 p. 40 et seq.)

It can be demonstrated experimentally, ho ever, that the first motion does travel with t velocity V_P in materials for which the elast constants can be determined independently, su as glass, steel, or aluminum, and, by observi with samples of different sizes, that this veloci is independent of length and diameter of samp and of transducer frequency within certa ranges of dimensions and of experimental a curacy. This has been done in the course of t present study, and earlier by students of ultr sonic delay lines and others [for example, *M son and McSkimin*, 1947; *Roth*, 1948; *Hugh Pondrom, and Mims*, 1949]. Probably the mo comprehensive investigation, though of rel tively low precision, is that of *Silaeva a Shamina* [1958].

Even for so nearly ideal a medium as sili glass, the first motion arrives gradually, with 'foot' which recedes toward shorter times as t amplification is increased. This is discussed more detail below; the principal limitation accuracy comes from this circumstance.

The first motion is followed by a long train disturbances which have not been much utiliz in the present work. Hughes and others (19

d later papers) have made use of a retarded rival formed by conversion of compressional ves (P) at the cylindrical boundary to shear ves (S) reflected at the critical angle, propating across the cylinder, and reconverted to mpressional waves by reflection at the other e; this disturbance may be called *PSP*. The ometrical theory, given by Hughes and others, ows that the delay of *PSP*, measured from the st arrival, should depend only on the diameter the bar and the two velocities V_P and V_S (of ear waves). Thus the determination of this lay leads to a determination of V_S. The diffilties with this method are of a practical nare. First, the moment of onset of *PSP* is even ore difficult to determine than that of P, as ere is usually some motion resulting from P eflections, scattering) at the time *PSP* arrives ee, for example, Fig. 2 below, or the figures in *ughes, Pondrom, and Mims*, 1949). Second, less the medium is isotropic and uniform, the rious paths for *PSP* will have different delays. The verification given by *Hughes, Pondrom, d Mims* [1949, pp. 1553, 1554] even for so od a medium as steel shows the probable limitions of accuracy. For the samples of different ngths, having a diameter of 2.54 cm, the delay *PSP* ranges from 6.50 to 6.86 microseconds rst delay) with a mean of 6.65; for the sames having a diameter of 3.645 cm, the delay nges from 9.62 to 9.92, with a mean of 9.79 icroseconds. The means are in the ratio 1.472, stead of 1.435, the ratio of diameters. Measements on several aluminum specimens, showg a comparable discrepancy, are shown below Table 2. For materials sufficiently uniform, otropic, and fine-grained, this method can be ed to find V_S with a probable accuracy of a w per cent, or to two significant figures. Either e use of shear-mode transducers with pulse citation or the measurement of frequency of rsional resonance gives V_S with greater reibility than the observation of *PSP*. This phase usually observable, however, and then prodes an easily obtained, if somewhat unreliable, easure of V_S under the same conditions as the servation of V_P.

Experimental details. The measurement of locity consists of the determination of travel ne of a compressional pulse through a short, lindrical specimen. A pulse of voltage is applied across a circular plate of polarized barium titanate ceramic (the transducer), exciting thickness modes of vibration. The transducer covers one end of the specimen, through which the disturbance is transmitted to a second transducer which converts the mechanical signal to an electrical one, finally amplified and displayed on an oscilloscope. The travel time is measured roughly on the face of the oscilloscope by comparison with calibrated time markers, more precisely by comparison with the travel time through a variable mercury delay line, as described below. The velocity V_P is the ratio of length of specimen to travel time of the first disturbance.

The specimens were 1.000 inch in diameter, from 2 to 4 inches long. Commercially available transducers could be used with no change except for light hand lapping of the flat surfaces to ensure even contact. The specimens of rock were first cored with diamond core drills, then ground to right circular cylinders with flat ends. They were jacketed with copper foil, usually 0.004 inch thick, soft-soldered at the seams. Transducers and backing pieces were then assembled in rubber tubing which was slipped over the jacketed cylinder to form the configuration shown in Figure 1.

The function of the rubber tubing is to exclude the pressure fluid from the spaces between transducers, backing pieces, and specimen. As the pressure is raised, these pieces are clamped together with normal stresses nearly equal to the hydrostatic pressure; at the same time, the edge of the tranducer is exposed to the pressure transmitted through the rubber. Thus the stress in the transducer is quasi-hydrostatic if the flat surfaces are sufficiently smooth. A light film of oil applied to these surfaces helps to fill small irregularities that may be present on the ends of the specimen. Under these conditions, the barium titanate disks show an indefinite useful life, usually ended only by mishandling on removal of the rubber.

The backing pieces, of aluminum, served as the ungrounded terminals for the transducers, the jacket of the specimen being grounded to the pressure chamber. Connections were made with coaxial cables; 'Microdot' 50-ohm cable, about 0.08 inch in diameter, was used inside the pressure chamber, connected to the usual pres-

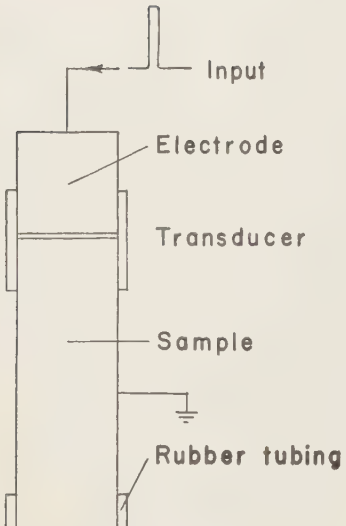

Fig. 1. Arrangement of specimen, backing pieces, and transducers.

sure-tight insulated stems for transmission to the outside system of RG58/U cable. The assembly of Figure 1 is mounted in a brass tube attached to a four-stem pressure-tight closure; this in turn is fitted in the pressure vessel and held in position by a screw.

The lower part of the pressure vessel, a thick-walled cylinder with inside diameter of 1.5 inch, outside diameter of 6 inches, serves for the generation of pressure by advance of a piston driven by a 6-inch ram. The general features of systems of this kind have been described by *Bridgman* [1949] and require little further elaboration. The pressure fluid was a mixture of kerosene and petroleum ether. Pressure was determined from the change in resistance of a calibrated manganin wire gage. Temperature was not controlled, except by the temperature of the room; all measurements were made between about 20° and 30°C.

Commercial electronic components were used throughout, except for the mercury delay line. A Hewlett-Packard model 212A pulse generator supplies a rectangular pulse of about 50 volts, variable in length from about 0.1 to 10 microseconds, to the sending transducer at the specimen and also to a similar transducer at one end of the mercury line. The signals received after passage through the specimen, and, in parallel, the mercury column, are independently amplified in two Tektronix type 121 preamplifiers and displayed simultaneously on the screen of a Tektronix type 535 oscilloscope with the aid of the switching unit of the type 53C two-channel amplifier. The combined rise time for the amplifiers is about 0.05 microsecond.

Mercury delay lines have been used by *McSkimin* [1950], *Laughton* [1957], and others. They have the merit of giving a transmitted signal with a continuously variable delay with respect to the original pulse. One transducer is fixed in the base, below the mercury column. The other is mounted on a slide, moved vertically with a screw; the position of the slide is read with a micrometer or dial gage and is easily controlled to within 0.001 inch. This distance, 0.001 inch, corresponds to a travel time in mercury of 1/57, or roughly 0.02, microsecond. The maximum delay for the line used in this work was about 20 microseconds, or a path in mercury of about 29 mm.

The accuracy of time measurement depends upon the quality of the signal and upon calibration of the mercury line. The response of a transducer is determined by its natural frequency and the damping; even for an ideally sharp voltage pulse, the mechanical response builds up gradually, and consists of an initial rise followed by damped oscillations; a similar response of opposite sign is produced by the following edge of the pulse. The mechanical oscillations produced by the two edges of the electrical pulse interfere with one another, and complex results can be obtained on varying the pulse width. If this is too short (less than about 0.6 microsecond for a transducer with a lowest natural frequency of 1 Mc/s), the full displacement is not reached before the trailing edge of the pulse starts motion in the opposite sense; the signal is consequently small. If the electrical pulse is longer than a microsecond or so, the

ial swing reaches a maximum but interfer-
es take place later. The optimum pulse length
; found to be about 0.6 microsecond for
Ic/s transducers, 0.2 microsecond for the 3-
/s transducers, these being the shortest which
e full initial swings with substantial cancella-
n of subsequent ones.

The transmitted signal is further affected by
pagation through the specimen. At 3 Mc/s,
wavelength is from 2 to 3 mm, comparable
the dimensions of the grains in many of the
rser rocks. Under these conditions, scatter-
becomes important in reducing the ampli-
e, especially of the high-frequency compo-
ts of the pulse, and in distorting later phases
h as *PSP*. Other processes of loss also dis-
minate against the high frequencies, so that
pulse becomes less sharp the greater the
h length.

The gradual onset of the 'first motion' is the
ncipal limitation on the accuracy of velocity
asurement. With high amplification, the un-
tainty can be reduced to about 0.05 micro-
ond or less in favorable cases, but it may be
ch greater at low pressure. The signal through
mercury line has a similar shape; the
thod of fitting the two signals together helps
reduce the uncertainty of setting which would
ne from attempting to place a vertical marker
the beginning of the signal. For times of 10
20 microseconds, as with the present samples,
accuracy is of the order of a few parts in a
usand at best.

The mercury calibration is accomplished with
aid of time markers from a crystal-controlled
illator such as the DuMont type 300 time
ibrator. Displacing the mercury signal across
set of microsecond time marks gives the
gth of path in mercury per microsecond. This
s carried out between 0° and 50°C; the re-
ts are in satisfactory agreement with the
re exact determinations of *Hubbard and*
omis [1928].

The zero setting of the delay line was ob-
ned by finding the settings corresponding to
first arrivals through steel samples of differ-
lengths and extrapolating to zero length;
s method eliminates errors of starting times
amplifier delays. The steel standards were
t from the same bar of 1-inch round annealed
ll rod, and designed to have travel times of

TABLE 1. Observations with the Mercury Delay Line on Steel Samples of Different Lengths

Length of Steel, in.	Setting of Delay Line, in.	Ratio V_P(steel)/V(mercury)
1.159	0.283	4.095
2.319	0.566	4.097
3.474	0.848	4.097
4.638	1.133	4.094
	Mean	4.096

Temperature of mercury, 30°C. Velocity, 1.446 km/sec. V_P(steel) = 4.096 × 1.446 = 5.92 km/sec.

about 5, 10, 15, and 20 microseconds, respectively. These measurements also give the ratio of velocities in mercury and steel. A sample set of readings is shown in Table 1; these were made after the zero of the dial gage had been adjusted to correspond with zero length of sample, but an arbitrary setting can be used equally well.

In the first design of the mercury line, diaphragms of shim steel 0.002 inch thick were placed between the transducers and the mercury, with the idea of minimizing the path in the steel and of ensuring good transmission from transducer to mercury. On repeating the calibration with steel samples, small changes of zero, of the order of a few thousandths of an inch of mercury, were occasionally found. These changes were traced by D. C. Tozer to deformations of the thin diaphragms. The condition was remedied by replacing the shim steel by steel disks 0.060 inch thick. Though, as expected, the amplitude of the mercury signal was reduced, this disadvantage was more than offset by the improvement of stability of the zero setting. Repeated checks against the steel samples have since shown no change of zero greater than 0.001 inch, about equal to the usual uncertainty of the setting.

Typical signals, with 1-microsecond markers, are shown on the two lower traces of Figure 2; the upper trace shows the same signal with more amplification and with the signal from the mercury line slightly displaced. The lower traces show, besides the first arrival at the left, the *PSP* arrival as a small signal of somewhat indefinite beginning, followed by a reflection of the first motion from the back of the aluminum

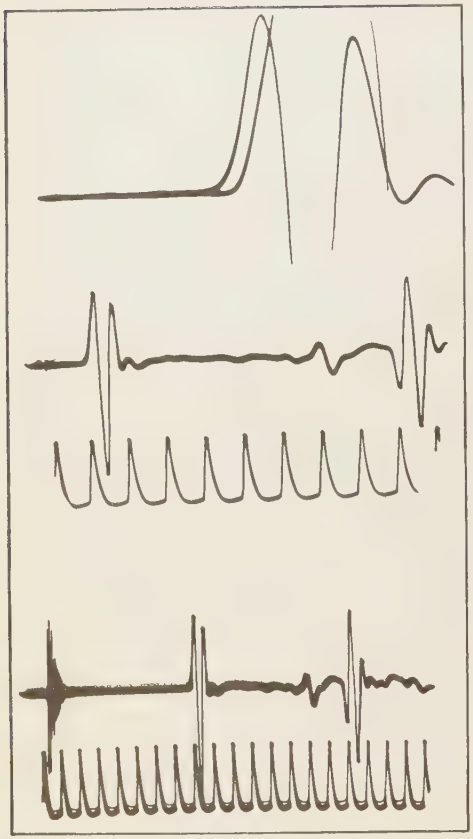

Fig. 2. Oscilloscope traces for Nippissing diabase at 8 kilobars. The lowest photograph shows microsecond timing marks on one trace; on the other, reading from the left, may be seen electrical pick-up from the pulse, the first arrival, *PSP*, and a reflection of *P* from the outer end of the backing piece. The middle photograph shows the same with a faster sweep, the pulse now displaced from the screen. The top photograph, with still faster sweep, shows only the first arrival, with the mercury signal slightly displaced from coincidence.

backing piece; this reflection comes too late to interfere with either the first arrival or with *PSP*. Final settings were made with much more vertical amplification and with faster sweep speed than can be shown in a photograph; about 20 times as much vertical gain was normally used, so that the virtual height of the first swing was some 20 to 50 cm. The sweep was usually set at 5 cm/microsecond; thus 0.001 inch on the scale of the mercury line gave a displacement of about 1 mm on the oscilloscope. The signals of Figure 2 are for a specimen of Nippissing diabase at 8 kilobars.

Some readings on a set of commercial aluminum alloy (2011-T3) specimens of different diameters, but of the same length, are recorded in Table 2; they serve to illustrate the limitations on the use of *PSP* for determining V_S, even in relatively ideal material. The ratio of the difference in setting between *P* and *PSP* to diameter should be constant; in fact, it shows a small systematic variation with diameter, in the same direction as shown by the observations of *Hughes, Pondrom, and Mims* [1949] referred to above.

The specimens were weighed and measured before jacketing; the densities were calculated from the mass and dimensions, and thus are 'bulk' densities. Velocities were then found in a clamping device which could load the specimens and transducers axially with as much as 600 psi, or roughly 40 bars; the standard clamping pressure was about 10 bars. Even this was enough to produce measurable changes of velocity and of quality of transmission in many of the specimens. Except for the most compact rocks, little significance should be attached to the velocities for pressures below 500 bars; they are not reliably reproducible to better than perhaps 10 per cent. Where very low values are recorded, the signal quality was also poor, so that one might question the identification as a true 'first arrival'; gradual application of pres-

TABLE 2. Observations on Samples of Aluminum Alloy
All samples, 2.500 inches long.

Diameter, in.	Mercury Line Settings, in.			Ratio Difference / Diameter	V_S, km/sec
	P	*PSP*	Difference		
1.250	0.575	1.096	0.521	0.416	3.04
1.000	0.575	0.988	0.413	0.413	3.06
0.500	0.575	0.776	0.201	0.402	3.12
0.250	(0.575)[1]				

[1] First arrival visible, but too small for precis reading.

V_P = 6.26 km/sec. Density, 2.828.

re, however, enables one to observe the con-uous transformation of a poor, slow signal a good, fast one, unquestionably the first rival. The change within a few hundred bars ay be striking; the low-pressure variation is own in some detail for a few specimens in gure 5, below.

After preliminary measurements of this kind, e specimens were jacketed, assembled with ansducers and backing pieces as shown in Fig-e 1, and mounted in the pressure vessel. Pres-re was then raised, at first by small increments 100 bars or so to 500 bars, then 1000, and ccessively to 2, 4, 6, 8, and 10 kilobars, then duced to 9, 7, 5, 3, and 1 kilobar, readings ing taken at each of these pressures, over a eriod of 10 to 30 minutes. A small 'drift' could ten be observed after a change of pressure, to-ard higher velocity after the pressure was ised, toward lower velocity after pressure was duced. The observed changes of this kind were the order of a few parts per thousand; their fect is probably largely eliminated by the ethod of averaging the data.

Description of materials. Many of the sam-les were large blocks originally assembled by . A. Daly, which have provided specimens for rlier studies [*Zisman*, 1933*a*, 1933*b*; *Ide*, 1936, 937; *Birch and Clark*, 1940; *Birch and Ban-roft*, 1938, 1940; *Birch*, 1943]. To these have een added an accumulation of samples from umerous localities, through the kindness of any geologists. Several groups of samples are oteworthy: the rocks of the southern Cali-rnia batholith, collected by Esper S. Larsen, r.; samples from the Bushveld Complex, col-cted with the aid of Louis T. Nel and C. M. chwellnus; a number of rocks from Ontario nd Quebec, collected with the help of Marland . Billings; rocks from the Chester quarry, near udlow, Vermont, picked out by Sydney P. lark, Jr. Samples of Westerly granite and entreville diabase, corresponding to the G-1 nd W-1 of the comprehensive studies by *Fair-airn and others* [1951], were obtained by E. C. obertson; the modal analyses of these rocks hown in Table 4 below are those of *Chayes* 1950]. The analysis shown for the Sacred Heart ranite is from *Lund* [1956, p. 1486]. The com-osition of the 'eclogite' from Tanganyika, col-cted by C. Bursill, was determined by C. van Zyl, of the Anglo-American Corporation, Johannesburg. The analysis of the Bethlehem granodiorite gneiss is by *Kruger* [1946, p. 182], who collected the sample.

The identification of the varieties of serpentine in the samples from Thetford, Quebec, and Ludlow, Vermont, was made by H. H. Hess. Much additional information on the eclogite from Healdsburg, California, is given in a paper by *Borg* [1956], and on the dunites by *Ross, Foster, and Myers* [1954]. The rocks of the Bushveld Complex have been described in classical papers, with many analyses [*Daly*, 1928; *Hall*, 1932] and those of the batholith of Southern California by *Larsen* [1948]. The massive grossularite from Connecticut is very similar to that described by *Agar and Krieger* [1932]. New analyses for the Japanese jadeite, obtained from Ward's Natural Science Establishment, and for the almandite-pyrope garnet, made by J. Ito, are shown in Table 3. The jadeite analysis is similar to an analysis of another Japanese jadeite by Zies [*Kracek, Neuvonen, and Burley*, 1951]. The red garnet was a single crystal, shattered and somewhat altered along the fractures, obtained from the collection of the Department of Mineralogy and Petrography, Harvard University. Its place of origin is not known. The two bronzitites closely resemble the samples from the Stillwater Complex and from Farm Jagdlust, Bushveld Complex, described in *Hess and Phillips* [1940].

A number of new Rosiwal analyses by Edwin

TABLE 3. Chemical Analyses

	Garnet	Jadeite, Japan
SiO_2	36.30	58.45
TiO_2	2.45	
Al_2O_3	20.18	23.51
Fe_2O_3	0.07	0.51
FeO	32.01	
MnO	1.74	Trace
MgO	4.75	0.78
CaO	2.02	1.33
Na_2O	...	13.59
K_2O	...	0.29
H_2O+	n. d.	0.20
H_2O-	0.27	1.24
	99.79	99.90

TABLE 4. Modal Analyses

Percentages by volume, Rosiwal method

Abbreviations

ab	albite	bi	biotite	gr	grossularite	om	omphacite
al	almandite	br	bronzitite	ho	hornblende	or	orthoclase
an	anorthite	ch	chlorite	hy	hypersthene	py	pyrope
and	andradite	en	enstatite	mi	microcline	qu	quartz
au	augite	fa	fayalite	mu	muscovite	serp	serpentine
				ol	oligoclase	sp	spessartite

The asterisk signifies marked alteration.

Sample	Quartz	Potash Feldspar	Plagioclase	Mica	Amphibole	Rest
Granite						
Westerly, R. I. (G-1)	27.5	35.4 mi	31.4 ol	3.2 bi 1.3 mu		1.2
Quincy, Mass.	26	63 ab and microperthite			10	1
Rockport, Mass.	28	64 microperthite			6	2
Stone Mt., Ga.	26	32 or	38 an_5	4 mu		
Chelmsford, Mass.	31	31 mi	31 ol	1 bi, 4 mu		2 ch
Hyderabad, India (B)	28	54 or	14 an_{20}			1 ch 3 hy
Barre, Vt.	26	25 or	37 ab	9 bi, 3 mu		
Sacred Heart, Minn.	26	41	27 an_{20}	3 bi		3
Barriefield, Ont.	20	70* or (ab)		2 bi		8 (ch 5)
Hyderabad, India (A)	30	47 or	19*			2 ch 2 hy
Latchford, Ont.	27	17 or	51 an_5*			3 ch 2 epidot
Granodiorite gneiss ('Bethlehem'), N. H.	20	20 or	40 an_{33}	16 bi, 2 mu		2 garnet
Quartz monzonite, Porterville, Cal.	34	27 or	33 an_{30}	4 bi		2
Granodiorite, Butte, Mont.	27	23 or	40 an_{30}	7 bi		2 ch
Charnockite, Pallavaram, India	46	8 or	38 an_{18}	1 bi		6 hy
Tonalite, Val Verde, Cal.	28		50 an_{45}	15 bi	7 ho	1
Quartz diorite						
San Luis Rey quad., Cal.	19		50 an_{50}	17 bi	13 ho	
Dedham, Mass.	13	6	48 an_{20}* (?)		21 ho*	12 (5 ch)

Gaucher are given in condensed form in Table 4, usually for single thin sections which may not adequately represent the specimens. The reported amount of serpentine for the Addie, N. C., dunite, for example, seems to be too high; it is not consistent with the density or velocity. More petrographic work would be desirable on many of the samples.

Several artificial materials are included: AD-99 is a high-density alumina ceramic produced by the Coors Porcelain Company; the silica glass is of delay-line quality; the diabase glass was produced by the General Electric Company from Holyoke diabase.

The lithographic limestone, presumably from Solenhofen, was in the form of an old lithographic plate. It appears to be of higher porosity than many specimens whose properties have been studied. The aragonite specimens were cored from a block of hot-spring sinter from Mexico, obtained through the kindness of C. S. Hurlbut, Jr. Of three specimens, only one was principally aragonite, as indicated by density and X-ray diffractometer pattern. The other two were mainly calcite and showed velocities approaching those of marble. The anhydrite was in the form of a 3-inch drill core, apparently very uniform and reasonably pure. The pyrophyllite was a specimen of the natural rock marketed under the name 'Lava' by the Ameri-

TABLE 4. (Continued)

Sample	Plagioclase	Mica	Amphibole	Pyroxene	Olivine	Rest
Aplitite, Sylmar, Pa.	98 an_{12}		2 actinolite			
Anorthosite, Stillwater Complex	93 an_{80}			7 br		
Augite syenite, Lake Superior District, Ont.	84 or, ab	1 bi		13 au	2	
Anorthosite, Bushveld Complex, Transvaal	86 an_{80}			14 br		
Gabbro, Mellen, Wis.	72 an_{60}	1 bi		14 diallage	11	2
Labase (W-1), Centreville, Va.	45 an 3 K-feldspar	1.8 bi		45 au		3.5 1.8 qu
Labase, Holyoke, Mass.	66 an_{54}			32 au		2
Norite, Bushveld Complex	53 an_{60}		1	46 (pigeonite-au-hy)		
Labase (Keweenawan) Sudbury, Ont.	70 an_{50}*	2 bi		18 au	1	9
Labase, Frederick, Md.	48 an_{67}	1 bi		49 (au-hy)	1	
Gabbro, French Creek, Pa.	51 an_{65}	1 bi		32 au, 15 hy		1
Pyroxenite, Sonoma Co., Cal.			1	93 diopside (diallage)	5 fa_{15}	2 serp
Pyroxenite, Stillwater Complex			4 ho	94 br	2	
Pyroxenite, Bushveld Complex	4 an_{80}		2 ho	92 br		2
Harzburgite, Bushveld Complex	1*	2 bi	2	42 au*	38 fa_{35}*	15 (9 serp)
Amphibolite, South Boulder Cr., Madison Co., Mont.			86 (75 tremolite-actinolite, 11 anthophyllite)		6 serp	8 ore, spinel

Sample	Olivine	Serpentine	Rest
Dunite			
Dun Mt., New Zealand	97 fa_9	3	
Webster, N. C.	78 fa_{10}	19 (?)	3
Balsam Gap, N. C.	97 fa_8	2	1
Addie, N. C.	80 fa_{12}	19 (?)	1
Twin Sisters Mt., Wash.	92 fa_{12}	0.5	7 pyroxene (en_{85})
(Hortonolite), Bushveld Complex	90 fa_{55}		9 bowlingite 1 ore

Sample	Pyroxene	Garnet	Rest
Eclogite			
Kimberley Distr., O. F. S.	70 om*	25 ($al_{30}py_{70}$)	5 (bi, ho, ch)
Healdsburg, Cal.	72 om	24 ($al_{57}py_{12}gr_{19}and_{10}sp_2$)	4
Sunnmöre, Norway	55 om* (alt. to feldspar)	26 ($al_{52}py_{26}gr_{18}and_4$)*	10 ho 8 qu 1 ch
Eclogite,' Sango Distr., Tanganyika	20 br-hy (en_{79})	12 ($al_{48}py_{45}gr_6and_1$)	35 epidote (clinozoisite) 20 ho 10 bi 2 qu

n Lava Corporation; it is much used in high-essure devices.

The magnetite samples are of massive ore; the uth African sample, from Magnet Heights in e Bushveld Complex, and the sample from ahawus, New York, are rich in titanium, with about 14 per cent TiO_2 and small amounts of silicate minerals. The Port Henry ore is remarkably pure, except for small amounts of silicate and apatite. The hematite specimen was cored from a piece of specular hematite, large enough to give only a single one of the required

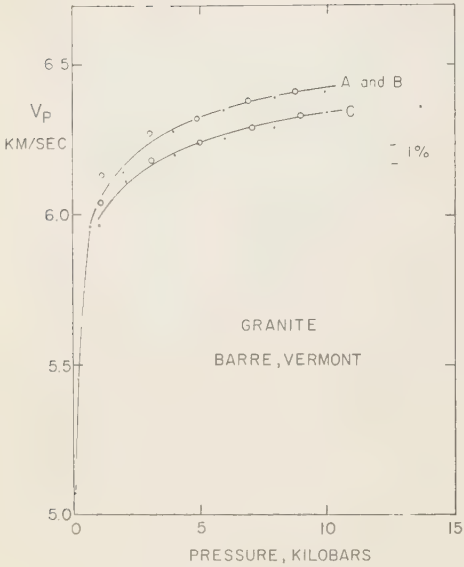

Fig. 3. Experimental points for two specimens of Barre granite. Dots indicate measurements with increasing pressure; circles, with decreasing pressure. The points for specimen *B* fall close to those for *A*.

size; the degree of anisotropy cannot be determined without additional measurements.

Numerical data. Table 5 contains the densities and velocities for the silicate rocks, regardless of classification as igneous, metamorphic, or sedimentary. The order is that of increasing mean density. Table 6 shows values for some other rocks and miscellaneous materials.

The large number of individual observations have been reduced to mean values at fixed pressures. Values obtained with increasing pressure are frequently somewhat different from those found with decreasing pressure, the latter being usually slightly higher for a given pressure. Examples are shown in Figures 3 and 4 for two granites. Departures from a smooth mean curve rarely exceed 1 per cent at pressures above 1 kilobar, or a few parts per thousand between 6 and 10 kilobars. Though three significant figures are recorded, the third figure may be affected by hysteresis and possibly by long-period time effects not adequately explored.

Because of these inherent uncertainties, some liberties have been taken in the reduction of the data. The velocity in mercury has been taken as 0.0570 inch/microsecond, or 1.448 km/sec, for all calculations for rocks. According to Hubbard and Loomis, this corresponds to a temperature of 27°C; 0.0571 inch/microsecond corresponds to 21°C, 0.0569 to 33°C. As the mercury temperature was usually between 25° and 30°C, the error introduced by the use of the single value 0.0570 will not exceed about 2 parts per thousand. If a higher precision were justified by more regular behavior of the samples, the mercury could be held to a fixed temperature with a suitable thermostat.

A correction for the change of length of specimen under pressure is of greater importance. The velocity may be written as $V = (L_0/t)(L/L_0)$, where t is the travel time, L the length under pressure, and L_0 the initial length at 1 atmosphere. The factor (L/L_0) is of course smaller than unity at high pressures, by about 6 parts per thousand for granites to about 3 parts per thousand for dunites at 10 kilobars. This correction has not been applied to the values of Tables 5 and 6, except for the measurements on glasses. The tabulated values are (L_0/t), thus higher than the true velocities by the indicated amounts. The greatest correction would be about 4 units in the last figure for granitic rocks at 10 kilobars; it is barely significant as far as absolute velocities are concerned, but the correction should be taken into account for the calculation of pressure coefficients. Rather than apply the correction for each meas-

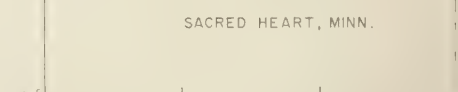

Fig. 4. Experimental points for two specimen of Sacred Heart granite. Dots and circles as fo Figure 3.

TABLE 5. Silicate Rocks, Velocity of Compressional Waves as Function of Pressure
The symbol ⊥ indicates propagation normal to foliation or schistosity. V_P in km/sec. P in bars.

Rock	Density	Velocity						
		P = 10	500	1000	2000	4000	6000	10,000
erpentinite	2.598	5.5		5.60	5.66	5.73	5.79	5.91
hrysotile)	2.603	5.8		5.83	5.88	5.96	6.03	6.15
hetford, Que.	2.601	5.5		5.59	5.65	5.71	5.78	5.93
mean	2.601	5.6		5.67	5.73	5.80	5.87	6.00
erpentinite	2.618	4.5	6.06	6.22	6.33	6.44	6.49	6.56
ntigorite)	2.620	4.0	6.00	6.16	6.28	6.41	6.46	6.57
udlow, Vt.	2.603	5.7	6.94	6.99	7.15	7.26	7.29	7.33
mean	2.614	4.7	6.33	6.46	6.59	6.70	6.75	6.82
ranite	2.621	3.8	5.58	5.84	6.02	6.19	6.26	6.35
Vesterly, R. I.	2.619	4.2	5.59	5.78	5.89	6.00	6.05	6.12
3-1'	2.618	4.2	5.71	5.89	6.00	6.11	6.16	6.23
mean	2.619	4.1	5.63	5.84	5.97	6.10	6.16	6.23
ranite	2.623	5.1	6.07	6.16	6.27	6.36	6.41	6.48
uincy, Mass.	2.618	5.0	6.01	6.06	6.13	6.25	6.32	6.42
mean	2.621	5.1	6.04	6.11	6.20	6.30	6.37	6.45
ranite	2.623	5.4	6.12	6.27	6.34	6.42	6.47	6.54
ockport, Mass.	2.622	4.9	5.84	6.14	6.27	6.38	6.42	6.50
	2.626	4.7	5.93	6.13	6.26	6.36	6.40	6.48
mean	2.624	5.0	5.96	6.18	6.29	6.39	6.43	6.51
ranite	2.625	3.7	5.57	6.00	6.20	6.32	6.36	6.42
tone Mt., Ga.	2.625	3.8	5.24	5.90	6.14	6.24	6.30	6.35
	2.626	3.6	5.46	5.93	6.14	6.26	6.33	6.43
mean	2.625	3.7	5.42	5.94	6.16	6.27	6.33	6.40
ranite	2.626	4.7	5.83	6.03	6.16	6.27	6.32	6.38
helmsford,	2.623	4.6	5.77	5.96	6.13	6.23	6.29	6.36
lass.	2.628	3.4	5.33	5.75	5.97	6.16	6.23	6.31
mean	2.626	4.2	5.64	5.91	6.09	6.22	6.28	6.35
neiss,	2.639	3.6	5.65	5.86	6.05	6.15	6.21	6.25
elham, Mass.	2.646 ⊥	2.9	5.54	5.83	5.96	6.09	6.15	6.25
	2.644	3.7	5.82	6.04	6.18	6.30	6.35	6.43
mean	2.643	3.4	5.67	5.91	6.06	6.18	6.27	6.31
uartz monzonite	2.644	5.1		5.90	6.04	6.17	6.24	6.31
orterville, Cal.	2.648	5.2		5.98	6.10	6.25	6.31	6.38
	2.641	5.1		5.96	6.08	6.23	6.30	6.41
mean	2.644	5.1		5.95	6.07	6.22	6.28	6.37
uartzite	2.648	5.3		6.13	6.16	6.21	6.25	6.32
	2.647	5.8		6.18	6.23	6.31	6.37	6.46
Iontana	2.647	5.8		6.03	6.07	6.13	6.17	6.26
mean	2.647	5.6		6.11	6.15	6.22	6.26	6.35
ranite	2.653	5.4	6.38	6.40	6.48	6.55	6.61	6.68
lyderabad, India	2.655	5.5	6.15	6.22	6.27	6.33	6.36	6.43
mean	2.654	5.4	6.26	6.31	6.38	6.44	6.49	6.56
ranite	2.657	4.8	5.92	6.08	6.17	6.28	6.35	6.41
arre, Vt.	2.655	5.2	5.79	6.10	6.17	6.27	6.34	6.42
	2.653	5.3	5.86	6.00	6.11	6.21	6.26	6.34
mean	2.655	5.1	5.86	6.06	6.15	6.25	6.32	6.39

TABLE 5. (Continued)

Rock	Density	Velocity						
		P = 10	500	1000	2000	4000	6000	10,000
[illegible]	2.659	3.8	4.8	5.18	5.36	5.58	5.71	5.89
[illegible], N. Y.	2.[illegible]	3.7	4.8	5.10	5.28	5.48	5.61	5.81
	2.665	4.3	5.3	5.54	5.68	5.83	5.94	...
mean	2.659	3.9	5.0	5.27	5.44	5.63	5.75	(5.85)
[illegible]	2.[illegible]	[illegible]5		4.73	5.02	5.38	5.58	5.89
Granite	2.679	6.0		6.12	6.16	6.22	6.27	6.34
Sacred Heart, Minn.	2.[illegible]	6.0		6.29	6.33	6.38	6.42	6.49
	2.[illegible]	5.7		6.31	6.36	6.41	6.44	6.51
mean	2.[illegible]	5.9		6.24	6.28	6.34	6.38	6.45
Granite	2.677	5.6	6.28	6.35	6.42	6.48	6.51	6.57
Barriefield, Ont.	2.670	5.9	6.20	6.27	6.32	6.38	6.42	6.47
	2.670	5.5	6.16	6.26	6.32	6.40	6.44	6.48
mean	2.672	5.7	6.21	6.29	6.35	6.42	6.46	6.51
Gneiss	2.[illegible] ⊥	4.5	5.76	5.83	5.94	6.05	6.10	6.26
Hell Gate, N. Y.	2.677	5.3	6.18	6.25	6.37	6.46	6.49	6.64
	2.684	5.6	6.25	6.31	6.39	6.47	6.53	6.61
mean	2.[illegible]	5.1	6.06	6.13	6.23	6.33	6.37	6.50
Granite	2.[illegible]	5.8		6.48	6.52	6.56	6.60	6.66
Hyderabad, India A)	2.681	5.5		6.36	6.40	6.46	6.50	6.57
	2.688	5.8		6.43	6.46	6.50	6.54	6.61
mean	2.676	5.7		6.42	6.46	6.51	6.55	6.61
'Granite'	2.[illegible]	6.1	6.34	6.41	6.43	6.47	6.52	6.61
Englehart, Ont.	2.[illegible]	6.2	6.34	6.41	6.45	6.50	6.54	6.62
	2.675	6.1	6.17	6.18	6.23	6.31	6.37	6.47
mean	2.679	6.1	6.28	6.33	6.37	6.43	6.48	6.57
Greywacke,	2.682	5.3	5.60	5.75	5.87	5.99	6.06	6.15
New Zealand	2.676	5.4	5.62	5.78	5.88	5.98	6.02	6.11
	2.682	5.4	5.66	5.75	5.87	5.98	6.04	6.13
mean	2.679	5.4	5.63	5.76	5.87	5.98	6.04	6.13
'Granite'	2.683	5.6	6.08	6.14	6.20	6.27	6.30	6.37
Latchford, Ont.	2.683	5.7	6.14	6.18	6.25	6.30	6.33	6.41
	2.683	5.9	6.18	6.24	6.29	6.33	6.38	6.44
mean	2.683	5.7	6.13	6.19	6.25	6.30	6.34	6.41
Albitite	2.694	6.45		6.72	6.74	6.77	6.79	6.83
Sylmar, Pa.	2.680	6.35		6.61	6.64	6.67	6.71	6.76
	2.688	6.40		6.53	6.56	6.61	6.66	6.70
mean	2.687	6.40		6.62	6.65	6.68	6.72	6.76
Granodiorite	2.708	4.7		6.22	6.32	6.40	6.46	6.54
Butte, Mont.	2.708	4.1		6.30	6.32	6.41	6.47	6.56
	2.700	4.5		6.30	6.41	6.47	6.51	6.58
mean	2.705	4.4		6.27	6.35	6.43	6.48	6.56
Graywacke	2.704	5.7		6.13	6.20	6.28	6.33	6.41
Quebec	2.709	5.2		5.87	6.01	6.14	6.20	6.27
	2.709	5.2		5.77	5.90	6.01	6.06	6.15
mean	2.705	5.4		5.92	6.04	6.14	6.20	6.28
Serpentinite	2.718	5.8		5.99	6.05	6.12	6.19	6.29
Cal.	2.684	5.9		6.05	6.12	6.18	6.24	6.35
	2.718	5.8		6.03	6.08	6.14	6.21	6.30
mean	2.710	5.8		6.02	6.08	6.15	6.21	6.31

TABLE 5. (Continued)

Rock	Density	Velocity						
		P = 10	500	1000	2000	4000	6000	10,000
ite	2.741	4.97		5.40	5.56	5.71	5.80	5.96
ambridge),	2.734	5.81		6.05	6.13	6.23	6.29	6.39
edford, Mass.	2.729	5.69		5.92	6.04	6.13	6.20	6.31
mean	2.734	5.49		5.79	5.91	6.02	6.10	6.22
harnockite'	2.717	6.09		6.22	6.26	6.30	6.35	6.41
llavaram, India	2.764	6.19		6.24	6.33	6.40	6.43	6.48
	2.738	6.17		6.26	6.32	6.37	6.41	6.49
mean	2.740	6.15		6.24	6.30	6.36	6.40	6.46
anodiorite	2.762 ⊥	3.6		5.74	5.87	6.01	6.08	6.17
eiss	2.768	4.9		6.14	6.22	6.30	6.36	6.43
Bethlehem), N. H.	2.745	4.8		5.98	6.12	6.16	6.19	6.31
mean	2.758	4.4		5.95	6.07	6.16	6.21	6.30
onalite	2.763	5.1		6.37	6.44	6.52	6.55	6.62
al Verde, Cal.	2.763	5.0		6.32	6.44	6.51	6.56	6.63
	2.763	5.1		6.31	6.38	6.45	6.50	6.56
mean	2.763	5.1		6.33	6.43	6.49	6.54	6.60
northosite	2.754	6.92		6.98	7.03	7.07	7.10	7.16
ahawus, N. Y.	2.754	6.77		6.92	6.95	6.98	7.01	7.05
	2.797	6.50		6.68	6.73	6.78	6.81	6.85
mean	2.768	6.73		6.86	6.90	6.94	6.97	7.02
northosite	2.735	6.3		6.78	6.82	6.86	6.88	6.92
illwater	2.842	6.6		7.03	7.09	7.14	7.17	7.20
omplex, Mont.	2.735	6.6		7.09	7.11	7.15	7.17	7.19
mean	2.770	6.5		6.97	7.01	7.05	7.07	7.10
ugite syenite	2.797	5.6		6.55	6.59	6.66	6.69	6.75
ntario	2.749	5.8		6.65	6.70	6.76	6.79	6.84
	2.795	5.7		6.53	6.61	6.68	6.72	6.77
mean	2.780	5.7		6.58	6.63	6.70	6.73	6.79
lica schist	2.795	6.1		6.48	6.53	6.59	6.62	6.69
oodsville, Vt.	2.796	4.6	⊥	6.05	6.10	6.17	6.22	6.31
	2.800	6.5		6.77	6.80	6.84	6.87	6.91
mean	2.797	5.7		6.43	6.48	6.53	6.57	6.64
rpentinite	2.820	6.6		6.68	6.73	6.80	6.86	6.94
udlow, Vt.	2.781	6.4		6.50	6.55	6.63	6.69	6.79
	2.792	6.2		6.35	6.44	6.57	6.68	6.79
mean	2.798	6.4		6.51	6.57	6.67	6.74	6.84
uartz diorite	2.801	5.1		6.45	6.53	6.61	6.66	6.73
an Luis Rey	2.796	5.1		6.45	6.54	6.63	6.67	6.73
ad., Cal.	2.797	5.2		6.40	6.49	6.56	6.60	6.68
mean	2.798	5.1		6.43	6.52	6.60	6.64	6.71
northosite	2.815	5.8	6.90	6.94	7.00	7.07	7.11	7.16
ushveld Complex	2.801	5.9	6.76	6.85	6.95	7.04	7.07	7.13
	2.806	5.5	7.09	7.16	7.21	7.27	7.30	7.35
mean	2.807	5.7	6.92	6.98	7.05	7.13	7.16	7.21
hlorite schist	2.773	3.8		6.40	6.49	6.66	6.76	7.02
hester Quarry, Vt.	2.805	5.4		6.77	6.88	6.98	7.02	7.10
	2.795	5.2		6.82	6.86	6.96	7.02	7.10
	2.897	3.3		6.52	6.61	6.70	6.75	6.82
	2.897	5.3		6.83	6.87	6.94	7.00	7.02
	2.877	5.9		7.17	7.23	7.30	7.32	7.36
mean	2.841	4.8		6.75	6.82	6.92	6.98	7.07

TABLE 5. (Continued)

Rock	Density	Velocity P = 10	500	1000	2000	4000	6000	10,000
Quartz diorite	2.902	5.4		6.48	6.55	6.60	6.66	6.71
Dedham, Mass.	2.912	5.6		6.45	6.51	6.58	6.63	6.71
	2.905	5.5		6.45	6.52	6.61	6.65	6.72
mean	2.906	5.5		6.46	6.53	6.60	6.65	6.71
Talc schist	2.919	5.0		6.23	6.45	6.62	6.74	6.93
Chester, Vt.	2.909	4.8		6.36	6.55	6.80	6.89	7.01
mean	2.914	4.9		6.30	6.50	6.71	6.82	6.97
Gabbro	2.917	6.7	6.92	6.95	6.97	7.00	7.04	7.11
Mellen, Wis.	2.948	6.8	7.20	7.23	7.25	7.28	7.32	7.36
	2.929	6.8	6.99	7.03	7.06	7.10	7.13	7.17
mean	2.931	6.8	7.04	7.07	7.09	7.13	7.16	7.21
Diabase	2.967	6.54		6.65	6.68	6.72	6.75	6.82
(Nippissing)	2.969	6.54		6.62	6.65	6.70	6.74	6.81
Cobalt, Ont.	2.956	6.58		6.66	6.68	6.72	6.75	6.82
mean	2.964	6.55		6.64	6.67	6.71	6.75	6.82
Diabase	2.981	6.14		6.73	6.78	6.84	6.87	6.94
Centreville, Va. 'W-1'	2.966	6.19		6.69	6.75	6.81	6.84	6.92
	2.980	6.10		6.69	6.76	6.82	6.86	6.92
mean	2.976	6.14		6.70	6.76	6.82	6.86	6.93
Diabase	2.981	6.32	6.43	6.47	6.51	6.55	6.59	6.66
Holyoke, Mass.	2.973	6.26	6.40	6.42	6.46	6.51	6.55	6.62
	2.977	6.16	6.37	6.41	6.45	6.50	6.54	6.61
mean	2.977	6.25	6.40	6.43	6.47	6.52	6.56	6.63
Norite	2.975	6.6	6.99	7.02	7.06	7.10	7.14	7.20
Pretoria	2.977	6.6	7.03	7.07	7.12	7.17	7.22	7.33
Transvaal	2.981	6.5	7.05	7.13	7.16	7.20	7.25	7.32
mean	2.978	6.6	7.02	7.07	7.11	7.16	7.20	7.28
Dunite (altered)	3.000	6.31		6.54	6.62	6.72	6.80	6.93
Webster, N. C.	2.962	5.46		6.07	6.18	6.28	6.40	6.62
	2.979	6.3		6.51	6.57	6.66	6.71	6.83
mean	2.980	6.0		6.37	6.46	6.55	6.64	6.79
Diabase	2.999	6.6	6.79	6.82	6.84	6.89	6.92	6.98
(Keweenawan)	3.005	6.4	6.60	6.64	6.69	6.74	6.77	6.85
Sudbury, Ont.	3.006	6.3	6.61	6.70	6.74	6.79	6.82	6.89
mean	3.003	6.4	6.67	6.72	6.76	6.81	6.84	6.91
Diabase	3.012	6.76		6.77	6.80	6.85	6.88	6.92
Frederick, Md.	3.012	6.78		6.77	6.80	6.84	6.88	6.93
	3.012	6.76		6.78	6.81	6.84	6.87	
mean	3.012	6.76		6.77	6.80	6.84	6.88	6.92
Gabbro	3.057	5.8	6.82	6.96	7.03	7.12	7.18	7.25
French Creek, Pa.	3.060	5.8	6.75	6.95	7.05	7.14	7.19	7.26
	3.042	5.7	6.65	6.87	6.98	7.08	7.13	7.19
mean	3.054	5.8	6.74	6.93	7.02	7.11	7.17	7.23
Amphibolite	3.108	6.09		6.61	6.65	6.72	6.77	6.83
Madison Co., Mont.	3.124	7.31		7.50	7.54	7.59	7.63	7.66
	3.129	7.26		7.41	7.45	7.49	7.52	7.57
mean	3.120	6.89		7.17	7.21	7.27	7.31	7.35

TABLE 5. (Continued)

Rock	Density	Velocity P = 10	500	1000	2000	4000	6000	10,000
Jadeite,	3.151	7.7		8.15	8.15	8.16	8.18	8.22
Japan	3.194	7.4		8.23	8.24	8.26	8.27	8.29
	3.196	7.7		8.25	8.26	8.27	8.28	8.33
mean	3.180	7.6		8.21	8.22	8.23	8.24	8.28
Actinolite	3.166	6.90		7.31	7.43	7.50	7.55	7.60
schist	3.217	5.62		6.62	6.75	6.84	6.92	7.01
Chester, Vt.	3.199	7.32		7.68	7.79	7.89	7.94	8.00
mean	3.194	6.61		7.20	7.32	7.41	7.47	7.54
Dunite	3.253	7.0		7.65	7.68	7.75	7.79	7.87
Webster, N. C.	3.275	6.9		7.42	7.46	7.51	7.57	7.63
	3.204	7.0		7.56	7.62	7.68	7.73	7.83
mean	3.244	7.0		7.54	7.59	7.65	7.69	7.78
Pyroxenite	3.239	6.7		7.72	7.79	7.87	7.94	8.00
Sonoma Co., Cal.	3.244	6.4		7.45	7.52	7.65	7.72	7.82
	3.259	7.2		8.03	8.06	8.11	8.14	8.20
mean	3.247	6.8		7.73	7.79	7.88	7.93	8.01
Dunite	3.262	7.3	7.38	7.45	7.48	7.54	7.60	7.66
Mt. Dun,	3.255	7.9	8.14	8.20	8.25	8.30	8.35	8.43
New Zealand	3.257	7.2	7.54	7.61	7.66	7.73	7.81	7.91
mean	3.258	7.5	7.69	7.75	7.80	7.86	7.92	8.00
Dunite	3.258	6.4	7.52	7.54	7.70	7.85	7.91	8.00
Balsam Gap, N. C.	3.269	6.5	7.55	7.70	7.84	7.96	8.04	8.15
	3.274	8.0	8.38	8.42	8.49	8.57	8.63	8.69
mean	3.267	7.0	7.82	7.89	8.01	8.13	8.19	8.28
Bronzitite	3.283	7.20		7.60	7.64	7.70	7.73	7.82
Stillwater	3.271	7.48		7.59	7.61	7.68	7.71	7.79
Complex	3.284	7.58		7.67	7.71	7.77	7.81	7.89
mean	3.279	7.42		7.62	7.65	7.72	7.75	7.83
Bronzitite	3.304	6.2	7.45	7.50	7.57	7.66	7.71	7.80
Bushveld Complex	3.297	5.9	7.30	7.40	7.53	7.70	7.85	8.12
	3.264	5.0 (?)	7.46	7.56	7.71	7.88	8.00	8.13
mean	3.288		7.40	7.49	7.60	7.75	7.85	8.02
Dunite	3.304	7.85	8.07	8.12	8.19	8.29	8.34	8.41
Addie, N. C.	3.306	7.90	8.23	8.30	8.35	8.41	8.44	8.51
	3.302	7.34		7.56	7.61	7.73	7.82	7.91
mean	3.304	7.70		7.99	8.05	8.14	8.20	8.28
Dunite	3.314	7.6	7.86	7.97	8.04	8.12	8.16	8.23
Twin Sisters	3.312	8.3	8.73	8.78	8.85	8.88	8.90	8.95
Peaks, Wash.	3.310	7.2	7.74	7.83	7.92	7.97	8.00	8.07
mean	3.312	7.7	8.11	8.19	8.27	8.32	8.35	8.42
'Eclogite'	3.338	6.67	7.40	7.47	7.52	7.62	7.68	7.76
Tanganyika	3.323	6.88	7.46	7.55	7.62	7.71	7.76	7.83
	3.324	6.36	7.03	7.13	7.24	7.37	7.42	7.53
mean	3.328	6.64	7.30	7.38	7.46	7.57	7.62	7.71
Jadeite	3.330	8.52		8.65	8.68	8.71	8.74	8.77
Burma	3.332	8.38		8.68	8.69	8.72	8.75	8.78
mean	3.331	8.45		8.67	8.69	8.72	8.75	8.78

TABLE 5. (Continued)

Rock	Density	Velocity P = 10	500	1000	2000	4000	6000	10,000
Eclogite Kimberley	3.338	6.6	7.49	7.56	7.65	7.79	7.85	7.92
Harzburgite,	3.380	6.7	7.61	7.65	7.70	7.73	7.77	7.82
Bushveld	3.356	6.6	7.76	7.80	7.82	7.87	7.91	7.97
Complex	3.371	7.3	7.84	7.89	7.91	7.96	8.01	8.05
mean	3.369	6.9	7.74	7.78	7.81	7.85	7.90	7.95
Eclogite	3.338	7.02	7.55	7.58	7.65	7.72	7.76	7.86
Kimberley	3.370	7.13	7.58	7.61	7.67	7.74	7.75	7.78
	3.420	7.35	7.82	7.84	7.87	7.91	7.94	7.98
mean	3.376	7.17	7.65	7.68	7.73	7.79	7.82	7.87
Eclogite	3.392	5.4		7.20	7.37	7.52	7.61	7.80
Sunnmöre, Norway	3.376	5.1		7.17	7.40	7.56	7.60	7.70
	3.361	5.1		7.01	7.13	7.31	7.41	7.58
mean	3.376	5.2		7.13	7.30	7.46	7.54	7.69
Eclogite	3.441	7.34		7.60	7.75	7.83	7.90	7.99
Healdsburg, Cal.	3.430	7.55		7.71	7.78	7.85	7.91	7.97
	3.452	7.05		7.77	7.91	7.98	8.02	8.07
mean	3.441	7.31		7.69	7.81	7.89	7.94	8.01
Garnet	3.574	6.2		8.46	8.53	8.68	8.80	8.98
(grossularite)	3.563	7.1		8.57	8.70	8.87	8.96	9.02
Conn.	3.545	5.5		8.21	8.41	8.60	8.73	8.96
mean	3.561	6.3		8.41	8.55	8.72	8.83	8.99
Dunite	3.737	6.6	7.12	7.15	7.20	7.26	7.28	7.33
Mooihoek Mine,	3.777	7.0	7.40	7.42	7.46	7.50	7.53	7.57
Transvaal	3.717	6.6	6.87	6.90	6.98	7.06	7.10	7.19
mean	3.744	6.7	7.13	7.16	7.21	7.27	7.30	7.36
Garnet (almandite-pyrope)	3.950	5.9		7.81	7.91	7.99	8.01	8.07

urement, it has seemed preferable to apply it only to the mean values for various groups of rocks, which are probably more significant for such problems as the composition of the crust as indicated by seismic velocities or the refraction of seismic rays [*Birch*, 1958].

The tabulated data will enable the reader to reproduce the mean curves from 1 to 10 kilobars with adequate precision. For some purposes, the course of variation below 1 kilobar may be of interest, especially where very large changes take place. A plot of velocity versus the logarithm of the pressure makes it possible to show the variation at the lowest pressures (Figure 5). A characteristic sigmoid curve is found, with most of the rise between a few hundred and 1000 bars, but there are great differences in the amount of rise. Such a plot suggests the possibility of useful extrapolation to higher pressures than 10 kilobars; it should be noted that the curves are slightly concave upward at high pressure, so that linear extrapolation on the log P plot tends to give lower limits whereas linear extrapolation of velocity versus pressure probably gives upper limits. These limits diverge as pressure increases, and beyond 100 kilobars or so they are so different as to have little value.

A few measurements were made to pressures above 10 kilobars in another pressure system [*Birch, Robertson, and Clark*, 1957]. Tozer made observations on high-purity aluminum to 15 kilobars and on iron (unknown purity) to 18 kilobars. The displacement of the mercury setting was linear with pressure for both metals

TABLE 6. Miscellaneous Materials, Velocity of Compressional Waves as Function of Pressure
V_P in km/sec, P in bars

Rock	Density	Velocity					
		$P = 10$	1000	2000	4000	6000	10,000
mestone	2.544	5.5		5.54	5.56	See text;	
thographic)	2.545	5.5		5.45	5.46	increasing P	
	2.541	5.6	5.59	5.63	5.66	only	
mean	2.543	5.5	5.59	5.54	5.56		
arble	2.705	4.7	6.48	6.53	6.58	6.59	6.60
anby, Vt.	2.703	5.9	6.69	6.76	6.81	6.84	6.87
	2.704	4.8	6.65	6.69	6.77	6.80	6.81
mean	2.704	5.1	6.61	6.66	6.72	6.74	6.76
olomite	2.843	5.6	7.04	7.09	7.14	7.19	7.26
Rutland'?), Vt.	2.845	5.8	7.04	7.08	7.13	7.18	7.25
	2.844	5.4	6.85	6.92	6.99	7.05	7.16
mean	2.844	5.6	6.98	7.03	7.09	7.14	7.22
ragonite mpure)	2.917	5.7	5.82	5.85	5.90	5.93	5.97
nhydrite	2.930	4.7	6.03	6.09	6.16	6.20	6.28
	2.925	4.8	5.97	6.04	6.14	6.19	6.27
	2.929	4.8	5.99	6.05	6.14	6.18	6.25
mean	2.928	4.8	6.00	6.06	6.15	6.19	6.27
lagnetite ore	4.52	5.7	6.25	6.33	6.41	6.48	6.57
itaniferous)	4.56	6.0	6.39	6.48	6.62	6.68	6.77
ransvaal mean	4.54	5.9	6.32	6.41	6.52	6.58	6.67
lagnetite ore itaniferous) ahawus, N. Y.	4.532	(2.3)	6.65	6.75	6.85	6.92	6.98
lagnetite ore	4.845	(4.5)	6.77	6.88	6.98	7.03	7.11
ort Henry, N. Y.	4.850	(3.3)	6.68	6.92	6.99	7.06	7.10
	4.905	(3.5)	6.85	6.90	6.99	7.04	7.12
mean	4.866	(3.8)	6.77	6.90	6.99	7.04	7.11
ematite	5.0	7.1	7.72	7.73	7.74	7.76	7.80
lumina (AD-99)	3.822	10.45					10.55
lica glass used silica)	2.213	5.97					5.53
bsidian, Modoc	2.376	5.80		5.78	5.73	5.70	5.62
iabase glass	2.750	6.30					6.30

about the precision of setting (0.001 inch). he changes were small, the total displacement or iron amounting only to 0.011 inch of the ercury, with about 3 times as much for the luminum. These measurements have been re-uced, taking into account the shortening of the ecimens, to give pressure coefficients of veloc-y $(1/V_P)(\partial V_P/\partial P)_T$. The values are: for iron, 1.1×10^{-6} per bar, or 1.1 per megabar; for aluminum, 2.7 per megabar. From the order of magnitude, it is clear that these coefficients cannot be used for extrapolation to pressures greater than perhaps 0.1 megabar. They may be compared with those found for V_S to 4 kilobars [*Birch*, 1937]: for drill rod, 0.89 per megabar; for commercial aluminum, 3.15 per megabar. A

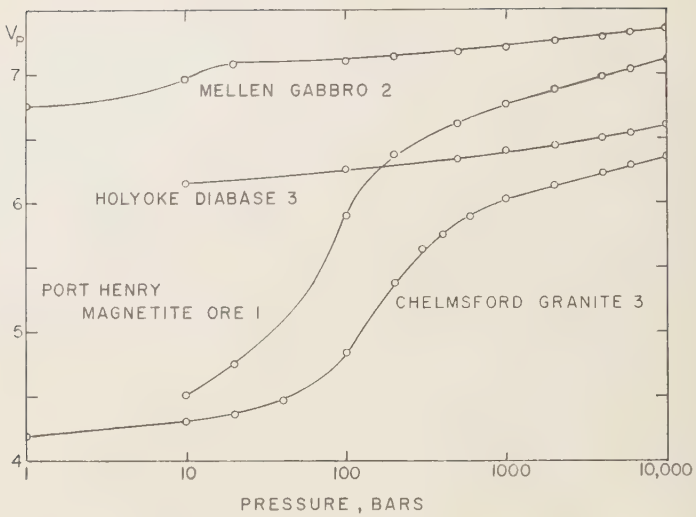

Fig. 5. Velocities versus log P for several materials.

more sensitive method is required for measuring such small changes; for fine-grained materials which can transmit frequencies of the order of 10 Mc/s or higher, it is preferable to adopt the procedure of *Lazarus* [1949]; or of *McSkimin* [1957].

It will be noticed that the entries for lithographic (Solenhofen) limestone in Table 6 are incomplete; this material exhibited anomalous behavior above about 5 kilobars, to be described in a separate report by Tozer.

Acknowledgments. Many individuals have contributed to these investigations. For aid in the collection of rocks, I am indebted to S. Balakrishna, T. F. W. Barth, M. P. Billings, C. Bursill, S. P. Clark, Jr., F. F. Evison, Clifford Frondel, H. H. Hess, C. S. Hurlbut, Jr., S. Katz, F. C. Kruger, Esper S. Larsen, Jr., Louis T. Nel, W. H. Pinson, J. C. Rabbitt, Eugene C. Robertson, E. I. Robertson, C. M. Schwellnus, A. Sergiades, B. Wasserstein, and H. S. Yoder. Also to J. P. Alexander, Cold Spring Granite Company, Cold Spring, Minnesota; W. A. Blomstran, Republic Steel Company, Port Henry, New York; S. O. Gross, National Lead Company, Tahawus, New York.

Most of the measurements were made by Eugene Herrin, Martin Bailyn, and David C. Tozer; T. J. Shankland, R. K. Verma, S. Balakrishna, and Robert Page also aided in the accumulation of data. The petrographic studies were done by Edwin Gaucher. The coring, grinding, and jacketing of specimens, and construction and maintenance of the mechanical parts, including the delay line, were accomplished by Harold and Arthur Ames. Charlotte Isaacs typed the interminable tables. The skill and care of all these collaborators are gratefully acknowledged.

A generous grant-in-aid from the American Petroleum Institute met part of the cost of the investigation. The samples from the Transvaal were collected during a visit to the Bernard Price Institute of Geophysical Research; I owe thanks to the Carnegie Corporation of New York for a travel grant, to B. F. J. Schonland for his kind invitation and hospitality, and to Louis T. Nel for guidance during an unforgettable tour of the Bushveld Complex.

References

Agar, W., and P. Krieger, Garnet rock near West Redding, Connecticut, *Am. J. Sci., 24,* 68–80 1932.

Balakrishna, S., Elasticity of some Indian rocks *Bull. Natl. Inst. Sci., India, 11,* 50–58, 1958*a*.

Balakrishna, S., Velocity of compressional waves in some Indian rocks, *Trans. Am. Geophys. Union, 39,* 711–712, 1958*b*.

Bancroft, Dennison, An electronic interval-timer for laboratory seismometry, *Trans. Am. Geophys. Union,* Part II, 695–696, 1940.

Birch, Francis, The effect of pressure on the modulus of rigidity of several metals and glasses *J. Appl. Phys., 8,* 129–133, 1937.

Birch, Francis, Elasticity of igneous rocks at high temperatures and pressures, *Bull. Geol. Soc Am., 54,* 263–286, 1943.

Birch, Francis, Physics of the crust, *Geol. Soc. Am Spec. Paper 62,* 101–117, 1955.

Birch, Francis, Interpretation of the seismic struc

ture of the crust in the light of experimental studies of wave velocities in rocks, *Contributions in Geophysics in Honor of Beno Gutenberg,* Pergamon Press, New York, pp. 158–170, 1958.

rch, Francis, and Dennison Bancroft, The effect of pressure on the rigidity of rocks, *J. Geol., 46,* 59–87 and 113–141, 1938.

rch, Francis, and Dennison Bancroft, New measurements of the rigidity of rocks at high pressures, *J. Geol., 48,* 752–766, 1940.

rch, Francis, and Harry Clark, The thermal conductivity of rocks and its dependence upon temperature and composition, *Am. J. Sci., 238,* 529–558 and 613–635, 1940.

rch, Francis, Eugene C. Robertson, and Sydney P. Clark, Jr., Apparatus for pressures of 27,000 bars and temperatures of 1400°C, *Ind. Eng. Chem., 49,* 1965–1966, 1957.

org, Iris, Glaucophane schists and eclogites near Healdsburg, California, *Bull. Geol. Soc. Am., 67,* 1563–1584, 1956.

ridgman, P. W., *The Physics of High Pressure,* 2nd ed., T. Bell. and Sons, London, 445 pp., 1949.

haves, F., Composition of the granites of Westerly and Bradford, Rhode Island, *Am. J. Sci., 248,* 378–407, 1950.

aly, Reginald A., Bushveld igneous complex of the Transvaal, Shaler Memorial Series, *Bull. Geol. Soc. Am., 39,* 703–768, 1928.

airbairn, H. W., and others, A cooperative investigation of precision and accuracy in chemical, spectrochemical and modal analysis of silicate rocks, *U. S. Geol. Survey Bull., 980,* 71 pp., 1951.

[all, A. L., The Bushveld igneous complex of the Central Transvaal, Department of Mines and Industries, Geological Survey, *Memoir 28,* 554 pp., The Government Printer, Pretoria, 1932.

[ess, H. H., and A. H. Phillips, Optical properties and chemical composition of magnesian orthopyroxenes, *Am. Minerologist, 25,* 276–285, 1940.

[ubbard, J. C., and A. L. Loomis, The velocity of sound in liquids at high frequencies by the sonic interferometer, *Phil. Mag., 5,* 1177–1190, 1928.

[ughes, D. S., and J. H. Cross, Elastic wave velocities at high pressures and temperatures, *Geophysics, 16,* 577–593, 1951.

[ughes, D. S., and H. J. Jones, Variation of elastic moduli of igneous rocks with pressure and temperature, *Bull. Geol. Soc. Am., 61,* 843–856, 1950.

[ughes, D. S., and H. J. Jones, Elastic wave velocities in sedimentary rocks, *Trans. Am. Geophys. Union, 32,* 173–178, 1951.

[ughes, D. S., and J. L. Kelly, Variation of elastic wave velocity with saturation in sandstone, *Geophysics, 17,* 739–752, 1952.

[ughes, D. S., and C. Maurette, Elastic wave velocities in granites, *Geophysics, 21,* 277–284, 1956.

[ughes, D. S., and C. Maurette, Variation of elastic wave velocities in basic igneous rocks with pressure and temperature, *Geophysics, 22,* 23–31, 1957*a*.

Hughes, D. S., and C. Maurette, Détermination des vitesses d'onde élastique dans diverses roches en fonction de la pression et de la température, *Rév. inst. franç. pétrole et Ann. combustibles liquids, 12,* 730–752, 1957*b*.

Hughes, D. S., W. L. Pondrom, and R. L. Mims, Transmission of electric pulses in metal rods, *Phys. Rev., 75,* 1552–1556, 1949.

Ide, John M., Comparison of statically and dynamically determined Young's modulus of rocks, *Proc. Natl. Acad. Sci. U. S., 22,* 81–92, 1936.

Ide, John M., The velocity of sound in rocks and glasses as a function of temperature, *J. Geol., 45,* 689–716, 1937.

Kracek, F. C., Neuvonen, K. J., and Burley, G., Thermochemistry of mineral substances, I, A thermodynamic study of the stability of jadeite, *J. Washington Acad. Sci., 41,* 373–383, 1951.

Kruger, F. C., Structure and metamorphism of the Bellows Falls Quadrangle of New Hampshire and Vermont, *Bull. Geol. Soc. Am., 57,* 161–206, 1946.

Larsen, Esper, S., Jr., Batholith and associated rocks of Corona, Elsinore, and San Luis Rey Quadrangles, Southern California, *Geol. Soc. Am. Mem., 29,* 1948.

Laughton, A. S., Sound propagation in compacted ocean sediments, *Geophysics, 22,* 233–260, 1957.

Lazarus, David, The variation of the adiabatic elastic constants of KCl, NaCl, CuZn, Cu, and Al with pressure to 10,000 bars, *Phys. Rev., 76,* 545–554, 1949.

Love, A. E. H., *A Treatise on the Mathematical Theory of Elasticity,* Cambridge University Press, 643 pages, 1927 (also Dover, New York, 1944).

Lund, E. H., Igneous and metamorphic rocks of the Minnesota River Valley, *Bull. Geol. Soc. Am., 67,* 1475–1490, 1956.

Mason, Warren, P., *Physical Acoustics and the Properties of Solids,* D. Van Nostrand Co., Princeton, N. J., 402 pp., 1958.

Mason, Warren, P., and H. J. McSkimin, Attenuation and scattering of high frequency sound waves in metals and glasses, *J. Acoust. Soc. Am., 19,* 464–473, 1947.

McSkimin, H. J., Ultrasonic measurement techniques applicable to small solid specimens, *J. Acoust. Soc. Am., 22,* 413–418, 1950.

McSkimin, H. J., Propagation of longitudinal waves and shear waves in cylindrical rods at high frequencies, *J. Acoust. Soc. Am., 28,* 484–494, 1956.

McSkimin, H. J., Ultrasonic pulse technique for measuring acoustic losses and velocities of propagation in liquids as a function of temperature and hydrostatic pressure, *J. Acoust. Soc. Am., 29,* 1185–1192, 1957.

Ross, C. E., M. D. Foster, and A. I. Myers, Origin of dunites and of olivine-rich inclusions in ba-

saltic rocks, *Am. Minerologist, 39,* 693–737, 1954.
Roth, W., Scattering of ultrasonic radiation in polycrystalline metals, *J. App. Phys., 19,* 901–910, 1948.
Silaeva, O. I., and Shamina, O. G., The distribution of elastic pulses in cylindrical specimens, (*Izvest. Akad. Nauk SSSR*), *Bull. Akad. Sci. USSR, Geophys. Ser.* (English ed.), *1,* 17–24, 1958.
Tocher, Don, Anisotropy in rocks under simple compression, *Trans. Am. Geophys. Union, 38,* 89–94, 1957.
Verma, R. K., Elasticity of some high-density crystals, *J. Geophys. Research, 65,* 757–766, 1960 (also Thesis, Harvard University, 1959).
Volarovich, M. P., and D. B. Balashov, Study of velocities of elastic waves in samples of rock under pressures up to 5000 kg/cm², (*Izvest. Akad. Nauk SSSR*), *Bull. Acad. Sci. USSR Geophys. Ser.,* (English ed.), *3,* 56–69, 1957.
Wyllie, M. R. J., A. R. Gregory, and L. W. Gard ner, Elastic wave velocities in heterogeneous an porous media, *Geophysics, 21,* 41–70, 1956.
Wyllie, M. R. J., A. R. Gregory, and G. H. F Gardner, An experimental investigation of fa tors affecting elastic wave velocities in poro media, *Geophysics, 23,* 459–493, 1958.
Zisman, W. A., Compressibility and anisotropy rocks at and near the Earth's surface, *Proc. Nat Acad. Sci. U. S., 19,* 666–679, 1933*a*.
Zisman, W. A., Comparison of the statically an seismologically determined elastic constants rocks, *Proc. Natl. Acad. Sci. U. S., 19,* 680–68 1933*b*.

(Manuscript received February 1, 1960.)

Radar Astronomy Symposium Report[1]

RAY L. LEADABRAND

Communication and Propagation Laboratory
Stanford Research Institute
Menlo Park, California

PREFACE

At the October 1959 meeting of the United ates National Committee of the International ientific Radio Union (URSI), a special sym- osium on radar astronomy was held. The mposium, which took the form of a panel scussion, was part of the technical program esented at the San Diego meetings by URSI ommission 3.

The purpose of the symposium was to call tention to the potential usefulness of radar in e exploration of the solar system and to re- rt on past work. Although the name 'radar tronomy' is relatively new, a number of ex- eriments of this class have been conducted for ore than 15 years. Recent improvement in dar systems and techniques, however, will on make it possible to extend new and im- rtant astronomical studies out to the far aches of the solar system.

To discuss this newly recognized field, a dis- nguished panel of experts was selected. Pro- ssor V. R. Eshleman of Stanford University rved as moderator, the other panel members ing Mr. B. Yaplee of the Naval Research aboratory, Dr. J. V. Evans of the Jodrell Bank xperimental Station of the University of Man- ester, Dr. R. B. Dyce of the Stanford Re- arch Institute, Dr. P. E. Green, Jr., of the ncoln Laboratory of the Massachusetts Insti- te of Technology, Professor W. E. Gordon of rnell University, and Dr. K. L. Bowles of the entral Radio Propagation Laboratory of the ational Bureau of Standards. The members of e panel were chosen because of their extensive owledge of past work in radar astronomy and because of the proposals several of them have made for future studies.

The subject of radar astronomy was divided for the purposes of the symposium into the topics: (1) radar studies of the moon; (2) radar studies of the planets; (3) radar studies of the exosphere and the interplanetary medium; (4) radar studies of the sun; (5) radar studies of meteors and auroras. After the opening remarks by the moderator, members of the panel were asked to review the present state of studies in each of the topic areas and to indicate the potentialities for future research. Comments and questions from the audience were then solicited, and, finally, the discussion was summarized by the moderator. In the following report an attempt has been made to give an accurate account of the speakers' remarks. However, the words are often those of the reporters, sometimes supplemented by written contributions from the panel members. The responsibility for any misquotation rests with the author of these proceedings.

INTRODUCTION

Von R. Eshleman (Moderator): Radar astronomy offers many interesting possibilities for studies of our solar system. Unlike visual and radio astronomy, radar astronomy does not depend upon emissions from the celestial objects that are to be investigated. Instead, it utilizes man-made emissions which are directed toward solar system objects, where some of the energy is scattered back to the sender. The added control inherent in the use of our own emissions makes possible new studies of solar system features as well as studies complementing and extending passive-astronomy and space-probe investigations.

Radar astronomical studies can be divided

[1] Fall Meetings, October 19–21, 1959, San Diego, alifornia, of USA Commission 3, Union Radio ientifique Internationale.

into two categories, depending in part on the wavelength used and on the type of object in the solar system to be studied: (1) the detection and study of solid bodies in the solar system by radar techniques (moon, planets, giant planet cores, asteroids, satellites, and space probes), and the measurement of solar system distances; (2) the detection and study of the ionized regions in the solar system by radar techniques (the sun and its corona, transitory solar streams of gas, the interplanetary medium, comets, planetary ionospheres, the regular and irregular components of the earth's exosphere, rockets and missiles during powered flight and re-entry, and gaseous markers released by deep space probes).

The measurements listed in the first category (solid bodies) can be accomplished best at microwave frequencies (400 to 2000 Mc/s), where the effects of the atmospheres of the earth and planets will be small, where very large antenna gains can be obtained, and where the new low-noise receiving devices are most important. The measurements listed in the second category (gaseous objects) would be best conducted at frequencies in the HF and lower VHF range (20 to 100 Mc/s). At such relatively low frequencies, the effects of the ionized regions in interplanetary space and near the sun and planets would be maximized. For example, radar studies of the sun are believed to be feasible only at the upper HF and lower VHF frequencies (e.g., between about 20 and 50 Mc/s), owing to the way in which absorption and reflection in the solar corona vary with frequency.

One of the most interesting features of radar astronomy is the relatively recent and simultaneous interest displayed by a number of researchers active in radio physics and upper atmospheric research. At least six groups in the United States and England are actively involved in radar astronomical research and are planning extensive future experiments. A meeting on radar astronomy was recently held by the Space Science Board of the National Academy of Sciences under the chairmanship of Professor Bruno Rossi. At this meeting, all facets of radar astronomy were discussed in the light of recommendations that should be made to the National Academy of Sciences. One interesting side feature which came out of the meetings was the definition of a new term of radar sensitivit —the millstone. One millstone is the sensitivit obtainable by the MIT Lincoln Laborator Millstone Hill radar, the radar used to obtai the first echoes from Venus.

The interest in radar astronomy follows natu rally from the fact that technological and sc entific progress has now made it possible t sound astronomical bodies beyond the moon. required about 70 db more system sensitivit to detect Venus than to detect the moon, an the time between the achievement of these goa was about 13 years, which amounts to a average increase of about 5 db per year in rad sensitivity. The increase is not linear, howeve and systems having sensitivities as great 10,000 millstones (an increase of 40 db) a now being built.

Radar Studies of the Moon

Von R. Eshleman: The first topic that will b discussed is the radar study of the moon. It w be introduced by Mr. Benjamin Yaplee and w be further discussed by Dr. John V. Evans ar Dr. Rolf B. Dyce.

Benjamin Yaplee: During the past 10 yea a continuously increasing effort has been ma to study and describe the properties of rad reflections from the moon. The major part this effort has been concentrated in the UH region and has used wide pulses or CW. Fro this study important information has been ob tained about the total electron content in th earth's ionosphere (to be discussed in det later in this meeting) and some conclusions ha been drawn about the extent and type of refle tion at the moon. From measurements of Far day rotation at 120 Mc/s, *Evans* [1959] fou that the electron content in the earth-moon pa was about twice that obtained from a paraboli layer model for the ionospheric electron distr bution. Both *Trexler* [1958] and *Evans* [195 have concluded that half the energy of the r flected lunar signal comes from a circular ar with a diameter equal to approximately a ten of the moon's disk. The moon's surface ther fore appears to be smooth. The data of Eva [*Browne, Evans, Hargreaves, and Murra* 1956] and Fricker [*Fricker, Ingalls, Maso Stone, and Swift,* 1960] and their colleagu show a definite correlation between librati

es of the moon and the fading rate of the ar echoes.

ystematic observations with narrow pulses l 10-cm waves were begun by Yaplee [*Yaplee, ıton, Craig, and Roman,* 1958; *Yaplee, Ro- n, Craig, and Scanlan,* 1958] in 1957 and by ghes [*Hey and Hughes,* 1958] in 1958. The se shape of the echoes confirmed that the on acted as a smooth reflector, but disagree- nt remains as to the reason why smooth re- tion occurs. *Senior and Siegel* [1958] have gested that the reflected signal is due to a discrete areas (perhaps five or six) and that first pulse in the received signal is generated a single area whose extent is about half a snel zone. The fluctuations of the signal plitude are presumed to be caused by the erent orientations of this area. Other investi- ors, including *Evans* [1959], believed that first reflected pulse is composed of the con- outions from several areas in a region deter- ned by the pulse width used, and that the ing is caused by interference of these local- l reflecting areas.

The range measurements, which are inti- tely tied up with the reflection mechanism l the assumed curvature of the moon, showed crepancies between the radar and the calcu- ed values. To obtain a broader understanding the reflection process and the effect of the pagating medium, and to put confidence lim- on the range measurements, a systematic dy of the whole problem of the reflection cess should be undertaken. Experiments for s purpose should use initially only narrow ses of the order of 1 to 5 microseconds so t adequate resolution would be obtained.

Knowledge of the type of specular reflection t is taking place at the moon could help to lain the observed range fluctuations. This y be tested in several ways which comple- nt and check each other:

1. Using two narrow pulses of 2 and 5 micro- onds alternately on one frequency, correla- n should be established if only one area tributes to the reflection. If several areas tribute to the echo, however, the wider pulse uld have larger fluctuation rates, since areas larger libration rates contribute to the re- ted signal.

2. Using two adjacent frequencies with the same pulse width should show no difference in return if one area of reflection is involved but should give different fluctuation rates if several areas are contributing to the return.

3. Using two widely separated frequencies, single-area reflection would cause larger fluctuations at the lower frequencies, since a larger area would reflect the signal. The opposite effect would be produced with several areas of reflection, and larger fluctuation rates would occur at the higher frequency.

4. Finally, the fluctuation rates of the moon echoes should be compared when the libration rate is a minimum and again when it is a maximum. For single-area reflection, there should be relatively little dependence of fluctuation rate on libration rate. But with several reflecting areas, large fluctuation rates would occur when the libration rate was a maximum. Assuming consistent results from these tests, a radar model of the moon could be constructed. If single-area reflection is obtained, an attempt should be made to correlate the radar echoes with visual regions on the lunar surface. By analyzing the complete video signal over long periods of time, the location and extent of other properly oriented reflected areas should be determined. The range differences of these discrete and localized areas could then describe the curvature of the moon. If no correlation with visual observation can be established, a corresponding electromagnetic model will be necessary. On the other hand, if it is found that energy in the initial pulse is made up of the reflection from several areas, a statistical model of these areas may be possible. In either event, the range of the leading edge will have more significance and an attempt can then be made to analyze the range discrepancies as a function of the reflection mechanism.

To obtain accurate range measurements with moderate transmitter power, a sequence of successively narrower pulses can be used which will make it possible to estimate the range of each successive pulse with greater accuracy. Thus, taking advantage of the high signal-to-noise ratio of wide pulses, it will be possible, knowing the repetition period and Doppler shift, to estimate the occurrence of narrower pulses even if they disappear into the noise. From fluctuation rate measurements of the gated

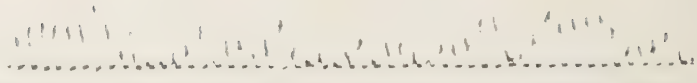

Fig. 1(*a*). Echoes strobed from the time base near transit showing rapid fading. Echoes are 1 second apart.

Fig. 1(*b*). Echoes strobed from the time base near moonrise where the fading is slow. Echoes are 1 second apart.

video in this region, it would be possible to determine the range with greater accuracy. This method would also provide a rapid means to measure the modulation loss as given by *Trexler* [1958]. By measuring the range over extended periods of time, the orbit of the moon can be determined with better accuracy, and from it improved values of various astronomical and geodetic constants can then be derived.

John V. Evans: In addition to range determinations, radar studies of the moon can give a statistical picture of the moon's surface. The work conducted at Jodrell Bank illustrates this ability. Figure 1(*a*) shows the relatively rapid fading of moon echoes near meridian transit; Figure 1(*b*) the slow fading of echoes at moonrise. Figure 2 shows the variation of moon libr tion rate for June 15, 1958, as compared wi the pulse-to-pulse correlation for echoes 1 se ond apart. It can be seen that the correlatic becomes much less during periods of high fadi rate or high moon libration rate. Figure 3 illu trates the observed autocorrelation function f 100-Mc/s moon echoes. The best-fitting cur for these data is a Gaussian function. Figure illustrates the power spectra of moon echoes observed at 100 and 120 Mc/s. These exper mental power spectra are compared with tl power spectrum of a uniformly bright mo (Lommel Seeliger) scattering. These curves lustrate the fact that at frequencies of the ord of 100 Mc/s the moon is limb dark, in contra to the optical picture, which is limb bright.

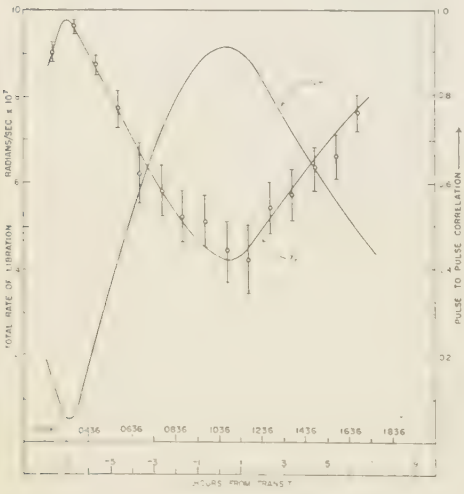

Fig. 2. The variation of the total libration $\dot{l}_T$ on June 15, 1958. Calculated using the expression given in the text. Also shown is the pulse-to-pulse correlation for echoes 1 second apart observed on this day.

The equipment used to obtain these resul consisted of the 250-foot radio telescope Jodrell Bank and a transmitter operating at 1 Mc/s with 8-kw peak power. A pulse length 25 milliseconds was used at a PRF of 1 cps. T receiver noise figure was 3 db, and the receiv bandwidth was 7 kc/s. Circular polarization w used to eliminate Faraday fading.

Rolf B. Dyce: Another technique for studyi the roughness of the moon surface uses spac receiving equipments. The moon may be r garded as a relatively small reflector (seve hundred kilometers in diameter) having an regular scattering pattern with very narr lobes. By observing the moon's reradiated pow distribution on the earth's surface, using spac receiving antennas, it should be possible, by t reverse logic, to determine the roughness of t moon's surface. On a test of this technique, t amplitude-time patterns of the pulse returns each of the three receiving locations were co pared using a 106-Mc/s moon radar with thr separate receiving antennas. (See Fig. 5 for ty

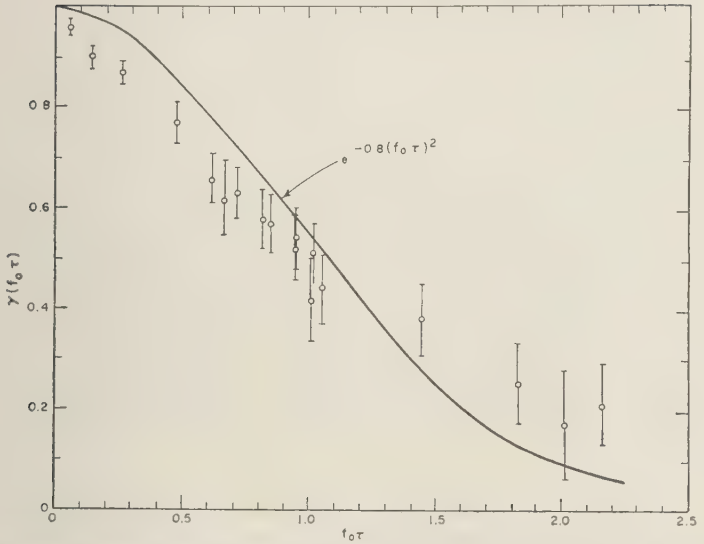

g. 3. The observed autocorrelation function $\gamma(f_0\tau)$ for echoes at 100 Mc/s. Also shown is a Gaussian function exp $[-0.8(f_0\tau)^2]$, which is the best fit to the observed points.

results.) It was found that correlation be-een the fading envelopes of the pulse patterns pped to 0.26 at a spacing of 1 km. This im-es a scattering fine structure of about 0.25 × $^{-5}$ radian, or an effective radius of the order 600 km.

This experiment may be of value to the moon-nce communication engineer, because it fixes spacing at which diversity antennas become ective for reducing the loss of intelligence due echo fluctuations.

Discussion of the study of the moon by radar ulted in a number of questions from the audi-e.

Question: Do the spaced receiving tests on on echoes agree with the results expected m libration and fading rate tests?

Answer: The correlation depends only upon roughness of the moon or the amount of the on's surface responsible for producing sig-s at the earth. The scattering pattern by the ced receiver method is in agreement with the ttering pattern obtained by computing the li-tion rate and measuring the fading rate at station.

Question: Why is the moon limb dark at radio quencies and not at optical frequencies?

Answer: There is a difference in wavelength of about 10^7 at optical frequencies. The moon, like terrestrial dust or rocks, scatters in all directions. At VHF, the lunar irregularities smaller than a meter are unimportant and the surface tends to reflect more like a silver sphere.

Question: Does the moon have an ionosphere?

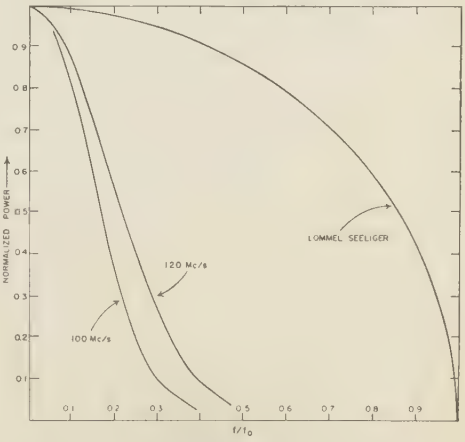

Fig. 4. The power spectra of moon echoes observed at 100 and 120 Mc/s [Browne, Evans, Hargreaves, and Murray, 1956]. The power spectrum produced by a uniformly bright moon (Lommel Seeliger) scattering is also shown.

Fig. 5. Echoes from the moon on 106.1 Mc/s showing uncorrelated fluctuations at separated receivers, January 11, 1958, 0500–0501 PST. The moon was near upper culmination: 177° azimuth, 47° elevation.

Answer: No. The experimental moon reflection data to date do not indicate the existence of a lunar atmosphere or ionosphere. The best measurements of this come from the study of the occultation of radio point sources by the moon.

Radar Studies of the Planets

Von R. Eshleman: The discussion of the possibilities of radar studies of the planets will be introduced by Dr. Paul Green. Dr. Green, a staff member of the MIT Lincoln Laboratory, is a coauthor of the paper announcing the first radar detection of Venus. The potentialities of radar astronomical studies of the solar system were made evident with this demonstration that radar is no longer limited to the earth-moon regions.

Paul E. Green, Jr.: My remarks will deal mostly with future possibilities, since so very little radar observation of planets has even been attempted to date. The radar range to Venus has been measured with some accuracy, but many experiments of a different and more remarkable type await the availability of more sensitive equipment.

Figure 6 tabulates a number of properties of the other planets in our solar system. Notice

BODY	CLOSEST DISTANCE (mile)	DIAMETER (mile)	ROTATION PERIOD	SYNODIC PERIOD (days)	ANGULAR SIZE (sec.)	NUMBER SATELLITES	OPTICALLY OBSER. TEMP. ON THE SUN-LIT SIDE (°K.)	CRITICAL FREQ. RELATIV TO EARTH FOR STANDARD IONOSPHERE
MERCURY	4.8×10^7 (conjunction) 9.3×10^7 (quadrature)	3.2×10^3	?	116	–	0	613	2.5
		"	–		9	–		
VENUS	2.6×10^7	7.6×10^3	?	584	67	0	370	1.4
MARS	3.5×10^7	4.2×10^3	$24^h\,37^m$	780	25	2	260	0.6
JUPITER	3.7×10^8	8.5×10^4	$9^h\,50^m$ (equator) $9^h\,55^m$ (temp. lats.)	399	50	11	143	0.3
SATURN	7.4×10^8	7.1×10^4	$10^h\,14^m$ (equator) $10^h\,38^m$ (lat. 35°)	378	20 (not including rings)	9	120	0.2
URANUS	1.7×10^9	3.1×10^4	$10^h\,49^m$	370	3.8	5	?	0.1
NEPTUNE	2.7×10^9	2.8×10^4	$15^h\,40^m$(?)	367	2.0	2	108	.05
PLUTO	3.5×10^9	3.7×10^3	16^h(?)	367	0.23	?	?	.025

Fig. 6. Planets as radar targets.

the rotation periods of two of our nearest ıbors, Venus and Mercury, are unknown. her, the nature of planetary surface condi- ; is almost completely unknown, Mars being aps the only exception. Rotation periods of ıard cores (if any) of the Jovian planets are ɔservable optically because of deep atmos- es. The sixth column in the table indicates the angular sizes are so small as to preclude some time any studies of the planets by lution of different portions with narrow an- a beams. The temperatures given are opti- derived; the current flurry of activity in measurement of radio temperature is pro- ng a series of figures which vary with wave- th and are generally higher than the optical es.

igure 7 lists the sun, all the major planets, e of their satellites, and some of the minor ets (asteroids). It shows along the abscissa radar detectability relative to 1 square er at 10,000 miles (the ratio of received to smitted RF power). As an arbitrary nor- ization, surface conditions on the target are ɔred in this computation, and a reflecting s section equal to the projected area is med. In actuality, one must be prepared the possibility of encountering high electri- losses in the planetary atmospheres, so that erved reflectivity could be disappointingly . The ordinate gives the time of flight of the al. (This time of flight becomes important n one begins to plan a radar detection in e detail; for example, the round trip to Pluto take more than 11 hours, and, therefore, the

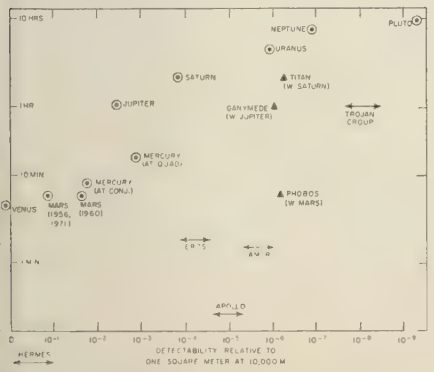

Fig. 7. Detectability of sun and planets.

earth's rotation will obviously hinder a radar probe of Pluto using long integration times from a single station.)

The minor planets tend to concentrate between Mars and Jupiter, but some are found outside this region. They become especially interesting when, as frequently happens, one of them makes an excursion to within a fairly small distance from the earth. During such passages they are of great usefulness to the astronomer. Besides being close, they have practically no disk, appearing instead as point sources, and so permitting very accurate measurements of parallax. Measurements on the minor planet Eros have constituted one of the best methods previously available for fixing the size of the astronomical unit, the mean radius of the earth's orbit about the sun. It frequently happens that a new minor planet is detected making a very close approach to the earth. For example, the minor planet Hermes came within half a million miles of the earth, only two moon distances away, and was subsequently lost. Such passages are usually unexpected and occur very rapidly, the body being lost again within a day or two. If radar observation capability can be mobilized quickly, observation of minor planets by radar could play an important part in the determination of distance. Also, since these bodies are optically point sources, the size must usually be inferred indirectly, e.g. by calculating the mass from observed perturbations by other bodies. Measurements of radar cross section would be very helpful in reckoning the mass of these bodies.

The minor planets are shown in Figure 6 in an approximate way because of this uncertainty about their diameter. Better knowledge of their surface properties is not completely uninteresting, but they almost certainly have no atmospheres, because of a low escape velocity.

The contemporary state of the art in high-powered transmitters, wide-aperture antennas, low-noise receiver input stages, and correlation detection techniques brings us at present to the point where Venus is just detectable, and that requires some 60 db more capability than the 1946 moon detection. As Figure 7 indicates, the number of other interesting targets will become available as sensitivity increases beyond that required for Venus. Indeed, by the time still

another 60 db in detectability becomes available, it should be possible to make radar contact with every planet but Neptune and Pluto.

Already at least two facilities with active radar capability are being planned whose intended performance offers exciting possibilities: the 1000-foot spherical dish with movable feed being planned by Cornell University for erection in Puerto Rico, and the Navy's 600-foot completely steerable facility at Sugar Grove, West Virginia. As presently planned, both these installations should provide about 45 db more predetection signal-to-noise ratio than the MIT Lincoln Laboratory's Millstone Hill radar used by *Price, Green, Goblick, Kingston, Kraft, Pettengill, Silver, and Smith* [1959], on Venus. It is hoped that these facilities will become usable within another 3 years.

Perhaps the simplest experiments, those requiring the most modest signal-to-noise ratio, involve distance measurement. The basic yardstick of the solar system is the astronomical unit—the mean radius of the earth's orbit—whose accuracy has been subject to steady refinement by optical means over a period of several centuries. Knowledge of the position of bodies in the solar system to 1 part in at least 10^6 or 10^7 is at present possible as long as the results are expressed in terms of the astronomical unit. The true size of this distance, however, has been in doubt by some 2 parts in 10^3. The extent of this disagreement is evident from Figure 8, which lists various proposed values of 'solar parallax,' the angle subtended at the sun by the earth's equator. (Shaded areas show claimed probable error; the IAU value is legislated number.) The difficulty lies in t fact that all previous nonradar methods of fixi the size of the astronomical unit depend parallax measurements, and, by virtue of t short base line obtainable on the earth and l cause of atmospheric refraction, they are lik to be permanently limited to about this order precision.

For some years, astronomers have regarc measurement of interplanetary distances as c of the first problems for a reasonable space rac program, and it was anticipated that the fi radar detection of any of the planets would i prove the precision of the astronomical unit at least one order of magnitude. For examp the previous uncertainty in the position of Ve was of the order of several times Venus's dia eter, so that, even if the atmosphere is fai thick and it is not known whether the ra return is obtained from the atmosphere or fr a reflecting surface somewhere beneath it, increase in distance accuracy still represents important contribution to the knowledge of solar system. Even more accurate measurem will be possible using a bare target such as M. especially if it can be assured that the retarc effect of interplanetary particles is negligibl can be corrected for. Such a correction could made using a multiple-frequency radar exp ment. If this can be done, it should be poss to measure the astronomical unit to the accuracy with which the speed of light i vacuum is known.

The next several years should see a numbe

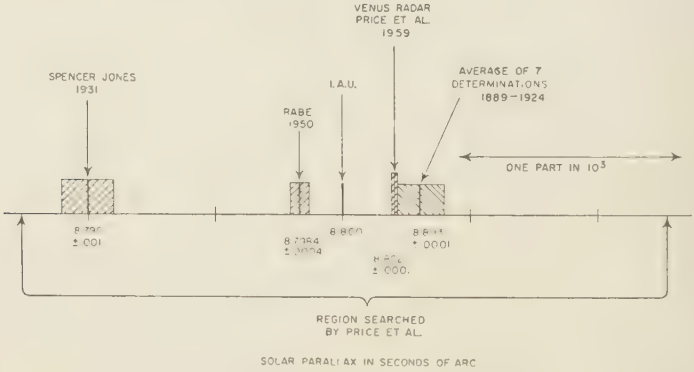

Fig. 8. Various proposed values of solar parallax.

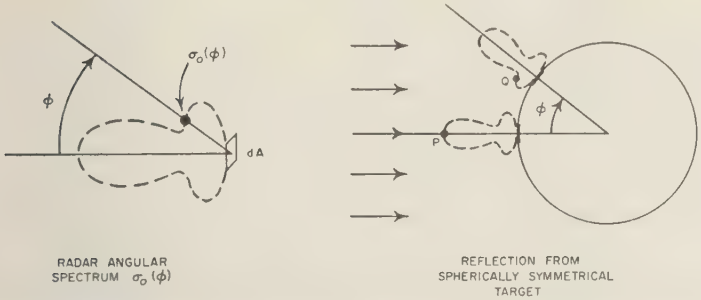

9. Depiction of way in which the radar angular spectrum $\sigma_0(\phi)$ of the planet influences the nature of the returned signal.

ies of distance to Venus, and later Mars, perhaps the minor planets. The technique making this measurement is to determine the of flight of the signal to the near face of planet. In getting the required degree of e resolution with peak powers that are likely e available, it will probably be desirable to pulse compression techniques for enhancing signal energy in each small range interval.

adar ranging on a planet at various places s orbit may help in fixing the orbital ele- ts more precisely. Ultimately the perihelion ion of Mercury and other planets might be sured with sufficient precision to assist in her experimental verification of general rela- y.

terplanetary radar techniques may very make their most spectacular contributions cience in the study of surface conditions on planets, since they seem to provide one of few methods for piercing cloudy atmos- es. The only planets whose visible surfaces known to be solid are the earth and Mars probably Mercury). Studies of conditions he solid surfaces (if any) of all the others t new non-optical experiments at wave- ths long enough to penetrate the atmos- es.

he resolution of individual surface features adar will have to rely on a high degree of e or Doppler resolution or both as we shall hortly, but a measurement of gross surface hness is relatively simple and should pro- a great deal of new information about a et.

et us define the time-average radar cross ion per unit area of a flat section of the planetary surface as $\sigma_0(\phi)$, where ϕ is the angle of incidence and reflection of the radar signal (see Fig. 9). We can call $\sigma_0(\phi)$ the *radar angular spectrum*, the fractional amount of radar energy returned per unit solid angle from a unit area of the surface as a function of ϕ, the deviation from normal incidence of the radar beam.

In general, $\sigma_0(\phi)$ will be different on different parts of the planetary surface. Oceans would give a high, narrow $\sigma_0(\phi)$, whereas rough, mountainous terrain would give a broad, low curve. The shape and magnitude of $\sigma_0(\phi)$ should yield considerable information about the surface. Thomas Gold has suggested that a frequency spectrum of σ_0 values might reveal something about the scale size of the material of which the surface is made, thus shedding some light on the nature of the terrain and perhaps even on whether vegetation is present. For illustrative purposes, Figure 4 shows a somewhat peculiar form of $\sigma_0(\phi)$.

There are several ways of determining the character of the radar angular spectrum experimentally. In particular, if we assume that the surface is uniform, that is $\sigma_0(\phi)$ is the same everywhere on the planetary surface, we can easily get $\sigma_0(\phi)$ either from the time-average return $\bar{\sigma}(\tau)$ due to a short transmitted pulse or (if the target rotates) from a related quantity $\bar{\sigma}(f)$, the average Doppler spectrum obtained from a long transmitted pulse.

Figure 9 shows how the total return is made up of reflections from different parts of the surface. The power returned from the near face of the planet (point P) will be proportional to $\sigma_0(0)$, whereas that from the other point at angle ϕ shown will be proportional to $\sigma_0(\phi)$.

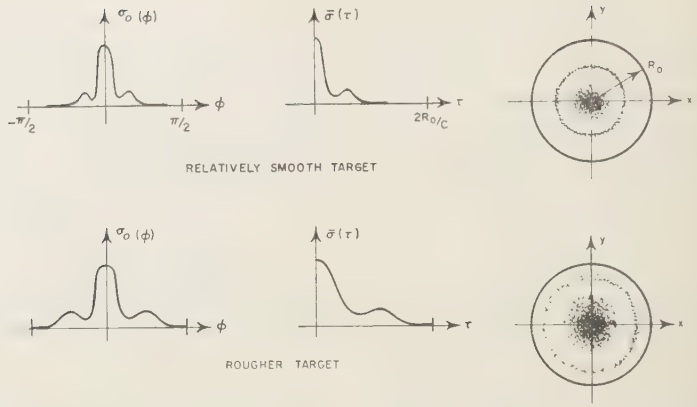

Fig. 10. Radar angular spectrum, pulse pattern, and 'surface illumination' for similar radar ang spectrum $\sigma_0(\phi)$.

The latter return will be characterized by a longer travel time and, if the planet is rotating, a Doppler shift.

The first way of determining $\sigma_0(\phi)$ then is by using pulse radar experiments to measure $\bar{\sigma}(\tau)$, the average cross section as a function of range, i.e., the pulse pattern. This is the method that has been most frequently employed with the moon.

If the surface of the planet is perfectly smooth and conducting, only the near face should be visible in the received pulse pattern. The depth will correspond to the first few Fresnel zones. On the other hand, extreme surface roughness will contribute some return all the way out to a value of delay $\tau = 2R_0/c$ corresponding to the limb of the planet. Figure 10 shows the way $\sigma_0(\phi)$ maps over into $\bar{\sigma}(\tau)$ for two different $\sigma_0(\phi)$ characteristics.

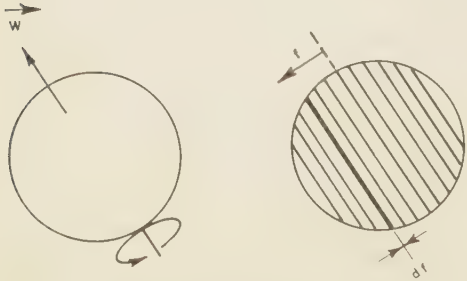

Fig. 11. The contours of equal Doppler frequency shift on a rotating sphere.

If the body is rotating with vector velo **W** (Fig. 11), strips on the surface paralle the axis will produce returns with var frequency displacements from the mean Dop shift associated with relative earth-planet mot The frequency displacement f is linearly portional to distance from the plane contai the axis and the line of sight. Depending on surface characteristic $\sigma_0(\phi)$ and the proje rotation vector $|W| \cos \alpha$ (α = angle betw axis and line of sight), an incident sine w will be mapped into a spread-out Dop spectrum $\bar{\sigma}(f)$. Knowing $\sigma_0(\phi)$ (perhaps f pulse measurements) and $\bar{\sigma}(f)$, one can dec $|W| \cos \alpha$. Or knowing $|W| \cos \alpha$, then $\sigma_0(\phi)$ be deduced from (f); this is the second of two methods enumerated a moment ago.

A lower limit on the rotation speed $|W|$ c be set from such a measurement, but ac determination of the vector **W** would rec the resolution of the ambiguity of values c M. H. Cohen of Cornell has proposed an inte ing method of almost completely resolving ambiguity by making these observations the planet at a number of different asp (different times during one synodic period).

In practice, one would abandon the notic spherical symmetry and be prepared for irreg surface conditions. The rotation period ca deduced from the resulting periodicities in l term radar records. Another possibility is pl in evidence by Figure 12, which shows a of $\bar{\sigma}(\tau, f)$, the time-averaged cross sectio

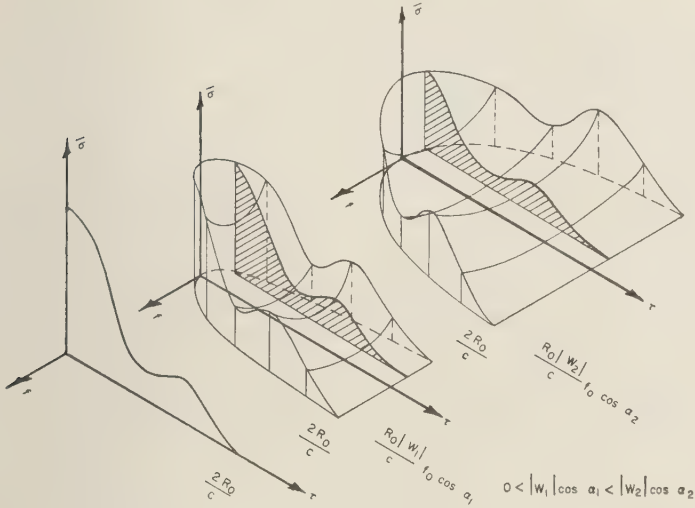

12. Three-dimensional plots of the time-averaged cross section of the target as a function of position in the range-doppler plane.

rget for an element of the range-Doppler $d\tau$ by df in size at range τ and Doppler f. previous quantity $\bar{\sigma}(\tau)$ is simply $\int_{-\infty}^{\infty}\bar{\sigma}(\tau, f)$ d $\bar{\sigma}(f)$ is $\int_{\infty}^{\infty}\bar{\sigma}(\tau, f)\,d\tau$.) A $\sigma_0(\phi)$ such as is in the bottom of Figure 10 is assumed in xample; rotation velocity is zero for the m at the left and has successively larger for the other two. The slice parallel range axis corresponds to the shaded region sphere in Figure 11. Thus, it is seen that on the surface of the sphere map over points in the range-Doppler plane. By le wave-form encoding techniques (pulse ression) it is possible to isolate small range- ency cells. Not only does this allow isolation given surface feature at a given time of vation, but, by exploiting the fact that as lanet rotates each feature will have a n trajectory in the range-Doppler plane, easurement of rotation period appears le in principle.

nasse [1959] of Lincoln Laboratory has sed an interesting series of experiments interferometers to determine the surface ion $\sigma_0(\phi)$ and the rotation vector **W**. The hand diagram of Figure 10, showing the n of returned signal strength on the surface planet, suggests the interferometer tech- of deducing $\sigma_0(\phi)$. The basis of the idea is as follows: It is well known that for small angles the far-field, voltage-gain pattern is the two-dimensional Fourier transform of the antenna aperture illumination. By analogy with this, the two-dimensional autocorrelation function of the illumination of the ground plane is the two-dimensional Fourier transform of the source distribution, assuming that the source is directly overhead. If the source is not directly overhead the two-dimensional autocorrelation function that would exist on a ground plane perpendicular to the line of sight is simply projected radially from the source on the actual ground plane.

From the right-hand diagrams of Figure 10, contour lines of the corresponding two-dimensional autocorrelation of the (perpendicular) ground pattern illumination would likewise be a series of concentric circles, but the circles would be larger for condition A than for condition B. The proposed method of finding this angular source distribution is to measure the autocorrelation function of the signals received at a pair of spaced receivers as a function of receiver separation and then take the Fourier transform of this autocorrelation function to find the shape of the source distribution. If the form of $\sigma_0(\phi)$ can be assumed and only the scale factor of the ϕ scale needs to be determined, a single pair of stations will suffice since they will give two

points on the space autocorrelation curve, one at zero and one at the value of spacing used. The rougher the target, the smaller the spacing required. The smallest value of spacing that would be necessary is the effective beamwidth on earth if the planet is regarded as a transmitting antenna, namely

$$D = 1.3\,(\lambda/\text{diameter})\ \text{range}$$

which for Venus is 0.2 mile at S band. Figures for angular size given in Figure 6 can be scaled accordingly to get the distance D for the other planets.

The vector **W** will be difficult to get from a single radar station but could be obtained by means of two interferometer measurements with crossed base lines, as has been proposed and analyzed in some detail by Manasse. The essence of the technique can be described by recalling the description in the preceding paragraph of the use of an interferometer for determining surface roughness. If we add to the picture the assumption that the target is rotating, the pattern of illumination produced at the earth sweeps across it at a vector velocity related to **W**. The cross correlation of signals received at two spaced receivers will be a maximum, not for zero delay of one signal relative to another, but for some new value of time delay equal to the projection of the receiver separation along the track of the pattern divided by the velocity of the pattern. The combination of two such measurements with effectively two different base lines then yields not only the scale of roughness (as described previously) but also a value of **W**.

It is not known whether any of the planets other than the earth have ionospheres, but it seems likely that they might, particularly those nearer the sun. A determination of electron density in the upper atmosphere of any planet would be a remarkable experiment and would provide one more piece of information about that planet's atmosphere to supplement the very few other bits of data we already have. The possible existence of the associated Van Allen radiation belts poses a serious problem to space travel.

A simple high-resolution pulse experiment at a suitably low frequency should show the ionosphere as a return from a range less than the planetary surface. The trick will be to get a signal outside the earth's ionosphere and yet have it reflect from the planetary ionosphere: carrier frequency f will have to be higher t sec θ times f_{oe} the critical frequency for densest layer of earth, and yet lower than critical frequency f_{cp} for the region of the pl tary ionosphere under inspection. The ang is the angle of penetration of our own i sphere. It can be expected that the valu f_{oe} will usually depend on the level of ioniza in the F_2 layer, and will vary from 2 or so m cycles at nighttime to around 12 to 15 at mid during the peak in the sunspot cycle, these ures being roughly halved during the trough the sunspot cycle.

Suppose we were to assume identical i spheres on all the planets. The rate of ion duction per unit volume is proportional to incident solar flux density, which is inve proportional to the square of the distance f the sun. Since critical frequencies are pro tional to the square root of ionization den the critical frequencies for the various pla would be in inverse proportion to their or radii. Figure 6 gives this crude figure relativ the earth. We see that it varies only over orders of magnitude from Mercury to P Almost certainly other factors will outweigh parameter.

One is tempted to look first at the inf planets, Mercury and Venus, particularly Ve since it is closest and is known to have a d atmosphere. At close approach (conjuncti however, we would be looking at the dark si the daytime. The frequency f_{oe} would be and f_{cp} would be low, so that it might no possible to find a proper frequency. Mar Jupiter would probably be better, since would be sunlit and observed at night du times of close approach (opposition). Jupit particularly suspicious because of the two t of peculiar electrical activity that have observed there at HF and at microwave quencies.

In principle, swept-frequency or mult frequency pulse experiments could reveal strength of the planetary magnetic field providing data on differences in time of fl critical frequency, or polarization of the r netoionically split components.

Almost limitless conjecture is possible on detailed experiments that might be done. W planetary radar studies become possible o

ive scale, the most important experiments robably be ones that we cannot now antici-

n V. Evans: There have been relatively attempts to obtain Venus echoes at Jod-ank. The 250-foot telescope was used with smitter of 50-kw power at 400 Mc/s. A of 1 cps was used with a 30-millisecond running continuously for 5 minutes and ff for 5 minutes. Theoretical considerations ted that a −10- to −15-db signal-to-noise should be expected. These results, although inary, indicated that Venus echoes were ed with a probability of 99 per cent.

AR STUDIES OF THE EXOSPHERE AND THE INTERPLANETARY MEDIUM

R. Eshleman: The exosphere of the earth is discussion is defined as all the ionosphere the height of the F_2 ionospheric layer num.

eral methods are possible for studying the here. The introductory discussion, to be ted by Dr. John V. Evans, will consist y of moon-echo results using the Faraday on technique. The description of a new que involving incoherent scattering from dual electrons will be presented by Pro- William Gordon and Dr. Kenneth Bowles. dditional technique which utilizes moon-studies but is independent of Faraday ro- will be presented from the floor by Dr. Gallagher.

n V. Evans: The amount of Faraday ro- observed by using moon echoes is a on of the earth's magnetic field and the on density of the medium. An examination e function $B \sec \chi \cos \theta$ vs. height, which rs in the equation for Faraday rotation

$$\Omega = \frac{1}{2\pi^2} \frac{e^3 c}{m^2 f^2} \int_d^h NB \cos \theta \sec \chi \, dh$$

tes that 98 per cent of the Faraday rota- would take place below 800-km height. lay rotation studies of moon echoes ob- l at Jodrell Bank suggest that there are times as many electrons above the layer num as below it. Such results would indi- that an appreciable portion of the iono- e extends to heights as great as 1000 km. *lliam Gordon:* Although the Faraday rota- technique indicates the integrated density in the region between 100 and 1000 km, it is not able to give an accurate shape of the curve of electron density vs. height. The free electrons in this region will scatter back a radar signal [*Gordon,* 1959]. Although the energy from an individual electron is quite small, the energy scattered by a large number of electrons is detectable provided that a relatively powerful radar is used.

A radar powerful enough to detect incoherent scattering from free electrons is to be constructed by Cornell University. The antenna will be spherical, 1000 feet in diameter, and will be built in an excavated earth depression in Puerto Rico. The spherical shape of the reflector will allow swinging of the beam up to ±20° of the zenith. The transmitter will have a peak power of 2.5 mw and will operate with a 10-millisecond pulse. The frequency of operation will be approximately 400 Mc/s.

Using this radar, not only will the electron density of the exosphere and interplanetary medium be obtained, but by measuring the Doppler spread of the radar returns from the electrons, a measure of the temperature of the ionized medium may be found.

Kenneth Bowles: For some months the National Bureau of Standards [*Bowles,* 1959] has been operating a very sensitive radar at Long Branch, Illinois, for the purpose of examining the nature of incoherent scattering from the ionosphere. The radar operates at 41 Mc/s with a peak power of 16 Mw. The antenna consists of an array of dipoles, 400 feet on a side, oriented to look at the zenith.

Incoherent echoes have been obtained from the ionosphere, and electron-density profiles have been constructed for heights up to 700 km.

As mentioned by the previous speaker, electron temperature measurements should be obtainable by observing the Doppler spread of the radar returns. These returns should be spread, on the basis of theoretical considerations, by as much as 400 kc/s. Experimental results, however, have yielded spreads as little as 4 kc/s. The difference between the experimental results and the theoretical predictions is believed to be due to coulomb attraction between the electrons and the positive ions.

An experiment that can produce more accurate results has been proposed for a location near the earth's magnetic equator so that propa-

gation normal to the earth's magnetic field can be observed. It is anticipated that it should be possible to measure the electron density vs. height, the electron temperature vs. height, the chemical composition of the ionized medium (based on the gyro rotation rate of the ions), and the magnetic field of the earth vs. height.

Philip Gallagher, Radio Propagation Laboratory, Stanford University (from the floor): The ionized medium between the earth and the moon is being studied at Stanford University by means of lunar radar echoes. Of prime interest is the ion density beyond the earth's ionosphere, i.e., in the interplanetary medium. There are several techniques based upon HF moon echoes for measuring the total integrated ion density between the earth and moon. The ionospheric part can be determined from Faraday rotation-of-polarization measurements and subtracted from the total, leaving a measure of the gas density in interplanetary space.

A straightforward method of measuring the total cislunar ion density would be to measure the delay time of an HF moon echo. The moon's radar range exceeds the true range because of group retardation, which is a measure of integrated ion density. Since the true range is not known very accurately, however, it would be better to send two pulses at different frequencies, the higher-frequency pulse serving as a time reference. The added delay of the lower-frequency pulse would then be directly proportional to the integrated ion density. The lower frequency should probably be below 50 Mc/s in order for the extra delay not to be masked by the effects of the rough lunar surface.

Since a single pulse is made up of energy spread over a band of frequencies, the differential delay could in theory be made with just a single pulse, the pulse dispersion or spreading in the echo being a measure of the gas density.

Although the above methods would be the most direct, they are not feasible with our present HF equipment because of the requirement of many megawatts of peak power to obtain strong echoes at short pulse lengths. Several equivalent CW methods have been contrived, so that the full average-power capability of our HF transmitter can be used effectively. In one method (equivalent to the pulse dispersion method), three equally spaced frequencies are sent in the form of a frequency-modulated wave. Their relative phases, and hence the chara of the modulation, are changed as the resu dispersion in the cislunar medium. The v of the modulation frequency at which a quency-modulated transmitted wave is cha to an amplitude-modulated echo would direct measure of the integrated cislunar density. This CW method has been tried a Mc/s for about 6 months. It is now evident path splitting during propagation between earth and the moon, or the roughness of lunar surface, causes more phase variation is produced by dispersion alone.

A different CW method will soon be tried, it is hoped that the above difficulties wil overcome. In this second method (equivale the differential delay of two pulses), Stan University's 23-Mc/s transmitter and a Mc/s transmitter belonging to Stanford search Institute will be modulated by the audio source, and the relative phases of echo waves will be compared. If this mea ment proves successful, it will be very inte ing to find how the density of the interplan medium changes with the ever-changing act of the sun.

Radar Studies of the Sun

Von R. Eshleman: The possibility of ob ing radar echoes from the sun was first disc by *Kerr* [1952] about 8 years ago. At that the sensitivity of the radar needed for the d tion of sun echoes may have seemed so pro tive (at least 50 db more sensitive than ne for moon echoes) as to make a solar rada periment of academic interest only. The d opment of higher-powered transmitters, antennas, and data-processing techniques, ever, makes such studies feasible. Several gr are now attempting or planning to obtain e from the sun: Stanford University, MIT coln Laboratory, and the Central Radio P gation Laboratory.

The introductory comments about sun e will be made by Dr. Kenneth Bowles.

Kenneth Bowles: On the basis of the com tive visual diameter of the sun and the n the radar required for sun echoes will ne be 50 db more sensitive than that require moon echoes. Since this is now viewed as n overwhelming difference, the possibility o taining sun echoes is most inviting. Theor

siderations by *Kerr* [1952] and the Russians ss *and Braude,* 1957] predict severe absorp- of radar signals in the sun's corona, the orption increasing with frequency, owing to greater penetration into the corona for the ier frequencies. Because of this absorption, frequency to be used should be as low as sible (provided that it will penetrate the h's ionosphere). A frequency in the 30-Mc/s ge has been predicted as most suitable for ar echoes from the sun.

s the effective noise temperature of the sun bout 10° degrees it will be necessary to have adar at least 70 db more sensitive than the ar needed for moon echoes. Owing to mag- ionic effects in the sun's corona, it is possible t a higher frequency (400 Mc/s) could be d for sun echoes.

ome characteristics of the sun's corona would icate that it might be quite rough, resembling rcupine quills. The quills would be irregular moving and changing with time. It might possible to get multiple echoes from the co- a and even to measure velocities of the par- es in various sections. Radar echoes from ividual gas clouds thrown out from the sun ght be possible.

The echoes from the sun, its corona, and from clouds will probably be much more complex n echoes from the planets. It is possible, refore, that the complex data-processing tech- ues used by MIT Lincoln Laboratory for aus echoes might not be practical for sun oes on account of Doppler broadening. If so, may be necessary to employ more sensitive ars for sun echoes than have previously been dicted.

William Abel, MIT Lincoln Laboratory (from floor): MIT Lincoln Laboratory has at El mpo, Texas, a 32-Mc/s, 300-kw CW transmit- . The possibility of using this transmitter for echoes has been recognized, and a large an- na array is being constructed for this pur- se. This radar should be in operation sometime arly 1960.

Philip Gallagher, Radio Propagation Labora- y of Stanford University (from the floor): e Radio Propagation Laboratory at Stanford iversity has been attempting to obtain sun oes for some time now, using a radar of mar- al capability. Magnetic tape recordings of the echo tapes are being processed on an elec- tronic computer to determine whether sun echoes have been obtained.

Radar Echoes from Meteors and Auroras

Von R. Eshleman: The subject of radar echoes from meteors and auroras will be introduced by Dr. Rolf Dyce of Stanford Research Institute.

Rolf B. Dyce: The study of meteor echoes is perhaps the first form of radar astronomy. Considerable work has been done to study the orbits of meteors, the ionization produced by the meteors, and the number and duration of meteor trails observable at about 90-km altitude. The much higher-powered radars described by the previous speakers may make it possible to obtain echoes from the meteoric particles before they enter the earth's atmosphere and destroy themselves. By such studies it may be possible to learn something of the nature of the particles and to compare it with the ionization trail formed by them.

Many radar studies of auroral ionization have been made in recent years. At present it is believed that the aurora is most likely initiated protons and electrons. The shape, position, and time variations of the 'outer' Van Allen belt suggest that this belt of trapped charges, at least along its outward or poleward edge, should be related to the aurora. This outer region, of which little is known, may represent an immense reservoir, filled occasionally by the sun and emptied frequently as an aurora down in the atmosphere. Future radar studies of the aurora using more sensitive radars may relate these trapped charges to the auroral ionization occurring in the ionosphere. It should be pointed out here that the parts of the Van Allen belt systems that are dangerous to man because of high particle energy actually have an electron density of only about 1 electron per cubic meter, a value only 10^{-12} that of the F region and certainly not adequate to return a radar echo. Even more interesting for future radar astronomy experiments of the aurora is the possible interrelation of auroral ionization, Van Allen charged particles, and the outer extensions of the sun's corona. Such studies appear to complement rocket probe experiments advantageously.

Fred L. Whipple and Gerald S. Hawkins, Harvard College Observatory (contributed in absentia): A three-station radar network has been

constructed at the Long Branch Field Station, Illinois, of the National Bureau of Standards for the study of meteors. At the central station a 10-Mc (peak) transmitter of the National Bureau of Standards is being used in conjunction with a trough antenna of 22-db gain.

The system is designed to measure the velocity, height, radiant point, and orbit of individual meteors, and the sensitivity limit is estimated to be eleventh magnitude. In addition the system will yield data on the ionization curve of the meteor and other measurements pertaining to the physics of the meteor process. It is also planned to make the system phase coherent to obtain data on upper-atmosphere winds and turbulence.

Conclusions

Von R. Eshleman: It would appear from the foregoing discussion that the relatively new field of radar astronomy is well under way at a number of organizations, and several more programs are in the planning stage.

The two-pronged attack needed for radar astronomical investigations has already been mentioned: the use of HF radar for the study of distances and solid surfaces and of LF radar for study of gaseous regions near the sun and planets and in space. The radar approach to astronomical studies in the solar system is fundamentally complementary to passive visual and radio astronomy. Even though the new information gained by radar to this date is somewhat limited, the future of this new approach to astronomy seems bright indeed.

It is hoped that those agencies of the government supporting research will recognize the potential usefulness of radar astronomy in their future programs. Not only will radar astronomical techniques be useful in their own right, but they should provide a useful supplement to the data obtained by space probes. The cost of radar astronomy programs such as those described in this meeting is less than that of one rocket space probe.

Acknowledgment. The author wishes to acknowledge the help of the chairman of USA Commission 3 of URSI, Professor L. A. Manning, for making it possible to hold this symposium. The help of Messrs. G. Parks, A. Fredriksen, M. Baron, and L. Dolphin of the Stanford Resear Institute in reporting on the symposium is al appreciated. The author is grateful to the par members who supplied written material and illu trations for use in this report. Much of the wo reported by the speakers was supported by t Advanced Research Projects Agency, the Air For Cambridge Research Center, the Naval Resear Laboratory, and the Rome Air Developme Center.

References

Bass, F. G., and S. I. A. Braude, On the questi of reflecting radar signals from the sun, *Ukra ian J. Phys., 2,* (2), 149–163, 1957.

Bowles, K. L., Incoherent scattering by free ele trons as a technique for studying the ionosphe and exosphere: Observations and theoreti considerations, *Natl. Bur. Standards Rept. 60* September 18, 1959.

Browne, I. C., J. V. Evans, J. K. Hargreaves, a W. A. S. Murray, Radio echoes from the moo *Proc. Phys. Soc., 69,* 901, 1956.

Evans, J. V., Research on moon echo phenomer *Final Rept. 5–1–56 to 5–1–59,* University of Ma chester, Jodrell Bank Experimental Station, 19

Fricker, S. J., R. P. Ingalls, W. C. Mason, M. Stone, and D. W. Swift, Measurement and co putation of the characteristics of moon-reflect UHF signals, Lincoln Laboratory, MIT, Lexin ton, Massachusetts, to be published, 1960.

Gordon, W. E., Incoherent scattering of rad waves by free electrons, *Proc. IRE, 46,* 182 1829, 1959.

Hey, J. S., and V. A. Hughes, Radar observatio of the moon at 10 cm wavelength, *Paris Sy posium Radio Astron.,* August 1958.

Kerr, F. G., On the possibility of obtaining rad echoes from the sun and planets, *Proc. IRE,* 660, 1952.

Manasse, R., The use of radar interferomet measurements to study planets, *MIT Linco Laboratory Group Rept. 312–23,* March 18, 19

Price, R., P. E. Green, Jr., T. J. Goblick, Jr., R. Kingston, L. G. Kraft, Jr., G. H. Pettengil, Silver, and W. B. Smith, Radar echoes fro Venus, *Science, 129* (3351), 751–753, 1959.

Senior, T. B. A., and K. M. Siegel, Radar refle tion characteristics of the moon, *Paris Sy posium Radio Astron.,* August 1958.

Trexler, J. H., Lunar radio echoes, *Proc. IRE,* 286, 1958.

Yaplee, B. S., R. H. Bruton, K. J. Craig, and N. Roman, Radar echoes from the moon at a wav length of 10 cm, *Proc. IRE, 46,* 293, 1958.

Yaplee, B. S., N. G. Roman, K. J. Craig, and T. Scanlan, A lunar radar study at 10 cm wav length, *Paris Symposium Radio Astron.,* Augu 1958.

(Manuscript received February 5, 1960.)

Corpuscular Radiation Experiment of Satellite 1959 Iota (Explorer VII)[1]

GEORGE H. LUDWIG[2] AND WILLIAM A. WHELPLEY

Department of Physics and Astronomy
State University of Iowa
Iowa City, Iowa

Abstract. Satellite 1959ι (Explorer VII) carries an apparatus prepared by the Department of Physics and Astronomy of the State University of Iowa for comprehensive spatial and temporal monitoring of total cosmic-ray intensity, geomagnetically trapped corpuscular radiation, and solar protons. In view of the successful operation of the equipment during the first 2 months of flight and the expectation of its continued operation until October 1960, we have considered it desirable and worth while to invite international participation in the recording and interpretation of the radiation observations. A full description of the apparatus is given, including detector calibrations, telemetry code, samples of actual recordings, and other pertinent information.

ntroduction. At 1530 UT on October 13, 9, earth satellite 1959ι (Explorer VII) was cessfully launched by its Juno II rocket. The ntific payload was planned by the United tes IGY Technical Panel on the Earth Satel- Program, and the flight was included in the ited States part of the International Geo- sical Cooperation, 1959. This satellite con- as a number of pieces of apparatus, one of ch is a charged particle radiation monitor pared by the Department of Physics and ronomy of the State University of Iowa II). It is the purpose of this paper to de- be the instrumentation so that any inter- d group can receive the signals from the llite and reduce them to a form suitable for ding, analysis, and interpretation. It is hoped t the dissemination of detailed instructions reducing this part of the satellite data will ke world-wide participation in the experi- nt possible. Also, the originating group at I will be grateful for telemetry records cover- periods of time during which no observa- ns are available from the present network. The instrumentation is designed for a 1-year rating lifetime, at the end of which the power supply is to be disconnected by means of an on-board timer. Of course, component failure may occur sooner, thus shortening the effective life.

Orbital characteristics of 1959ι (Explorer VII). The orbital characteristics are exemplified by Table 1 for the epoch 1540 UT, November 28, 1959 (courtesy National Aeronautics and Space Administration).

Predictions of equatorial crossings are prepared weekly by NASA. But since the orbit is nearly circular and the effect of atmospheric drag very small, we find it easy to construct satisfactory predictions for several days in advance by extrapolations of local station observations.

Telemetry. The payload carries two transmitters. The higher-frequency one (108 Mc/sec) was powered by chemical batteries only and operated for 36 days of orbital life until they were exhausted. The lower-frequency transmitter and all the equipment connected to it are powered by a bank of chemical batteries which is recharged by an array of solar cells whenever the payload is in sunlight. The lifetime of the system is limited only by the on-board timer (1 year) and by possible component failure. This transmitter operates at a frequency of 19.994 Mc/sec and has an output power of 0.6 watt. It drives a crossed dipole antenna which is circularly polarized. The transmitted carrier

Assisted by United States IGY Project 32.1 of National Science Foundation and the National demy of Sciences and by the National Aero- tics and Space Administration.
[2] Research Fellow of the U. S. Steel Foundation.

TABLE 1

Anomalistic period	101.32 min
Rate of change of period	−0.00037 min/day
Inclination	+50.35°
Right ascension of ascending node	+316.18°
Motion of ascending node	−4.211°/day
Argument of perigee	+208.71°
Motion of perigee	+3.415°/day
Mean anomaly	+271.66°
Eccentricity	+0.03648
Semimajor axis	1.128694 earth radii
Perigee altitude	558.2 km
Apogee altitude	1083.5 km

is amplitude-modulated by the summed output of four frequency-modulated subcarrier oscillators (nominal center frequencies 560, 730, 960, and 1300 cycles per second).

The remainder of this paper is concerned only with the SUI corpuscular radiation experiment. The operation of the instrumentation is illustrated schematically in the block diagram of Figure 1. Two Geiger-Müller counters are used, a small one (Anton type 302), associated with a large scaling factor, which is 'on scale' in the presence of the highest expected intensity in the radiation belts, and a larger counter (Anton type 112), used with a smaller scaling factor, which is useful in the range from cosmic-ray intensity to an intermediate level. Over the part of the dynamic range in which the counters overlap an absorption coefficient can be determined, since they are covered by different but known thicknesses of absorber.

The output voltages of the two Geiger counter channels frequency-modulate the 1300 cycles per second subcarrier oscillator. No other data are applied to this channel. The oscillator has four discrete frequency 'states,' as determined by the combination of the two scaler output voltages. Each of these four states correspon to a unique combination of the two states the final stages of the two scaling circuits, listed in Table 2 and illustrated in Figure 2. T SCO frequencies given in Table 2 may va slightly as the temperature of the instrumen tion varies. They are typical of those observ during the first 2 months of orbital flight. change in state of the 112 counter scaler caus a change in subcarrier frequency of 40 to cycles per second; a change in state of the 3 counter scaler causes approximately a 90 cy per second frequency shift. Therefore the t scaler outputs are readily distinguished, ev when the absolute frequencies are not measur

Detector characteristics. Both Geiger-Mül counters were manufactured by Anton El tronic Laboratories, Inc. They are haloge quenched and have an essentially unlimit operating lifetime. The temperature of our d tector assembly on the satellite has thus been within the range −20° to 57°C, which well within the operating range of the counte and associated circuits.

The characteristics and dimensions of t counters are listed in Table 3, and a summa of the absorbers surrounding the counters given in Table 4. The omnidirectional flux

$$J_0 = R/\epsilon G_0$$

TABLE 2. Telemetry Code

State	SCO Frequency, cycles/sec	112 Counter Scaler	302 Counter Scaler
1	1219	Off	Off
2	1256	On	Off
3	1304	Off	On
4	1368	On	On

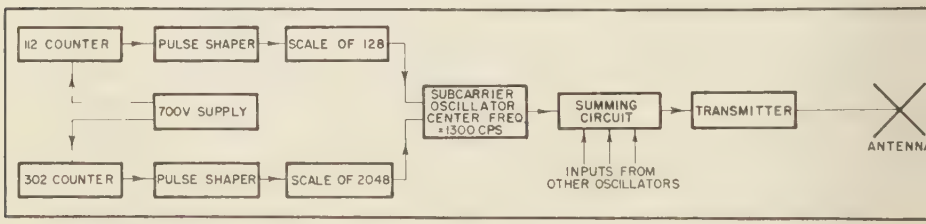

Fig. 1. Block diagram of the SUI charged particle radiation experiment of satellite 1959ε.

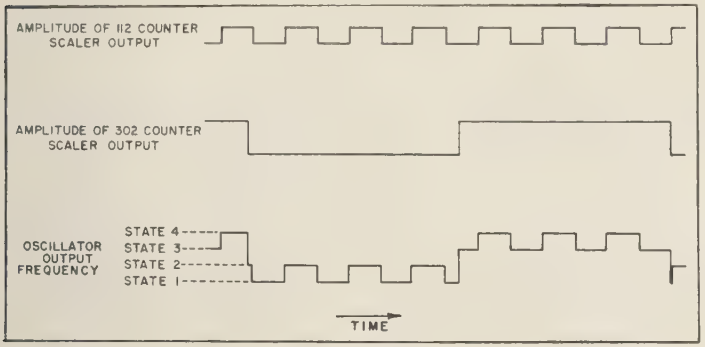

ig. 2. Illustration of the method of combining the two scaler outputs on a single telemetry channel in satellite 1959ι.

here ϵ and G_0 are as listed in Table 3. R is the ue counting rate, which is defined as the ounting rate of a counter and scaler having ero dead time but with otherwise identical haracteristics. The instrumentation was cali- rated with an X-ray source before flight to btain the relationship between r, the apparent ounting rate, and R. The data are accurately epresented by the semi-empirical expressions sted in Table 5, where the values of τ are orrect at 23°C and at the nominal primary ower supply voltage (6.5 volts). These values f τ vary somewhat with temperature and upply voltage. The effect is to change the urves by an amount which is trivial at low R nd which increases as R increases. For the 112

TABLE 3. Characteristics of Geiger-Müller Counters

	112 Counter	302 Counter
ffective diameter (a), cm	1.82 ± 0.01	0.65 ± 0.03
ffective length (l), cm	5.27 ± 0.1	0.94 ± 0.1
mnidirectional geometric factor (G_0), cm²	9.02 ± 0.19	0.61 ± 0.09
bsolute efficiency (ϵ) for energetic charged particles	0.81 ± 0.03	0.84 ± 0.05
mnidirectional flux (J_0) for energetic charged particles	$0.137R_{112}$	$1.95R_{302}$
caling factor (s)	128	2048

counter at $R = 2000$ sec^{-1} the temperature coefficient of r is about +1.5 percent °C^{-1}, and its supply voltage coefficient is about +1.7 per cent for a one per cent change in supply voltage. The temperature and supply voltage are expected to always be within the ranges −20° to 60°C and 5.8 to 7.2 volts. Temperature and supply voltage corrections of the 302 counter data are trivial for R less than 5000 sec^{-1} and small for R less than 10,000 sec^{-1}. The value of r is obtained from the telemetry records; it is simply

$$r = ns/t(n)$$

where s is the scaling factor and $t(n)$ is the time for n full cycles of the scaler output wave form. It should be noted that the relationship between R and r is a double-valued function. It is expected that the counting rate of the 302 counter will always remain on the ascending part of the curve. The ambiguity in the 112 counter data can nearly always be resolved by the use of auxiliary data: spatial dependence of counting rate, the simultaneous rate of the 302, and the statistical fluctuations of the 112 rate. It should be further noted that the values of J_0 given in Table 3 are meaningful only if all counts are produced by energetic particles passing directly through the counters. Other detection processes require a different relationship between J_0 and R. If, for example, the counts are due only to the bremsstrahlung from 60-kev electrons stopped in the walls of the equipment,

$$J_0 = (4 \times 10^5)R_{302}$$

TABLE 4. Absorbers Listed in Order from Counter Outward

Item	Material	Absorption, (mg/cm²)	Solid Angle, ster
		112 Counter	
Counter cathode	28% Cr 72% Fe	40 for 81% of cathode surface 241 for 19% of cathode surface	...
Counter ends	Ceramic	0.4 cm thick	...
Absorber	Al	260 ± 3	4π
Absorber	Pb	1150 ± 30	4π
Detector box	Mg	140 ± 40	4π
Payload structure	Mostly Al	>1700	3.9
Instrument column	Mostly Al	>3000	0.84
		302 Counter	
Counter wall	28% Cr 72% Fe	402 ± 20	*
Detector box	Mg	140 ± 40	4π
Payload structure	Mostly Al	>1700	3.9
Instrument column	Mostly Al	>3000	0.84

* The section of the counter wall having this absorption is 0.57 cm long. The remainder of the wall an the ends are a combination of stainless steel, ceramic, and aluminum having several times this absorptio

Receiving equipment. Any reasonable antenna and sensitive receiver are capable of receiving the telemetry signal from satellite 1959*ι*. At the SUI receiving station, an omnidirectional, circularly polarized antenna is located on the roof of the physics building. On the antenna mast is a radio-frequency preamplifier, and a Collins R-390 receiver is in the basement, about 100 feet from the preamplifier. Pre- and post-detection receiver bandwidths of about ±2000 cycles per second are used.

The output of the receiver is the sum of the subcarrier oscillator frequencies. This can be tape-recorded for later reduction, or passed directly through a data reduction system. The data reduction system used at SUI includes a bandpass filter centered at 1300 cycles per second and having a width of ±7½ per cent to separate this subcarrier channel from the other channels. Following this is a narrow band (BW = 60 cycles per second) FM discriminator to demodulate the subcarrier signal. The resultin output is recorded as a function of time by moving-pen oscillograph. Alternatively, a simpl 'comb' filter, consisting of four LC tuned narro bandpass filters (15 cycles per second BW connected with their inputs in parallel, has bee found capable of producing a high-quality oscil lograph record. Each of the four filters is tune to a different one of the four discrete frequencie listed in Table 2. The outputs of the individua filters are rectified, passed through RC integra tors, and combined in such a way that the tw information channels are available separatel for recording on a multichannel oscillograph.

The importance of recording accurate an reliable time on all magnetic tapes and oscillo graph records cannot be overstressed. Th orbital information is obtained as a function o time. Therefore the time correlation of all dat is necessary in order to establish the cor respondence between a particular bit of dat

TABLE 5. Conversion from True Rate R to Apparent Rate r

Counter Channel	Range of Applicability, sec^{-1}	Formula	τ_1, sec	τ_2, sec
112	R = 0–5000	$r = R/(1 + R\tau_1)$	7.30×10^{-4}	...
112	R = 4000–20,000	$r = (R/[1 + R\tau_1])(e^{-R\tau_2})$	5.04×10^{-4}	6.2×10^{-5}
302	R = 0–100,000	$r = R/(1 + R\tau_1)$	3.64×10^{-5}	...
302	R > 100,000	R is not expected to exceed 100,000		

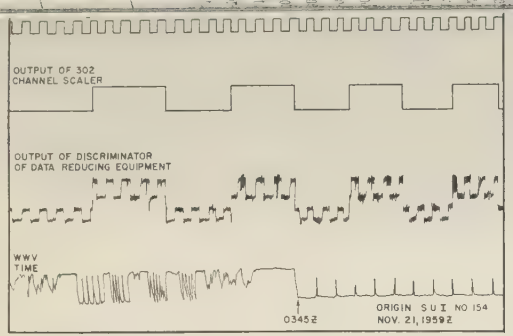

Fig. 3. Sample data recording and analysis, with a medium ratio of 112 to 302 scaler output rates and a moderately high signal-to-noise ratio. The form of the WWV time display used on the oscillographic recordings is also shown.

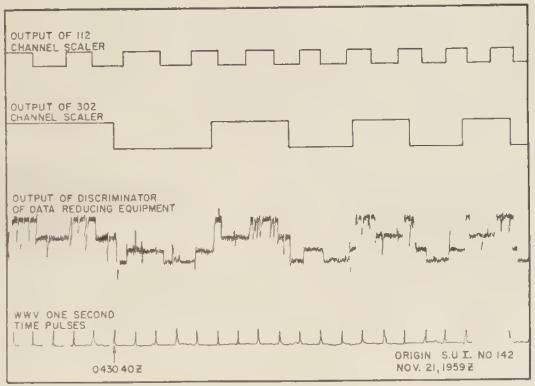

Fig. 4. Sample data recording and analysis, with a moderately low ratio of 112 to 302 scaler output rates and a moderately high signal-to-noise ratio.

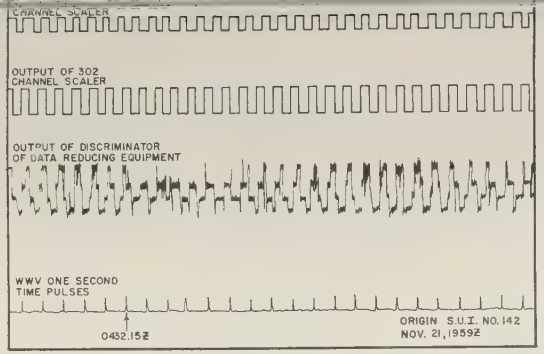

Fig. 5. Sample data recording and analysis, with a near-unity ratio of 112 to 302 scaler output rates and a moderately high signal-to-noise ratio.

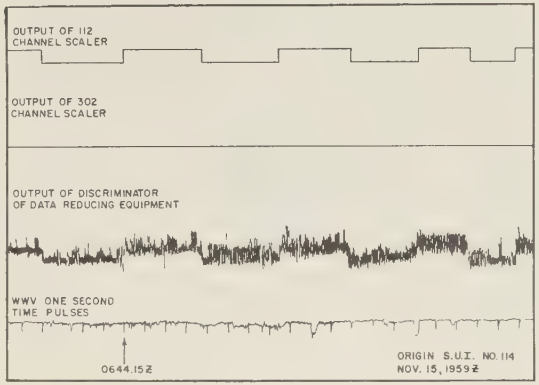

Fig. 6. Sample data recording and analysis, with a high ratio of 112 to 302 scaler output rates and a rather low signal-to-noise ratio.

and the location of the satellite at the time of receipt of the data. Whenever this correspondence cannot be established, the data are usually worthless. A time base must be recorded on recordings at the time of signal reception. Neither a local voice announcement of the time nor a manually applied mark on the records has proved satisfactory. By far the simplest and most practical system is to record the output of a WWV or other standard time signal receiver on a second channel of the recordings. All recordings should include an absolute time announcement by the standard time station. Then, if care is taken to record the universal date on the records, the time information is complete and unambiguous.

The simple receiving station outlined above produced an average of 4.5 usable recordings each day during the 2-month period from October 14 to December 14. The duration of readable data has averaged 7.2 minutes per pass, many passes continuing for more than 12 minutes. Reception during the night is usually superior to that during the day, owing presumably to more favorable ionospheric conditions.

Data reading. The output of the FM discriminator on the ground is, in the absence of noise, of the same form as the subcarrier oscillator output, illustrated in Figure 2. Noise makes the wave form more difficult to read, but, since it is a composite of two rectangular wave forms, good discrimination against noise spikes can be made by a trained data reader. Samples of actual recordings are included as Figures 3, 4, 5 and 6, along with their interpretations, in order to illustrate the method of reading the data.

In Figure 3 the ratio of 112 to 302 scaler output switching rates is 7.4, and the signal-to-noise ratio is large. Under these conditions the data are easily readable. This record also illustrates the manner in which the WWV time signal is recorded on the oscillograph records. A coded time announcement is shown followed by the 1-second markers. In Figure 4 the scaler output ratio is somewhat lower (2.6), and in Figure 5 it is nearly equal to unity (1.03). In both cases the data are still easily readable. Note that in Figures 3 and 4 the rates change appreciably during the 25 second intervals.

Figure 6 shows the appearance of the data in the presence of considerably more noise. In th recording segment no switching of the 302 scal output is observed. The 112 rate can be dete mined reasonably well.

Concluding remarks. A great variety of lar and small temporal fluctuations of radiation i tensity has been observed during the first months of orbital life of 1959ι, especially in hi latitudes. We believe that others will find t study of the spatial and temporal dependenc of intensity of considerable geophysical a astrophysical interest. The establishment of receiving station for the reception of the co puscular radiation data from satellite 1959ι a reasonably modest undertaking, and the da are quite easily read and reduced to usable for Interested groups are invited to participate the use of this instrumentation for their ov investigations and in order to expand the cove age of the present net of receiving stations. Da from central Africa, the Near East, the USS China, Japan, India, the East Indies, and t South Pacific are especially needed. Persons o taining usable data and wishing to make the available to the State University of Iowa a urged to send a list of available recordin specifying the date and time of recording a the quality of the data, to:

Dr. J. A. Van Allen
Department of Physics and Astronomy
State University of Iowa
Iowa City, Iowa, USA.

We will then ask for records for which we ha no duplicate coverage. It is preferred that r cordings sent to SUI be in the form of origi magnetic tape recordings or tape copies of t original recordings. If procurement of magne recording tape is a problem, tapes will be r turned after analysis at SUI on request.

Acknowledgments. The authors wish to tha Dr. J. A. Van Allen for his assistance in the pl ning of this experiment and in the preparation this paper, and Mr. J. W. Freeman for his ass tance in the calibration of the detectors. In ad tion, the assistance of many individuals at t Army Ballistic Missile Agency, Huntsville, A bama, in the form of over-all payload engineeri provision of the telemetry and power supply s tems, conduct of the payload environmental te ing, and launching of the payload, is gratefu acknowledged.

(Manuscript received December 30, 1959.)

On the Theory of Protons Trapped in the Earth's Magnetic Field

ERNEST C. RAY

Department of Physics and Astronomy
State University of Iowa
Iowa City, Iowa

Abstract. A differential equation of transport is written for protons losing energy in an atmosphere but not scattering. It is solved under the approximation that a proton loses a negligible amount of energy while it drifts once around the earth in longitude. Three cases are treated: the equilibrium solution with input and loss rates equal; the solution for impulsive injection at $t = 0$, the intensity then dying away; and the solution for the intensity zero initially, the input mechanism being turned on at $t = 0$. No numerical work bearing on the geometry of the source function is included. The treatment is an improvement over previous ones in that it adequately treats the particles as moving along their actual trajectories. A detailed comparison with observations over South Africa shows that the altitude dependence of intensity is roughly consistent with the view that the particles seen by the unshielded Geiger tube on 1958ϵ are protons supplied by a weak source (for example, by decay of albedo neutrons) which are lost to the detector when their energy is reduced below the detection threshold by absorption. The atmosphere required has a temperature of about 2000°K at 400 km if it is pure dissociated nitrogen. At some height between about 1100 and 1300 km the scale height sharply increases in a way consistent with the view that at this height the composition changes to pure dissociated hydrogen. Only relative intensities are used in these comparisons.

Introduction. Recently, a region of very intense radiation has been discovered near the earth by means of a Geiger tube carried in satellite 1958α [*Van Allen, Ludwig, Ray, and McIlwain,* 1958]. Its properties have been extensively studied by a large number of investigators. We mention here only the experiments carried out in some of the early satellites and space probes [*Vernov, Vakulov, Gorchakov, Logachev, and Khudakov,* 1958; *Van Allen, McIlwain, and Ludwig,* 1959; *Van Allen and Frank,* 1959].

It has been suggested independently by *Vernov* [1958], by *Singer* [1958] and by *Kellogg* [1959] that the decay products of secondary cosmic-ray neutrons might be trapped in the earth's magnetic field in sufficient numbers to account for the observed intensities.

In addition, it is now clear that at least the so-called outer zone must contain major contributions from extraterrestrial particles, if these are not indeed the only important source.

The present paper explores in some detail the properties that protons trapped in the earth's magnetic field and interacting with the earth's high atmosphere should exhibit. This is done for a general spatial and angular dependence of the source. Of the previous treatments of this problem [*Singer,* 1958; *Kellogg,* 1959; *Vernov, Grigorov, Ivanenko, Lebedinskii, Murzin, and Chudakov,* 1959], the present one is most nearly like that of Singer. Indeed, the solution found for the equilibrium case is the same as Singer's. However, the present work adequately includes the effects of varying air density along a particle trajectory in the earth's magnetic field, while from the previous derivation it was necessary to assume, as noticed by Singer, that the solution was only good for particles with small excursions in latitude.

The transport equation. We neglect elastic scattering and assume that the only important loss mechanism is the loss of energy suffered by the protons in passing through the tenuous atmosphere present at the heights where the radiation is encountered. We approximate this loss as continuous, using the Bethe-Bloch formula in the usual way.

Denote by $\tau\ d\mathbf{x}\ d\mathbf{p}$ the number of protons in the volume element $d\mathbf{x}\ d\mathbf{p}$, where $\mathbf{x}$ is the position vector, and $\mathbf{p}$ is the free-space momentum of a

particle in the presence of a magnetic field. Then the differential equation for τ, as given for example by *Jeans* [1954], is

$$\frac{d\tau}{dt} + \tau \sum_{s=1}^{3} \left\{ \frac{\partial \dot{p}_s}{\partial p_s} + \frac{\partial \dot{q}_s}{\partial q_s} \right\} = G \qquad (1)$$

where $G\, d\mathbf{x}\, d\mathbf{p}$ is the number of particles added to $d\mathbf{x}\, d\mathbf{p}$ per second. The sum in equation 1 gets contributions from the earth's magnetic field and from the dissipation by the absorbing atmosphere. *Swann* [1933] has shown that the contributions from the magnetic field add up to zero, even though the momenta are the free-space rather than the canonical ones. Then equation 1 is

$$\frac{d\tau}{dt} + \tau \sum_{s=1}^{3} \frac{\partial \dot{p}_s^{(D)}}{\partial p_s} = G \qquad (2)$$

where $\dot{p}^{(D)}$ is the force responsible for the dissipation by the atmosphere. This force must be in the direction $(-\mathbf{p}/p)$ and of such magnitude that $dE/dt = \rho v\, dE/dx$, where E is the kinetic energy of the particle, ρ is the air density, v is the particle speed, x is path length in g/cm², and $-dE/dx$ is given by the Bethe-Bloch formula. This means that

$$\dot{p}^{(D)} = 3p^{-1}(dE/dx)\mathbf{p} \qquad (3)$$

If this is substituted in (2), using the correct relativistic formula relating kinetic energy and momentum, a simple rearrangement yields

$$\frac{d}{dt}\left[\tau p^2(-dE/dx)\right] = (-dE/dx)p^2 G \qquad (4)$$

It is shown by *Jánnosy* [1950] that τp^2 is the differential directional intensity per unit energy, per steradian per unit area per second. If we denote it by j and at the same time put $ds = v\, dt$, (4) becomes

$$\frac{d}{ds}\left[(-dE/dx)j\right] = (p^2/v)(-dE/dx)G \qquad (5)$$

Once the trajectory is known, the solution of (5) can be written in terms of a quadrature, but this is not convenient. It is known from the work of *Alfvén* [1950] that the coordinates of a particle trapped in the earth's field are periodic functions of s. This result is approximate but of good accuracy. It is still true when the particle loses energy provided that it loses a negligible amount during one cycle. We now make this assumption.

Let us average equation 5 over a cycle, assuming that the energy is constant during the cycle. Then

$$(\Delta s)^{-1}\Delta\left[(-dE/dx)j\right] = (-dE/dx)\bar{S}(E) \qquad (6)$$

where

$$\bar{S} \equiv (\Delta s)^{-1} \oint (p^2/v)G\, ds$$

Let us also assume that during a cycle E changes sufficiently little that (6) can be approximated adequately as

$$(d/ds)\left[(-dE/dx)j\right] = (-dE/dx)\bar{S}(E) \qquad (7)$$

Now,

$$ds = (dE/dx)^{-1}\bar{\rho}^{-1}\, dE$$

Then equation 7 becomes

$$(d/dE)\left[(-dE/dx)j\right] = -\bar{\rho}^{-1}\bar{S}(E) \qquad (8)$$

with $\bar{\rho} = (\Delta s)^{-1} \oint \rho\, ds$ to adequate accuracy in the approximation of small energy loss per cycle. Equation 8 is the equation to be solved, and all details of the particle trajectory have been taken care of in the averaging process.

Equilibrium solution. To solve this equation for the equilibrium case, it is only necessary to notice that letting the source operate at constant strength for an infinite length of time produces the equilibrium state. This is achieved by integrating equation 8 from $E = \infty$ to E, taking $j = 0$ at $E = \infty$. Then

$$j = \bar{\rho}^{-1}(-dE/dx)^{-1} \int_E^\infty \bar{S}(E)\, dE \qquad (9)$$

is the desired solution. Applications are discussed in later sections.

Solution for impulsive injection. We now treat the case where the radiation is deposited all at once in the magnetic field. The time behavior of the solution will furnish one possibility of defining a lifetime of trapped protons. For this case we solve equation 8 with $\bar{S} = 0$. This gives, with j_0, E_0 referring to the time of injection,

$$j = j_0(-dE/dx)_0(-dE/dx)^{-1}$$

If we specialize this to the nonrelativistic case by approximating $-dE/dx$ as kE^{-1}, where k is an appropriate constant,

$$j = (E/E_0)j_0(E_0) \tag{10}$$

'e must now calculate the dependence of on time. From $dE/dx = -k/E$ we get $= -(k\bar{\rho}v)^{-1}E\ dE$. Now, $v = (2/m)^{1/2}E^{1/2}$. hus

$$E_0 = (E^{3/2} + C\bar{\rho}t)^{2/3} \tag{11}$$

ith

$$C \equiv \tfrac{3}{2}k(2/m)^{1/2}$$

quation 10 becomes

$$= j_0([E^{3/2} + C\bar{\rho}t]^{2/3})E(E^{3/2} + C\bar{\rho}t)^{-2/3} \tag{12}$$

here $j_0(E_0)$ is the input spectrum. If E is in ev, $\bar{\rho}$ in g/cm², and t in seconds, $C = 10^{12}$.

Solution for constant source before equilibrium. ippose that there is a time-independent source. ippose further that at $t = 0$ the trapping gion is sufficiently disturbed that essentially l the particles are removed from it. We now btain the solution that describes the way in hich it fills up again.

We evidently obtain the desired result by tegrating equation 8 from E_0 to E and using e time dependence of E from the previous ction. The result is

$$j = -\bar{\rho}^{-1}k^{-1}E\int_{E_0}^{E}\bar{S}(E)\ dE \tag{13}$$

here we have again approximated dE/dx as kE^{-1}. By replacing E_0, using equation 11, e time dependence is exhibited.

Mean air density. All the above results epend on the mean over a cycle of the air den-ty. We now calculate the mean approximately. ssume that

$$\rho = \rho_a \exp\,[-\mu g(r)] \tag{14}$$

ves the air density as a function of r, the dis-nce from the center of the earth, and that this the only coordinate on which the density epends. For the case of a constant temperature th height, but including the variation of avity,

$$g(r) = 1 - r_a/r \tag{15}$$

here r_a is a constant. Fitting (14) to the satellite ag density values of *Harris and Jastrow* [1959] elds $\mu = 106$, $\rho_a = 6 \times 10^{-14}$ g/cm³, $r_a = 6650$ n.

The particles drift very little in longitude while excuting one period in latitude, so that it is a good approximation to treat them as spiraling along a line of force. We shall calculate $\bar{\rho}$ for a quarter oscillation in latitude. If it is desired to include effects due to the nondipole nature of the field, the expression obtained can then be averaged over longitude. We shall not do that here.

We have

$$\bar{\rho}\ \Delta s = \int_{r=r_R}^{r_0}\rho\ ds \tag{16}$$

where r_R is the value of r at the point where the reflection of the particle occurs, and r_0 is the value of r at the point where the magnetic field, as a function of position along the line of force, has a minimum. We can evaluate this integral approximately using Laplace's method [*Erdélyi*, 1956]. At r_R, $dr/ds = 0$ and $d^2r/ds^2 > 0$. Then

$$\bar{\rho}\ \Delta s = \rho_R\left[\frac{\pi}{2\mu\ d^2g/ds^2}\right]_{r=r_R}^{1/2} \tag{17}$$

where ρ_R is the air density at r_R and (14) has been used for ρ. At r_R, $dr/ds = 0$, so $(d^2g/ds^2)_R = (dg/dr)_R(d^2r/ds^2)_R$. From elementary geometry, in a dipole field,

$$\frac{dr}{ds} = 2\left(\frac{1-r}{4-3r}\right)^{1/2} \cdot[1 - \sin^2\alpha_0(4-3r)^{1/2}r^{-3}]^{1/2} \tag{18}$$

In this equation, all lengths are in units of r_0, the distance from the center of the earth to the point where the line of force crosses the equator. Also, α_0 is the angle between **B** and the velocity as the particle crosses the equator. Then

$$\left(\frac{d^2r}{ds^2}\right)_R = \frac{3}{r_0}\frac{\sin^2\lambda}{(1+3\sin^2\lambda)^2}\frac{3+5\sin^2\lambda}{\cos^2\lambda}$$

where we have used the equation of a line of force in a dipole field, $\cos^2\lambda = r/r_0$. Then

$$\left(\frac{d^2g}{ds^2}\right)_R = \frac{3}{r_0}\frac{\sin^2\lambda}{\cos^2\lambda}\frac{3+5\sin^2\lambda}{(1+3\sin^2\lambda)^2}\left(\frac{dg}{dr}\right)_R \tag{19}$$

By using (15) we obtain

$$\left(\frac{d^2g}{ds^2}\right)_R = \frac{3}{r_0^2}\frac{\sin^2\lambda}{\cos^4\lambda}\frac{3+5\sin^2\lambda}{(1+3\sin^2\lambda)^2}\frac{r_a}{r} \tag{20}$$

where all quantities in the right member of this equation and in (18) and (19) as well are to be evaluated at the mirror point. Then, from (17),

$$\bar{\rho}\,\Delta s = \rho_R \sqrt{\frac{\pi}{6\mu}} \left(\frac{r}{r_a}\right)^{1/2} \cdot \frac{\cos^2\lambda}{\sin\lambda} \frac{1 + 3\sin^2\lambda}{(3 + 5\sin^2\lambda)^{1/2}} \qquad (21)$$

with Δs in units of r_0.

We now compute Δs. We have

$$\Delta s = \int_{r=r_R}^{r_0} ds \qquad (22)$$

with ds given by (18). This expression becomes infinite at both limits of the integral. Write the integral as

$$\Delta s = \int_{r=r_R}^{r_1} ds + \int_{r=r_1}^{r_0} ds \qquad (23)$$

and make an appropriate variable change in each. For the integral from r_R to r_1, put

$$\chi = [1 - \sin^2\alpha_0(4 - 3r)^{1/2} r^{-3}]^{1/2} \qquad (24)$$

The variable χ is the cosine of the angle between **B** and the velocity vector. For the other integral, put

$$\psi = (1 - r)^{1/2} \qquad (25)$$

The variable ψ is $\sin\lambda$, where λ is the geomagnetic latitude. Then

$$\Delta s = \frac{2}{3\sin^2\alpha_0} \int_0^{\chi_1} \frac{4 - 3r(\chi)}{8 - 5r(\chi)} \frac{r^4(\chi)\, d\chi}{[1 - r(\chi)]^{1/2}} + \int_0^{\psi_1} [4 - 3r(\psi)]^{1/2} \cdot [1 - \sin^2\alpha_0\{4 - 3r(\psi)\}^{1/2} r^{-3}(\psi)]^{-1/2}\, d\psi \qquad (26)$$

where $r(\chi)$ is obtained from (24) and $r(\psi)$ from (25). These integrals can be evaluated for sufficiently high latitudes as follows. Expand the square bracket which appears to the power $-1/2$ in the second integral by the binomial theorem, keeping terms through $\sin^2\alpha_0$, and integrate term by term. Expand the integrand of the first integral in powers of χ^2, keeping terms through χ^4, and integrate term by term. Choose $\chi(r_1) = 1/2$. This also fixes the value of $\psi(r_1)$. The term in the result which is proportional to χ_1^5 then contributes less than 10 per cent to Δs for latitudes greater than 30°, while the term proportional to $\sin^2\alpha_0$ also contributes less than 10 per cent. The result is given in Table 1. From the table, in the range of latitude from 30° to 70°, $\Delta s \cong 1$ with an error of less than about 30 per cent. Recall that Δs as here calculated is given in units of r_0.

TABLE 1. Path Length along a Trajectory in a Dipole Field

Latitude of reflection, °	30	37	44	53	64	72
Δs	1.0	1.1	1.1	1.2	1.3	1.3

Using Δs as given in Table 1 together with equation 21, we obtain $(\bar{\rho}/\rho_R)(r_a/r_R)^{1/2}$ as shown in Figure 1. The values of λ_R given on the horizontal axis are the latitudes at which reflection occurs; they were calculated from the equation of a line of force in a dipole field, namely

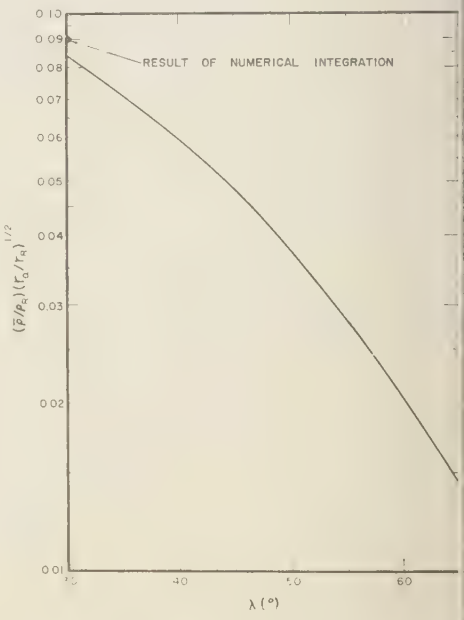

Fig. 1. The ratio of the average of the atmospheric density over a period of the motion of a charged particle to the density at the mirror points. The calculation was carried out using a dipole field and the interim atmosphere of *Harris and Jastrow* [1959].

$\cos^2 \lambda_R = r_R/r_0$. The point shown at $\lambda_R = 30°$ is the result of numerical integrations of equations 26 and 16. The agreement is satisfactory.

Power-law input spectra. In this section we will specialize the various results to the case of a source function which is the product of a function of the coordinates alone by some power of the kinetic energy. That is,

$$S = M(\mathbf{x})E^{-\alpha}$$

Then

$$\bar{S} = \bar{M}E^{-\alpha} \tag{27}$$

where

$$\bar{M} = (\Delta s)^{-1} \oint M \, ds \tag{28}$$

Equation 9, the equilibrium solution, becomes

$$j = (\bar{M}/k\bar{p})(\alpha - 1)^{-1}E^{2-\alpha} \tag{29}$$

This result is the same as that of *Singer* [1958], except that it has now been shown to be correct for the particle oscillating over any range of latitudes, provided only that the particle makes many oscillations while its energy changes appreciably. In addition, the factor $\bar{M}$, as defined in (28), now offers the possibility of routinely treating the spatial and angular dependence of the source under the same restriction of small energy loss per oscillation. In (29), we have put $dE/dX = -k/E$ for the nonrelativistic case.

The result given in equation 29 together with the mean air density depicted in Figure 1 shows that, if a model for the inner zone is assumed, based on equilibrium with a weak source like the decay products of neutron albedo, the falling off of intensity in the inner zone at constant height with increasing latitude is not a natural feature produced simply by a spherically symmetric atmosphere. Several conjectures have been made about the cause of this feature of the observations. Singer reports [semiprivate communication] that $\bar{M}$ is of such nature for the albedo hypothesis that it decreases toward higher latitudes. He has also suggested [*Singer*, 1959], as has *Vernov* [1959], that, as one goes to higher latitudes, the adiabatic invariant, $\sin^2 \alpha/B$, may break down more and more, permitting the escape of protons from the trapping regions. Two other widely discussed possibilities are that either the atmosphere has a suitable latitude dependence or there are time variations of the magnetic field of sufficient magnitude and sufficiently short time scale that the leakage from the trap at higher latitudes is suitably enhanced.

Let us also put the result (29) in a slightly different form. Suppose we have a detector that responds to all particles with energy above a least energy E_c. Suppose that it is sensitive only to particles arriving from within a narrow range of solid angle. Then we can define an intensity from this counter, I (cm² sec sterad)⁻¹, which is a differential intensity as far as solid angle is concerned but an integral intensity with respect to energy,

$$I = \int_{E_c}^{\infty} j \, dE$$

Now, the number of particles added to a unit volume per second per steradian with energy greater than E_c is

$$N = \int_{E_c}^{\infty} \bar{S}(E) \, dE$$

Using these two equations together with (29) and (27), we obtain

$$I = \{E_c^2/[k\bar{p}(\alpha - 3)]\}N$$

Notice that this equation can only be used with $\alpha > 3$. If α is too close to 3, a correct relativistic formula must be used for $-dE/dx$ instead of the k/E used here. If $\alpha \leq 3$, the input energy spectrum is absurd and must be modified.

Now specialize to a power law in the energy the case of impulsive injection. Equation 12 becomes

$$j = M[E^{3/2} + C\bar{p}t]^{-(2/3)(\alpha+1)}E \tag{30}$$

Whether or not this model has anything to do with reality, this is, for the case of a power-law input spectrum, the equation from which the 'lifetime' of the particles in the trapping region is determined. Since the expression on the right is not an exponential, a lifetime cannot be defined in the usual sense. Alternatively, the lifetime is a function of time. As an example of the way to calculate this quantity for a given detector, we offer the following, where the integrals are especially simple.

Suppose that we have a detector, like the d-c scintillator in 1958ϵ [*Van Allen, McIlwain, and Ludwig*, 1959], that measures the energy flux carried by the particles. Let us suppose that the entire flux measured by this hypothetical detector is due to protons. (This is just for illustration and not supposed to represent reality.) Suppose further that the detector measures all the energy carried by particles with energies greater than E_t (which particles therefore must stop in the detector) but does not measure any of the energy of particles below this critical value. Then, if the detector accepts only a narrow range of solid angles, and if F denotes its response per unit solid angle,

$$\frac{1}{F}\frac{dF}{dt} = \left[\int_{E_t}^{\infty} jE\, dE\right]^{-1} \frac{d}{dt}\int_{E_t}^{\infty} jE\, dE$$

If we substitute j from equation 30, and carry out the integrations and the differentiation, we obtain

$$\frac{1}{F}\frac{dF}{dt} = -\frac{2}{3}(\alpha - 2)t^{-1}(\Gamma + 1)^{-1} \cdot \frac{2(\alpha + 1)\Gamma + 3}{(2\alpha - 1)\Gamma + 3} \qquad (31)$$

provided that α is greater than 2. The quantity Γ is $E^{3/2}(C\bar{\rho}t)^{-1}$. If $\Gamma \leq 1$, little error is made by putting

$$(1/F)(dF/dt) = -\tfrac{2}{3}(\alpha - 2)t^{-1} \qquad (32)$$

The reciprocal of this quantity is a reasonable value for lifetime of the present detector. It is evidently not in any sense approximately constant. Similar though more complicated results are obtained for a particle counter.

Finally, we specialize the solution (13) to the case of a power law in the energy. Putting in (27) as well as (11), we obtain

$$j = [k(\alpha - 1)\bar{S}]^{-1}\bar{M}E[E^{-(\alpha-1)} - (E^{3/2} + C\bar{\rho}t)^{-(2/3)(\alpha-1)}] \qquad (33)$$

This equation is useful in studying certain possible theories that depend on geomagnetic disturbance. For example, suppose we wish to consider the possibility that the region of the slot is relatively free of particles because of occasional large magnetic disturbances, with the slot slowly filled with neutron albedo protons. (The neutron albedo protons in this case would be taken as the source of the inner zone.) This theory predicts that as one goes away from the earth, in the absence of any loss other than the Bethe-Bolch energy loss, the intensity will steadily increase. Let us suppose that at $t = 0$ the trapped radiation is removed down to about 0.5 earth radius but is not disturbed below that. Then how long would it take for the neutron albedo source to build up the intensity to, say, 1/4 the equilibrium value? The answer is found by putting $j(t)$ from (33) equal to 1/4 the equilibrium value, from which

$$C\bar{\rho}t = E^{3/2}[(4/3)^{(3/2)[1/(\alpha-1)]} - 1]$$

Take the case $\alpha = 2.6$, $E = 30$ Mev. Then with $\bar{\rho} = 10^{-16}$ g/cm^3, $t = 6$ days, with $\bar{\rho} = 10^{-18}$, $t \cong 2$ years, with $\bar{\rho} = 10^{-20}$, $t \cong 200$ years. The lower values of density seem the most reasonable, so that the theory can survive this test provided that the magnetic disturbances occur more closely spaced than every year or so. The assumption is implicit in this argument that the equilibrium value in the slot would be greater than the peak value in the inner zone.

Computation of directional intensity from omnidirectional intensity. In order to compare this theory with observations, it is desirable to compute j_n, the directional intensity in the direction perpendicular to the line of force, from the observed quantities. It seems reasonable to suppose that in the inner zone the response of the unshielded Geiger tube on 1958ϵ is due mostly to protons. However, this detector is roughly an omnidirectional detector. Hence the easily obtained quantity is $J(B)$, the omnidirectional intensity as a function of magnetic field strength along a particular line of force. This is then related to $j(B, \cos\alpha)$ by

$$J(B) = 4\pi \int_0^1 d\cos\alpha\, j(B, \cos\alpha) \qquad (34)$$

This integral equation can be solved in the following way. Change variables in the integral by using $(\sin^2\alpha)/B = (\sin^2\alpha_0)/B_0$. Define

$$\mathcal{J}(B_0/B) \equiv J(B)$$

Now define $B_0/B \equiv x$, $\sin^2\alpha_0 \equiv t$. Then (34) becomes

$$\frac{1}{2\pi}x^{1/2}\mathcal{J}(x) = \int_0^x (x - t)^{-1/2} j(t)\, dt \qquad (35)$$

This is known as Abel's equation and was solved by him. *Volterra* [1959] obtains the solution as follows. Multiply both sides by $(\xi - x)^{-1/2}\,dx$, and integrate from 0 to ξ. Interchange the order of integration in the right member. Change the integration variable x in the right member to t by the relation $x = t + (\xi - t)u$. Then (35) becomes

$$\frac{1}{\pi}\int_0^\xi x^{1/2}(\xi - x)^{-1/2} J(x)\,dx = \int_0^\xi dtj(t)\int_0^1 (u - u^2)^{-1/2}\,du$$

The integral from 0 to 1 with respect to u is equal to π. Differentiate both sides with respect to ξ. The result is

$$j(\xi) = \frac{1}{2\pi^2}\frac{d}{d\xi}\int_0^\xi x^{1/2}(\xi - x)^{-1/2} J(x)\,dx$$

Now restore the original variables.

$$j(\sin^2\alpha_0) = \frac{1}{2\pi^2}\frac{d}{d\sin^2\alpha_0}\cdot\int_0^{\sin^2\alpha_0}\sqrt{\frac{B_0}{B}}\left(\sin^2\alpha_0 - \frac{B_0}{B}\right)^{-1/2}\cdot J\left(\frac{B_0}{B}\right)d\left(\frac{B_0}{B}\right)$$

Let B_R denote the magnetic field strength at the point where the particle at α_0 reflects. Then $\sin^2\alpha_0 = B_0/B_R$, and our result can be written

$$j_n(B) = -\frac{1}{2\pi^2}B^2\frac{d}{dB}B^{-1}\int_1^\infty \frac{J(Bx)\,dx}{x^2\sqrt{x-1}}$$

or

$$j_n(B) = -\frac{1}{\pi^2}B^2\frac{d}{dB}B^{-1}\cdot\int_0^\infty (y^2+1)^{-2}J(B[y^2+1])\,dy \qquad (36)$$

where in the first of these we have put $B/B_R = x$, in the second we have put $x - 1 = y^2$, and in both we have dropped the subscript on B_R. To use this result, we fit the observations of $J(B)$ along a particular line of force with some convenient function. We substitute in that function $3(y^2 + 1)$ for B and put the result into (36).

Comparison with observations. *Hess* [1959] has studied the energy spectrum of trapped protons in the following way. He calculated the source spectrum by using measurements he and others had made of neutron intensities in the atmosphere together with a diffusion equation to calculate neutron intensities above the atmosphere. From these intensities he obtained the decay density and hence the proton source function. From the energy spectrum of this source, using Singer's method of calculating the equilibrium trapped spectrum, he obtained the spectrum $E^{-1.3}$ for the number of protons per cubic centimeter per Mev in the energy range from about 80 to about 700 Mev. The corresponding intensity spectrum would have j proportional to $E^{-0.96}$ in this energy range, since, as quoted by Hess, the velocity in this energy range is approximately proportional to $E^{0.344}$. This procedure is equivalent to putting $S \sim E^{-2.55}$, the source function of Hess, into equation 9 of the present paper, using $(-dE/dX) \sim E^{-0.59}$ in this energy range, after Hess, and regarding all the spatial dependence as residing in an unknown multiplicative constant. If this spectrum of $E^{-0.96}$ is compared with the values of this quantity measured by *Fredan and White* [1959] the following situation is found. At energies greater than about 200 Mev there is conclusive disagreement between the theory and experiment. Hess takes the seven points of Fredan and White between 80 and 200 Mev as agreeing with the theory. These seven points alone, however, do not fix the exponent with any reasonable accuracy, and the true exponent might differ from the theoretical one by a factor of 2. Indeed, Fredan and White find a fit with an exponent of -1.84 to all their data, and the fit is perfectly satisfying in this energy range. In view of Hess's belief that there is a hint of agreement at the low-energy end of the measurements of Fredan and White, it would be useful to have measurements of the spectrum down to lower energies.

Let us now consider the spatial dependence of the intensity as determined by the unshielded Geiger tube on 1958ϵ. Figure 2 is a plot of $N(B)/B^2$ as a function of B along the line of force that passes through the point on the earth's surface at latitude 27°S, longitude 15°E. $N(B)$ is the counting rate in counts per second. The points shown were obtained by locating on various passes recorded by South African

Fig. 2. The dependence of N/B^2 on B along the line of force that hits the earth's surface at 27°S, 15°E. The quantity N is the counting rate of the unshielded Geiger tube in satellite 1958ϵ; B is the magnetic field strength.

receiving stations those points for which both the integral invariant, I [*Northrup and Teller*, 1959], and B have the same value that they have for some point on the chosen line of force.[1] The dispersion in the points is due to inaccuracies in this procedure.

We assume that the counting rate of this counter is related by a constant factor to the omnidirectional intensity due to all protons with energy greater than some threshold energy. We can then use (36) after replacing both intensities by relative intensities. We use $N(B)$ for counting rate and $n_n(B)$ for directional counting rate. J can then be obtained from N and j from n by dividing the counting rates by 0.7 cm².

A good fit to $N(B)$ in the range $0.26 \text{ gauss} \geq B \geq 0.19$ gauss is obtained with

$$N = B^2 \exp(26.9 - 83B) \tag{37}$$

Using this for $J(B)$ in (36) gives

$$n_n = (0.81B^{1/2} - 0.0049B^{-1/2}) \cdot B^2 \exp(26.9 - 83B) \tag{38}$$

Insignificant errors are made by putting this approximately as

$$n_n \cong 0.81B^{5/2} \exp(26.9 - 83B) \tag{39}$$

[1] We are indebted to E. H. Vestine for supplying us with tables of I, B, and lines of force which were indispensable in this procedure.

Then

$$j_n \cong 1.16B^{5/2} \exp(26.9 - 83B) \tag{40}$$

Notice especially that these results apply only in the range of B given above.

The properties of the atmosphere at the heights to which these data refer, and in this latitude region, are not well known. Let us assume provisionally that the atmospheric loss mechanism as treated in this paper is the correct one, and see what scale height is required in order that the observed altitude dependence be produced.

First, take the theoretical expression for j from (9). Integrate with respect to energy from the threshold energy of the detector to infinity. Then the spatial dependence arises in two ways. There is the spatial dependence of $\bar{\rho}$, and that of the average over the source function. This last is not at all well known, since the angular dependence of the neutron intensity is not known. We will omit it here. Then $(d \ln j)/dr \cong -(d \ln \bar{\rho})/dr$. From the calculations of Δs given earlier for a dipole field, we can replace this with good accuracy by $(d \ln j)/dr = -(d \ln \bar{\rho}\, \Delta s)/dr$. For present purposes, an alternative expression for $\bar{\rho}\, \Delta s$ is convenient. Recalculate $(d^2g/ds^2)_R$, see (17), in the following way. We have as before $(d^2g/ds^2)_R = (dg/dr)_R$. But $dr/ds = (B_r/B)\cos\alpha$, and by using Alfvén's adiabatic invariant and $g = 1 - r_a/r$ we obtain

$$(d^2g/ds^2)_R = (r_a/r_R)(B_r/B)_R^2(2r_RB_R)^{-1}(-dB/dr)_R$$

We denote the radial component of the magnetic field by B_r. Then

$$\bar{\rho}\, \Delta s = \rho_R \left[\frac{\pi}{\mu}\frac{r_R}{r_a}\left(\frac{B}{B_r}\right)_R^2 (rB)_R \left(-\frac{dB}{dr}\right)_R^{-1}\right]^{1/2} \tag{41}$$

Now, if H is the scale height,

$$H^{-1} = -(d \ln \rho)/dr - \frac{d}{dr}\ln \bar{\rho}\, \Delta s + \frac{1}{2}\frac{d}{dr}\ln\left[r^2B^3B_r^{-2}\left(-\frac{dB}{dr}\right)^{-1}\right] \tag{42}$$

Since $(d \ln \Delta s)/dr$ is negligible, we replace the first term in the right-hand member by $-(d \ln \bar{\rho})/dr$, and that is approximately $(d \ln j)/dr$. Now, use

j) for j. Then the scale height required to produce the observed intensity variation is given by

$$H^{-1} = \frac{5}{2} B^{-1} \frac{dB}{dr} - 83 \frac{dB}{dr} + \frac{1}{2} \frac{d}{dr} \ln \left[r^2 B^3 B_z^2 \left(-\frac{dB}{dr} \right)^{-1} \right]$$

We must now evaluate dB/dr, not over South America, but rather on the given magnetic shell at the point where it dips closest to the earth. The appropriate point, when $B = 0.25$ gauss, is 45°S, 31°W, $h = 400$ km. Then $dB/dr \cong -10^{-4}$ gauss/km, and $H \cong 130$ km. If the atmosphere at this plate is taken to be pure dissociated nitrogen, the temperature is then about 2000°K. This result does not have high accuracy because of the neglect of the spatial dependence of the source function. A probably much less important error arises from the failure to average the air density properly over the longitudinal drift of the particles.

The scale height undergoes a sudden increase to a height somewhere between 1100 and 1300 km. This is shown by the sharp change of slope between $B = 0.19$ and $B = 0.17$ in Figure 2. There are not enough points on the upper part of the curve to fix the new slope with precision, but it is quite consistent with the change in scale height that would be produced if the composition changed from dissociated nitrogen to dissociated hydrogen. It has been shown by *Johnson* [1960] that this change in composition should occur at this height.

The scale height obtained in this fashion is twice the value obtained at the same height from satellite drag by *Groves* [1959] and by *King-Hele* [1959].

A thorough study along these lines is in progress on all the data from 1958ε; it should yield much information on the range of latitude and altitude over which the loss mechanism discussed here is applicable.

Acknowledgments. I am indebted to J. A. Van Allen, C. E. McIlwain, G. H. Ludwig, and P. Stothwell for many helpful discussions about the experimental techniques used and the meaning of the results. The work was markedly advanced by J. H. Vestine, who supplied me with tables of the integral invariant I, of B, and of lines of force which he had calculated. R. Lynch computed by hand the value of $\bar{\rho}$ shown as a point in Figure 1.

References

Alfvén, H., *Cosmical Electrodynamics,* Chapter II, Clarendon Press, Oxford, 237 pp., 1950.

Erdélyi, A., *Asymptotic Expansions,* section 2.4, Dover, New York, 108 pp., 1956.

Fredan, S. C., and R. S. White, Protons in the earth's magnetic field, *Phys. Rev. Letters, 3,* 9–11, 1959.

Groves, G. V., Air density in the upper atmosphere from satellite orbit observations, *Nature, 184,* supp. 4, 178–179, 1959.

Harris, I., and R. Jastrow, An interim atmosphere derived from rocket and satellite data, *Planetary Space Sci., 1,* 20–26, 1959.

Hess, W., Van Allen belt protons from cosmic-ray neutron leakage, *Phys. Rev. Letters, 3,* 11–13, 1959.

Jánnosy, L., *Cosmic Rays,* p. 268, Clarendon Press, Oxford, 1948.

Jeans, J. H., *The Dynamical Theory of Gases,* p. 70, Dover, New York, 444 pp., 1954.

Johnson, F. S., The ion distribution above the F_2 maximum, *J. Geophys. Research, 65,* 577–584, 1960.

Kellogg, P. J., Possible explanation of the radiation observed by Van Allen at high altitudes in satellites, *Nuovo cimento,* [10] *11,* 48–66, 1959.

King-Hele, D. G., Density of the atmosphere at heights between 200 km. and 400 km., from analysis of artificial satellite orbits, *Nature, 183,* 1224–1227, 1959.

Northrup, T. G., and E. Teller, Stability of the adiabatic motion of charged particles in the earth's field, research report UCRL-5615, Lawrence Radiation Laboratory, University of California, Livermore, California, 1959.

Singer, S. F., Trapped albedo theory of the radiation belt, *Phys. Rev. Letters, 1,* 181–183, 1958.

Singer, S. F., Cause of the minimum in the earth's radiation belt, *Phys. Rev. Letters, 3,* 188–190, 1959.

Swann, W. F. G., Application of Liouville's theorem to electron orbits in the earth's magnetic field, *Phys. Rev., 44,* 224–227, 1933.

Van Allen, J. A., and L. Frank, Radiation around the earth to a radial distance of 107,400 km., *Nature, 183,* 430–434, 1959.

Van Allen, J. A., G. H. Ludwig, E. C. Ray, and C. E. McIlwain, Observation of high intensity radiation by satellites 1958α and γ, *Jet Propulsion, 28,* 588–592, 1958.

Van Allen, J. A., C. E. McIlwain, and G. H. Ludwig, Radiation observations with satellite 1958ε, *J. Geophys. Research, 64,* 271–286, 1959.

Vernov, S. N., Special lecture, Fifth General Assembly of CSAGI, Moscow, July 30–August 9, 1958.

Vernov, S. N., A talk given at the meeting of the commission on cosmic radiation of the International Union of Pure and Applied Physics, Moscow, July 1959.

Vernov, S. N., N. L. Grigorov, I. P. Ivanenko, A. I.

Lebedinskii, V. S. Murzin, and A. E. Chudakov, Possible mechanism of formation of 'terrestrial corpuscular radiation' by the action of cosmic rays, *Doklady Akad. Nauk SSSR, 124,* 1022–1025, 1959.

Vernov, S. N., P. V. Vakulov, E. V. Gorchakov, Y. I. Logachev, and A. E. Chudakov, The study of the soft components of cosmic rays beyond the limits of the atmosphere, *Artificial Satellites of the Earth,* no. 2, Academy of Sciences, USSR, Moscow, 1958. (This has been translated by J. I Zygielbaum under the title: Astronautics infor mation, translation no. 2, artificial earth satel lites, Jet Propulsion Laboratory, California In stitute of Technology, September 1959.)

Volterra, V., *Theory of Functionals and of Integro and Integrodifferential Equations,* section 4 Dover, New York, 226 pp., 1959.

(Manuscript received January 12, 1960.)

Radiation Information from 1958δ_2

R. P. BASLER, R. N. DEWITT, AND G. C. REID

Geophysical Institute, University of Alaska
College, Alaska

Abstract. The telemetered radiation information from the satellite 1958δ_2 (Sputnik III) has been analyzed for 62 separate passes recorded in College, Alaska. The data indicate a dependence of radiation intensity on altitude in the range 250 to 500 km. Both the high- and the low-energy components apparently contribute to the over-all increase of intensity with altitude, but the presence of a continuous afterglow in the scintillating crystal prevented detailed interpretation of the results.

Introduction. The Geophysical Institute at e University of Alaska has recorded the radio nal from the satellite 1958δ_2 (Sputnik III) ce it was launched on May 15, 1958. The ntinuously telemetered radiation data from is satellite have been analyzed for 62 separate sses recorded in College, Alaska (64° 52'N, 7° 50'W), from May 18 until the partial ilure of the telemetering system on June 17, 58. This analysis was made on the basis of the formation presented at the Rocket and Satel- e Symposium during the Fifth Reunion of the mité Spécial de l'Année Géophysique Inter- tionale held in Moscow, July 30 to August 9, 58. Much of the relevant material presented this symposium has since been published ewhere [*Vernov, Chudakov, Gorchakov, Lo- chev, and Vakulov*, 1959].

Data reduction. The satellite's 20 Mc/s bea- n radio transmission consists of a recurring ries of three telemetry pulses and a marker lse, repeating at intervals of 1.23 seconds. e durations of the second and third pulses ve a measure of the radiation intensity inci- nt on a sodium iodide crystal as recorded by photomultiplier. The second pulse changes ngth in response to the anode current of the otomultiplier, and the third pulse changes response to the current at one of the dinodes. or high-energy pulses the relation between ese currents is nonlinear, so that the difference tween the radiation intensities recorded by e two channels at the same time should give measure of the fraction of the radiation oc- rring in the form of high-energy pulses. For details of the telemetry system, the reader is referred to *Vernov and others* [1959].

The radio signal strength was recorded on a Sanborn 150 recorder at a chart speed of 10 mm/sec. The individual pulses could readily be identified and their relative durations measured directly from the chart. These durations were tabulated for the entire readable part of each record and reduced to values of radiation intensity using the published code. A typical graph of this information is shown in Figure 1.

The area under each curve represents the total energy released in the sodium iodide scintillating crystal during the recording. The true value of this energy is given by channel 3, the curve for channel 2 being somewhat lower, owing to the nonlinearity in the later stages of the photomultiplier tube. The oscillations in the two curves are those referred to by *Vernov and others* [1959] as due to the satellite's tumbling in the earth's magnetic field, thus affecting the sensitivity of the photomultiplier.

The average radiation intensity values were determined for each of the 62 recordings. These averages were taken from all the available data from any one recording without regard to which parts of the tumbling cycle were sampled, since it was sometimes difficult to determine the position of the crests and troughs of these cycles, especially in a short record. The error introduced by this averaging, however, cannot exceed the tumbling modulation, which is of the order of 10 per cent.

It should be noted that the intensity values recorded are not the actual intensities, but are

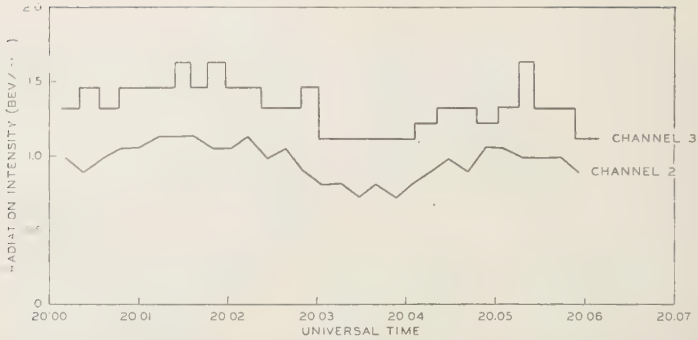

Fig. 1. Radiation intensity observed on channels 2 and 3 during a typical passage of 1958δ_2 ov College, Alaska, on June 5, 1958. The points for channel 2 represent a 12.3-second (10 telemeterin cycles) average of the telemetered intensities. Closest approach occurred at 20:03:09 Universal Tim

somewhat higher, owing to the perpetual afterglow in the scintillating crystal. Since this afterglow is largely due to the high-intensity radiation encountered during the north-south crossings of the geomagnetic equator, it will have decayed near its minimum value when the satellite pass over Alaska. The decay is never complete partly because the crystal is constantly irrad ated, but mostly because the time constant f the afterglow is comparable with the satellit period; thus, the crystal is re-exposed to t high-intensity radiation at the magnetic equ tor before it has had time to recover from i previous exposure. The intensities recorded channel 3 can therefore be considered only upper limits for the actual intensities.

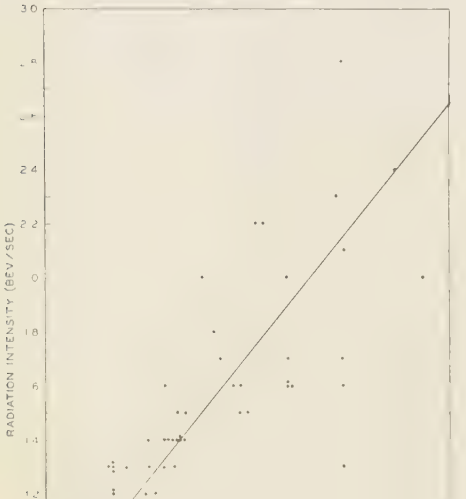

Fig. 2. Observed dependence of total radiation intensity on altitude. The straight line represents a least-squares fit to the data.

Altitude dependence. The satellite's positi during each of the recordings was determin from the orbital information supplied by t Space Track Control Center at the L. G. Han com Field in Bedford, Massachusetts. The heig of the satellite at its point of closest approa to College is therefore known for each pass, b since all the recordings were made during t first weeks following the launching, before t orbit was well established, the heights given a probably not accurate to better than 20 k Unfortunately, no accurate ephemeris is ava able for the early months of 1958δ_2, and so present there is little hope of refining the estimates.

Figure 2 shows the average radiation intensi plotted against the closest-approach altitude f each satellite passage. The possible height rors, together with the fact that the radiati intensity values have been rounded off to t nearest 0.1 bev/sec, would be expected to pr duce some scatter in the points. However, t

scatter, especially at higher altitudes, can- be explained on the basis of inaccurate data. gure 2 indicates that there is an increase adiation with altitude, but no definite func- al relationship is apparent. A straight line is to be a good first approximation. There as to be a tendency toward decreasing slope igher altitudes, but this might be due to the ced effect of the afterglow during these es since they are farther removed from magnetic equator.

is interesting to compare Figure 2 with altitude-intensity curve published by *Mere-*, *Gottlieb, and Van Allen* [1955] for rockoon t number S.U.I. 20 on August 30, 1953. a were at very nearly the same geomagnetic ude, and, although the rockoon data are a much lower altitude (up to about 100 , both show a nearly linear increase of in- ity with altitude.

igh-energy intensity. As described above, telemetering system in 1958δ₂ was designed hat the combined information on channels nd 3 would serve to determine the portion the total energy that is released in the tillating crystal in the form of pulses whose vidual amplitude is greater than 1 to 2 Mev. description of this system by *Vernov and ers* [1959] is incomplete, but apparently it intended that the intensity due to pulses

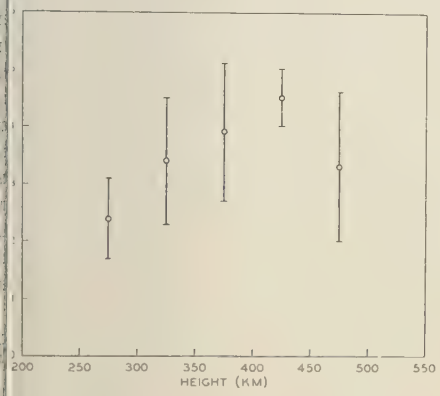

ig. 3. Observed altitude dependence of the ponent of the total radiation intensity due to es larger than 1 to 2 Mev. Each point repre- s the weighted mean of all the observations in a 50-km height interval. The vertical bars esent the standard deviations.

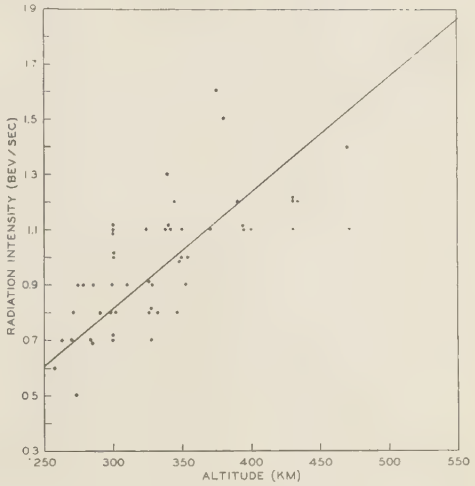

Fig. 4. Observed altitude dependence of the component of the total radiation intensity due to pulses smaller than 1 to 2 Mev. The straight line represents a least-squares fit to the data.

greater than 1 to 2 Mev be given approximately by the difference in the intensities indicated on channel 2 and channel 3. But the previously mentioned afterglow in the scintillating crystal prevented operation in this fashion by introducing a continuous component in the photomultiplier current which lowered the energy required for a pulse to exceed the linear response range of the anode current. This caused channel 2 to indicate a lower intensity than channel 3, thus indicating a spuriously high intensity of high-energy radiation.

If the high-energy pulses are assumed to be entirely due to galactic cosmic rays, their intensity would be expected to be constant and independent of altitude in the range encountered during passages over Alaska. However, the recorded high-energy intensity values range up to 40 per cent. of the total intensity, and seem to have an altitude dependence, as shown in Figure 3. The corresponding dependence of the low-energy intensity on altitude is shown in Figure 4. Both the high- and the low-energy components are seen to contribute to the previously noted general increase of intensity with altitude, although, as before, the wide scatter of the observed points makes the form of the increase uncertain. As in Figure 2, the tendency toward

decreasing slope at higher altitudes in Figures 3 and 4 might be due to the reduced effect of the afterglow during these passes.

The values of intensity in Figures 3 and 4 are from all the recordings except those for which the total intensity exceeded the limit of the telemetering system; that is, the relay changing in response to the anode current switched more than once per cycle (1.23 sec). A more detailed analysis in the manner of *Herz, Ogilvie, Olley, and White* [1959] would probably yield this increased switching rate, but their technique does not seem warranted in our case since it would be necessary in only a few instances and would involve a much more elaborate scaling technique than we used. Also, on account of the effect of the afterglow, the information on channel 2 is of questionable value, at least as an indicator of high-energy intensity. At best, the difference between channels 2 and 3 can be regarded as the lower limit for the true intensity, the value from channel 3 already having been mentioned as the upper limit.

Discussion. Since the inclination of the satellite's orbit (65°) was very close to the latitude of College, Alaska, only a limited latitude range was sampled in all our observations, so that no systematic intensity variation with latitude could be detected.

The intensities sampled ranged from 0.7 to 2.8 bev/sec, much lower than the average intensity over the complete orbit, reported as 300 bev/sec [*Vernov and others*, 1959], but comparable with what was recorded in the USSR. In all our recordings the counting circuit was overloaded, indicating that the ionosphere over Alaska from 60° to 65° latitude is also characterized by the permanent low-energy (100 kev) electron flux observed at similar geographic latitudes by *Vernov and others* [1959].

Efforts were made to interpret the radiation observations in relation to ionospheric, magnetic, and solar activity, but there was no ob vious correlation, and our data were too limi to warrant a statistical approach. This wa period of very little activity in any of th fields, however, and there were no major so flares, magnetic storms, or radio wave abso tion events. Moreover, the ionosphere o Alaska was constantly sunlit during the per of our recordings.

The general increase of intensity with a tude, represented in Figure 2, might be due an increase in the number of geomagnetica trapped particles at greater heights. This crease would result from the reduced absorpt in the less dense higher atmosphere and fr an increased sampling of trapped particles, t is a sampling of particles with mirror heig up to and including the altitude of the satell The most that can be said about the scatter points in Figure 2 is that there is an appar time variation of intensity at any given a tude.

Acknowledgments. The authors wish to tha the staff members of the Geophysical Institute their helpful comments and to express their a preciation to Mrs. Catherine Hiland for her h in scaling the data.

This work was supported by the National S ence Foundation under Grant Y/32:42/268.

References

Herz, A. J., K. W. Ogilvie, J. Olley, and R. White, Radiation observations with satel 1958δ₂ over Australia, *Nature, 184,* 391, 1959

Meredith, L. H., M. B. Gottlieb, and J. A. V Allen, Direct detection of soft radiation abo 50 kilometers in the auroral zone, *Phys. Re 97* (1), 201, 1955.

Vernov, S. N., A. E. Chudakov, E. V. Gorchak J. L. Logachev, and P. V. Vakulov, Study of cosmic-ray soft component by the 3rd Sov earth satellite, *Planetary and Space Sci., 1* (86, 1959.

(Manuscript received December 28, 1959.)

The Determination of Ionospheric Electron Content and Distribution from Satellite Observations Part 1. Theory of the Analysis

OWEN K. GARRIOTT

Radio Propagation Laboratory
Stanford University
Stanford, California

Abstract. Two techniques are described which permit the integral of the electron density up to the satellite height to be deduced from the satellite radio transmissions. One method is based on the rate of polarization rotation due to the Faraday effect. The other method depends on a measurement of the total angle of polarization rotation at the time of closest approach of the satellite. If useful results are to be obtained, a number of corrections to assumptions made in the simplified analysis are necessary to account for path splitting between the two magneto-ionic components, error in the 'high-frequency approximation,' refraction, and satellite-antenna motion. Owing to the slow rotation of the satellite perigee position, the height of the passage at any given latitude varies. Variations of the integrated electron density with height can then be related to the electron-density profile. The results of the observations of Sputnik III radio signals in an 8-month period are included in part 2.

1 INTRODUCTION

easurements of the total ionospheric elec- content and estimates of the electron- ty profile above the height of maximum ty in the F layer are now possible utilizing radio transmissions from earth satellites. polarization of the received satellite signals nd to rotate, owing to propagation through irefringent ionosphere. From the observa- of this rotation the integral of the electron ty up to the satellite height may be de- l. For satellite passages at heights in excess out 1000 km, the total ionospheric electron nt is measured. The height of the satellite ny particular observing latitude usually s quite slowly as the result of the rotation ie perigee position. The variations of the rated electron density as a function of the ite height obtained over a period of weeks onths can then be related to the average on-density profile.

e observations of Faraday polarization ro- n are made in two different ways: by meas- the total angle of polarization rotation at convenient time; and by measuring the of polarization rotation [*Bowhill*, 1958; *ison and Weekes*, 1959]. These measure- s can be related to the integrated electron density in a rather simple manner, although a number of corrections to the simplified theory are a necessity if useful results are to be obtained. Therefore, after the simplified equations are found, the remainder of this paper will be devoted to a consideration of the approximations involved and the corrections that are required. Part 2 will present the results of the measurements of electron content and an estimate of the average electron-density profile above the F-layer maximum density.

2 SIMPLIFIED THEORY

A Rotation-angle measurement. An expression for the rotation of polarization per unit distance was given by Lorentz in 1906 in a series of lectures dealing with optical phenomena [*Lorentz*, 1952]. This same expression is frequently applicable at radio frequencies; it can be written

$$\frac{d\Omega}{ds} = \frac{\pi(\Delta\mu)}{\lambda_0} \approx \frac{K}{f^2} NH \cos\theta, \quad \frac{\text{rad}}{\text{meter}} \qquad (1)$$

where

$$K = \frac{e^3\mu_0}{8\pi^2 m^2 c\epsilon_0} = 2.97 \times 10^{-2}, \qquad \text{mks.}$$

f = wave frequency, cps.
N = electron density, elec/m^3.
H = magnetic field intensity, amp-turns/m.
θ = angle between the magnetic field and the direction of propagation.
λ_0 = free-space wavelength.
Ω = angle of polarization rotation, radians.
ds = sec χ dh = element of path length.
$(\Delta\mu)$ = difference in the values of the refractive index for ordinary and extraordinary waves.
$\approx XY_L$ (high-frequency, Q-L approximation).
$X = (f_0/f)^2$.
$f_0^2 = (Ne^2)/(4\pi^2 m\epsilon_0)$.
$Y_L = Y_H \cos\theta$.
$Y_H = (\mu_0 eH)/(2\pi fm)$.

This expression can be integrated along the ray path between the satellite and the receiver in order to determine the ionospheric electron content up to the satellite height. Many times the following approximation may be used [*Evans*, 1957]:

$$\Omega = \frac{K}{f^2}\int_0^{h_s} NH\cos\theta\, ds \qquad (2)$$

$$\approx \frac{K}{f^2}\overline{H\cos\theta\sec\chi}\int_0^{h_s} N\, dh \qquad (3)$$

The manner in which the rotation angle varies during a satellite passage is suggeste Figure 1. When the satellite is far to the s the rotation angle is relatively large, since cos θ and sec χ in equation 3 are large. W the satellite is at the point of closest appr (PCA), the rotation angle is found to be sm owing largely to the reduction in sec χ. As satellite continues its travel to the north, ever, the rotation angle still continues to decr because the reduction of cos θ more than of the increase in sec χ. As the ray path becc transverse to the magnetic field the total rota angle has been reduced to a small fractio the overhead value. In this region propaga is termed quasi-transverse (Q-T) and the po zation, in general, is found to be elliptical.

The variations in the total rotation angle a passage of Sputnik III have been easily served. When two horizontal, orthogonal dip were connected to separate receivers, and t outputs were recorded on chart paper, a re similar to the upper two channels in Figu was frequently obtained. At the right of Fi 2 the usual fading pattern is observed, whic dicates that the received signals were pl polarized and that the plane of of polariza was rotating. Assuming that the satellite ante was oriented in a fixed direction in space,

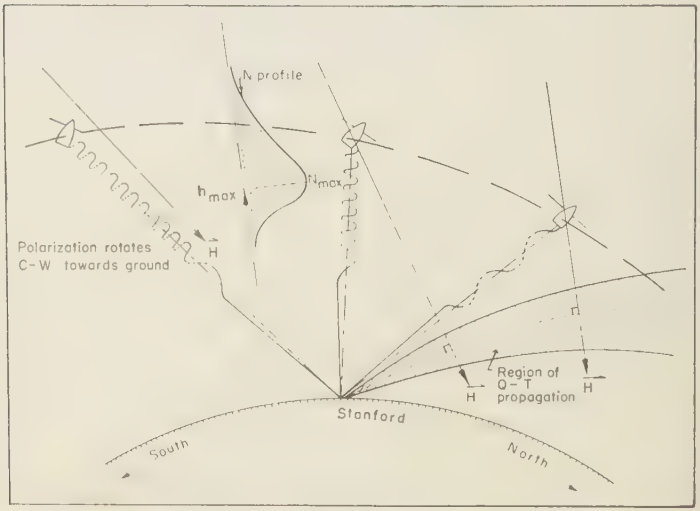

Fig. 1. Pictorial sketch of the way in which the rotation angle varies during a satellite passage

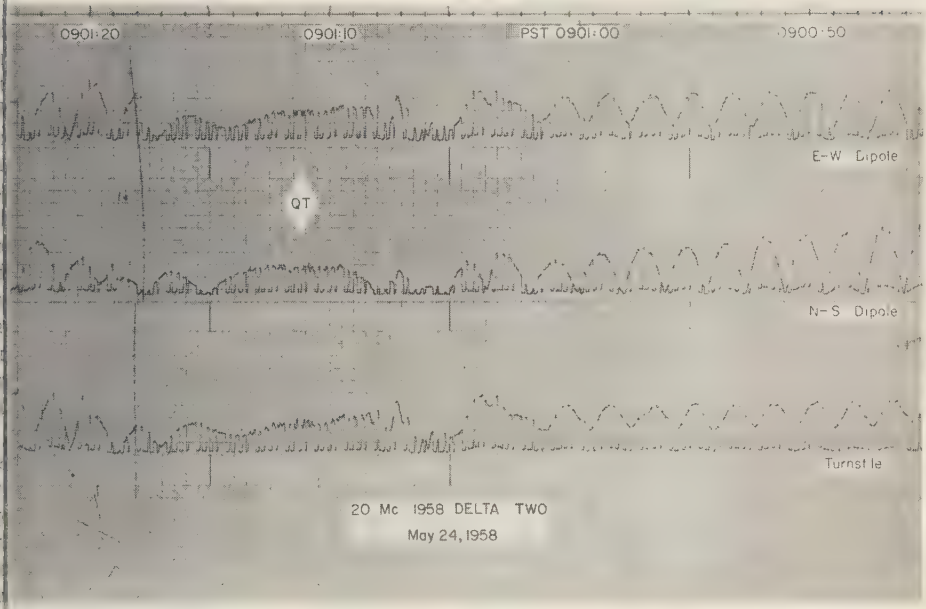

2. Faraday fading record, showing the region of quasi-transverse propagation. The relative phase of the fading reveals the direction of the polarization rotation. Passage is from south to north.

corresponds to an increase or a decrease of dians in the total rotation angle.

his ambiguity can be eliminated by noting *phase* of the fading on the two orthogonal nnas. If a satellite happens to be in either ie two vertical planes containing the dipoles, relative phase of the Faraday fading will be and it will be impossible to decide in which tion the polarization is rotating. But for any r satellite position, the two antennas do not *ar* orthogonal as viewed from the satellite. results in a relative fading phase other 90° and permits the direction of rotation e deduced. For example, at the time the rd in Figure 2 was taken, Sputnik III was oximately at an azimuth of 330° and at levation angle of 17° from the receiving lo- n at Stanford University. Assuming that rotation rate is constant, the phase of the g on the E-W dipole will lead that of the dipole by about 37° if the direction of rota- is CCW as viewed from the satellite.

seen in the earliest part of Figure 2 (at right) the rotation direction is CCW (E-W E-SW to N-S). It may be determined that, for propagation in the same direction as the magnetic field, the transmitted polarization will be rotated CW in passing through the ionosphere.[1] A CCW rotation of polarization at the ground implies that the total rotation angle is decreasing, which is consistent with the previous arguments for a S-N passage.

Near the center of Figure 2 can be seen the region of quasi-transverse propagation. The regular fading pattern due to polarization rotation changes to one of a nearly constant elliptical polarization. Beyond this point, the polarization again becomes plane and the direction of rotation continues CCW, indicating both that the longitudinal component of the magnetic field has changed sign and that the total rotation angle is increasing in the CCW direction.

Now a very simple method of determining the total rotation angle is seen. Suppose that a

[1] This conclusion may be reached from the following considerations. For propagation in the direction of the magnetic field, the ordinary wave is polarized CCW circular and travels with a smaller phase velocity than the extraordinary component [*Snyder and Helliwell*, 1952].

record of the variations in signal strength has been obtained from the time a satellite passes overhead to a point in the north where Q-T propagation is observed. The number of fades between these two times, multiplied by π, is (very approximately) equal to the total rotation angle that exists at the PCA overhead. This is related by equation 3 to the electron density integrated up to the height of the satellite.[2]

A number of assumptions have been made in this simplified approach, and they must be either justified or modified. Therefore, each of the following topics will be considered:

1. A majority of the records obtained do *not* show a region of Q-T propagation. Instead, the rotation angle (or, more precisely, one-half the difference in the phase path lengths of the two magnetio-ionic components) reaches some minimum value, then the direction of rotation reverses and the rotation angle begins to increase. Figure 3 is an example of this; the reversal in the direction of rotation is indicated by a change in phase of the Faraday fading with intermediate Q-T propagation in evidence. The minimum rotation angle is frequently 30 to 50 per cent of the overhead value, rather than zero as indicated by the simple analysis above. A method for estimating the minimum rotation angle relative to that at the PCA is discussed in section 3A.

2. Equation 2 assumes that both magneto-ionic components follow the same ray path between the satellite and the receiver. In some cases this path separation appears to be significant; in fact, this is believed to be the cause of the rotation reversal prior to an observation of Q-T propagation. Section 3B discusses the significance of this magneto-ionic path splitting to the measurement of the rotation angle.

3. Equation 2 has assumed implicitly that the wave frequency is always much larger than

[2] This same technique has been noted independently by *Blackband, Burgess, Jones, and Lawson* [1959].

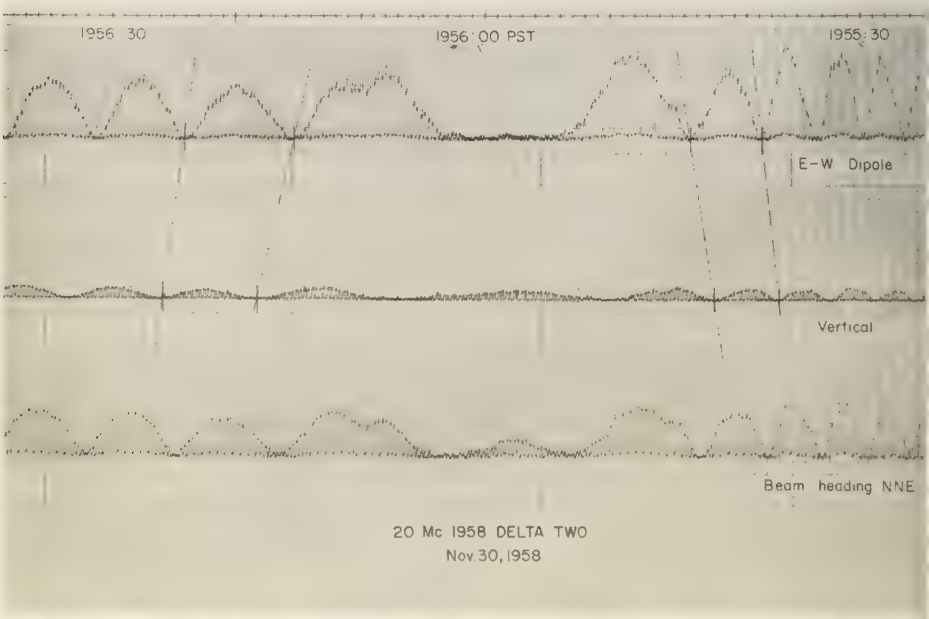

Fig. 3. Faraday fading record, showing a reversal in the direction of polarization rotation. P sage is from north to south. The approximate position of the satellite at this time was at an azim of 330° and an elevation angle of 30° from Stanford University. The direction of rotation is first C (S-N to vertical to E-W), then it reverses to CW at the left.

rna frequency ($f \gg f_0$). When this is so, the
x of refraction can be expressed as

$$\left[1 - \frac{X}{1 \pm Y_L}\right]^{1/2} \approx 1 - \frac{1}{2} X \pm \frac{1}{2} X Y_L \qquad (4)$$

the result is used in equation 1. Many times
'high-frequency approximation' is not
iently accurate and must be corrected if
ıl values of electron content are to be
ined. This correction is considered in section

The effects of refraction are considered in
ion 3*D*.

If the satellite antenna structure does not
ıtain a fixed spatial orientation, additional
s *may* be introduced in the signal-strength
ds. This, of course, leads to some inaccuracy
ıe measurement of the total rotation angle.
ion 3*E* discusses one means of determining
much, if any, correction is necessary to
unt for motion of the satellite antenna.

The effect of horizontal gradients in the
sphere is briefly considered in section 3*F*.

Rotation-rate measurement. Within several
nptions, *Bowhill* [1958] has related the rate
ıraday rotation to the electron density inte-
d vertically up to the satellite height. These
nptions are: (*a*) flat earth; (*b*) horizontal
spheric stratification; (*c*) horizontal satellite
ity; (*d*) $f \gg f_0$; (*e*) refraction neglected.
derivation has been slightly modified
iott, 1959] in order to include the effect of
atively small vertical velocity component.
following equation is obtained by following
procedure used by Bowhill:

$$= \frac{K}{f^2}\left\{\frac{H_x v_x}{z}\int N\,dh + H_L \sec\chi\, N_{\text{local}}\, v_s - \frac{(xH_x + yH_y)v_z}{z^2}\int N\,dh\right\} \qquad (5)$$

quantities x, y, and z are shown in Figure 4.
H_y, and H_L are the components of the earth's
netic field resolved along $\hat{i}$, $\hat{j}$, and $\overline{OP}$.
$_{\text{al}}$ is the electron density in the vicinity of
satellite. The first term on the right in (5)
e expression derived by Bowhill; the last
s are corrections for the vertical velocity
onent.

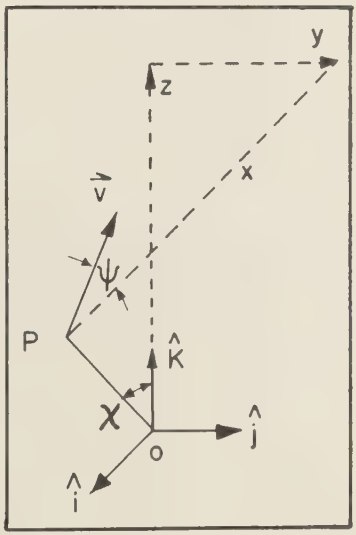

Fig. 4. Geometry for the analysis of Faraday rotation rate. The satellite velocity is parallel to the x-z plane.

When the rotation rate is measured at the PCA ($x = 0$), equation 5 can be solved for the integrated electron density:

$$\int_0^{h_s} N\,dh = \frac{\{(d\Omega/dt) - (K/f^2)H_L \sec\chi\, N_{\text{local}}\, v_s\}\gamma}{(K/f^2 h_s)[H_x v_s - H_y \tan\chi v_s]} \qquad (6)$$

The multiplier γ has been inserted in equation 6 in order to correct for the error in assuming that $f \gg f_0$. This factor will be discussed more fully in section 3*C*. The value of N_{local} must be estimated, but this will not seriously affect the result for small v_s. For satellite orbits with a sufficiently large eccentricity, it may be possible to solve (6) for the local electron density. Since this derivation includes all the assumptions made in the rotation-angle measurements the discussion of the required corrections given in the following sections is applicable to both techniques.

3. Corrections to Approximations

A. Minimum rotation angle. When Q-T propagation can actually be observed, the minimum difference in the phase path lengths be-

tween the two magneto-ionic components (or the rotation angle) is relatively small and can be reasonably well estimated. However, by far the majority of the satellite passages reveal (at 20 Mc/s) a change in the direction of polarization rotation at some point between the zenith and the direction of transverse propagation in the north. Figure 3 was a typical example of such a case. Since the minimum rotation angle (which occurs at the time of the reversal in the direction of polarization rotation) may be a relatively large fraction of the rotation angle when the satellite is at the PCA, it cannot be neglected. Some means of estimating the minimum difference in phase path lengths is therefore necessary.

It has been found desirable to make use of a digital computer for the estimation of the minimum difference in phase path length, and this is accomplished in the following manner. An electron-density profile is assumed of the form

$$N = N_{\max} \exp \tfrac{1}{2}[1 - z - e^{-z}] \qquad (7)$$

and

$$z = (h - h_{\max})/H' \qquad (8)$$

where the values of $N_{\max}$, $h_{\max}$, and H' are arbitrary input constants. Near the time of each satellite passage a vertical-incidence ionospheric sounder has been preset to record an ionogram. Each ionogram has been reduced to a true height profile, and from this the values of $N_{\max}$, and $h_{\max}$ and the best-fitting value of H' are used in the computer program.

Three geographic coordinates are also supplied to the computer: P_0, the observer's location (Stanford University); P_I, the satellite position at the point of closest approach (PCA); P_{II}, the satellite position at the time of Q-T propagation or, more frequently, near the time of a reversal in the direction of polarization rotation. The geographic coordinates or P_I and P_{II} are determined from an ephemeris made available in advance of publication by Dr. R. M. Adams of the Smithsonian Astrophysical Observatory. Errors in the tabulated positions of Sputnik III are believed to be less than 20 km at all times (private correspondence). The computer first determines the isotropic ray paths (i.e., neglecting the earth's magnetic field) between P_0 and P_I and between P_0 and P_{II} (ray paths I and II, respectively). Then the total Faraday rotation angle along each path is estimated by integ ing equation 1:

$$\Omega_I' = \frac{K}{f^2} \int_I NH \cos\theta \sec\chi \, dh$$

$$\Omega_{II}' = \frac{K}{f^2} \int_{II} NH \cos\theta \sec\chi \, dh \qquad (9$$

Although the values of Ω_I' and Ω_{II}' may closely correspond to the true values Ω_I and (which are, of course, unknown), it should true that their ratio is considerably more curate than their absolute values. This is duced from the fact that cos θ and sec χ cha very little along a ray path, particularly for path I, where the zenith angle is small. The er in these quantities due to refraction is pri pally a function of $N_{\max}$, which is determi for each passage from the corresponding ve cal-incidence ionogram. Therefore, it is assur that

$$\phi \equiv \Omega_{II}'/\Omega_I' = \Omega_{II}/\Omega_I \qquad (1$$

From the record of signal strength obtai during a satellite passage the number of fa due to polarization rotation between positi P_I and P_{II} (defined as ΔF) can be counted. T is related to the total rotation angle at the P by

$$\Omega_I = [(\Delta F)\pi]/(1 - \phi) \quad \text{radians} \qquad (1$$

The same computer program also relates to the integral of the electron density as follo

$$\Omega_I \cdot \gamma = \frac{K}{f^2} \int_I NH \cos\theta \sec\chi \, dh \qquad (1$$

$$= \left(\frac{K}{f^2}\right) G_I \int_0^{h_*} N \, dh \qquad (1$$

G_I is some function affected by both the elect distribution and the magnetic field along path I. It is obtained for the assumed distri tion of N and the magnetic field model (dip adjusted to match the observer's dip and va tion) from the following equation:

$$G_I = \frac{\int_I NH \cos\theta \sec\chi \, dh}{\int_I N \, dh} \qquad (1$$

e ($H \cos \theta$ see χ) is relatively constant all g the ray path, the value of G_1 will be quite sitive to variation in the electron-density le.

addition, the computer is programmed to ulate the quantity γ, which is the correction or for the error introduced by the high- uency approximation (section 3C). Finally, solution for the integrated electron density tained by combining (12), (14), and (15).

Magneto-ionic path splitting. In the pre- s section the number of polarization rota- s between the satellite and the observer (or rotation angle) was estimated by integrat- a function along the isotropic ray path be- n the two points in question (equations 9 10). More correctly, the phase path length each magneto-ionic component should be d separately. Unfortunately, it is rather ult to determine these two ray paths, and accuracy is required in the computations. individual phase path lengths may differ nly 10 to 100 wavelengths along a total path th of 10^5 wavelengths. Integrating along the opic ray path (which is comparatively easy etermine) does not require taking the dif- ice between two nearly equal, large quanti- and thereby reduces the accuracy required. latter method is seen to have certain ad- ages if it can be shown that neglecting the

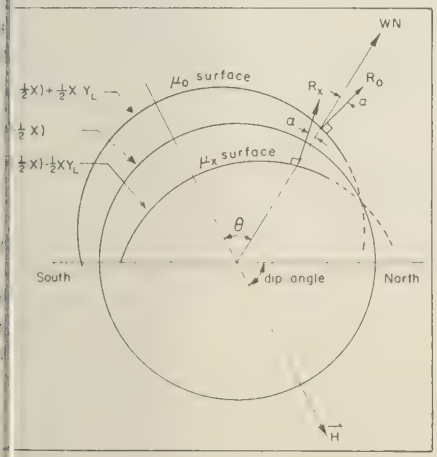

g. 5. μ surfaces for determining the ray di- ons, assuming high wave frequency and Q-L itions.

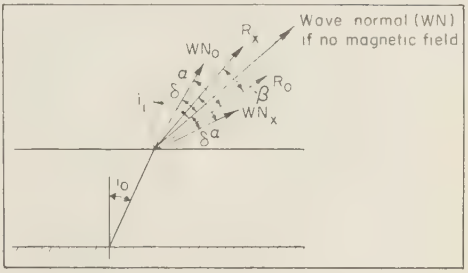

Fig. 6. A single ray incident on the lower edge of a semi-infinite, homogeneous ionosphere.

path splitting between the two magnetoionic components does not result in serious error.

In order to investigate analytically the importance of path splitting, a very simple ionospheric model has been selected: a semi-infinite homogeneous slab of electrons commencing at height h above a flat earth. The satellite height is constant at 2 h. For this situation the various path lengths can be derived and a general feeling for the effect of path splitting obtained.

First, it is noted that the ordinary and extraordinary (O and X) rays must depart from the satellite at slightly different angles in order to converge at the ground receiver. Although it can be demonstrated from this point of view, a more convenient method is to consider propagation from observer to the satellite. The two rays will differ in direction from their respective wave normal directions along portions of their paths. The angle α between wave normal and ray can be determined with the aid of Figure 5.

This figure is a plot of the 'μ surfaces' for O and X waves, assuming Q-L conditions. Each surface (in three dimensions) represents the magnitude of the index of refraction in that particular direction. For a wave normal drawn from the origin to any point on a μ surface, the corresponding ray direction is given by the gradient of the μ surface at that point [*Ratcliffe*, 1959]. Looking to the north (and at zenith angles less than the magnetic dip angle) the ordinary ray is seen to be bent toward the horizontal by an angle α with respect to its wave normal and toward the vertical for the extraordinary ray, where

$$\alpha = \tfrac{1}{2} X Y_H \sin \theta \qquad (16)$$

The conditions required for convergence of the rays at the satellite can be found using Figure 6, which shows a single ray incident on the lower edge of the ionized slab. In the absence of the earth's magnetic field, the angle of refraction would be

$$i_1 = i_0 + \epsilon \tag{17}$$

where

$$\epsilon \approx (1 - \mu) \tan i_0 \approx \tfrac{1}{2} X \tan i_0 \tag{18}$$

The inclusion of the earth's field results in slightly different wave normal directions for the two magnetoionic components. The ordinary wave normal is refracted less, by an amount δ measured with respect to i_1, and the refraction is greater for the extraordinary wave normal, where

$$\delta = \tfrac{1}{2} X Y_H \cos \theta \tan i_0 \tag{19}$$

The angle between the two rays is therefore given by

$$\begin{aligned} \beta &= (2\alpha - \delta) \\ &= X Y_H (\sin \theta - \cos \theta \tan i_0) \end{aligned} \tag{20}$$

With the satellite at height $2h$, and assuming that α and δ do not change for small variations in i_0, the *initial* ordinary-ray direction must be *decreased* by $\beta/4$, and the extraordinary ray direction increased by $\beta/4$, in order to converge at the satellite. These changes are shown in Figure 7.

Now the two phase path lengths can be computed. For either ray, the phase path length is given by the following expression, where the integration is performed along the ray path:

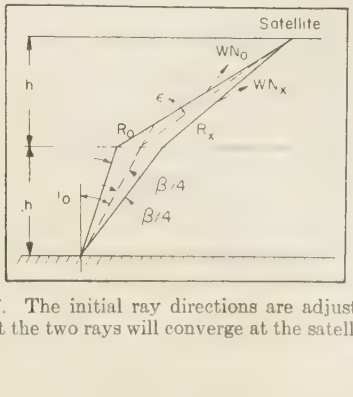

Fig. 7. The initial ray directions are adjusted so that the two rays will converge at the satellite.

$$P = 2\pi \int \frac{ds}{\lambda_r} = 2\pi \int \frac{f\, ds}{v_r} \text{ radians} \tag{2}$$

and v_r = ray velocity[3] $= c/(\mu \cos \alpha)$

$$P = \frac{2\pi}{\lambda_0} \int \mu \cos \alpha \, ds \tag{2}$$

The difference in the phase path lengths alo the two rays is

$$\Delta P = P_O - P_X \tag{2}$$

$$\begin{aligned} &= \frac{2\pi h}{\lambda_0} \left\{ \sec \left(i_0 - \frac{\beta}{4} \right) - \sec \left(i_0 + \frac{\beta}{4} \right) \right. \\ &\quad + \mu_0 \cos \alpha \sec \left(i_1 + \frac{\beta}{4} \right) \\ &\quad \left. - \mu_X \cos \alpha \sec \left(i_1 - \frac{\beta}{4} \right) \right\} \end{aligned} \tag{2}$$

$$\begin{aligned} \Delta P \left(\frac{\lambda_0}{2\pi h} \right) \approx & -\frac{\beta}{2} \sec i_0 \tan i_0 \\ & + \left(1 - \frac{\alpha^2}{2} \right) \left[\left(1 - \frac{X}{2} \right) \right. \\ & \cdot \left(\frac{\beta}{2} \sec i_1 \tan i_1 \right) \\ & \left. + X Y_L \sec i_1 \right] \end{aligned} \tag{2}$$

It can now be seen that terms involving α not important and can be neglected. This plies that the phase velocity is a suitable proximation to the ray velocity in these cal lations.

The above equation is then reduced to

$$\Delta P \left(\frac{\lambda_0}{2\pi h} \right) \approx X Y_L \sec i_1 + \frac{X\beta}{2} (\sec i_0 \tan^3$$

(

It should be noted that the first term on right side of (26) is simply the approximate pression for $(\Delta\mu)$ integrated along the isotro ray path. The additional term is a correction path splitting.

As a satellite travels north the rotation ar (which is proportional to ΔP) is observed to crease as indicated in (26) by the reductior

[3] The ray velocity is defined as the velocity phase propagation in ray direction.

n the first term. However, the second term eventually increase more rapidly than the s term decreases and thereby cause the total ber of rotations to increase. The two terms ne right in (26) and their sum are shown in re 8 as a function of the zenith angle i_0. can be seen from this figure, the total ro- n angle begins to increase beyond $i_0 \approx 45°$ value of $X = 0.25$. However, the magnitude e second term, which is increasing rapidly, ll considerably less than the magnitude of irst term at the point where the rotation begins to increase.

om this example several useful observations be made. First, the effect of magneto-ionic splitting is to increase the phase-path- h difference when looking northward and by to *reduce* the rate of polarization rota- Second, the magnitude of the effect is large gh to reverse the direction of polarization ion as is observed. Third, the path splitting rly negligible for zenith angles less 40° but ases rapidly for zenith angles greater than Fourth, owing to the rapid increase in the of the path-splitting contribution, its mag- de is still much smaller than the velocity dis- on term at the time of the minimum phase- -length difference.

e observed variations in the rotation angle quite well with the calculations above. principal difference is that the polarization rsal' occurred at zenith angles greater than 50° to 60° was more frequently found. cally, the rotation rate during a S-N pas- remained relatively constant, then slowed reversed direction rather abruptly at some to the north (Fig. 3). The magnitude of otation rate was frequently greater after eversal than it had been previously. This ment suggests that magneto-ionic path ing becomes a significant factor (at a geo- etic latitude of about 45°) only at zenith s greater than about 40°.

High-frequency approximation. When the frequency and the plasma frequency be- comparable in size, considerable error is duced by the use of the approximate ex- ion for the index of refraction given by However, a correction factor can be found very straightforward manner. With suffi- accuracy for most purposes,

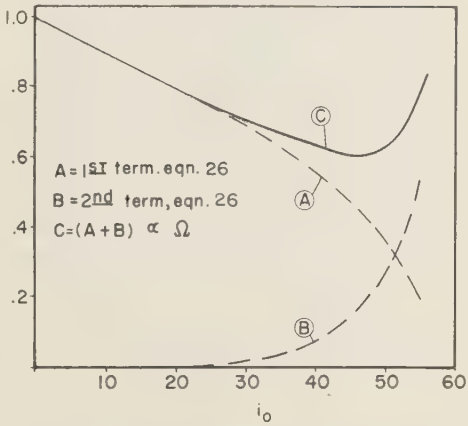

Fig. 8. Relative contribution of the dispersion and path-splitting terms to the rotation angle.

$$\mu = \left[1 - \frac{X}{1 \pm Y_L}\right]^{1/2} \approx [1 - X(1 \mp Y_L)]^{1/2} \qquad (27)$$

Expanding each magneto-ionic component in a binomial series (subscripts O and X refer to the ordinary and extraordinary modes, respectively) we obtain

$$(\Delta\mu) = \mu_O - \mu_X = Y_L[X + \tfrac{1}{2}X^2 + \tfrac{3}{8}X^3 + \tfrac{5}{16}X^4 + \cdots] \qquad (28)$$

in which third powers of Y_L have been neglected in the last two terms. By retaining only the first two terms in the binomial expansion [one term in $(\Delta\mu)$], the usual 'high-frequency' expression can be obtained.

If additional terms are retained, the rotation angle becomes a function of the distribution of electrons as well as of their total number. Furthermore, the rotation angle is not proportional to $1/f^2$ as indicated by the high-frequency approximation, and this is a characteristic frequently observed with satellite transmissions at 20 and 40 Mc/s. However, the effect of the distribution of electrons on the total rotation angle can be determined surprisingly well from a single parameter, e.g., the critical frequency of the layer. Expressed from another viewpoint, the layer critical frequency permits a relatively accurate estimate to be made of the contribution of the first-order term in (28) as compared with

the sum of all the terms. Knowing the fractional contribution of the first-order term permits the calculation of the integrated electron density, regardless of the layer shape. The observed rotation angle Ω is simply multiplied by this fraction, and the 'reduced' Ω is inserted in the high-frequency equation, as was done in (6) and (13) without prior justification.

Substituting (28) into (1), the more exact expression for the rotation angle becomes

$$\Omega = \frac{\pi Y_L}{\lambda_0} \cdot \int [K'N + \tfrac{1}{2}(K'N)^2 + \tfrac{3}{8}(K'N)^3 + \cdots] \, ds \tag{29}$$

where $K' = 80.6/f^2$ (mks). The contributions of each term can be considered individually for any layer shape. One layer profile which is frequently not a bad approximation to true height curves of the lower ionosphere is that of a simple attachment-like Chapman region:

$$N = N_{\max} \exp [1 - z - e^{-z}] \tag{30}$$

where

$$z = (h - h_{\max})/H' \tag{31}$$

It also has the useful advantage of being integrated easily, as are all its powers. This distribution has been inserted in (29), integrated as function of the height variable z, and evaluat term by term, for various values of $N_{\max}$.

Figure 9 is a plot of the ratio of the fir order term to the sum of the first four terms (28). Each curve is parametric in $X_{\max} = K'N_{\max}$ For small $X_{\max}$, the first-order term is the o important one, indicating good accuracy in high-frequency approximation. However, $X_{\max}$ increases, higher-order terms rapidly come important. For these curves to be usef they must be shown to be largely independe of the electron-density profile. Therefore, simi computations have been made for several p files, including a 'parabolic' layer in which upper semithickness was twice that of lower. The curves in Figure 9 provided proper correction for the parabolic layer with 10 per cent at all heights.

An important characteristic of the curves their flatness above the layer maximum (z 0). In order to obtain the proper 'reducing f tor' (γ), it is necessary to assume a value of in order to compute the height of the satellite units of z. But the value of H' is one of quantities we wish to obtain from the satell observations. Since the curves of Figure 9 relatively flat above the layer maximum, value of H' which is assumed in order to obt γ will not be too important. (H' equal to km is reasonable in equation 31.)

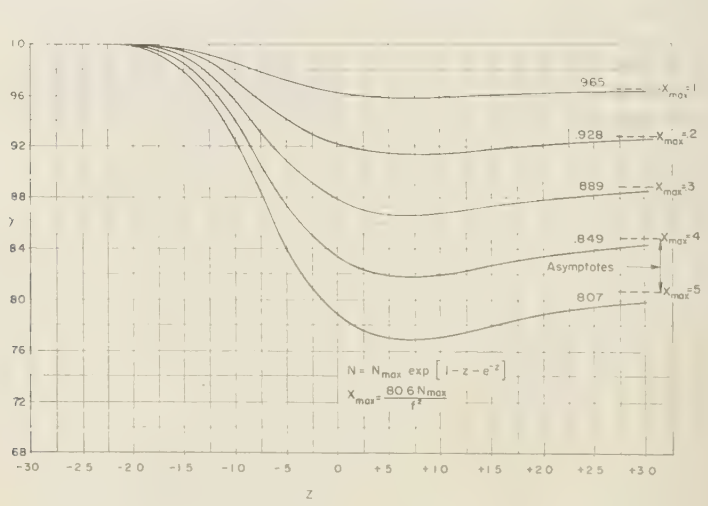

Fig. 9. Fractional contribution of the first-order term in ($\Delta\mu$).

hen the Faraday rotation rate at both 20 and Mc/s is measured, a check can be made on accuracy of the correction. After multiply- 20-Mc/s rate by the fraction γ, the 20-Mc/s should be approximately 4 times the 40- 's rate, although refraction and path-splitting ts may still alter this ratio at large zenith es.

. Refraction. The effects of refraction are ely taken into account in the rotation-angle surements by the computer analysis out- in section 3*A*. Refraction is automatically uded when the isotropic ray path between satellite and the receiver is computed. Since rotation-rate equations derived in section do not include the effect of refraction, the tion rate should be measured at the time he satellite's closest approach in order to imize refraction error.

. Satellite-antenna motion. The motion of transmitting antenna about the center of vity of a satellite may or may not affect the rage rate of polarization rotation. The 'free- y' motion of a cylindrical satellite may be ected to decay into a propellerlike spin about e nearly perpendicular to the cylinder axis *acewell and Garriott,* 1958]. A dipole at- ed to the cylinder will generate a cone about axis of rotation.

o an observer, the dipole will rotate or simply llate depending on whether or not a line wn between satellite and observer lies inside generated cone [*Thomson,* 1958]. If the ole is observed to rotate, the fading rate of received signals will be increased (or de- sed) by twice the spin rate of the satellite. he dipole merely oscillates, the average fad- rate (over one spin period) will be unaf- ed by the rotation of the satellite's antenna, ough some amplitude modulation may be d.

he night-time observations of Sputnik III eal very slow Faraday fading due to the small spheric electron content. The errors due to action, magneto-ionic path splitting, and the n-frequency approximation are quite small hese times, and the Faraday fading should ow the $(1/f^2)$ relation closely. In some cases, t-time observations at both 20 and 40 Mc/s e made it possible to determine whether or a correction for satellite-antenna motion was necessary, based on the ratio of the fading rates. In the daytime, the Faraday fading was usually much faster than the satellite half-spin period (about 40 sec), making a correction unnecessary.

F. Horizontal ionospheric gradients. Another factor that affects the results of both rotation-angle and rotation-rate measurements is horizontal ionospheric gradients. An estimate of the magnitude of the gradient has been made from the variation in skip distance as a function of azimuth obtained from the *H-F* backscatter records at Stanford University [*Peterson, Egan, and Pratt,* 1959]. This horizontal gradient is then included in the model ionosphere used in the computer calculations outlined in section 3*A*. Furthermore, rotation-angle measurements become inherently insensitive to horizontal gradients when the Faraday fading can be used to a point near the Q-T region in the north.

The rotation-rate measurements do not include any correction for these gradients, and the errors incurred become very appreciable near such times as sunrise when large horizontal variations are known to exist.

4. Conclusions

Two methods have now been analyzed which will provide values of the integrated electron density from the observation of satellite radio transmissions. Each of the methods is susceptible to error in varying degrees on account of the approximations made. Thus the two techniques are to some extent independent and should provide a useful cross check on the values of integrated electron density that are obtained.

Acknowledgments. The advice of Professors O. G. Villard, Jr., A. M. Peterson, and R. N. Bracewell, as principal investigators in the research program under which this work was performed, is very much appreciated. A number of discussions with Professor R. A. Helliwell have also been most helpful. Financial support for most of the work has come from National Science Foundation Grant Y/32.43/269. The program has been extended in 1960 by a grant from the National Aeronautics and Space Administration.

References

Aitchison, G. J., and K. Weekes, Some deductions of ionospheric information from the observations of emissions from satellite 1957α_2, I, The

theory of the analysis, *J. Atmosphric and Terrest. Phys., 14* (3 and 4), 236–243, 1959.
ics Laboratory, Stanford University, November 3, 1959.

Blackband, W. T., B. Burgess, I. L. Jones, and G. J. Lawson, Deduction of ionospheric electron content from the Faraday fading of signals from artificial earth satellites, *Nature, 183,* 1172, 1959.

Bowhill, S. A., The Faraday rotation rate of a satellite radio signal, *J. Atmospheric and Terrest. Phys., 13* (1 and 2), 175, 1958.

Bracewell, R. N., and O. K. Garriott, Rotation of artificial earth satellites, *Nature, 182,* 760–762, 1958.

Evans, J. V., The electron content of the ionosphere, *J. Atmospheric and Terrest. Phys, 11* (3 and 4), 259–271, 1957.

Garriott, O. K., The determination of ionospheric electron content and distribution from satellite observations, *Tech. Rept. 1,* Stanford Electron-

Lorentz, H. A., *The Theory of Electrons,* p. 163 Dover Publications, 1952.

Peterson, A. M., R. D. Egan, and D. S. Pratt, The IGY three-frequency backscatter sounder, *Proc IRE, 47,* (2), 300-314, 1959.

Ratcliffe, J. A., *The Magneto-Ionic Theory and Its Applications to the Ionosphere,* chapter 8 (Q-L and Q-T approximations) and chapter 18 (relation between ray direction and μ surfaces) Cambridge University Press, 1959.

Snyder, W., and R. A. Helliwell, Universal wave-polarization chart for the magneto-ionic theory *J. Geophys. Research, 57,* 73, 1952.

Thomson, J. H., The rotation of the first Russian earth-satellite, *Phil. Mag., 3,* (32), 912, 1958.

(Manuscript received January 8, 1960.)

The Determination of Ionospheric Electron Content and Distribution from Satellite Observations Part 2. Results of the Analysis

OWEN K. GARRIOTT

Radio Propagation Laboratory
Stanford University
Stanford, California

Abstract. The results of observations of the radio transmissions from Sputnik III ($1958\delta_2$) in an 8-month period are presented. The measurements of integrated electron density are made in two ways, described in part 1. The measurements reveal the diurnal variation of the total ionospheric electron content; also, the ratio of the total content to the content of the lower ionosphere below the height of maximum density in the F layer is obtained. An estimate of the average electron-density profile above the F-layer peak is made possible by the slow variation in the height of the satellite due to rotation of the perigee position. The gross effects of large magnetic storms on the electron content and distribution are found.

Introduction. In part 1 two methods were escribed in which the observations of radio gnals from earth satellites were related to the ntegral of the electron density up to the satel- te height. In one method an estimate is made f the total angle of polarization rotation ue to the Faraday effect at the time of the osest approach of the satellite. The second ethod relates the rate of polarization rotation bserved at the receiver to the integrated elec- on density. A number of corrections are ap- lied to the simplified analysis in each case. This aper will present the results of an analysis of early 8 months' data in the period September 958, to April 1959.

Observational results. In the above period ie NW to SE (descending) passages of Sput- ik III ($1958\delta_2$) were at heights greater than 200 km at the observing latitude (37.4°N). The alues of the integrated electron density (N_s) hat were obtained are therefore essentially the ntire ionospheric electron content. The diurnal ariation of the electron content is observed, wing to the westward motion of the nodes at n average rate of about 15 minutes per day. igure 1 shows the computed values of N_s, ach of which is defined as the number of elec- rons in a vertical column of unit cross section p to the satellite height. The local time of each bservation increases to the right, resulting in he date of the observation increasing to the left.

The rotation-angle measurements have been made by counting the number of fades on the signal-strength record in a certain interval of time. This interval is between the satellite's point of closest approach and a point somewhat to the south of the reversal in the direction of polarization rotation. From this basic observation, equations 12, 14, and 15 of part 1 are solved for the integrated electron density. These values are plotted as circles in Figure 1. The rate of polarization rotation at the point of closest approach is related to the integrated electron density by equation 6 of part 1, and these values of N_s are shown as dots. Vertical lines connect the measurements made on the same satellite passage. The values of the integral of the electron density up to the height of maximum density in the F layer have been obtained from the calculated true height profiles. Each of these quantities is defined as N_b and is plotted as a cross. The smoothed curves through the points of N_s and N_b represent the average ionospheric behavior in the period of the observations.

The ratio of the values of these two curves (N_s/N_b) at any time is also a quantity of interest, especially since this ratio has previously been measured by moon echo techniques [*Evans*, 1957; *Bauer and Daniels*, 1958, 1959]. A pronounced diurnal variation of the ratio is illustrated in Figure 2, although the average

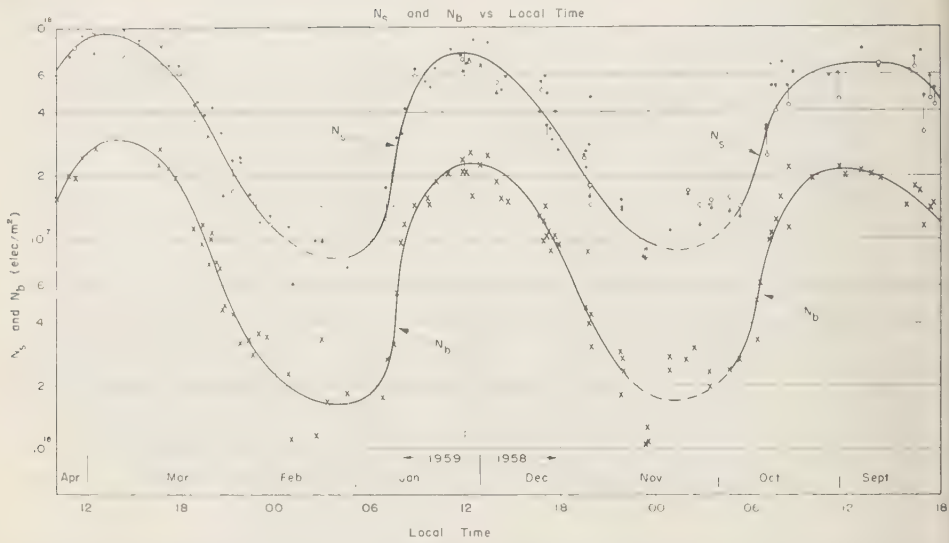

Fig. 1. N_s and N_b vs. local time for the NW to SE (high) satellite passages. Circles refer to rotation-angle measurements and dots to rotation-rate measurements. The dashed parts of the curves are less reliable.

value is about 4 as found by Evans. The ratio tends toward 3:1 in the daytime and 5:1 at night, with a rather sharp decrease at sunrise. This is consistent with the variations noted in the later work of *Bauer and Daniels* [1959], although their values are somewhat higher.[1]

Figure 3 is of the same type as Figure 1, except that the curves are for SW to NE passages of Sputnik III. In the 8-month period considered, the satellite height varied from less than 300 km to over 900 km at the observing latitude. As the height increased, the ratio (N_s/N_b) varied from about unity up to the same value as that for the descending passages. The variation of this ratio with height provides a means of obtaining the average electron-density profile for the top of the F_2 layer.

[1] The ratio used by Bauer and Daniels $n_a/n_b = (N_s/N_b) - 1$.

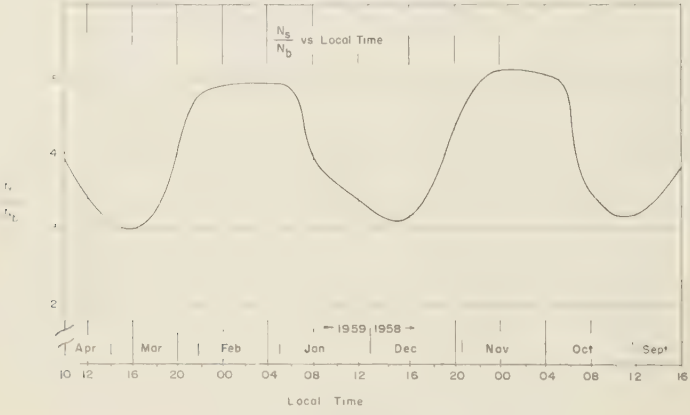

Fig. 2. N_s/N_b vs. local time.

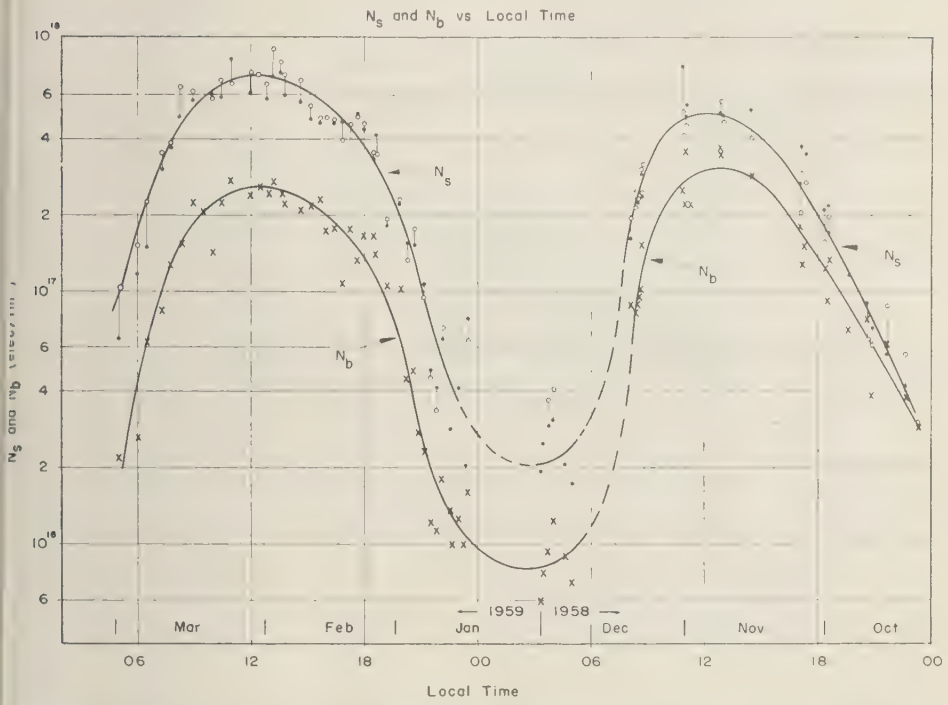

Fig. 3. N_s and N_b vs. local time for the SW to NE (low) satellite passages. Circles refer to rotation-angle measurements and dots to rotation-rate measurements. The dashed parts of the curves are less reliable.

The value of $(N_s - N_b)$ is the number of electrons per meter column between the height of maximum electron density (h_{max}) and the satellite height (h_s). If normalized by dividing by N_{max}, the quantity

$$y \equiv (N_s - N_b)/N_{max} \qquad (1)$$

is the 'equivalent column height' of a meter column of electrons containing the number $(N_s - N_b)$ but compressed to a density of N_{max}. The observed values of y plotted as a function of

$$x \equiv h_s - h_{max} \qquad (2)$$

are shown in Figure 4 for the SW to NE satellite passages. Days of high magnetic activity have been excluded and will be discussed separately. It should be noted that the values of y are independent of the electron-density distribution and content of the lower ionosphere below h_{max}. The values of y appeared to have very little dependence upon local time; therefore, no distinction has been made between day and night-time observations. The NW to SE (high) passages, which are not plotted, gave an average value of equivalent column height of 280 km. When averaged separately, the night values were about 10 per cent greater and the daytime values 10 per cent less than this number.[2]

If it is assumed that the electron-density profile for the top part of the ionosphere has some constant *shape* (but not necessarily the same N_{max}), then the integral of the normalized profile is some function,

$$y = f(x) \qquad (3)$$

where y and x are defined above. Furthermore,

$$dy/dx = f'(x) \qquad (4)$$

is the value of the normalized electron density at any height x. In other words, the function

[2] From the value of y and an assumed temperature profile, *Burkard* [1958] has described a method for obtaining the atmospheric scale height at the level of the maximum electron density.

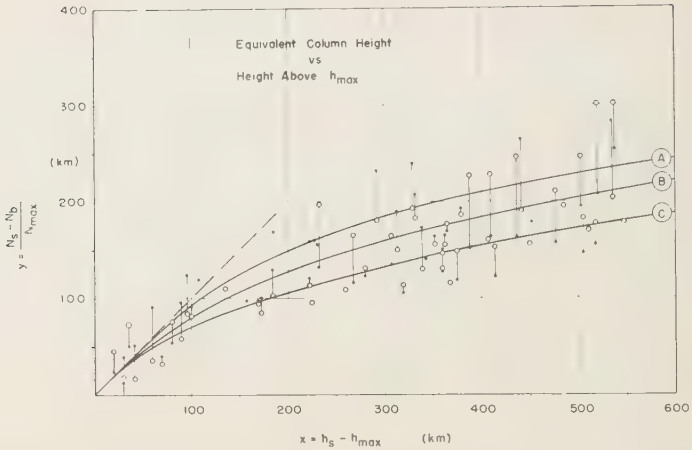

Fig. 4. Equivalent column height (y) vs. height above h_{max} (x) for the SW to NE satellite passages.

$f'(x)$ is the normalized electron-density profile.

One method of obtaining $f'(x)$ would be to fit a least-mean-square-error polynomial to the observed points and find its first derivative. However, this excludes a considerable amount of a priori knowledge relating to $f(x)$. First, the value of $y_{(0)}$ must be zero by the very definition of y. Second, since the electron-density profile has been normalized to N_{max}, it must be true that

$$(dy/dx)_{x=0} = 1 \tag{5}$$

Third, since the electron density decreases below h_{max} and presumably above h_{max}, the point $y_{(0)}$ must be an inflection point. Thus

$$(d^2y/dx^2)_{x=0} = 0 \tag{6}$$

Now, the first three coefficients of the polynomial $f(x)$ are known:

$$y = a + bx + cx^2 + dx^3 + hx^4 + \cdots \tag{7}$$

where $a = c = 0$ and $b = 1$.

Furthermore, $f'(x)$ should become small at large x and also should never have a negative value (implying a negative electron density) or a positive value greater than unity (implying an electron density in excess of N_{max}.) A polynomial of the form (7) would have to have a rather large number of terms in order to satisfy all the above requirements in the region of x that is of interest (perhaps $0 < x < 1000$ km.)

However, by reversing the functional relationship to

$$x = g(y) = A + By + Cy^2 + Dy^3 + Hy^4 + \cdots \tag{8}$$

all the restrictions can be met with relatively few terms. The same arguments used before lead to

$$A = C = 0 \quad \text{and} \quad B = 1$$

The general form of the desired polynomial is now

$$x = y + Dy^3 + Hy^4 \cdots \tag{9}$$

The normalized electron-density profile is obtained from

$$N/N_{max} = 1/(dx/dy)$$

Several different functions of the form (9) have been plotted in Figure 4. All these trial functions have been forced to pass near the average value of the equivalent column height (y) determined from the NW to SE, high passages.

The equations for these trial function are:

$$\text{Curve } A \quad x = y + (10^{-7})y^4$$

$$\text{Curve } B \quad x = y + (35 \times 10^{-6})y^3 \tag{10}$$

$$\text{Curve } C \quad x = y + (10^{-4})y^3 - (2 \times 10^{-7})y^4$$

The normalized electron-density profiles corresponding to these trial functions are shown in

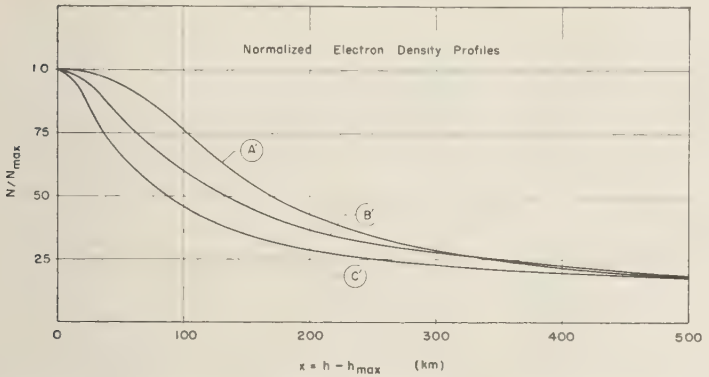

Fig. 5. Normalized electron-density profiles corresponding to the trial functions of Figure 4.

gure 5. For the best-fitting curve (B and B' Figs. 4 and 5) the electron density has deeased to about 50 per cent of its maximum alue 135 km above the height of h_{max}. It as also dropped to 20 per cent of N_{max} about 50 km above the height of the maximum denty.

These profiles may be compared with similar estimates made by several Russian workers. *Gringauz* [1958] has reported the results of a daytime rocket flight which gave electron-density profile up to a height of 475 km. *Al'pert, Dobriakova, Chudesenko, and Shapiro* [1958] have estimated the electron concentration of the upper ionosphere from observation of the time of 'radio rise and set' of Sputnik I. An entirely

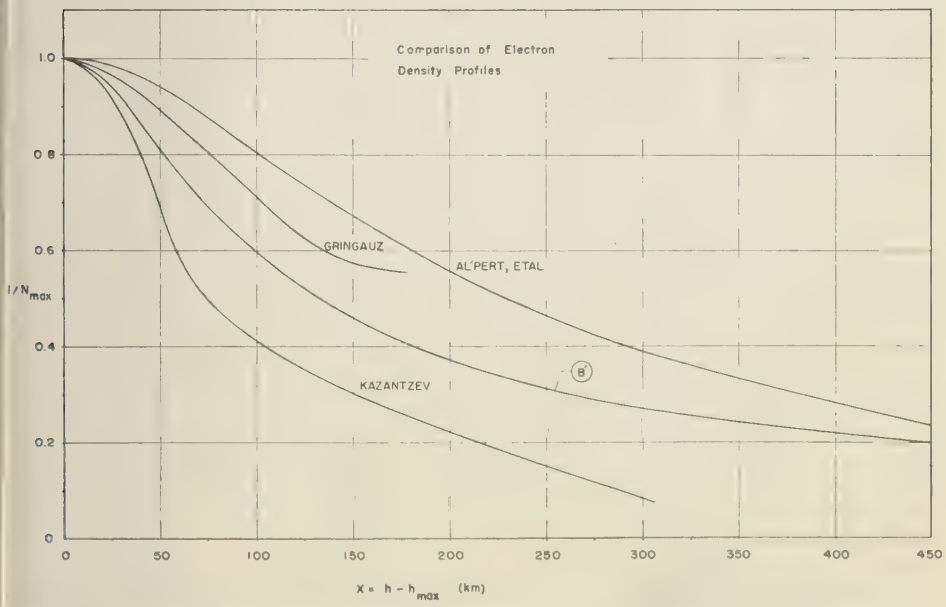

Fig. 6. Comparison of the electron-density profiles found by several authors. The profiles attributed to the Russian investigators have been scaled from their curves given in the references. It is hoped that this has not led to any appreciable inaccuracy.

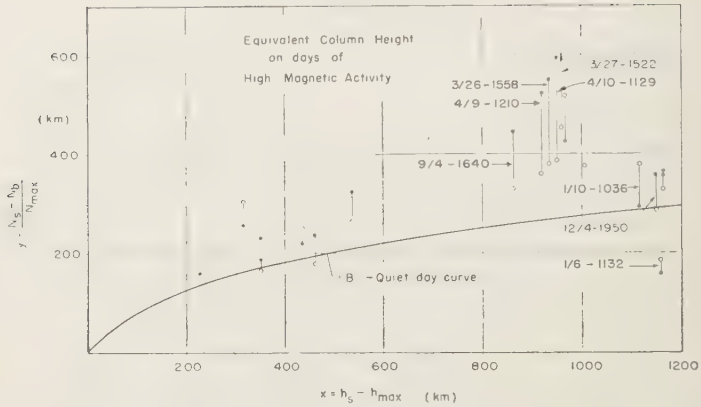

Fig. 7. Values of equivalent column height on days of high magnetic activity. The unusually large discrepancies between rotation-rate and rotation-angle observations suggest that significant horizontal ionospheric gradients may exist.

different technique was employed by *Kazantsev* [1959], who measured the received field strength of the first two Soviet satellites. By comparing the field strength as a function of range and satellite height, an estimate of the total ionospheric absorption was made. After subtraction of the amount of absorption believed due to the lower ionospheric layers, the remainder was related to the electron content above the height of maximum density. The various profiles, obtained in these very different manners, are shown in Figure 6.

As previously implied, the values of y on magnetically active days showed a marked departure from those on quiet days. Major magnetic storms in this 8-month period occurred on September 3–5, 1958, March 26–28, 1959, and April 9–10, 1959. In each case a large decrease in the F_2-layer critical frequency (or N_{max}) was found. For these larger storms a reduction to 25–40 per cent of the quiet-day N_{max} is frequently observed [*Maeda and Sato*, 1959]. Yet the calculated values of the total electron content N_t were near normal. This implies a severe distortion of the shape of the quiet-day electron-density profile. The values of y on magnetically active days, shown in Figure 7, can be compared with the solid curve which is a plot of the quiet-day curve (B in Fig. 4.).

The wide scatter of points appears to be related to the magnitude of the depression of N_{max}. All the active dates with large depressions in N_{max} show abnormally high values of equivalent column height y. On December 4, 1958, and January 6, 1959, both moderately active days, no depression in N_{max} occurred and the equivalent column height was equal to or less than that of the average quiet day. No attempt has been made to obtain an average active-day electron-density profile since the magnitude of the distortion of the quiet-day profile apparently varies widely. However, a reduction of N_{max} to even 50 per cent of the quiet-day value accompanied by the normal value of electron content requires that the electron density decrease very slowly for 300 to 400 km above h_{max}. A more rapid decrease in electron density would not provide an adequate electron content.

On the dates of all three of the major magnetic storms mentioned above, unusually large discrepancies are found between the rotation rate and rotation angle measurements. They may be due to relatively large horizontal gradients in the ionosphere with a larger electron content to the south than to the north.

Discussion. The comparison of the values of N_t obtained from the Faraday rotation-rate and rotation-angle observations indicates that both methods represent useful techniques in ionospheric investigation. It is essential, however, that a number of corrections to the simplified analysis be made.

The rotation-rate measurements become questionable at times when large horizontal iono-

spheric gradients are found to exist. The rotation-angle measurements are particularly sensitive to magnetoionic path splitting at the greater zenith angles and also are appreciably affected by the model of the magnetic field that is assumed. The computer program used in the rotation-angle calculations is currently under revision in order to include the effect of path splitting by computing the phase path length of each magnetoionic component separately. Such a program has been recently developed by *Lawrence and Little* [1959]. In both methods the night-time values are probably less accurate, on a percentage basis, than the daytime values, owing to the satellite-antenna motion. It was possible to correct for this motion by simultaneous 20- and 40-Mc/s observations on only a portion of the passages analyzed. Sometimes four measurements were made on a single passage in order to estimate the electron content up to the satellite height: rotation-rate and rotation-angle measurements at both 20 and 40 Mc/s. In most of these cases all values were within ± 10 per cent of the mean value, but a significant number showed larger deviations and the reasons for this need further investigation.

It seems reasonably certain that measurements of the local electron density (e.g., in the vicinity of the vehicle) will soon be available from satellite data as well as from rocket flights. The electron-density profile obtained in this work can then be checked. It should be remembered that the profile has been obtained only with the assumption that there is no seasonal or diurnal variation in the *shape* of the profile above the height of maximum electron density. The observations suggest that these were reasonable assumptions in the period considered, but additional confirmation would be desirable. If the shape of the electron-density profile for the upper part of the F layer is constant, the variations of the ratio (N_s/N_b) observed in Figure 7 must be attributed largely to diurnal variations in the profile of the lower ionosphere. Measurements of the total ionospheric electron content will continue to be useful, and it is expected that Faraday rotation observations will remain a valuable technique for this purpose although not necessarily in exactly the same manner employed here. Transmissions from a satellite in a near equatorial orbit with a period of 23 to 25 hours would be very desirable for these electron-content measurements. The changes in electron content could be observed continuously for periods of a week or longer over large portions of the globe with such a satellite.

Acknowledgments. As noted in part 1 of these papers, the advice of Professors O. G. Villard, Jr., A. M. Peterson, and R. N. Bracewell has been most helpful and is very much appreciated. In addition, Mr. D. M. Annett is responsible for much of the equipment installation and Messrs. S. C. Hall and O. Lie have accomplished a large portion of the data recording and analysis. Financial support has come from research grants by the National Science Foundation and the National Aeronautics and Space Administration.

References

Al'pert, Dobriakova, Chudesenko, and Shapiro, On the results of determining the electron concentration of the outer regions of the ionosphere by means of observations on the radio signals of the first satellite, *Doklady Akad. Nauk SSSR, 120* (4), 743–746, 1958.

Bauer, S. J., and F. B. Daniels, Ionospheric parameters deduced from the Faraday rotation of lunar radio reflections, *J. Geophys. Research, 63* (2), 439–442, 1958.

Bauer, S. J., and F. B. Daniels, Measurements of ionospheric electron content by the lunar radio technique, *J. Geophys. Research, 64* (10) 1371, 1959.

Burkard, O., Studien zum neuen Modell der Ionosphare: I, *Geofis. pura e appl., 41* (III), 133–140, 1958.

Evans, J. V., The electron content of the ionosphere, *J. Atmospheric and Terrest. Phys., 11* (3 and 4), 259–271, 1957.

Gringauz, K. I., Rocket measurements of the electron concentration in the ionosphere using an ultra-shortwave dispersion interferometer, *Doklady Akad. Nauk SSSR, 1206,* 1234–1237, 1958.

Kazantsev, A. N., Absorption and electron distribution in the F_2 layer determined from measurements of the transmitted radio signals from earth satellites, *J. Planetary and Space Sci., 1* (2), 130–135, 1959.

Lawrence, R. S., and C. G. Little, On the analysis of polarization rotation recordings of satellite radio signals, Paper presented at URSI-IRE meeting in San Diego, California, October 21, 1959.

Maeda, K. I., and T. Sato, The F region during magnetic storms, *Proc. IRE, 47* (2), 232–239, 1959.

(Manuscript received January 8, 1960.)

Vertical Transport of Electrons in the F Region of the Ionosphere[1]

SUSHIL CHANDRA, J. J. GIBBONS, AND E. R. SCHMERLING

Ionosphere Research Laboratory
Pennsylvania State University
University Park, Pennsylvania

Abstract. From the equation of continuity for free electrons, an expression is developed for the vertical transport velocity which can be evaluated, subject to some limitations, from electron-density-height profiles. A few numerical computations of the vertical drift velocities determined for the four IGY stations Huancayo and Talara, Peru; Panama, Canal Zone; and Washington, D. C., are presented. It is shown that the velocity is predominantly downward during the night and upward during the day at the equatorial stations. There is an apparent phase reversal from summer to winter at Washington. The order of magnitude of the vertical-velocity amplitude is 25 m/sec. There is substantial agreement between the values calculated here from ionospheric data and those deduced from S_q data on the dynamo theory.

Introduction. It has been known for more an 20 years that the behavior of the F_2 layer quite different from that of the other layers the ionosphere. The *Chapman* [1931] theory, spite of its simplicity, was remarkably suc-ssful in explaining the main features of the E ad F_1 layers. It cannot, however, account for ven the major features of the F_2 layer. *Martyn* 1947] suggested that it might be possible to ccount for some of the peculiar characteristics this layer in terms of the vertical transport of ectrons occasioned by the electrodynamic rces and 'winds' associated with the iono-heric current system. The existence of the nospheric current system is manifested by the aily variation of the magnetic field of the arth. Its origin and its effect on vertical trans-ort have been discussed in detail by *Martyn* 1953], *K. Maeda* [1955], *H. Maeda* [1955], *Hirono* [1955], and *Hirono and Maeda* [1955]. At present, however, our knowledge of the ertical transport of electrons from either the-ry or experiment is much too limited to permit formulation of an acceptable theory of the F_2 layer. We shall, therefore, attempt in this aper to develop a method which allows the ertical transport to be deduced from experimental data with a minimum of theoretical assumptions.

We shall make no distinction between the F_1 and F_2 layers, both of which we shall denote by 'region F,' since, by the theory of *Bradbury* [1938], both layers are considered to arise from the same mechanism of electron production. Experimental evidence for this view has been presented by *Ratcliffe, Schmerling, Setty, and Thomas* [1956]. We shall refer to this paper later as *RSST*.

It is further assumed that the factors controlling region F are mainly electron production and electron loss, with the vertical transport of electrons acting as a perturbation. The detailed behavior of the electron density as a function of time at various heights is then used to deduce information about the vertical transport. In this report a method is presented for determining the velocity of vertical transport, and some specific results are discussed.

Solution of the continuity equation. The continuity equation for the electron density may be written as follows:

$$\partial N/\partial t = Q - L - D - \text{div}\,(Nv) \qquad (1)$$

where Q is the production function, L the loss function, D the diffusion under gravity, N the electron density, and div (Nv) contains the terms

$$\frac{\partial}{\partial x}(Nv_x),\ \frac{\partial}{\partial y}(Nv_y),\ \frac{\partial}{\partial z}(Nv_z)$$

[1] The research reported in this paper has been sponsored by the U. S. National Committee for the IGY under Project 6.9, and the preparation of the report, in part, by the Geophysics Research Directorate of the Air Force Cambridge Research Center, Air Research and Development Command, under Contract AF19(604)-3875.

From an examination of electron-density–height or N-h profiles from different stations we conclude that the mean horizontal gradients $\partial N/\partial x$ and $\partial N/\partial y$ are negligible in comparison with the vertical gradient $\partial N/\partial z$. This enables us to neglect the terms containing horizontal-velocity components. Under these circumstances, integration of equation 1 leads to the following expression for the vertical velocity amplitude v at any height h:

$$v = (N_0 v_0/N) - (I_0^h/N) \qquad (2)$$

where

$$I_0^h = \int_{h_0}^{h} \left(\frac{\partial N}{\partial t} + L + D - Q\right) dz$$

N_0 and N are electron densities at heights h_0 and h, respectively; v_0 and v are the corresponding vertical velocities. The above expression shows that, even if the production, loss, and diffusion terms are known for different heights, the velocity v can be calculated only in terms of the velocity at an arbitrary lower height. Once the velocity at any height is known, it can be computed for all heights. It is not possible to calculate the absolute velocities from the electron-density data above unless some assumption is made about the velocity profiles. This amounts to determining the constant of integration v_0 in equation 2. We shall return to this point later. In the following we shall consider the production, loss, and diffusion terms separately.

Production and loss mechanisms. It is assumed that electrons are produced by the absorption of solar ionizing radiation, and their rate of production, Q, is given by the formula of *Chapman* [1931]:

$$Q = Q_0 \exp(1 - z - e^{-z} \sec \chi) \qquad (3)$$

where Q_0 is the maximum rate of electron production for a vertically overhead sun ($\chi = 0$) and z is the reduced height given by $z = (h - h_0)/H$, where h_0 is the level of maximum production when $\chi = 0$ and H is the scale height.

The following values of Q_0, h_0, and H for F-region heights have been adopted as obtained by Grant and Schmerling (private communication, 1957):

$Q_0 = 600$ electrons/cc sec

$h_0 = 180$ km

$H = 40$ km

These values are consistent with those found in *RSST*.

According to *RSST*, the loss of electrons above 250 km is proportional to N, with coefficient β. It has been shown by *Schmerling* [1955] that the coefficient β above 250 km very nearly satisfies the equation

$$\beta(h) = 2.2 \times 10^{-5} + 0.25e^{-h/37} \qquad (4)$$

This is in close agreement with the formula

$$\beta(h) = 10^{-4} \exp[(300 - h)/50]$$

given by *RSST* for heights between 250 and 350 km. Below 250 km the loss is of the recombination type with coefficient α and is proportional to αN^2.

The effective $\beta = (\alpha N)$ for the height range 160 to 260 km is calculated as follows. Taking the value of $\alpha = 4{\cdot}10^{-9}$/sec at 160 km, as given by *Bates and Massey* [1946], we start with different values of αN at 160 km and draw smooth monotonic curves to join them with the curve starting from 260 km as given by equation 4. To calculate the effective β at any height we note the value of N at 160 km and follow the corresponding curve. This is illustrated in Figure 1.

Effect of diffusion. *Ferraro* [1946] has shown that the expression for diffusion $D(h)$ may be written in the form

$$D(h) = -\frac{b}{n} \sin^2 I \left(\frac{d^2N}{dh^2} + \frac{3}{2H}\frac{dN}{dh} + \frac{N}{2H^2}\right) \qquad (5)$$

where $b = 10^{19}$/cm sec is a constant derived from the theory of diffusion and

n = molecule density at height h.
H = scale height.
N = electron density.
I = magnetic dip angle.
h = height.

This expression can be evaluated if the molecular height distribution is known.

In view of the uncertainties existing in the various parameters, it was decided to avoid the introduction of additional uncertainties due to

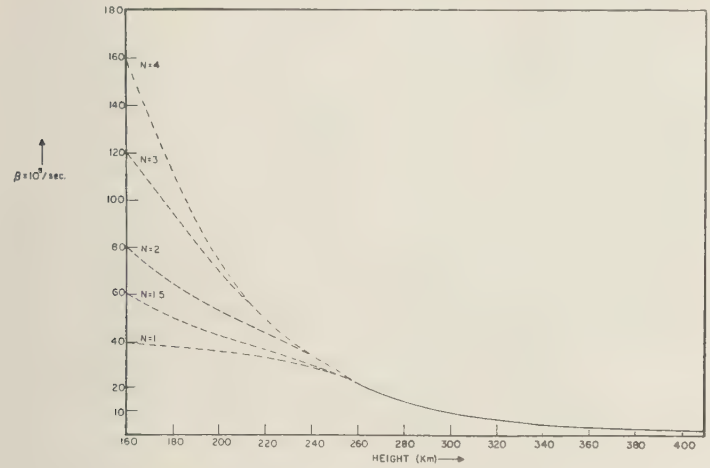

Fig. 1. Height variation of loss coefficient. N = electrons/cc $\times$ 10^{-5}.

ffusion parameters. Our values of v, therefore, clude the velocity due to tidal and electrodynamic forces as well as diffusion. We shall fer to this as the vertical-transport velocity. he diffusive effect can, obviously, be separated asily, if desired. The stations Huancayo, Tara, and Panama are close to the magnetic quator, so that the diffusion term is very small n view of the factor $\sin^2 I$ in equation 5. The ame is not true, of course, for Washington,). C.

Numerical evaluation of vertical-transport elocities. The formula for v, previously deuced, may be rewritten as

$$= \frac{N_0 v_0}{N} - \frac{1}{N}\int_{h_0}^{h}\left(\frac{\partial N}{\partial t} + \beta N - Q\right) dz \quad (6)$$

As was pointed out before, a unique solution an be found only if (1) the velocity v is known t some height h_0 or (2) the form of the velocty-height variation is known. It will be shown ater that the simple assumptions of constant elocity or constant velocity gradient do not, in general, lead to self-consistent solutions.

A family of solutions of equation 6 may be btained by starting with a set of arbitrary values of v_0. Each of the resulting curves represents a valid, self-consistent solution, subject only to the physical limitation that the resulting velocities must have reasonable values. Apart from this, in the absence of any other information, there can be no reason for preferring any one curve of the family over the others.

It might be thought that a good approximation could be obtained by assuming a set of constant-velocity segments over small height ranges, thus approximating the true velocity-height curve. On such an assumption, the constant of integration is apparently evaluated automatically. If this is done, however, the solution picks out the most nearly constant segments of the family of possible solutions, jumping from one curve to another. The resulting velocity-height curve is then not, in general, a valid solution of equation 6 for the entire height range. The same situation, of course, applies on the assumption of constant velocity gradient over small height ranges.

We have here chosen the starting values, v_0, bounded by ± 20 m/sec. The corresponding curves converge with increasing height. At greater heights the uncertainty of 40 m/sec which exists at the start is reduced to a much smaller value, of the order of 10 m/sec, or even less. It may be pointed out that our limits on v_0 of ± 20 m/sec are based on the fact that the magnitude of the vertical-transport velocity, estimated so far by various authors [*H. Maeda*, 1955; *K. Maeda*, 1955; and *Martyn*, 1959], is of the order of ± 15 m/sec. During the day we are able to extend our analysis down to 180 km.

The variation of electron density at this height and below is approximately Chapman-like. During the night, the lower height to which we can extend our analysis ranges from 240 to 300 km. Even for this height range the limits of ±20 m/sec seem to be reasonable.

A few computations have been carried out using models of Q and β as described above and electron-density–height profiles obtained under IGY project 6.9 [*Schmerling*, 1958, 1959].

Figures 2 to 9 show velocity profiles every hour at Talara for typical magnetically quiet summer and winter days. These curves are drawn for $v_0 = 20, 10, 0, -10$, and -20 m/sec. Figures 10 to 15 show velocity profiles for Huancayo, Panama, and Washington, D. C., at a few selected hours on the same days. These curves are drawn for $v_0 = 20, 0$, and -20 m/sec. From Figures 2 to 15 it can be seen that the profiles converge with increasing height, thus reducing the uncertainty there to lower values. It is also apparent that the velocity profiles are not, in general, linear; and it is easily seen how attempts to fit the profiles by linear sections often result in jumping from one solution to another.

Figures 16 and 17 show the diurnal variations for the four stations Huancayo, Talara, Panama, and Washington, D. C., for typical quiet summer and winter days, respectively. The limits of uncertainty are given by the upper and lower curves, which correspond, respectively, to $v_0 = +20$ and -20 m/sec. It is to be noted that, even with this uncertainty in v_0, except for Washington, D. C., in December, the velocities are predominantly positive (upward) during the day and predominantly negative (downward) during the night. The velocities for every station show a dip at sunrise. This may be partly due to the fact that the values of Q are not calculated accurately at sunrise and sunset, since we have not made corrections for curvature of the earth.

Effects on the drift profiles due to changing Q_0. In the previous section we have developed a method for deducing the velocity profiles. It is clear that these depend on the values chosen for β and Q_0. We have used our best estimates of these parameters to evaluate a number of velocity profiles. Since our estimates of Q_0 and β are subject to some uncertainty, we shall now examine the effects of making rather drasti changes in these parameters.

In Figure 18 we illustrate the effect of chang ing Q_0 by a factor of 2. Profiles are drawn fo $Q_0 = 300$, 600, and 1200 electrons/cc sec, th other parameters remaining unchanged. Figure 19 and 20 are the diurnal plots of the vertica velocity at fixed heights calculated from th same models. It is seen that, except for Wash ington, D. C., in winter, the profiles corre sponding to $Q_0 = 1200$ electrons/cc sec hav very large gradients between 180 and 240 km This result does not appear to be physicall reasonable. The maximum daytime velocitie are between 60 and 80 m/sec as compared wit the night-time values ($Q_0 = 0$), which rang between -8 and -10 m/sec. It can safely b concluded that, for the β model adopted in thi computation, $Q_0 = 1200$/cc sec is too high value for Talara in summer and winter, and fo Washington, D. C., in summer.

The profiles corresponding to $Q_0 = 300$/cc se seem to be very well behaved, but they kee the velocity negative throughout the day. It i hard to imagine any physical process that woul cause a downward transport over 24 hour particularly near the magnetic equator, wher the diffusion term is hindered by the term sin I in equation 5. The velocity curves correspond ing to $Q_0 = 600$ give the daytime maximu velocity between 10 and 30 m/sec. Though th upper limit is a little high, the order of magni tude is not unreasonable. From the foregoin considerations, we are inclined to think tha with the values of β given in Figure 1, the valu of Q_0 between 500 and 600 electrons/cc sec i very reasonable for equatorial stations and fo stations in middle latitudes during summer.

It is difficult to draw any definite conclusion from the Washington, D. C., winter records. I seems that during the night there is a sligh upward tendency for the drift velocity. It woul not be unreasonable to assume $Q_0 = 600$/cc se even in this case, which keeps the velocit reasonably negative throughout the day excep at sunrise where the value is of the order o -40 m/sec. This is not easily accounted fo unless some special mechanism of electron re lease is postulated for sunrise.

It is interesting to note that a negative ve locity of -10 m/sec can cause the noon electro

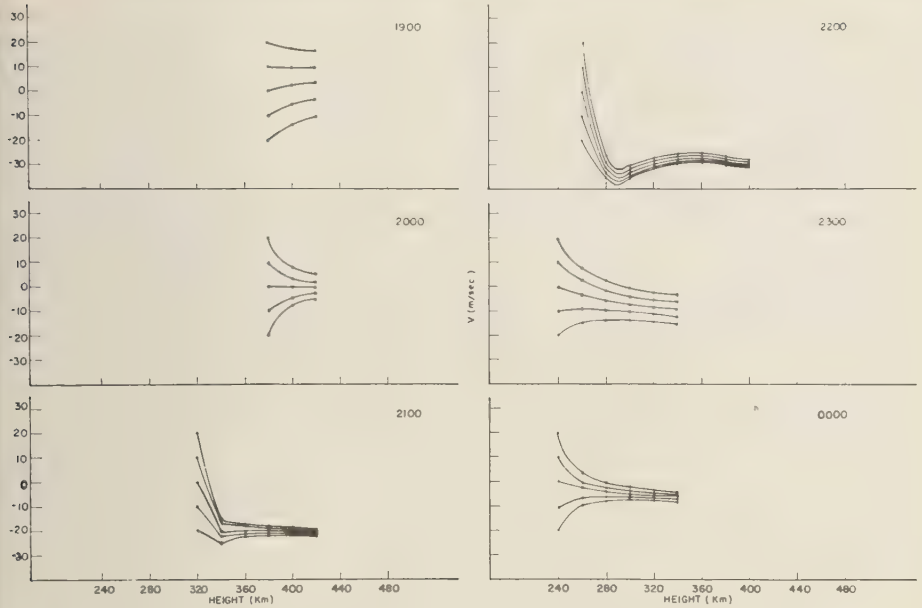

Fig. 2. Velocity profiles, Talara, July 27, 28, 1957.

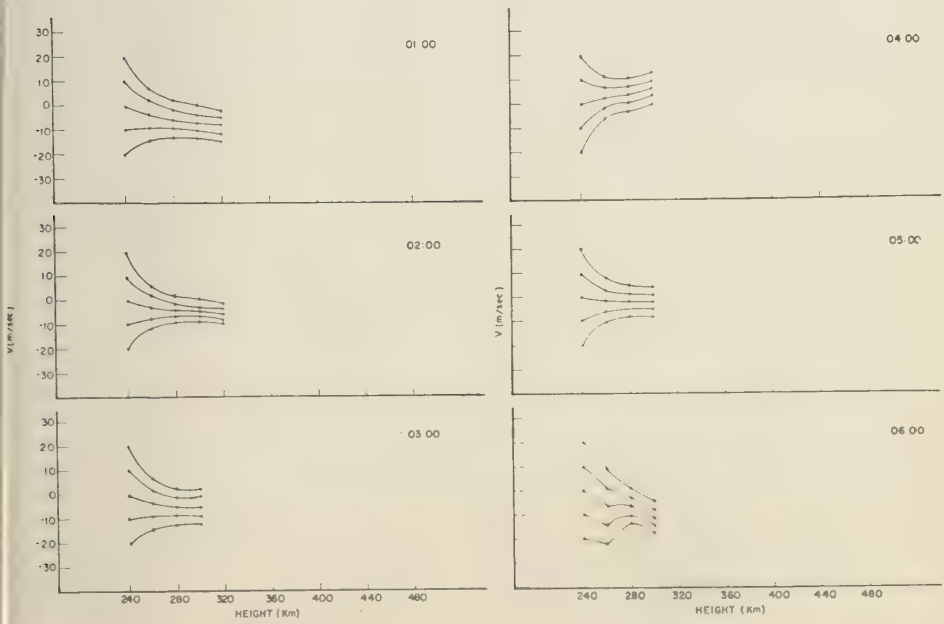

Fig. 3. Velocity profiles, Talara, July 28, 1957.

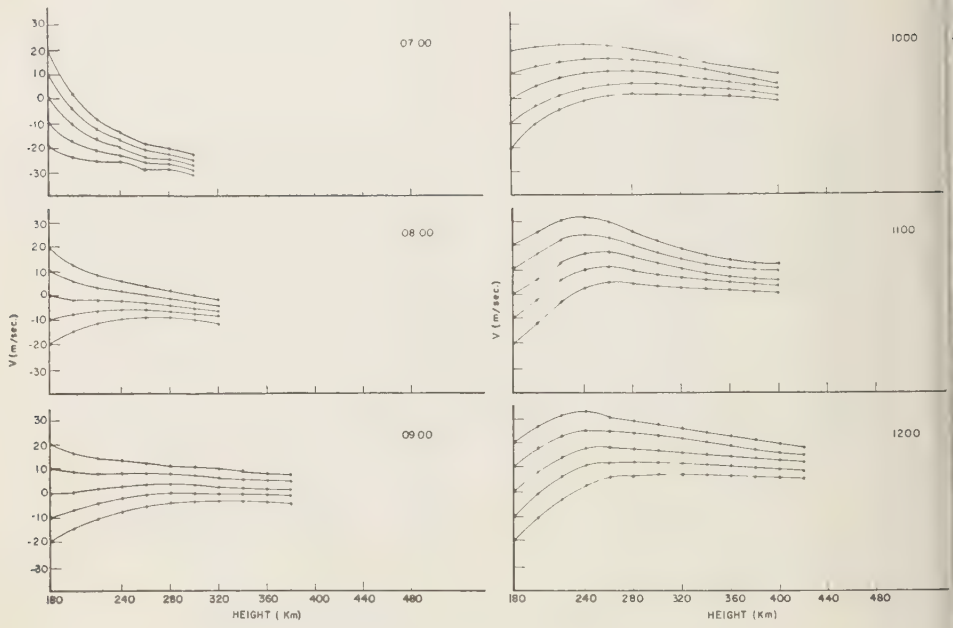

Fig. 4. Velocity profiles, Talara, July 28, 1957.

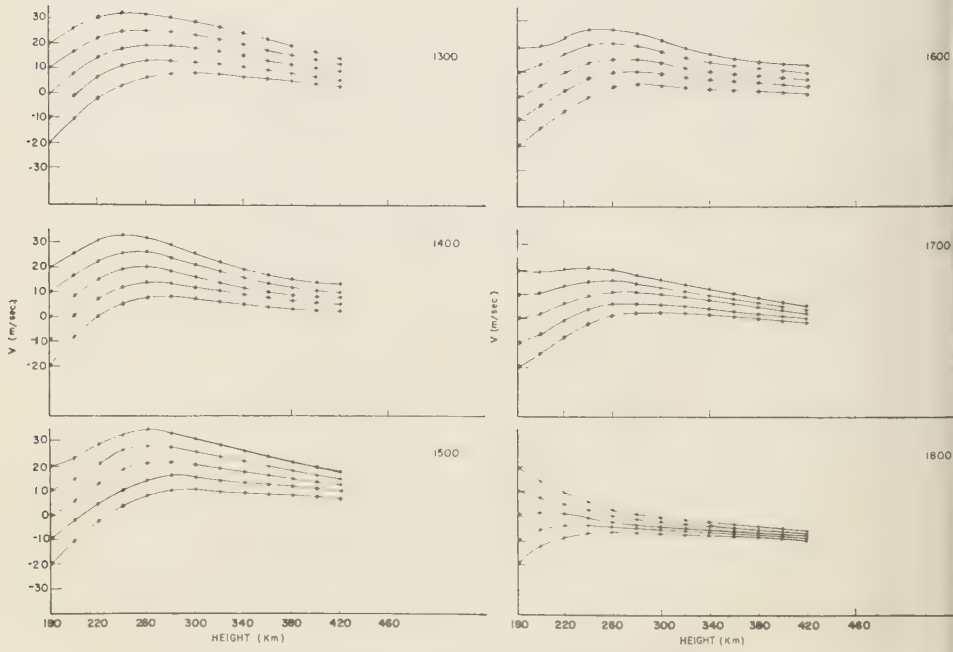

Fig. 5. Velocity profiles, Talara, July 28, 1957.

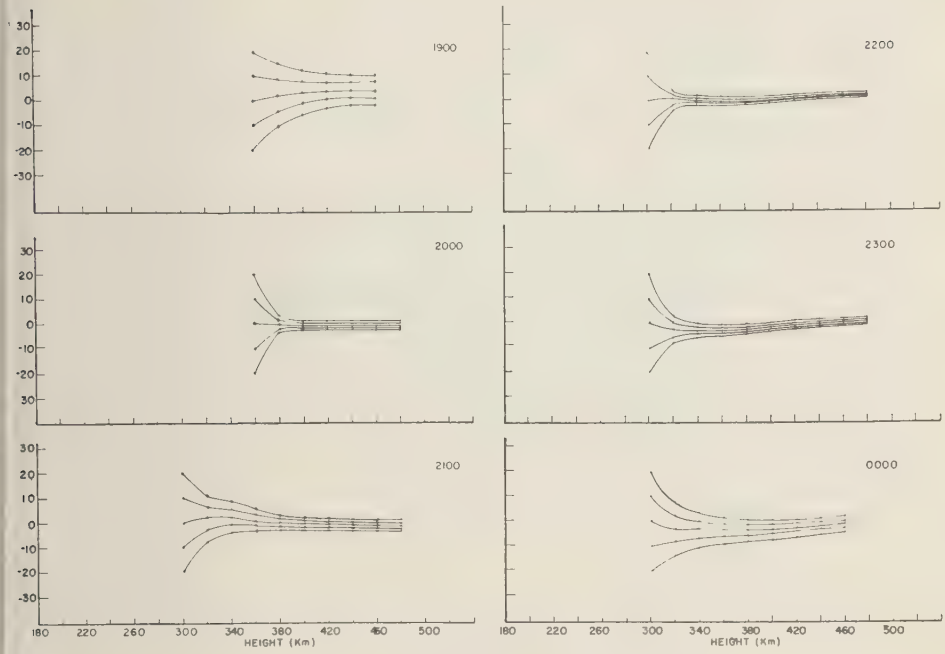

Fig. 6. Velocity profiles, Talara, December 22, 23, 1957.

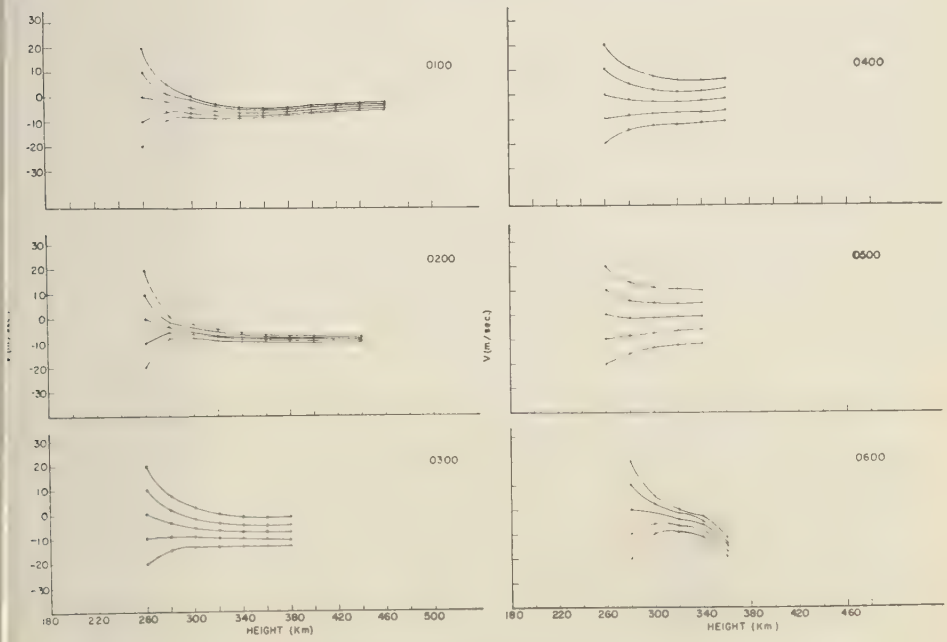

Fig. 7. Velocity profiles, Talara, December 23, 1957.

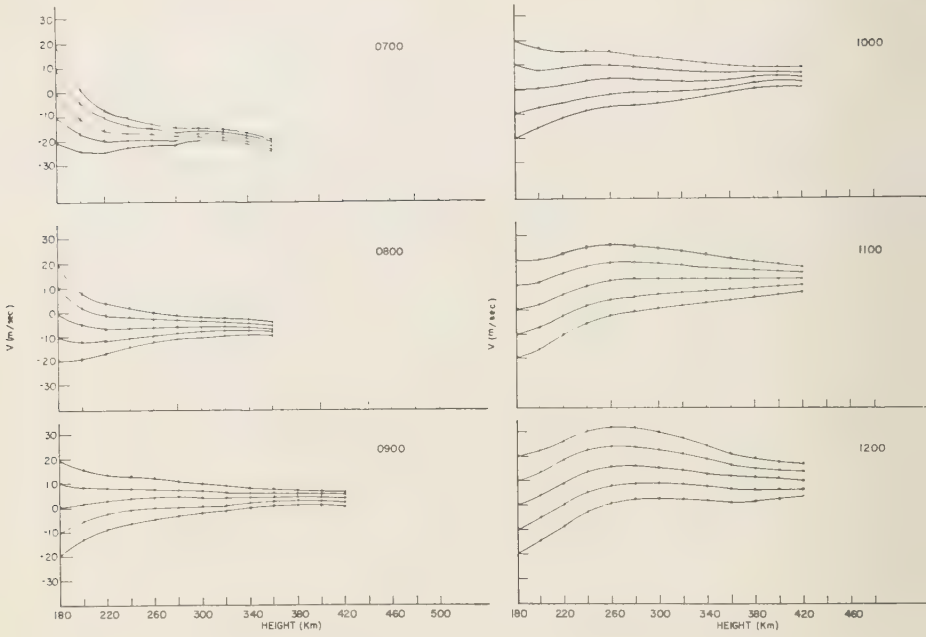

Fig 8. Velocity profiles, Talara, December 23, 1957.

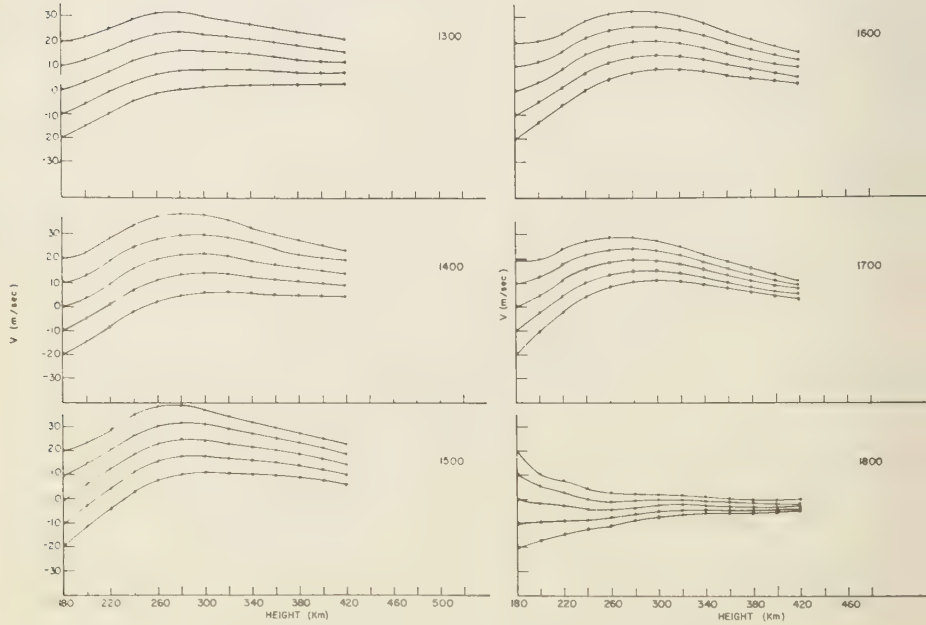

Fig. 9. Velocity profiles, Talara, December 23, 1957.

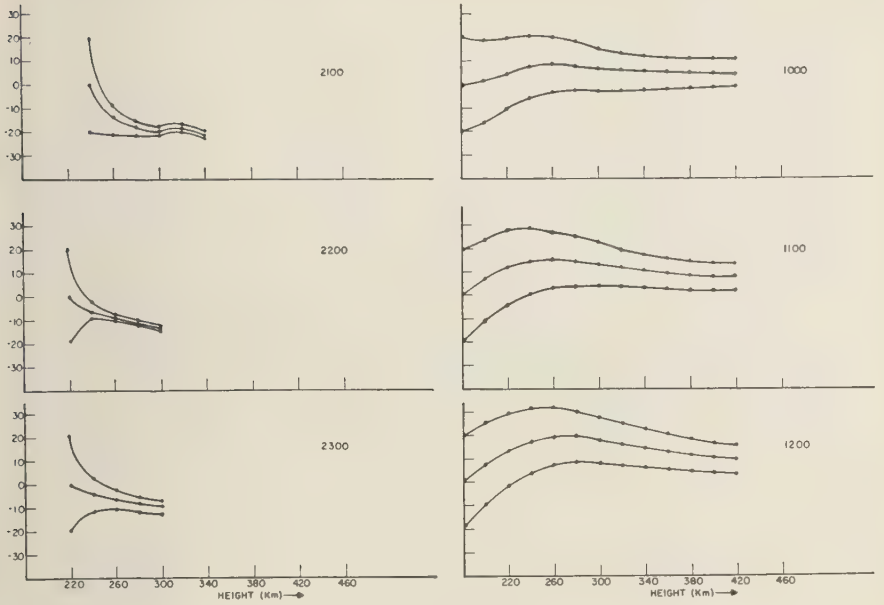

Fig. 10. Velocity profiles, Huancayo, July 27, 28, 1957.

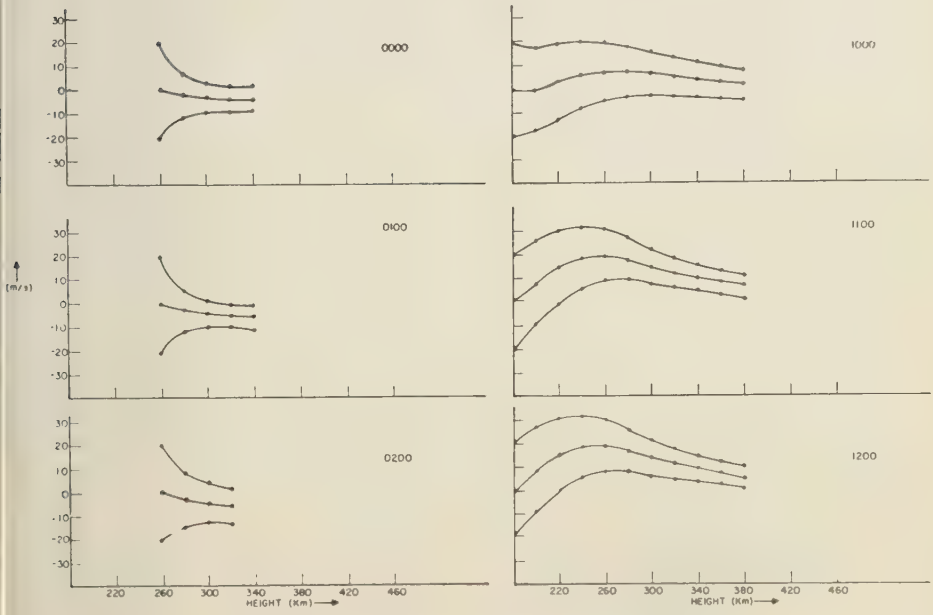

Fig. 11. Velocity profiles, Panama, July 27, 28, 1957.

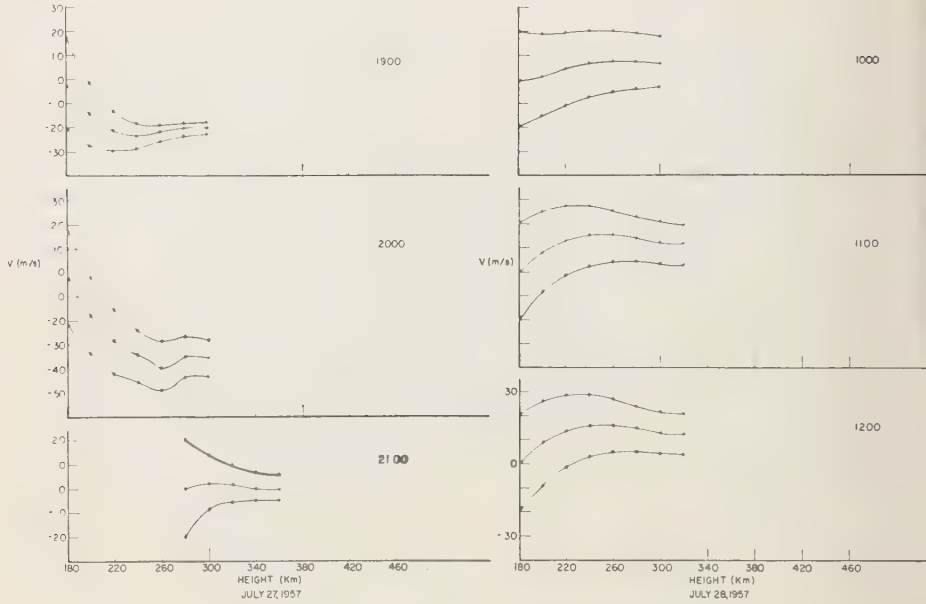

Fig. 12. Velocity profiles, Washington, D. C.

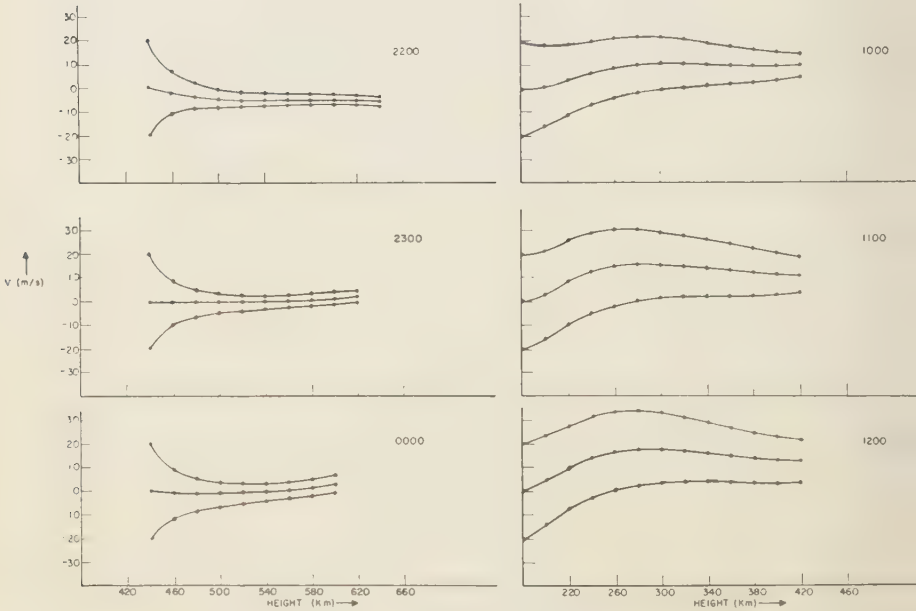

Fig. 13. Velocity profiles, Huancayo, December 22, 23, 1957.

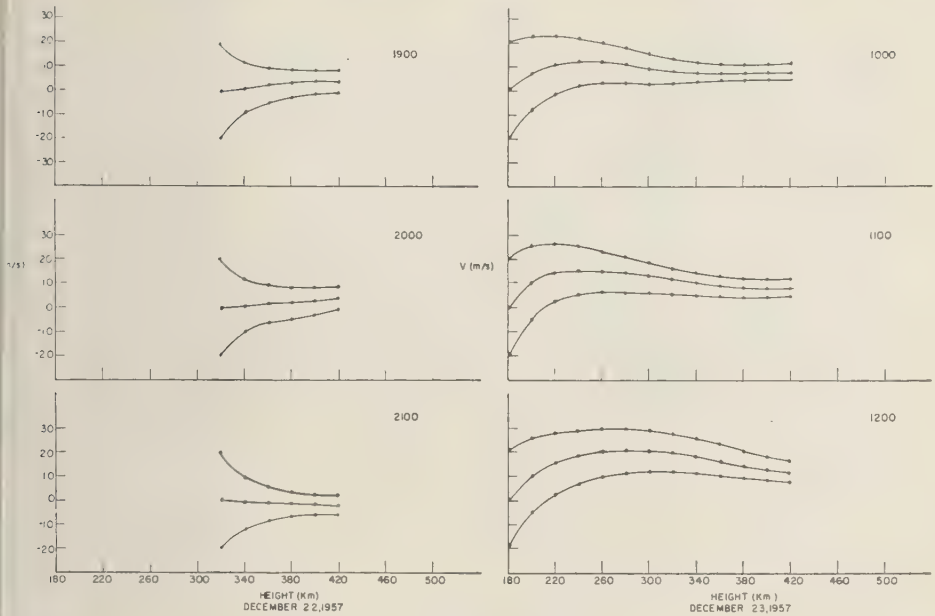

Fig. 14. Velocity profiles, Panama.

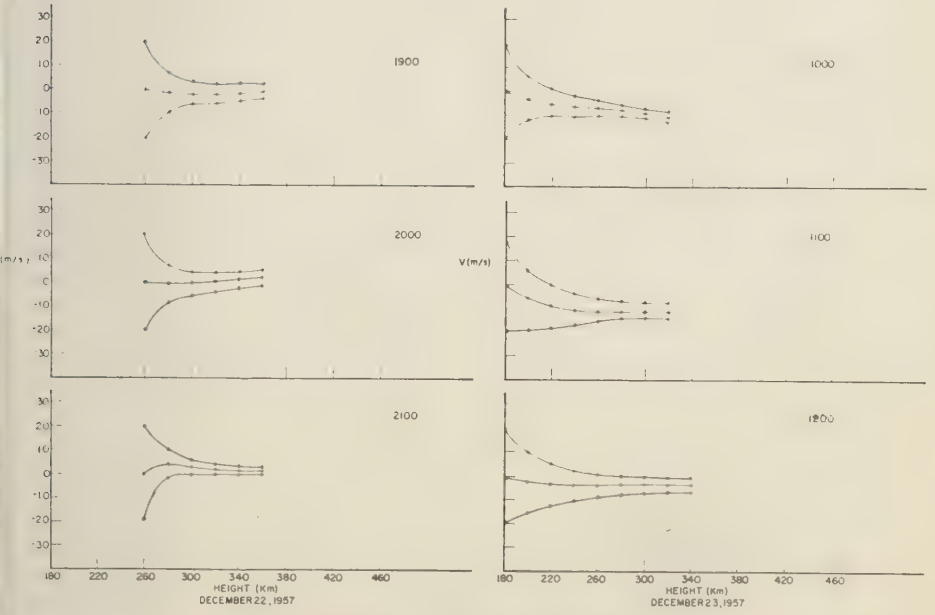

Fig. 15. Velocity profiles, Washington, D. C.

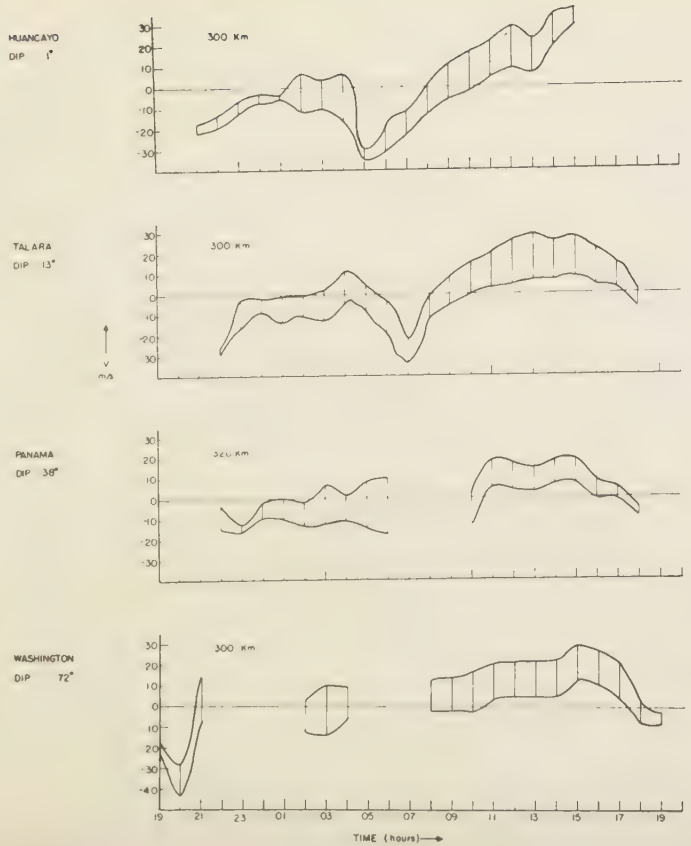

Fig. 16. Vertical transport velocities, July 27, 28, 1957.

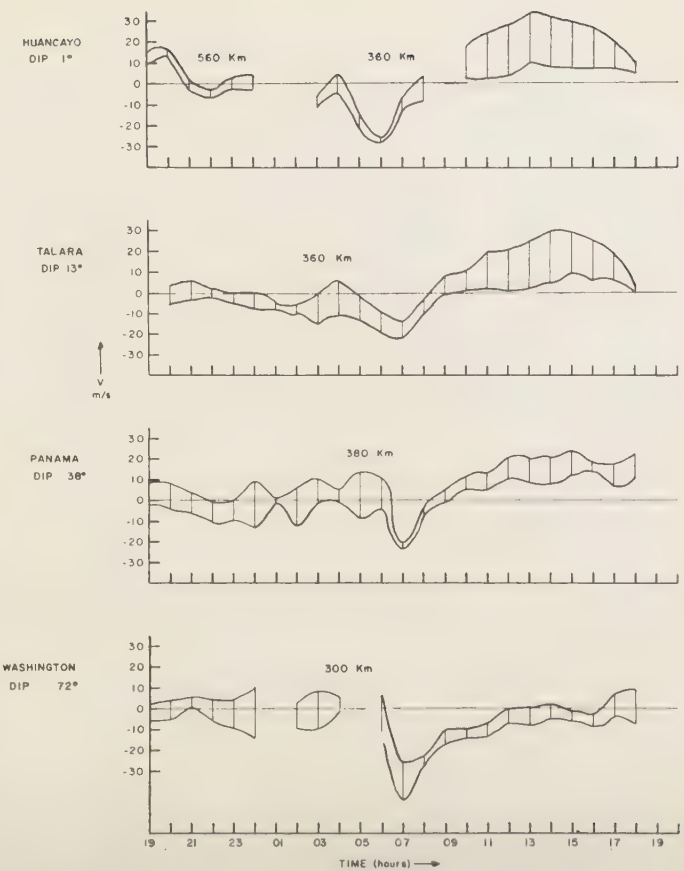

Fig. 17. Vertical transport velocities, December 22, 23, 1957.

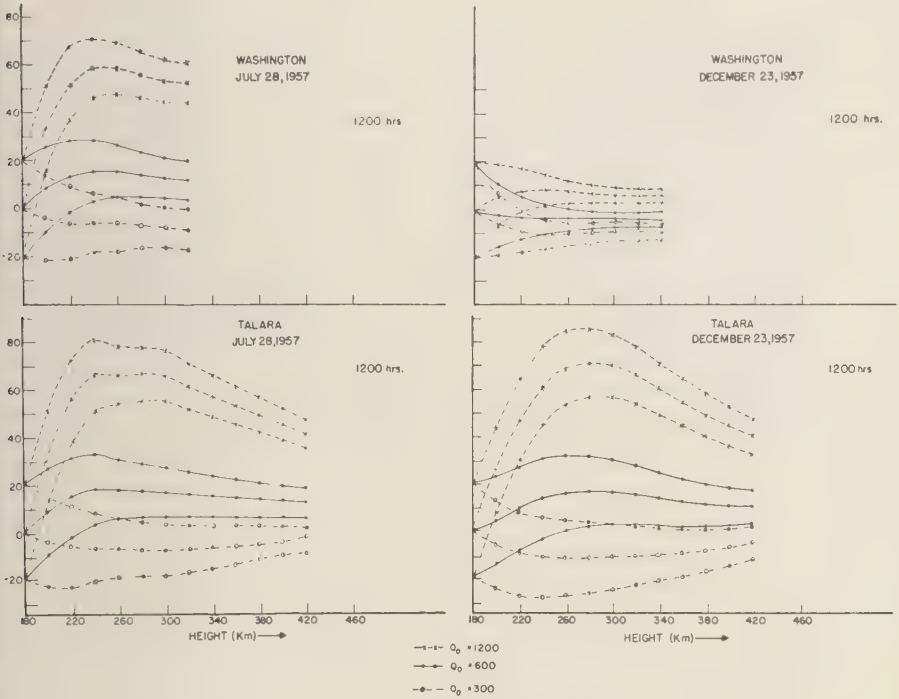

Fig. 18. Velocity profiles for different values of Q_0.

lsity to be greater by a factor of 3 as com-ed with summer values, and can thus ac-nt for the so-called summer and winter omaly. This conclusion is purely tentative l should be examined in greater detail. It is y desirable to obtain data on total electron tent from satellite measurements, or any er source, in order to establish that no real omaly exists in the production processes, and t the observed increase of electron density ow the height of the maximum is caused irely by downward drift.

Effects of changing β. Figures 21 and 22 strate the change of computed drift with nges of β, other parameters being kept con-nt. The parameters for the production term the same as above, and calculations are de for the values of β as given in Figure 1 l then multiplied by a factor of 0.1. It is parent from an examination of these curves t a decrease of β by a factor of 10 does not se any appreciable change in the nighttime velocities. The effect of a decreased β during the night is equivalent to increasing the velocity by about 3 m/sec in the positive direction. This is quite understandable for the equatorial stations where the increase and decrease of electron density during the night hours are so great that it is almost safe to conclude that the distribution of electron density is entirely controlled by movements and not by loss. For Washington, D. C., the situation is not so clear-cut.

The effect of β is very significant on the daytime velocity. A decrease of β by factor 10 raises the maximum velocity to about 35 to 60 m/sec. In order to keep the velocity at a reasonable positive value, Q_0 should be assumed to be of the order of 300 electrons/cc sec. This is illustrated in Figure 23.

It is thus evident that we cannot place limits on Q_0 and β simultaneously, but if one of them is reasonably certain, it is not difficult to estimate the other.

Estimation of vertical-drift velocities from

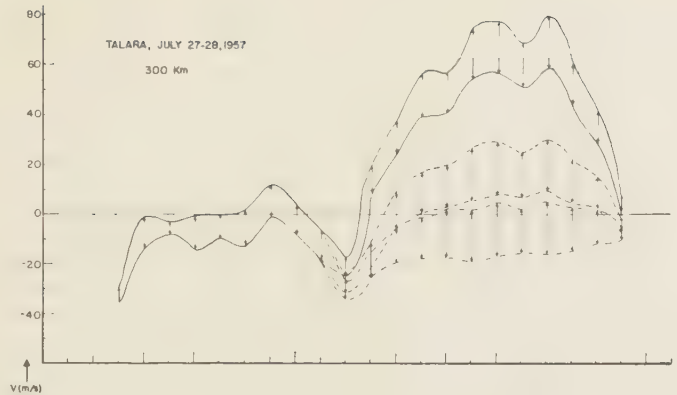

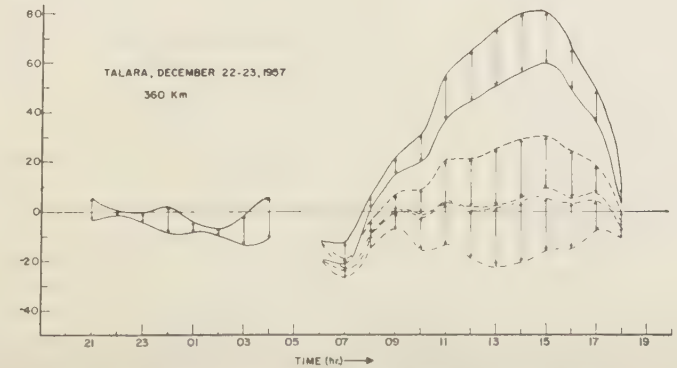

Fig. 19. Vertical drift velocities for different values of Q_0.

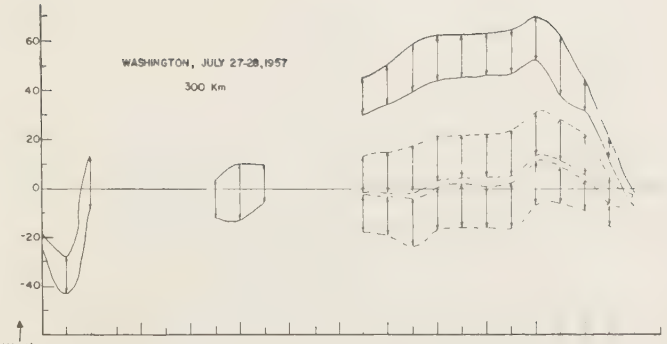

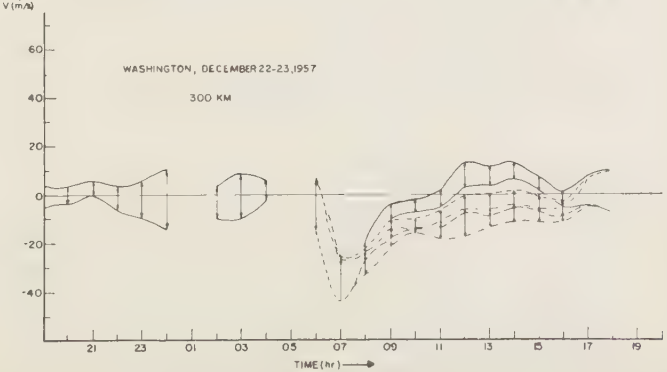

Fig. 20. Vertical drift velocities for different values of Q_0. Solid curves, $Q_0 = 1200$ electrons/cc sec; dash line, $Q_0 = 600$ electrons/cc sec; dot-and-dash line, $Q_0 = 300$ electrons/cc sec.

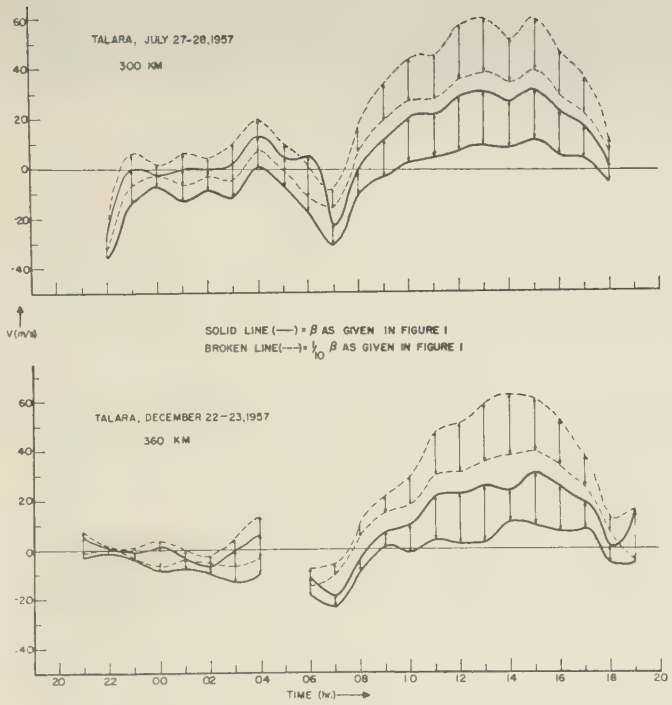

Fig. 21. Vertical drift velocities for different values of loss coefficient.

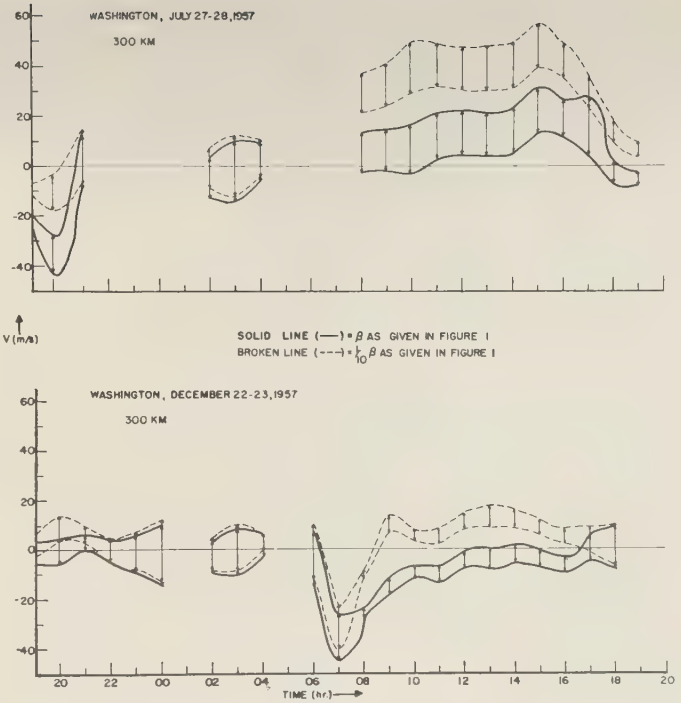

Fig. 22. Vertical drift velocities for different values of loss coefficient.

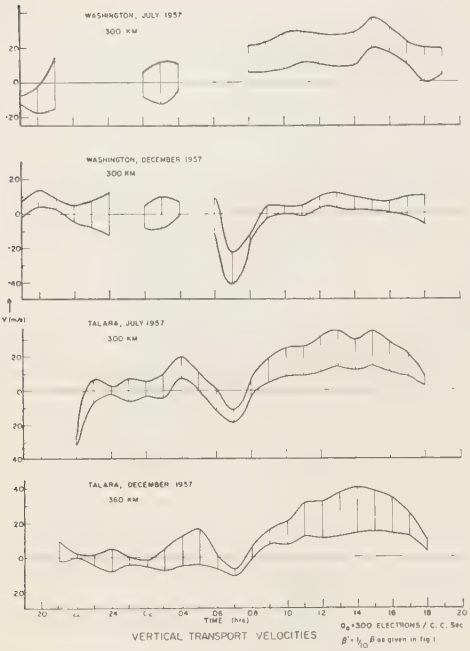

Fig. 23. Vertical transport velocities. $Q_0 = 300$ electrons/cc sec. $\beta' = 0.1\beta$ as given in Figure 1.

the S_q current. It is instructive to compare our results with those obtained by *H. Maeda* [1955], who calculated the vertical drift from S_q data based on an analysis of geomagnetic fluctuations; see Figure 24. In view of the fact that his calculations are based on many simplifying assumptions and correspond to a 'mean' wind, the comparison cannot be very close. Nevertheless, there is reasonable agreement between our results and his, both in phase and in magnitude.

For middle-latitude stations, Maeda obtains negative velocities during the day and positive velocities during the night, which approximately corresponds to our Washington, D. C., winter results. These very encouraging preliminary results suggest that further work be done on the analysis of S_q data with the minimum of assumptions.

Conclusions. 1. Integration of the continuity equation leads to an expression for vertical-drift velocity which remains indeterminate by a constant of integration even when full data on electron-density distribution, electron pr duction, and electron loss are available.

2. An effort to evaluate this constant of i tegration by assuming zero or contant gradie within small height intervals does not, in ge eral, lead to self-consistent solutions.

3. By assuming reasonable values of v_0, whi we have considered as ± 20 m/sec, velocit height profiles can be computed. They conver with increasing height. This feature enables to estimate the velocity with less uncertainty greater heights.

4. A diurnal plot of velocity, even with t unavoidable residual uncertainty, shows a pr dominantly downward velocity during the nig and a predominantly upward velocity duri the day, both in summer and in winter, at the stations except Washington, D. C., where t velocities are negative in winter during the da

5. The effects of changes of Q_0 and β on t

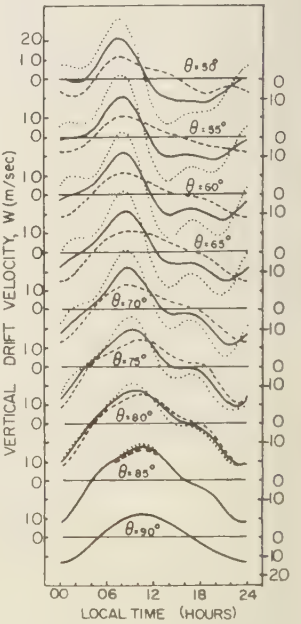

Fig. 24. Daily variations of the vertical dr velocity of electrons in the ionospheric F regi for each of the following three cases: (1) no ti oscillation exists in the F region (solid lines); (the same tidal oscillation exists in the F region in the E region (dotted lines); (3) the tidal os lation in the F region is the opposite of that in t E region (dashed lines). (By H. *Maeda*, 1955.)

city profiles and diurnal plots are consid-
, and it is concluded that it is not possible
place definite limits on both parameters
ultaneously. But if one of them is known,
other can be estimated within reasonable
ts.

It is suggested that the increase of winter-
electron densities at middle-latitude stations
a factor of 3 as compared with the summer-
values may be due to a phase reversal of
city from summer to winter.

. The vertical-transport velocities calculated
n the S_q data by Maeda are compared with
s. In view of the limitations of the calcula-
ns, there is quite good agreement between the
results, which gives added support to the
amo theory.

References

es, D. R., and H. S. W. Massey, *Proc. Roy. Soc. London, A, 187,* 261, 1946.

dbury, N. E., *Terrestrial Magnetism and Atmospheric Elec., 43,* 55, 1938.

Chapman, S., *Proc. Roy. Soc. London, 43,* 26, 1931.

Ferraro, V. C. A., *Terrestrial Magnetism and Atmospheric Elec., 50,* 215, 1946.

Hirono, M., *Rept. Ionosphere Research Japan, 9,* 95, 1955.

Hirono, M., and M. Maeda, *Rept. Ionosphere Research Japan, 9,* 86, 1955.

Maeda, H., *J. Geomagnetism and Geoelec., 6,* 121, 1955.

Maeda, K., *Rept. Ionosphere Research Japan, 9,* 69, 1955.

Martyn, D. F., *Proc. Roy. Soc. London, 189,* 241, 1947.

Martyn, D. F., *Phil. Trans. Roy. Soc. London, A, 246,* 306, 1953.

Martyn, D. F., *Proc. IRE, 47,* 2, 129, 1959.

Ratcliffe, J. A., E. R. Schmerling, C. S. G. K. Setty and T. O. Thomas, *Phil. Trans. Roy. Soc. London, 248,* 621, 1956.

Schmerling, E. R., Ph.D. Thesis, Cambridge University 1955.

Schmerling, E. R., *Penn. State Univ. Ionosphere Research Lab. Sci. Repts. 105* and *118,* 1958 and 1959, and IGY time-height tables.

(Manuscript received December 23, 1959; revised January 25, 1960.)

ionospheric Absorption Investigations at Hawaii and Johnston Island

A. FREDRIKSEN AND R. B. DYCE

Communication and Propagation Laboratory
Stanford Research Institute, Menlo Park, California

Abstract. Measurements of ionospheric absorption by the cosmic-noise monitoring method show that, at certain tropical latitudes, an irregular component of absorption is often present in the evening hours. If the variable absorption is present at one observing site (Johnston Island), then variations are also likely to be present at another station about 1325 km away (Hawaii). The individual variations of absorption as a function of time are not correlated at the two stations, however, suggesting that the scale of the patches causing the absorption must be less than about 1000 km.

An attempt is made to find a correspondence between hourly averages of the apparent absorption with other ionospheric parameters. Both a nighttime and daytime absorption are observed. A greater nighttime component appears at Johnston Island than at Hawaii, implying the existence of a latitude dependence. Correlation with spread F or with sporadic E on the basis of ionosonde data from Maui was not found, although a correlation is apparent between cosmic-noise absorption and ionosonde minimum reflection frequency during geomagnetically quiet periods. There is good correlation between average hourly values of the absorption and F_2 critical frequency f_oF_2. This latter observation is explainable by the shielding effect of the F region.

troduction. Several 'riometers'—devices for suring cosmic-noise absorption—were oper- in the Pacific during Operation Hardtack sreel in the summer of 1958. In the intervals veen nuclear tests, after shot effects had dis- eared, the riometers remained in operation revealed curious absorption variation ap- ntly characteristic of the latitude of John- Island (Fig. 1).

The riometer [*Little and Leinbach,* 1959] is a self-regulating device for matching the power output of a noise generator (a temperature-limited diode) to the power appearing at the antenna terminals. By recording the generator input as a function of time, cosmic-noise level is automatically and continuously recorded. To measure absorption, a 'quiet-day' curve is first derived by taking the value of maximum cosmic

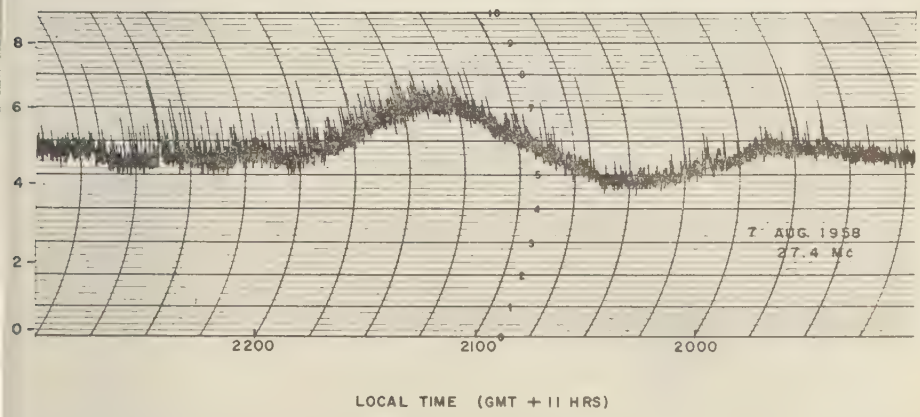

Fig. 1. Example of rapid fluctuation of absorption observed at Johnston Island.

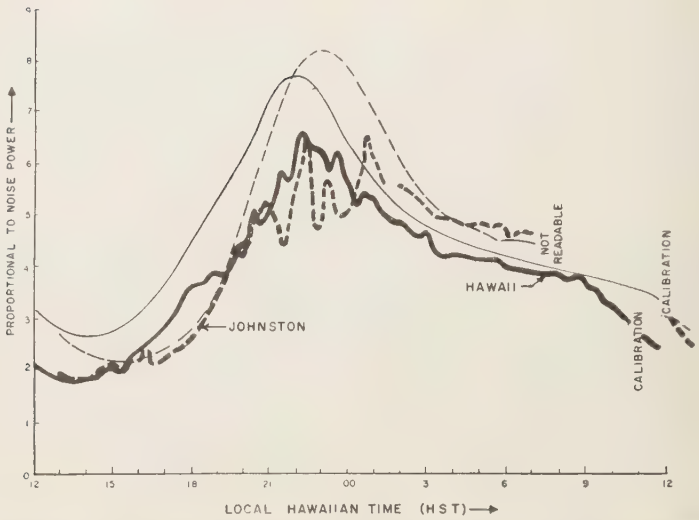

Fig. 2. Comparison of the fluctuations observed on August 5, 1958, at the Johnston Island and Haw stations, which are separated by a distance of 1325 km.

noise that has ever been observed at a given time of the sidereal day. This curve is taken to represent the level to which the riometer record would return if there were no absorption. Depressions below this curve can be interpreted as equivalent absorption integrated over the solid angle viewed by the antenna. This procedure is valid if based upon an entire year's data so that the solar and sidereal variations of noise level can be resolved. The present study is consid ably more risky because only a few weeks' d were available.

Observations. At times when the shot effe were absent, the riometer often recorded a nig time irregular fluctuation of the cosmic-no power amounting to about 1 db at 27.5 M and changing at a rate of about 1 cycle hour. From visual inspection, a few gene

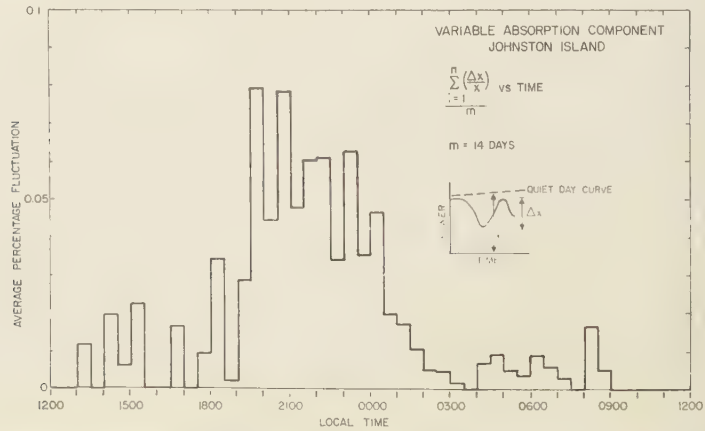

Fig. 3. Percentage fluctuation of absorption observed at Johnston Island showing maximum activi in early evening hours.

nents can be made about the variable com-
ut of absorption. These features are illus-
l in Figure 2.

The variations commence at about 1900
time and terminate gradually soon after
midnight (see also Fig. 3).

The variations are greater at Johnston
l than at either Hawaii (at a higher geo-
etic latitude) or Bikini (at a lower lati-
. Observations at Antigua, at an even
r latitude, show even less variability. It is
esting to note that the latitude of Johnston
o the latitude of maximum F-region ioniza-
[*Rawer*, 1956], while Bikini lies partly in
quatorial trough.

A day showing generous fluctutations at
tation also tends to show generous fluctua-
at another station.

The individual fluctuations at Johnston
d do not correlate with those of Hawaii,
km to the northeast.

An attempt was made to find correspond-
between the individual absorption fluctua-
and the short-term variations of iono-
ric variables taken from the ionospheric
der at Maui (150 km east of the Hawaiian
eter). (*a*) As sporadic E is present for such
periods of time, no conclusive relationships
be drawn. Sporadic E, however, tends to
a daytime maximum at this latitude, so
a relationship would be surprising if pres-
(*b*) Insufficient data are on hand for min-

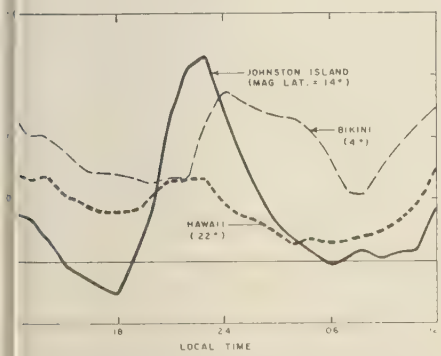

g. 4. Average hourly absorption for Hawaii
y–August 1958), Johnston Island (July–August
), and Bikini (April–May 1958). Johnston
nd, at an intermediate latitude, tends to show
e absorption than the two other sites.

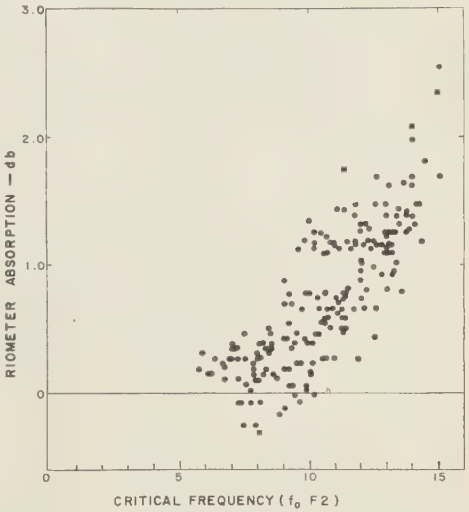

Fig. 5. Hourly values of riometer absorption versus F_2-layer critical frequency (f_0F_2). The riometer and ionosonde were separated by about 250 km.

ute-by-minute comparison because spread F often obscures the ionosonde record. (*c*) Although spread F can appear and disappear in the course of a 15-minute interval, no significant relationship to the absorption fluctuations could be found.

Hourly values of the absorption measured by the riometer were manually integrated for comparison with ionospheric variables. This procedure is dangerous because the quiet-day curve cannot be determined with precision using only a few weeks' data. The following conclusions are reached when fluctuations shorter than 1 hour are integrated out:

1. For periods in which simultaneous data were available, the total amounts of absorption at Johnston Island and at Hawaii were not significantly different. The absorption exceeds 1 db at Johnston 16 per cent of the total time.

2. Diurnal curves for each station show an evening maximum in addition to the expected noon maximum (Fig. 4).

3. Hourly values of absorption show a strong correlation with critical frequency of the F region (Fig. 5). This is in agreement with observations on 18.3 Mc/s by *Mitra and Shain* [1953]. There is a tendency for the critical frequency

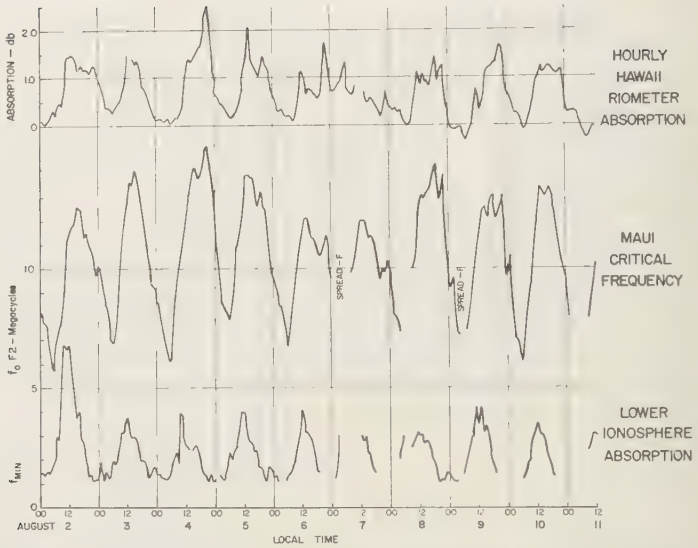

Fig. 6. Comparison of Hawaii riometer absorption with Maui F_2-layer critical frequencies (f_o) and lower ionosphere absorption (f_{min}). Geomagnetic activity was particularly low during this per August 2 data may be affected by the high-altitude nuclear burst of August 1.

to have not only an early afternoon peak (expected) but also another component extending into the evening hours (Fig. 6). Unusually large intervals of absorption were exactly accompanied by an unusual peak of critical frequency.

4. Only during quiet geomagnetic conditions was there correlation between f_{min} and riometer absorption (high values of each near noon).

5. The correlation with K index is not defined, although, if there is any dependence would appear to be negative (Fig. 7). Suc result, however, would be a likely conseque of the fact that geomagnetic disturbances associated with low F-region critical frequen and high critical frequencies have been shown be related to increased absorption.

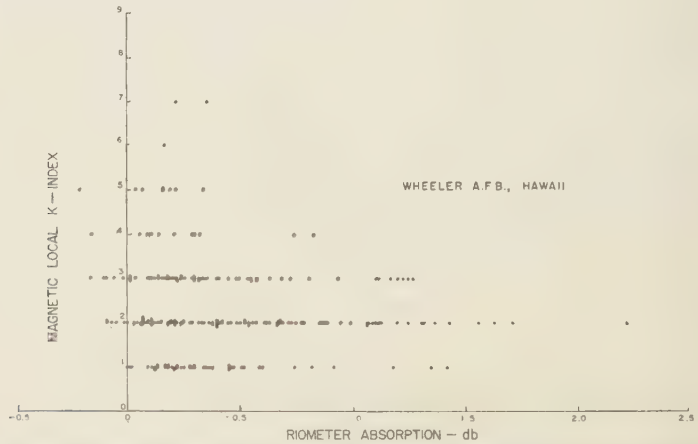

Fig. 7. Scatter plot of riometer absorption (averaged over a 3-hour interval) and local magnetic index showing absence of positive correlation.

The correlation of absorption with high critical frequency might be explained by the fact that the ionosphere may shield the receiver from high cosmic-noise temperatures outside the ionosphere and reflect portions of relatively cool earth into the antenna beam. For example, if the F-region critical frequency is 15 Mc/s, energy will be arriving from cosmic sources (more than 10,000°K) only within the cone of half-angle 60° centered on the zenith. The solid angle viewing the sky is now only one-half of the solid angle of the observed hemisphere. For rays below this critical angle, the antenna would view the earth's surface, which, in the absence of thunderstorm activity, might appear at 300°K. If the riometer antenna is assumed to have a beamwidth of 90°, to have a $\cos\theta$ beam shape, and to be pointed at the zenith, the received noise power would be reduced to about 75 per cent of its original value, or about -1.25 db. This number could be even greater when the center of the galaxy is located at a lower angle in the sky. Thus an intensely ionized F region is expected to give rise to an apparent 'absorption.'

Some part of the observed absorption may be occurring in the F region. It can be shown that an intensely ionized F region can be responsible for about 1 db of absorption [*Mitra and Shain,* 1953]. Short-term variations of this order are not likely to be due to this cause because the F-region critical frequency is known to vary in a more gradual manner.

Conclusions. Ionospheric absorption on 30 Mc/s measured in the tropics shows a variable nighttime component that is not correlated in detail between stations (suggesting a scale less than 1000 km), has an apparent latitude dependence that is maximum at Johnston Island, and is not obviously related to geomagnetic activity. A study of hourly values of absorption (tending to integrate over the above variations) shows both a nighttime and a noontime maximum. There appears to be no correlation with sporadic E or spread F, although, during magnetically quiet times, correlation with $f_{\min}$ is apparent. There is a strong correlation between riometer 'absorption' and F-region critical frequency that is statistically in agreement with the 'absorption' latitude dependence. This observation may be largely explained by blocking of the incident cosmic noise by a reflecting F region.

Acknowledgment. The authors express thanks to the IGY Ionospheric Data Center, CRPL, Boulder, Colorado, in particular to Sidney Ostrow, for the use and interpretation of certain ionosonde records. This research was made possible by Air Force Cambridge Research Center Contract AF 19(604)-3462, whose support is greatly appreciated.

References

Little, C. G., and H. Leinbach, The riometer—a device for the continuous measurement of ionospheric absorption, *Proc. IRE, 47* (2), 315–319, 1959.

Rawer, K., *The Ionosphere,* Frederick Ungar Publishing Company, New York, English translation, p. 114, 1956.

Mitra, A. P., and C. A. Shain, The measurement of ionospheric absorption using observations of 18.3 Mc/s cosmic radio noise, *J. Atmospheric and Terrest. Phys., 4,* 204–218, 1953.

(Manuscript received December 8, 1959; revised February 3, 1960.)

Refraction of Radio Waves at Low Angles within Various Air Masses

B. R. BEAN, J. D. HORN, AND L. P. RIGGS

National Bureau of Standards
Boulder, Colorado

Abstract. The refractive index structure and bending of radio rays within air masses of nonexponential refractive index height structure is treated in terms of the value expected in an average atmosphere of exponential form. It is demonstrated that refraction differences within air masses arise from departures of refractive index structure from the normal exponential decrease with height. The effect upon radio ray refraction of these departures from the normal exponential refractive index structure is most pronounced for small initial elevation angles of the radio ray.

ntroduction and background. It has been own for some time that the radio field engths beyond the horizon vary with different masses [*Englund, Crawford, and Mumford,* 8; *Hull,* 1935, 1937]. Further, characteristic fractive index profiles of various air masses ve been presented by *Gerson* [1948], and ny studies have been made of mean refrac- e index profile characteristics for such regions the United Kingdom [*Stickland,* 1946], Ja- a [*Tao,* 1957], Canada [*Hay,* 1958], France *lisme,* 1958], and the United States [*Bean,* 53].

More recent studies have led to the evalua- n of radar elevation angle errors in different mates and air masses [*Schulkin,* 1952; *Fannin d Jehn,* 1957]. In general, these studies did t emphasize the relation between air mass fractive index structure and the *refraction* of dio waves within the air mass. For example, ean angular bendings for radio rays passing mpletely through the earth's atmosphere are ven for extremes of air mass types and a range initial elevation angles, θ_0, on Figure 1 *chulkin,* 1952]. It is seen that maritime tropi- l air produces 30 per cent more bending than ntinental polar air at initial angles of arrival departure of about 10° (175 milliradians) d that this difference increases to about 70 r cent at zero initial elevation angle. Further, e magnitude of the total bending increases pidly with decreasing values of θ_0.

Figure 1 does not make it clear that differ- ces in radio ray refraction arise from differ- ces in the refractive index profiles of the two air masses. It is the purpose of this paper to show that various air masses have characteristic refractive index profiles and that the radio ray refraction within each air mass is mirrored by the difference of the actual refractive index structure from a standard atmosphere of exponential form.

Refraction of radio rays. The angular bending of a radio ray, $\tau_{1,2}$ (see Fig. 2) between two points in the atmosphere of refractive indices n_1 and n_2 is given by the geometrical optics formula [*Smart,* 1931; *Schulkin,* 1952]

$$\tau_{1,2} = -\int_{n_1}^{n_2} \cot \theta \, dn \qquad (1)$$

under the assumption that $n - 1 << 1$ and θ is the local elevation angle. It is also assumed that n is spherically stratified and concentric

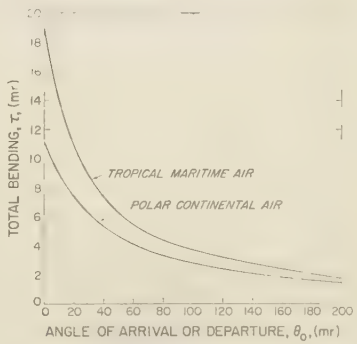

Fig. 1. Comparison of total angular bending of radio rays within air masses. After *Schulkin* [1952].

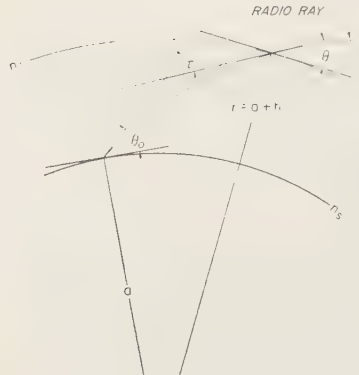

Fig. 2. Geometry of radio ray refraction.

with the earth. The value of cot θ is determined from Snell's law, and $\tau_{1,2}$ is completely determined from a knowledge of the variation of n with height. An empirical formula to describe the long-term average variation of n with height is[1]

$$\overline{N(h)} = \overline{[n(h) - 1]}10^6 = 313 \exp\{-h/6.95\} \quad (2)$$

where h is the height above the earth's surface in kilometers and 313 is the long-term average value of $(n - 1)10^6$ at the earth's surface for the United States. In practice it is convenient to utilize this average $\overline{N(h)}$ function to refer the observed $N(h)$ data to the common level of $h = 0$ by means of

$$A(h, 313) = N(h) + 313\,[1 - \exp\{-h/6.95\}] \quad (3)$$

This new quantity, $A(h, 313)$, is analogous in concept to potential temperature but utilizes the normal N gradient rather than the adiabati gradient of the potential refractive modulus o *Lukes* [1944] and *Katz* [1951]. The notatio $A(h, 313)$ is used to indicate that A is deter mined from the refractive index at the heigh h and the 313 exponential atmosphere. It ha been found to be advantageous to use severa atmospheres of exponential form in application involving different climatic regions [*Bean an Dutton*, 1960]. The particular form of (3) em phasizes departures of N structure from norma as shown by recent studies of synoptic varia tions of $N(h)$ about frontal systems [*Bea Riggs, and Horn*, 1959] and, in addition, pe mits direct calculation of radio ray bending fo any observed refractive index structure. Whe $A(h, 313)$ is introduced into equation 1 for ra bending, one obtains

$$\tau_{1,2} = -\int_{h_1}^{h_2} \frac{10^{-6} \cot\theta}{n}\, dA(h, 313) + \tau(h, 313) \quad (4$$

which indicates that the bending can be r garded as the resultant of the bending in th normal atmosphere, $\tau(h, 313)$, and a perturba tion component representing departures of r fractive index structure from that of the 31 exponential atmosphere. The value of $\tau(h, 313$ can be obtained from refraction tables [*Bea*

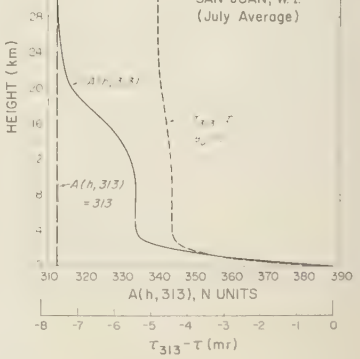

Fig. 3. Comparison of $A(h, 313)$ profiles wi departures from normal bending of radio wav for maritime tropical air. After *Byers* [1944].

[1] The *n-height* distribution given by (2) is actually the result of the examination of considerable meteorological data [*Bean and Thayer*, 1959*a*], the 313 representing the average of nearly 2,000,000 individual observations of N at the earth's surface from all parts of the United States and the scale height of 6.95 km determined as the best value for a single exponential representation of $N(h)$ for $N(0) = 313$.

l Thayer, 1959b], and the perturbation term
be evaluated by graphical methods to yield
over-all accuracy of a few per cent in esti-
ting $\tau_{1,2}$ [*Bean and Dutton,* 1960].
$A(h, 313)$ profiles were prepared from typical
nperature, pressure, and humidity distribu-
ns within a range of air masses as published
the literature [*Byers,* 1944; *Willett,* 1944;
ewartha, 1943] and climatic summaries of
per air data [*Ratner,* 1945]. Two of these
files, one for maritime tropical air and the
ner representing continental tropical air, are
tted on Figures 3 and 4 to represent the ex-
mes of $A(h, 313)$ profiles. These profiles
arly show that the two air masses have quite
ferent refractive index structures. The dif-
rence is most pronounced near the ground. At
ights of 20 km, however, $A(h, 313)$ rapidly
proaches the asymptotic value of 313, regard-
s of air mass type. The radio ray bending is
so plotted on these figures relative to the value
pected in the $N(h) = 313 \exp\{-h/6.95\}$ at-
osphere. Near the ground, bending departures
e seen to be mirrored by the A unit profiles.
hat is, a *negative* gradient of N or A produces
positive increase of bending. Above a few kilo-
eters, however, the bending departures ap-
roach a fixed, usually nonzero, value. It is

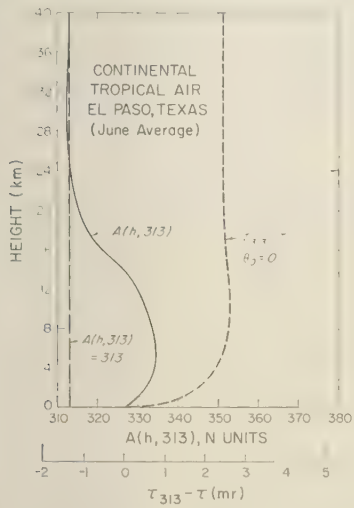

Fig. 4. Comparison of $A(h, 313)$ profiles with departures from normal bending of radio waves for continental tropical air. After *Ratner* [1945].

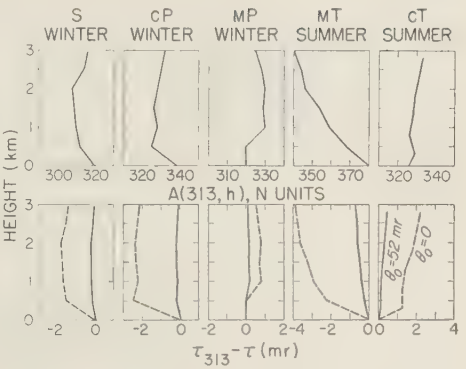

Fig. 5. Comparison of $A(h, 313)$ profiles with departures from normal bending of radio rays for the several air masses.

apparent that the asymptotic value of $\tau_{313} - \tau$ at large heights is determined by the bending in the first few kilometers, where 60 to 75 per cent of the low-angle bending normally occurs. The marked differences in air mass n structure and bending are confined, therefore, to the first few kilometers above the earth, as is illustrated by Figure 5. The distribution of the meteorological elements within each air mass is reflected in the $A(h, 313)$ profiles. For example, the steep humidity gradient characteristic of maritime tropical air is reflected by the rapid decrease of $A(h, 313)$ with height. Comparatively, the high ground-level temperatures and rapid decrease of temperature with height in continental tropical air is reflected by the increase of $A(h, 313)$ with height within that air mass. These, and A-profile characteristics of other air masses, are listed in Table 1 and are evident from the form of the equation for the refractive index at radio frequencies [*Smith and Weintraub,* 1953].

$$N = (n - 1)10^6 = (77.6/T)(P + [4810e/T]) \quad (5)$$

where total air pressure P, and vapor pressure e, are in millibars, and the temperature T is in degrees Kelvin. The average decrease of pressure, temperature, and humidity with height produces a normal decrease of N. If, however, the temperature increases with height, as in a temperature inversion, N decreases more rapidly and radio rays are superrefracted, dependent, of course, upon the vapor pressure. Conversely, an

TABLE 1. Refractive Characteristics of Air Masses

Air Mass	Reference	Meteorological Characteristics	Refractive Characteristics
Superior (S) S/mT, typical of Gulf coast (Lake Charles, La.)	[*Byers*, 1944]	Formed from subsidence of high-level air with resulting dry adiabatic temperature lapse rate and low humidity. Often found overlying other, more humid air masses that show a resultant characteristic drying with height in the lower levels.	Rapid decrease of N and A with height in the lowermost layer produces a superrefractive* layer. The overlying superior air is nearly normal in bending characteristics.
Continental Polar (cP) source region	[*Willett*, 1944]	Characterized by low temperature and humidity with a pronounced temperature inversion at the surface created by progressive nocturnal cooling during the arctic night.	Ground-based superrefractiv layer arising from the temperature inversion.
Maritime Polar (mP), typical low-level ground modification (Seattle, Wash.)	[*Byers*, 1944]	Cool air, nearly saturated to a height of several kilometers. Example shows typical drying in lower levels when this air mass moves over land. Overlying mP has increasing humidity and decreasing temperature with height.	Surface layer produces near-normal bending. Increasing N in the overlying mP air produces an elevated subrefractive layer.
Continental Tropical (cT) source region (El Paso, Texas)	[*Ratner*, 1945]	Characterized by superheated lower layers, rapid decrease of temperature with height, and very low humidity.	Strong temperature lapse produces a subrefractive layer reaching to several kilometers.
Maritime Tropical (mT) source region (Pensacola, Fla.)	[*Byers*, 1944]	Relatively warm air, high water-vapor content in lowest layer, which decreases rapidly with height. Moderate changes in temperature and humidity structure produce large refractive gradient changes.	Strong superrefraction to great heights arising chiefly from rapid decrease of humidit with height.

* Normal refraction is taken to mean $\tau(h, 313)$, superrefraction to mean $\tau(h) > \tau(h, 313)$, and sub refraction $\tau(h) < \tau(h, 313)$.

unusually rapid decrease of temperature, or an increase of humidity, with height produces a subnormal decrease of N with height, or subrefraction of radio waves. In any event it is evident from these figures that A-profile effects on ray bending are most pronounced at $\theta_0 = 0$, are significantly less pronounced at $\theta_0 = 52$ mr ($\sim 3°$), and continue to diminish with increasing θ_0 until, at $\theta_0 = \pi/2$, there is no bending at all and consequently all departures are zero.

Conclusions. The work of Schulkin and others has shown that characteristic total bending differences in radio ray refraction exist between various air masses. The present study extends Schulkin's conclusion by identifying abnormal bending of radio rays with departures of re fractive index structure from average in th lowermost layers of the air masses. Considera tion of departures of both ray bending and re fractive index structure from their value in standard exponential atmosphere results in suitable method of cataloguing air masses i terms of either refractive index structure c bending characteristics.

References

Bean, B. R., The geographical and height distribu tion of the gradient of refractive index, *Pro IRE, 41*, 549–550, 1953.

Bean, B. R., and E. J. Dutton, On the calculatio

of the departures of radio wave bending from normal, *J. Research NBS, D,* Radio Propagation, 1960.

an, B. R., L. P. Riggs, and J. D. Horn, Synoptic study of the vertical distribution of the radio refractive index, *J. Research NBS, 63D,* 249–254, 1959.

an, B. R., and G. D. Thayer, On models of the atmospheric radio refractive index, *Proc. IRE, 47,* 740–755, 1959*a*.

an, B. R., and G. D. Thayer, C.R.P.L. exponential atmosphere, National Bureau of Standards Monograph 4, U. S. Government Printing Office, Washington 25, D. C., 1959. A digest of this monograph appeared in *J. Research NBS, 63D* (3), November–December, 1959.

ers, H. R., *General Meteorology,* McGraw-Hill Book Co., New York, pp. 255–277, 1944.

nglund, C. R., A. B. Crawford, and W. W. Mumford, Ultra-short-wave radio transmission through the non-homogeneous troposphere, *Bull. Am. Meteorol. Soc., 19,* 1938.

nnin, B. M., and K. H. Jehn, A study of radar elevation angle error due to atmospheric refraction, *Trans. IRE, AP-2, 1,* 71–77, 1957.

erson, N. C., Variations in the index of refraction of the atmosphere, *Geofis. pura e Appl., 13,* 1948.

ay, D. R., Air-mass refractivity in central Canada, *Can. J. Phys., 36,* 1678, 1958.

ull, R. A., Air-mass conditions and the bending of ultra-high-frequency waves, *QST, 19,* 13–18, 1935.

ull, R. A., Air-wave bending of ultra-high-frequency waves, *QST, 21,* 16–18, 1937.

atz, I., Gradient of refractive modulus in homogeneous air, potential modulus, pp. 198–199 in *Propagation of Short Radio Waves,* by D. E. Kerr, McGraw-Hill Book Co., New York, 1951.

Lukes, G. D., Radio meteorological forecasting by means of the thermodynamics of the modified refractive index, Third Conference on Propagation, November 16–17, 1944, Washington, D. C., Committee on Propagation, NDRC, pp. 107–113, 1944.

Misme, P., Essai de radioclimatologie d'altitude dans le nord de la France, *Ann. Telecommunications, 13* (11–12), 1958.

Ratner, B., Upper air average values of temperature, pressure, and relative humidity over the United States and Alaska, U. S. Weather Bureau, Washington, D. C., May 1945.

Schulkin, M., Average radio-ray refraction in the lower atmosphere, *Proc. IRE, 40* (5), 554–561, 1952.

Smart, W. M., *Spherical Astronomy,* Cambridge University Press, London, 1931.

Smith, E. K., and S. Weintraub, The constants in the equation for atmospheric refractive index at radio frequencies, *Proc. IRE, 41,* 1035–1037, 1953.

Stickland, A. C., Refraction in the lower atmosphere and its applications to the propagation of radio waves, Conference on Meteorological Factors in Radio-Wave Propagation, The Royal Institute, London, pp. 253–267, 1947.

Tao, Kazuhiko, Meteorological influences on the hourly median field strength of ultra-short waves in the diffraction region, *J. Radio Research Labs., 4,* (16), 155–254, 1957.

Trewartha, G. T., *An introduction to Weather and Climate,* McGraw-Hill Book Co., p. 206, 1943.

Willett, H. C., *Descriptive Meteorology,* Academic Press, New York, pp. 190–220, 1944.

(Manuscript received January 15, 1960; revised January 22, 1960.)

A Comparison of Intracloud and Cloud-to-Ground Lightning Discharges

N. KITAGAWA AND M. BROOK

New Mexico Institute of Mining and Technology
Socorro, New Mexico

Abstract. Lightning discharges were investigated with high time-resolution equipment on both electric-field and electric-field-change meters.

The analysis of the electrical records reveals that the late stages of intracloud discharges are very similar to those of cloud-to-ground discharges during the periods between successive return strokes (junction process) and during the period after the last return stroke (final process). In contrast, the initial portion of the field change of an intracloud discharge bears little or no resemblance to the initial portion of the leader field change of a discharge to ground. It is suggested that the difference in the initial breakdown characteristics results from variations in the relative populations of water drops and ice particles as they affect the internal impedence of the region of cloud where breakdown occurs.

The difference in the initial field-change characteristics of intracloud and cloud-to-ground discharges is so distinct that from the first 10 msec of the electric-field-change record one can predict with over 95 per cent certainty whether a discharge will reach ground or remain within the cloud.

Introduction. As part of a research program
thunderstorm electrical phenomena and cloud
ysics, the authors have engaged in the study
the lightning discharge and its relationship
the electrical and meteorological structure of
underclouds. One approach, described in this
aper, has been the study of the fine structure
electric-field changes associated with cloud-
-ground and intracloud discharges.

Considerable progress has been made during
ie past 30 years toward understanding the
ature of cloud-to-ground lightning [see, for
ample, the review by *Schonland,* 1956], but
vestigations into the nature of intracloud
scharges have been very rare [*Sourdillon,*
)52; *Smith,* 1957].

In this paper, the cloud-to-ground discharge
ill usually be referred to as a ground discharge,
l other discharges (e.g., intracloud, cloud-to-
oud, and cloud-to-air) being distinguished as
oud discharges.

Electric-field changes from approximately
)00 lightning discharges of all types were cor-
lated with simultaneous visual observations.
n the basis of these correlations, the authors
ave developed reliable criteria which allow
ositive identification of cloud and ground dis-
harges where visual correlations are absent.

Two types of in-cloud discharge processes are associated with each ground discharge: (1) the initial portion of the first leader and (2) the discharge process (junction or *J* process) between and after the strokes of a multiple ground discharge. *Malan and Schonland* [1951] first studied the latter process, offering it in explanation of the intermittent discharge mechanism which produces multiple ground strokes. Subsequently, *Malan* [1955] and the authors [*Kitagawa,* 1957*b*; *New Mexico Inst. Mining Technol.,* 1957] discussed the fine structure of this discharge process.[1]

If we consider the first-leader process in ground discharges, it can be seen that the duration of the electric-field change is much longer than that of the out-of-cloud portion as photographed by high-speed cameras [*Pierce,* 1955; *Kitagawa,* 1957*a*; *Clarence and Malan,* 1957]. *Clarence and Malan* [1957] tried to explain this discrepancy in duration between electric and photographic records in the following way. They assumed that before the stepped leader proceeds to ground the initial breakdown process takes place between the main negative

[1] Evidence that the fine structure is not spurious or due to corona discharge will be the subject of a future paper.

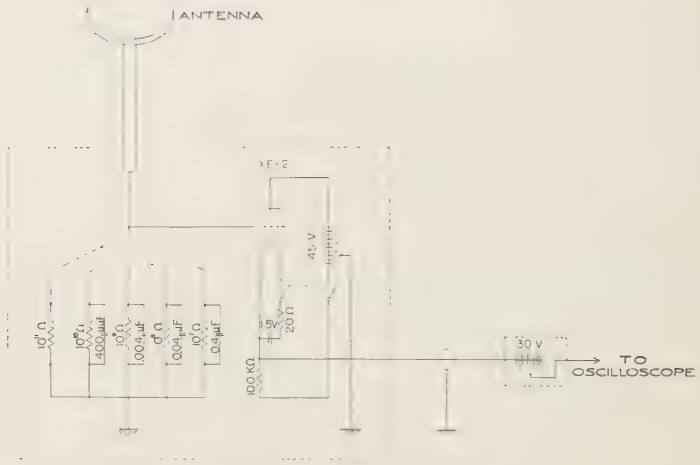

Fig. 1. Circuit diagram of the electric-field meter (slow antenna).

charge center and a small, localized positive charge near the cloud base. They recorded the whole pre-return-stroke field change, using a field-change meter of high sensitivity and high time resolution. The prestroke field change was divided into three portions: the *B* (breakdown) portion, the *I* (intermediate) portion, and the *L* (leader) portion. Only the *L* portion, it was suggested, corresponds to the stepped leader recorded photographically.

In this paper, detailed comparisons are made between the electric-field records of cloud and ground discharges; in particular, between the cloud discharge and the in-cloud portion of the ground discharge.

The observations reported were carried out at the New Mexico Institute of Mining and Technology, Socorro, New Mexico, covering the two thunderstorm seasons of 1957 and 1958.

Apparatus. The apparatus and techniques used to record field changes during a lightning discharge have been described earlier [*NMIMT*, 1959]. Brief mention is made here of the main features of the apparatus. Figure 1 is the circuit diagram of the electric-field meter used to record the slow electric-field change due to a lightning discharge. Essentially, the circuit consists of a flat-plate antenna and an electrometer tube operated as a cathode follower. The output is coupled directly to one input of a Tektronix type 535 oscilloscope. The time constant of t grid circuit is adjusted to 4 seconds, a peri long enough to reproduce faithfully field chang associated with lightning, yet short enough maintain the oscilloscope trace on scale duri such slow field changes as those occurring b tween successive lightning discharges. Five di ferent capacitor voltage dividers are used vary the sensitivity over a range of 80 db. T frequency response of the electrometer circu (hereinafter called the slow antenna) exten from dc to better than 20 kc/s.

The oscilloscope trace is allowed to free-r at the desired rate (usually 50 msec per swee and is photographed on a continuously advan ing film. The time resolution is at least 0.5 ms and is limited only by the slow film-transpo speed of approximately 24 in./min. The came accepts 1000-ft lengths of 35-mm film and, wi the stated film-transport speed, runs contin ously for approximately 8 hours on a single loa

Fast electric-field changes are studied by second flat-plate antenna (fast antenna). Du ing 1957 the fast antenna was connected direct to the second input of the dual-trace oscill scope (Tektronix type 535), and both slow a fast records were photographed simultaneous The very high sensitivity of the fast anten and the short time constant (0.3 msec) of t antenna circuit combine to emphasize the fa

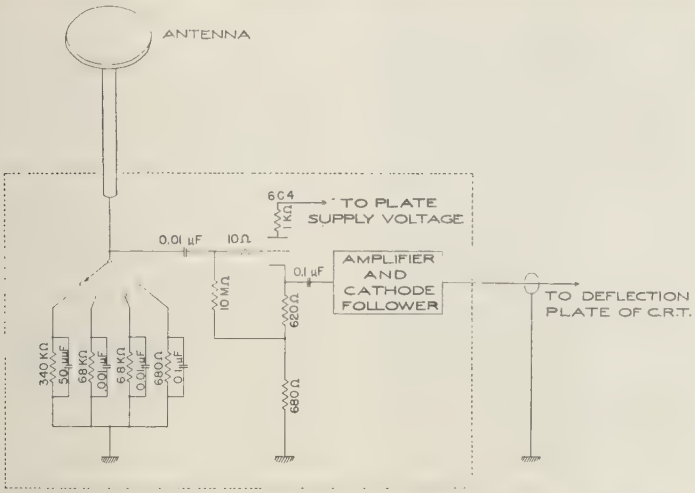

Fig. 2. Circuit diagram of the electric-field-change meter (fast antenna).

hanges in the field during lightning. Thus, the st antenna reveals many fine-structure details hich the slow antenna cannot resolve, but the ery fast components associated with each step- ise movement of a stepped leader are not re- olved. In 1958, in order to increase the time esolution for the observation of the stepped ader, the fast antenna was connected to a eparate oscilloscope (Tektronix type 535) hrough the cathode follower and amplifier hown in Figure 2. The time constant was adjusted to 70 μsec, and the frequency response of the circuit was extended to above 1 Mc/s. Gain of the system was varied over an 80-db range by means of a capacitor voltage divider. A resolution of 10 μsec was obtained by using a 2-msec sweep combined with the higher film-transport speed of 9 in./sec.

General character of field change due to ground discharges. Figure 3 illustrates the general character of the field change of a ground discharge recorded simultaneously by the fast

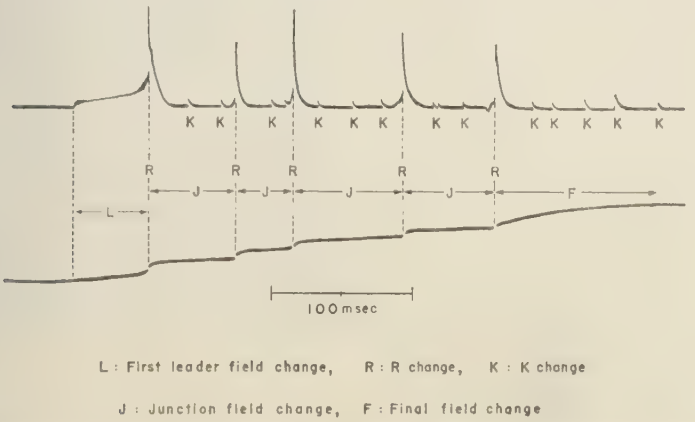

L : First leader field change, R : R change, K : K change

J : Junction field change, F : Final field change

ig. 3. Diagram of the typical field change of the ground discharge. The upper and lower traces are recorded simultaneously by the fast and slow antennas, respectively.

Fig. 4. The field change of a ground discharge recorded simultaneously by the fast and slow antennas. Both the fast and slow traces run in parallel from left to right and from top to bottom.

and slow antennas. In representing the various portions of the field change, the writers adopt the notation used by *Schonland* [1956]. Two features most characteristic of the field change of a ground discharge are (1) several large, rapid, positive field changes called R (return) changes, which are caused by return strokes, and (2) characteristic first-leader field changes, which occur before the first R change. This first-leader field change consists of a series of pulses, some of which are associated with the stepped leader. In addition, the interval between successive return-stroke field changes is overlapped by a series of small, rapid field changes (K changes) spaced from 2 to 20 msec apart [*Kitagawa*, 1957*b*]. The K changes are found similarly during the final field change (F change).

Figures 4 and 5 show examples of field changes due to ground discharges recorded with the sweep rate of 50 and 2 msec per sweep, respectively. In both figures, time increases from left to right and from top to bottom. The positive increase in the field deflects the trace downward. Figure 4 contains two traces recorded simultaneously by the slow and fast antennas and covers the whole duration of the discharge. The characteristic first-leader field change can be seen as a fuzzy or grassy portion. Figure 5 shows the earliest part of the fast-antenna trace, which includes the first-leader field change and the first R (return stroke) field change. It can clearly be seen that the first-leader field change consists of pulses usually associated with each step streamer of the stepped leader. Owing to the high sensitivity, the R change appears as a swift downward off-scale deflection; shortly afterward, the trace is seen to return at a rate determined by the time constant of the antenna circuit. Among the three features of the ground-stroke field change mentioned above, the first and second are well known. The third and somewhat novel feature (the small, rapid field changes between and

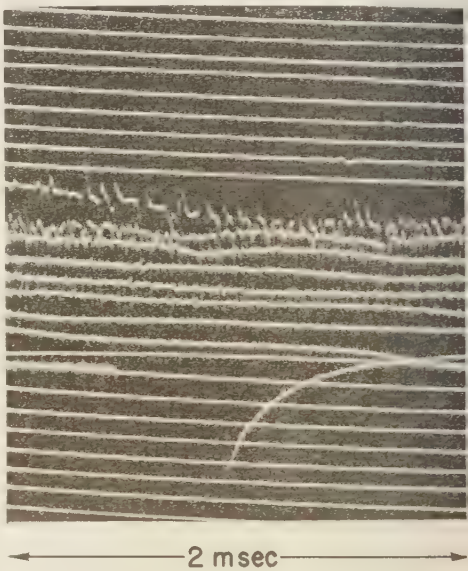

Fig. 5. The first-leader field change and R (return stroke) change recorded by the fast antenna.

after successive return strokes) will be discussed in detail.

Malan and Schonland [1951] suggested that during the periods between successive strokes a slow streamer (junction streamer), starting from the top of the ionized channel made by the preceding strokes, penetrates into a fresh region of the negative charge and renders this new region sufficiently conducting to discharge to ground as a following stroke. *Malan* [1954] also pointed out that a relatively large and long-lasting slow field change, which he designated as *F* or final field change, often follows the last *R* (return stroke) change. By recording the field changes simultaneously with the slow and fast antennas, the writers find that the *J* (junction) or *F* (final) field change is overlapped always by several small, rapid changes (*K* changes) [*Malan*, 1955; *Kitagawa*, 1957*b*; and *NMIMT*, 1959]. When nearby discharges were recorded with relatively high sensitivity, *K* changes were also present on the slow-antenna traces. In such cases, the electric field showed stepwise changes corresponding to the characteristic *K* changes on the fast-antenna trace. Even if *K* changes are not distinguishable on the slow trace, because of inadequate sensitivity, the sense of the *J* field change recorded by the slow antenna usually coincides with the sense of the *K* changes recorded by the fast antenna. These results are cited as strong evidence for the view advanced by the writers [*NMIMT*, 1957] that the greatest portion of the slow field change is actually the integrated sum of the individual *K* changes recorded by the fast antenna during the same interval.

General character of field changes due to cloud discharges. The writers have analyzed approximately 1400 cloud discharges in considerable detail, using the records obtained by operating the fast and slow antennas simultaneously. Figure 6 illustrates the typical electric-field change of the cloud discharge. The upper and lower traces were recorded by the fast and slow antennas, respectively.

This type of field change can be divided into 3 portions: (1) an initial portion, (2) a very active portion, and (3) a later or *J* (junction)-type portion. The initial portion is characterized by pulsations of a wide range of intervals and of relatively small amplitude. In the very active portion the pulse amplitude becomes much larger, and the pulse shapes and pulse intervals become more irregular. In this very active portion the electrostatic field change recorded by the slow antenna is largest and contains a number of relatively rapid changes corresponding to very large pulses on the fast-antenna record. In the later portion, the field change becomes less active and is similar to the *J* (junction) portion of the ground discharge; because of this similarity, it is appropriately designated the *J*-type portion. The *J*-type portion is characterized also by a series of small, rapid field changes (*K* changes) between quiescent intervals of from 2 to 20 msec duration. When the *J*-type portion is compared with the initial and very active portions, the difference in character is very distinct. The difference, however, between the initial and very active portions is not always well marked, the transition from one to the other usually being more or less gradual.

Figure 7 is a typical example of a field change recorded by both fast and slow antennas with

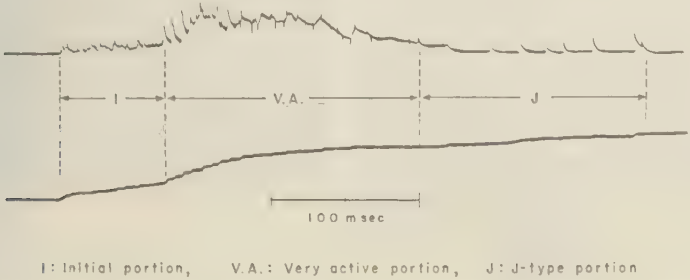

Fig. 6. Diagram of the typical field change of the cloud discharge. The upper and lower traces are recorded simultaneously by the fast and slow antennas, respectively.

a 50-msec sweep. Time increases from left to right and from top to bottom, and the downward deflections of both traces represent positive increases in field.

Figure 8 shows another typical example of a field change due to a cloud stroke. In this case, the field change consists of only two distinctive portions, a very active and a *J*-type portion. The initial portion is apparently absent. Figure 9 is an example of a field change which lacks both the very active and *J*-type portions. The

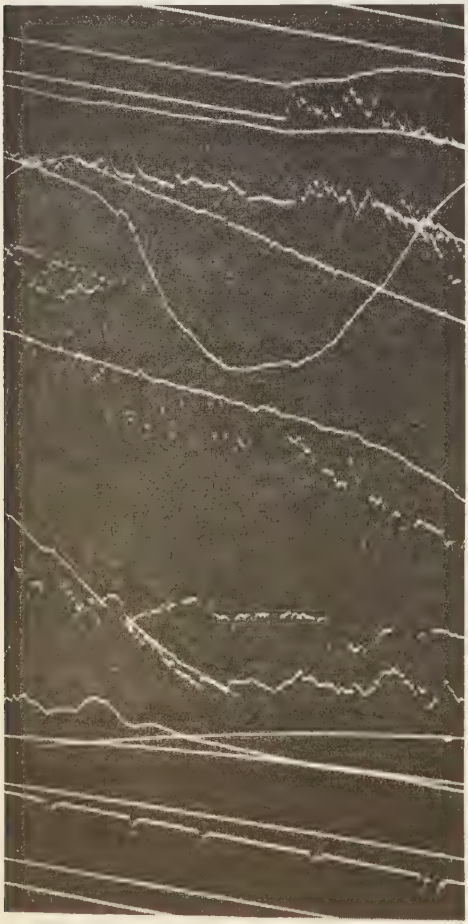

Fig. 7. An example of the field change of the cloud discharge which consists of three distinctive portions.

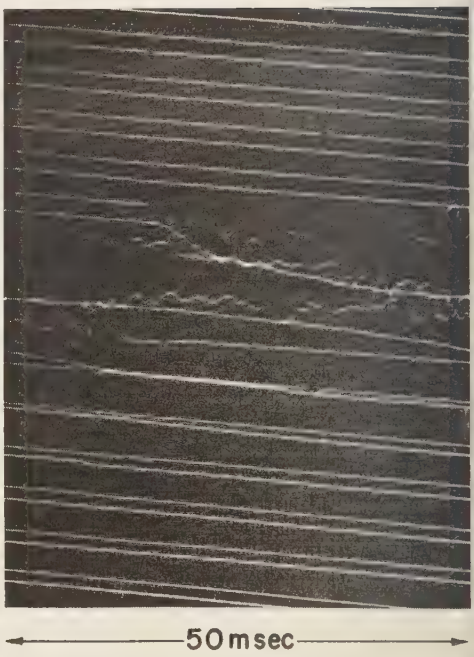

Fig. 8. An example of the field change of the cloud discharge which consists of two distinctive portions.

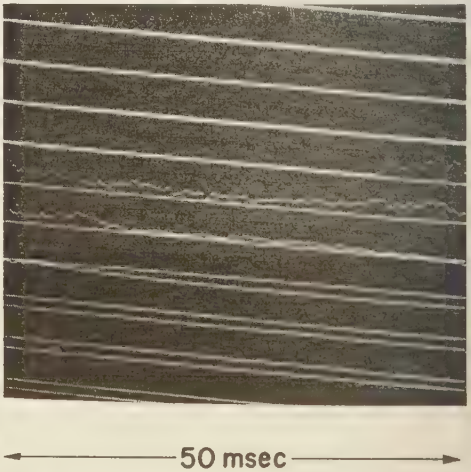

Fig. 9. An example of the field change of the cloud discharge which lacks both very active and *J* portions.

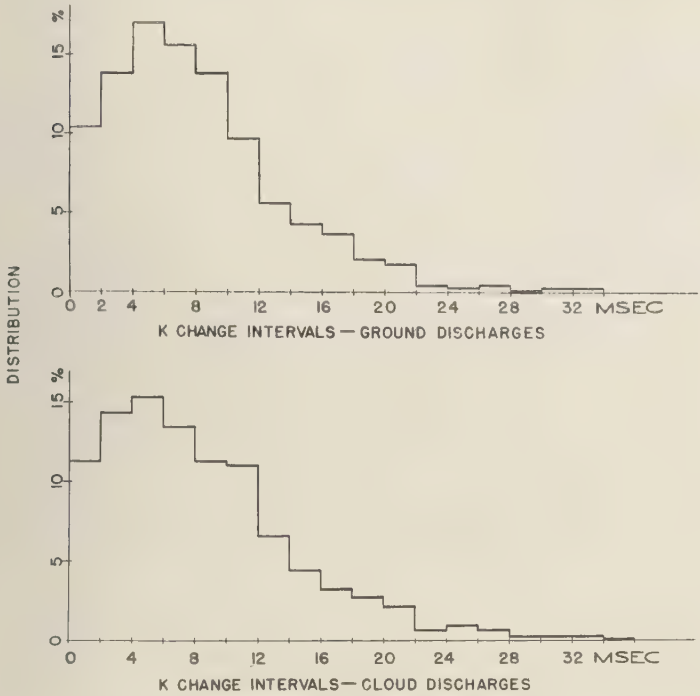

Fig. 10. Frequency distribution of K-change intervals for both ground and cloud discharges.

entire field change is representative of what has been classifield as the initial portion. Field changes of this type were seldom recorded.

Out of a total of about 1400 cloud discharges 50 per cent contain all 3 portions, 40 per cent consist of very active and J-type portions, and the remaining 10 per cent lack the J-type portion and consist of either the initial or very active portion, or both.

Comparison of ground and cloud discharge. It has already been mentioned that the junction process of the ground discharge and the later portion of the cloud discharge are very similar. The histograms shown in Figure 10 offer excellent support for this view. The upper histogram shows the frequency distribution of the K-change intervals representative of 671 ground discharges. The lower histogram shows the distribution of K-change intervals in the J-type portion of 1318 cloud discharges. The similarity between the two distributions is striking; it strongly suggests that the discharge mechanism of the junction process of ground discharges and that of the later portion of cloud discharges are essentially the same. The very active portion of the field change of cloud discharges, however, bears no resemblance to any portion of the field change of the ground discharge.

When the initial portion of a cloud discharge and the first-leader field change of a ground discharge are compared, cursory examination may lead one to conclude that the initial portion is similar to the first-leader field change, since the amplitude is relatively small and the periodicity of pulse repetition is fairly regular. Careful comparison, however, reveals two definitely different and readily distinguishable characteristics.

The first difference is in the duration. The histograms of Figure 11 show the distribution of the duration of initial portions and that of the first-leader field change. It should be noticed that the entire pre-first-stroke field change, which *Clarence and Malan* [1957] classified into

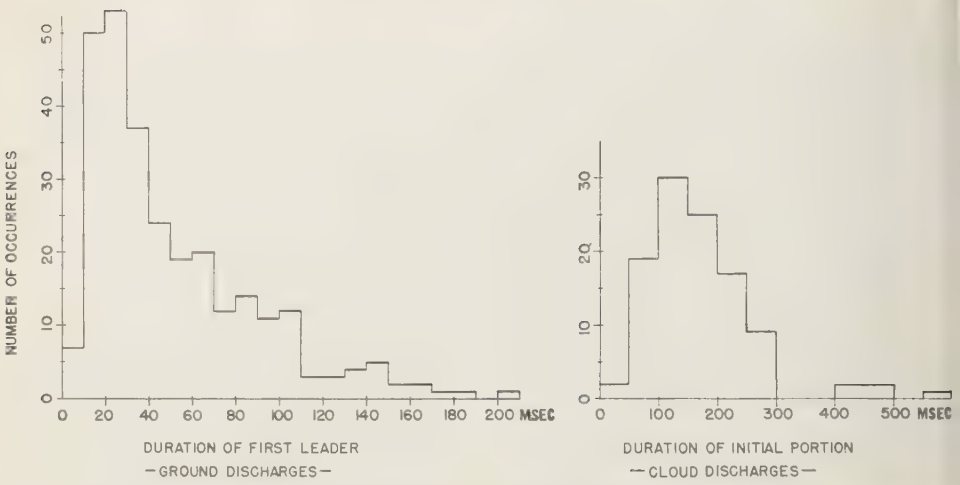

Fig. 11. Frequency distribution of the duration of the first-leader field change of the ground discharge and that of the initial portion of the field change of the cloud discharge.

three different stages (*B*, breakdown; *I*, intermediate; and *L*, leader), is here called the first-leader field change. The duration of the initial portion of the cloud discharge ranges from 50 to 300 msec, whereas the first-leader field change of the ground discharge ranges from 10 to 150 msec. Thus, it is seen that the initial cloud-discharge field change is from 2 to 5 times longer in duration than the first-leader field change.

The second notable difference is in the period of pulse repetition. The histograms on the left side of Figure 12 show the distribution of pulse intervals of the first-leader field change as recorded by the fast antenna with 10-μsec resolution. Full lines represent the results in New Mexico and dotted lines those for Japan, quoted from an earlier paper [*Kitagawa*, 1957*a*]. These histograms show a most frequent interval of from 40 to 60 μsec and offer excellent evidence that the pulses on the leader field change are to be associated with the photographically measured steps of the stepped leader. Because of the asymmetric distribution, the mean intervals are slightly longer than the most frequent values; for example, the mean interval for New Mexico storms is about 80 μsec.

The right histogram of Figure 12 shows the distribution of pulse intervals in the initial portion of cloud discharges. In the case of cloud discharges, the pulse intervals spread over a very wide range, the upper limit extending to 10 msec. The observable lower limit is about 10 μsec and is, of course, determined by the time resolution of the recording apparatus. To compare the pulse intervals from the first leader with the pulse intervals from the initial portion of the cloud discharge it was necessary to adopt two different scales for the abscissas in Figure 12. A linear time scale was used to plot the first-leader pulse intervals, whereas a logarithmic scale was adopted in order to cover the full range of pulse intervals present in the initial portion of the cloud discharge. It should be emphasized that in the histogram on the right the mean value cannot be obtained by dividing the area into two equal parts. An independent calculation shows the mean pulse interval to be about 680 μsec for the cloud discharge. In comparing the two distributions, we find the pulse intervals of the initial portion of the cloud discharge to be much longer than those of the leader field change, both in most frequent and mean values; and the upper range of pulse intervals of the initial-portion field change is about 30 times longer than that of the leader field change.

The large difference in pulse intervals is il-

Fig. 12. Frequency distribution of the pulse intervals for the first-leader field change of the ground discharge and for the initial portion of the field change of the cloud discharge.

lustrated in Figures 13 and 14, which show typical examples of the leader field change of a ground discharge and of the initial portion of a cloud discharge. The initial-portion field change is characterized as follows. (1) Pulses appear as several or scores of groups, which are separated by relatively long, quiescent time intervals ranging from 0.3 to 10 msec. (2) Within each group, the pulse intervals are somewhat similar to those of the leader field change. In contrast, pulse activity is much more uniform throughout the leader field change, as can be seen in Figure 13 and also in Figure 5. Figure 5 is an example of a leader of short duration (19 msec), and Figure 13 represents a leader of long duration (80 msec). The regularity and uniformity of the pulse intervals exhibited in the two figures are very striking; these are prominent characteristics of all leader field changes, regardless of their durations.

There are, of course, exceptions in the character of the field changes described above. In the case of a cloud discharge, the field change occasionally presents a relatively long train of pulses, very much like the first-leader field change. But usually the duration of a train of pulses of this type does not exceed 4 msec. Only in very rare cases (about 1.6 per cent of the number of cloud discharges) were long-lasting leader-type field changes (longer than 20 msec) found. For ground discharges there were also exceptional leader field changes in which the very beginning portion showed a character similar to the initial-portion field change of the cloud discharge. These exceptional leader field changes were confined to those discharges which exhibited first leaders of duration longer than 120 msec. Out of 80 field changes recorded by the fast antenna, 11 leader field changes exceeded 120 msec in duration; these are listed in Table 1.

The character of the field change is distinguished in the table as being either of the cloud type or normal. All the leaders, however, exhibited regular first-leader pulse activity within the last 20 msec before the first return stroke.

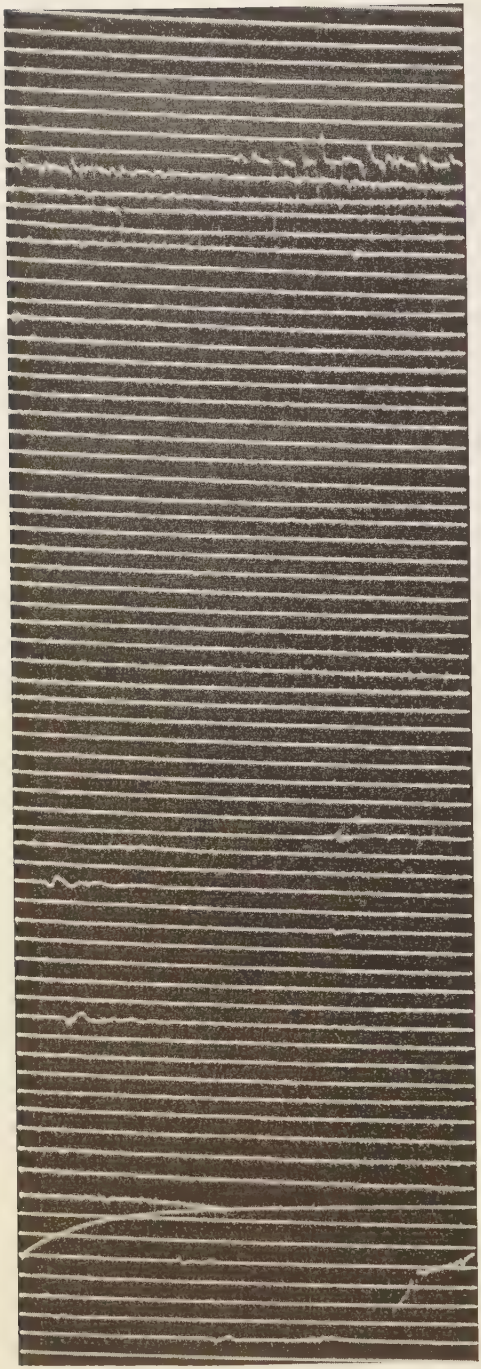

Fig. 13. The fast-antenna record of a first-lead field change of relatively long duration.

TABLE 1. List of First-Leader Field Changes with Very Long Duration (Longer than 120 msec

Duration in msec	Character of Beginning Par
250	Cloud type
180	Cloud type
144	Normal leader type
122	Normal leader type
700	Cloud type
350	Normal leader type
160	Cloud type
150	Normal leader type
167	Normal leader type
270	Cloud type
150	Normal leader type

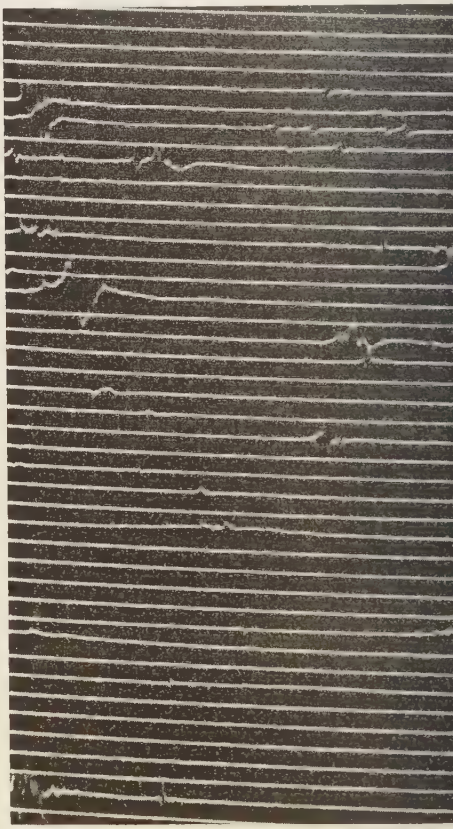

Fig. 14. The fast-antenna record of the initi part of a cloud discharge.

Approximately 6 per cent of the first leaders in ground discharges exhibited early parts similar to the initial portions of cloud discharges. It should be noted that the 6 per cent figure was derived from a relatively small sample of 80 ground discharges recorded during one thunderstorm season. The mean duration of the remaining 94 per cent of the leaders was found to be 4 msec.

In contrast with the present measurements, *Schonland* [1956] reported a time separation of about 50 μsec for radiation pulses from intracloud and cloud-to-air discharges and suggested that this pulse interval indicates extensive stepped-streamer processes. The appearance of 50-μsec pulse intervals from cloud strokes similar to the stepped-leader pulses is, as indicated earlier, relatively infrequent in New Mexico storms. A similar result, which also emphasizes the difference in the pulse intervals between intracloud and cloud-to-ground discharges, has been found by *Isikawa and Takagi* [1954] for storms in Japan.

The above mentioned differences between the initial portion of the cloud discharge and the first-leader field change of the ground discharge suggest that either (1) the mechanisms are entirely different (e.g., positive versus negative streamer processes) or (2) the mechanism is the same in both cases but is modified by certain environmental factors. These possibilities will be discussed in the following section.

Discussion of the results. The similarities and differences between cloud and ground discharges discussed in earlier paragraphs offer some clues as to the nature of the discharge processes within the cloud. The characteristic *J*-type field change of the cloud discharge suggests strongly that in its later stage the mechanism is very similar to that of the junction process of the ground discharge. Two main features of the junction process in a ground discharge should be emphasized at this point: (1) The *J*-process is characterized by a slow field change whose magnitude is in general smaller than the preceding *R* change, and (2) the discharge is assumed to take place between the tip of the ionized channel left by the previous return stroke and the nonconducting, neighboring charged region of the cloud. The junction streamers presumably start from the tip of the channel and penetrate into fresh regions of negative charge [*Malan and Schonland*, 1951].

The small magnitude and relatively quiescent and simple nature of these field changes (*J* and *J*-type) indicate that only limited regions of charge are involved. As is evident from the *J*-type portion of the field change shown in Figure 7, the *K* changes are usually unidirectional and well separated in time. This behavior is characteristic of both the *J*-type field change of the cloud discharge and the *J* and *F* field changes of the ground discharge.

In the earlier stage of the cloud discharge, especially in the very active portion, the field change exhibits constant pulse activity, with few or no quiescent periods. The polarity of the pulses exhibits no unidirectional tendency; negative and positive pulses appear throughout. This complex character is attributable to the simultaneous progression of many streamers, the existence of which may be interpreted as reflecting a complicated charge distribution in the cloud. This interpretation is consistent with the view that the charge distribution is closely connected with the cellular cloud structure [*Workman and Reynolds*, 1949*a*, *b*; *Kitagawa*, 1957*b*], in which the cells are estimated to be about 300 meters in diameter.

It was expected that the very beginning portion of the first-leader process associated with a ground stroke (the *B* or breakdown process) might reflect the same discharge characteristics as the process which produces the initial field-change portion during the course of the cloud discharge. This has been found not to be the case. The question arises as to why the characteristics of the initial portion of the first-leader process in a ground discharge should differ so markedly from the initial portion of the cloud discharge. Several possible reasons can be suggested:

1. The proximity of the ground may have an important influence on the initiation of a ground discharge, whereas its effect upon a cloud discharge may be negligible. In the case of first leaders of duration less than about 20 msec which approach ground with a uniform velocity (α-type leader), the effect of the ground is possibly important. As the leader approaches the earth, the electric field between the leader tip and the earth increases, thus enhancing the prob-

ability that the leader will contact the ground. But for most first leaders, whose velocities are nonuniform and usually greatest in the earliest stages (β-type leaders [*Schonland,* 1956]), the effect of the ground must be assumed to be negligible, at least during the initial breakdown portion.

2. Some investigators have considered the possibility that the proximity of a small positive charge located below the main negative charge and near the cloud base has an influence upon the nature of the early breakdown process in ground discharges. Such a charge distribution, it has been suggested, would account for some of the characteristics of the first-leader field changes [*Schonland,* 1956; *Loeb,* 1953; *Clarence and Malan,* 1957], as well as facilitate launching the stepped leader to ground. If we assume that all other conditions are constant, the effect of merely reversing the position of two charge centers does not offer, however, a reasonable explanation of the difference in discharge characteristics in the two cases.

An explanation of the marked difference between the initial breakdown processes may be sought in a detailed study of the meteorological environment in which the two types of discharges originate. For instance, the measurements of *Workman, Holzer, and Pelsor* [1942] and *Reynolds and Neill* [1955] indicate that the mean height of the dipole involved in intracloud discharges is located approximately 2 km above the mean height of negative charge centers involved in strokes to ground. This difference in height is equivalent, for New Mexico thunderstorms, to a temperature difference of about 12°C. The negative charge center involved in ground discharges is found to be, on the average, at a temperature of −6°C and at a height of 6 km (msl). For the center of the dipole involved in the intracloud discharge, the temperature is −18°C at a mean height of 8 km (msl). This large difference in the two temperature environments also leads to a large difference in the nature and population of precipitation elements and to an expected difference in the nature of the breakdown process, as will be shown.

From the work of *Macky* [1931] and the later work of *English* [1948] and *Loeb* [1953], it has been established that the presence of water drops considerably lowers the breakdown fiel necessary for the initiation of a discharge. Mack found that at atmospheric pressure the presenc of water drops of 1.4-mm diameter or greate reduced the breakdown field from a value o 30,000 v/cm for dry air to a value of 10,00 v/cm. It must be emphasized that the value o 10,000 v/cm for the breakdown field is applica ble only to a region of cloud in which wate drops of 1.4-mm diameter or greater are pres ent. For smaller droplets the minimum break down field increases; the smallest drop studie by Macky had a diameter of 0.85 mm, and th field necessary to produce a spark was 13,20 v/cm.

The cloud may be considered to be divide into two portions, that which lies above th −16°C isotherm and that which lies below i From the work of *Heverly* [1949] it appea that only droplets of 400-μ diameter or small will exist in liquid form at this temperature. A a temperature of approximately −18°C, th mean temperature location associated with clou discharges, only droplets smaller than 250 μ ca exist in liquid form. Thus, the breakdown fie value of 10,000 v/cm based on Macky's work valid only in the cloud region warmer tha −16°C. For the colder regions, it is not at a certain that the peculiar action of water dro in initiating lightning discharges is the contro ling factor.

In progressively colder regions of the clou the population of liquid water drops decreas in favor of the solid phase. It has been show by *Bandel* [1951] that, although negative an positive coronas from ice points are possibl the currents are exceedingly small. The coro currents are limited, of course, by the high r sistivity of ice. Similar measurements we carried out in these laboratories with the sam results. It appears, as *Loeb* [1953, p. 163] i dicated, that although 'ice points will probab contribute to some ionization in the cloud adequate electric stress . . . at fairly low fiel because of the sharp points . . . ice coronas w certainly not initiate discharge, as liquid wat does.' The absence of adequate numbers of lar drops of liquid water in the cold regions of th cloud should, for the above reasons, serious alter the manner and rate in which the dischar develops. The mean pulse interval during th

itial stages of cloud discharges was found to 680 μsec; the mean pulse interval for stepped ders to ground was 60 μsec. These values y well reflect the differences in the internal pedence of the region as determined by the rture of the precipitation elements in which oud and ground discharges are initiated. The rk of Macky needs to be extended to drop es considerably smaller than 250 μ, and to nperatures well below freezing, in order that te role of supercooled water droplets in a htning discharge may be evaluated. Such a ogram is now under way.

Summary. A cloud discharge manifests an rly and a late stage. The earlier stage is char- terized by intense and irregular pulse activity id by large, irregular electrostatic field changes, oth of which are indicative of a very compli- ted and nonhomogeneous charge distribution. he discharge mechanism of the later stage of ie cloud discharge is very similar to the junc- on process of the ground discharge.

The initial breakdown process of the cloud scharge is definitely different in nature from ie breakdown process which launches the epped leader and leads to a ground stroke. It suggested that the difference between the two itiation processes is directly attributable to the ifference in the relative concentration of water rops and ice particles as they affect the internal npedence of the highly charged regions of the loud.

Whether or not a discharge will reach ground r remain within the cloud is, surprisingly, al- eady determined in the first 10 msec of its xistence.

Acknowledgments. This work was supported y the Signal Corps of the U. S. Army and by a rant from the National Science Foundation. We re indebted to Dr. E. J. Workman for his sug- estions and advice throughout the course of the ork.

References

Bandel, H. W., Corona from ice points, *J. Appl. Phys., 22,* 984–986, 1951.

Clarence, N. D., and D. J. Malan, Preliminary discharge processes in lightning flashes to ground, *Quart. J. Roy. Meteorol. Soc., 83,* 161–172, 1957.

English, W. N., Corona from a water drop, *Phys. Rev., 74,* 179–189, 1948.

Heverly, J. R., Supercooling and crystallization, *Trans. Am. Geophys. Union, 30,* 205–210, 1949.

Isikawa, H., and M. Takagi, On the fine structure of atmospherics from near origins, *Proc. Research Inst. Atmospherics, Nagoya Univ.,* 1954.

Kitagawa, N., On the electric field-change due to the leader processes and some of their discharge mechanism, *Papers Meteorol. and Geophys. Tokyo, 7,* 400–414, 1957*a*.

Kitagawa, N., On the mechanism of cloud flash and junction or final process in flash to ground, *Papers Meteorol. and Geophys. Tokyo, 7,* 415–424, 1957*b*.

Loeb, L. B., Experimental contributions to the knowledge of charge generation, *Thunderstorm Electricity,* Univ. Chicago Press, Chicago, 150–192, 1953.

Macky, W. A., Some investigations on the deformation and breaking of water drops in strong electric fields, *Proc. Roy. Soc. London, A, 133,* 565–587, 1931.

Malan, D. J., Les décharges orageuses intermittentes et continues de la colonne de charge négative, *Ann. géophys., 10,* 271–281, 1954.

Malan, D. J., Les Décharges lumineuses dans les nuages orageux, *Ann. géophys., 11,* 427–434, 1955.

Malan, D. J., and B. F. J. Schonland, The electrical processes in the intervals between the strokes of a lightning discharge, *Proc. Roy. Soc. London, A, 206,* 145–163, 1951.

New Mexico Institute of Mining and Technology Reports, Thunderstorm electricity, *Signal Corps Research Proj. 172B,* no. 1, 1956; no. 7, 1957; Final report, 1959.

Pierce, E. T., Electrostatic field-changes due to lightning discharges, *Quart. J. Roy. Meteorol. Soc., 81,* 211–228, 1955.

Reynolds, S. E., and H. Neill, The distribution and discharge of thunderstorm charge-centers, *J. Meteorol. 12,* 1–12, 1955.

Schonland, B. F. J., The lightning discharge, *Handbuch der Physik, 22,* Springer Verlag, Berlin, 576–628, 1956.

Smith, L. G., Intracloud lightning discharges, *Quart. J. Roy. Meteorol. Soc., 83,* 103–111, 1957.

Sourdillon, M., Étude à la chambre de Boys de "l'éclair dans l'air" et du "coup de foudre à cime horizontale," *Ann. géophys., 8,* 349–364, 1952.

Workman, E. J., R. E. Holzer, and G. T. Pelsor, The electrical structure of thunderstorms, *Tech. Note Natl. Advis. Comm. Aeronautics, no. 864,* 1942.

Workman, E. J., and S. E. Reynolds, Electrical activity as related to thunderstorm cell growth, *Bull. Am. Meteorol. Soc., 30,* 142–144, 1949*a*.

Workman, E. J., and S. E. Reynolds, Time of rise and fall of cumulus cloud tops, *Bull. Am. Meteorol. Soc., 30,* 359–361, 1949*b*.

(Manuscript received November 16, 1959.)

Some Aspects of Lightning Activity and Related Meteorological Conditions

M. BROOK AND N. KITAGAWA

New Mexico Institute of Mining and Technology
Socorro, New Mexico

Abstract. Lightning statistics are used to define a thunderstorm activity index. The index is based upon (1) the total duration and (2) the frequency of occurrence of lightning discharges. It is suggested that the horizontal extent of a storm may be inferred from the shape of the frequency-distribution curve, whereas the mean duration of discharges is related to the vertical convective activity.

The bipolar thunderstorm model of Holzer and Saxon is extended to account for the occurrence of multiple discharges to ground. A relationship between the number of intracloud discharges and the total number of separate return strokes in ground discharges may be predicted from the model. Good agreement is found with the predictions in some, but not all, storms. Statistics are cited which suggest that the ratio of intracloud to cloud-to-ground discharges may reflect the type of storm (e.g., 'frontal' or 'local air mass').

Introduction. In the foregoing paper [*Kitagwa and Brook,* 1960] we discussed several pects of the fine structure of lightning discharges and indicated variations in the nature the electric field changes which may reflect ferences in the meteorological environment. the present paper we present statistical studwhich are concerned with some of the grosser pects of thunderstorm activity, and again we empt to relate electrical with meteorological rameters.

Electric-field and field-change measurements. he dual-record presentation of the slow and st field changes (described in the foregoing ticle) is uniquely suitable for the study of th the fine structure of lightning (resolution 300 μsec) and the chronology of electrical ents in a thunderstorm over a period of sevral hours. The fast-antenna record, with its gh amplification, is especially suitable for the easurement of lightning-stroke durations. *ierce and Wormell* [1953] have shown that the rliest part of electrostatic-field changes in htning discharges is most often slowly varyg; using very low frequency recording (down 1 cps), they were able to show that the duraon of the pre-return-stroke field change had reviously been grossly underestimated because he equipment had insufficient low-frequency sponse. Intense pulse activity, on the other hand, always accompanies the initial breakdown phase of a discharge when observed with wide-bandwidth, high-gain equipment [*Clarence and Malan,* 1957; *NMIMT,* 1958]. Indeed, the precise onset of lightning activity is detected more readily by the pulse activity on the high-frequency record than by the low-frequency record. The low-frequency record, at best, indicates a gradual change in slope, and the high-frequency record is superior with respect to defining the cessation of the lightning discharge [see Fig. 4 of *Kitagawa and Brook,* 1960]. The *K*-change pulses are detectable on the fast-antenna record after changes in slope on the slow-antenna trace are no longer recognizable. We now define the duration of a discharge as the time interval between the first burst of pulse activity and the last detectable *R*- or *K*-change pulse.

Total duration of lightning discharges. The distribution of durations for all types of lightning discharges (intracloud and cloud-to-ground) is shown in Figure 1. The curve represents data from 784 discharges. The median duration is 0.5 sec, a value twice as large as the 0.25 sec given by *Bruce and Golde* [1941], *Schonland* [1956], and *Pierce* [1955]. This large discrepancy can be attributed to differences in instrumental sensitivity and frequency response, as discussed in the preceding section. Inasmuch as the field change during the earlier part of the

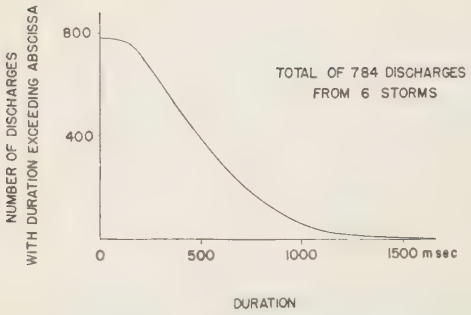

Fig. 1. Distribution of total durations for all types of lightning discharges.

discharge is generally larger than the final field change, the discrepancy is principally due to an underestimate of the duration of the final portion. In the present investigation, the final portions in both cloud and ground discharges v often exceed 200 msec.

Duration and frequency of discharges in dividual storms. Histograms showing the tribution of frequencies and durations of charges for three individual storms are sho in Figure 2. These storms were chosen beca they are representative of three degrees lightning activity from relatively isolated s tems. The active storm of August 30, 1957, p duced discharges with a mean duration of ab 0.7 sec; the greatest number of discharges curred within 10 sec of each other. In contra the storm of August 26, 1957 was a 'margir storm in which the mean duration of dischar was 0.3 sec, with no discharges occurring m often than one every 30 sec. The mean ti interval between discharges in the margi storm was greater than 1 min. The storm

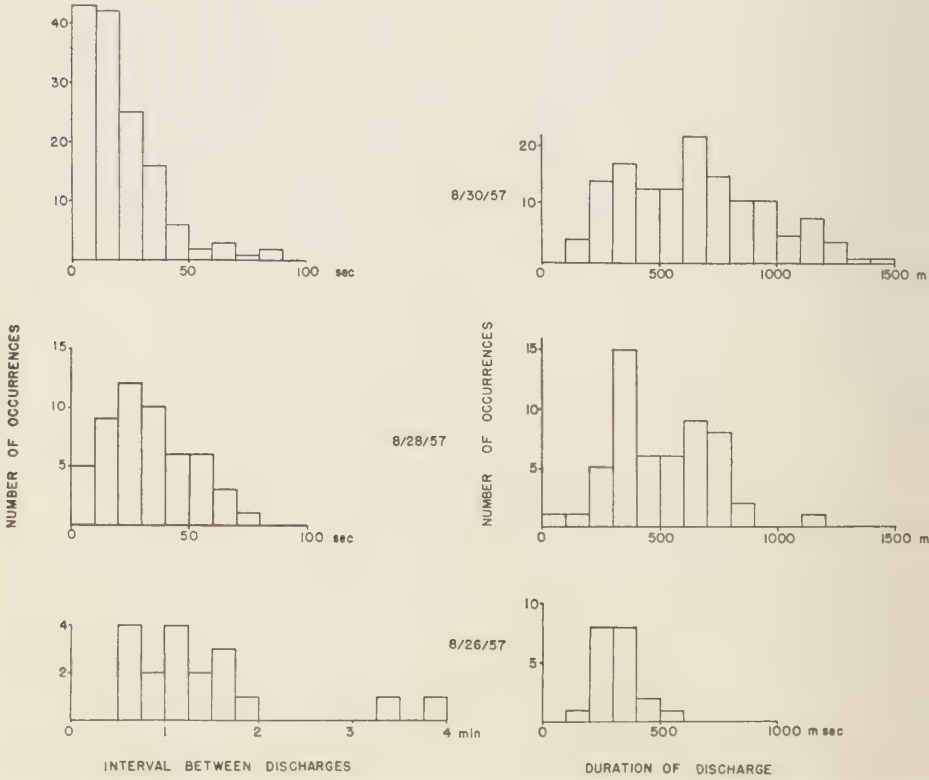

Fig. 2. Histograms showing distribution of frequencies and durations of discharges for three isolat storms.

gust 28, 1957, is representative of moderate htning activity and may be called an 'average' rm. The mean duration of discharges was 0.5 , and the most frequent time interval between em was approximately 30 sec.

For the three storms chosen, we note the following apparent relationship: The mean duration increases as the frequency of the lightning scharges increases. We suggest that the mean ration is proportional to the average amount charge Q involved in the discharges. The frequency of discharges, on the other hand, may influenced by two factors: the rate of charge paration in a single storm cell and the number independent storm cells in progress at any ven time. Thus, frequent lightning activity ay be produced by a very active single storm ll or by an aggregation of storm cells of small moderate activity.

The storms represented in the histograms of igure 2 were chosen because they were observed be isolated cloud systems of limited horizontal tent. For isolated storms the relationship mened earlier appears to hold: As the frequency lightning increases, the duration of the indidual lightning discharges also increases. It is be expected that the value of the measured rations will be influenced somewhat by the equency of the discharges if the time between scharges approaches a value comparable with e mean duration. Certainly, in the limit as e frequency increases indefinitely, individual events merge and we approach a 'continuous' discharge.[1] If a Poisson distribution about a mean duration of 0.5 sec and a high rate of occurrence of one discharge every 5 sec are assumed, calculations show that overlapping discharges affect the mean value of the measured durations by only 1 per cent. Consequently, for the values assumed, the frequency of occurrence and the durations may be considered statistically independent.

The histograms for the widespread storm of September 10, 1957, bear out the above conclusion (Fig. 3). We note the very high frequency of lightning discharges; yet the mean duration of discharges is 0.5 sec, which is the same as that for discharges from the average storm of August 28, 1957. We postulate, therefore, that *the shape of the frequency distribution curve is related to the horizontal extent of the storm.* In particular, if two storms which have the same values of mean discharge duration are compared, the median interval between discharges is an inverse function of the horizontal extent of the storm. The widespread storm of September 10 had a median interval of 7 sec between discharges, whereas the median interval for the isolated system of August 28 was 30 sec.

[1] Very high rates of lightning have been reported for Midwestern storms and for thunderstorm activity in the vicinity of tornadoes. Perhaps the 'continuous' lightning so reported is really an overlap in stroke durations, as discussed above.

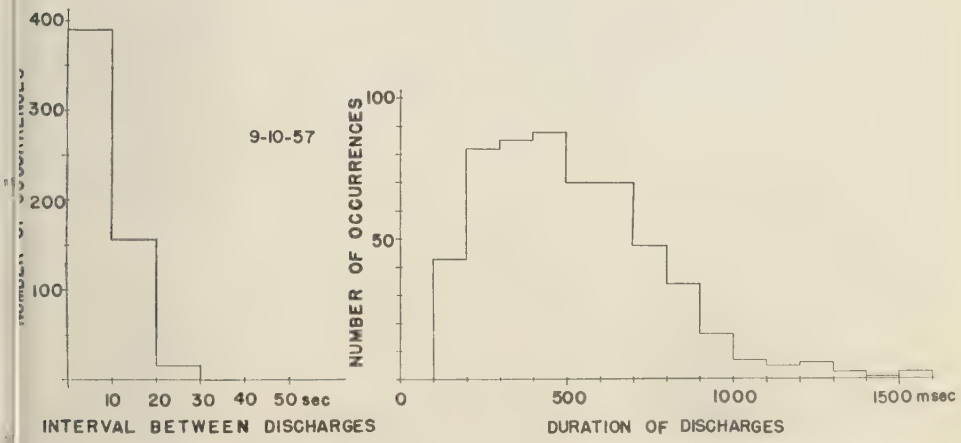

Fig. 3. Histograms of frequency and duration for the widespread storm of September 10, 1957.

From physical considerations the above postulate is quite reasonable. Single cells, such as occurred in the storm of August 26, have been observed to exhibit an active life of about 30 min. The activity from a single cell may vary considerably throughout its entire life cycle. Although the frequency of discharges may at times exceed 6 per min, usually there are intervals of time of the order of 1 min in which no lightning is produced. The lack of long time intervals in the frequency histogram of Figure 3 implies that many cells are active simultaneously. Thus, a narrow spread in lightning-discharge intervals implies a storm of large horizontal extent.

On the other hand, previous work [*Reynolds and Brook,* 1956; *Brook,* 1957; *Vonnegut, Moore, and Botka,* 1959] has demonstrated a direct relationship between vertical convection and electric fields in isolated thunderstorms. Although, as we have already shown, the frequency of observed lightning discharges is not a unique measure of the rate of charge separation in complex storm systems, it must certainly be a measure of the rate of charge separation in isolated storm systems. For isolated storms, the relationship between the frequency and mean duration of lightning discharges is apparent. We suggest, therefore, that the mean value of the duration is a measure of the extent and intensity of vertical convection.

Thunderstorm activity index. It is desirable that an over-all index of thunderstorm activity combine both the durations of individual discharges and the frequency of discharges. Such a combined index may be obtained if we plot the cumulative durations versus time for each 5-min interval of a storm. Figure 4 is such a diagram for the storms of August 26, 28, and 30 and September 10, 1957. The solid lines represent the total durations summed over each 5-min interval, and the dashed lines represent the sum of the number of discharges recorded during the same interval. (Note that the ordinates differ by a factor of 2. When the solid and dashed lines coincide, the mean duration during the interval is equal to 0.5 sec.)

It is obvious from the histograms in Figure 4 that the area under the curves is greatest for the storm of September 10. This, of course, indicates that the total amount of charge involved in discharges in this storm was greatest simply

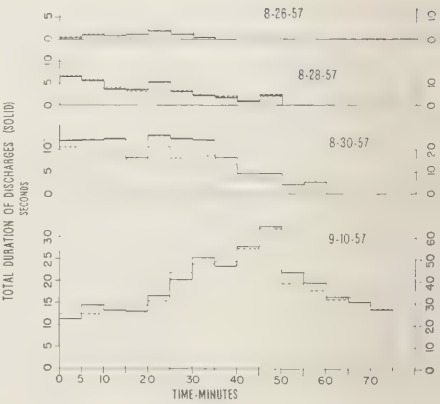

Fig. 4. Cumulative durations and cumulat number of lightning discharges versus 5-min ti intervals for four thunderstorms.

because of the preponderant number of d charges. The dashed lines are, on the avera the same distance below and above the so lines, indicating that the mean duration was sec. The specific intensity of electrical activ of all or any part of a storm might be defin as the average value of stroke duration for th interval; thus, a storm with mean duration 0.5 sec would have a specific intensity of On this basis, the specific intensity of the sto of August 30 was 0.7, whereas the specific tensities of the storms of August 26 and 28 a September 10 were 0.3, 0.5, and 0.5, respective The specific intensity may be particularly u ful when the activities of various portions of t same storm are compared. The total activity the storm is defined as the area under the h togram of the cumulative duration versus tir

In future studies we hope to relate the speci and total intensity to the precipitation int cepted at the ground. Some interesting corre tions have been made by *Israël and Tev* [1957] relating electrical activity and total ra fall.

Activity variations within a given storm. R ferring again to Figure 4, we note that t frequency of lightning discharges in the sto of August 26 increased steadily from the b ginning of the storm and reached a peak a proximately 25 min after the start of the el trical activity. A similar increase in activity to be noted for the storm of September 10

45 min after initial activity, followed by a dual decrease and a very abrupt cessation discharges. The storm of August 28, in con-t, exhibited the highest initial frequency of tning during the first 5 min of its life and reased essentially monotonically thereafter. storm of August 30 differed from the others hat the activity was virtually constant (ex-t for one 5-min interval) for about 30 min, reasing thereafter.

The histograms demonstrate that large varia-ns in the rate of occurrence and in the total nber of discharges may be expected within ngle storm; the specific intensity, however, as ined earlier, appears to be much less variable. suggest the use of the specific intensity as a tinguishing index of a thunderstorm.

Ratio of the number of intracloud to cloud-ground lightning discharges. Figure 5 shows

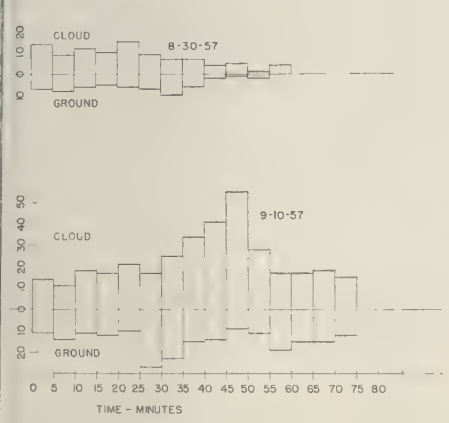

Fig. 5. Cumulative number of intracloud and oud-to-ground discharges versus 5-min time in-vals for the storms of August 30 and Septem-r 10, 1957.

o histograms in which the number of occur-nces of lightning, plotted against time, have en broken down to intracloud and cloud-to-ound discharges. In the histogram of August we again note the relatively constant rate at nich discharges occurred within the first 30 to min. The ratio of intracloud to cloud-to-ound discharges is approximately 1.5 and re-ains constant during the first 35 min, after nich time it is difficult to attach significance this ratio because of the small number of discharges involved. The number of discharges was far greater in the storm of September 10; here we see that the average ratio of intracloud to cloud-to-ground discharges was 1.5 during the first 25 min. At 25 min an abrupt change occurred in this ratio: from 25 min to 50 min, the ratio changed from less than 1 to very much greater than 1; from 55 to 75 min, the ratio was about 1. The histogram is particularly striking because it indicates three distinct phases of activity, each phase lasting some 25 to 30 min. These three phases of electrical activity are undoubtedly associated with thunderstorm cells whose lifetime is approximately 30 min [*Workman and Reynolds*, 1949]. The three phases of activity are separately characterized by an almost constant rate of lightning occurrence. The lower histogram shows an almost constant number of discharges for each of the 5-min intervals during the first 25 min; at the beginning of the second 25-min period the rate increased markedly, but the increased rate remained almost constant; in the last period, the number of discharges per 5-min interval decreased, but remained constant throughout that period. It appears, therefore, that the number of cloud and ground discharges in any period is not independent; an increase in cloud discharges is accompanied by a decrease in ground discharges. The interval from 25 to 50 min of the storm of September 10, 1957, is a good illustration of this behavior, inasmuch as the ratio of intracloud to cloud-to-ground discharges varied over a very wide range of values during this time, and the total number of discharges per 5-min interval remained essentially constant. The recognition of this variability casts some doubt upon the technique of estimating lightning activity (as was done recently in cloud-seeding programs) by counting only the total number of ground discharges.

Convective model of the negative column. Holzer and Saxon [1952] presented an analysis of a simple bipolar model of a thunderstorm in which conduction currents to and from the storm were included. A bipolar current generator within the cloud and a conductivity in the external atmosphere which varies exponentially with altitude were assumed in the model. On the basis of their analysis, a marginal thunderstorm is one in which the convection supply current

TABLE 1. Number of Intracloud Discharges, Cloud-to-Ground Discharges, and Component Return Strokes of the Storm of August 30, 1958

Time Interval		Number of Intracloud Discharges	Number of Cloud-to-Ground Discharges	Number of Return Strokes
From	To			
15 25 30	15 43 40	14	15	45
15 43 40	15 46 58	20	7	19
15 46 58	15 50 58	19	9	20
15 50 58	15 55 00	20	7	20
15 55 00	16 00 45	22	5	28
16 00 45	16 11 00	9	8	14
Totals		104	51	146

within the cloud just balances the loss due to conduction currents. If such a marginal situation is maintained, with no lightning, the lower negative charge becomes larger than the upper positive charge because of the increase in conductivity with altitude. Consequently, the electric field is no longer a pure dipole field, and the cloud now acquires a net negative charge. If a cloud stroke occurs, the system is left with a net negative charge $-q$, assuming that an amount of charge Q^- and Q^+ has been destroyed by the stroke. We have applied the above considerations to the marginal storm of August 26, 1957, as well as to some of the storms of 1958, in an attempt to account for the occurrence of multiple strokes in a discharge to ground.

We assume that the height of the current generator remains relatively stationary during a series of successive cloud discharges. If the time interval between discharges is sufficiently great, the regions of net negative charge (produced by the separate cloud strokes) will be separated in height by an amount approximately equal to the fall velocity of charge-bearing precipitation times the time between strokes. For example, if three cloud strokes occur approximately 30 sec apart, the regions of concentrated negative charge might be displaced by the amount of 30 sec $\times$ 10 m/sec, or 300 meters. If a cloud-to-ground discharge should now occur, we might look for this discharge to contain three return strokes, each originating in one of the regions of negative charge produced by the previous cloud strokes. It is most convenient in the above simple analysis to take the total charge volved in the cloud-to-ground discharge as $-$ This assumes that a net charge of $-q/n$ been involved in each of the n cloud discharg

An examination of the chronology of stro in the simple storm of August 26, 1957, rev that a total of 20 discharges was recorded, cloud discharges and 7 cloud-to-ground charges. There was little correlation between number of return elements in any one discha to ground with the cloud strokes which mediately preceded it. On the other hand total of 10 return strokes was involved (se rate R elements), as compared with 13 cl strokes. Thus, the agreement appears to better when we sum over the entire storm t it is between the individual ground strokes the preceding cloud strokes.

The chronology of the more active storm August 30, 1958, is very interesting. Table 1 summary of the number of cloud strokes, clo to-ground discharges, and component ret strokes for a number of time intervals cover the entire storm.

It can be seen from the totals in Table 1 t there is little correspondence between the val in the first and last columns. If we disrega however, the initial and final portions of storm, the correspondence is excellent. Omitt the first and last period, we obtain for the t in column 1, 81 cloud strokes, for column 2, cloud-to-ground discharges, and for column 87 return strokes.

On the other hand, the analysis of the sto of August 2, 1958, given in Table 2 shows real correspondence between columns 1 and

TABLE 2. Number of Intracloud Discharges Cloud-to-Ground Discharges, and Component Return Strokes of the Storm of August 2, 195

Time Interval		Number of Intracloud Discharges	Number of Cloud-to-Ground Discharges	Nu be o Ret Stro
From	To			
17 10 00	17 20 00	14	9	16
17 20 00	17 30 00	8	15	5
17 30 00	17 40 00	6	9	2
Totals		28	33	9

further check on the proposed relationship tween the number of cloud strokes and the nber of return strokes is made possible by the of two sets of independent measurements. In proposed model, the separation of regions negative charge S in a vertical column may computed by multiplying the time between cessive cloud strokes Δt_c by the fall velocity precipitation V_p. In addition, if these same ons of negative charge are involved in suc- ive return strokes, the time between return okes multiplied by the effective velocity of junction streamer V_j should also yield a value the separation S. Thus, $V_p \Delta t_c = S$, and $\Delta t_r = S$.

For V_p we choose the range 5 to 15 m/sec. e median time between discharges (moderate rm) is 30 sec. The above values yield $S =$ to 450 meters.

The average velocity of the junction streamer *honland,* 1956] is 2×10^4 m/sec, and the e between return strokes Δt_r falls most often the range 0.01 to 0.04 sec. From these values, obtain $S = 200$ to 800 meters. It is seen that the model a distance of separation consistent h the calculated value obtained from meas- ments of return-stroke intervals and junc- n-streamer velocities is predicted.

Figure 6 is a composite diagram of the field nge during the progress of thunderstorms er Japan. The figure is taken from the work *Tamura* [1940] and is used for comparison h our own data, the $\Delta F-$ field changes being erpreted as cloud discharges and the $\Delta F+$ ground discharges. Averaged over the entire rm, the number of cloud discharges exceeds number of ground discharges by a factor of Since the average number of return strokes r ground discharge is 3, we have here excellent reement with the proposed nonhomogeneous del of a negative column.

Pierce and Wormell [1955] classified the per- ntage of field changes from frontal and heat cal air mass) storms. The measurements at mbridge yield, for storms of the frontal type, per cent ground discharges and 71 per cent ud discharges. (The other 3 per cent could t be classified.) Again, multiplying the num- r of ground discharges by 3 to obtain the tal number of return strokes, we get 71 per nt cloud strokes as against 3×26, or 78 per

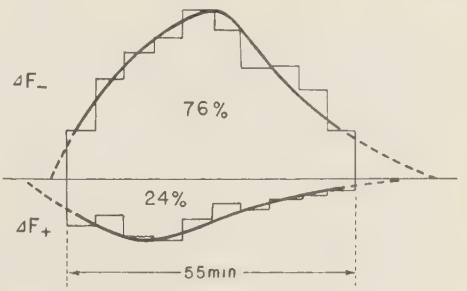

Fig. 6. Occurrence of intracloud and cloud-to-ground discharges versus time for 18 thunderstorms over Japan (from Y. Tamura).

cent, return strokes. Here again, the correspondence between the number of cloud strokes and return strokes is striking.

For the storms which *Pierce and Wormell* [1955] classified in the heat category, we find 46 per cent ground discharges as against 51 per cent cloud discharges. Thus, there appears to be a very definite distinction between frontal and local-air-mass storms. Further studies of the similarities and differences in lightning activity from these two types of storms are needed.

Conclusions. The authors are aware that the relationships suggested in this paper are based upon a relatively small and local sample of a very variable phenomenon. It is hoped that some of the relationship will be examined by investigators in other parts of the world.

Acknowledgments. The work described in this paper was supported by the U. S. Army Signal Corps and by a grant from the National Science Foundation. We are indebted to Dr. E. J. Workman for his suggestions and advice throughout the course of this work.

References

Brook, M., The relationship between the initial radar echo and the initial electric field in isolated thunderstorm cells, *Proc. Sixth Weather Radar Conf.*, Mass. Inst. Technol., Cambridge, 61–68, 1957.

Bruce, C. E. R., and R. H. Golde, The lightning discharge, *J. Inst. Elect. Engrs. London, 88,* 487–505, 1941.

Clarence, N. D., and D. J. Malan, Preliminary discharge processes in lightning flashes to ground, *Quart. J. Roy. Meteorol. Soc., 83,* 161–172, 1957.

Holzer, R. E., and D. S. Saxon, Distribution of electrical conduction currents in the vicinity of

thunderstorms, *J. Geophys. Research, 57,* 207–216, 1952.

Israël, H., and G. Tewes, Niederschlags- und Ladungsbildung in Gewitter, *Geofis. pura e appl., 37,* 197–204, 1957.

Kitagawa, N., and M. Brook, a comparison of intracloud and cloud-to-cloud lightning discharges, *J. Geophys. Research, 65,* 1189–1201, 1960.

New Mexico Institute of Mining and Technology Reports, Thunderstorm electricity, *Signal Corps Research Proj. 172B,* no. 8, 1958.

Pierce, E. T., Electrostatic field changes due to lightning discharges, *Quart. J. Roy. Meteorol. Soc., 81,* 211–228, 1955.

Pierce, E. T., and T. W. Wormell, Field changes due to lightning discharges in, *Thunderstorm Electricity,* edited by H. R. Byers, Univ. Chicago Press, Chicago, 251–266, 1953.

Reynolds, S. E., and M. Brook, Correlation of th initial electric field and the radar echo in thun derstorms, *J. Meteorol., 13,* 376–380, 1956.

Schonland, B. J. F., The lightning discharge *Handbuch der Physik, 22,* Springer Verlag, Ber lin, 576–628, 1956.

Tamura, Y., Charge distribution in thundercloud (in Japanese), *Chikyubutsuri, 4,* 181–226, 194(

Vonnegut, B., C. B. Moore, and A. Botka, Pre liminary results of an experiment to determin initial precedence of organized electrificatio and precipitation in thunderstorms, *J. Geophys Research, 64,* 347–357, 1959.

Workman, E. J., and S. E. Reynolds, Electrica activity as related to thunderstorm cell growth *Bull. Am. Meteorol. Soc., 30,* 142–144, 1949.

(Manuscript received November 16, 1959.)

Note on the Spectrum of Lightning in the Region 3670 to 4280 A[1]

L. WALLACE

Yerkes Observatory, University of Chicago
Williams Bay, Wisconsin

Abstract. Examination of the near-ultraviolet lightning spectrum has revealed the presence of the CN violet bands and a large number of unidentified features in addition to confirming most of the previous identifications.

INTRODUCTION

During the early evening of July 25, 1959, a well-exposed spectrogram, covering the range from 3670 to 4280 A, of an overhead lightning storm was obtained. The spectrogram, which was built up of the reflections, from clouds, of a large number of lightning strokes, was obtained in the third order of the 9-inch $f/0.8$ Schmidt-Cassegrain spectrograph at about 22 A/mm. (*Chamberlain* [1955] has previously described this instrument.) A review of the literature concerning the lightning spectrum in this region [*Dufay and Mao-Lin*, 1949*a* and *b*; *Dufay*, 1947 and 1949; *Israel and Wurm*, 1945; *Nicolet*, 1943; and several others referred to in these works] showed that, although a large number of features have already been identified, a comparably large number registered on this spectrogram have not previously been noted. This wealth of detail prompted the present investigation.

IDENTIFICATIONS

The wavelengths of the most easily measured features were determined in the usual manner by reference to an argon comparison spectrum. The results of these measurements and the identification of the features, using the works of *Moore* [1945] and *Pearse and Gaydon* [1950] as wavelength authorities, are summarized in Tables 1 and 2. Densitometer tracings of the spectrum are given as Figure 1. No characteristic curves were available for the determination of relative line intensities.

(*a*) *CN violet system.* Superposed on the very strong and highly developed 0-0 first negative N_2^+ band are a series of five features which can only be the $\Delta v = 0$ sequence of the CN violet system. Some of the heads of this sequence have been identified previously with N_2^+, but none with CN. The lower resolution of the previous work is undoubtedly the reason why this sequence has been overlooked. The difficulty in identifying the $\Delta v = -1$ sequence does not invalidate the identification of the $\Delta v = 0$ sequence, because the former is faint compared with the latter and probably is blended with other features.

(*b*) *N_2^+ first negative system.* The strong development of the N_2^+ sequences, noted in greatest detail by *M. Dufay* [1949], is not apparent on this spectrogram. The tail structure of the 0-0 band, however, is highly developed and is overlapped by the $\Delta v = 0$ sequence of the CN violet bands, the 0-2, 1-3, and 2-4 second positive N_2 bands, and a few other faint features. However, an estimate of the rotational temperature can be made from the observation that the average plate density in the region 3900 to 3905 A is the same as that in the region 3825 to 3835 A after allowance has been made for the faint feature at about 3825.5 A. The 3900 A region should be clear of any serious overlap, but the 3825 A region may be enhanced somewhat by the tail structure of the CN bands. By comparison, the contribution of the 1-1, 2-2, and 3-3 N_2^+ bands should be negligible. Within this limitation the intensity relations given by *Herzberg* [1950] and the rotational line wavelengths and constants given by *Childs* [1932] can be used to

[1] The research reported in this paper was supported by the Geophysics Research Directorate of the Air Force Cambridge Research Center, Air Research and Development Command, under Contract AF 19(604)-3044 with the University of Chicago.

TABLE 1. Identified Features

The identifications marked '?' are uncertain; the observed wavelengths marked 'd' are features that appear either diffuse or double.

λ_{obs}	λ_{lab}	Emitter
3709.8	3710.5	N_2 second pos. 2–4
54.6	55.4	N_2 second pos. 1–3
3804.0	3804.9	N_2 second pos. 0–2
30.	?30.4	N I, 11, $3s^2P$–$3p'\ ^2P^0$
50.3	50.9	CN violet 4–4
54.6	54.7	CN violet 3–3
61.0	61.9	CN violet 2–2
70.9	71.4	CN violet 1–1
83.0	83.4	CN violet 0–0
93.8	94.6	N_2 second pos. 3–6
3914.1	3913.5	N_2^+ 0–0
18.7	19.0	N II, 17, $3p^1P$–$3d^1P^0$
41.7	?43.0	N_2 second pos. 2–5
47.6	47.3	OI, 3, 3^5S^0–4^5P
55.4d	?55.9	N II, 6, $3s^3P^0$–$3p^1D$
73.0	73.1	N II, 38, $3d^3F^0$–$4f^3F$
83.0	82.3	N II, 38, $3d^3F^0$–$4f^3F$
94.9	95.0	N II, 12, $3s^1P^0$–$3p^1D$
98.4	98.4	N_2 second pos. 1–4
4025.5d	4026.1	N II, 40, $3d^3F^0$–$4f^1G$
4035.0	4035.1	N II, 39, $3d^3F^0$–$4f^3G$
41.3	41.3	N II, 39, $3d^3F^0$–$4f^3G$
43.8	43.5	N II, 39, $3d^3F^0$–$4f^3G$
58.7	59.4	N_2 second pos. 0–3
4100.1	4099.9	N I, 10, $3s^2P$–$3p'\ 2D^0$
09.9	4110.0	N I, 10, $3s^2P$–$3p'\ 2D^0$
37.4d	37.6	N I, 6, $3s^4P$–$4p^4S^0$
52.2	51.5	N I, 6, $3s^4P$–$4p^4S^0$
67.1	?67.8	CN violet 3–4
80.8	?81.0	CN violet 2–3
97.0	?97.2	CN violet 1–2
4216.1d	?4216.0	CN violet 0–1
	15.9	N I, 5, $3s^4P$–$4p^4P^0$
22.8	23.0	N I, 5, $3s^4P$–$4p^4P^0$
24.6	24.7	N I, 5, $3s^4P$–$4p^4P^0$
37.2	36.5	N_2^+ 1–2
41.4	41.8	N II, 47, 48, $3d^3D^0$–$4f^1F$, $4f^3F$
54.8d	54.7	N I, 4, $3s^4P$–p^4D^0
78.3	78.1	N_2^+ 0–1

obtain a rotational temperature. On the assumption that no correction for the CN bands is necessary, equal intensity in these two regions yields a temperature of 50,000°K. This temperature is no doubt falsified by the CN bands because the apparently rapid drop-off in intensity beyond about 3790 A (corresponding to $K = 60$ in the R branch) would not occur at 50,000°. Taking this drop-off into consideration, a maximum temperature seems to be around 30,000°. Adopting a further correction of a factor of 2 for the CN bands gives a temperat of 9300°, and a factor of 3 correction gi 5800°. Consequently, it appears that a ro tional temperature in the neighborhood of 6 to 30,000°K is valid for this band. It may that no single rotational temperature is a quate for the description of this band, but observations are not of high enough quality check on this possibility.

Confirmatory evidence for a high rotatio temperature is found in the ability to trace the rotational structure of the 0-1 band to = 50 (4159 A) in the R branch. The reg short of 4222 A is seriously overlapped w features other than the 0-1 band, however, a the intensities of the rotational lines depart c siderably from a regular variation. It is cl from the 0-0 band that the rapid fall-off in tensity beyond $K = 50$ should make the det tability of these lines in the 0-1 band diffic because of the overlapping features.

The N_2^+ 1-2 band head is clearly present, a the influence of its tail structure can be s in the augmented intensity in the region 42 to 4234 A and the gap in the region 4217 4221 caused by the perturbation at appro mately $K = 13$ in the $v' = 1$ level [*Coster a Brons*, 1932]. Another perturbation at appro mately $K = 39$ in $v' = 0$ [*Childs*, 1932] m

TABLE 2. Unidentified Features

The features marked 'd' are diffuse or double.

λ	λ
3888.5	4125.9
3924.6	29.3
89.0	33.4
4009.2d	40.8
15.3	44.2d
19.1	56.4
30.0	59.7
49.1	63.4
52.4	70.4
62.7	73.7
69.3	77.6
72.7	87.7
76.8	93.8
82.1	4200.0
86.5	06.0
90.2	09.1
4112.6	11.8
17.0	19.7
20.5	

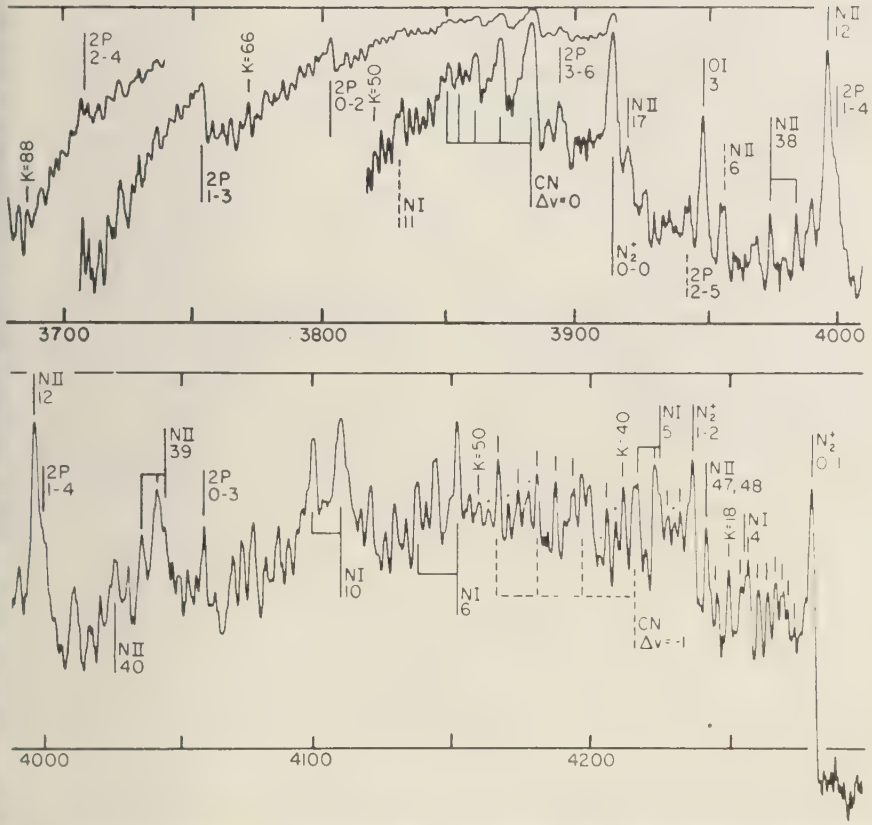

Fig. 1. Densitometer tracings of the spectogram. The labeled rotational lines refer to the R branches the 0–0 and 0-1 N_2^+ bands. The unlabeled short leading lines and full circles indicate rotational lines the 0–1 N_2^+ band with even and odd K, respectively.

the cause of the intensity minimum at 3897.6 in the 0-0 band P branch, but does not seem affect appreciably the 0-1 band P branch. he same perturbation in the R branches of ie 0-0 and 0-1 bands is masked by other atures.

(*c*) *Other molecular bands.* Beyond a few latively faint N_2 second positive band heads, other molecular constituents could be identi-ed, in spite of the presence of several groups features having the appearance of band ructure.

(*d*) *Atomic lines.* The identifications of the -4*p* and 3*s*-3*p*′ transition arrays constitute all ie would expect to find in this region from N I. he N II ion is quite well represented in this region by the 3*s*-3*p*, the 3*p*-3*d*, and the 3*d*-4*f* transition arrays. Only the 3947.3 A line of O I and no lines at all of O II could be identified with certainty.

Summary

The present work has confirmed the previously reported general characteristics of the lightning spectrum in this region—the intense N_2^+ bands with high rotational development, and the presence of neutral and singly ionized nitrogen and oxygen, the oxygen lines generally being weak compared with the nitrogen. The CN violet system represents the only new band system identified. Most of the identifications previously made have been confirmed. The use

of higher dispersion has required a long exposure over many lightning strokes, and, consequently, many of the features previously identified in spectra of single strokes could not be identified with certainty. The presence of a large number of faint lines not previously listed in the literature has been noted; few of them have been identified.

References

Childs, W. H. J., Perturbations and rotational constants of some first negative nitrogen bands, *Proc. Roy. Soc. London, A, 137,* 641–661, 1932.

Chamberlain, J. W., The ultraviolet airglow spectrum, *Astrophys. J., 121,* 277–286, 1955.

Coster, D., and H. H. Brons, Die negativen Stickstoffbanden, *Z. Physik, 73,* 747–774, 1932.

Dufay, J., and T. Mao-Lin, Recherches sur les spectres des éclairs, I, Étude des spectres, de 3830 à 6570 A, au moyen de spectrographes à fente, *Ann. géophys., 5,* 137–149, 1949*a*.

Dufay, J., and T. Mao-Lin, Spectres des éclai de 3830 à 6570 A, *Compt. rend., 228,* 330–3 1949*b*.

Dufay, M., Sur le spectre des éclairs dans l régions violette et ultraviolette, *Compt. ren 225,* 1079–1080, 1947.

Dufay, M., Recherches sur les spectres des éclai II, Étude du spectre dans les régions violette ultraviolette, *Ann. géophys., 5,* 255–263, 194

Herzberg, G., *Spectra of Diatomic Molecules,* 2r ed., D. Van Nostrand Co., New York, 658 p 1950.

Israel, H., and K. Wurm, Das Blitzspektrur *Naturwissenschaften, 29,* 778–779, 1941.

Moore, C. E., A multiplet table of astrophysic interest, revised ed., *Contrib. Princeton Uni Obs.,* No. 20, 1945.

Nicolet, M., Le spectre des éclairs, *Ciel et terr 95,* 91–98, 1943.

Pearse, R. W. B., and A. G. Gaydon, *The Ident fication of Molecular Spectra,* 2nd ed., Chapma and Hall, London, 276 pp., 1950.

(Manuscript received January 25, 1960.)

The Modes of Release of Available Potential Energy in the Atmosphere

BARRY SALTZMAN AND AARON FLEISHER

Department of Meteorology
Massachusetts Institute of Technology
Cambridge, Massachusetts

Abstract. We have obtained the space spectra of the fields of vertical motion and temperature in the free atmosphere for February 1959, and have estimated from these the conversions between available potential energy and kinetic energy as a function of wave number.

Introduction. Given the daily hemispheric fields of the thickness between 850 and 500 mb and the individual pressure change at 600 mb, we have calculated the following quantities: (*i*) the available potential energy as a function of wave number around latitude circles; (*ii*) the rate of conversion between potential and kinetic energy showing the effects of the mean meridional circulations and the eddy circulations of different scales.

The basic energy equations in which these quantities appear and discussions of their significance for the general circulation are given by *Lorenz* [1955], *White and Saltzman* [1956], and *Saltzman* [1957, 1958].

Formulas and data. We shall use these symbols:

λ = longitude
ϕ = latitude
p = pressure
t = time
n = wave number around a latitude circle
∇ = surface spherical gradient operator on an isobaric surface
ω = dp/dt = individual pressure change
w = vertical velocity
$\mathbf{v}$ = horizontal wind vector
T = temperature (deg Abs)
ρ = density
g = the acceleration of gravity
C_P = specific heat at constant pressure
R = gas constant

$$B(n, \phi, p, t) = (2\pi)^{-1} \cdot \int_0^{2\pi} T(\lambda, \phi, p, t)e^{-in\lambda}\, d\lambda$$

= complex Fourier coefficient for the temperature

$$\Omega(n, \phi, p, t) = (2\pi)^{-1} \cdot \int_0^{2\pi} \omega(\lambda, \phi, p, t)e^{-in\lambda}\, d\lambda$$

= complex Fourier coefficient for ω

$$[x] = (2\pi)^{-1} \int_0^{2\pi} x\, d\lambda$$

= zonal average of x

$$x' = x - [x]$$

= deviation from the zonal average

$$\{x\} = (\sin\phi_2 - \sin\phi_1)^{-1} \int_{\phi_1}^{\phi_2} x \cos\phi\, d\phi$$

= meridional average of x between latitudes ϕ_1 and ϕ_2

$$x'' = x - \{x\}$$

= deviation from the meridional average

$$\{[x]\}$$

= area average over a constant pressure surface

$$x^* = x - \{[x]\}$$

= deviation from the area average

$$\bar{x} = \tau^{-1} \int_0^{\tau} x\, dt$$

= time average (τ = length of record)

$$x''' = x - \bar{x}$$

$$= \text{deviation from the time average}$$

$$\sigma(x) = (\overline{x^2} - \bar{x}^2)^{1/2}$$

$$= \text{standard deviation}$$

$$\gamma = (\{[T]\} - p^{C_p R^{-1}} \partial\{[T]\}/\partial p)^{-1}$$

The total available potential energy per unit area per unit pressure difference is [*Lorenz*, 1955; *Saltzman*, 1957]

$$\mathbf{P} = \frac{C_P \gamma}{2g} \{[T^{*2}]\}$$

$$= P_Z + P_E$$

where

$$P_Z = \frac{C_P \gamma}{2g} \{[T]'^2\}$$

is the *zonal* available potential energy and

$$P_E = \frac{C_P \gamma}{2g} \{[T'^2]\}$$

is the total *eddy* available potential energy. The contribution to the total eddy available potential energy from temperature variations of wave number n is

$$\mathcal{P}(n) = \frac{C_P \gamma}{g} \{|B(n)|^2\}$$

which satisfies

$$P_E = \sum_{n=1}^{\infty} \mathcal{P}(n)$$

We call $\mathcal{P}(n)$ the 'spectral function' for eddy available potential energy.

The total rate of conversion from available potential energy to kinetic energy per unit area and per unit pressure difference is [*Lorenz*, 1955]

$$\mathbf{C} = -\frac{R}{pg} \{[\omega T]\}$$

The average is to be taken over a closed pressure surface (i.e., $\phi_1 = -\pi/2$, $\phi_2 = \pi/2$) and can be expressed as a sum of subaverages in the manner,

$$\mathbf{C} = C_E + C_Z + C_0$$

where

$$C_E = -\frac{R}{pg} \{[\omega' T']\}$$

is the rate of conversion from eddy available potential energy to eddy kinetic energy,

$$C_Z = -\frac{R}{pg} \{[\omega]''[T]''\}$$

is the rate of conversion from zonal available potential energy to zonal kinetic energy, and

$$C_0 = -\frac{R}{pg} \{[\omega]\}\{[T]\}$$

C_0 is identically zero, since

$$\{[\omega]\} = \int_0^p \{[\nabla \cdot \mathbf{v}]\}\, dp = 0.$$

In practice, we can measure these quantities over only a limited region of the globe (in our case, the belt between 20°N and 80°N). If, however, the region is large enough to capture most of the significant scales of variations of ω and T (as we believe is the case here) we can have confidence that the values obtained for C_E and C_Z are fairly representative of what would be obtained if the entire pressure surface were sampled. On the other hand, $\{[\omega]\}$ and hence C_0 need not vanish for such a limited region because of systematic variations of ω with latitude. Such a non-zero value of C_0, however valid for the particular region, cannot, a priori, be correct for the entire pressure surface. For these reasons we take as our estimate of $\mathbf{C}$ the measured value $(C_E + C_Z)$, which we denote by $\mathbf{C}_{\mathrm{EST}}$. We shall take up the question of representativeness again.

The quantity C_E can be expanded in terms of a spectral function measuring the rate of conversion from eddy available potential energy of a given wave number to eddy kinetic energy of disturbances of the same wave number [*Saltzman*, 1957]. This spectral function is

$$\mathcal{C}(n) = -\frac{R}{pg} \{\Omega(n)B(-n) + \Omega(-n)B(n)\}$$

which satisfies

$$C_E = \sum_{n=1}^{\infty} \mathcal{C}(n)$$

TABLE 1. Mean values and standard deviations of the zonally averaged individual pressure change $[\omega] = \Omega(0)$, in 10^{-4} g cm^{-1} sec^{-3}, and of the zonally averaged temperature $[T] = B(0)$, in deg Abs., both as a function of latitude, for February 1959 (Fig. 1)

ϕ	80	75	70	65	60	55	50	45	40	35	30	25	20
$\overline{[\omega]}$	−344	+43	−325	−781	−403	−300	+425	+782	+565	+643	+204	−300	−406
$(\pm)$	1167	957	795	1032	809	1276	845	1158	785	718	460	397	348
$\overline{[T]}$	244.01	245.59	247.13	248.62	250.26	252.19	254.62	257.71	261.61	265.74	269.77	273.37	276.88
$(\pm)$	1.68	1.02	1.04	1.06	1.03	1.06	1.06	0.73	0.56	0.15	0.23	0.42	0.55

The functions **P**, **C**, and their components were evaluated for the month of February 1959. The data comprised the 850- to 500-mb thickness in centimeters, denoted here by h, and the 600-mb individual pressure change ω in g cm^{-1} sec^{-3}, computed from the two-parameter, quasi-geostrophic, adiabatic, frictionless model of the Joint Numerical Weather Prediction Unit. We are indebted to the JNWP Unit for these data and to Mr. B. Lewis and Mr. V. Murino of the Extended Forecast Section of the U. S. Weather Bureau for the computer program that interpolates these quantities from the JNWP grid to intersections at every 5° of longitude and 10° of latitude from 20°N to 80°N. The computations began with a Fourier analysis of h and ω in 15 wave numbers around latitude circles.

The fields of both ω and the mean temperature equivalent to h were taken to apply in the vicinity of 600 mb. The hydrostatic approximation to the equivalent temperature is

$$T = 0.64 \times 10^{-3} h$$

We have set γ equal to 10^{-3} deg Abs^{-1}, which corresponds roughly to the normal value of $\partial\{[T]\}/\partial p$ at the midtroposphere.

The ω field and the available potential energy. (*a*) The ω field: The mean values and standard deviations of $[\omega]$ are given in Table 1 and Figure 1 as a function of latitude (a sine scale is used in all graphs having latitude as the abscissa). This is a representation of the monthly mean zonally averaged meridional circulation. Two large cells in low through middle latitudes and the suggestion of a third cell in high latitudes are visible. The maximum vertical velocity of these cells, computed from the approximate formula $w = -(\rho g)^{-1}\omega = -1.3\omega$, is about 0.1 cm sec^{-1}. This pattern resembles the picture of the mean meridional circulation first suggested by *Ferrel* [1856] and later modified by *Rossby* [1941]. Since heat sources and friction are not included in the computation of ω, the meridional cells obtained can only be the result of imbalances caused by meridional eddy transports of heat and momentum. However, if the direct forcing effects of the zonally averaged heat sources and friction were included, the

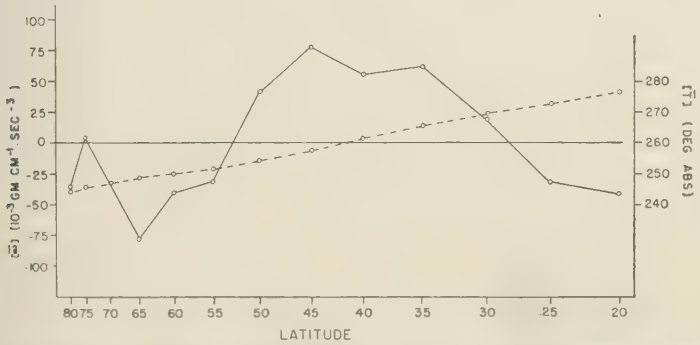

Fig. 1. Mean values of [ω] (solid curve) and of [T] (dashed curve) for February 1959. See Table 1.

TABLE 2. Mean values and standard deviations of the Amplitude Spectrum of the individual pressure change $2\,|\,\overline{\Omega(n)}\,|$, in 10^{-4} g cm^{-1} sec^{-3}, and of the temperature $2\,|\,\overline{B(n)}\,|$, in deg, around the three latitude circles, 30, 50, and 70°N, for February 1959 (Figs. 2 and 4)

		Wave Number, n														
	ϕ	1	2	3	4	5	6	7	8	9	10	11	12	13	14	15
	70	1661	1761	2189	2140	2034	1702	1322	1208	859	732	526	372	371	248	167
$2\,\lvert\overline{\Omega(n)}\rvert$	50	1526	1933	1669	2038	1502	2403	2660	3335	2892	2674	2198	1951	1606	1549	1413
	30	1163	1653	2098	1837	2613	2721	2588	2334	2690	2490	2113	2248	1969	1840	1998
	70	998	1069	976	1190	846	962	847	791	648	303	308	235	202	147	97
σ (±)	50	889	919	982	1264	1041	1112	1361	1888	1315	1888	1109	958	783	983	752
	30	662	924	968	848	1286	1112	1403	921	1218	1388	956	1201	964	1067	886
	70	4.03	6.21	1.78	1.45	1.22	0.78	0.49	0.39	0.33	0.22	0.14	0.13	0.08	0.07	0.05
$2\,\lvert\overline{B(n)}\rvert$	50	3.60	6.10	4.62	2.37	2.16	1.77	1.18	1.25	0.88	0.63	0.59	0.49	0.42	0.34	0.34
	30	2.86	2.25	1.71	1.53	1.04	1.59	1.07	0.95	0.69	0.67	0.48	0.43	0.29	0.37	0.26
	70	2.02	2.34	1.07	0.61	0.70	0.36	0.25	0.22	0.17	0.11	0.09	0.06	0.04	0.04	0.03
σ (±)	50	1.90	1.21	1.63	1.25	0.84	1.07	0.53	0.73	0.32	0.36	0.30	0.26	0.16	0.21	0.17
	30	0.92	1.08	0.73	0.53	0.53	0.65	0.41	0.39	0.33	0.39	0.23	0.22	0.15	0.20	0.13

results probably would not be changed very much [*Phillips*, 1954, 1956; *Kuo*, 1956].

The area under the curve in Figure 1 is proportional to $\{\overline{[\omega]}\}$, which we said should be zero for a closed pressure surface. Our value of $\{\overline{[\omega]}\}$ is slightly positive (+.0098 g cm^{-1} sec^{-3}) indicating a net mean sinking motion for the region of roughly 0.01 cm sec^{-1}. It would appear from Figure 1, however, that the systematic negative values which are likely to be found in tropical regions below 20°N would bring $\{\overline{[\omega]}\}$ closer to zero.

To obtain some idea of the eddy variations of the ω field the monthly mean amplitude spectrum of ω around three latitude circles 30, 50, and 70°N, and their standard deviations were computed and are listed in Table 2. A graphical representation is shown in Figure 2. Please observe that this and all subsequent spectra are line spectra. It is notable that in middle and low latitudes the contribution of the high wave numbers to the total zonal variability of ω is quite large. The mean zonal variance $\overline{[\omega'^2]}$ around all the latitude circles studied is given in Table 3 and Figure 3.

(*b*) The available potential energy: The mean values and standard deviations of the zonally averaged temperature around latitude circles are listed in Table 1. The graph of these data is shown in Figure 1. The monthly mean amplitude spectrum of T around three latitude circles, 30, 50, and 70°N, and their standard deviations are listed in Table 2, and a graphical representa-

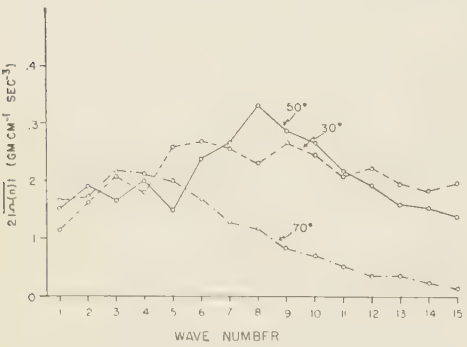

Fig. 2. Mean amplitude spectrum of the individual pressure change, $2|\Omega(n)|$, at the three latitudes, 30, 50, and 70°N, for February 1959. See Table 2.

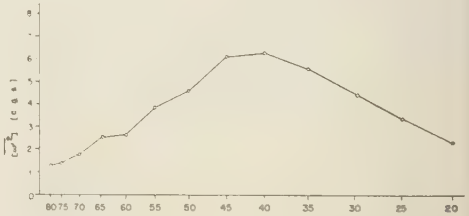

Fig. 3. Mean variance of the individual pressure change around latitude circles, $[\omega'^2]$, for February 1959. See Table 3.

TABLE 3. Mean values and standard deviations of $[\omega'^2]$ in 10^{-3} cgs units, $[T'^2]$ in deg^2, and $[\omega' T']$ in 10^{-3} g cm^{-1} sec^{-3} deg, as a function of latitude, for February 1959 (Figs. 3, 5, and 8)

ϕ	80	75	70	65	60	55	50	45	40	35	30	25	20
$\overline{[\omega'^2]}$	128	140	178	252	264	392	459	615	639	563	449	344	237
σ (±)	144	78	120	158	226	186	199	275	258	170	157	115	87
$\overline{[T'^2]}$	16.8	27.0	37.5	47.0	52.4	55.6	51.3	40.3	26.9	18.9	15.0	9.7	4.1
σ (±)	10.2	13.5	14.1	16.9	13.3	9.1	8.3	8.6	6.2	4.6	4.1	3.5	1.6
$\overline{[\omega' T']}$	−599	−530	−572	−700	−746	−1109	−854	−1156	−1105	−603	−337	−45	−41
σ (±)	995	482	706	457	540	687	648	568	576	418	291	210	167

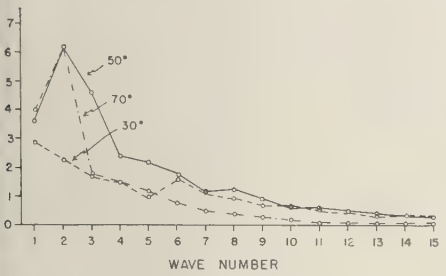

Fig. 4. Mean amplitude spectrum of the temperature, $2\overline{|B(n)|}$, at the three latitudes, 30, 50, and 70°N, for February 1959. See Table 2.

on is shown in Figure 4. The maximum zonal ariability occurs at the longer wavelengths and higher latitudes. The latitude dependence of ie zonal variability is more clearly evident in able 3 and in Figure 5, which gives the eridional profile of $[\overline{T'^2}]$.

The monthly mean values of $\mathbf{P}$, P_Z, P_E, and (n) and their standard deviations are given Table 4. Figure 6 is a graph of the mean ectral function $\overline{\mathcal{P}}(n)$. The largest store of vailable potential energy resides in the zonal omponent P_Z; the longer wavelengths (especially ave number 2, which is the scale of the major ontinents and oceans) contain most of the eddy available potential energy. We find that the mean total available potential energy is about 5 times as great as the total kinetic energy measured for the same region of the northern hemisphere [cf. *Lorenz*, 1955]. The largest contribution to $\bar{P}_E$ comes from variations of the temperature in middle to high latitudes (Fig. 5).

The energy conversions. The mean values of the conversion integrals C_Z, C_E, $\mathcal{C}(n)$, and $\mathbf{C}_{\text{EST}}$ and their standard deviations are listed in Table 5. Figure 7 is a graph of the spectral function $\mathcal{C}(n)$, showing the modes of release of eddy available potential energy. We have

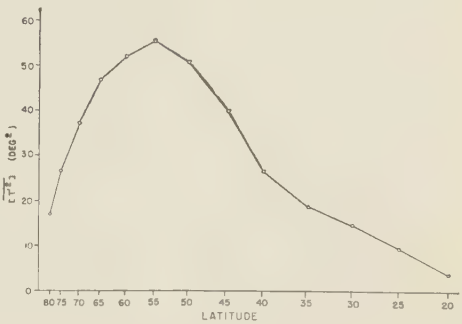

Fig. 5. Mean variance of temperature around latitude circles $[T'^2]$, for February 1959. See Table 3.

TABLE 4. Mean values and standard deviations of the total, zonal, and eddy available potential energy and of the spectral function for eddy available potential energy, in units of 10^3 ergs cm^{-2} mb^{-1}, for February 1959 (Fig. 6)

	$\bar{P}$	$\bar{P}_Z$	$\bar{P}_E = \sum_{n=1}^{15} \overline{\mathcal{P}}(n)$
	6903	5280	1623
σ (±)	402	333	151

n	1	2	3	4	5	6	7	8	9	10	11	12	13	14	15
$\overline{\mathcal{P}}(n)$	331	622	269	113	82	87	35	36	17	12	7	6	4	3	2
σ (±)	104	208	99	74	46	57	15	21	10	8	4	3	2	1	1

TABLE 5. Mean values and standard deviations of the rate of conversion from available potential energy to kinetic energy, in units of 10^{-3} ergs sec^{-1} cm^{-2} mb^{-1}, for February 1959 (Fig. 7)

	$\bar{C}_Z$	$\bar{C}_E = \sum_{n=1}^{15} \bar{c}(n)$	$\bar{C}_{E\,ST}$
	−196	+2878	+2682
σ (±)	567	715	...

n	1	2	3	4	5	6	7	8	9	10	11	12	13	14	
$\bar{c}(n)$	+210	+355	+181	+297	+317	+509	+251	+309	+184	+140	+42	+36	+16	+20	+
σ (±)	189	240	254	280	280	426	280	294	172	164	78	68	39	50	

defined these quantities so that a positive value signifies a conversion from potential to kinetic energy.

In accordance with the remarks made above, we take $(C_Z + C_E)$, given in the last column of Table 5, as the estimate of the net rate of conversion. This value is 2.682 ergs sec^{-1} cm^{-2} mb^{-1}, which agrees in order of magnitude with estimates of the rate of frictional dissipation made, for example, by *Brunt* [1941]. (The net conversion rate, in the long-time average, must be equal to the net rate of dissipation; see, for example, *White and Saltzman* [1956].) Almost all of this net conversion is due to the release of eddy available potential energy (+2.878 ergs sec^{-1} cm^{-2} mb^{-1}), the conversion of zonal available potential energy being an order of magnitude smaller and of opposite sign. (−0.196 ergs sec^{-1} cm^{-2} mb^{-1}). We recognize that these measurements do not properly weight the processes in low latitudes. To estimate the effect of this omission we have assigned to $[\bar{\omega}]$ a constant value (12.9×10^{-3} g cm^{-1} sec^{-3}) from 20°N to the equator, which makes $\{[\bar{\omega}]\} = 0$, and have extended the mean temperature profile linearly to the equator with the slope observed at 20°N.

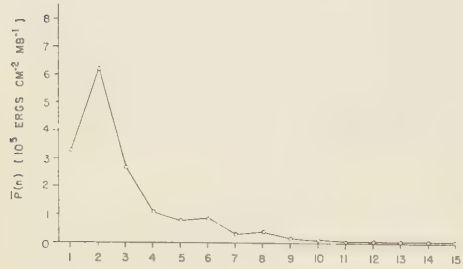

Fig. 6. Mean spectral function for eddy available potential energy for February 1959. See Table 4.

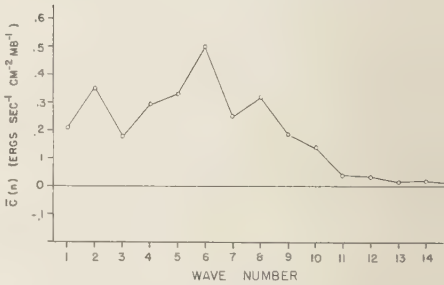

Fig. 7. Mean spectral function for rate of co version from eddy available potential energy eddy kinetic energy for February 1959. See Table

The value of C_Z that results from this mea field is +0.294 ergs sec^{-1} cm^{-2} mb^{-1}, which still 1 order of magnitude less than $\bar{C}_E$. Th suggests that, over the whole hemisphere, it primarily the large-scale eddy motions, rath than the zonally averaged motions, which gro directly at the expense of the available potenti energy [cf. *Starr*, 1954].

These results are substantially the same those obtained by *White and Saltzman* [195 using data from a more restricted region (t sector of the North American continent betwe latitudes 35°N and 60°N and between longitud 70°W and 120°W). Their values for $\bar{C}_Z$ and were larger but of the same sign as obtained he (−2000 × 10^{-3} and +6800 × 10^{-3} ergs sec cm^{-2} mb^{-1}, respectively). The larger value $\bar{C}_E$ is probably due to two factors: (1) compare with other sectors of the hemisphere, the Nor American sector is particularly active in t baroclinic development of eddies and (2) t data coverage for this particular sector is mu better than for the hemisphere as a whol permitting the use of 5° grid spacing in longitu and giving a more accurate representation of t

ller-scale cyclogenetic processes which prob-
y contribute to the over-all conversion rate.
e larger negative value of $\bar{C}_Z$ is a consequence
the fact that the region is located entirely
hin middle latitudes where the Ferrel cell
dominates, and hence includes little of the
itive energy-releasing effects of the Hadley
.

Although our coverage is much more extensive
n was the case in the study by White and
tzman, it is still deficient in the sense that
region is not 'closed,' as is evident from the
n-zero value of $\{[\bar{\omega}]\}$. The simple extrapolation
cribed above indicates that if latitudes down
the equator were sampled $\bar{C}_Z$ would become
itive, owing to the fuller inclusion of the
ect Hadley cell, but would remain small. The
crease of the eddy correlation between ω and
toward lower latitudes (Fig. 8) shows that
is slightly over-estimated on this account.
wever, the value of $\bar{C}_E$ may, on another
count, be somewhat underestimated as a
ult of the failure to include as detailed a
presentation of smaller-scale phenomena as
s done in the study by *White and Saltzman* [956]. It is also possible that positive contri-
tions could be made by scales of variations
ich are even smaller than those considered
either study (cumulus convection, for ex-
mple).

We emphasize that our measurements apply
ly to a single level in the mid-troposphere.
these measurements are to be a fair estimate
the rate of conversion for the entire atmos-
ere, we must assume that the events occurring
all other levels, weighted by mass and inte-
ated, would give very much the same result
at we obtain by taking the 600-mb level to
present the entire atmosphere. We think we
n assume that this is so. However, the dif-
rences at other levels are of interest. In the
ratosphere there is some indication of a reversal
the correlation between ω and T which gives
se to a small negative value of $\bar{C}_E$ [*White and olan*, 1960]. At lower levels, on the other hand,
e observed convergence into warm lows and
vergence from cold highs may be reflected in
higher correlation between ω and T than is
und in the mid-troposphere.

The spectral resolution of $\bar{C}_E$ is shown in
igure 7. For this month the kinetic energy of

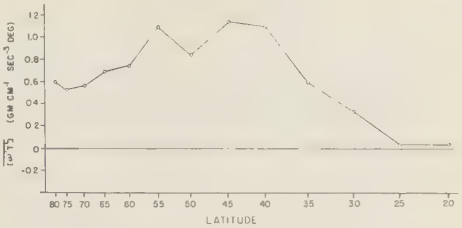

Fig. 8. Mean covariance between the individual pressure change and the temperature around latitude circles, $-[\omega' T']$, for February 1959. See Table 3.

eddies of all scales grows at the expense of available potential energy. Eddies of wave number 6 are most active, in general agreement with the linear theory of baroclinic instability which predicts a maximum growth rate for waves of roughly intermediate scale. The maximum conversion occurs from scales which store comparatively little available potential energy (Fig. 6). In the long run the total store of available potential energy must be maintained through generation by diabatic processes. It is of interest to know the modes of this generation and the manner in which the available energy is exchanged among the modes. The expressions for these processes have been discussed by *Saltzman* [1957].

The marked decrease in $\bar{C}(n)$ beyond wave number 10 may be due in part to lack of detail in the analysis of hemispheric charts. Concerning the long-wave end of the spectrum, Mr. A. Wiin-Nielsen has informed us that, when the diabatic component of the ω field is considered, a large reduction or even a reversal in the sign of $\bar{C}(n)$ probably occurs. If this is the case, these long waves must, on the average, obtain energy from the scales of motion which do have potential energy sources (for example, wave numbers 5 to 10) in order to overcome their losses through friction and by transfer to the zonal current [*Saltzman and Fleisher*, 1960]. A discussion of the nonlinear processes whereby such an energy transfer can occur was given by *Saltzman* [1959].

It is of interest to note the comparatively small standard deviation of the daily values of C_E from the monthly mean (Table 5). This is a reflection of the fact that the release of potential energy by the eddy circulations is a rather steady process, contrary to the often expressed

belief that this release is a more-or-less sporadic event after which the atmosphere 'coasts' barotropically for a comparatively long period. As it appears from these computations, some part of the atmosphere is continuously involved in overturnings which release energy at a fairly steady rate.

The computations reported here for the single month of February 1959 probably reveal most of the essential features of the long-time mean winter hemispheric fields of ω and T and of the conversion process. However, in order to establish greater significance for these statistics and to determine the seasonal variations, we plan to consider a longer record of data. It seems that most of the limitations of this study (the adiabatic method of computing ω, the incomplete sampling in the horizontal and the vertical, the exclusion of smaller-scale variations) will not be substantially removed in the very near future.

Acknowledgments. We thank the staff of the M.I.T. Computation Center for providing the IBM 704 computer time and for running our program, Lt. Col. P. D. Thompson, Mr. G. 'Arnason, Mr. L. Carstensen, Mr. A. Wiin-Nielsen, and Dr. G. Cressman of the Joint Numerical Weather Prediction Unit, and Mr. B. Lewis and Mr. V. Murino of the Extended Forecast Section, United States Weather Bureau, for their cooperation in securing the data and for supplying the information necessary for coding the problem.

During the time we were doing this work we learned that Mr. A. Wiin-Nielsen was engaged in a similar study. We are grateful to him for the opportunity to discuss the problem and to compare results.

This research was sponsored by the Geophysics Research Directorate, Air Force Cambridge Research Center, under Contract No. AF 19(604)-4958.

References

Brunt, D., *Physical and Dynamical Meteorology*, Cambridge Univ. Press, London, 1941.

Ferrel, W., Essay on the winds and ocean currents, *Nashville J. Med. and Surg., 11,* 287–301, 375–389, 1856.

Kuo, H.-L., Forced and free meridional circulations in the atmosphere, *J. Meteorol., 13,* 561–568, 1956.

Lorenz, E. N., Available potential energy and the maintenance of the general circulation, *Tellus, 7,* 157–167, 1955.

Phillips, N., Energy transformations and meridional circulations associated with simple baroclinic waves in a two-level, quasi-geostrophic model, *Tellus, 6,* 273–286, 1954.

Phillips, N., The general circulation of the atmosphere: a numerical experiment, *Quart. J. Roy. Meteorol. Soc., 82,* 123–164, 1956.

Rossby, C.-G., The scientific basis of modern meteorology, *Climate and Man: Yearbook of Agriculture,* U. S. Govt. Printing Off., Washington D. C., 38–55, 1941.

Saltzman, B., Equations governing the energetics of the larger scales of atmospheric turbulence in the domain of wave number, *J. Meteorol., 14,* 513–523, 1957.

Saltzman, B., Some hemispheric spectral statistics, *J. Meteorol., 15,* 259–263, 1958.

Saltzman, B., On the maintenance of the large-scale quasi-permanent disturbances in the atmosphere, *Tellus, 11,* 425–431, 1959.

Saltzman, B., and A. Fleisher, Spectrum of kinetic energy transfer due to large-scale horizontal Reynolds stresses, *Tellus, 12,* in press, 1960.

Starr, V. P., Commentaries concerning research on the general circulation, *Tellus, 6,* 268–272, 1954.

White, R. M., and G. F. Nolan, A preliminary study of the potential to kinetic energy conversion process in the stratosphere, *Tellus,* in press, 1960.

White, R. M., and B. Saltzman, On conversions between potential and kinetic energy in the atmosphere, *Tellus, 8,* 357–363, 1956.

(Manuscript received December 28, 1959.)

The Effect of Meteorological Variables upon the Vertical and Temporal Distributions of Atmospheric Radon

HARRY MOSES,[1] ANDREW F. STEHNEY,[2] HENRY F. LUCAS, JR.[1]

Argonne National Laboratory
Lemont, Illinois

Abstract. Hourly values of radon concentrations were obtained simultaneously at four levels above ground up to 39.9 meters on the Argonne Meteorology Tower on three separate days. Twenty-seven consecutive hourly measurements were made on the first two days, and 17 on the third. Radon samples were obtained by adsorption on activated charcoal and were measured by means of scintillation counters. This technique, developed at Argonne, allowed direct measurement of radon instead of the common procedure of calculating radon values from measurements of daughter products.

The large amount of meteorological data routinely obtained at the Argonne Meteorology Laboratory makes it possible to carry out detailed case studies on the relationship between radon concentration and the meteorological variables. This work has provided information on the heterogeneity of the horizontal distribution of radon. An inverse fumigation phenomenon was also observed. Under very stable nighttime conditions with light winds the radon concentrations observed at the top of the tower remained very low—about the same as during the daytime. Shortly after sunrise, with an increase in vertical mixing, the concentrations rose sharply. At a height of about 5.72 meters the radon concentrations on the clear nights were larger by a factor of 20 than concentrations on the clear days. During cloudy conditions nighttime values were about twice as large as daytime values.

INTRODUCTION

Ever since *Elster and Geitel* [1901] reported that the atmosphere contains radioactive substances, investigators have measured the content of radon and radon daughters in the lower atmospheric layers. Much of this work was done by German investigators during the first half of this century, but within the last decade interest in problems associated with radioactive fallout has given new impetus to the study of atmospheric radioactivity in this country. Many of the fundamental relations between meteorological variables and radon concentrations were treated in the early work. Some types of data on radon concentrations are extremely rare. An example of this is data on hourly vertical concentration gradients.

It is commonly agreed that radon observed in the lower layers of the atmosphere comes from the soil. The concentration of atmospheric radon at any location is a function of the following factors: (1) the emanation rate from the soil, (2) the atmospheric diffusion rate, (3) the advective rate, that is, the rate at which radon is brought in over the station by the horizontal component of the wind, and (4) the radioactive decay rate. The first three factors are markedly influenced by meteorological variables.

For a vertical air column of unit cross-sectional area a balanced equation for radon concentration under steady-state conditions may be written as

$$\int_0^\infty [\bar{\mathbf{V}}\cdot\nabla_h N + \nabla_h\cdot K\nabla_h N]\, dZ + E = \int_0^\infty \lambda N\, dZ$$

where Z equals height; $\bar{\mathbf{V}}$ equals the mean wind velocity; ∇_h is the horizontal operator, $\mathbf{i}(\partial/\partial x) + \mathbf{j}(\partial/\partial y)$; K is the eddy diffusion coefficient; N is the concentration of radon per unit volume; E is the emanation rate; and λ is the radioactive decay constant.

The term $\bar{\mathbf{V}}\cdot\nabla_h N$ represents the radon brought in or removed from the sides of the column by advection, and the term $\nabla_h\cdot K\nabla_h N$ represents the amount of radon entering or leaving the sides by eddy diffusion. During a

[1] Radiological Physics Division.
[2] Chemistry Division.

major portion of the time these terms are very small.

Much remains to be learned about the mechanisms which remove radon from the soil. For example, the effect of atmospheric pressure changes is considered important by some [*Lester,* 1925; *Wright and Smith,* 1915] and discounted as unimportant by others [*Baver,* 1956]. The effect of wind speed or soil temperature gradients is also in need of further investigation. It is commonly agreed that rainfall retards the emanation of radon by clogging the capillary pores in the soil, but insufficient data are available to establish quantitative relationships between rainfall or soil moisture and the diminution of radon emanation.

The vertical diffusion rate of radon in the atmosphere is primarily determined by wind speed, atmospheric stability, and surface roughness. An added complicating factor was suggested by *Israel* [1951]. He pointed out that radon may become adsorbed on particulates, and therefore the vertical distribution of radon would be influenced by particle pickup, velocity of fall of particles, or upwind sources of particles.

Previous investigators [*Becker,* 1934] have shown that the trajectory of the air influences radon concentration at a point. However, the emphasis has been on the differences between air of continental and air of maritime origin. The data presented below indicate that substantial horizontal discontinuities may occur in air which has had a land trajectory only.

Three case studies of the variation of radon concentrations from hour to hour at four different levels above ground are presented in this paper. The Meteorology Tower at the Argonne National Laboratory was used as a platform for measurements of radon up to 39.9 meters. Also available for use in this investigation is the rather large amount of meteorological data routinely taken by the Meteorology Group at the laboratory. The first two studies occurred on days when there was strong daytime heating accompanied by pronounced nocturnal radiation. The third study was made on a cloudy day. Difference in types of days is patently shown in the patterns of radon concentration.

In these studies only radon was measured, rather than a combination of radon and daughter products, as was considered by other investigators. Since radon has a half-life of 3.825 days, it may be considered a conservative constituent of the atmosphere for short-period studies and may serve as an excellent tracer of air motions by showing rates of diffusion. It is superior to moisture, for example, which may undergo a change in phase from gas to liquid.

Radon and Its Decay Products in the Atmosphere

The radioactive decay of Rn^{222} leads to several shorter-lived species (the daughter products) whose half-lives and main modes of decay may be indicated as follows:

$$Rn^{222} \xrightarrow[3.825\ d]{\alpha} Po^{218} \xrightarrow[3.05\ min]{\alpha} Pb^{214} \xrightarrow[26.8\ min]{\beta}$$

$$Bi^{214} \xrightarrow[19.7\ min]{\beta} Po^{214} \xrightarrow[1.5 \times 10^{-4}\ sec]{\alpha} Pb^{210}$$

Although Pb^{210} is also radioactive, its half-life of 22 years is long compared with its residence time in the atmosphere, and the activity of Pb^{210} remains 2 to 3 orders of magnitude smaller than that of radon in air. On the other hand, the activity of the shorter-lived species approaches that of radon. These daughter products tend to become attached to particulate matter which may be filtered from an air stream or precipitated electrostatically. Thus, a measure of the concentration of radon in air may be obtained by collection of the daughter products and observation of alpha particles emitted from Po^{214} and Po^{218} or of beta particles from Pb^{214} and Bi^{214}. Such procedures have been successfully used in monitoring air for radiological protection [*Harley,* 1953; *Tsivoglou, Ayer, and Holaday,* 1953] and in obtaining a continuous record of atmospheric radioactivity [*Gale and Peaple,* 1958; *Wilkening,* 1959]. However, the numerous variables which enter into the relationship between the counting rates of collected particulate matter and radon in air make it difficult to obtain great accuracy for radon or reliability during atmospheric changes. The more direct procedure of collecting radon gas and measuring its activity was used here.

A brief discussion of the variables involved

n measurements of radon from daughter products is given here to indicate why this method s not considered suitable for the present work. n making the necessary calibration measurements and derivations of radioactive decay ormulas, the concentration of radon at a point n air is assumed to be constant, and the following factors, listed somewhat chronologically, nust be known or reproducible:

1. The degree of radioactive equilibrium between radon and its daughter products.
2. The uniformity of attachment of daughter products on particulate matter.
3. The efficiency of collection of daughter products.
4. The degree of saturation of daughter products on the collection medium attained at a known rate of sampling of air for a known period of time.
5. The relative activities of the daughter products at the time of counting.
6. The efficiency with which alpha or beta particles, or both, are counted.
7. The concentration of other airborne sources of radioactivity, such as thoron and radioactive fallout material from bomb debris.

In principle, the counting rate to be expected for a particular set of conditions may be calculated exactly, although the formulas involving several decay constants and efficiency factors may be somewhat complicated. In practice, some calibrations with known amounts of radon or of the daughter products are necessary, the most direct procedure being measurement of the concentration of radon in the air being sampled and comparison with the counting rate obtained from a well-defined procedure of collection and counting of daughter products. Such calibrations are valid only for the set of conditions existing at that time, and the extent of variation of such conditions is of interest.

Items 1, 4, and 5 relate primarily to the decay constants of the daughter products and the time sequence of the measurement. Sudden changes in the radon content of the air would cause these factors to vary from their standard values, with a subsequent error in interpretation of counting rates. Since instances were found in this work in which the concentration of radon changed as much as fourfold in consecutive measurements 1 hour apart, estimates were made of the errors that would be introduced by a sudden increase in radon content. Calculations[3] were made of the fraction of the increase which would be observed at later times if the radon concentration had been constant at its previous level for several hours and collection of daughter products continuous during the entire period under consideration. If the change were initially unaccompanied by a similar increase in daughter products, only 24 per cent of the increased radon concentration would be apparent if the alpha particles were counted on the collector after 30 minutes, and 42 per cent after 60 minutes. For beta particles, one would observe 21 per cent of the increase after 30 minutes and 40 per cent after 60 minutes. These results were calculated for the case of counting daughter products as collected; similar percentages would be obtained if counting were done 30 minutes after collection.

The somewhat more complicated calculations corresponding to a linear increase of radon content should provide similar values for the percentage of increase observed at the end of an hour, because an abrupt change in the middle of the period is a sufficiently close approximation to a continuous rise over a period of 1 hour for Pb^{214} and Bi^{214}; the shorter-lived Po^{218} would be close to equilibrium at the final level of radon in either case.

A change in radon concentration accompanied by a corresponding change in daughter products would be more quickly reflected in the counting rates as a simple build-up of daughter products on the collector. For counting of either alpha particles or beta particles, collection periods of 30 minutes and 60 minutes would provide ap-

---

[3] The formulas used for these calculations are

$$A_n = R A_1^{\,c} \sum_{j=2}^{n} \left[\tau_j - (T) \prod_{\substack{k=2 \\ k \neq j}}^{n} \frac{\lambda_k}{\lambda_k - \lambda_j} e^{-\lambda_j t} \right]$$

for $n = 2, 3, 4,$

where $T = \tau_j + t$ for the case of daughter products absent at $t = 0$, and $T = \tau_j$ for the case of daughter products in equilibrium at all times.

Subscripts 1, 2, 3, and 4 refer to Rn^{222}, Po^{218}, Pb^{214}, and Bi^{214}, respectively; A_n = activity of the nth nuclide on the filter at time t; R = volume rate of filtering; $A_1^{\,c}$ = activity of radon per unit volume of air; and τ_j = mean life of jth nuclide $= 1/\lambda_j$. At start of filtering, $t = 0$.

proximately 45 per cent and 70 per cent, respectively, of the increase in activity which would be observed for collection to saturation. If the technique applied involved filtering for only 1 hour, then, of course, the daughter products on the filter would reach the full value of the activity corresponding to the new level of radon 1 hour after the change occurred. This case of a sudden change of both radon and daughter products is evidently the situation for which *Gale and Peaple* [1958] calculated almost 100 per cent detection 1 hour after a sudden change in radon for filtering periods of 1 hour.

Although it is generally assumed that radon and its daughter products are in equilibrium under 'normal' conditions in the atmosphere, Gale and Peaple did find nonequilibrium (of nonspecified degree) in 3 out of 10 samplings by a procedure which would not have revealed small deviations from equilibrium. It appears likely that changes in the radon content of the atmosphere will be accompanied by corresponding changes in the daughter products when a new mass of air moves into the sampling zone. However, this may not be so in the important case of a change from unstable to stable atmospheric conditions in which the vertical transport rate of radon decreases. Radon then accumulates near the ground surface from which it emanated and is presumably deficient in daughter products.

The factors listed as 2, 3, and 6 above are necessarily interrelated because the size and concentration of the particulates in air and the type of collection medium will affect both the retention efficiency for daughter products and the efficiency with which radiations (particularly the easily absorbed alpha particles) from the accumulated products will be counted. Some indication of incomplete or nonuniform attachment of daughter products on particulates has been reported [*Gale and Peaple*, 1958], but studies of this nature indicate an acceptably reproducible distribution of daughter products on filterable particulate matter (±20 per cent) for a given set of atmospheric particulate conditions [*Gale and Peaple*, 1958; *Harley*, 1953]. On the other hand, *Harley* [1953] found that for Whatman 41 filters the retention and counting efficiency of radon daughter products, under low particulate conditions, was only 20 per cent of that for normal or high particulates; even with molecular filters, a twofold reduction in over-all efficiency was noted. *Wilkening* [1952, 1959] reported very little about the efficiency or reproducibility of his electrostatic precipitation system, but it is noteworthy that he considered radon concentrations obtained from a sampling point 0.8 meters above ground surface to be the same as those at ground surface [*Wilkening*, 1959]. Data presented in this paper show radon concentrations at ground surface to be 2 to 5 times greater than those at 1 meter. It is at just these lowest levels that one might expect the greatest differences in degree of saturation of daughter products on particulates.

Little need be said about interference from sources of radioactivity in the atmosphere (item 7) when collection periods of less than an hour are employed. The counting rate of thoron daughter products is only a small percentage of that of the radon chain, and fallout activity is even smaller except for brief periods in which interference from bomb debris should be recognizable.

To sum up the very general discussion above, the various investigators appear to be justified in concluding that radon concentrations well within a factor of 2 of the correct value are usually deduced from measurements of daughter products. Furthermore, measurements of particulate activity as such may have valuable meteorological applications, but the reliability of these techniques in measuring radon as an atmospheric tracer for short-term changes is open to question.

In the present work, it was necessary to obtain accurate values of radon concentration in air at known times for detailed comparison with meteorological variables. The apparent uncertainties in relating counting rates of collected particulate matter to radon in air led to a preference for the more direct procedure of collecting radon gas and measuring its activity. This appears to be the first detailed study of radon in air in which such a procedure was used.

Experimental Technique

Twenty-minute averages of radon concentrations were obtained during the three periods: 0900 May 20 to 1110 May 21, 0950 July 16 to 1210 July 17, and 1550 August 27 to 0810

TABLE 1. Summary of Times and Heights above Ground of Radon Measurements

Experiment	Date and Time Began	Date and Time Ended	No. of Samples	Levels Sampled 0.32 cm	0.97 m	5.72 m	23.8 m	39.9 m
I	0900 5/20/58	1110 5/21/58	27		X	X	X	X
II	0950 7/16/58	1210 7/17/58	27	X*	X	X		X
III	1550 8/27/58	0810 8/28/58	17	X	X		X	X

* Measurements during the first three periods were at 6.35 cm.

August 28. Most of the measuring periods began at 10 minutes before the hour and ended at 10 minutes after the hour. Measurements were made at 0.32 cm, 0.97 meters, 5.72 meters, 23.8 meters, and 39.9 meters above the ground except in one run in which three measurements were made at 6.35 cm above the ground. Dates, hours, and levels sampled are summarized in Table 1.

Radon Measurements

The radon concentration in the air from each level was obtained by drawing air through 6.4- and 9.5-mm copper tubing, attached to the Meteorology Tower and leading to a small shack located beside the tower. The radon in the 50 to 100 liters of air per sample was quantitatively absorbed on 7 grams of cooled, activated cocoanut charcoal as shown schematically in Figure 1.

In this system the Drierite-Ascarite column removed water and CO_2 from the air, and the two dry-ice-cooled, dip-type freeze traps removed the final traces of water. The water and radon traps were immersed in a dry-ice-cooled 1:1 mixture of carbon tetrachloride and chloroform. Under these conditions the radon was quantitatively retained by the activated cocoanut charcoal [*Stehney and others,* 1955]. The volume of each sample was measured with a wet-test meter,[2] and corrections to standard conditions (STP) were made. The volume of each sample was obtained to an accuracy of 0.3

[2] Precision Wet Test Meter, Fisher Scientific Company, 217 Forbes Street, Pittsburgh 19, Pennsylvania.

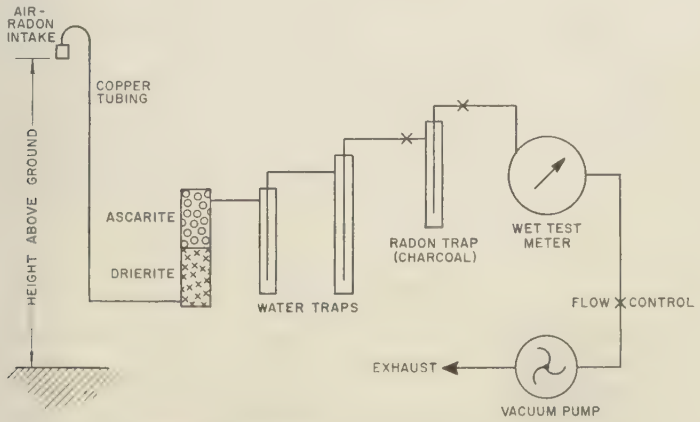

Fig. 1. Diagram of apparatus for collection of radon on charcoal.

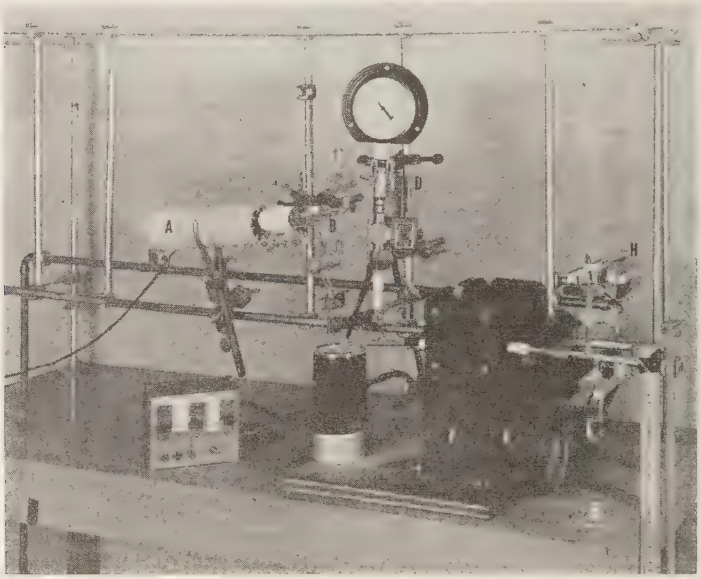

Fig. 2 System used to transfer radon from charcoal to radon counter bottle.

per cent or better. The wet-test meter dials were photographed to minimize reading errors.

The charcoal (radon) trap was removed from the sampling apparatus and taken to the laboratory for analysis. In the analysis procedure the charcoal trap containing the radon sample was evacuated in a 5-minute interval to about 0.03 mb while immersed in a dry-ice-cooled bath. Loss of radon was less than 0.3 per cent. The trap was then placed in the system shown in Figure 2 and the radon was transferred to the counter by the following procedures. The charcoal trap (B) was heated for 5 minutes by the furnace (A) at 500°C. Meanwhile, the transfer line and radon counter were flushed with helium and then evacuated. A 15-cm^3 portion of helium from reservoir (D) was then added to the charcoal trap. Pump (F)[3] transferred approximately 90 per cent of this helium carrier gas to the counter (H) in 1 minute. Since the volume of the counter is 96 cm^3, about 6 cycles were necessary to bring the pressure within the counter to 1 atmosphere. Quantitative transfer of radon was complete before the pressure in the counter reached 1 atmosphere, since less than 0.1 per cent of the radon remained in the charcoal trap after 3 of the 6 helium flush cycles routinely used. Four samples per hour may be transferred by one person using this apparatus [*Lucas,* 1957].

The counter was then sealed, removed, and allowed to stand 2 hours for growth of radon daughters. The radon content was then determined by placing the window of the counter bottle in contact with the window of a Dumont 6292 photomultiplier tube, covering with a light-tight cover, and counting for 50 to 60 minutes. This system has an efficiency of 5.46 $\pm$ .05 cpm/$\mu\mu$c radon and a reproducibility of $\pm$1 per cent. Counting rates from 300 to 16 cpm were observed, resulting in counting errors of 2 to 5 per cent with 90 per cent confidence. All values were corrected for radon decay and a background counting rate of about 0.1 cpm.

Meteorological Measurements

The instrumentation used to obtain the meteorological measurements was straightforward and is summarized in Table 2. All the recorders were housed in the Meteorology Laboratory.

For determining atmospheric stability the

[3] Sigmamotor Pump, Model T6S, Catalog No. R-4367X, Schaar and Company, 754 W. Lexington, Chicago, Illinois.

TABLE 2. Summary of Meteorological Instrumentation

Meteorological Element	Sensor	Levels of Measurement	Recorder
Wind speed and direction, Type 1	Aerovane wind system	5.72, 11.4, 22.9 and 45.7 meters above ground	Esterline-Angus
Wind speed and direction, Type 2	Modified AN/GMQ-1 wind system; speed, 3-cup anemometer with ac generator; direction-vane driving contactor of potentiometer	2.01 meters above ground	Esterline-Angus
Atmospheric stability (temperature difference)	Lower thermocouples-copper constantan (No. 16 wire); upper thermocouples-copper constantan (No. 36 wire); upper and lower thermocouples connected in opposition	1.68–4.63 meters, 1.68–10.4 meters, 1.68–22.0 meters and 1.68–43.9 meters above ground	Minneapolis-Honeywell strip chart, Electronik potentiometer
Ambient temperature	Thermopile made of 5 copper constantan thermocouples (No. 36 wire)	1.68 meters above ground	Minneapolis-Honeywell strip chart, Electronik potentiometer
Soil temperature	Leeds and Northrup Thermohms (100-ohm copper resistors)	0.01, 0.10, 0.20, 0.50, 1.00, 3.05 and 8.84 meters below ground surface	Leeds and Northrup Micromax
Atmospheric pressure	Bendix Friez microbarograph	227.4 meters above sea level	Clock-driven drum
Dew point	Foxboro Dewcels	1.68, 5.72, 11.4, 22.9 and 39.9 meters above ground	Minneapolis-Honeywell strip chart self-balancing Wheatstone bridge
Intensity of solar radiation on a horizontal surface	Eppley 50-junction pyrheliometer	1.83 meters above ground	Leeds and Northrup Micromax
Net radiation flux	Beckman and Whitley net radiometer	1.83 meters above ground	Minneapolis-Honeywell strip chart, Electronik potentiometer

temperature difference between a reference level of 1.68 meters and each of four other levels was measured by pairs of thermocouples connected in opposition. The thermocouples at the reference level were mounted on a mast about 160 feet from the Meteorology Tower and the others were mounted on the tower. Also mounted on the tower were the aerovanes and the dewcels.

Discussion of Data

The radon data as a function of time and height for the three experiments are shown in Figure 3. Although the meteorological conditions during the first two series of measurements were similar in a number of respects, some striking differences in the radon concentration patterns appeared. During the third experiment the differences in the radon distribution and weather variables were markedly different from those of the other two.

Statistical Summary of Radon Measurements

Table 3 is a statistical summary of the data shown in Figure 3. A discussion of elements contained in this table follows.

Maximum and minimum radon concentrations ($\mu\mu c/l$) and times of occurrence. The magnitudes of the radon concentration maxima were highest near the ground and decreased rapidly with height. It is of interest to note that the highest hourly value recorded, 3.93 $\mu\mu c/l$, was observed 0.32 cm above the ground on July 16, 1958. During the August run, when the vertical diffusion rates were very high, the highest value observed at 0.32 cm above the ground was 1.07 $\mu\mu c/l$. Maximum values were

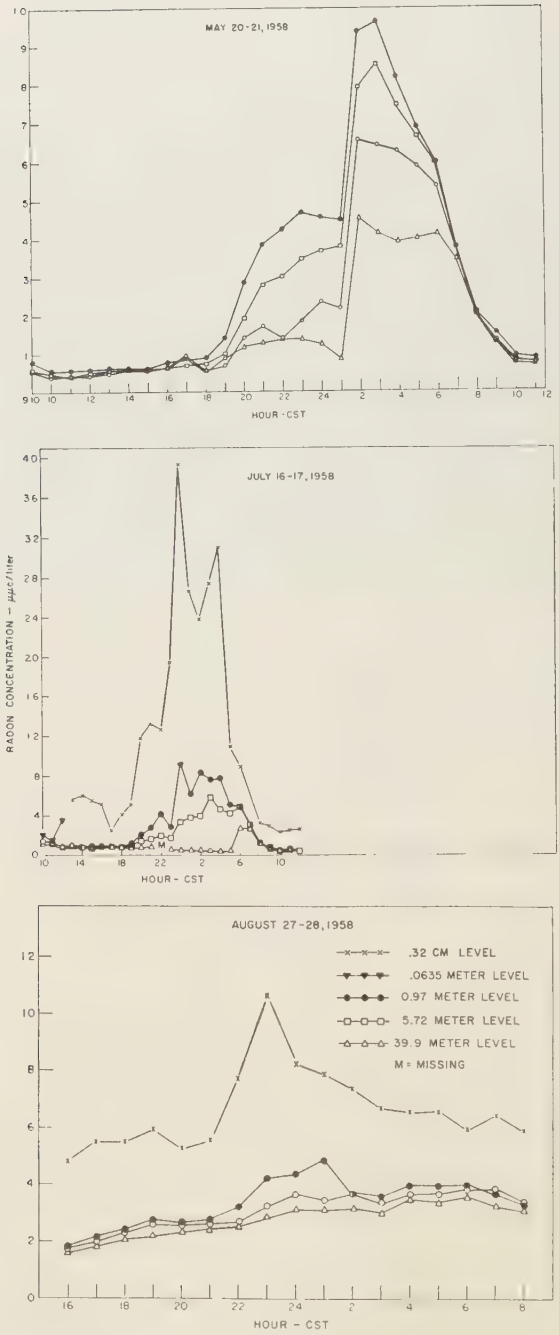

Fig. 3. Hourly values of radon concentration at indicated levels. Hourly values are determined from 20-minute averages centered about indicated times.

TABLE 3. Statistical Summary, Radon Concentration Measurements

	May 20–21, 1958 Tower Levels				July 16–17, 1958 Tower Levels				August 27–28, 1958 Tower Levels			
	0.97m	5.72m	23.8m	39.9m	0.32cm	0.97m	5.72m	39.9m	0.32cm	0.97m	23.8m	39.9m
ximum concentration, μμc/liter	0.960	0.850	0.650	0.445	3.93	0.928	0.582	0.276	1.07	0.488	0.383	0.355
ne of maximum (CST)	0300	0300	0200	0200	2400	2400	0300	0600	2300	0100	0600	0600
nimum concentration, μμc/liter	0.053	0.039	0.039	0.039	0.223	0.047	0.038	0.034	0.484	0.181	0.174	0.159
te	5/20	5/20	5/20	5/20	7/17	7/17	7/17	7/17				
ne of minimum (CST)	1000	1100	1000	1000	1000	1200	1000	1000	1600	1600	1600	1600
nge: Max. minus min.	0.907	0.811	0.611	0.406	3.71	0.881	0.544	1100 0.242	0.523	0.307	0.209	0.196
tio: Max/min.	18.1	21.8	16.7	11.4	17.6	19.7	15.3	8.1	2.2	2.7	2.2	2.2
ax. build-up rate, μμc/liter/hour	0.492	0.416	0.436	0.365	1.97	0.647	0.184	0.234	0.30	0.101	0.055	0.044
ours CST	01–02	01–02	01–02	01–02	23–24	23–24	02–03	05–06	22–23	22–23	22–23	03–04
ax. decline rate, μμc/liter/hour	0.218	0.229	0.168	0.146	2.00	0.314	0.190	0.157	0.25	0.119	0.042	0.032
ours CST	06–07	06–07	06–07	07–08	04–05	24–01	06–07	07–08	23–24	01–02	07–08	06–07

	May 20–21, 1958 Tower Levels			July 16–17, 1958 Tower Levels			August 27–28, 1958 Tower Levels		
	0.97–5.72m	5.72–23.8m	23.8–39.9m	0.32cm–0.97m	0.97–5.72m	5.72–39.9m	0.32cm–0.97m	0.97–23.8m	23.8–39.9m
aximum gradient, μμc/liter/meter	0.0308	0.0118	0.0147	3.116	0.1253	0.0156	0.6757	0.0064	0.0036
me of maximum gradient (CST)	0200	0300	0400	2400	2400	0300	2300	0100	0700

ecorded during the dark hours in the lower yers of the atmosphere. However, at 39.9 neters during the July run and at 23.8 meters nd 39.9 meters during the August experiment, ne maxima were recorded at 0600 CST.

The minima for the August runs are not gnificant, since observations for the part of he day during which minima generally occur ere not made. During the May and July runs he minima ranged from 0.03 to 0.05 μμc/l at evels from 0.97 meters and above. A markedly igher value of 0.22 μμc/l was observed at the .32-cm level, but this is extremely close to the round. At all levels the minima occurred in the ime interval between 1000 and 1200 CST.

It is to be noted that, although the magnitudes of the radon concentration maxima decreased markedly with height, the variation with altitude of the radon minima was slight.

Ranges and ratios of radon concentration. The ranges of radon concentration values (maxima minus minima) decreased with height. This s to be expected, since above 0.32 cm the values of the minima remained nearly the same but the maxima varied widely. For this reason the height variation of the ranges reflect the changes of the maxima. Ratios of maxima to minima show that the maxima were 15 to 22 times as great as the minima below the 39.9-meter level. At this level the ratios are only one-half as large.

Maximum rates and gradients of build-up and decline. During the May run the maximum rate of build-up substantially exceeded the rate of decline, but the two rates were comparable during the other runs. The horizontal advection of a pronounced radon concentration discontinuity (increase) during the May run probably accounts for this difference. It is to be noted that the changes taking place in 1 hour may represent a substantial fraction of the maximum value observed. For example, at the 0.32-cm level on July 16, from 2300 to 2400 CST, there was a change of 1.97 μμc/l which is approximately one-half the maximum value observed of 3.93 μμc/l. Similar instances may be noted in Table 3. It is also of interest that the May and July runs were characterized by

the occurrence of very marked changes in radon concentration from one hour to the next. This is not true of the August run.

The maximum gradients within the lowest layers are more pronounced than those in the upper layers. The July and August runs show that from 0.32 cm to 0.97 meters above ground the maximum radon concentration gradient was about 200 times as large as the maximum concentration gradient at the upper levels of the tower.

Additional Features Shown by the Radon Data

Advective effects. In the May run a sharp rise in radon concentration occurred at all levels from 0100 to 0200 CST. The fact that the rise occurred simultaneously at all levels and was associated with a sharp change in wind dire tion indicates that the rise was probably due the advent of air over the station with greater radon concentration. There is some ev dence of a similar occurrence in the July r from 2300 to 2400 CST.

Patterns of diurnal variation. The May a July runs were made during sunny days a clear nights. The strong convection during t day transferred the radon upward rapidly that low concentrations were observed in t layers up to the top of the tower. As a resu of strong nocturnal cooling during the nigh the atmosphere became very stable and vertic mixing was suppressed. A high radon conce tration, therefore, developed in the lower laye During the August run radiational heating a

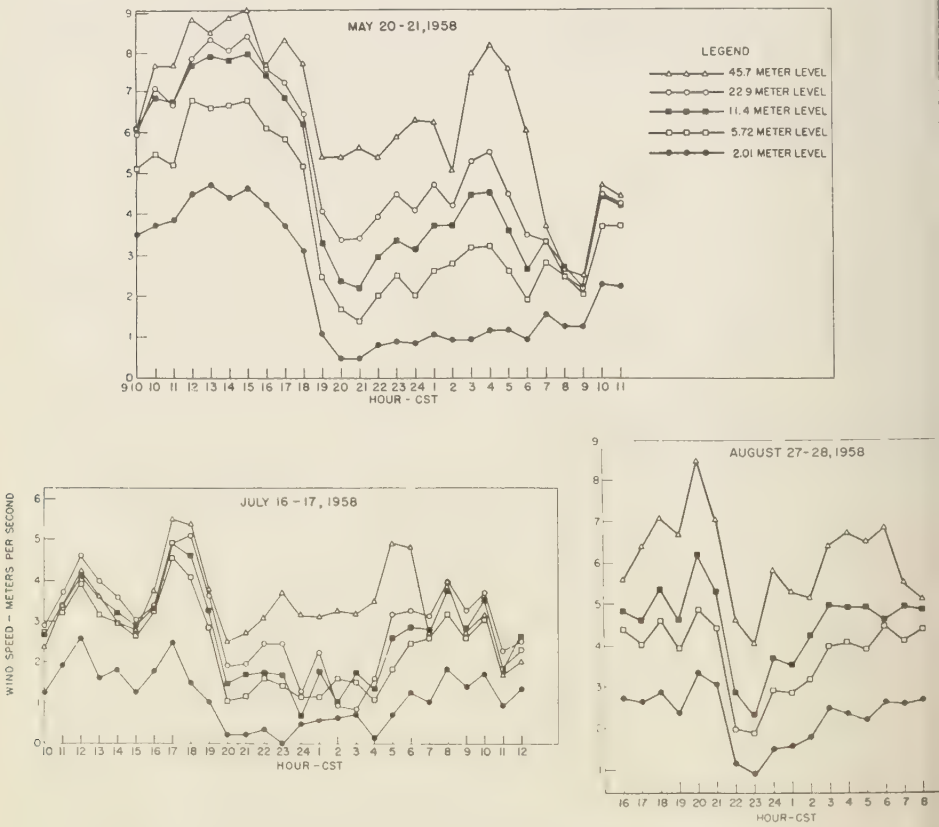

Fig. 4. Hourly values of wind speed at indicated levels.

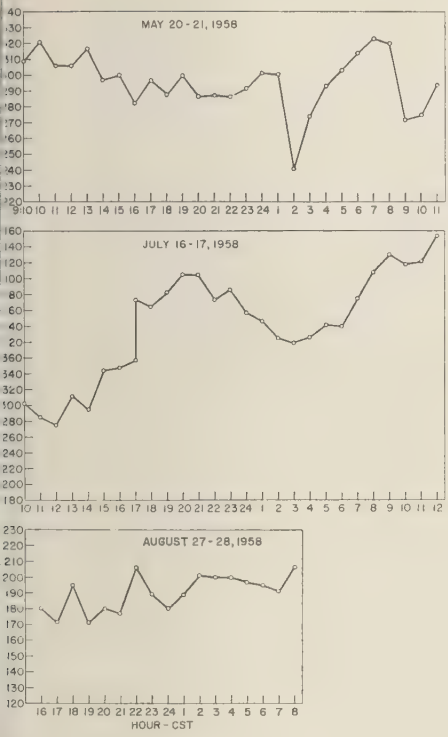

ig. 5. Hourly values of wind direction at 22.9-meter level, Meteorology Tower.

ooling were smaller. Consequently, the amplitude of the diurnal variation of radon concentration at all levels was markedly smaller.

Meteorological Relationships

Wind

The graphs of the wind speed and direction shown in Figures 4 and 5 are based on 20-minute averages taken during the radon observation periods. Only the direction at 22.9 meters is shown. The reading of direction at this level was arbitrarily assumed to be representative of the air layer under study.

An examination of the hourly values of wind speed at the levels measured shows the typical pattern of high values during the daytime and low values at night. Superimposed on this pattern are minor fluctuations. Since the gross aspects of radon concentration curves are nearly 180° out of phase with the wind-speed curves, one might expect a similar relation between correspondence of the minor fluctuations of the wind speed and the radon concentrations. Many instances of such correspondence appear when the radon and wind data are compared. For example, minima for wind speeds at 2.01 meters correspond roughly to maxima of radon concentration at the 0.32-cm level. Examples of this occur at 2100 CST on July 16, 0400 CST on July 17, and 2300 CST on August 27. However, some exceptions appear.

The correspondence between minima of wind speed and maxima of radon concentration is not surprising when one considers the reduction in the vertical exchange coefficient due to a diminution of mechanical turbulence with a decrease in wind speed. This, of course, allows an increased accumulation of radon near the ground.

The degree of roughness of the terrain differs with direction from the station. It is therefore to be expected that turbulent structure and diffusion rates in the atmosphere differ with winds from various directions. For this reason even if the emanation rate of radon from the soil were uniform in time and space, wind from a different direction would bring in air with different concentrations of radon. Examples of this may be seen during the periods 0100–0200 CST May 20, 1600–1800 CST July 16, and 2100–2400 CST August 27. The pronounced wind shift of July 16 was characteristic of a microfront associated with the onset of a sea breeze. As is shown in Figure 5, the wind direction for each of the runs was different: west northwest for the May run; northwest up to 1700 CST and then east for the July run; and approximately south for the August run.

Vertical Temperature Differences, Stability

Figure 6 shows the hourly values of temperature difference between the tops and bottoms of the layers from 1.68 to 4.63 meters, 1.68 to 10.4 meters, 1.68 to 22.0 meters, and 1.68 to 43.9 meters. These temperature differences represent 4-minute averages of the stability within the indicated layer. An examination of the radon data and the temperature difference or stability traces brings to light a number of interesting relationships which may be summarized as follows:

Variation of radon concentration with stabil-

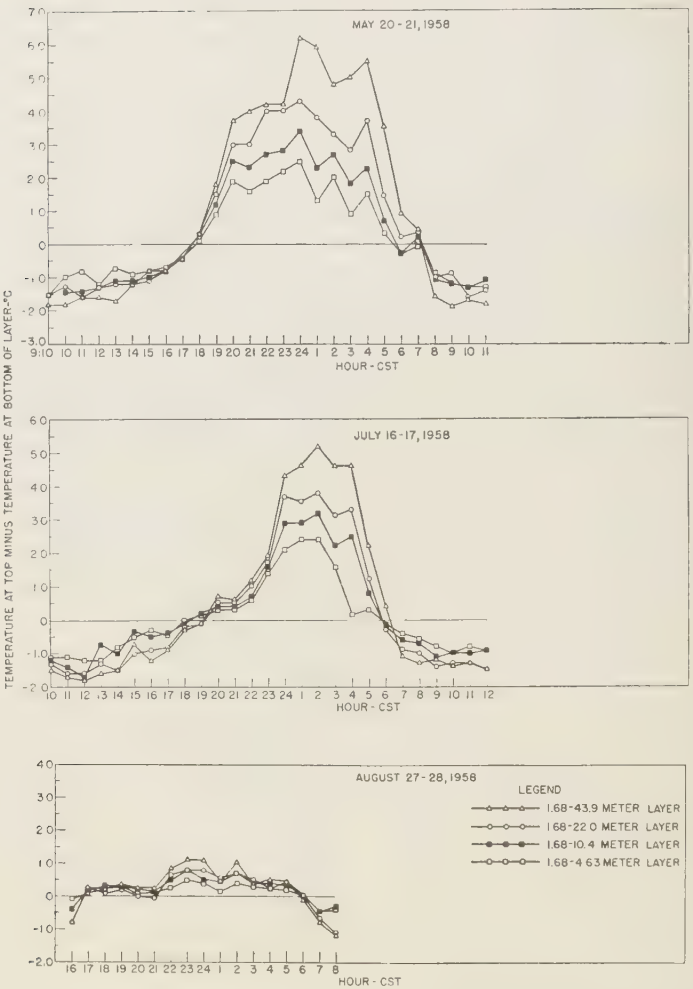

Fig. 6 Hourly values of atmospheric stability as denoted by temperature difference between top and bottom of indicated layers. These data are based on the average of two 2-minute readings within the 20-minute radon-measuring period.

ity. Examination of the gross features of stability and radon curves shows that a marked similarity exists. The strong relationship between radon concentrations and stability has been observed in the past [*Gale and Peaple*, 1958]. When the stability is high the radon concentration is high, and vice versa. It may be noted that during the night when the radon concentration was highest, May 21, the stability was greatest. Similarly the nighttime radon concentrations were lowest when the nocturnal inversion was weakest.

Radon concentration rise with completion of lapse to inversion transition. During the transition period between lapse and inversion conditions, the temperature variation with height was irregular; that is, in the layer from 1.68 to 43.9 meters some sublayers were stable while others were unstable. In all three runs it was found that a sharp rise of radon concentration

curred when the temperature increased with ght throughout the entire layer. In other rds, the transition was complete. Note the e in radon concentration and the stability rves at 2000 CST during the May and July ns and 2200 CST during the August runs.

Decline in radon concentration with morning eak-up of the inversion. It is most interest- g that a maximum or a peak in the radon ncentration occurred at 0600 CST in all the ns. When the inversion broke up, the flux of lon increased because of the increased vertical nsport. There was a transition period during ich the radon-laden air from the layers a few ntimeters above the ground was carried up- rd, thus giving rise to the observed peak in lon concentration at 39.9 meters. During this riod the concentration of radon fell in the ry lowest layers. This phenomenon may be nsidered an 'inverse fumigation condition.' dinarily fumigation conditions occur shortly er sunrise. Concentrations are brought to the und from several hundred meters above. In is case, foreign material was brought to the per layers from high concentrations near the rface. This is the inverse of the normal fumi- tion phenomenon.

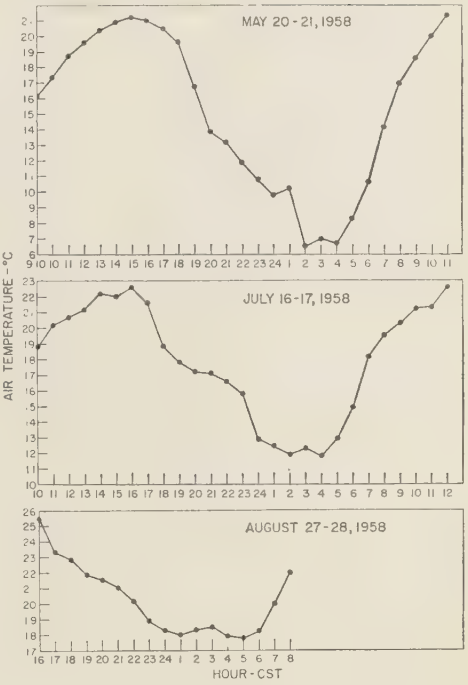

Fig. 7. Hourly values of ambient air temperature at 1.68 meters above ground.

r Temperature

The temperature readings shown in Figure 7 present 20-minute averages taken during the me time interval as that of the radon meas- ements. A comparison of the gross features the temperature and radon charts shows a iking inverse relationship. This is especially ue of the radon concentrations at the 0.32-cm d 0.97-meter levels. In a substantial majority the cases hourly rises in temperature were sociated with hourly falls in radon concentra- n, and vice versa.

An interesting chain of events takes place th feedback at various steps to produce the served changes in temperature. The radia- nal cooling at night which causes the temper- ure to fall in the lowest atmospheric layers oduces stability. As a result, vertical motions d the downward transport of momentum are ppressed. As this continues, the wind speed comes lower and turbulent transport or mix- g is reduced further, thus favoring a strength- g of the inversion. This process results in a reduction of the turbulent exchange coefficients and the accumulation of radon at the lower layers. Thus the same factors which operate to reduce the air temperature result in an increase in radon concentration. A similar line of reasoning may be employed to explain the reduction in concentration near the surface as the ground and lower layers are warmed.

Soil Temperature

Hourly values of soil temperature at 0.01, 0.10, 0.20, 0.50, 1.00, 3.05, and 8.84 meters for the periods of the experiments are shown in Figure 8. The soil temperature data are based on 2-minute averages taken either during the period of radon observation or within 3 minutes. Only the readings for the 3.05- and 8.84-meter levels, where the hourly temperature changes are very small, were made outside the radon measuring period. The data from each level are recorded in sequence for 2 minutes.

The temperature of the upper layers of the

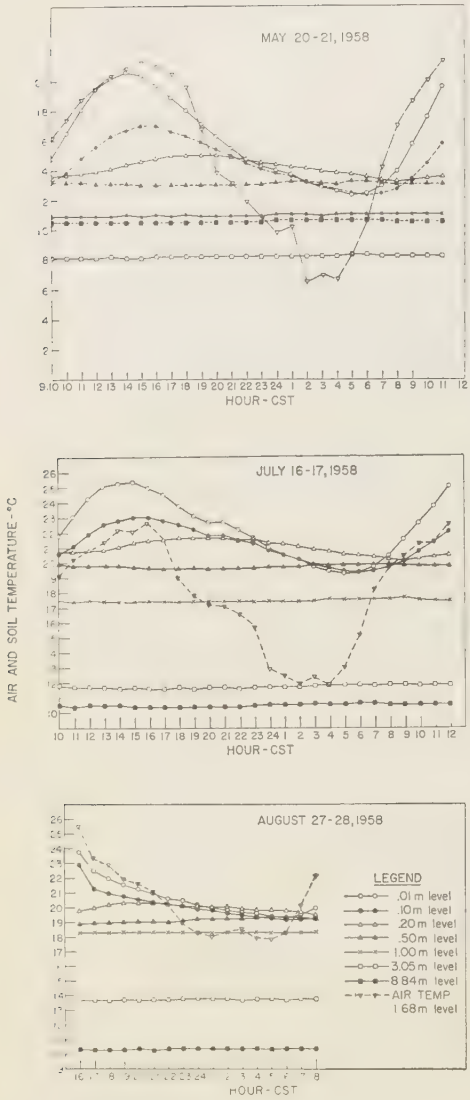

Fig. 8. Hourly values of air and soil temperature at indicated levels.

soil may contribute to the concentration of radon in two ways:

1. The release of the radon formed in the soil is affected by the temperature, since the soil aeration is a function of this variable [*Baver*, 1956].

2. The heat flux from the soil to the air depends on the temperature distribution within the soil, among other variables. Since the amount of heat released by the soil influences the air temperature, it is part of the chain of events which determines the rate of diffusion of radon within the lower layers of the atmosphere.

Soil temperatures near the surface were lowest during the May run, but the values during the July and August experiments were comparable with each other. In the May and August runs the air temperature at 1.68 meters above the surface was lower than the soil temperature at 1 cm during the night but higher during the day; in the July run the soil temperature at 1 cm was higher during the entire measuring period.

Atmospheric Pressure

Hourly value of atmospheric pressure are shown in Figure 9. The pressure chart shows a rise after the passage of a microfront associated with the onset of a sea breeze in the July run. The effect of pressure upon the concentration of radon appears to be undetectable from a gross examination of the data.

Atmospheric Moisture

The distribution of moisture with height is of importance as a factor contributing to the concentration of radon at a given level. The flux of terrestrial radiation is a function of water vapor pressure and consequently the variation of temperature with height depends on this variable. High moisture values found during the August run no doubt contributed to the reduced rate of nocturnal cooling in the lower layers. As a result, only a weak inversion formed and smaller radon concentrations were observed. No similarity was observed in plots of the dew point and radon concentration data.

Solar radiation and net radiation flux

The solar radiation measurements during the May and July experiments show that the days were mostly sunny. During the night of the May run the net radiation flux upward was relatively high, indicating the absence of clouds. In the dark hours of the July and August runs the net radiation flux upward increased during the latter half of the night. This was associated

ith an increase in stability and in radon concentrations.

Summary and Conclusions

The following is a summary of the information provided by the radon measurements which may be of use to others concerned with this problem:

1. The radon measurements provided information concerning the heterogeneity of the horizontal distribution of radon. The heterogeneity was brought out clearly in the May experiment. When the wind direction changed, thus changing the immediate trajectory near the measuring point, the radon concentrations increased markedly.

2. The data also reveal the fact that large changes of radon concentration may occur at a given station from one hour to the next. Although large changes were more likely to occur in the lower levels, large hourly changes did occur at the 39.9-meter level. In addition to advection as a cause of large hourly changes, a sudden clearing at night allows a rapid inversion build-up and may also result in a rapid increase of radon in the lower layers.

3. On the night of July 16–17, when the atmosphere was very stable and the winds were relatively light, the large accumulation of radon did not reach the 39.9-meter level. Typically low daytime concentrations were observed at this level until after sunrise.

4. All three sets of data showed a peak in radon concentration at the 39.9-meter level at 0600 CST, shortly after sunrise. The most obvious explanation is that with the onset of daytime heating turbulent vertical transport increased and brought up the radon-laden air—an inverse fumigation. The knowledge that the radon concentrations may increase at a level of about 40 meters above the ground shortly after sunrise simultaneously with a sharp decrease at the lower levels may prove useful to those conducting scientific work in laboratories located in the upper stories of tall buildings where the radon background may be a factor.

5. The data also bring out rather interesting information concerning the ratios of daytime to nighttime radon concentrations. At about 6 meters, the height of the second or third story of a conventional building, the radon concentrations at night were larger by a factor of 20 as compared with the daytime values when the skies were clear. During cloudy conditions the nighttime values were only about twice as large.

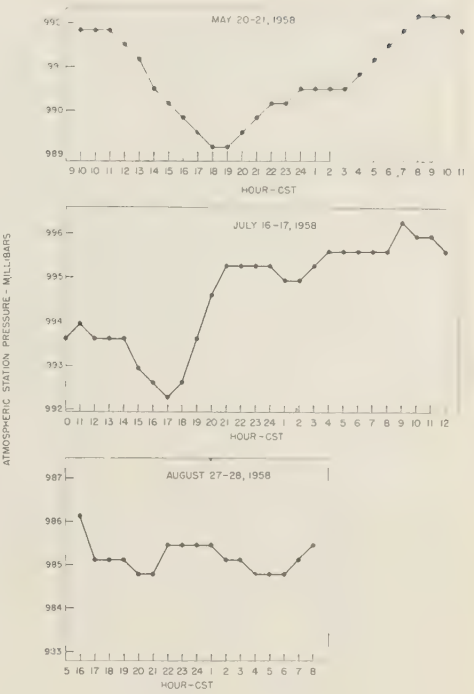

Fig. 9. Hourly values of atmospheric station pressure.

6. The graphs showing the hourly values of ambient air temperature served as a rough index of the variation of radon concentration. One must not conclude from this that the radon concentration is a function of the ambient air temperature. Rather, as explained above, the same factors which contribute to rises or falls of the surface air temperature (provided same air mass remains over the station) contribute to changes in the radon concentration. One might suspect that within the same air mass under dry conditions the daily range of temperature would correlate highly with the daily range of radon concentration at a given level near the ground.

7. The relationships between the radon concentrations and the other meteorological variables pertinent to the assessment of the diffusive

capacity of the atmosphere, such as wind and stability, indicate that the radon is an excellent tracer for studying the diffusion process in the atmosphere.

Acknowledgments. The help of Peter E. Wasko, Frank C. Kulhanek, Gunther A. Zerbe, and Hugh G. Daubek of the Meteorology Group and F. Ilcewicz of the Radiochemistry Group in making the measurements is acknowledged. Thanks are also due Martha C. Sundquist for her part in preparing the figures and making numerous calculations connected with these studies. The authors are grateful for the helpful comments and suggestions given by Dr. Horace R. Byers of the University of Chicago.

This work is sponsored by the Atomic Energy Commission.

References

Baver, L. D., *Soil Physics,* 3rd. edition, p. 210, John Wiley & Sons, New York, 489 pp., 1956.

Becker, F., Messungen des Emanationsgehaltes der Luft in Frankfurt a.M. und am Taunus-Observatorium, *Beitr. Geophys., 42,* 365–384, 1934.

Elster, J., and H. Geitel, Uber eine fernere Analogie in dem elektrischen Verhalten der naturlichen und der durch Becquerelshtrahlen abnorm leitend gemachten Luft, *Phys. Z., 2,* 590–593, 1901.

Gale, H. J., and L. H. J. Peaple, A study of the radon content of ground-level air at Harwell, *Intern. J. Air Pollution, 1,* 103–109, Pergamon Press, London, 1958.

Harley, J. H., Sampling and measurement of ai borne daughter products of radon, *Nucleoni 11,* no. 7, 12–15, 1953.

Israel, H., Radioactivity of the atmosphere, *Co pendium of Meteorology,* Am. Meteorol. So Boston, 1334 pp., 1951.

Lester, O. C., A rapid and accurate method of co recting measurements with emanation electr scopes for ordinary changes in temperature ar pressure, *J. Opt. Soc. Am., 11,* 637–640, 1925.

Lucas, Henry F., Jr., Improved low-level alp scintillation counter for radon, *Rev. Sci. Instr 28,* 680–683, 1957.

Stehney, A. F., W. P. Norris, H. F. Lucas, Jr., ar W. H. Johnston, A method for measuring th rate of elimination of radon breath, *Am. Roentgenol. Radium Therapy Nuclear Me 73,* 774–784, 1955.

Tsivoglou, E. C., H. E. Ayer, and D. A. Holada Occurrence of nonequilibrium atmospheric mi tures of radon and its daughters, *Nucleonics, 1* 40–45, 1953.

Wilkening, M. H., A monitor for natural atmo pheric radioactivity, *Nucleonics, 10,* no. 6, 36–3 1952.

Wilkening, M. H., Daily and annual courses natural atmospheric radioactivity, *J. Geophy Research, 64,* 521–526, 1959.

Wright, J. R., and O. F. Smith, The variation wit meteorological conditions of the amount radium emanation in the atmosphere, in th soil gas and in the air exhaled from the surfa of the ground at Manila, *Phys. Rev., 5,* 459-48 1915.

(Manuscript received December 1, 1959; revise January 18, 1960.)

Indications of Deep Pacific Circulation from the Distribution of Properties at Five Kilometers[1]

WARREN S. WOOSTER

Scripps Institution of Oceanography
La Jolla, California

AND

GORDON H. VOLKMANN

Woods Hole Oceanographic Institution
Woods Hole, Massachusetts

Abstract. A description of the deep Pacific Ocean, based on 145 deep oceanographic stations, is presented, showing the distributions of *in situ* temperature, potential temperature, salinity, and dissolved oxygen at a depth of 5 km. At this depth the open Pacific appears to consist of four major connecting basins. Bottom water is introduced at high southern latitudes from the deep Indian Ocean; initially it has the following characteristics: *in situ* temperature, 0.9°C; potential temperature, less than 0.5°C; salinity, 34.7‰; dissolved oxygen, 5.0 ml/l.

Salinity variations at this depth are little greater than measurement errors, the average value for the whole open Pacific being 34.695‰ with a standard deviation of 0.034‰. *In situ* temperature increases from south to north, the rate of increase being much greater in the central basin than in either the southern or the northern basin. This increase is attributed to heat flow through the sea floor and to mixing with overlying waters. Both the change of temperature and the observed northward decrease of dissolved oxygen content are consistent with a northward drift of bottom water. The deep water of the eastern North Pacific is presumably the 'oldest' water of the open ocean, its properties having been most extensively modified: *in situ* temperature, 1.6°C; potential temperature, 1.1°C; dissolved oxygen, 3.4 ml/l.

Introduction. Classically, the deep ocean circulation has been indirectly studied by inference from the distributions of temperature and dissolved substances at great depths. Our limited knowledge of the deep Pacific is due to the use of this method by *Wüst* [1937] and by *Sverrup, Johnson, and Fleming* [1942]. Today, promising new techniques are being applied, such as the direct measurement of deep flow (*Swallow,* 1955; *Swallow and Worthington,* 1957] and the use of artificial and natural isotopic tracers for the study of transfer phenomena in the sea [*Craig,* 1957].

Nevertheless, a re-examination of the distribution of properties seems warranted, since (1) the number of deep oceanographic observations in the Pacific has more than doubled since 1942, so that one can now describe abyssal conditions in greater detail than heretofore, and (2) the new techniques, although promising, do not yet give unequivocal answers. Furthermore, the observations are so expensive and time consuming that it will be many years before a systematic body of data is available from the whole Pacific. Meanwhile, knowledge of the characteristics of deep ocean waters provides a framework to which the new measurements can be referred.

Sources and treatment of data. A search of the sources of Pacific oceanographic data yielded 145 stations which reached depths of approximately 5 km and whose data appeared to be sufficiently reliable to provide usable information (Table 1). These observations were made during the last 30 years and, although irregularly spaced, are widely distributed throughout the Pacific basin (Fig. 1).

For each station temperatures were plotted against depth, and salinities and dissolved oxygen concentrations were plotted as functions of

[1] Contribution from the Scripps Institution of Oceanography and the Woods Hole Oceanographic Institution. This work was supported by the Office of Naval Research.

Fig. 1. Distribution of *in situ* temperature (°C, upper number) and dissolved oxygen (ml/l, lower number, when available) at 5 km. Sources of data are indicated by symbols and listed in Table 1. Dashed line is arbitrary flow line (see text).

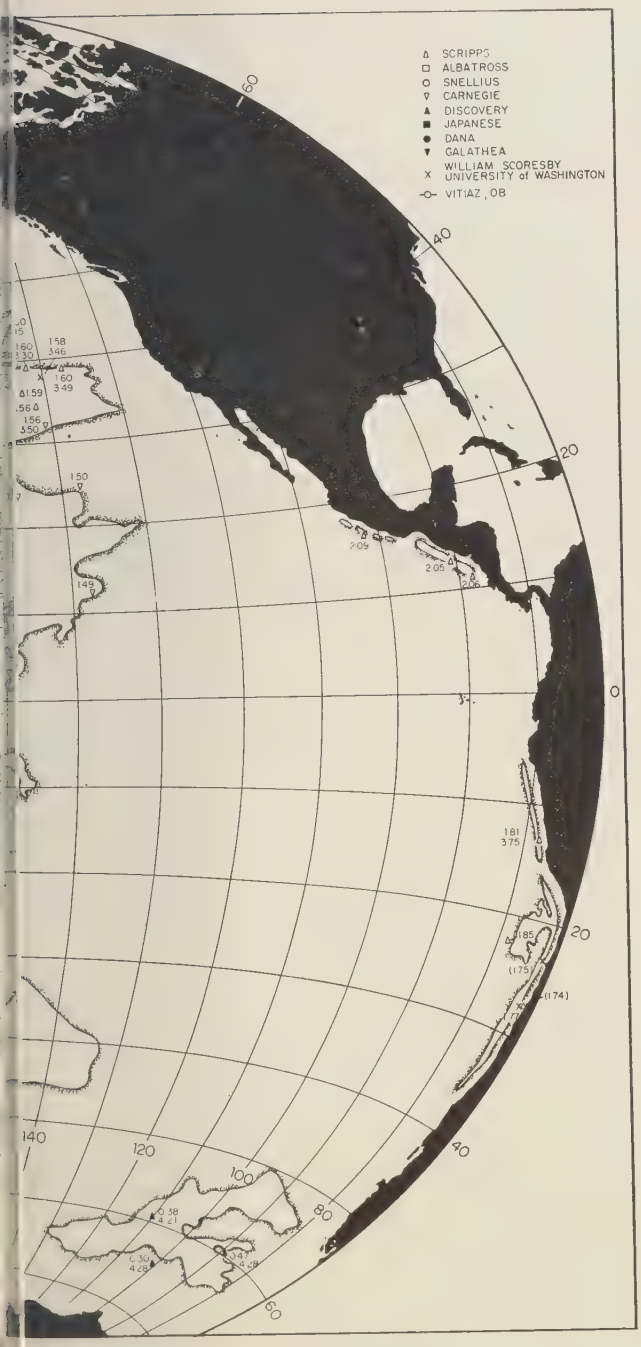
SCRIPPS
ALBATROSS
SNELLIUS
CARNEGIE
DISCOVERY
JAPANESE
DANA
GALATHEA
WILLIAM SCORESBY
UNIVERSITY of WASHINGTON
VITIAZ, 08
60
40
20
0
20
40
60
80
100
120
140
158
346
160
349
150
149
205
205
206
181
375
185
(175)
(174)

temperature. In the drawing of the station curves, data from neighboring stations were used to facilitate interpolation. It is estimated that the values read at 5 km are subject to the following random errors: temperature, ±0.03°C; salinity, ±0.04 ppm; oxygen, ±0.05 ml/l.

Values of temperature and dissolved oxyg were plotted on an equal-area chart along wi the 5-km isobath (Fig. 1). Salinity values we not plotted, since, as will be discussed late spatial variations in salinity are little great than the uncertainty in the reported data.

Configuration of the Pacific abyss. The 5-k

TABLE 1. Sources of Data Used in Study of Five-Kilometer Surface

Identification	Year	Stations	Reference
Albatross	1947–8	105, 123, 128, 133, 138, 162	*Bruneau et al.* [1953]
Carnegie	1929	116, 119, 137, 139, 142, 146, 148, 151, 156, 162	*Fleming et al.* [1945]
Dana	1928–9	3580, 3628, 3676, 3683, 3745	*Carlsberg Found.* [1937]
Discovery II	1932	972, 974, 976	*Discovery Comm.* [1941]
	1938	2217	*Discovery Comm.* [1947]
	1950–1	2735, 2769, 2819, 2823, 2824, 2825	*National Inst. Oceanog.* [1957]
Galathea	1951–2	412, 433, 677	*Bruun and Kiilerich* [1955]
*Japanese**	1933–5	24–15, 28, 68, 83; 27–35; 30–18; 31–88, 95; 32–B77, B84	*Japan, Maritime Safety Agency* [195(
	1935–7	33–46, 51; 34–107; 35–11, 33; 36–32, 78; 38–92; 42–143; 43–78	*Japan, Maritime Safety Agency* [195
	1938	52–24, 94	*Japan, Maritime Safety Agency* [195
Ob	1958	361, 393	Data from IGY World Data Center A, College Station, Texas
Scripps	1952–3	*Capricorn* 7, 26 *Transpac* 11, 24, 59, 99	Data on file, Scripps Institution
	1954	*Cusp* B, C *Acapulco Trench* 8, 12, 15	
	1955	*Norpac* 5, 43	
	1956	*Equapac* 9, 17, 28 *Chinook* 2, 4, 5, 6, 7, 10, 11, 12, 13, 13a, 14	
	1957	*Mukluk* 1, 10	
	1958	*Downwind* 28, 31, 32	
Snellius	1929–30	47, 48, 52, 53, 76, 180 197, 210, 212, 229, 235, 251, 260, 262, 264, 265, 272, 275, 301, 321, 362, 365	*Van Riel et al.* [1950] *Postma* [1959]
Vitiaz	1953–5	B, D.	*Brujewicz* [1957]
Vitiaz	1957–8	3625, 3631, 3634, 3686, 3689, 3726, 3728, 3746, 3759, 3778, 3780, 3795, 3805, 3812, 3818, 3823, 3827, 3831, 3876	Data from IGY World Data Center A, College Station, Texas
	1958	4066, 4096, 4120	mss data, courtesy N. N. Sysoev
Washington	1954, 7	64–26; 176–1, 8, 10, 15	Data on file, Univ. Washington
	1958	199–11, 14	
William Scoresby	1931	612, 629	*Discovery Comm.* [1949]

* Oxygen data from these stations were furnished by Dr. Y. Miyake.

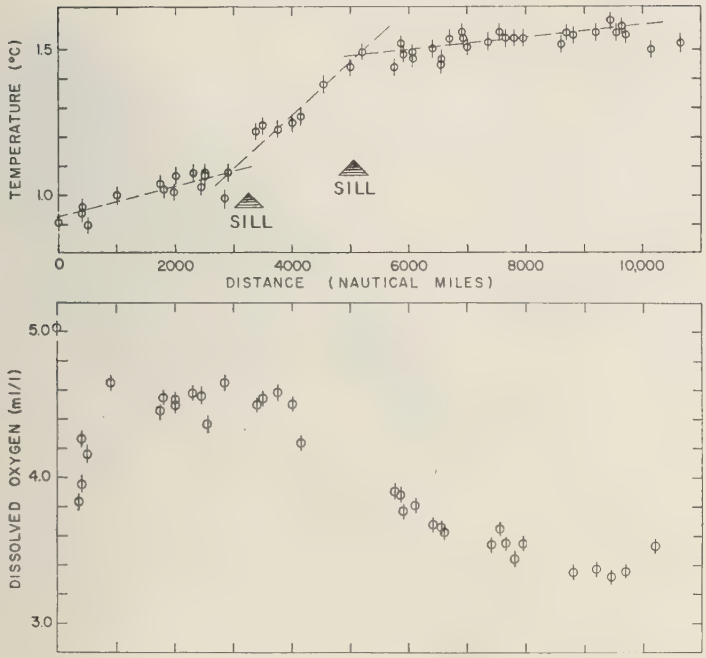

Fig. 2. *In situ* temperature (°C) and dissolved oxygen (ml/l) at 5 km along arbitrary flow line. stance in nautical miles from origin at 55°S, 170°E. Arrows indicate positions of supposed sills be- een southern and central basins (at 3200 miles) and between central and northern basins (at 5000 les.

bath used in this study (Fig. 1) was derived m an unpublished chart of H. W. Menard. at portion of the open Pacific deeper than km appears to be divided into four major sins: a southern basin extending from 60°S to °S, a central basin extending from 10°S to arly 20°N, a northern basin reaching north- rd to 50°N from 140°E to 130°W, and an stern basin lying between 10° and 20°N, east 170°W. It is possible that the northern basin further divided into an eastern and western rt by a chain of topographic highs extending m Hawaii to Kamchatka.

Division into the four major basins is not vays based on detailed soundings, and the istence and character of the dividing sills must accepted with reservations at this time. How- er, as will be seen later, the existence of the ls between the southern and central basins d between the central and northern basins es seem to be supported by the temperature ta.

Other large areas deeper than 5 km include the Bellingshausen Basin in the eastern South Pacific, and the Philippine Sea Basin in the western tropical Pacific.

Distribution of temperature. The distribution of temperature at 5 km is described in three ways: individual station values are plotted on an equal-area chart (Fig. 1); temperatures on stations near an arbitrary flow line are plotted against distance from the origin of this line at 55°S (Fig. 2); the distribution of potential temperature is shown on an equal-area chart (Fig. 3). The arbitrary flow line (Fig. 1), which we have introduced as a convenience in discussing the distributions of temperature and oxygen, stems from the general picture of circulation in the Pacific abyss, which is discussed later.

The lowest values of *in situ* temperature at 5 km in the Pacific, 0.30° to 0.47°C, are found in the Bellinghausen Basin in the eastern South Pacific; the highest, 3.83°C, occurs in the iso-

Fig. 3. Distribution of potential temperature at 5 km (based on stations shown in Fig

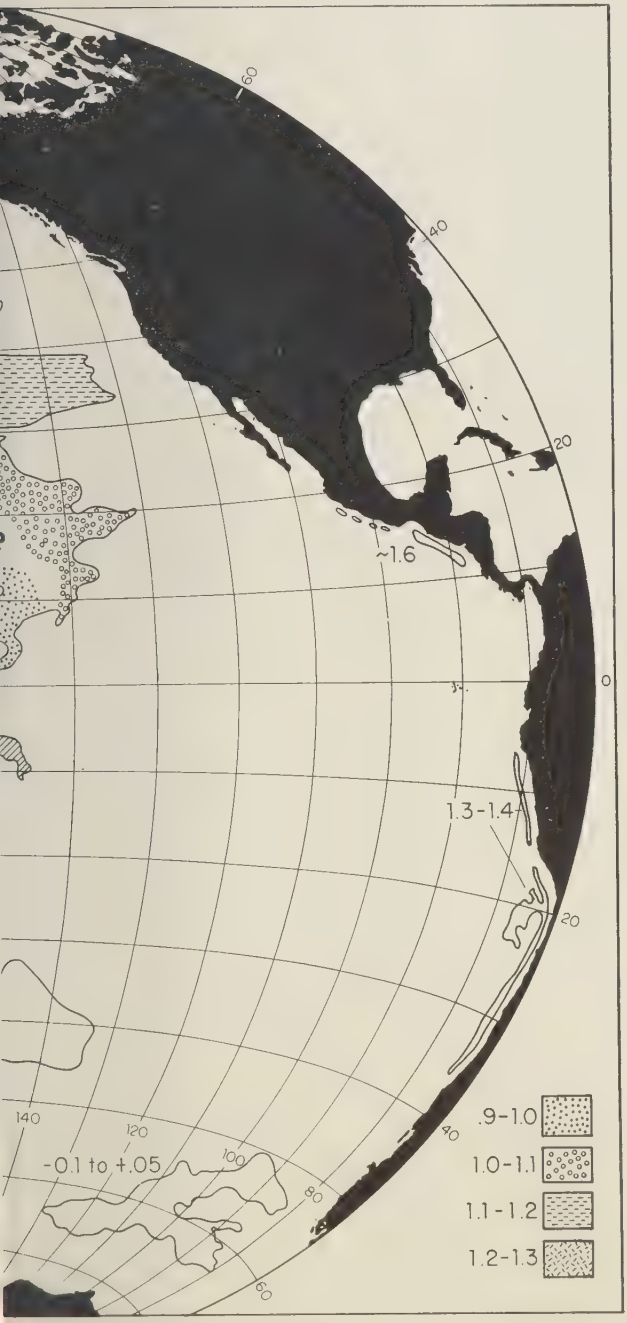
60
40
20
0
20
~1.6
1.3-1.4
140
120
100
80
60
-0.1 to +0.05
.9-1.0
1.0-1.1
1.1-1.2
1.2-1.3

lated Celebes Basin of the Malay Archipelago. The range is much smaller in the major basins of the open ocean; the temperature increases from about 0.9°C south of 50°S to 1.6°C in the eastern North Pacific. Along the arbitrary flow line the increase is not uniform (Fig. 2), being about $0.03°/10^3$ km in the southern basin, $0.10°/10^3$ km in the central basin, and $0.01°/10^3$ km in the northern basin. Changes from one rate of temperature increase to another take place near the supposed sills between basins; there is also a suggestion (Fig. 1) of an abrupt increase in temperature (from 1.08° to 1.22°C) across the sill between the southern and central basins, although the data are too sparse to establish this definitely.

In the eastern basin, beyond the arbitrary flow line, the water at 5 km is slightly cooler than it is farther north, the few available values falling between 1.52° and 1.37°C. The temperature in the Aleutian Trench is similar to that in the northern basin with which it connects, whereas in the more isolated Middle America and South America Trenches high average values are found (2.08° and 1.78°C, respectively).

Potential temperatures were computed from an unpublished table of R. B. Montgomery. In order to determine the absolute value of potential temperature, it is necessary to know accurately the coefficient of thermal expansion —the factor which varies more with temperature and pressure than the other pertinent quantities. *Eckart* [1958] pointed out that this value is seriously in doubt, especially at low temperature and elevated pressure. In our use of potential temperature, at constant pressure and with a small horizontal temperature range, this uncertainty presumably does not adversely affect the significance of the distribution (Fig. 3).

The distribution of potential temperature does not, of course, differ markedly from that of *in situ* temperature, the difference between the two values being relatively constant (0.40° to 0.45°C) at this depth throughout the basin. Again it is evident that in the major basins through which the principal circulation takes place the highest temperatures occur in the eastern part of the northern basin.

Although more detailed, the picture is similar in its general features to the 4-km potential-temperature chart of *Wüst* [1937], which was based for the most part on earlier data. Only east of Japan and the Kuriles, where Wüst shows a region of low potential temperature (less than 0.6° to 1.0°C), do the two charts differ markedly. The modern data do not confirm the existence of this low-temperature area even at 4 km, which is the average depth of the deep temperature minimum in the western North Pacific.

Distribution of salinity. The available salinity data are surprisingly similar everywhere in the deep Pacific. On the 86 stations with reliable salinity data in the open Pacific the average value at 5 km was 34.695‰ with a standard deviation of 0.034‰. This range of variation is not much greater than measurement errors in the conventional salinity method. For example, in a recent study based on field data *Wooster and Taft* (in press) concluded that the upper limit of measurement errors could be estimated as 0.018‰ (standard deviation). Until more accurate salinity data are available from the deep Pacific it does not seem profitable to plot salinity values on the 5-km chart.

Salinity data from the various basins were examined for evidence of downstream change (Table 2). Although there appears to be a slight decrease of salinity downstream, the data are inadequate to establish significant differences.

Distribution of dissolved oxygen. The distribution of dissolved oxygen at 5 km is shown as individual station values (Fig. 1) and as a function of distance along the arbitrary flow line (Fig. 2). The extreme range is from 1.62 ml/l in the isolated Celebes Basin (where the highest temperatures were also observed) to about

TABLE 2. Salinity Data

Area	No. of Observations	Average Salinity, ‰	Standard Dev., ‰
Southern Basin	15	34.710	0.043
Central Basin	11	34.710	0.033
Western Northern Basin	25	34.693	0.029
Eastern Northern Basin	33	34.686	0.035
Open Pacific	86	34.695	0.034

0 ml/l in the western South Pacific. The open ean range is, of course, much smaller, from 0 ml/l down to low values of about 3.4 ml/l the eastern North Pacific.

It is evident that a pronounced decrease in ssolved oxygen content parallels the increase temperature from south to north through ne major basins. A region of high oxygen con- nt (more than 4.5 ml/l) extends from 60°S roughout the southern basin and up to the quator in the central basin. It should be noted at within this region there are four anomalous alues south of 50°S. All these values are from *Discovery II*, in 1938 and 1951, and are lower an all other oxygen values at 5 km in the estern South Pacific.

North of the region of high oxygen content ne rate of decrease of dissolved oxygen is large about 0.15 ml/l per 10^3 km). This sharp de- rease appears to begin somewhere beyond the ll between the southern and central basins. In ne North Pacific the rate of oxygen decrease rom west to east seems to be somewhat smaller. Data from the Scripps *Transpacific* Expedition how a parallel increase in inorganic phosphorus ontent at 5 km, from 2.51 μg atoms/l on *Transpacific* 99 (at 140°E) to 3.04 μg at- ms/l on *Transpacific* 11 (at 140°W). Unfor- nately, no deep oxygen data are available rom the eastern basin.

Discussion. Knowledge of the Pacific abys- al circulation was summarized by *Sverdrup, ohnson and Fleming* [1942, pp. 751–755]. Deep nd bottom waters of high density are formed nly in high latitudes; in the North Pacific this oes not occur because of low surface salinities. lthough it has not been demonstrated con- lusively that no bottom water is formed in the acific sector of the Antarctic, it is generally ccepted that Pacific bottom water originates n the Weddell Sea and to the south of the ndian Ocean [*Deacon*, 1937]. This water then nters the Pacific basin between Tasmania and ntarctica. The Pacific and Indian Oceans are eparated by a ridge extending southward from asmania, with a greatest depth of about 3500 eters (U. S. Navy Hydrographic Office Chart o. 2562, 1956). Recent carbon-14 measure- ents in this region [*Brodie and Burling*, 1958] uggest that the entering waters are several housand years old, but the published observa- tions were taken at too shallow a depth and were too few to be conclusive.

Some fraction of the Antarctic bottom water flows northward into the southern and central basins. Sverdrup suggested that a sluggish northward flow takes place on the western side of the ocean with return flow to the south on the eastern side. The exchange of deep and bottom water across the equator is believed to be very small, the average velocities of flow being estimated as fractions of a centimeter per second.

A somewhat different picture is presented by *Stommel* [1958] in a recent theoretical discussion of abyssal circulation. He envisions a balance between two 'point sources' of deep water (in the North Atlantic and the Weddell Sea) and an oceanwide 'sink' with upward flux everywhere across the 2-km surface. If the sources are connected with this distributed sink in a way consistent with the dynamics of a fluid on a rotating sphere, it appears that the meridional component of velocity in the deep sea is everywhere directed away from the equator, where it vanishes, except in the western parts of oceans where intense boundary currents occur. In the western Pacific such a strong current flowing northward across the equator toward the 30°N parallel is suggested; north of it there is an oppositely directed boundary current [Fig. 2 of *Stommel*, 1958].

Unfortunately, the present description of the distribution of properties on the 5-km surface cannot be used for a direct and convincing test of these ideas of the deep Pacific circulation. We believe, however, that it can contribute to an understanding of some aspects of the problem.

If one assumes that all bottom water enters the Pacific through the passage between Australia and Antarctica, its initial properties in the Pacific at 5 km are those observed south of New Zealand: *in situ* temperature about 0.9°C, potential temperature less than 0.5°C, salinity slightly greater than 34.7‰, and dissolved oxygen content about 5.0 ml/l.

The low values of oxygen content in this region found by *Discovery II* in 1938 and 1951 are not consistent with the two recent *Ob* values or with the widespread presence of more highly oxygenated water north to the equator. A possi-

ble explanation is that the oxygen content of the entering water differs from year to year. However, such variation is not reflected in the other values of the southern basin, all of which from 1929 to 1957 are uniformly higher than the *Discovery II* values.

The temperature of bottom water can be expected to increase downstream because of (1) heat flow through the sea floor and (2) mixing with overlying warmer waters. Thus the increase of temperature along the arbitrary flow line on the western side of the deep Pacific is consistent with flow from south to north. As noted before, the rate of increase is not everywhere the same, being much greater in the central basin than it is in either the southern or the northern basin; the changes in rate appear to occur near the supposed positions of the sills between basins. At a lesser depth (4 km) the rate of increase is constant (about 0.05°C per 10^8 km) throughout the southern and central basins; in the northern basin there is no temperature increase at this depth.

The observed changes in rate of temperature increase imply that the speed of flow is not the same in all basins, or that the rate of adding heat, either through the sea floor or from above, is not everywhere the same. The speed of flow in the various basins cannot easily be determined from the present data, but it is obvious that the rate of heating is not uniform everywhere. The available measurements of heat flow through the sea floor show at least 50-fold variation [*Von Herzen*, 1959]. In the northern basin, where the rate of temperature increase is very small, heating from below must be important because at all deep stations in that region *in situ* temperature *decreases* upward to a deep temperature minimum at a depth of about 4 km. Such a temperature minimum is not evident in the central basin, where the rate of temperature increase is greatest, or in the southern basin.

The dissolved oxygen content of bottom water can be expected to decrease downstream because of (1) consumption in oxidative processes (respiration, decomposition) and (2) mixing with overlying, more poorly oxygenated waters. Decreasing oxygen concentrations along the arbitrary flow line tend to support the temperature data in indicating northward flow of the bottom water. The rate of decrease is about the sam at both 5 and 4 km, although the oxygen con centration is usually higher at the greater depth

In the northern basin changes in the proper ties of bottom water are smaller, and the natur of the circulation is not clear. The slight west to-east increase in temperature across the Nortl Pacific is compatible with the classical pictur of clockwise circulation, as is shown by th arbitrary flow line. A slight decrease in oxyge content (and an increase in that of inorgani phosphorus) is also consistent with the indi cated direction of flow. On the other hand temperature data from the eastern basin sug gest that waters there are derived from th central basin rather than from the eastern par of the northern basin. In either case, it seem likely that bottom water of the eastern Nortl Pacific, with the highest temperature and low est oxygen concentration, is the 'oldest' botton water of the open Pacific.

References

Brodie, J. W., and R. W. Burling, Age determina tions of southern ocean waters, *Nature, 181,* 107 108, 1958.

Brujewicz, S. W., On certain chemical features o waters and sediments in northwest Pacific *Proc. UNESCO Symp. Phys. Oceanog.,* 1955 Tokyo, 277–292, 1957.

Bruneau, L., N. G. Jerlov, and F. F. Koczy, Physi cal and chemical methods, *Rept. Swed. Deep Sea Exped., 3*(4), 99–112, I-LV, 1953.

Bruun, A. F., and A. Kiilerich, Characteristics o the water masses of the Philippine, Kermade and Tonga Trenches, *Papers Marine Biol Oceanog., Deep-Sea Research, suppl. 3,* 418–425 1955.

Carlsberg Foundation, Hydrographical observa tions made during the "Dana" Expedition 1928 1930, *Dana Rept., 2* (12), 1–46, 1937.

Craig, Harmon, Isotopic tracer techniques fo measurement of physical processes in the se and the atmosphere, in *The Effects of Atomi Radiation on Oceanography and Fisheries,* NAS NRC Publ. no. 551, 103–120, 1957.

Deacon, G. E. R., The hydrology of the southern ocean, *Discovery Rept., 15,* 1–124, 1937.

Discovery Committee, Station list 1931–1933, *Dis covery Rept., 21,* 1–226, 1941.

Discovery Committee, Station list 1937–1939, *Dis covery Rept., 24,* 197–422, 1947.

Discovery Committee, Station list R. R. S. "Wil liam Scoresby" 1931–1938, *Discovery Rept., 25* 143–280, 1949.

Eckart, Carl, Properties of water, Pt. II, The equations of state of water and sea water at low

temperatures and pressures, *Am. J. Sci., 256,* 225–240, 1958.

Fleming, J. A., C. C. Ennis, H. U. Sverdrup, S. L. Seaton, and W. C. Hendrix, Observations and results in physical oceanography, Oceanography I-B. *Carnegie Inst. Wash. Publ. 545,* 315 pp., 1945.

Japan, Maritime Safety Agency, The results of oceanographic observations in the northwestern Pacific Ocean. No. 3. 1931–1935, *Hydrogr. Bull.,* Publ. no. 981, Spec. no., 1–139, 1950.

Japan, Maritime Safety Agency, The results of oceanographic observations in the northwestern Pacific Ocean. No. 4. 1935–1938, *Hydrogr. Bull.,* Publ. no. 981, Spec. no. 8, 1–143, 1951.

Japan, Maritime Safety Agency, The results of oceanographic observations in the northwestern Pacific Ocean. No. 5. 1938–1941, *Hydrogr. Bull.,* Publ. no. 981, Spec. no. 9, 1–194, 1952.

National Institute of Oceanography, Station list 1950–1951, *Discovery Rept. 28,* 299–398, 1957.

Postma, H., Tables. Oxygen, hydrogen ion, alkalinity and phosphate, *Snellius Rept., 4,* 1–35, 1959.

Stommel, H., The abyssal circulation, *Deep-Sea Research, 5,* (1), 80–82, 1958.

Sverdrup, H. U., M. W. Johnson, and R. H. Fleming, *The Oceans, their Physics, Chemistry, and General Biology,* Prentice-Hall, New York, 1087 pp., 1942.

Swallow, J. C., A neutral-buoyancy float for measuring deep currents, *Deep-Sea Research, 3,* 74–81, 1955.

Swallow, J. C., and L. V. Worthington, Measurements of deep currents in the western North Atlantic, *Nature, 179,* 1183–1184, 1957.

Van Riel, P. M., H. C. Hamaker, and L. Van Eyck, Tables. Serial and bottom observations. Temperature, salinity and density, *Snellius Rept., 2*(6) 1–41, 1950.

Von Herzen, R., Heat-flow values from the southeastern Pacific, *Nature, 183,* 882–883, 1959.

Wooster, W. S., and B. A. Taft, On the reliability of field measurements of temperature and salinity in the ocean, *J. Marine Research Sears Foundation, 17,* in press.

Wüst, Georg, Bodentemperatur und Bodenstrom in der pazifischen Tiefsee, *Veroff. Inst. Meeresk. Univ. Berl., Neue Folge, A. Geogr.-naturwiss.,* (35), p. 56, 1937.

(Manuscript received January 11, 1960.)

The Effect of the Gulf of Mexico on Rayleigh Wave Dispersion

D. H. SHURBET

Seismological Observatory, Texas Technological College
Lubbock, Texas

Abstract. The dispersion of Rayleigh waves crossing the Gulf of Mexico was measured. It is shown that the observed dispersion can be accounted for by considering the presence of unconsolidated sediments. The average sediment thickness required to account for the dispersion is 7 km.

Introduction. The velocity of Rayleigh waves of very long period is strongly influenced by the properties of the earth's mantle. It was shown by *Ewing and Press* [1954] that dispersion curves for Rayleigh waves with periods longer than about 75 sec are identical for both continental and oceanic paths.

Investigation of Rayleigh waves which have traversed only continental paths show reasonably consistent dispersion in the period range from about 10 sec to about 75 sec, and the dispersion of oceanic Rayleigh waves in the period range from about 75 sec to about 35 sec also agrees very closely with that predicted by theoretical curves [*Ewing, Jardetzky and Press,* 1957].

Ewing and Press [1956] showed that the observed dispersion of continental Rayleigh waves does not exactly fit the theoretical curve of Figure 1. For periods of 18 to 30 sec the observed points lie slightly above the theoretical curve. This is explained by an increase of velocity with depth in the crust. For periods greater than about 38 sec the observed points are below the theoretical curve by a small amount, which increases with increasing period. This discrepancy is accounted for by a velocity gradient in the mantle.

Oliver and Ewing [1958*b*] showed that much of the observed slowing of waves with periods shorter than 10 to 15 sec, to velocities below the theoretical curve of Figure 1, can be accounted for by considering the contribution of the sedimentary layers.

The purpose of the present study is to compare the observed dispersion of Rayleigh waves crossing the Gulf of Mexico with the theoretical and observed dispersion curves for typical oceanic and continental paths.

Presentation of data. The method of obtaining the dispersion data for the present report was to read through the Rayleigh wave train, plotting the arrival time of each consecutive peak, trough, or zero. The slope of the resulting curve gives a measure of wave period, and the corresponding group velocity can be calculated. The method is discussed by *Ewing and Press* [1952].

The U. S. Coast and Geodetic Survey epicenter data for each earthquake used in the study are shown in Table 1, in which the numbers assigned to the earthquakes correspond to the numbers assigned to the paths shown in Figure 2. In Figure 1 the solid-line curves show the theoretical dispersion of oceanic and continental Rayleigh waves as taken from *Ewing, Jardetzky, and Press* [1957]. The observed data points

TABLE 1. U. S. Coast and Geodetic Survey Epicenter Information

Earthquake Number	Deg N	Deg W	Depth of Focus, km	Origin Time, UT	Date
1	11½	86½		09 31 33	April 24, 1959
2	12	87		14 42 11	October 24, 1956
3	12½	87½	100	04 41 24	May 3, 1959
4	15½	91	150	18 16 22	February 20, 1959
5	17½	95	100	09 54 51	April 12, 1959
6	16	97		13 52 13	February 11, 1959

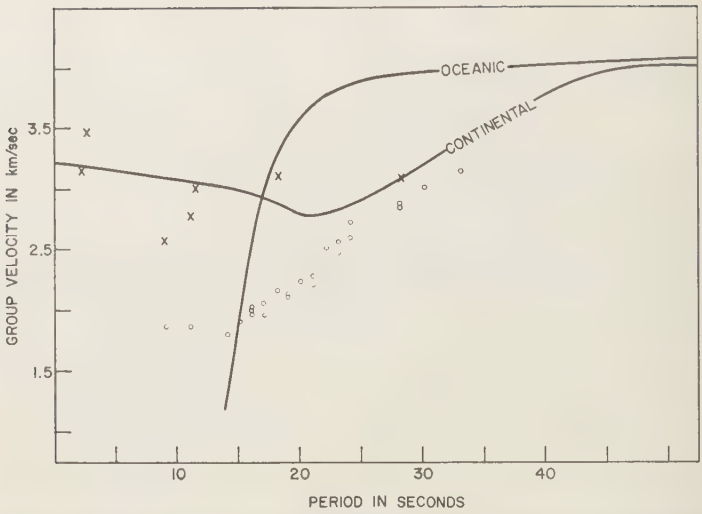

Fig. 1. Uncorrected dispersion data of earthquakes listed in Table 1 compared with theoretical Rayleigh wave dispersion curves.

Fig. 2. Map showing geographic location of epicenters and the Rayleigh wave paths to Lubbock, Texa

own with the curves of Figure 1 are from the rthquakes listed in Table 1. All data points e taken from the seismograms for the vertical strument ($T_0 = 10$ sec and $T_g = 90$ sec) ex- pt the very short waves of earthquake 6. hese waves were read from the short-period ertical seismogram ($T_0 = 1$ sec and $T_g = 1$ c).

The dispersion data of earthquake 6, plotted crosses in Figure 1, show that the southern art of the North American continent is similar other areas already explored by this method. here are no very long period waves, but the elocity of waves with periods between 18 and 0 sec is slightly above the theoretical curve of igure 1. For periods near 10 sec the observed oints fall below the theoretical curve, as is to e expected for sediments of average thickness *Oliver and Ewing,* 1958*b*]. The very short eriod waves which arrive early approximately t the *M*2 dispersion curve of *Oliver and Ewing* 1958*a*]. The belief that the structure of the outhern part of the continent is not extremely ifferent from average continental structure is trengthened by the study of other earthquakes long the coast of Mexico to about latitude 25°N. The dispersion details of these earthquakes are not included in the present study. However, for periods shorter than 10 sec the velocities 'tail off' below the theoretical curve, an indication of about average continental sediments [*Oliver and Ewing,* 1958*b*]. The very short period waves roughly fit the *M*2 theoretical curve.

The observed data for earthquakes 1, 2, 3, 4, and 5 are plotted as points in Figure 1. It is seen that these points do not lie close to the theoretical curve for oceans or the curve for continents. This is to be expected, as it is seen in Figure 2 that earthquakes 1, 2, 3, 4, and 5 have slightly different proportional amounts of Gulf of Mexico structure in the path to Lubbock. The outline of the physiographic provinces of the Gulf of Mexico as shown in Figure 2 is taken from *Ewing, Ericson, and Heezen* [1958]. These provinces are used to make corrections to the observed dispersion data of Figure 1. It is commonly accepted that an appropriate line of demarkation between continental and oceanic structure is the 1000-fathom curve or the edge of the continental slope. Therefore the edge of the continental slope (Fig. 2) is

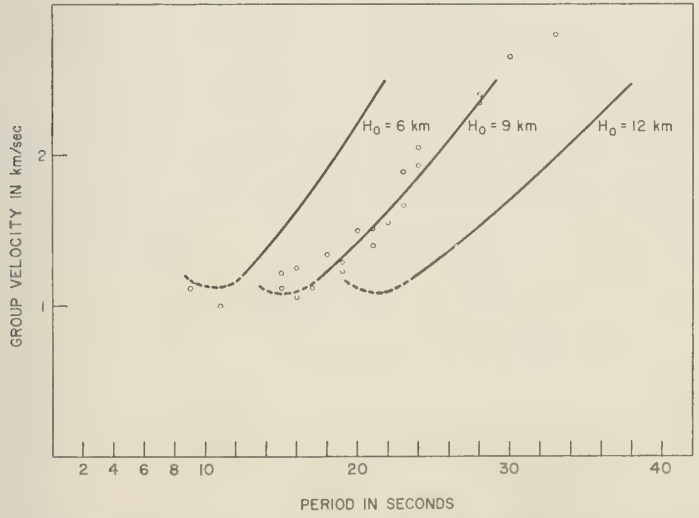

Fig. 3. Corrected dispersion data of earthquakes listed in Table 1 compared with calculated group-velocity curves. Points indicate velocities calculated by subtracting times required to traverse land and abyssal path segments from the total observed travel time. Curves are obtained by differentiation of curves of Figure 4.

TABLE 2. Computed Values of k (Wave Number) for Selected Values of C (Phase Velocity)

C, km/sec	k				
	H_0 = 3 km	6 km	9 km	12 km	18 km
1.60	1.320	0.662	0.442	0.333	0.221
1.70	.907	.455	.305	.231	.157
1.80	.7215	.364	.245	.186	.124
1.90	.6221	.313	.212	.161	.109
2.0	.5435	.275	.187	.142	.096
2.1	.4846	.247	.168	.128	.086
2.28	.401	.209	.143	.111	.073
2.35	.3805	.199	.136	.103	.0695
2.4	.3665	.1925	.131	.100	.067
2.66	.294	.1615	.111	.084	.0565
2.7	.287	.158	.108	.082	.055
2.75	.275	.153	.105	.080	.0535
2.8	.267	.149	.102	.078	.052
2.85	.252	.145	.0995	.076	.051
2.9	.245	.141	.097	.073	.049
2.97	.237	.136	.094	.071	.048
3.04	.226	.131	.090	.069	.046
3.15	.210	.124	.086	.065	.044

H_0 = depth of liquid, km.
H_1 = intermediate layer thickness = 10 km.
V_p in liquid = 1.52 km/sec.
V_p in intermediate layer = 5.5 km/sec.
V_p in infinitely thick lower layer = 8.1 km/sec.

taken as the boundary between continental and oceanic structures. The observed velocities are corrected by assuming that from the coast line to Lubbock and from epicenter to coast line the waves travel with typical continental velocities. Across the abyssal zone the velocities are assumed to be typical of oceanic structures. The travel times for these segments of the paths are subtracted from the total travel time, leaving the time required for the waves to cross the path segment between the coast line and the ocean side of continental slope. Sediment effects were included in the land-path segment in the amount indicated by the data from earthquake 6. The dispersion data of earthquake 6 do not exactly fit the theoretical continental curve, but the variations are those explained in the introduction and are taken into account in the correction of observed data. Scatter in the corrected data is not considerably less than in the uncorrected data. The lack of scatter in the uncorrected data reflects the fact that there is no great variation in the proportional amount of Gulf structure included in each path. The corrected dispersion data for earthquakes 1, 2, 3, 4, and 5 are plotted as points in Figure 3. These points are calculated by subtracting from the observed travel time the time required for the waves to traverse abyssal and land-path segments.

Figure 4 shows phase-velocity curves calculated for cases of different liquid depths (H_0) using the method of *Jardetzky and Press* [1953]. The calculations were made for case I of Jardetzky and Press, and the calculated values of k (wave number) for selected values of C (phase velocity) are shown as Table 2. The group velocity is obtained by graphical differentiation of the phase-velocity curves and the resulting group-velocity curves where H_0 (liquid depth) is 6 km, 9 km, and 12 km are shown in Figure 3. The corrected dispersion data closely fit the theoretical curve for the case H_0 = 9 km. This layer includes both water and unconsolidated sediments, and the average sediment thickness can be calculated by subtracting the average water depth along the path from the total thickness of the liquid layer. Bathymetric charts of the Gulf show that a good value of average water depth along the paths is about 2 km. This gives an average value of 7 km for the thickness of unconsolidated sediments along the paths.

Colle and others [1953] showed that the sedi-

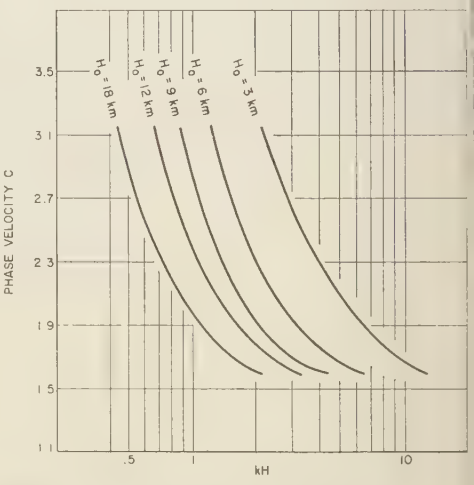

Fig. 4. Calculated phase-velocity curves for various liquid layer thicknesses.

nts at the Texas Gulf coast are about 14 km
ck, and *Ewing, Worzel, Ericson, and Heezen*
955] concluded that the main basin of the
ulf of Mexico is typically oceanic, modified by
e addition of about 7 km of sediments.

The present study agrees well with the 7-km
lue for average sediment thickness and there-
re adds little new information on the struc-
ral picture of the Gulf of Mexico. However,
is case is a significant example of the value of
is method for measuring sediment thickness.

Conclusions. 1. The study of Rayleigh wave
spersion is a valuable method of measuring
e thicknesses of sedimentary columns. 2. A
itable distribution of stations around the Gulf
Mexico would make possible improved accu-
cy of similar measurements and greater areal
verage.

References

olle, Jack, W. F. Cooke, Jr., R. L. Denham, H. C. Ferguson, J. H. McGuirt, Frank Rudy, Jr., and Paul Weaver, Sedimentary volumes in Gulf Coastal Plains of United States, part IV, Volume of Mesozoic and Cenozoic sediments in western Gulf Coast Plains of United States, *Bull. Geol. Soc. Am., 63,* 1193–1200, 1953.

wing, M., D. B. Ericson, and B. C. Heezen, Sediments and topography of the Gulf of Mexico, in *Habitat of Oil,* Am. Assoc. of Petrol. Geologists, Tulsa, Okla., June 1958.

Ewing, M., W. Jardetzky, and F. Press, *Elastic Waves in Layered Media,* McGraw-Hill, New York, 1957.

Ewing, M., and F. Press, Crustal structure and surface wave dispersion, part II, *Bull. Seism. Soc. Am., 42,* 315–325, 1952.

Ewing, M., and F. Press, Mantle Rayleigh waves from the Kamchatka earthquake of November 4, 1952, *Bull. Seism. Soc. Am., 44,* 471–479, 1954.

Ewing, M., and F. Press, Surface waves and guided waves, *Encyclopedia of Physics, 47,* Geophysics I, 119–139, Springer-Verlag, Berlin, 1956.

Ewing, M., J. L. Worzel, D. B. Ericson, and B. C. Heezen, Geophysical and geological investigations in the Gulf of Mexico, part I, *Geophysics, 20,* 1–18, 1955.

Jardetzky, W. S., and F. Press, Crustal structure and surface wave disperson, part III: Theoretical disperson curves for suboceanic Rayleigh waves, *Bull. Seism. Soc. Am., 43,* 137–144, 1953.

Oliver, J., and M. Ewing, Normal modes of continental surface waves, *Bull. Seis. Soc. Am., 48,* 33–49, 1958*a*.

Oliver, J., and M. Ewing, The effect of surficial sedimentary layers on continental surface waves, *Bull. Seism. Soc. Am., 48,* 339–354, 1958*b*.

(Manuscript received September 2, 1959; revised January 27, 1960.)

The Seismic Sea Wave of July 9, 1956, in the Greek Archipelago

N. N. AMBRASEYS[1]

Department of Fluid Mechanics and Hydraulic Works
National Technical University of Athens
Athens, Greece

Abstract. The earthquake of July 9, 1956 (magnitude 7½, epicentral intensity VIII-IX MM), with epicenter at 36°54′N, 26°12′E, was followed by a severe seismic sea wave which originated near 36°49′N, 26°09′E. The wave was probably produced by a series of landslides on the steep banks of the submarine trench of Amorgos. The amplitude of the wave near its source was 100 feet, and the agitation of the sea within the central area lasted several days. A list of seismic sea waves in the Greek archipelago and adjacent seas is given in the Appendix.

Introduction. The Greek archipelago contains numerous islands, many of which are of volcanic origin and are well known for their seismicity. On the morning of July 9, 1956, these islands experienced one of the most disastrous seismic sea waves in their contemporary history. The wave was of local origin and followed the violent earthquake of the same date.

Many other seismic sea waves have occurred in the Greek archipelago, but most of them caused no serious damage. Several seismic sea waves, however, have been severe enough to cause loss of life, damage to property, and in some cases devastation of entire towns. Noteworthy were the waves that wiped out many towns in Crete, among which were probably Knossos and its landing place, Amnisos; the date of the event is not accurately known but it appears to have been circa 1400 B.C. [*Marinatos,* 1934, 1939; *Galanopoulos,* 1957, 1958] Historians and writers of the classic Hellenistic, Roman, and Byzantine periods described the destruction of many towns in Greece by such waves, for instance, the destruction of Potidaea (or Cassandreia) in Chalcidice in 479 B.C., some towns in Euboea in 426 B.C., and Hiera in A.D. 62 or 66. Pausanias described how in 373 B.C. the town of Helice perished under the waters of the Gulf of Corinth, where '. . . the population was drowned to a man.'[2] Diodorus Siculus described the deluge of Samothrace where the inhabitants of the island had time to take refuge in the mountains and save themselves. Great waves caused catastrophes in A.D. 365, 1650, and 1821. In the Appendix a number of seismic sea waves which have occurred in the Greek archipelago and adjacent seas are listed chronologically.

There is little doubt that the coasts of Greece and Asia Minor are often subject to such calamities, the severity of which is mainly attributable to the lack of local dissipative zones and the abundance of narrow passages and V-shaped bays which characterize these coasts.

The severity of the waves of July 9, 1956, was not uniform. It varied greatly from place to place and over rather short distances. Waves up to 100 feet in height were observed, and many casualties were reported. The area affected by the waves exceeded 40,000 square miles, and the disturbance of the sea lasted over 24 hours.

Characteristics of the seismic sea wave. The earthquake which preceded or coincided with the seismic sea wave of July 9, 1956, occurred at 03 11 38 GMT (Local time = GMT + 2 hours) with an epicenter at 36°54′N, 26°00′E. The magnitude of the shock was 7½, and it was followed, at 03 24 05 GMT by a strong aftershock of magnitude 7, the epicenter of which was at 36°48′N, 25°12′E [*National Observatory, Athens,* 1956, 1957].

In the Greek archipelago there are occasional large earthquakes at unusually great depths. The most recent previous earthquakes occurred on June 26, 1926 (magnitude 8.2), with a focal

[1] Now at Imperial College of Science and Technology, London.

[2] Pausanias vii; 25.8, cf. Senec. *Quest. Nat.* lib. 6.25.

depth of 100 km; next in magnitude was the earthquake of July 9 which, however, appears to have been relatively shallow [*Richter*, 1958].

Arrival times from a number of stations furnished by the *Hydrographic Service of the Royal Hellenic Navy* [1956], the *National Observatory in Athens* [1956, 1957], and *Galanopoulos* [1956] made it possible to determine analytically that the seat of the disturbance was at 36°49′N, 26°09′E. It is shown in Figure 1 together with the wave fronts computed from arrival times and the topography of the sea bed. The latter was obtained from charts issued by the *Hydrographic Service, R.H.N.* [1953] and the *Hydrographic Department, R.N.* [1956–1957] as well as from pilot reports of the area under consideration [*Hydrographic Department, R.N.*, 1955].

It should be pointed out that the wave fronts shown in Figure 1 were computed by means of Lagrange's equation for long waves. Waves produced by submarine landslides, however, do not fall into the class of long waves, since dipolar[3] disturbances produce waves whose velocity is not independent of their length. Such waves after they have traveled a short distance from their source can be considered Cauchy-Poisson waves. Hence, the wave fronts shown in Figure 1 represent only approximately the development of the actual wave fronts.

The shape of the zero-time wave front approximates an ellipse, and it was found to have

[3] Disturbances of dipolar type are produced by the sudden transfer of material within the disturbed medium without any change in its initial total volume.

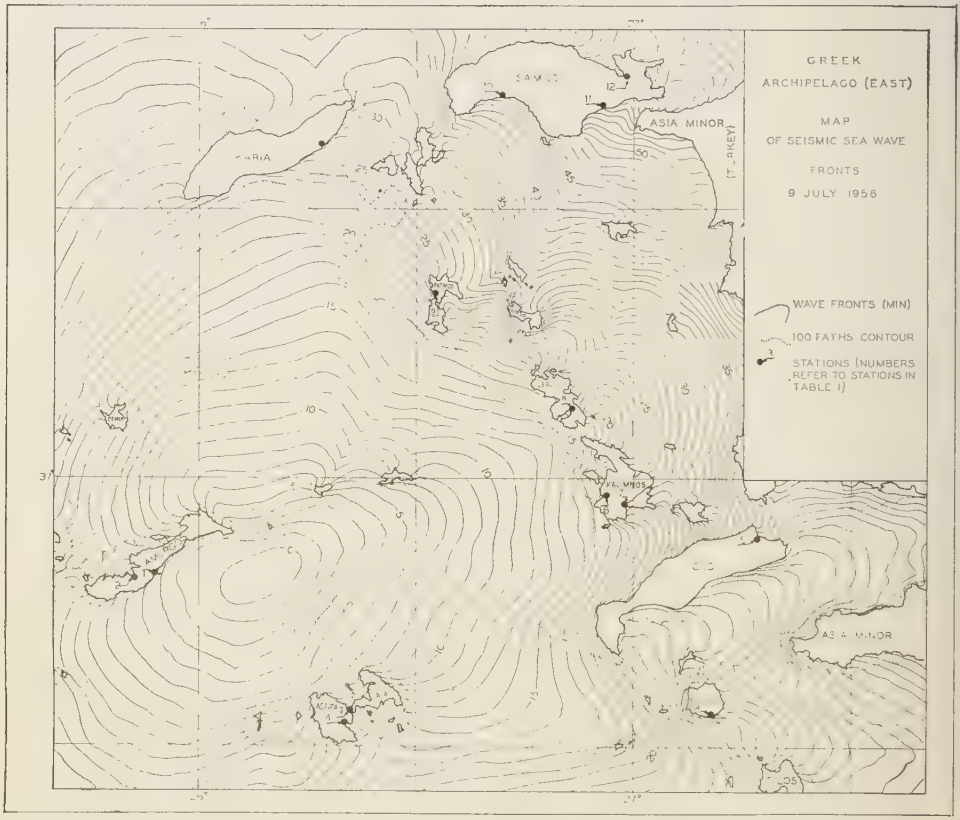

Fig. 1. Greek archipelago (east). Map of seismic sea wave fronts, July 9, 1956.

en formed at 03 11 42 GMT, or nearly at the me time as the first shock. The principal axis the ellipse is situated over the deepest part the submarine trench of Amorgos and coinides with the trough of the trench, which is er 400 fathoms deep. This region was obrved during the phenomenon to be most agited, and waves near the southeast coast of the and of Amorgos up to 100 feet in height were ported by the Observatory stations. A strong rbidity of the sea which was observed in this gion lasted for several days.

In his report to the Academy of Athens, *alanopoulos* [1956] inferred from the evidence n the phenomenon that the cause of the wave ust be sought in a submarine landslide or ers of landslides triggered by the seismic shock. he fact that the depth of the focus should ave been in layers of low velocity and that the picentral intensity of VIII to IX MM is rather nall in comparison with the seismic magnitude d Galanopoulos (private communication) to xclude any advance of the crustal dislocation the seabed.

It is most probable that the cause of the wave was not a unipolar disturbance, such as a subsidence or caving in of the seabed, but rather a series of submarine landslides. The steep slopes[4] of deposits on the banks of the submarine trench of Amorgos could easily have been made to slide under the influence of a shock as intense as that of July 9. The fact that the duration of the surface disturbance of the sea near the source of the wave was so long (over 28 hours) indicates that the source ought to have been of a dipolar type, since waves produced by submarine subsidences or fault-drops are feeble and die out easily.

Disturbances of dipolar type should require the surface waves to advance from their source with a crest always formed first, followed by a trough from 1 to 3 times the amplitude of the first crest, followed by a crest of about the same amplitude as the trough. From the available information on the mode of agitation of the sea on the coasts near the source, it appears that

[4] The mean slope of the banks of the trench vary between 10° to 20° near the coast of Amorgos and 25° near the northeastern end of the island.

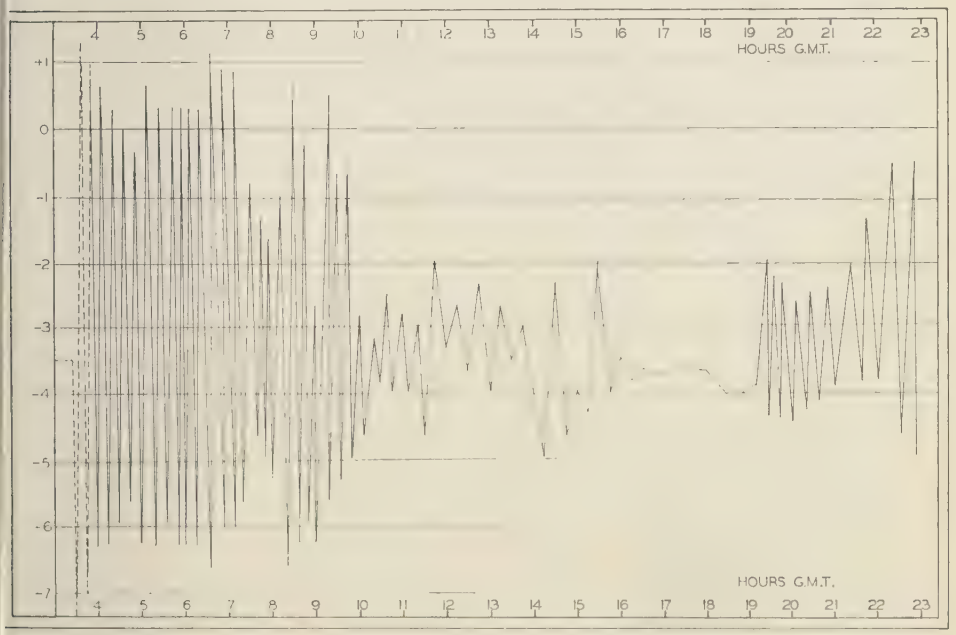

Fig. 2. Sea-level fluctuations, Laki station, Leros.

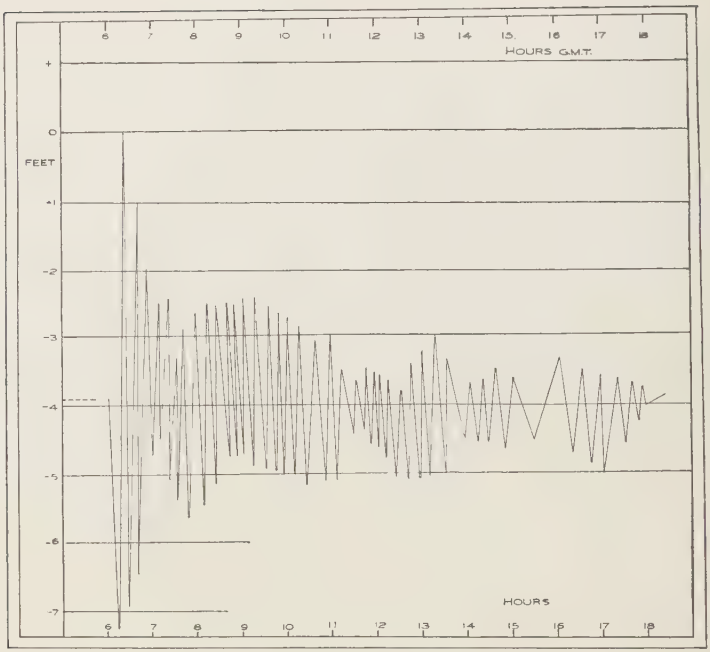

Fig. 3. Sea-level fluctuations, Souda station, Crete.

the first movement of the sea was a recession, which does not agree with a dipolar disturbance. The information concerning the initial stage and development of the wave was supplied by observers and not by instrumental records. It is therefore most probable that the observers who reported the mode of attack of the first wave front near the source missed the initial stage of the phenomenon owing to its short period and small amplitude as compared with the period and amplitude of the following trough. It has been noticed in the past that, though reports from observers showed that the first effect of the wave was a trough, tide-gage records in the same region showed that the first actual effect was a crest [*Shepard and others*, 1950]. In the present case, however, this cannot be checked, since neither of the two tide gages functioned in the affected area during the whole day of July 9. Both instruments were rendered temporarily useless by the seismic shock.

Accurate readings of the sea level taken at short intervals at two stations (Souda and Laki) by the Hydrographic Service, R.H.N. (private communication), as well as from *Galanopoulos's* [1956] report, made it possible to reproduce the fluctuations of the sea level at these stations (Figs. 2 and 3). In both cases the initial part of the marigram was missing.

A phenomenon usually observed during the development of seismic sea waves is that although the initial movement of the sea near the source of disturbance is a recession, at a distance it may appear to be an advance, or vice versa. A possible explanation of this phenomenon lies in the refraction-reflection properties of waves as well as in the scattering of the wave front on islands and reefs. Waves traveling from one island to another by different paths may arrive at a given locality after being reflected. Their phase at the moment of arrival will greatly contribute to their final size and phase. A series of intersections of a major wave of, say, negative initial elevation, with a number of reflected minor waves of positive elevation may finally result in the formation of a wave traveling crest first. This is particularly true for islands shadowed by intermediate obstacles, as are most of the islands of the Greek archipelago.

A summary of the reported characteristics of

e wave is given in Table 1, and Figure 4 shows e locations of the stations listed in Table 1. Since the available data are few and their curacy rather low, a more extensive treat- ent of the phenomenon is thought to be un- rranted.

Effect of the waves on islands of the archi- lago. On Kalimnos, and in the town of Kalim- os, the wave was felt most strongly and the mage inflicted there was rather severe. In e town of Pothea the sea retired first and then se with a great swell, flooding the shore and e entire town. The height of the wave was 8 et on land, and its impulse was so severe that ocks of residential buildings on the harbor as ell as small shipbuilding installations 100 yards land were badly damaged. Over thirty fishing oats and one large sailing ship were tossed on nd and crushed. Three times the sea receded id advanced in the first hour, carrying debris id furniture 1 mile inland. A person was seized id carried by the wave ¾ mile inland; three her persons were drowned. Extensive areas of ultivated land at various places on the island ere washed away.

At Porto-Scala on the island of Astipalaia, the rst wave was 16 feet high on land and surged 00 yards into the town. A large number of shing boats were crashed on shore and debris as carried over 500 yards inland. In other arts of the island hundreds of acres of culti- ated land were washed away. Two persons ere injured and a number of houses damaged. ne house collapsed.

At the town of Katapola on Amorgos island, he wave was 9 feet high and caused consider- ble damage to harbor works and houses near he sea front. Four large sailing ships were hrown onto the quay and four others were recked on shore. The pavement of the quay ettled and the quay proper was damaged. The each near the town and the land behind it ere littered with trunks and limbs of trees, and ultivated land farther inland was washed up. t the southeast coast of the island waves up to 00 feet in height crashed against the rocky liffs of the coast. This part of the island is parsely populated, and, because of the rocky opography of the coast, villages are perched igh on the rocks. No casualties were reported.

On the island of Antiparos the sea over- lowed the shores and also the town of Kastro, which stands on a ridge near the northern end of the island. Little damage was done to build- ings near the coast, but the quay was washed away and other parts of the pier settled con- siderably. A motorboat was taken by the waves and crashed on the rocks 15 yards inland, and a score of fishing boats were taken offshore.

On the island of Lipso the sea advanced 700 yards, and many houses were damaged. In Sokora a large number of cattle were taken by the wave and drowned. In the harbor of Lipso

TABLE 1. Characteristics of the Seismic Sea Wave of July 9, 1956

No.	Station	A	B	C	D	E	F
1.	AMORGOS	−	100				
2.	Katapola	+	9	10			
3.	ASTIPALAIA	−	67				
4.	Porto-Scala	−	16	17	10		11
5.	COS	+	3	2			
6.	KALIMNOS	−	12	17		3	
7.	Pothea	−	8	8		3	
8.	LEROS, Laki	−	4	4			
9.	PATMOS, Scala	−	13	50			
10.	SAMOS						
	Marathokambos	−	7	7	8		
11.	Tigani	−	3	5	8		
12.	Vathi	−	2	3	10		
13.	KASSOS,						
	Ag. Marina	−	4	5	5		
14.	NISYROS,						
	Mandraki	(?)	9				
15.	KIMOLOS	−	4	5			
16.	FOLEGANDROS	−	33	26			
17.	PAROS, Parikia	−	4	5			
18.	IOS	+	5	10	15		
19.	ERMIONI	(?)	3	3	8		6
20.	KYTHIRA,						
	Kapsalos	+		3	5		
21.	SERIFOS	+	3	2	5		
22.	NAXOS	+	4	3			
23.	SKOPELOS	(?)	1	1	8		
24.	CRETE, Sitia	+	5	5	5		
25.	Ag. Nikolaos	−	3	4	6		
26.	Palaiokastro	+	12	13			
27.	Heraclion	+	7				
28.	Souda	−	4	3	6		6
29.	Chania	(?)	3	2			
30.	Rethymnon	(?)	4	6	10		7
31.	ATTICA, Voula	−		1	5		
32.	TINOS	(?)	10				
33.	POROS	(?)			10		

A Reported initial movement of the sea level; (−) ebb, (+) tide.
B Maximum amplitude of tide observed (in feet).
C Maximum amplitude of ebb observed (in feet).
D Mean period of wave observed (in minutes).
E Number of waves observed in open sea.
F Velocity of waves observed (in miles per hour).

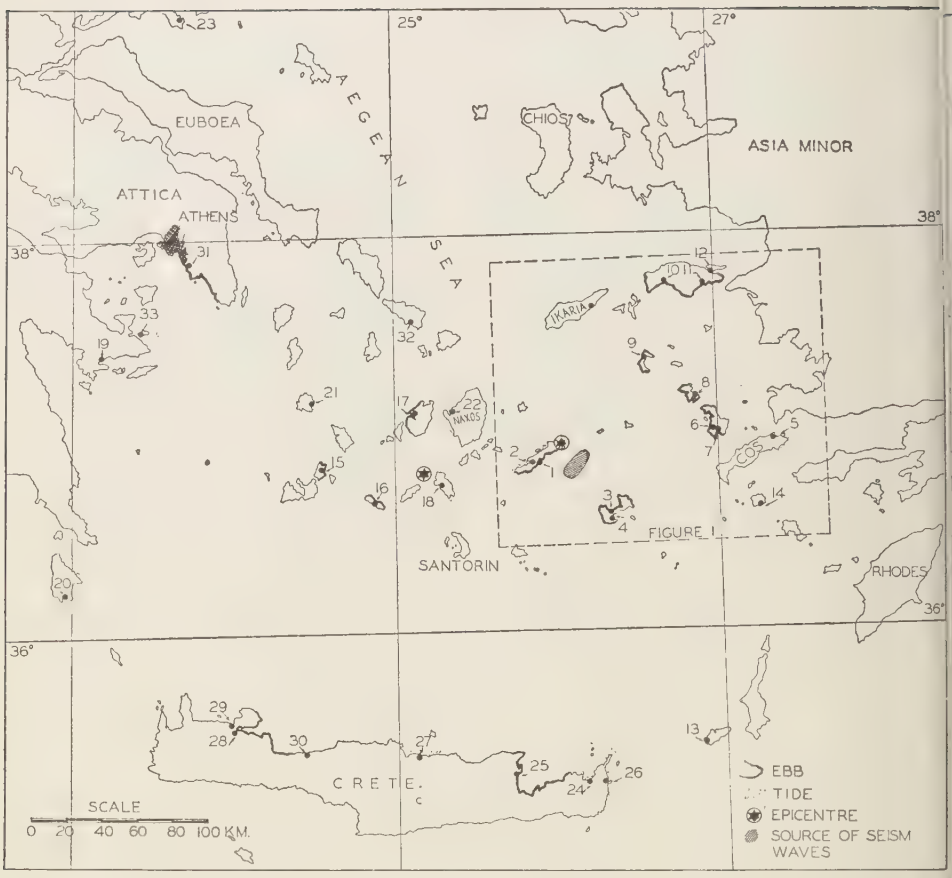

Fig. 4. Locations of the stations listed in Table 1.

the wharf and quay were demolished and harbor facilities were severely damaged. One house collapsed.

Near Laki, on Leros island, the first movement was a retreat of the sea. Although the height of the waves was only 4 feet, many houses around the harbor were damaged and goods stored on the wharfs were taken away by the waves. Ten fishing boats were taken by the waves and destroyed. Many fishing villages on the island were flooded.

In the town of Foiniki, on Karpathos island, the wave was so severe that it demolished the breakwater and anchorage of the harbor. The height of the wave there was over 20 feet; many villages were flooded, with severe damage to houses, and thirty cattle were drowned.

On the southwest promontory of the island of Rhodes the islet of Prasonisos, which was connected with the island by a narrow belt of land 1000 feet long, was detached shortly after the shock, the stretch of land connecting it with Rhodes subsiding more than 30 feet underwater. It is not clear whether this subsidence was the result of the seismic shock. It appears, however, that the isthmus of Prasonisos subsided because of spreading of the soft material of which it was composed.

Appendix

The following is a list of seismic sea-waves which have occurred in the Greek archipelago

ig. 5. Locations of seismic sea waves which have occurred in the Greek archipelago and adjacent seas.

nd adjacent seas. Entries prior to A.D. 1400 re the only ones found for the region under onsideration in classic works and chronicles of ie time. It is believed, however, that the list is ncomplete, in particular for the time prior to .D. 1200.

In early times, chronicles referred for the ost part to widespread disasters and, since mall disasters caused by seismic sea waves were ever chronicled or, if they were, were disguised n various texts, only the large ones are traceale. A considerable number of such references have been found during the author's search in many texts, but they are not included in the following list because their origins are obscure and their dates uncertain. Such allegorical statements can be found, for instance, in Homer (*Iliad* v; 638–651, xiv; 234–258), in Strabo's *Geography* (xvi; 2.26-28, xvi; 4.23), in Diodorus Siculus' *Histories* (v; xlvi), and in Procopius' *Histories of the Wars* (8;25), not to mention those found in ecclesiastic archives which are most difficult to interpret. It is believed, however, that further research in early

TABLE 2. Seismic Sea Waves in the Greek Archipelago and Adjacent Seas

Date	Location
c. 1400 B.C.	SANTORIN, CRETE, Amnisos, Knossos
c. 1300 B.C.	TROAD
479 B.C.	CHALCIDICE, Potidaea
426 B.C.	MALIACOS, OPUNTIAN gulfs, ATALANTA, PEPARATHOS Isl.
373 B.C.	Gulf of CORINTH, Helice
222 B.C.(227?)	RHODES, TILOS Isls., Carian and Lycian towns
62 A.D.(65?)	CRETE
77 A.D.	CYPRUS, Episkopi
365 21 Jul.	CRETE, ASIA MINOR
543 6 Sept.	ASIA MINOR, Kyzicos
551 7 or 9 Jul.	MALIACOS Gulf
554	COS, DODECANESE Isls.
558 14 Dec.	MARMARA Sea, Constantinople
740 26 Oct.	MARMARA Sea, Constantinople
1050	CYCLADES Isls., SANTORIN
1222 25 Dec.	CYPRUS, Paphos
1344 14 Oct.	Constantinople
1389 20 Mar.	CHIOS, LESVOS Isls., Smyrna
1481 3 May	RHODES. DODECANESE Isls.
1509 14 Sept.	BOSPORUS Sea, Constantinople
1612 8 Nov.	Sea of CRETE, CRETE
1622 5 May	IONIAN Isls., ZANTE
1646 5 Apr.	Constantinople
1650 29 Sept.	SANTORIN
1748 14 May	Gulf of CORINTH, Aiyion
1805 8 Jan.	Gulf of PATRAS, Patras
1817 23 Aug.	Gulf of CORINTH, Aiyion
1821 9 Jan.	IONIAN Isls., ZANTE
1856 13 Nov.	AEGEAN Isls., CHIOS
1859 20 Oct.	Pireaus
1861 26 Dec.	Gulf of CORINTH
1866 22 Jan.	CHIOS
1866 28 Jan.	SANTORIN
1866 Oct.	MIRTOON Sea, KITHERA Isl.
1867 10 Apr.	Lixouri
1867 20 Sept.	IONIAN Isls., SYROS
1871 5 Oct.	Gulf of CORINTH
1878 15 Apr.	Nikomedia, Prussa
1893 28 Jan.	SAMOTHRACE Isl.
1894 16 Apr.	SKIATHOS, ATALANTI Isls.
1914 27 Nov.	IONIAN Isls., Lefkas
1928 25 Apr.	Piraeus
1932 26 Sept.	Gulf of STRIMON, Ierissos
1933 23 Apr.	COS, DODECANESE Isls.
1948 9 Feb.	KARPATHOS, DODECANESE Isls.
1948 22 Apr.	IONIAN Isls., LEFKAS
1956 9 Jul.	AEGEAN Isls., CRETE

Hellenistic and Byzantine literature may pro rewarding, and it is hoped that a more comple list of seismic sea waves for the Greek arch pelago may be presented soon.

References to the occurrences listed in Table are so numerous and of such a nature that it considered unwarranted to present them her Dating of early events and, in many instance the historical checking of such occurrences r quire that so many references and commentari be quoted a detailed presentation of the even in Table 2 is by itself a subject of historical r search. It will be treated as such elsewhere.

There are, however, many references whic can be mentioned here, for instance, *Heck* [193 1947], *Schmidt* [1879], *Galanopoulos* [1955 and Philipson and Osswald's 'Seimisch-geologisc Übersichtskarte von Griechenland,' as well a reports of the Commission pour l'Etude des Ra de Marée and the Matériaux pour l'Etud des Calamités. In none of the references is th original source of information given, save i Schmidt's catalog, and in many instances th dating of the events is incorrect. Schmidt's an Galanopoulos's lists of earthquakes in Greec contain many references to seismic sea wave and it can be said that they are the most com plete catalogs for this region.

Figure 5 shows the locations listed in Table Since the consulting of atlases is difficult whe there is a variety of spelling in use, place name are given as in the *Mediterranean Pilot* [1955 of the Royal Navy. In Table 2 place names ar given as reported in the texts which were con sulted; entries in capital letters indicate name of regions affected by the waves and the name following refer to towns.

Acknowledgements. The subject matter of thi paper is condensed from data compiled for th investigation of the seismic stability of harbo works in the Greek archipelago while the autho was a member of the staff of the Department o Fluid Mechanics, National Technical Universit of Athens (1954–1956).

I wish to acknowledge the help given by Pro fessor A. Galanopoulos of the Seismological Lab oratory, University of Athens, and by Captain E Colokythas R.H.N. of the Hydrographic Servic of the Royal Hellenic Navy.

References

Galanopoulos, A., Erdbebengeographie von Grie chenland, *Ann. géol. Pays Helléniques, 6*, 83 121, 1955 (in Greek with summary in German)

anopoulos, A., The seismic sea-wave of July 9, 956, *Proc. Acad. Athens, 32,* 90–101, 1956 (in reek).

anopoulos, A., Zur Bestimmung des Alters der antorinkaldera, *Neues Jahrb. Geol. u. Paläon-ol., 9,* 419–420, 1957.

anopoulos, A. Zur Bestimmung des Alters der antorinkaldera, *Ann. géol. Pays Helléniques, 9,* 35–188, 1958.

ck, N., List of seismic sea-waves, *Ann. Comm. our l'Etude des Raz de Marée,* no. 4, 20–41, 'aris, 1934.

ck, N., List of seismic sea-waves, *Bull. Seism. oc. Am., 37,* 270, 1947.

drographic Service of the Royal Hellenic Navy, Chart of South Aegean Sea, Votanikos, Athens, 953.

drographic Service of the Royal Hellenic Navy, Report on the seismic phenomenon of July 9th, 956, near Amorgos island, *Interim report,* 1956 in Greek).

drographic Department Royal Navy, Admiralty, *Mediterranean Pilot, 4,* London, 1955.

Hydrographic Department Royal Navy, Admiralty, Charts N.1866/1956, N.2682/1957, N.2836*a*/1957, London, 1956–1957.

Marinatos, S., Amnisos die Hafestadt des Minos, *Forsch, u. Fortschr., 10,* 341–343, 1934.

Marinatos, S., The volcanic destruction of Minoan Crete, *Antiquity, 13,* 425–439, Gloucester, 1939.

National Observatory, Athens, *Bull. Prelim. de l'Inst. Seism. Athènes,* July 1956.

National Observatory, Athens, *Bull. Seism. Inst.,* no. 7, 1957.

Richter, C., *Elementary Seismology,* W. H. Freeman Co., San Francisco, 618–619, 1958.

Schmidt, J., *Studien über Erdbeben,* Alwin Georgi, Leipzig, 1879.

Shepard, F., C. McDonald, and D. Cox, The tsunami of April 1, 1946, *Bull. Scripps Inst. Oceanog. Univ. Calif., 5,* 404–406, 1950.

(Manuscript received November 5, 1957; revised September 23, 1959.)

Seepage into Ditches from a Plane Water Table Overlying a Gravel Substratum[1]

DON KIRKHAM

Iowa State University, Ames, Iowa

Abstract. The problem of flow of ponded water over a stratum of homogeneous soil overlying a stratum of gravel, the gravel in turn overlying an impermeable layer, is solved for the case in which equally spaced ditches penetrate into the gravel. Flow nets are obtained, as are formulas giving the quantity of water seeping through the ground into the ditches. The theory shows that unless the ditches are closer together than about three times the depth of the stratum of soil overlying the gravel, the proportion of water entering the ditches through the ditch walls is small compared with that reaching the ditches by way of the underlying gravel stratum.

ntroduction. The solution of the problem of seepage of water from a plane water table drainage ditches has been given by the au- [*Kirkham,* 1950]. A similar problem is t with in the present paper and is indicated Figure 1. A related problem has been dealt n experimentally by *Youngs* [1959], using an tric-analog technique. In his problem, steady nfall replaces the ponded water of Figure 1, tile drains replace the ditch drains.

nalysis. In Figure 1 a series of drainage hes at distance apart $2s$ are cut into a homogeneous soil stratum overlying highly permeable material which we may consider to be gravel. The ditches just reach or penetrate into the gravel, and water stands in them to a height h above a plane separating the gravel from the upper layer of soil. The thickness of this upper layer of soil is d. The soil is completely waterlogged to the surface and has a layer of surface water of thickness t. The problem is to analyze the flow and, in particular, to obtain flow nets and expressions for the quantity of water reaching the ditches for different values of s, d, and h.

We assign the origin and x, y axes of a coordinate system as shown in Figure 1. If we take the reference level for hydraulic head (potential) to be the plane $y = 0$ and the hydraulic conductivity of the gravel to be infinite, and if

Contribution from the Department of Agron-, Iowa State University. Journal Paper No. 96 of the Iowa Agricultural and Home Eco- ics Experiment Station, Ames, Iowa. Project 998.

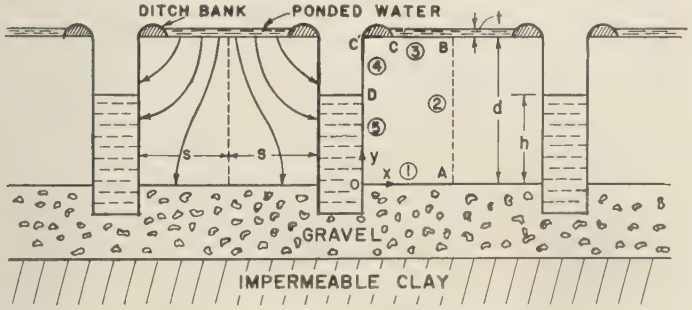

Fig. 1. Geometry for drainage ditches in soil overlying gravel, the gravel in turn overlying impermeable clay; streamlines are schematic; circled numbers refer to boundary conditions above equation of the text.

we consider the semisection $OABCC'DO$ between successive ditches, the boundary conditions are seen to be

1. Along OA $(0 < x < s, y = 0)$, $\phi = h$
2. Along AB $(0 < y < d, x = s)$, $\partial\phi/\partial x = 0$
3. Along BC', if CC' is infinitesimal,
$(0 < x < s, y = d)$, $\phi = d + t$
(Finite CC' will be considered later.)
4. Along $C'D$ $(h < y < d, x = 0)$ $\phi = y$
5. Along DO $(0 < y < h, x = 0)$ $\phi = h$

Laplace's equation for this two-dimensional problem is

$$\partial^2\phi/\partial x^2 + \partial^2\phi/\partial y^2 = 0 \qquad (1)$$

Let A_n $(n = 1, 2, 3, \ldots)$ be arbitrary constants. Then, as the reader may verify, a solution of equation 1 which satisfies boundary conditions 1, 2, and 3 is

$$\phi = h + [(d + t - h)/d]y - \sum_{n=1}^{\infty} A_n \frac{\cosh [n\pi(s - x)]/d}{\cosh n\pi s/d} \sin n\pi y/d \qquad (2)$$

To satisfy boundary condition 4, equation 2 becomes

$$y = h + \frac{d + t - h}{d} y - \sum_{n=1}^{\infty} A_n \sin \frac{n\pi y}{d}, \qquad h < y < d$$

and to satisfy boundary condition 5, equation 2 becomes

$$h = h + \frac{d + t - h}{d} y - \sum_{n=1}^{\infty} A_n \sin \frac{n\pi y}{d}, \qquad 0 < y < h$$

Reversing the order of the last two equations and simplifying them, we find

$$[(d + t - h)/d]y = \sum_{n=1}^{\infty} A_n \sin n\pi y/d, \qquad 0 < y < h$$

$$h + [(t - h)/d]y = \sum_{n=1}^{\infty} A_n \sin n\pi y/d, \qquad h < y < d$$

If we define $f(y)$ by

$$f(y) = [(d + t - h)/d]y, \quad 0 < y < h \qquad (3$$

$$= h + [(t - h)/d]y, \quad h < y < d \qquad (3$$

we have a Fourier half-range series for determining the A_n, namely

$$f(y) = \sum_{n=1}^{\infty} A_n \sin n\pi y/d, \qquad 0 < y < d$$

where, as is known, the A_n are given by

$$A_n = \frac{2}{d} \int_0^d f(y) \sin \frac{n\pi y}{d}\, dy$$

Using (3a) and (3b) in (4), we find, after performing the integration and simplifying,

$$A_n = 2\, dn^{-2}\pi^{-2} \sin (n\pi h/d) - 2tn^{-1}\pi^{-1} \cos n\pi \qquad (4$$

Our solution, then, which satisfies all the boundary conditions, is equation 2, with the given by equation 5.

Equations 2 and 5 enable us to plot the equipotentials. In order to plot the streamlines we must determine the stream function ψ. The function (see advanced calculus books) is related to ϕ by the Cauchy-Riemann equations

$$\partial\phi/\partial x = \partial\psi/\partial y \qquad (5$$

$$\partial\phi/\partial y = -\partial\psi/\partial x \qquad (6$$

By inspection of (2), (6), and (7), a suitable form of ψ is seen to be

$$\psi = -[(d + t - h)/d]x - \sum_{n=1}^{\infty} A_n \frac{\sinh [n\pi(s - x)/d]}{\cosh n\pi s/d} \cos n\pi y/d \qquad (7$$

We can add an arbitrary constant to the right hand side of (8), if we wish, without upsetting the validity of (6) and (7). The right-hand side of (8) is negative because the flow enters a 'sink' rather than leaves a 'source.' The source situation is conventional for a positive sign. Flow nets obtained from (2), (5), and (8) will presently be given.

Quantity of water entering the ditches. The volume of water $Q/2$ *entering* one side of a ditch per unit time (Q being that entering from both sides) is the same as the volume of water ente

the soil surface between $x = 0$ and $x = s$. ce we have

$$Q/2 = (-) \int_0^s - k(\partial\phi/\partial y)_{y=d}\, dx \qquad (9)$$

t is, utilizing (2) and (5), we have

$$= 2ks\left[\frac{d + t - h}{d} - \frac{1}{s}\sum_{n=1}^{\infty}\left(\frac{2d}{n^2\pi^2}\sin\frac{n\pi h}{d} - \frac{2t}{n\pi}\cos n\pi\right)\cdot\tanh\frac{n\pi s}{d}\cdot\cos n\pi\right] \qquad (10)$$

ere the quantity in parentheses under the mation sign is A_n of equation 5.

ince, in equation 10, $t/s = (t/d)/(s/d)$, wing that t/s may be expressed as a function $/d$ and s/d, and since other geometric quanes in the brackets occur as ratios h/d and , we may write the last equation in the form

$$Q = ksF(t/d,\ h/d,\ s/d) \qquad (11)$$

ere F is the coefficient of ks in the right-hand e of (10).

f in equation 11, $t = 0$ the right-hand side the equation becomes

$$Q_{t=0} = ksF(h/d,\ s/d) \qquad (12)$$

ere, as is seen from (10) and (12),

$$h/d,\ s/d) = 2(d - h)/d - \frac{2}{s}\sum_{n=1}^{\infty}\frac{2d}{n^2\pi^2}\sin\frac{n\pi h}{d}\cdot\tanh\frac{n\pi s}{d}\cdot\cos n\pi \qquad (13)$$

ABLE 1. Values of F, Equation 13, for Comting Q, the Flow into a Ditch, by Equation 12

	s/d					
	0	0.5	1.0	2.0	3.0	∞
)	2.000	2.000	2.000	2.000	2.000	2.000
!	2.000	1.906	1.772	1.688	1.660	1.600
(	2.000	1.772	1.514	1.358	1.308	1.200
)	2.000	1.548	1.202	1.002	0.936	0.800
)	2.000	1.106	0.772	0.588	0.524	0.400
)	0	0	0	0	0	0

Values of $F(h/d,\ s/d)$ are given in Table 1, for which the column headed by $s/d = 0$ needs some explanation.

To obtain the values in the column headed $s/d = 0$, we make use of the fact that when $s \to 0$ in the right-hand side of (13), tanh $n\pi s/d \to n\pi s/d$; so that F becomes

$$F_{s\to 0} = 2(1 - h/d) + \frac{4}{\pi}\left(\sin\frac{\pi h}{d} - \frac{1}{2}\sin\frac{2\pi h}{d} + \frac{1}{3}\sin\frac{3\pi h}{d} - \cdots\right)$$

That is, since [see *Dwight*, 1947, formula 416.07]

$$[\sin \pi h/d - (1/2)\sin 2\pi h/d + \cdots] = \pi h/2d$$

we have

$$F_{s\to 0} = 2 \quad \text{when} \quad h/d < 1$$
$$= 0 \quad \text{when} \quad h/d = 1$$

An important point to note in Table 1 is that the entries in the column for $s/d = 3$ are roughly the same as the entries in the column for $s/d = \infty$. This means that practically all the flow goes into the gravel in both the latter cases, the proportion entering the walls of a ditch being negligible.

There is another point of interest in Table 1. When $s/d = \infty$ and $t = 0$, values of F are seen to be directly proportional to $(d - h)/d = 1 - h/d$, and, in fact, it is seen that they are then equal to $2(1 - h/d)$, also seen from equation 13. Since these F values for $s \to \infty$ are directly proportional to $d - h$, we see that, for $s \to \infty$, the influence of the ditches on the flow stems only from the head of water in them, and not from the leakage through their walls.

A table of values associated with the flow into a ditch which shows more clearly how Q varies with s is that given by a quantity $G(h/d,\ s/d)$ defined by

$$G(h/d,\ s/d) = (s/d)F(h/d,\ s/d) \qquad (14)$$

With G so defined, we see from (11) and (13) that

$$Q/kd = G(h/d,\ s/d) \qquad (15)$$

Thus, using the G form, we see that, with constant d, the values of G are directly propor-

TABLE 2. Values of G, Equation 14, for Computing Q, the Flow into Both Sides of a Ditch, by Equation 15

	s/d				
h/d	0	0.5	1.0	2.0	3.0	∞
0	0	1.000	2.000	4.000	6.000	∞
0.2	0	0.953	1.772	3.376	4.980	∞
0.4	0	0.886	1.514	2.716	3.924	∞
0.6	0	0.774	1.202	2.004	2.808	∞
0.8	0	0.553	0.772	1.176	1.572	∞
1.0	0	0	0	0	0	0

tional to the flow. Table 2 gives values of G. It has been obtained from Table 1 by multiplying the entries there by s/d. Table 2 shows that for $h/d = 0$ the flow is directly proportional to s, there being zero leakage through the ditch walls.

Flow net. A flow net for $t = 0$ is shown in Figure 2. Here the ditches are close together at semispacing $s = d$. The ditches are half full and, for this close spacing, we see that more than 50 per cent of the flow enters the wall of the ditch, less than 50 per cent reaching the gravel substratum. Instead of thinking of the ditches as such, we can think of them as vertical slots, made, for example, by a mole plow or by vertical mulching equipment [*Spain and McCune,* 1956]. The figure shows that slots that are closely spaced and vertical will be helpful promoting drainage if they can run reasonab ($h<0.5d$) freely. Rather than using ditches, ho ever, it would be better to place an underdr in the gravel, keeping the underdrain running atmospheric pressure. In this latter event would have, effectively, the situation $h/d =$ For this, we see in equation 10 that with $t =$ a maximum value of Q would result, since wi $h/d = 0$ and $t = 0$ the subtractive summati term in the right-hand side of (10) would vani

In the flow net shown, the stream function not given as determined from (8) but is giv in such a way that 100 per cent of the fl enters the ditch from one side. The actual valu of ψ determined from (8), which correspond $\psi = 0$, 25, 50, 75, and 100 in Figure 2, a $\psi = 0.73$, 0.05, -0.64, -1.32, and -2.00, r spectively. The last value, -2.00, is exactly $-$ because the summation in (8) is zero wh $x = s$ (and because of the choice of values the figure for d, h, and s).

Consideration of width of ditch banks. far we have considered the width of the dit banks to be zero and $t = 0$. If t is not zero, should expect that, for zero thickness of dit wall in Figure 1, the velocity of the water e tering the ditch near the point ($x = 0$, $y =$ would be infinite. To show that it is infinite, have from (8) and (5), when $y = d$ and $x =$

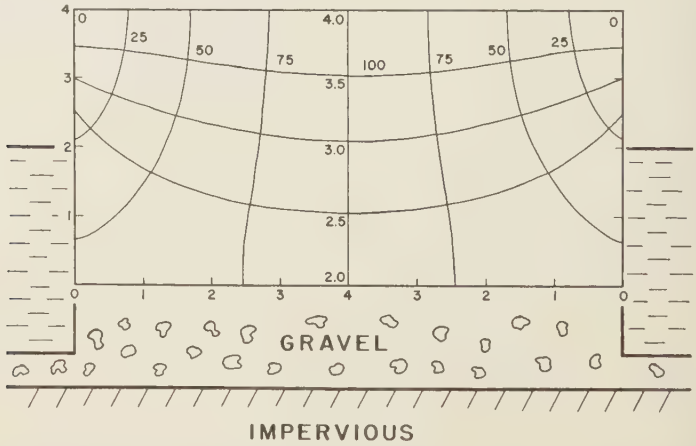

Fig. 2. Flow net for Figure 1 when t, the surface water thickness, is zero. The stream lines 0, . . . , are percentages with reference to the flow to one side of a ditch; the equipotentials 2, 2.5, 3 . . . , are in feet of hydraulic head if the dimensions in the drawing are feet.

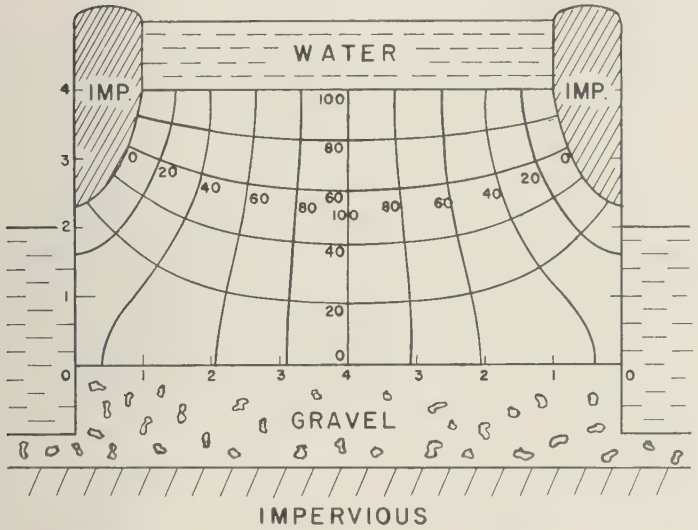

Fig. 3. Flow net for Figure 1 when $t/d = 1/4$, $s/d = 1$, and $h/d = 1/2$; situation corresponds to a ver limit of true flow, since the region indicated as impervious under the ditch banks will, in prac- e, not be impervious.

$$= -\sum_{n=1}^{\infty} (2d/n^2\pi^2) \sin n\pi h/d \cdot \tanh n\pi s/d \cdot \cos n\pi + \sum_{n=1}^{\infty} (2t/n\pi) \cos n\pi \cdot \tanh n\pi s/d \cdot \cos n\pi$$

re the first sum converges; but the second n, because $\cos^2 n\pi = 1$, becomes

$$\sum_{n=1}^{\infty} (2t/n\pi) \tanh n\pi s/d$$

ere $\tanh n\pi s/d$ approaches 1 as n increases. see that this last series diverges, suppose that, er the first three terms, $\tanh n\pi s/d = 1$ to lesired degree of approximation, say 3 deci- ls (which would be true for $s/d > 1/3$); then terms after the first three terms in the series

$$(2t/\pi)(1/4 + 1/5 + 1/6 + \cdots)$$

ich is a series the value of which is known to infinity.

To keep the stream function finite, we may npute its value for decreasing values of x wn to some finite value $x = \epsilon$ near $x = 0$. To erpret ϵ physically, we may consider that the dth of the ditch bank is of value ϵ, the material in the ditch bank being impervious. If we further imagine the material under the ditch bank to the left of a streamline passing through the point $(x = \epsilon, y = d)$ as given by equation 8 to be impervious, we can construct a flow net for the case $t \neq 0$. Based on these interpretations of ϵ, the flow net shown in Figure 3 has been obtained. The value of ϵ has been taken for convenience to be $h/2$, with the other geometrical values as in Figure 2. The case for $t \neq 0$ is presented, among other reasons, for its value in filter problems.

The approximate value of the flow reaching both sides of the ditch in the case of a ditch bank of thickness ϵ is, when an impermeable region below the ditch bank is assumed as in Figure 3 (compare equation 9),

$$Q = 2 \int_{\epsilon}^{\cdot} - k(\partial\phi/\partial y)_{y=d}\, dx$$

That is, using (10) and integrating, we have

$$Q = 2k(s - \epsilon)\left[\frac{d + t - h}{d} - \frac{1}{s - \epsilon} \sum_{n=1}^{\infty} A_n \cos n\pi \frac{\sinh n\pi(s - \epsilon)/d}{\cosh n\pi s/d}\right] \quad (16)$$

The values of Q given by the right-hand side of (16) will be somewhat low, since in actuality the material under the wall of the ditch bank and lying to the left of the streamline passing through the point $x = \epsilon$, $y = d$, is not impervious, as we have postulated, but is of the same permeability as the stratum of thickness d under consideration.

Surface drainage. Although our analysis has shown that subsoil drainage is helped by the ditches, especially if they are close together, it is clear that surface drainage will be a more effective method for removing ponded water than subsurface drainage.

Conclusions. Referring to Figure 1, we conclude:

1. Unless the drainage ditches are closer together than $s = 3d$, the proportion of water entering the ditches through the ditch walls, when $t = 0$, will be small compared with that reaching the ditches by way of the underlying gravel, even when the width of the ditch banks approaches zero (but not when $t \neq 0$ and the width of the ditch banks approaches zero).

2. If in addition to $t = 0$ we have also $h = 0$, then no water will seep through the ditch walls, regardless of whether s is large or small, provided the gravel may be considered to be infinitely permeable compared with the overlying soil.

3. If s is greater than $3d$, the influence of t ditches on drainage will primarily be a con quence of the height of water in them; the fore, for obtaining maximum seepage flow, t height of water in the ditches should be kept or below the level of the gravel.

4. If s is greater than $3d$, subsurface dra kept at atmospheric pressure will remove wa almost as fast as will the ditches when runni at $h = 0$, provided the ditches do not acc surface runoff and t is small compared with t width of the ditch banks.

5. If there is ponded water, $t \neq 0$, then su face drainage (width of ditch banks zero) w remove the water faster than will subsurfa drainage.

References

Dwight, H. B., *Tables of Integrals and other Ma ematical Data*, Macmillan, New York, 1947.

Kirkham, Don, Seepage into ditches in the case a plane water table and an impervious su stratum, *Trans. Am. Geophys. Union, 31,* 42 430, 1950.

Spain, J. M., and D. L. McCune, Something n in subsoiling, *Agron. J., 48,* 192–193, 1956.

Youngs, E. G., Water table heights in a drain homogeneous soil overlying an infinitely perm able layer, *J. Soil Sci., 10,* 101–104, 1959.

(Manuscript received January 21, 1960.)

Application of the Multiple Regression Approach in Evaluating Parameters Affecting Water Yields of River Basins

A. L. SHARP,[1] A. E. GIBBS,[2] W. J. OWEN,[1] AND B. HARRIS[3]

[1] *U. S. Department of Agriculture, Lincoln, Nebraska*
[2] *U. S. Department of the Interior, Lincoln, Nebraska*
and
[3] *Department of Mathematics, University of Nebraska Lincoln, Nebraska*

Abstract. The efficacy of the use of the multiple correlation and regression approach in evaluating parameters affecting water yields of river basins is examined. Results of several analyses of annual and monthly streamflow of the Delaware River Basin in Kansas are presented to provide a background for an examination of the method. Hydrologic data, in general, and factors affecting water yield, in particular, may not fit the premises upon which the multiple regression method of analysis is based: (1) There are no errors in the independent variables; errors occur only in the dependent variable. (2) The variance of the dependent variable (streamflow) does not change with changing levels of the independent variables (precipitation, for example). (3) The observed values of the dependent variable are uncorrelated random events.

Hydrologic data may not fit the further assumption implicit in tests of significance of multiple correlation and regression coefficients, that is, that the dependent variable (streamflow) is normally distributed about the regression line for fixed levels of the independent variables under consideration.

It is concluded that (1) although the multiple regression approach will result in a line of best fit and best estimating equation for hydrologic data, it is not safe to place too much reliance on values estimated by such equations, particularly at levels far removed from the mean, despite very high correlation coefficients and (2) some of the more modern statistical procedures may be better tools than the multiple regression approach for evaluating effects of watershed parameters on water yield.

INTRODUCTION

'or many years multiple linear (or curvilin-) regression analyses have been used in dying streamflow, forecasting water supplies n snowmelt, and estimating flood peaks. 'Co-rative Water Yield Procedures Study,' a nt effort of the Agricultural Research Serv- and the Soil Conservation Service of the De-rtment of Agriculture and the Bureau of clamation of the Department of the Interior, also employed these methods in its project analytic hydrology. The objectives of the ject are to develop methods of estimating cts of conservation practices and treatment land on the flow of streams and rivers.

Multiple regression analysis is a valuable tool many kinds of studies. It permits evaluation the combined effects of many parameters on a dependent variable. Relative effects of each parameter can be determined, and over-all efficiency can be measured by coefficients of determination. The significance of the relation between each independent variable and the dependent variable can be obtained. A 'best' estimating equation can be derived. These many desirable attributes of the method commended its use in the Cooperative Water Yield Procedures Study project.

In this project the method has been applied to many river basins in the Great Plains with the purpose of attempting to detect changes, if any, in streamflow resulting from changes in the use and treatment of land. Results of applying the method in various ways to the Delaware River Basin, Kansas, are shown, and the applicability of the method is examined.

Delaware River Basin

The Delaware River Basin in Northeast Kansas has a drainage area of 922 square miles above the U. S. Geological Survey's gaging station at Valley Falls, Kansas. Standard rain gages were operated by the U. S. Weather Bureau at Valley Falls, where the stream gage is located, at Horton, on the eastern edge of the watershed, at Holton, on the western edge, and at Centralia, which is just outside the upper (north) end of the watershed, during the period of runoff records, July 1922 to July 1959. Average annual precipitation, largely concentrated in the spring and summer months, is about 32 inches. Most of the watershed is cultivated or in pasture. A small area in the southwest corner is wooded and some woods also occur along the stream channels. Crops are mostly corn and small grain.

Soils of the watershed include thin loessial caps on the ridges, clay loams on the slopes, and colluvium along the streams. Topography of the watershed varies from flat on some wide ridge tops to gently rolling, and to steeply rol along the 'breaks' adjacent to the stream-ch nel bottom lands. Erosion has been a ser problem in the watershed. A Civilian Conse tion Corps camp was established in the mi 1930's and the Soil Conservation Service local Soil Conservation Districts have been tive since that time in combating the ero problem. About 25 per cent of the needed servation work has been accomplished, acc ing to estimates of local technicians and dents. This includes installation of small st tures, grassed waterways, and terraces. It includes adoption of improved crop rotati seeding eroded areas to grass, increasing leg inous crops, fertilizing, liming, strip cropp and contour tillage.

Analyses performed. Early exploratory a yses of the rainfall-runoff relations of the D ware River Basin were made on a calen year basis. Parameters included were

X_1 = annual streamflow (1 unit = 1 acre-feet), the dependent variable

TABLE 1. Results of an Exploratory Multiple Regression Analysis of Calendar-Year Runoff and O Data of the Delaware River Basin, Kansas

Condition	Regression Equation	Coef. of Determination	Standard Error	Avera Annu Runo
	With Linear Values of Variables	R^2 [a]	$\bar{S}$ [b]	$\bar{X}_1$
Thiessen wtd. precip.	$X'_1 = 23.10^{**} X_2 + 0.34^{*} X_3 + 3.41X_4 - 580$	0.810	100.7	281
Correlation wtd. precip.	$X'_1 = 24.30^{**}X_2 + 0.33^{*}X_3 + 2.85X_4 - 613$	0.833	94.4	281
	With Logarithmic Values of Variables			
			Log Units	Log
Thiessen wtd. precip.	$\log X'_1 = 2.71^{**} \log X_2 + 0.23^{**} \log X_3 + 0.09 \log X_4 - 2.25$	0.829	0.156	2.32
Correlation wtd. precip.	$\log X'_1 = 2.85^{**} \log X_2 + 0.23^{**} \log X_3 + 0.08 \log X_4 - 2.45$	0.861	0.141	2.32

** Indicates significance at the 1 per cent level.

* Indicates significance at the 5 per cent level.

[a] The coefficient of determination, R^2 (unadjusted for small sample), indicates the variability in dependent variable explained by the independent variables used. The coefficient of nondetermina in per cent, 100 $(1 - R^2)$, represents the variation in the dependent variable due to error and other varia not included in the analysis. R^2 is a measure of the efficiency of the regression equation.

[b] $\bar{S}$ indicates standard error adjusted for small sample.

= annual precipitation (1 unit = 0.1 inch) computed by use of Thiessen weights or weighted by correlations between individual rain-gage records and runoff
= average December and January (essentially base) flow to reflect long-time antecedent conditions of the watershed (1 unit = 1000 acre-feet)
= a numerical progression, 1 to 31, to reflect changes in soils, land use, land treatment, etc., with time

linear- and logarithmic-transformation yses were made with the results shown in e 1.

will be noted that in no case was the nucal progression significantly related to run- Both X_2, precipitation, and X_3, average ember-January runoff (base flow as a re- or of antecedent watershed conditions) were ficantly related to runoff. It appears from e results that logarithmic values are more il than linear values. Logic indicates, how-, that this may not be so. First, logarithmic sformations of variables should be adopted when and if such transformations truly re- the relations between the variables, that is n such relations are exponential. Second, the tion of logs is multiplication. It is not be- d to be logical that precipitation, anteced- watershed conditions, and a numerical pro- sion should be multiplied to obtain runoff.

will also be noted the determination of rshed-precipitation by weights obtained by elating the precipitation at each station runoff is seemingly better than the use of ssen weights, as judged from values of and $\bar{S}$. This procedure, however, uses up tional degrees of freedom, and it is entirely ible that the larger coefficients of determina-, R^2, are less significant statistically than e obtained when Thiessen weighted precipita- is used.

mple correlations were next computed be- en watershed-precipitation (obtained by ssen weights) and runoff for water years nning with the first of the 12 separate ths of the year.[4] A 36-year record was avail-

Based on an unpublished paper presented by D. L. Brakensiek, ARS, at the December 1957 ting of the American Society of Agricultural ineers.

TABLE 2. Results of Choosing Different Times to Begin the Water Year, Delaware River Basin, Kansas

Water Year	Coef. of Determination r^2	Water Year	Coef. of Determination r^2
Jan. 1 to Dec. 31	0.834	July 1 to June 30	0.876
Feb. 1 to Jan. 31	.826	Aug. 1 to July 31	.667
Mar. 1 to Feb. 28	.850	Sept. 1 to Aug. 31	.734
Apr. 1 to Mar. 31	.880	Oct. 1 to Sept. 30	.780
May 1 to Apr. 30	.895*	Nov. 1 to Oct. 31	.746
June 1 to May 31	.874	Dec. 1 to Nov. 30	.812

* Indicates 'best' water year.

able for study. It was found that the 'best' hydrologic year extended from May 1 to April 30, inclusive, with a correlation coefficient r of 0.946. The 'worst' year was August 1 to July 31, with $r = 0.817$. The normal water year, October 1 to September 30, had $r = 0.883$, whereas for the calendar year, $r = 0.913$. Squaring the correlation coefficients to obtain coefficients of determination resulted in the values given in Table 2 for 12 different water years.

These coefficients of determination indicate that precipitation in the 'best' hydrologic year supposedly explains 90 per cent of the variability in runoff, whereas in the 'worst' year only 67 per cent is explained. The 'best' years is 12 percentage points better than the normal water year, October 1 to September 30.

It appeared from this study and from an examination of platted precipitation and hydrographs that the best time to begin the hydrologic year is in the spring when the watershed is well soaked. Following this reasoning, we developed rainfall, runoff, and other parameters for a variable water year beginning in April, May, or June, when rainfall and runoff data indicated that the watershed soils were wettest. There was no overlap in time.

This variable hydrologic year did not prove to be as good as the 'best' hydrologic year of uniform length and dates insofar as precipitation and water-yeld relations are concerned.

The coefficients between precipitation and runoff were $r = 0.892$ and $r^2 = 0.796$. These values may be compared with $r = 0.946$ and $r^2 = 0.895$ for the 'best' constant-length water year, May 1 to April 30.

These data were further analyzed by multiple regression methods, with the following results.

$$X_1' = 0.15^* X_2 + 64^{**} X_3 + 2.50^* X_4 - 0.54 X_5 - 0.13 X_6 - 0.18 X_7 + 0.036 X_8 - 0.88$$

$$R^2 = 0.926, \qquad \bar{S} = 1.40, \qquad \bar{X}_1 = 5.52$$

where

X_1 = annual runoff in inches per variable year
X_2 = total precipitation in inches per variable year
X_3 = the sum of precipitation in each month in excess of 5 inches per month (a kind of index of storm size and intensity)
X_4 = base flow in inches per year
X_5 = change in ground-water storage from beginning of year to beginning of the following year in inches
X_6 = water in ground-water storage at the beginning of the year in inches
X_7 = average annual temperature in °F
X_8 = time, last 2 digits of year number

Again it will be noted that expressions of precipitation and base flow (X_2, X_3, and X_4 only) are significantly related to runoff (* = 5 per cent level, ** = 1 per cent level). The change in water in ground-water storage at the beginning of each year, X_6, was not significantly related to the annual water yield. Annual temperatures did not, apparently, affect annual runoff. The effects of omitting some of the variables were tested. The results on R^2 are shown in Table 3.

It can be seen from Table 3 that omission of nonsignificantly related variables, singly or in groups, had no appreciable effect on R^2 but that omission of a significantly related variable, X_4, reduced R^2 somewhat more.

It was thought that using an arithmetic progression did not actually portray effects of the use and treatment of land or of vegetative-cover conditions. Data were obtained on these factors

TABLE 3. Effects of Omitting Variables, Si and in Combinations, on the Coefficient of De mination, R^2, Delaware River Basin, Ka

Condition	R^2
Using all variables	0.9
Omitting X_8, time	.9
Omitting X_7, temperature	.9
Omitting X_6, water in ground storage	.9
Omitting X_5, change in ground-water storage	.9
Omitting X_5 and X_7	.9
Omitting X_5, X_6, and X_7	.91
Omitting X_5, X_6, X_7, and X_8	.91
Omitting X_4*, X_5, X_6, X_7, and X_8	.8

* This variable, base flow, was significa (5 per cent level) related to runoff

for use in the above analysis. The three par eters significantly related to runoff, X_2, and X_4 (precipitation, precipitation ove inches per month, and base flow), were retai X_9, percentage of the watershed in row cr X_{10}, miles of terrace per square mile of wa shed (times 1000), and X_{11}, average perc age normal of pasture at the first of each mo during the growing season, as reported by A cultural Marketing Administration, were ad to the analysis, with the following results.

$$X_1' = 0.14 X_2 + 0.72^{**} X_3 + 1.73^{**} X - 0.01 X_9 + 0.00016 . + 0.029 X_{11} - 4.97$$

$$R^2 = 0.918, \qquad \bar{S} = 1.44, \qquad \bar{X}_1 = 5.$$

Not only were use and treatment of land vegetative factors not significantly related runoff but some signs appear to be wrong. I generally believed that row crops increase r off; hence the regression coefficient of X_9 sho have a positive sign. In the above equation i negative, indicating an inverse relationship tween percentage of the watershed in row cr and runoff. According to popular concepti runoff should be inversely related to the amo of terraces in the watershed, but it was r Also, quality of grass was directly related runoff, whereas it is generally considered t quality of vegetative cover should be invers related to runoff. It will also be noted that to

cipitation is no longer significantly related runoff. Precipitation in excess of 5 inches per nth, X_3, has apparently acquired all effects of cipitation. This frequently occurs in multiple ression analysis with the inclusion of two iables, such as X_2 and X_3, which are highly related with each other. Even wrong signs y be obtained for regression coefficients un- such circumstances. In this instance the cor- ation between total precipitation, X_2, and cipitation in excess of 5 inches per month, X_3, s 0.803** (significant at 1 per cent level).

t was thought that a precipitation index ght be a better parameter than total precipi- ion. It was reasoned that some amount of ly precipitation is intercepted by vegetation, used in wetting the soil surface or in supply- ; depression storage. To test this, 0.2 inch was ducted from each day's precipitation. The ac- mulated remainder was substituted for X_2 in above analysis, with the following results.

$$X_1' = 0.18\ X_2 + 0.70^{**}\ X_3 + 2.03^{**}\ X_4 - 0.001\ X_9 - 0.0005\ X_{10} + 0.17\ X_{11} - 12.9$$

$$R^2 = 0.918, \qquad \bar{S} = 1.44, \qquad \bar{X}_1 = 5.52$$

The use of a precipitation index instead of tal precipitation did not improve R^2, it being 918 in both cases. Row crops and pasture con- ion still have the wrong signs, but terraces ve the correct sign in this case.

It was apparent from all the above analyses at in a study of relations between runoff and her watershed parameters on an annual basis e effects, if any, of agricultural practices on ter yields would not be detected. It was ought that a study of monthly values might sult in such a determination, if such effects ist. This was tried.

Because base flow in the Delaware River ries considerably from season to season and om year to year, it was decided to eliminate it om the dependent variable, X_1, in this monthly udy. Ground-water recharge, however, takes toll of some storms. In order to have the tual disposition of precipitation, ground-water charge in each month, if it occurred, was added surface (storm) runoff. This new quantity, orm runoff plus ground-water recharge, was used as the dependent variable, X_1, in the monthly study.

Three different variables for monthly precipitation were also tried. These included total monthly precipitation, accumulated monthly precipitation in excess of 0.2 inch per day, and accumulated precipitation in excess of 0.5 inch per day. These daily deductions eliminated many small daily rains and resulted in precipitation indices that perhaps more nearly reflect runoff-producing precipitation. These three separate parameters expressing precipitation were used in analyses of data for May and June, the months of greatest runoff in the Delaware Basin. No single one of the three expressions was better than the others, as judged from values of R^2; hence total monthly precipitation was used in the balance of the monthly analyses.

In all, 16 variables in various combinations were used in exploratory studies of data for May and June. These monthly data were studied in detail in order to provide a basis for selection of a practical number of parameters to use in analyses of the remaining monthly data. It should be pointed out here that inclusion of too many variables in a multiple regression analysis often leads to difficulty in the physical interpretation of the results and is often not good practice.

On the basis of these exploratory studies of May and June data, the parameters selected and the results obtained are those shown in Table 4.

It will be noted that results of this monthly anaylsis are inconsistent as regards the cultural factors. In March and April the pasture variable was related to runoff at the 10 and 20 per cent levels of significance, but the signs are different; the sign for March is negative and that for April is positive. Both should be negative, since it is generally thought that the more and better the grass the lower runoff should be. In July and August, terraces were related to runoff at the 20 per cent level. Both signs are negative, as it is thought they should be. In January and February, however, the signs of the terrace variable were positive. Row crops were related to runoff at the 20 per cent level of significance in January, March, April, and November and at the 5 per cent level in July and September. January, February, July, August, November, and

TABLE 4. Summary of Analyses of Monthly Data, Delaware River Basin, Kansas

Month		X_2	X_7	X_8	X_{10}	X_{11}	X_{13}	X_{17}	X_{18}	R^2	$\bar{S}$	$\bar{X}_1$	Re Cons
Jan.	b[1]	2.75**	0.0	0.95*	1.38*	6.55	−1.20	0.06	16.11‡	.735	188.1	148.0	−7
	t[2]	6.97		2.60	2.50	1.13	−.47	1.02	1.35				
Feb.	b	1.02†	0.0	2.74**	.44	−5.62	−1.71	.02	8.42	.765	178.4	213.3	−
	t	1.70		7.05	.70	−.91	−.68	.34	.72				
Mar.	b	3.00***	0.0	1.72‡	3.86**	−30.36*	−9.72†	−.02	−33.50‡	.687	366.6	375.2	17
	t	5.21		1.36	2.90	−2.10	−1.78	−.19	−1.43				
Apr.	b	2.06**	5.54***	.47	.41	−49.00*	16.85‡	−.12	−31.83‡	.913	367.2	650.7	21
	t	3.07	4.22	.60	.26	−2.20	1.58	−.92	−1.26				
May	b	2.31**	1.75‡	1.12**	3.34*	−10.40	−4.48	−.11	−18.56	.823	355.7	618.6	3
	t	3.31	1.31	2.84	2.65	−.42	−.40	−.91	−.73				
June	b	−.235	7.12***	1.12*	1.60	−19.17	4.84	−.20‡	9.45	.951	433.9	1343.9	8
	t	−.198	5.00	2.40	.87	−.62	.49	−1.47	.34				
July	b	1.43†	3.49*	.60†	9.64***	44.48‡	−5.93	.07	−58.82*	.843	432.6	403.7	−29
	t	1.97	2.44	1.85	4.43	1.37	−.61	.51	−2.22				
Aug.	b	.68†	1.64**	.60*	.47	18.83	1.59	−.09‡	2.24	.817	217.0	321.4	−18
	t	1.88	2.88	2.43	.40	1.09	.44	−1.23	.16				
Sept.	b	1.67**	.08‡	.83*	8.97**	16.18	−2.05	−.01	−50.58*	.801	327.9	376.0	−9
	t	3.08	1.32	2.48	3.67	.70	−.32	−.13	−2.34				
Oct.	b	1.33*	3.32*	.03	7.70***	18.45	−3.63	−.06	−6.40	.805	413.7	380.3	−11
	t	2.12	2.34	.08	4.71	.88	−.56	.41	−.24				
Nov.	b	1.62**	10.88***	.03	1.58‡	−6.14	2.32	−.04	32.44‡	.914	309.2	377.9	−6
	t	3.39	6.47	.08	1.55	−.36	.44	−.37	1.68				
Dec.	b	2.78***	0	.71*	.73	1.12	4.39	−.03	2.96	.592	270.5	165.3	−5
	t	4.92		2.31	.82	.09	.94	−.37	.18				

X_1 = Surface runoff plus ground-water recharge, inches × 1000
X_2 = Monthly precip., inches × 100
X_7 = Monthly precip., over 5", inches × 100
X_8 = First antecedent month's precip., inches × 100
X_{10} = Ground water in storage, inches × 1000
X_{11} = Monthly temp., °F
X_{16} = Percentage of watershed in row crops
X_{17} = Terraces, mi. per sq. mi. × 1000
X_{18} = Percentage in pasture × % condition/100

* Relations of t to level of significance:

t (25 degrees of freedom)	.86	1.32	1.71	2.06	2.78	3.71
Level of significance	40%	20% ‡	10% †	5% *	1% **	0.1% ***

[1] Regression coefficients.

[2] The t-test can be used to determine whether the regressi coefficient is statistically significantly different from zer t = regression coef./std. error of regression coefficient.

December had positive signs, as is believed proper. All the other months, including the two with highest significance, July and September, had negative signs.

It will also be noted that, for most months, precipitation and ground-water variables are significantly related to water yield. Temperatures are infrequently significantly related to runoff.

Coefficients of determination, R^2, vary through the year. They are low for the winter months, December through March, and high for the spring and summer months. This would be expected, since in this area some of the winter precipitation occurs as snow and may not appear as streamflow until much later. It is also worth noting that the standard error, $\bar{S}$, is as large as, or larger than, average runoff, $\bar{X}_1$, in about half of the months. It varies downward to about one-third $\bar{X}_1$ in the other months. This means that rather large errors could resu if runoff were estimated by use of the regressio equations, despite relatively high R^2 valu (Fig. 1). Values of X_1 estimated by the multip regression equation of Table 4 for the mont of June are plotted against observed values X_1. The scatter of the points about the line equal values is indicative of errors despite a R^2 of 0.951. For smaller events, some errors estimate exceed 100 per cent. Even negati runoff estimates are obtained.

These monthly data for the Delaware Riv Basin were combined by seasons and furth analyzed. Results are shown in Table 5. It w be noted, again, that those factors pertainin to climate are, in general, consistently ar significantly related to X_1. It will also be not that the cultural variables, X_{16}, X_{17}, X_{18}, ro crops, terrace expressions, and pasture, a not consistently and significantly related to X

en more important, the signs of these regres-
n coefficients are not consistent. Values of R^2
tained by seasons are no greater than those
tained for individual months; hence it may
concluded that combining months into sea-
ns does not improve the relations.

Conclusions regarding the Delaware River Basin. It may be concluded from the above that the analyses made of annual and monthly data of the Delaware River Basin fail to indicate whether or not the installed program of conservation practices and treament of land affects streamflow. It may be that the amount of conservation and treatment of land in the water-

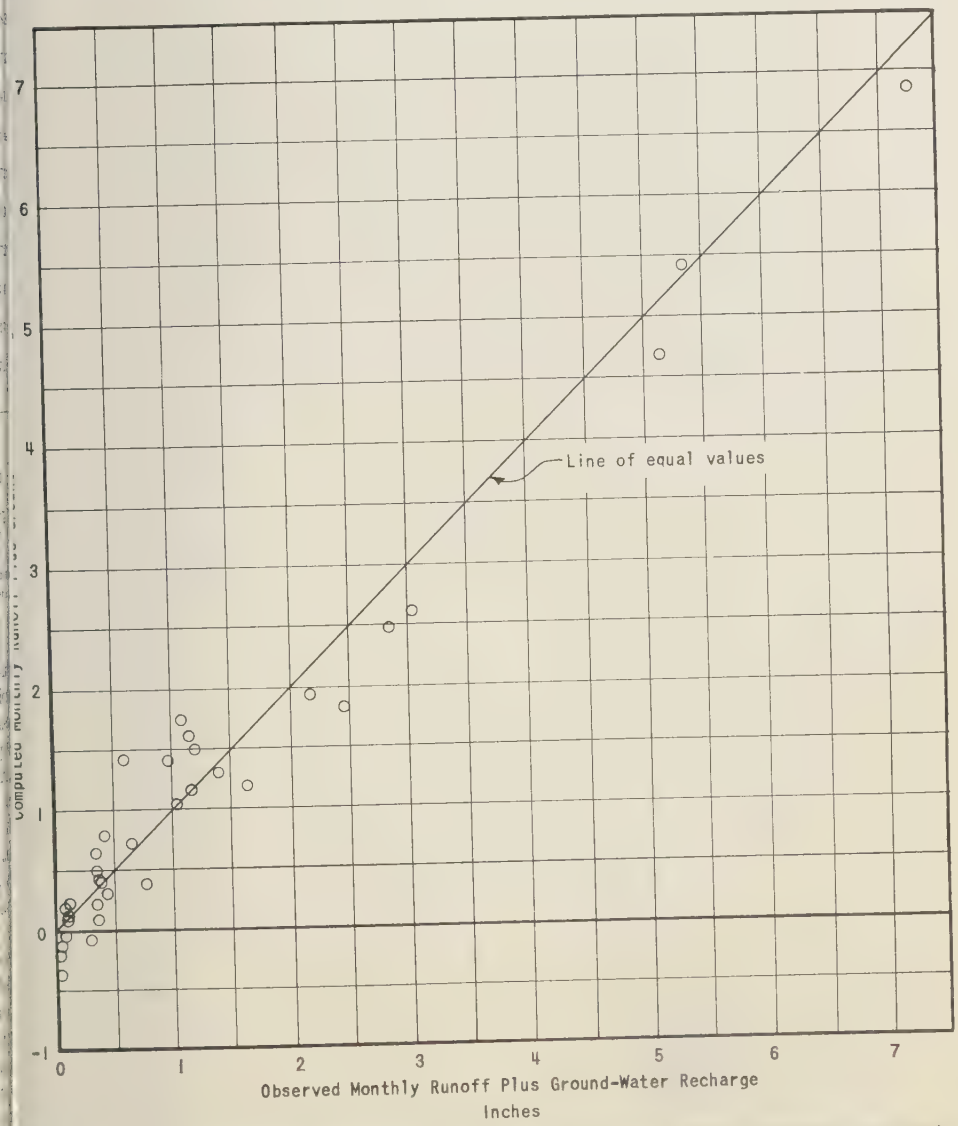

Fig. 1. Observed and computed June storm runoff plus ground-water recharge, Delaware River Basin, Kansas. Computed values were obtained by use of multiple regression equation in Table 4.

TABLE 5. Summary of Analysis of Seasonal Data, Delaware River Basin, Kansas

Season	Regression Coefficients								Other Values			
	X_2	X_7	X_8	X_{10}	X_{11}	X_{18}	X_{17}	X_{16}	R^2	$\bar{S}$	$\bar{X}_1$	Reg. Const. a
April, May, June	1.35**	+5.03**	+1.11**	+2.68**	−23.33**	+4.43§§	−.10‡	−5.8	.912	398.3	871.1	+830.2
July, August, Sept.	.92**	+1.61*	+.78**	+6.81**	+1.99	−4.77‡	+.002	−39.7	.705	402.8	367.0	+183.6
Oct., Nov.	1.96**	+4.60**	−.34‡	+4.74**	+1.64	−1.05	−.02	−29.8	.776	439.8	379.1	−866.7
Dec., Jan., Feb., March	2.71**		+.89**	+1.70**	−2.82§	−1.63	+.006	−8.1§	.552	287.2	225.4	+15.8

X_1 = Surface runoff plus ground-water recharge, inches × 1000
X_2 = Monthly precip., inches × 100
X_7 = Accumulated monthly precipitation in excess of 5 inches per month × 100
X_8 = First antecedent month's precip., inches × 100
X_{10} = Ground water in storage, inches × 1000
X_{11} = Monthly temp., °F
X_{16} = Percentage of watershed in row crops
X_{17} = Terraces, mi. per sq. mi. × 1000
X_{18} = Percentage in pasture × % condition/100
* Significant at 5% level
** Significant at 1% level
‡ Significant at 20% level
§ Significant at 40% level

shed is too small to be detected in these an
yses. It may also be that parameters not i
cluded in the studies, or random errors in t
parameters used, have effects large enough
mask those due to conservation practices a
treatment of land. It is possible that there a
interactions between parameters that have n
been considered or that the type of analy
used is not the proper one for the type of da
available. This will be discussed later in th
paper.

Applicability of Multiple Regression Analysis Methods

The results presented above were all obtain
by the use of correlation, simple regression, a
multiple regression analyses. The same metho
have been utilized in many other river bas
studies on annual, monthly and storm bas
The method, on the face of it, is well adapted
such studies. It also lends itself well to the e
ployment of electronic computers, which ha
been profitably utilized in this project.

Correlation and regression methods of an
ysis were largely developed from studies of bi
metrical data and are based upon reasonab
normally distributed data—the familiar be
shaped distribution curve. Hydrologic da
seem to be rarely normally distributed, hov
ever; they may be somewhat skewed and c
be severely skewed. In the sense intended her
skewness of hydrologic data refers to the cha
acteristically great number of relatively sm
events and only a few large events. Another ty
of skewness is discussed later in this paper. Th
few large events have a disproportionate effe
on the slopes of regression lines and correlatio
coefficients, as discussed below. As shown earli
high coefficients of correlation and determin
tion, per se, are not necessarily good indicato
of the quality of the estimating equation fo
predicting values far removed from the ave
ages. The confidence band about the regressio
line is bounded by sections of hyperbolas abov
and below the line. A high correlation coefficie
indicates that reasonably good individual est
mates can be made near the means, but as est
mates are made for values farther and farthe
removed from the means, probable errors i
crease enormously. Little confidence can b
placed in such estimates.

These considerations are very significant i

udies of water yields in the more arid parts of e country because it is the large events that oduce the bulk of the water. The few large flood ents produce over half the total streamflow the Washita River at Clinton, Oklahoma, for stance. Runoff during a 24-hour period (May 5–16, 1951) was equal to the total runoff for consecutive months subsequent to July 1, 951.

As an extreme example of what can happen hen standard methods of correlation and regression analysis are applied to hydrologic data, nd perhaps inappropriately interpreted, Figre 2 is shown. It will be noted that, if all vents are included, runoff, X_1, is highly signifiantly correlated with watershed precipitation, X_2. Omitting the one large event, however, reults in relations not reaching the 5 per cent evel of significance. Omitting the one event changes the regression coefficient (the slope of the line of best fit) from 6.04 to 1.59, or only 26 per cent as much. It also changes the y intercept from -1.88 to 1.69. In this case, an estimate of storm runoff based on the one equation would be nearly four times as large as one based on the other equation, for large events. For small events, the changed regression constant, a, would make great inverse differences in estimates. It was only by chance that the one large event occurred. Another period of record of similar length could have no such events, or several. There is no way of knowing which relation is the true one, or if either is. The different results obtained are not due to a breakdown of the method but rather to the use of a poor sample and to placing too much reliance on a highly significant correlation coefficient.

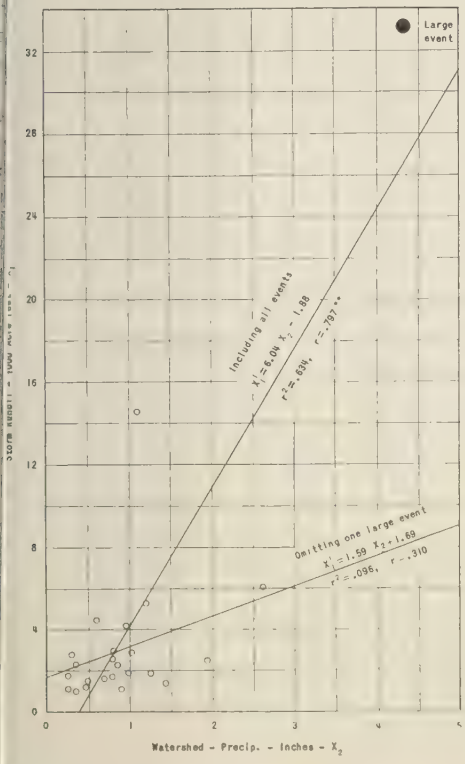

Fig. 2. The effect of omitting one large event on the runoff-precipitation relationship for July storms, upper Washita River Basin, Texas-Oklahoma.

The monthly runoff plus ground-water recharge values used to obtain the results shown in Tables 4 and 5 are also extremely skewed. This is shown in Figure 3, a plotting of distribution of monthly runoff events about the means of 35 years of record. The abscissa shows, by size classes, the ratios of individual events to mean values, and the ordinate shows the number of events in each class. It is readily apparent that the means are unduly influenced by the few larger events. About 75 per cent of the events in each month are smaller than the means, indicating extreme skewness in the data.

The distribution of the several other variables for the month of June, used in the study of monthly values in the Delaware River Basin, was also tested. The results of these tests are shown in Figure 4. The variables are the same as those shown in Tables 4 and 5. It will be noted that X_{11}, X_{16}, and X_{18}, monthly temperature, per cent of basin in row crops, and the pasture-area-condition index (percentage of watershed in pasture times per cent normal of pasture condition), are closely 'bunched' around their means and have no very large isolated values. All others are severely skewed in the sense that there are relatively large numbers of small values and a few very large values. Two variables, X_7, precipitation in excess of 5 inches per month, and X_{17}, terraces, have large numbers of zero values. There was no measurable amount of terracing in the watershed from 1923 to 1939, inclusive; hence for the first 17 years of record this variable was zero. In 17 of the

Fig. 3. Distribution of monthly storm runoff plus ground-water recharge about the means, Delaware River Basin, Kansas, showing extreme skewness.

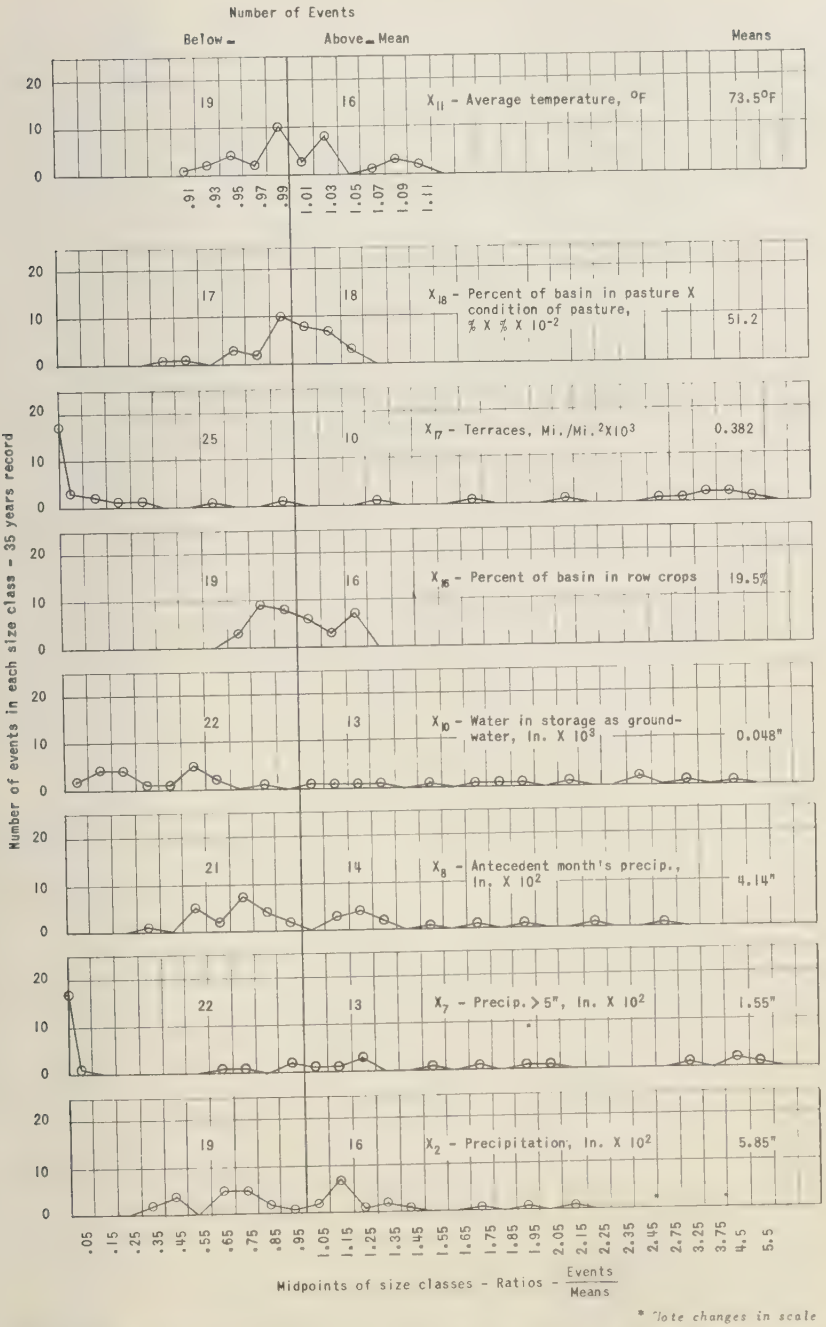

Fig. 4. Distribution of variables about their means, June, Delaware River Basin study reported in Table 4.

35 years, precipitation in June did not exceed 5 inches; hence this value was zero in 17 cases.

Installation of terraces in the watershed was begun in quantity in 1940. The rate of installation increased through the years. This variable, a cumulative one, rose rapidly to nearly 2 miles of terrace per square mile of watershed area in 1957. The distribution, or quantity, of this parameter with time is similar to the distribution of other conservation measures that might be applied to land in most river basins. These conservation variables will be zero up to the late 1930's or early 1940's. Subsequently, such parameters will probably increase in size (or amount) in some form of progression. This will introduce special problems into any statistical procedures.

To account for some of this skewness it was thought that data might be stratified, particularly as regards water yield, in order to reduce the skewness. All large events, all small events, etc., could be grouped. If, however, annual or monthly values are being studied, the number of cases is so reduced that no degrees of freedom will be left for testing significance. Thirty-six years of data could be divided into three groups of 12 small, medium, and large events. The effects of only one or two independent variables could be tested for each group. The least number of variables that should be tested, however, include precipitation and one or more of its characteristics, such as intensity, antecedent conditions, land use, vegetative conditions, and an index reflecting conservation treatment (terraces, for example). This is a minimum of six independent variables. Inclusion of so many variables would preclude stratification of data where only 20 to 40 events have occurred.

The possibility of combining monthly data, for example, into seasons immediately arises. This raises other questions. What seasons? Which months are to be included? How can we derive and introduce a parameter to reflect effect of season, if such an effect exists? And does any given month belong in the same season every year?

Another possibility is that of studying individual storms and the streamflow associated with such storms. This was done for the Washita River Basin in Texas and Oklahoma. This procedure introduces one major source of error into the data. It is impractical to install enough rain gages in a large watershed to adequately portray watershed-precipitation on a storm basis. It has been rather well demonstrated that relatively few rain gages will indicate annual or seasonal precipitation reasonably accurately. As the time period is shortened however, errors in estimated watershed-precipitation increase enormously, unless the number of gages is increased proportionately.

This potential error in estimating storm precipitation is indicated in Figure 5, isohyetal maps of the Washita Basin. The upper map was prepared from the data available from the rain gages in operation in 1936 when the streamgaging record was begun. The lower map was developed from data from all gages in operation in 1954 when the storm occurred. Watershed-precipitation, as estimated from the original 12 gages within and adjacent to the watershed, was 3.3 inches. Using the 20-odd gages in operation in 1954 gave an estimate of 4.7 inches of watershed-precipitation, an increase of 1.4 inches or 42 per cent. Introducing such potentially large errors into the most important independent parameter, watershed-precipitation, could well defeat the purpose of using storm data in a study to evaluate effects on water yields of changes in land use and treatment.

Attributes of Statistical Methods of Analysis

Inherent in the application of the multiple regression methods of analysis to the hydrologic problems discussed earlier in this paper are three tacit assumptions:

1. There are no errors in the independent variables; errors occur only in the dependent variable.

2. The variance of the dependent variable (runoff) does not depend on the values of the independent variables.

3. The observed values of runoff are uncorrelated random variables.

In the application of tests of significance, a fourth assumption is made: The population of the dependent variable (runoff) is normally distributed about the regression line for any fixed level of the independent variables (precipitation, for instance) under consideration. This is illustrated in Figure 6. It is the second type of

kewness mentioned earlier in this report. The nly information available about the distribu- ion of the population is that provided by the sample. In hydrologic data there simply are not enough large events in the relatively few years of record of streamflow, precipitation, and other factors to afford reliable information about the distribution of the dependent variable about the regression line. This fourth assumption may therefore be suspect, and high coefficients of correlation and determination and high t-test values may be misleading. Confidence limits, for values of the independent variable far from the mean, are so wide that runoff values esti-

STORM ISOHYETAL MAP USING ORIGINAL RAIN GAGES ONLY.
STORM WATERSHED - PRECIPITATION - 3.3"

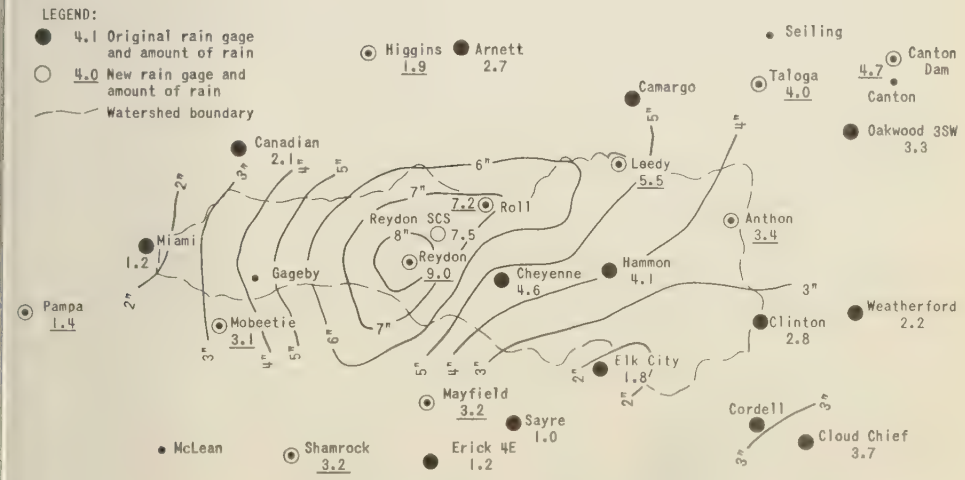

STORM ISOHYETAL MAP USING ALL AVAILABLE RAIN GAGES.
STORM WATERSHED - PRECIPITATION - 4.7"

Fig. 5. Effects on computation of precipitation of including new rain-gage stations in network of gages (storm of April 1954, upper Washita River Basin, Oklahoma and Texas).

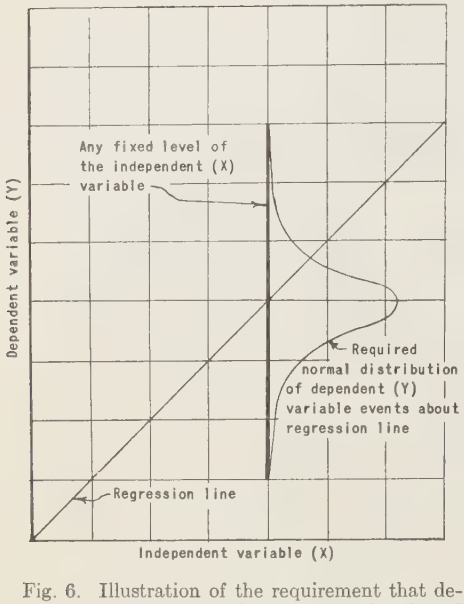

Fig. 6. Illustration of the requirement that dependent variable values be normally distributed about the regression line for any fixed level of the independent variables for significance to be reliable.

mated by use of the regression equation may bear little resemblance to the unknown true values.

In the case of streamflow, the third assumption is suspect. Streamflow, whether it be on an annual, monthly, storm, or daily basis, is not unrelated to preceding events. What occurred yesterday affects what happens today. June and July streamflow of the Delaware River, for instance, have a correlation coefficient of 0.616 whereas June and July precipitation are correlated to the extent of 0.412. Occurrences of runoff may not be uncorrelated random events; they may explain some of their own variance.

In the instance of the second assumption, the variance in runoff values is not entirely unaffected by the values of the independent variables. Small values of precipitation, for instance, are associated with low values and variance of runoff, but great precipitation events tend to generate runoff events with large variance.

The first assumption, that there are errors in the dependent variable only and not in the independent variables, is obviously violated by hydrologic data. Watershed-precipitation, land use, vegetative conditions, amounts of conservation treatment, and other variables pertaining to watersheds all contain certain amounts of error. This differs from swine-feeding experiments, for instance, where the amounts of different kinds of feed consumed can be very closely approximated. The failure of hydrologic data to meet this criterion is 'circumvented' by considering each set of independent variables as indices, not exact values.

It is possible that the attribute of runoff data (second assumption) may be corrected by using some type of variance-stabilizing transformation. It may be that the application of some of the more modern methods of multiple time series analyses will overcome the interrelation of runoff events (third assumption). Preliminary studies of the data reported in this paper indicate that the time series structure of the problem is a relevant consideration and that the application of these techniques should be investigated further. Studies of the 420-month record of precipitation and runoff of the Delaware River Basin, however, have shown that the relations are nonstationary, and this will introduce some difficulties.

It is possible that the development of mathematical models to simulate the hydrologic processes involved in the precipitation-runoff relationship will offer chances to test estimates of the parameters involved. This may result in more applicable parameters and means of testing significance.

Conclusions

In conclusion, it can be said that the multiple regression method of analysis will result in a 'best fit' equation, but that tests of significance may well be obviated by skewness in the data. Limited reliance should be placed on t-tests and coefficients of determination and correlation until the absence of skewness in the data is established. If severe skewness is present, such values may be meaningless.

There are several other methods of statistical analysis, particularly the more modern techniques, that may be more applicable to the problems of Cooperative Water Yield Procedures Study than the multiple regression methods. We plan to explore these possibilities.

(Manuscript received July 8, 1959; revised December 18, 1959.)

Limitations on the Composition of the Upper Mantle

PAUL W. GAST

Department of Geology, University of Minnesota
Minneapolis, Minnesota
and
Lamont Geological Observatory[1]
Columbia University
Palisades, N. Y.

Abstract. New determinations of the isotopic composition of strontium and of the concentration of K, Rb, Cs, Sr, and Ba rocks and meteorites are given. The isotopic abundance of Sr^{87} in the upper mantle and the crust appears to be lower than that found for chondrites. Furthermore, for a chondritic earth model, the concentrations of potassium, rubidium, and cesium in the earth's crust are anomalous when compared with those of uranium, barium, and strontium. These two concurring arguments indicate that the upper mantle and crust of the earth do not contain K, Rb, Cs, U, Ba, and Sr, in the proportions found in chondrites, and that the alkali metals are depleted relative to U, Sr, and Ba. This depletion may be an indication of a nonchondritic earth composition; it may also result from an earth differentiation in which K, Rb, and Cs were concentrated or retained in the lower mantle.

INTRODUCTION

The hypothesis that the average composition of either the whole earth or the mantle is similar to that of chondrites has been adopted in a number of geophysical and geochemical studies. Evidence supporting this hypothesis has recently been given by *Ringwood* [1958] and *MacDonald* [1959*a*]. The most direct evidence in its favor appears to be the near equality of the heat escaping from the earth with that produced by radioactivity in a chondritic earth in thermal equilibrium.

The chondrite hypothesis will be examined here, by comparing the terrestrial and meteoritic distribution of radiogenic Sr^{87} and by comparing the distribution and abundance of the elements K, Rb, Cs, Sr, Ba, and U in the crust with the distribution and abundance to be expected in a chondritic earth. Implicit in such comparisons is the assumption that the crust of the earth is derived from the present mantle or from a primitive upper mantle. In other words, it is assumed that the composition of the earth's crust as a whole, as well as that of certain volcanic rocks, is related to the composition of the upper mantle.

In a given chemical system the isotopic abundance of Sr^{87} is determined by four parameters: the isotopic abundance at a given initial time, the Rb/Sr ratio of the system, the decay constant of Rb^{87}, and the time elapsed since the initial time. The isotopic composition of a particular sample of strontium, whose history may or may not be known, may be the result of time spent in a number of such systems or environments. In any case the isotopic composition is the time-integrated result of the Rb/Sr ratios in all the past environments. Local differences in the Rb/Sr ratio will, in time, result in local differences in the abundance of Sr^{87}. Mixing of material during transport and rock-forming processes will tend to homogenize these local variations. Once homogenization occurs, the isotopic composition is not further affected by these processes. Because of this property and because of the time-integrating effect, isotopic compositions lead to useful inferences concerning the Rb/Sr ratio of the crust and of the upper mantle. It should be noted that similar arguments can be made for the radiogenic isotopes of lead, which are related to the U/Pb ratio and time.

As a check on the relative abundance of Rb and Sr, inferred from isotopic compositions, estimates of the crustal abundance of Rb and Sr, as well as K, Cs, Ba, and U, have been made from direct measurements of the abundance of these elements in common rocks.

A comparison of (1) the crustal Rb/Sr ratio

[1] Lamont Geological Observatory, Contribution No. 403.

and the associated isotopic abundance of Sr^{87}, (2) the relative abundance of geochemically similar elements, in this case, K, Rb, and Ba, and (3) the crustal concentrations of certain highly enriched elements (U, Ba, and Tl) with those expected in a differentiated chondritic earth places certain limitations on the distribution of these elements within the earth. The validity of these limitations may be a test of the chondrite hypothesis.

The abundances of radiogenic isotopes are further significant because they are directly or indirectly related to the distribution of the radioactive isotopes which are the source of a significant fraction of the heat escaping from the interior of the earth. The distribution of radiogenic lead is directly related to the distribution of uranium and thorium; Sr^{87} is indirectly related to potassium because of the chemical similarity of potassium and rubidium. This interrelation of the heat problem and th abundance of radiogenic isotopes places certai restrictions on earth models.

In the sense that they test a specific hypothesi the arguments given here are negative. Observe abundances of elements and isotopes are com pared with those expected from the chondrit model; thus the validity of this model is teste No specific compositions for alternative mode are suggested.

Data on Abundance of Isotopes and Elements

A number of new determinations of strontiu isotope compositions in rocks and meteorites a well as new determinations of the abundance c the alkali and the alkaline earth metals are give in this paper. These data along with other dat used in the arguments which follow are sum marized in Tables 1 to 4.

TABLE 1. Present and Initial Isotopic Abundance of Sr^{87} in Granitic Rocks

Sample	Present Sr^{87}/Sr^{86}	Rb/Sr	Age, m. y.	Initial Sr^{87}/Sr^{86}
Westerly granite Westerly, R. I.	0.720 ± .002	0.85	200 ± 20[a,b]	0.713 ± .002
Sixmile granite Llano County, Tex.	0.744 ± .004	0.64	1050 ± 70[c]	0.717 ± .005
Quartz Creek granite Gunnison, Colo.	0.936 ± .005	3.62	1400 ± 150[c]	0.729 ± .023
Rapakivi granite Virojoki, Finland	0.806 ± .005	1.43	1600 ± 80[d]	0.713 ± .007
Bodom granite Espoo, Finland	0.972 ± .005	3.86	1600 ± 80[d]	0.719 ± .014
Kaavi granite Vihitajarvi, Kaavi, Finland	0.737 ± .004	0.23	1800 ± 80[d]	0.718 ± .004
Pernio granite Pernio, Finland	0.863 ± .005	2.16	1800 ± 80[e]	0.705 ± .009
Gneissic granite Pointe Dubois, Manitoba	0.768 ± .004	0.60	2650 ± 100[f]	0.704 ± .003
Augen gneiss N. Bighorn Range, Wyo.	0.749 ± .003	0.35	2750 ± 100[f]	0.711 ± .004
Gneissic granodiorite Fort Victoria, S. Rhodesia	1.003 ± .003	2.62	>2650[g]	<0.721

[a] Age inferred from geologic relations.

[b] Uncertainties given here are estimated from combined determinations, zircons, biotite, etc., whe available.

[c] *Aldrich and others* [1958]; age for Sixmile granite inferred from Petrick granite. See also *Hutchinso and others* (1955).

[d] *Kouwo* [1958].

[e] Gast, unpublished determination.

[f] *Gast and others* [1958].

[g] Age inferred from Bikita pegmatite [*Holmes*, 1954; *Aldrich and others*, 1958].

Aside from the determinations made in connection with Rb-Sr age determinations, relatively few determinations of the isotopic composition of strontium are available, particularly in igneous and metamorphic rocks. The analyses reported here were made as part of a survey of representative and common types of rock. *Schumacher* [1956], *Herzog and Pinson* [1956], and *Webster, Morgan, and Smales* [1958] have reported the isotopic composition of strontium in two chondrites and three achondrites.

The lack of, or relatively small, variation found in the isotopic compositions of other metallic elements [lithium, *Cameron,* 1955; zinc, *Blix, Ubisch, and Wickman,* 1957; copper, *Walker, Cuttitta, and Senftle,* [1958] suggests that natural variations in the abundance of the nonradiogenic strontium isotopes should be small compared with those found for the radiogenic isotopes. No evidence of variations in the abundance of the nonradiogenic strontium isotopes was found in this study.

The abundance of Sr^{87} is given here in terms of the Sr^{87}/Sr^{86} ratio because this ratio is least susceptible to experimental difficulties. The experimental uncertainties given in Tables 1 to 3 are estimated both from the mean deviation for a large number (25 to 80) of individual scans and from the deviation between duplicate runs.

The observed isotope ratios and Rb/Sr ratios for a group of 10 granitic rocks, the ages of which range from 200 to 2700 m.y., are given in Table 1. The initial Sr^{87}/Sr^{86} ratios for these granitic rocks have been determined from the measured age and the observed ratios of elements and isotopes (cf. equation 4, below). The uncertainty in the measured age and in the Rb/Sr ratio results in a relatively high uncertainty for the initial Sr^{87}/Sr^{86} ratios of the most radiogenic samples. Nevertheless, it is apparent that the initial ratios for most granites are quite similar.

The Sr^{87}/Sr^{86} ratios for a number of limestones and mafic igneous rocks are given in Table 2. The data on the limestones have been previously discussed [*Gast,* 1955]. A 1.2 per cent increase in Sr^{87} over 3 b.y. was found. It is seen that the ratios for the basalts are similar to those found for limestones. The rubidium and strontium content of the individual basaltic rocks listed in Table 2 has also been determined. In every case, the Rb/Sr ratio is low enough so that there could have been no significant change in the Sr^{87}/Sr^{86} ratio during the history of the rock. A comparison of the Sr^{87}/Sr^{86} ratio in two relatively old rocks, the Keewatin pillow lava and the Stillwater anorthosite, with those found for recent mafic igneous rocks shows no evidence of a time-dependent increase in the Sr^{87}/Sr^{86} ratio. If such a time-dependent increase exists, it is probably masked by other variations.

TABLE 2. Isotopic Abundance of Sr^{87} in Basalts and Limestones

Sample	Sr^{87}/Sr^{86}	Rb/Sr
Basalts		
Olivine basalts Kilauea, Hawaii	0.708 ± 0.002	0.020
Olivine basalt Mid-Atlantic Ridge	0.705 ± 0.003	0.009
Leucite basalt Lake Kivu region Belgian Congo	0.708 ± 0.002	0.102
Diabase sill Centreville, Va.	0.710 ± 0.003	0.12
Greenstone, pillow lava Pointe Dubois, Manitoba	0.711 ± 0.003	0.043
Eclogite, Robert Victor Mine Kimberley, S. Africa	0.711 ± 0.003	...
Anorthosite layer Stillwater complex Stillwater, Montana	0.711 ± 0.003	0.02
Limestones		
Bulawayan limestone S. Rhodesia	0.704 ± 0.002	...
Grenville limestone Ontario, Canada	0.709 ± 0.002	...
Newland ls. Belt series	0.709 ± 0.002	...
Ordovician limestone Perry County, Texas	0.713 ± 0.003	...
Ocean water	0.712 ± 0.002	...

The Sr^{87}/Sr^{86} ratios for a number of meteorite samples are shown in Table 3. Both chondrites and achondrites were studied. Three achondrites, classified as howardites or eucrites, that is calcium-rich achondrites, have similar Sr^{87} abundances, and the Sr^{87}/Sr^{86} ratios for all three samples are identical within experimental error. *Herzog and Pinson* [1956] and *Schumacher* [1956] also determined the isotopic composition of strontium from the meteorite Passamonte.

TABLE 3. Isotopic Abundance of Sr^{87} in Stone Meteorites

Sample	Sr^{87}/Sr^{86}
Chondrites	
Forest City	0.755 ± 0.003
Modoc	0.757 ± 0.003
Holbrook	0.739 ± 0.004
Richardton	0.756 ± 0.003
Beardsley	0.811 ± 0.002
Achondrites	
Pasamonte	0.7004 ± 0.002
Sioux County	0.7015 ± 0.002
Nuevo Laredo	0.7027 ± 0.002

The ratio reported here agrees with the Sr^{87}/Sr^{86} ratio of 0.703 reported by Herzog and Pinson; it does not agree with the value of 0.687 reported by Schumacher. This discrepancy is not understood. The ratio reported here is the average of three different determinations (0.7011, 0.7005, and 0.6995) made on two different mass spectrometers. No blank correction was necessary in any of these determinations.

The Sr^{87}/Sr^{86} ratios of five chondrites are more variable than the ratios of the achondrites. The ratio for Beardsley, in particular, is higher than that of the others. The Sr^{87}/Sr^{86} ratio for Forest City is in good agreement with the ratio of 0.754 reported by *Schumacher* [1956]. The Rb-Sr ages derived from these data and the Rb and Sr contents of these meteorites will be discussed in some detail elsewhere. For the present discussion it will be sufficient to note that, with the exception of Beardsley, the chondrites 4.5 b.y. ago had a Sr^{87}/Sr^{86} ratio similar to that now seen in the achondrites. Beardsley is unusual in other ways; its K content appears to be higher than that of other chondrites [*Edwards and Urey,* 1955]. Its Th content also appears to be higher [*Bate, Huizenga, and Potratz,* 1959]. It is thus omitted from the average ratio for chondrites; including it would only strengthen the arguments which follow.

Data on the abundance of six different elements are summarized in Table 4. Three different composite samples were made from a collection of about 250 basaltic rocks investigated by *Turekian and Kulp* [1956]. The potassium, rubidium, cesium, strontium, and barium contents of these composite samples have been determined. The uranium content of one of these composite samples has also been determined. All six elements were also determined for two composite 'granite' samples, the first consisting of 27 Finnish granites and granite gneisses and the second consisting of 50 Precambrian granitic or gneissic rocks from western United States. All determinations except those for uranium were made by the method of stable-isotope dilution, the experimental error being less than ±10 per cent. Uranium was determined fluorometrically. The abundances of elements in meteorites given in Table 2 are averages of recent determinations which, with the exception of potassium, have

TABLE 4. Elemental Abundances in Composite Rocks and Meteorites

Sample	K, per cent	Rb, ppm	Cs, ppm	Sr, ppm	Ba, ppm	U, ppm
Composite basalt I	0.89	26	1.1	460	340	...
Composite basalt II	0.94	30	1.0	469	300	1.4 ± 0.3
Composite basalt III	1.01	32	1.2	454	359	...
Composite granite I	3.29	133	3.63	348	570	3.5 ± 0.2
Composite granite II	3.04	125	2.77	283	685	2.3 ± 0.3
Chondrites	0.0830[a]	2.8[b,e]	0.09[b,e]	11.4[g]	3.6[c]	0.011[e]
Basaltic achondrites	0.03[d,e]	0.25[e]	0.0012[e]	74[g]	30[c,g]	0.11[e]
Olivine basalt, Mid-Atlantic Ridge	0.14	0.98	0.04	102	50	0.08[f]
Olivine basalt, Hawaii	0.36	6.45	0.10	312	98	...

[a] *Edwards and Urey* [1955]
[b] *Webster and others* [1958]
[c] *Hamaguchi and others* [1957]
[d] *Geiss and Hess* [1958]
[e] *Gast* [1960]
[f] *Carr and Kulp* [1953]
[g] *Gast* (unpublished data)

been made by the isotope-dilution or the neutron-activation method. Experimental techniques and detailed descriptions of individual samples used in the new measurements reported here will be discussed elsewhere.

Inferences Concerning the Composition of the Upper Mantle

Implications of the isotopic abundance of Sr^{87}. Time-dependent variations in the isotopic abundance of Sr^{87} are quite analogous to those observed for the radiogenic lead isotopes. *Russell and Allan* [1955] derived completely general equations for the variations in the abundances of lead isotopes. Their equation 4.1 may be applied to the variation of the Sr^{87} abundance. In order to avoid confusion, a different set of symbols will be used for the present case: the Sr^{87}/Sr^{86} ratio is denoted by r, the present-day Rb^{87}/Sr^{86} ratio is denoted by R, and the subscript zero refers to an arbitrarily assumed starting time, for example, 2000 m.y. ago. The decay constant for Rb^{87} is taken as 1.39×10^{-11} $years^{-1}$ [*Aldrich, Wetherill, Tilton, and Davis,* 1956]. The time-dependent variation of the Sr^{87}/Sr^{86} ratio is then given by

$$r = r_0 + \int_t^{t_0} \lambda R e^{\lambda t}\, dt \qquad (1)$$

Because $\lambda t \rangle\rangle (\lambda t)^2/2$ for all intervals of geologic time, $e^{\lambda t}$ may be expressed by the two-term expansion $1 + \lambda t$; equation 1 then becomes

$$r = r_0 + \int_t^{t_0} R(1 + \lambda t)\lambda\, dt \qquad (2)$$

In the case where R does not vary except for the radioactive decay of Rb^{87}

$$r = r_0 + R\lambda(t_0 - t) + R(\lambda^2 t_0^2 - \lambda^2 t^2)/2 \qquad (3)$$

and the second term may again be neglected. This approximation introduces a maximum error of 3 per cent for the largest values of λt. In the case where R changes due to a geologic process, for example, an igneous differentiation,

$$r = r_0 + \bar{R}\lambda(t_0 - t) \qquad (4)$$

where

$$\bar{R} = \frac{1}{t_0 - t}\int_t^{t_0} R\, dt \qquad (5)$$

Unless otherwise stated, it will be assumed that the primeval Sr^{87}/Sr^{86} ratio for the earth is similar to that found in the achondrites. It is readily shown from the Rb and Sr contents that the variation in the Sr^{87}/Sr^{86} ratios of achondrites over the last 4.5 b.y. is negligible.

Various conclusions may be drawn from a comparison of the terrestrial and meteoritic Sr^{87} abundances. A cursory examination of the data shows that strontium in many terrestrial occurrences is less radiogenic than that found in chondrites. In fact, in several cases, terrestrial strontium is similar to that found in the three achondrites.

The abundance of Sr^{87} in six basaltic rocks (Table 2) is quite uniform and not much higher than that assumed for the primeval earth. This observation is inconsistent with the suggestion of *Rubey* [1951] and *Ringwood* [1958] that basaltic magmas result from partial melting of a chondritic mantle. If basaltic magmas are derived from the upper mantle, we may infer that the abundance of Sr^{87} in the part of the mantle represented by these volcanic rocks is relatively low. The apparent values of R represented by the six samples range from 0.041 to 0.17; these correspond to Rb/Sr ratios ranging from 0.014 to 0.060. Clearly these are much lower than the average ratio for chondrites (0.25) given in Table 4.

A more comprehensive comparison of terrestrial and meteoritic Sr^{87} abundances requires some knowledge of the distribution of radiogenic strontium within the earth. In particular, some estimate of the amount of Sr^{87} stored in silicic continental rocks must be made.

The average present-day Sr^{87} abundance of the ten silicic rocks listed in Table 1 cannot be used as an average for silicic rocks. The average Rb/Sr ratio of this group is 1.63; this is 6 times higher than the average Rb/Sr ratio derived from the data of *Horstmann* [1957] and *Turekian and Kulp* [1956]. It is also 8 times higher than the mean Rb/Sr ratio of the composite granites listed in Table 4. The amount of radiogenic strontium found (Table 1) is thus much greater than that expected for typical silicic rocks. This result was not unexpected, since most of the rocks listed in Table 1 were chosen on the basis of age determinations available before 1957. It was not possible to choose many

representative plutonic rocks from such a limited sample. In any event, the *initial* Sr^{87}/Sr^{86} ratios given in Table 1 will be useful in estimating the amount of radiogenic strontium now within the crust. The constancy of the initial ratios suggests that radiogenic strontium was accumulated after the formation of these silicic rocks. An average Sr^{87}/Sr^{86} ratio for silicic rocks may then be found from an average Rb/Sr ratio and an average age. It will be assumed that the latter parameters are independent of each other.

The analysis of the composite granites given in Table 4 furnishes one estimate of the Rb/Sr ratio of silicic rocks. The mean for composites I and II is 0.41. The rubidium content of silicic rocks is best estimated by combining the K/Rb ratio found for the composites (Table 4) with the large number of potassium determinations available for silicic rocks. Using the mean potassium content (2.9 per cent) for 794 silicic and 635 intermediate igneous rocks given by *Nockolds and Allen* [1954], we find an average Rb content of 120 ppm. The abundance of strontium in silicic rocks was investigated by *Turekian and Kulp* [1956]. They suggested a value of 440 ppm for the silicic crust. The latter values give a Rb/Sr ratio of 0.27. A ratio of 0.33 will be adopted here.

A crude estimate of the average age of silicic continental rocks may be made from a large number of age determinations published in recent years. In North America, relatively few rocks older than 2700 m.y. have been found. The areal extent of younger rocks, 1400 and 1000 m.y. old for example [*Tilton and Davis*, 1959], is at least as great as that of older rocks. An average age of 1500 m.y. for the North American continent is probably a good first approximation. Although there are fewer data for other continents, the distribution of ages appears roughly similar to that found in North America. It seems improbable that the average age of the silicic continental rocks exceeds 2000 m.y.

If we use an initial Sr^{87}/Sr^{86} ratio of 0.714 (the weighted average of the values in Table 1), an average Rb/Sr ratio of 0.33, and an average age of 2000 m.y., we find a present-day Sr^{87}/Sr^{86} ratio of 0.742 for the silicic crust. Thus, even in the most silicic parts of the earth, the estimated present-day Sr^{87}/Sr^{86} ratio is slightly lower than the present-day ratio for chondrites. The details of this calculation are undoubtedly open to question and revision. It does, however, show the difficulty involved in trying to balance the low abundance of Sr^{87} in some parts of the earth with a higher abundance in the silicic parts. For a crustal model consisting of equal parts of mafic and silicic material, both of which have approximately equal strontium contents, the average Sr^{87}/Sr^{86} ratio is 0.726, if we assume a ratio of 0.710 (Table 2) for the mafic portion. Furthermore, if the Sr^{87}/Sr^{86} ratio in oceanic basalts is representative of the upper mantle, the average ratio for the crust plus upper mantle is further reduced. It seems clear that the Sr^{87}/Sr^{86} ratio in the upper part of the earth is lower than that found in chondrites. If this observation is to be reconciled with a chondritic Rb/Sr ratio for the earth as a whole, it implies an early separation of Rb and Sr in the earth (prior to 4.0 b.y. ago) and retention of Rb in the lower mantle; no samples of such mantle material have been found in surface rocks. Alternatively, it may be an indication of a nonchondritic earth composition.

Since potassium and rubidium are geochemically similar, inferences concerning the distribution of rubidium may also apply to the distribution of potassium. In particular, the present observations suggest that in the upper mantle and crust of a chondritic earth potassium is less enriched than strontium. If, for example, the strontium remaining below the crust is evenly distributed in the shell, designated layer (B) by *Bullen* [1947], and if the strontium in this layer has a Sr^{87}/Sr^{86} ratio of 0.710, more than half of the earth's rubidium must be below this layer, and a similar proportion of the earth's potassium would also be expected to be below this zone. It is of some interest to note the implications which this situation may have for the earth's heat balance. *MacDonald* [1959*b*] found that approximately one-third of the radioactive heat sources of the earth must be deeper than 600 km for a differentiated, chrondritic earth, in which no heat is lost by convection. At present, potassium-40 furnishes about three- fifths of the heat due to radioactivity in a chondritic earth, so the retention of approximately one-half of the earth's potassium below 400 km satisfies the

istribution of heat sources suggested by Mac-Donald for the conditions stated above.

The near equality of the lowest terrestrial Sr^{87}/Sr^{86} ratios and those of the achondrites is f further interest. It suggests that, if the earth's omposition is chondritic or if the earth was ini-ially derived from matter having a chondritic Rb/Sr ratio, the time of separation of the stron-ium from rubidium or the time when the mate-ial making up the planet was separated or lerived from pre-existing materials was about .5 b.y. ago. This is in agreement with a simi-ar argument based on ratios of lead isotopes *Patterson*, 1956].

Implications of the crustal abundances of U, Ba, K, Rb, Cs, and Tl. The distribution of uranium in the earth was discussed by *Birch* [1958]. He showed that if the mean uranium ontent of the earth is the same as that of chon-drites a large fraction of the earth's uranium s above the Mohorovicic discontinuity. This en-richment of uranium in the crust implies an extensive differentiation of the earth at some ime in the past. The argument Birch gave for uranium will be reviewed and extended to other lements in this section. All the calculations are based on the assumption that the entire mass of the earth, 6.0×10^{27} grams, has a mean com-position similar to that of chondrites. A mean composition based on an iron core and a chon-dritic mantle will not materially change the argument. In fact, an improbable situation re-sults, where 100 per cent of the earth's uranium s in the crust. To find the proportion of the earth's potassium, rubidium, etc., which is now n the crust, we must estimate the abundance of these elements in the crust. Such estimates are admittedly uncertain because they depend on the validity of a particular crustal model.

The calculations made here are based on a simplified version of the crustal model proposed by *Poldervaart* [1955]. It is assumed that the crust consists of equal parts of mafic (basalt) and intermediate (granodiorite) rock, having a total mass of 2.4×10^{25} grams. The concentra-tion of the various elements in the composite samples reported in Table 4 are used in esti-mating the abundance of these elements in the mafic and silicic portions of the crust. The abundances of K, Rb, Cs, Sr, and Ba in the mafic portion of the crust are taken to be the average concentration in the three basalt com-posites. The uranium content used for the mafic portions of the crust (1.2 ppm) is an average of the concentration in Composite Basalt II and the mean concentration in 34 basic rocks reported by *Evans and Goodman* [1941]. Chemical an-alyses of the granitic composites given in Table 2 show that they are more silicic than average intermediate or granodioritic rocks. Thus the analyses of the granitic composites cannot lead directly to estimates of abundances for a grano-dioritic crust.

As is indicated above, a value of 2.9 per cent will be adopted for the potassium content of the granodioritic crust. The rubidium and cesium contents are interpolated from this potassium content and from the K/Rb and K/Cs ratios of the granitic composites. Uranium and barium in the granodioritic crust are taken as 2.2 ppm and 550 ppm, respectively. The strontium con-tent is taken as 440 ppm, mainly from the work of *Turekian and Kulp* [1956]. The average crustal abundances derived from these figures are given in Table 5. These abundances and the concentrations given for chondrites (Table 4) lead to the proportions shown in the second column of Table 5. Sixty-two per cent of the earth's uranium and 49 per cent of its barium are in the crust of the model chosen here. Thus, even though barium and uranium are not diadochic, they are similarly enriched in the earth's crust. The enrichment of both elements is so extreme that it seems to require a rather efficient chemical differentiation of the earth.

Perhaps more significant for the present argu-ment is the apparent difference between the alkali metals and the elements strontium, bar-ium, and uranium. Unlike barium and uranium,

TABLE 5. Crustal Abundance and Enrichment of Six Lithophilic Elements for a Chondritic Earth

Element	Crustal Abundance	Fraction Now in Crust
K	1.9 per cent	0.093
Rb	74 ppm	0.105
Cs	1.5 ppm	0.089
Sr	450 ppm	0.16
Ba	440 ppm	0.49
U	1.7 ppm	0.62

the three alkali metals are only moderately enriched in the earth's crust. The apparent enrichment of the alkali metals is 5 and 8 times lower than that of barium and uranium, respectively; even strontium is more strongly enriched than the alkalis. These differences appear to be inconsistent with the observed geochemical behavior of these elements.

The abundances of a number of lithophile elements—the heavy alkali metals, barium, uranium, thorium, and lead, for example—are generally greater in silicic than in mafic rocks. The similar behavior of barium and potassium is of particular interest in this discussion. In igneous rocks, the main hosts for barium are potassium feldspars and micas, in which barium substitutes for potassium. *Goldschmidt* [1954] suggested that during a fractional crystallization sequence the Ba/K ratio will remain constant or will slowly decrease as crystallization proceeds. Thus the end products in which potassium is concentrated may in some cases be depleted in barium. In a study of over 15 different magmatic rock sequences, *Nockolds and Allen* [1953, 1954, 1956] found that the behavior of barium and potassium is similar to that suggested by Goldschmidt, with few significant deviations from the general rule. *Engel and Engel* [1958] found a similar relation between potassium and barium in a sequence of metamorphic rocks. The calculated fivefold enrichment of barium over potassium in the crust of the earth is thus inconsistent with the behavior of these elements in observed igneous processes.

The work of Nockolds and Allen also shows that strontium is generally depleted in rock that are most differentiated. The calculated twofold enrichment of strontium relative to potassium in the crust is thus also inconsistent. These inconsistencies suggest that the crustal rocks evolved from a source having a lower abundance of alkali metals, relative to strontium and barium, than that found in chondrites. This conclusion is valid for a rather wide range in the proportions of the various types of rocks making up the crust, because the concentrations of potassium, barium, and uranium change 'sympathetically' in the range from mafic to silicic rocks. Thus, in a completely basaltic crust, the apparent enrichment of barium would be 3 times that of potassium and rubidium.

This argument, which is independent of the strontium-isotope evidence, indicates that the heavy alkali elements may, in general, be depleted with respect to the heavy alkaline earth elements in the upper parts of the earth.

Both the extent and variation of the apparent crustal enrichments (Table 5) indicate that similar comparisons for other elements may be of interest. *Reed, Kigoshi, and Turkevich* [1959] recently determined the concentration of thallium in a number of stone meteorites. They reported a concentration of about 3×10^{-4} ppm for five normal chondrites. The abundance of thallium in crustal rocks can be estimated from the recent studies of *Heier and Taylor* [1959] and *Zlobin* [1958], as well as from earlier work [*Shaw*, 1952]. Thallium, like rubidium, is primarily contained in potassium minerals. The Rb/Tl and K/Tl ratios of rocks are thus less variable than the Tl concentration itself. Heier and Taylor reported that the mean Rb/Tl ratio is about 100 for a large number of potassium feldspars. Zlobin reported an average K/Tl ratio of $3.6–0.7 \times 10^4$ for 21 samples from the Sandyk complex of peralkaline rocks. If these results are typical for silicic rocks, they lead to a Tl content of 1.2 and 0.8 ppm for the silicic portion of the crust, for the Rb and K contents given above. *Shaw* [1952] estimated a Tl content of 3.1 ppm for granitic rocks; granodiorites and granitic gneisses contain about 0.6 ppm Tl according to his measurements. Three different estimates of the abundance of Tl in the silicic crust are thus in fairly good agreement. If the abundance of 1 ppm is assumed, the thallium in 1.2×10^{25} grams of silicic crust exceeds the amount in a chondritic earth by approximately a factor of 7. Thus, if the chondrite hypothesis is correct, (1) the analytical results must be in error or (2) a very steep vertical gradient in the crustal Tl concentration must be postulated. The observed variations in the abundance of Tl suggest no such gradient. It seems more reasonable in this case to doubt the chondrite hypothesis.

Relative abundance of the alkali metals. In the preceding discussion, certain similarities between the earth and the calcium-rich achondrites are indicated. *Gast* [1960] has shown that the K/Rb and the K/Cs ratios for these achondrites are much higher than those of the chondrites. It is thus of some interest to compare the relative distribution of potassium and ru-

idium in the earth with that seen in meteorites. *Ahrens, Pinson, and Kearns* [1952] found hat the ratio of potassium to rubidium in a ariety of rocks was similar to that in chondrites. Using stable-isotope-dilution techniques, *Herzog nd Pinson* [1956] concurred with the conclu- ion of Ahrens. A more careful comparison, ased on a number of new determinations of ubidium in chondrites [*Webster, Morgan, and Smales,* 1958; *Gast,* 1960] and on the determi- nations given in Table 4, suggests that the early conclusions may have involved some oversimpli- fication. *Horstmann* [1957] found some evidence of increases in the K/Rb ratio with decreasing potassium content. He reported an average K/Rb ratio of 240 for 66 granitic rocks having an average potassium content of 4.1 per cent and 310 for 15 gabbroic rocks with an average potassium content of 0.93 per cent. The composite samples, the analyses of which are reported in Table 2, show distinct evidence of similar changes. The K/Rb ratios of the three composite basalts range from 310 to 340; those of the two composite granites are 250 and 245. Thus there appears to be a systematic decrease of at least 30 per cent in the K/Rb ratio in the range from basalt to granite.

An average K/Rb ratio of 340 for more than 50 rocks (Composite Basalt I) clearly implies that ratios exceeding 400 are not uncommon. Two individual analyses of oceanic basalts (Table 4) exhibit unusually high K/Rb ratios and give some indication of the possible range of K/Rb ratios in igneous rocks. *Webster, Morgan, and Smales* [1958] determined the rubidium content of 12 different chondrites. If we exclude the extremely low rubidium content of the Bluff meteorite, their rubidium values and the potassium determinations of *Edwards and Urey* [1955] and *Edwards* [1955] give an average K/Rb ratio of 315 ± 30. *Gast* [1960], in a study of five chondrites, found an average K/Rb ratio of 280. If one unusually low value (Beardsley) is excepted, an average of 310 is obtained. Thus the K/Rb ratio of a number of basaltic rocks is higher than that of chondrites. The data on the K/Rb ratios from both the present study and the earlier study of Horstmann suggest that igneous and metamorphic processes which concentrate potassium generally concentrate rubidium to an equal or greater degree. If this generalization applies to a large-scale differentiation of a chondritic earth in which the alkali elements are enriched near the surface, it may be expected that the K/Rb ratio of the upper mantle would be similar to or somewhat less than that of chondrites, that is, probably less than 300. The alkali metal content of basaltic magmas is presumably somewhat greater than that of their source region. If we assume that most basaltic magmas originate in the mantle, we may infer from the K/Rb ratios given in Table 4 that the K/Rb ratio of the upper mantle is probably greater than 400. In this case the K/Rb ratio of the upper mantle inferred for a simply differentiated chondritic earth is incompatible with that suggested by surface rocks.

Discussion

In summary, it appears that the abundance of alkali metals, relative to strontium, barium, and uranium, is and always has been much lower in the upper mantle than in chondrites. In addition, it seems that the abundance of cesium and rubidium, relative to potassium, is lower in the upper mantle than in chondrites.

Both of these relationships are also found in basaltic achondrites. In comparison with chondrites, achondrites are generally depleted in potassium [*Edwards,* 1955; *Geiss and Hess,* 1958]. The depletion of rubidium and cesium is even greater than the depletion of potassium. The Sr^{87}/Sr^{86} ratio indicates that the loss of rubidium, relative to strontium, took place about 4.5 b.y. ago. Thus the observations made here are apparently in accord with the earth model proposed by *Lovering* [1958]. He assumed that the mantle is made up of material similar to achondritic meteorites, the upper 60 per cent of the mantle having a composition similar to the basaltic achondrites. However, closer examination shows that Lovering's model is not completely adequate. Difficulties similar to but more serious than those involved in the chondrite hypothesis are found, namely a complete differentiation of the mantle to account for the cesium and rubidium content of the crust. Given a crustal abundance of 74 ppm of rubidium (Table 5) and an average concentration of 0.25 ppm of rubidium (Table 4) in the basaltic achondrites, Lovering's model can account for only 55 per cent of the rubidium now in the crust. Similarly, it implies that virtually

all of the earth's cesium is now in the crust. It seems unreasonable, then, to equate the composition of the basaltic achondrites to that of the earth's mantle.

The existence of the basaltic achondrites demonstrates the existence of conditions which resulted in the type of element fractionation implied by the data given here at some points in the solar system about 4.5 b.y. ago. *Urey and Craig* [1953] and *Urey* [1951] postulated that, during the formation of the planets, some differential volatilization of the silicate and metal phases occurred, resulting in different ratios of silicate to metal phase. Such a process could result in some separation of the volatile and nonvolatile elements in the silicate phase. More specifically, volatile compounds of potassium, rubidium, and cesium could be lost from the silicate phase. In this case, the difference between the earth and the achondrites would be the amount of volatile material that was lost.

G. J. F. MacDonald (personal communication) has suggested that at the high pressures obtained in the mantle the chemical behavior of the alkali elements may be different from that observed near the surface. Under such conditions, rubidium, cesium, and perhaps potassium may not be concentrated in the silicic or late-crystallizing fraction of a silicate melt. If this is the case and if the behavior of uranium and barium does not change at high pressures, a large-scale differentiation of the earth could result in relatively low concentrations of the alkali elements, particularly Rb and Cs, in the upper mantle. Some support for this suggestion comes from the work of *Clark* [1958], who found that at more than 12,000 bars the melting points of the chlorides of potassium, rubidium, and cesium are in the reverse order of those found at ordinary pressures. If applied to the achondrites, this explanation implies that the achondrites were derived from a large, well-differentiated body.

In conclusion, it appears that at present two explanations of the apparently low abundance of potassium, rubidium, and cesium in the upper mantle must be considered. The first is that the chemical composition of the earth is different from that of chondrites, the low abundance of the alkali metals being characteristic of the whole mantle. It is suggested that this may be due to the differential retention of the volatil and nonvolatile elements of the silicate phas In the second explanation it is assumed that th earth has the same composition as chondrites. large-scale differentiation of the earth is im plied, during which potassium, rubidium, an cesium were retained or concentrated in the in terior of the earth.

Acknowledgments. The author is grateful fo the suggestions and criticisms of F. Birch, W. W Broecker, S. R. B. Cooke, and G. J. Wasserburg who read the manuscript. B. J. Mason, L. Silver and H. H. Nininger furnished the meteorite sam ples listed in Table 3. Their cooperation is ac knowledged.

The work reported here was supported by Na tional Science Foundation Grant No. G3479. W Barringer and J. M. Wampler assisted in some o the measurements given in Tables 1 to 4.

Finally, the author is grateful to J. L. Kulp whose support and encouragement made possible the work reported here.

References

Ahrens, L. H., W. H. Pinson, and M. M. Kearns, Association of rubidium and potassium and their abundance in common igneous rocks and meteorites, *Geochim. et Cosmochim. Acta, 2,* 229–242, 1952.

Aldrich, L. T., G. W. Wetherill, G. R. Tilton, and G. L. Davis, Half life of Rb^{87}, *Phys. Rev., 103,* 1045–1047, 1956.

Aldrich, L. T., G. W. Wetherill, G. R. Tilton, and G. L. Davis, Radioactive ages of micas from granitic rocks by Rb-Sr and K-A methods, *Trans. Am. Geophys. Un., 39,* 1124–1134, 1958.

Bate, G. L., J. R. Huizenga, and H. A. Potratz, Thorium content of stone meteorites, *Science, 126,* 612–614, 1957.

Bate, G. L., J. R. Huizenga, and H. A. Potratz, Thorium in stone meteorites by neutron activation analysis, *Geochim. et Cosmochim. Acta, 16,* 88–100, 1959.

Birch, F., Differentiation of the mantle, *Bull. Geol. Soc. Am., 69,* 483–486, 1958.

Blix, R., H. V. Ubisch, and F. E. Wickman, A search for variation in the relative abundance of the zinc isotopes in nature, *Geochim. et Cosmochim. Acta, 11,* 162–164, 1957.

Bullen, K. E., *An Introduction to the Theory of Seismology,* Cambridge, Univ. Press, 276 pp., 1947.

Cameron, A. E., Variation in the natural abundance of the lithium isotopes, *J. Am. Chem. Soc., 77,* 2731–2733, 1955.

Carr, D. and J. L. Kulp, Age of Mid-Atlantic Ridge basalt boulder, *Bull. Geol. Soc. Am., 64,* 253–254, 1953.

Clark, S. P., Jr., Melting point of alkali halides

at high pressure, *Ann. Rept. of the Director Geophys. Lab., Carnegie Inst. Wash. Year Book, 57,* 174–176, 1958.

Edwards, G., Sodium and potassium in meteorites, *Geochim. et Cosmochim. Acta, 8,* 285–294, 1955.

Edwards, G., and H. C. Urey, Determination of alkali metals in meteorites by a distillation process, *Geochim. et Cosmochim. Acta, 7,* 154–168, 1955.

Engel, A. E. J., and C. G. Engel, Progressive metamorphism and granitization of the major paragneiss, northwest Adirondack Mountains, New York, *Bull. Geol. Soc. Am., 69,* 1369–1410, 1958.

Evans, R. D., and C. Goodman, Radioactivity of rocks, *Bull. Geol. Soc. Am., 52,* 459–490, 1941.

Gast, P. W., Abundance of Sr^{87} during geologic time, *Bull. Geol. Soc. Am., 66,* 1449–1459, 1955.

Gast, P. W., Alkali metals in stone meteorites, *Geochim. et Cosmochim. Acta,* (in press) 1960.

Gast, P. W., J. L. Kulp, and L. E. Long, Absolute age of early Precambrian rocks in the Bighorn Basin of Wyoming and Montana, and southeastern Manitoba, *Trans. Am. Geophys. Union, 39,* 322–334, 1958.

Geiss, J., and D. C. Hess, Argon-potassium ages and the isotope composition of argon from meteorites, *Astrophys. J., 127,* 224–236, 1958.

Goldschmidt, V. M., *Geochemistry,* Oxford Univ. Press, 730 pp., 1954.

Hamaguchi, J., G. W. Reed, and A. Turkevich, Uranium and barium in stone meteorites, *Geochim. et Cosmochim. Acta, 12,* 1–28, 1957.

Heier, K. S., and S. R. Taylor, Distribution of Li, Na, K, Rb, Cs, Pb, and Tl in southern Norwegian Pre-Cambrian alkali feldspars, *Geochim. et Cosmochim. Acta, 15,* 284–304, 1959.

Herzog, L. F., and W. H. Pinson, Rb/Sr age, elemental and isotopic abundance studies of stony meteorites, *Am. J. Sci., 254,* 555–556, 1956.

Holmes, A., The oldest dated minerals of the Rhodesian Shield, *Nature, 173,* 612–614, 1954.

Horstmann, E. L., The distribution of lithium, rubidium, and cesium in igneous and sedimentary rocks, *Geochim. et Cosmochim. Acta, 12,* 1–28, 1957.

Hutchinson, R. M., Discussion; Symposium on Precambrian correlation and dating, *Geol. Assoc. of Can., Proc., 7,* 130–132, 1955.

Kouvo, O., Radioactive age of some Finnish Pre-Cambrian minerals, *Comm. Geol. Bull., 182,* 1–70, 1958.

Lovering, J. F., The nature of the Mohorovicic discontinuity, *Trans. Am. Geophys. Union, 39,* 947–955, 1958.

MacDonald, G. J. F., Chondrites and the chemical composition of the earth, in *Researches in Geochemistry,* (P. H. Abelson, ed.) John Wiley & Sons, New York, 476–494, 1959*a*.

MacDonald, G. J. F., Calculations on the thermal history of the earth, *J. Geophys. Research, 64,* 1967–2000, 1959*b*.

Nockolds, S. R., and R. Allen, The geochemistry of some igneous rock series, Part I, *Geochim. et Cosmochim. Acta, 4,* 105–141, 1953.

Nockholds, S. R., and R. Allen, The geochemistry of some igneous rock series, Part II, *Geochim. et Cosmochim. Acta, 5,* 245–285, 1954.

Nockolds, S. R., and R. Allen, The geochemistry of some igneous rock series, Part III, *Geochim. et Cosmochim. Acta, 9,* 34–77, 1956.

Patterson, C., Age of meteorites and the earth, *Geochim. et Cosmochim. Acta, 10,* 230–237, 1956.

Poldervaart, A., Chemistry of the earth's crust, *Geol. Soc. Am. Spec. Paper, 62,* 119–144, 1955.

Reed, G. W., K. Kigoshi, and A. Turkevich, Tl, Rb, Bi, and U Contents of meteorites (abstract), *J. Geophys. Research, 64,* 1121, 1959.

Ringwood, A. E., The constitution of the mantle, III: Consequences of the olivine spinel transition, *Geochim. et Cosmochim. Acta, 15,* 195–213, 1958.

Rubey, W. W., Geologic history of sea water, *Bull. Geol. Soc. Am., 62,* 1111–1147, 1951.

Russell, R. D., and D. W. Allan, The age of the earth from lead isotope abundances, *Monthly Notices Roy. Astron. Soc., Geophys. Suppl., 7,* 80–101, 1955.

Schumacher, E., Quantitative Bestimmung von Rubidium und Strontium in Steinmeteoriten mit massenspektrometrischer Isotopen Verdünnungsmethode, *Helv. Chim. Acta, 39,* 538–547, 1956.

Shaw, D. M., The geochemistry of thallium, *Geochim. et Cosmochim. Acta, 2,* 118–154, 1952.

Tilton, G. R., and G. L. Davis, Geochronology, in *Researches in Geochemistry,* (P. H. Abelson, ed.) John Wiley & Sons, New York, 190–216, 1959.

Turekian, K. K., and J. L. Kulp, The geochemistry of strontium, *Geochim. et Cosmochim. Acta, 10,* 230–237, 1956.

Urey, H. C., *The Planets,* Yale Univ. Press, 1951.

Urey, H. C., Diamonds, meteorites, and the origin of the solar system, *Astrophys. J., 124,* 623–637, 1956.

Urey, H. C., and H. Craig, The composition of the stone meteorites and the origin of the meteorites, *Geochim. et Cosmochim. Acta, 15,* 150–153, 1953.

Walker, E. C., F. Cuttitta, and F. Senftle, Some natural variations in the relative abundance of copper isotopes, *Geochim. et Cosmochim. Acta, 15,* 183–194, 1958.

Webster, R. K., J. W. Morgan, and A. A. Smales, Some recent Harwell analytical work on geachronology, *Trans. Am. Geophys. Union, 38,* 543–545, 1957.

Webster, R. K., J. W. Morgan, and A. A. Smales, Cesium in chondrites, *Geochim. et Cosmochim. Acta, 15,* 150, 1958.

Zlobin, B. I., Geochemistry of thallium in alkalic rocks, with Mt. Sandyk massif as an example, *Geochemistry,* 560–573, 1958.

(Manuscript received August 27, 1959; revised January 26, 1960.)

Letters to the Editor

Statement of Agreement regarding the Ring-Current Effect

C. O. HINES

Radio Physics Laboratory
Defence Research Telecommunications Establishment
Defence Research Board
Ottawa, Canada

AND

E. N. PARKER

Enrico Fermi Institute for Nuclear Studies and Department of Physics
University of Chicago
Chicago 37, Illinois

In an earlier communication [*Hines and Parker*, 1958], we recorded discrepant views garding the possible magnetic effects at the und caused by a hypothetical ring current in earth's exosphere. This followed upon earlier tements by *Parker* [1956, 1958*a* and *b*] to effect that only an increase of geomagnetic d could be produced in a reasonably short ne by such a current, as a consequence of spheric shielding, and conflicting statements *Hines* [1957] and *Hines and Storey* [1958] the effect that geomagnetic field changes of ner sense could be propagated rapidly through exosphere by hydromagnetic waves. In view the interest that this controversy appears to re raised, and because of the basic importance the consequences in geomagnetic storm the-, we wish now to record a reconciliation of ws, to the effect that circulating charge high he exosphere can indeed be associated with a rease of geomagnetic field at ground level in easonably short time and, therefore, may eed be responsible for the main phase of a magnetic storm.

n order to clarify the basic features of the troversy most readily, the original discrepant ws will be restated briefly in application to y extreme models where each in turn un-ubtedly applies. It should be noted, however, t each view can in turn be justified for other dels which bear a much closer resemblance he circumstances of nature, and the separate conclusions were originally formulated with these other models in mind.

As a first example, Parker's earlier conclusions [*Parker*, 1956, 1958*a* and *b*] would certainly be valid in an extreme model where the geomagnetic field is essentially confined to some lower region of the exosphere and where a ring current is established well beyond that field. The field of the ring current would in this case push back the ionized gas as it expands from the ring, and the gas would in turn push back the geomagnetic field and transmit only an increase of that field to ground level. The sequence of events is indicated in Figure 1. The disturbance field surrounding the ring current could *eventually* diffuse through the exosphere and the geomagnetic field, and so could ultimately produce a decrease in the apparent geomagnetic field at ground level, but it would do so only in a time of the order $R^2\mu\sigma$, where R is the distance from the ring to the earth, and μ is the permeability and σ the effective conductivity of the exosphere in mks units. This time would be very long if the exosphere is fully ionized, so it led to Parker's original conclusion that the ring current could not produce the main-phase decrease of a geomagnetic storm in a reasonably short time. He therefore directed attention away from possible currents, toward stresses that might be exerted by the ionized gas on the geomagnetic field.

An extreme example of a model to which the

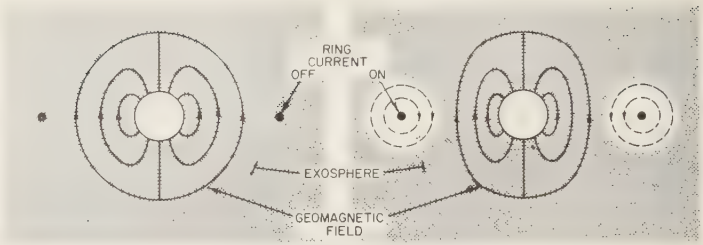

Fig. 1.

arguments of *Hines* [1957] and *Hines and Storey* [1958] would apply without question is one wherein the ring current is established well within the domain of the geomagnetic field, the exospheric ionization is confined to a region below the ring current, and the disturbance field of the ring current is very small compared with the geomagnetic field at the boundary of, and within, the exosphere. The disturbance field can then propagate readily through the exosphere in the form of a hydromagnetic perturbation of the geomagnetic field. The disturbance field can cause an increase or a decrease of the measured geomagnetic field at ground level, depending only on the sense of the current flow, and it can do this in a very short time. Hines and Storey were led by this conclusion to dismiss the question of time scale as a pertinent argument against a ring-current hypothesis for the main-phase decrease of a geomagnetic storm. (See Fig. 2.)

In an attempt to understand the basic differences between the two views, *Hines and Parker* [1958] explored together a further model in which a line current was embedded in a highly conducting gas in the presence of a strong magnetic field, but once again the discrepant conclusions were reached.

We do not feel that it is fruitful now to pu sue these original arguments further, if or because we can readily reach agreement on t behavior of a new model which we believe more in keeping with the natural phenomenc This model, described elsewhere by *Dessler a Parker* [1959], involves the trapping of blo of solar gas in the geomagnetic field. During t period of influx of the blobs, an increase of fie strength would be expected at ground level b cause of the extra pressure exerted from wit out on the exposure, and so on the geoma netic field [*Parker*, 1958*c*]. We believe that th increase would diminish in intensity and possib reverse locally as the blobs filtered through tl upper geomagnetic field lines and ultimate diffused onto them and merged with the gener exospheric ionization. The time required for th merging process would be of the order $L^2\mu$ where L is an effective linear dimension of blob, and it could be fairly short; it might co respond to the transition time of a geomagnet storm between initial and main phases.

Once the excess matter has merged with th exospheric ionization, it would be expected t follow trapped orbits in the geomagnetic fiel as discussed originally by *Singer* [1957] an more recently by *Dessler and Parker* [1959]

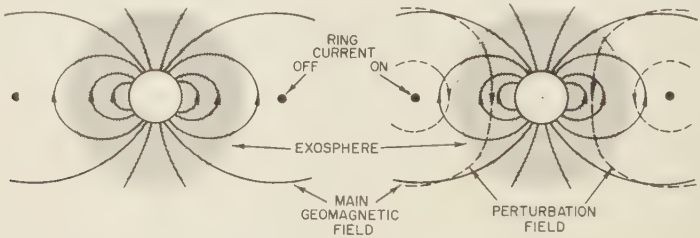

Fig. 2.

ger and Wentworth [1959], and *Akasofu* 960]. In following these orbits it would estab- a circulation of charge which might be med a ring current, although in its details it parts significantly from earlier, simpler, con- ts of the ring current.

Although we might choose different terms in scribing the local interaction of the circulating arge with the geomagnetic field, we do now ee that the disturbance it produces will pagate rapidly through the exosphere to the th and can there produce the main-phase crease of a geomagnetic storm.

We wish to acknowledge the contribution of . A. J. Dessler, who acted as intermediary in exchange of ideas which led to the foregoing tement of agreement.

References

asofu, S. I., *J. Geophys. Research, 65,* 535–543, 960. Also *Proc. Symposium on Physical Processes in the Sun-Earth Environment,* Defence Research Board of Canada, Ottawa, 1960.

Dessler, A. J., and E. N. Parker, Hydromagnetic theory of geomagnetic storms, *J. Geophys. Research, 64,* 2239–2252, 1959. Also *Proc. the Symposium on Physical Processes in the Sun-Earth Environment,* Defence Research Board of Canada, Ottawa, 1960.

Hines, C. O., *J. Geophys. Research, 62,* 491, 1957.

Hines, C. O., and E. N. Parker, *J. Geophys. Research, 63,* 691, 1958.

Hines, C. O., and L. R. O. Storey, *J. Geophys. Research, 63,* 671, 1958.

Parker, E. N., *J. Geophys. Research, 61,* 625, 1956.

Parker, E. N., *J. Geophys. Research, 63,* 437, 1958*a*.

Parker, E. N., *J. Geophys. Research, 63* 683, 1958*b*.

Parker, E. N., *Phys. Fluids, 1,* 171, 1958*c*.

Singer, S. F., *Trans. Am. Geophys. Union, 38,* 175, 1957.

Singer, S. F., and R. C. Wentworth, *J. Geophys. Research, 64,* 1807–1813, 1959. Also *Proc. of the Symposium on Physical Processes in the Sun-Earth Environment,* Defence Research Board of Canada, Ottawa, 1960.

(Received February 4, 1960.)

Visual Confirmation of the Junction Process in Lightning Discharges

M. BROOK

New Mexico Institute of Mining and Technology
Socorro, New Mexico

AND

B. VONNEGUT

Arthur D. Little, Inc.
Cambridge, Massachusetts

An unusual opportunity to observe the in-cloud and out-of-cloud paths of lightning was afforded the writers on the night of August 30, 1958. Atmospheric electricity measurements were in progress on Socorro Mountain (alt. 7200 ft msl), near Socorro, New Mexico, when a very active line of thunderstorms, subtending an angle of perhaps 70°, developed about 40 to 70 miles to the south and east. The mountain peak affords an excellent view in this direction, and on this occasion no intervening clouds obstructed the view. The writers were amazed at the detailed spectacle which unfolded before them.

The junction, or *J* process [*Schonland*, 1956], in which a streamer moves slowly upward in the intervals between the return strokes of a multiple discharge to ground, was clearly visible as it penetrated the remote regions of the cloud. The uppermost region from which the return stroke originated was observed to move (in steps reminiscent of darts) upward and outward, illuminating new regions of cloud, before a new section was added to the channel of the previous return stroke and a new stroke occurred. Some discharges to ground appeared to originate from a vertical column, but by far the greater number were seen to progress horizontally or inclined at about 30° to the horizontal. These observations are consistent with the electric-field measurements of *Pierce and Wormell* [1953]. The horizontally progressing junction streamer occurred about 3 times as often as the vertical streamer.

The manner of horizontal spread of the junction streamer is also of interest. It appeared sometimes to progress horizontally in diver directions, and, although the in-cloud paths distinct and separate, and often quite long, return strokes were seen to follow the same low-cloud path to ground. This observatio important because it shows that light strokes may often bridge individual convec cells when many thunderstorms are simult ously active along a line. Thus, one light flash may tap the electrical energy stored multiplicity of storm cells [*Workman, Br and Kitagawa*, in press].

The intermittent dartlike manner in w the junction streamer progressed is excel evidence that the slow junction field cha first observed by *Malan and Schonland* [19 is actually the sum of the individual *K* cha observed on field meters of high time resolu [*Malan*, 1955; *NMIMT*, 1956; *Kobayashi Kitagawa*, 1958]. Photomultiplier studies nocturnal lightning [*NMIMT*, 1957; *Kitag* 1957] also associate luminosity with the changes.

Such unusually favorable visibility condit are quite rare in our experience. Photogra taken on a moving-film camera would have plemented these observations with direct m urements of the effective velocity of the junc streamer. Nevertheless, it is refreshing, in age of data-taking machines and digitalizing vices, to be able to report a simple visual servation which appears to have scientific wo

REFERENCES

Kitagawa, N., On the mechanism of the cloud and junction process in flash to ground, *Pa*

teorol. and Geophys. Tokyo, 7, 415–424, 1957.
yashi, M., and N. Kitagawa, Preliminary
dies of variation in luminosity and field-
nges due to lightning flashes, *Papers Mete-
l. and Geophys. Tokyo, 9,* 29–34, 1958.
n, D. J., Les décharges lumeneuses dans les
ges orageux, *Ann géophys., 11,* 427, 1955.
n, D. J., and B. F. J. Schonland, The electri-
processes in the intervals between strokes of
ghtning discharge, *Proc. Roy. Soc. London,
206,* 145–163, 1951.
MT, *Thunderstorm Electricity, Rep. 3,* New
xico Inst. Mining and Technology, October
6.
MT, *Thunderstorm Electricity, Rep. 7,* New
Mexico Inst. Mining and Technology, October 1957.
Pierce, E. T., and T. W. Wormell, Field changes due to lightning discharges, (H. R. Byers, editor), in *Thunderstorm Electricity,* Univ. Chicago Press, 251–274, 1953.
Schonland, B. F. J., The lightning discharge, *Handbuch der Physik, 22,* 576–627, Springer-Verlag, Berlin, 1956.
Workman, E. J., M. Brook, and N. Kitagawa, Lightning charge storage, *J. Geophys. Research,* in press, 1960.

(Received February 1, 1960.)

Correction to the Paper, 'The Height of F-Layer Irregularities in the Arctic Ionosphere'

HOWARD F. BATES

Geophysical Institute, University of Alaska
College, Alaska

Recent analyses of vertical incidence $h'—f$ records indicate that the values of 350 to 500 km for the actual heights of the observed F-region irregularities, as reported in my recent paper [*Bates,* 1959], are a bit optimistic. Two of the assumptions made have been examined critically and do not hold.

First, it was assumed that the least time path passes close to the layer maximum; a subsequent calculation (based on a parabolic layer) has shown that it penetrates only five- to seven-tenths of the distance to the layer maximum. This lowers the actual height by 25 to 50 km.

Another factor was the assumption that the presence of the E layer would not materially affect the virtual height of the base of the F layer; again it was assumed that the F layer is roughly parabolic. Thus the height of the base of the F region was assumed to be the minimum virtual height of the F-layer vertical incidence trace.

Analyses of vertical incidence records by the 10-point method [*Schmerling,* 1958], using the material supplied by the National Bureau of Standards [*Wright and Norton,* 1959], have shown that this latter assumption introduc serious error when the F-region critical quency is low. Thus it is apparent that th regularity heights must be revised downwar the region of 250 to 400 km.

In appendix I of the paper an estimat 425 km was made for the height of the irr larities producing the IF echo shown in Fig 1E. The vertical incidence trace shown in ure 1E was analyzed by means of the 10-p method, and the resulting height for the irr larities was between 350 and 375 km.

REFERENCES

Bates, H. F., The height of F layer irregular in the arctic ionosphere, *J. Geophys. Resea 64,* 1257–1265, 1959.

Schmerling, E. R., An easily applied method the reduction of $h—f$ records to $N—h$ profile cluding the effects of the earth's magnetic f *J. Atmospheric and Terrest. Phys., 12,* 8–16, 1

Wright, J. W., and R. B. Norton, Analysis of i spheric vertical soundings for electron den profile data, *Tech. Note 14,* Boulder Lab tories, National Bureau of Standards, 1959.

(Received February 1, 1960.)

o Tropical Storms Play a Role in the Water Balance of the Northern Hemisphere?

H. E. LANDSBERG

Office of Climatology, U. S. Weather Bureau
Washington, D. C.

his presidential address before the Royal orological Society, *Sutcliffe* [1956] stated: ccounts of the general circulation it (the cal cyclone) is usually ignored or added as mbroidery of no basic importance except reas subject to its violence.' He also called tion to the importance of tropical storms imatic elements. As part of the same paper uotes data from J. K. Bannon on the pre- able water contents of the atmosphere in ary and July over the two hemispheres. r the northern hemisphere the average pitable water in midwinter and midsummer nts to 20 mm and 35 mm, respectively. For southern hemisphere the spread is much ler. The midwinter value is the same as in north, but the summer value is only 5 mm r.

though Sutcliffe does not specifically state e idea that the tropical storms are the bal- wheels in the seasonal water vapor dis- tion is very appealing. The writer has essly called attention to this possibility *dsberg, 1958a, b*]. Under this hypothesis tropical storms essentially reduce the water r contents from summer to winter condi- . This view fits a number of climatic facts: Most tropical storms occur after the warm- month of the year; (*ii*) the (continental) hern hemisphere has warmer summers than (primarily oceanic) southern hemisphere; e more water evaporates and more vapor is stored in the northern atmosphere, as Bannon's figures show; (*iii*) the northern hemisphere has many more tropical storms than the southern hemisphere; (*iv*) tropical storms deposit extraordinarily large amounts of precipitation; (*v*) the water vapor conversion is a major part of the driving energy of tropical storms, although other circumstances in the general circulation are essential as starter mechanisms. Although we have no quantitative information on the precipitation cycle over open water areas, the figures for island and coastal stations in tropical storm zones can act as guide. Tropical storms, even though they pass over a fixed point only occasionally, will be of influence on monthly totals and their long-term averages. This can be illustrated, for example, by data for the station at Key West, Florida, or for the averages of the island of Puerto Rico. These are shown in Table 1, where the monthly average totals are expressed as percentages of the annual totals.

The autumn peak is well pronounced. Similar data could be given for the Virgin Islands and for stations in the Far East.

As far as the tropical storms alone are concerned, some of the investigations of the National Hurricane Research Project have produced data which permit a semiquantitative check on the hypothesis. These sources of information yield some reasonable assumptions on size, path length, and precipitation of tropi-

BLE 1. Monthly Relative Precipitation at Key West, Florida, and over the Island of Puerto Rico, in Terms of Annual Total, in Per Cent

Month	Jan.	Feb.	Mar.	Apr.	May	June	July	Aug.	Sep.	Oct.	Nov.	Dec.
West												
906–1958)	4.6	4.3	3.7	4.5	8.2	10.9	9.6	11.6	17.1	15.1	6.0	4.4
to Rico												
899–1930)	5.3	4.2	5.0	6.6	9.6	8.9	9.6	10.3	11.7	11 7	10.6	6.5

TABLE 2. Moisture Balance at Three Stations (after Ivanov)

	Jan.	Feb.	Mar.	Apr.	May	June	July	Aug.	Sep.	Oct.	Nov.	D
Jacksonville, Fla.												
Mean precip., mm	70	80	75	60	100	135	170	145	190	110	50	
Evaporation, mm	50	65	85	110	120	100	90	95	75	75	65	
$p - e$, mm	20	15	−10	−50	−20	35	80	50	115	35	−15	
p/e, per cent	140	123	88	55	83	135	190	160	250	147	77	
Barbados, W. I.												
Mean precip., mm	85	55	50	40	70	110	130	190	195	195	165	
Evaporation, mm	95	100	105	120	125	90	100	90	95	95	90	
$p - e$, mm	−10	−45	−55	−80	−55	20	30	100	100	100	75	
p/e, per cent	90	55	48	33	56	123	130	210	205	205	183	
Tokyo, Japan												
Mean precip., mm	60	75	110	135	150	170	140	180	255	200	90	
Evaporation, mm	50	55	65	70	75	65	70	80	60	60	60	
$p - e$, mm	10	20	45	65	75	105	70	100	190	140	30	
p/e, per cent	120	135	170	193	200	260	200	225	390	335	150	

cal storms in the Atlantic and the Caribbean [*Haggard and Cry*, 1958; *Cry and others*, 1959; *Schoner and Molansky*, 1956]. If these are taken as representative, an estimate for the whole hemisphere can be made. All values in the following calculations are rounded to about two significant figures.

The area of the hemisphere is 2.55×10^8 km^2 or 2.55×10^{14} m^2. The summer to winter difference of precipitable water is 15 mm, so that the hemispheric water surplus is about 3.9×10^{15} liters.

The assumed standard characteristics of tropical storms are as follows: diameter 150 km, path length 4000 km, central rainfall 100 liters per square meter (100 mm, or 4 inches). This leaves out of consideration all rainfall in the fringe areas of the tropical storm, but instead, for ease of computation, it is assumed that all the center area receives uniform amounts.

With these values the area swept by a storm amounts to $1.5 \times 10^2 \times 4 \times 10^3$ km^2 or 6×10^{11} m^2. Hence the total rainfall per storm is 6×10^{13} liters. For the assumed annual number of 45 storms the value is $6 \times 45 \times 10^{13}$ liters or 2.7×10^{15} liters. This represents about 70 per cent of the summer-winter vapor surplus.

There are, of course, some loopholes in this calculation, but most of the assumptions on the storms are conservative. The assumed diameter of the storm center is probably small; the average number, considering the incomplete statistics in the Pacific and Indian Oceans, is perhaps higher than was assumed (30 North Pacific North Atlantic, 5 Indian Ocean). The aver rainfall of 100 mm (4 inches) is likely to be r istic in view of the statistics by *Schoner Molansky* [1956]. These indicate for 47 of major hurricanes which hit the United Stat mean maximum of 7.3 inches per 10,000 squ miles per 24 hours. *Hughes* [1952] in his e mates also arrives at larger amounts. There of course, never an even distribution, and some cases extreme variability exists [cf. *Jor and Shiroma*, 1959].

In moisture balance considerations the pr lem of evaporation cannot be left out. H again we have no precise data, but some gu ance can again be obtained from land stati Many stations in the tropical storm zones sh a very large preponderance of precipitation o evaporation. In a very comprehensive st *Ivanov* [1958] recently published moisture ances for a large number of tropical stati From his tables the monthly figures for th selected stations in the tropical storm zone reproduced here (Table 2).

The very high surplus of precipitation o evaporation during the months of tropical sto is pronounced. In Jacksonville in Septembe is 250 per cent, in Barbados it is over 200 cent from August through September, and Tokyo it reaches over 300 per cent in Sept ber and October. This permits at least assumption that the extraordinary precipita attributable to tropical storms does not ret

diately in vapor form to the atmosphere. conclusion, it seems quite acceptable to bute to the tropical storms a definite role e general circulation of the atmosphere. dissipate an important portion of the po- al (latent) energy stored in form of water r by the high absorption of solar energy the land-rich northern hemisphere.

Knowledgment. I am indebted to my collab- rs Mr. George Cry, for furnishing me many l data on the characteristics of tropical s, and Mr. P. H. Putnins, for interpretation anov's book.

References

G. W., W. H. Haggard, and H. S. White, rth Atlantic tropical cyclones, tracks and quencies of hurricanes and tropical storms, 6–1958, *U. S. Weather Bur., Tech. Paper 36,* 59.

gard, W. H., and G. W. Cry, A climatological index for North Atlantic tropical storm activity, *Proc. Tech. Conf. on Hurricanes,* Am. Meteorol. Soc., A1–1 to A1–10, 1958.

Hughes, L. A., On the low-level wind structure of tropical storms, *J. Meteorol. 9,* 422–428, 1952.

Ivanov, N. N., Atmosfernoe Uvlazhnenie Tropicheskikh i sopredelnykh stran zemnogo shara, *Izvest. Akad. Nauk SSSR, Ser. Geog., 18,* 311 pp., 1958.

Jordan, C. L., and M. Shiroma, A record rainfall at Okinawa, *Bull. Am. Meteorol. Soc., 40,* 609–612, 1959.

Landsberg, H. E., Climatology, *Encyclopedia Britannica,* 1958*a*.

Landsberg, H. E., *Physical Climatology,* pp. 111–120, 1958*b*.

Schoner, R. W., and S. Molansky, Rainfall associated with hurricanes, *Preprinted Rept., Natl. Hurricane Research Proj. 3,* 305 pp., U. S. Weather Bureau, Washington, D. C., 1956.

Sutcliffe, R. C., Water balance and the general circulation of the atmosphere, *Quart. J. Roy. Meteorol. Soc., 82,* 385–395, 1956.

(Received January 14, 1960.)

A Variant Least-Squares Method of Solution of a System of Observation Equations

J. L. STEARN AND H. RICHARDSON

U. S. Coast and Geodetic Survey
Washington, D. C.

Introduction. The theory of least squares is specifically designed for application to systems in which the probability distribution of the errors is known to be gaussian and free of systematic errors. Consequently one seeks to remove any observation which has a systematic error or a large random error.

In this note we shall show a mathematical device for using a suspect observation equation as a quasi-normal equation, so that if desired, this equation which is placed last in the normal equations, may be dropped from the solution, thereby precluding the necessity for the formation of a new set of normal equations and a new forward solution for the effect of the removal of the suspected observation.

Theoretical development. Given r observation equations $v = Ax + n$ and the suspect observation equations $V = Bx + M$, the problem is to minimize the weighted sum of squares of residuals

$$F \; v'Wv + V'\overline{W}V$$

$$F = x'A'WAx + 2x'A'Wn + n'Wn + x'B'\overline{W}Bx + 2x'B'\overline{W}M + M'\overline{W}M$$

$$\frac{1}{2}\frac{\partial F}{\partial x} = A'WAx + A'Wn + B'\overline{W}Bx + B'\overline{W}M = 0$$

The classical least-squares solution is [*Wright*, 1884]

$$x = -(A'WA + B'\overline{W}B)^{-1} \cdot (A'Wn + B'\overline{W}M)$$

Now rearrange the solution to form a set of normal equations in which $V = Bx + M$ is treated as a system of quasi-normal equations. This solution in matrix form is

$$\begin{bmatrix} A'WA & B' \\ B & -\overline{W}^{-1} \end{bmatrix} \cdot \begin{bmatrix} x \\ \overline{W}V \end{bmatrix} = -\begin{bmatrix} A'W \\ M \end{bmatrix}$$

where A is a weighted matrix and B amd M unweighted.

In the general case where one has, in addition to a system of observation equations, restraints in the form of conditions, $Lv + k = 0$, one minimize $v'Wv + V'\overline{W}V + (Lv + k)'C$ where C is an undetermined Lagrangian vector. The system of normal equations including the condition set is

$$\begin{bmatrix} A'WA & A'L' & B' \\ LA & 0 & 0 \\ B & 0 & -\overline{W}^{-1} \end{bmatrix} \cdot \begin{bmatrix} x \\ C \\ \overline{W}V \end{bmatrix} = -\begin{bmatrix} A' \\ Ln \\ M \end{bmatrix}$$

See *Stearn and Braaten* [1948].

The numerical example given below is a simple fictitious one to illustrate the technique developed above; the solution is carried out by the well-known Gauss-Doolittle elimination method. Note that $x_3 = +0.14866$ and, from the relation $x_3 = \overline{W}V$, we get $V = +1$. The deletion of the quasi-normal equation yields a greatly improved vector v.

Conclusions. The variant method is well adapted for least-squares solution and practical application in the fields of geodesy and geophysics. With a large system of equations the variant method is more efficient and economical; and, because of the tremendous volume of computations being run by the high-speed machines today, it is believed that the method is preferable to the standard method

Observation Equations

$\sqrt{w}$	x_1	x_2	n
1	+1	+ 1	− 4.30
1	+4	+ 5	−19.28
.7	+4.286	− 2.857	+ 2.214
.3	−6.67	+10	−15.67 suspect

Weighted Observation Equations

				I − v	II − v
1	+1	+ 1	− 4.30	−.170	−.168
1	+4	+ 5	−19.28	−.071	+.037
.7	+3	− 2	+ 1.55	+.688	+.011

Quasi-Normal Equation

B		M	V
−6.67	+10	−15.67	+1.652

Solution of Normal Equations

x_1	x_2	x_3	N	Σ
+26	+15	−6.67	−76.77	−42.44
−1	−.57692	+.25654	+2.95269	+1.63231
	+30	+10	−103.80	−48.80
	+21.3462	+13.8481	−59.5096	−24.3153
	−1	−.64874	+2.78783	+1.13909
		−11.1111	−15.67	−23.4511
		−21.8060	+ 3.2417	−18.5643
		−1	+.14866	−.85134

I–Vector x $\begin{bmatrix} +1.43811 \\ +2.69139 \end{bmatrix}$

Quasi-vector +.14866

II–Vector x $\begin{bmatrix} +1.34434 \\ +2.78783 \end{bmatrix}$

References

arn, J. L., and N. F. Braaten, A method of imultaneous solution of a system of observation nd condition equations, *Trans. Am. Geophys. Union, 29,* 157–162, 1948.

Wright, T. W., *A Treatise on the Adjustment of Observations,* D. Van Nostrand, New York, 437 pp., 1884.

(Received September 30, 1959; revised January 6, 1960.)

History of Manning's Formula

Ralph W. Powell

Rocky Mountain Hydraulic Laboratory, Allenspark, Colorado

Several years ago *Chow* [1955] published a short note on the history of the Manning formula, which led to further discussion [*Rouse and others,* 1956] but left several links in the development missing. More recently the writer [*Powell,* 1958] added some new material which was further extended in the discussion. This traced the Manning formula, as we now use the term, back to *Buckley* [1911]. The writer has now been able to consult a copy of this book and found that in support of his recommendation of Manning's formula, Buckley quoted *Willcocks and Holt* [1899]. After some correspondence, a copy of this rare book was located in the Library of Congress.

On page 10 of this book the statement is made:

> The simplicity, the regularity and the easy adaptability of Manning's formula mark it out as one of the best formulas of the day. It is based on the law that the velocity does not vary as $R^{1/2}$ but as $R^{2/3}$, and taking Kutter's value for $1/n$, $V = R^{2/3} S^{1/2}/n$ for metric units. This formula is also applicable to water moving in pipes. If Kutter's formula is examined, it will be found that, when $R = 1$ metre, the coefficient c is independent of the slope, which is extraordinary. Beyond this, the coefficient c increases with the slope for values of R less than 1 metre and decreases as the slope increases for values of R greater than 1. This is difficult to explain, and is due to some weakness in the formula. Any way, it leads to the conclusion that it is possible that the slope does not affect the coefficient, as Bazin and Manning state. For combination of theory and practice, Manning's formula is one of the best in use today. Its use is recommended.

So apparently Buckley's only original contribution was adding the 1.486 to reduce to English units. Willcocks and Holt were probably the first to recommend the above equation as Manning's in English, but they referred back to *Flamant* [1891]. Flamant had seen an 1890 preprint of Manning's paper [1891] and gave $V = C\,R^{2/3}S^{1/2}$ (in our notation) as Manning's formula and added that C is the reciprocal Kutter's n. In a footnote he said that this a simplification of Manning's longer form which included the height of the mercury rometer. I believe 'approximation' would ha been a better word than 'simplification.' should be emphasized that it was this lon formula which Manning would have wished bear his name. In his second paper on the su ject [*Manning,* 1895] the longer formula w used, and no mention was made of the form with the two-thirds power.

The chronology of what we now call the Ma ning formula would then seem to be as follo

1868 Gauckler proposed the formula $V = R^{2/3} S^{1/2}$ but limited it to values of S l than 0.0007.

1881 Hagen (apparently independently) rived the same formula (but for values of S) from Kutter's data.

1889 Manning derived the same formula was not satisfied with it and reco mended a formula which included height of the barometer.

1890 Flamant saw a pre-publication copy Manning's paper, liked the exponent equation, and recommended it in his 18 book.

1899 Willcocks and Holt published their ha book, repeating Flamant's recommen tion in English.

1911 Buckley converted the equation from metric system into English units, giv the present-day form of the equation

1915 Parker published the same material the United States.

Perhaps the writer has improperly criticiz Manning for not giving credit to earlier auth of the same formula. It has been many ye since he read the paper, but it is his reme brance that Hagen was not mentioned in

ginal paper but that in the discussion some-
e asked if Cunningham had not proposed the
o-thirds power formula in 1882. Manning's
bly was that he had derived it independently
1885 before seeing Cunningham's paper, and
e latter was based on *Hagen* [1881]. I believe
ne of them knew of Gauckler's still earlier
rk [1868].

The writer wishes to thank P. Ackers of the
ydraulics Research Station, Wallingford, Eng-
nd, and C. J. Posey of the State University of
wa for help in this research.

References

ickley, R. B., *Design of Channels for Irrigation or Drainage,* Spon, London, 1911.
now, Ven Te, A note on the Manning formula, *Trans, Am. Geophys. Union, 36,* 688, 1955.
Flamant, A., Mécanique appliquée—Hydraulique, Paris, 1891.
Hagen, G. W., Neuere Beobachtung über die gleichförmige Bewegung des Wassers, *Z. Bauwesen, 31,* 403–408, Berlin, 1881.
Manning, Robert, On the flow of water in open channels and pipes, *Trans. Inst. Civ. Engr. Ireland, 20,* 161–207, 1891, and *24,* 179, 1895.
Parker, Philip à Morley, *Control of Water,* Van Nostrand, New York, 1915.
Powell, Ralph W., About the "Manning formula," *Civil Engineering, 28,* 441, 1958, with discussion, 767, 1958.
Rouse, Hunter, J. M. Robertson, James C. I. Dooge, and Ven Te Chow, Discussion of "A note on the Manning formula," *Trans. Am. Geophys. Union, 37,* 327–330, 1956.
Willocks, Sir William, and P. Holt, *Elementary Hydraulics,* National Printing Office, Cairo, Egypt, 74 pp, 1899.

(Received November 25, 1959.)

Abstracts of the papers presented at the Pacific Northwest Regional Meeting, American Geophysical Union Corvallis, Oregon, November 5-6, 1959 listed in the order of the last name of the first author

DONALD L. BENDER AND J. A. ROBERSON (Hydraulic Laboratory, Washington State College, ullman, Wash.) *The Use of a Dimensionless Unit Hydrograph to Derive Unit Hydrographs for Some Pacific Northwest Basins.* In many areas, and articularly in the Pacific Northwest, short-period torms suitable for deriving unit hydrographs are are. Therefore, the use of the unit hydrograph or predicting runoff would increase if a method or deriving the unit hydrograph from long-period torms could be developed.

This paper presents the development of a dimensionless unit hydrograph for some Pacific Northwest basins. It then makes use of the dimensionless unit hydrograph to derive unit hydrographs from long-period storms. The method is adaptable to electronic computers and has been successfully tested on the IBM 650 computer.

G. L. BODHAINE (U. S. Geological Survey, Tacoma, Wash.) *Flood Frequency Relationships in the Pacific Northwest.* This paper describes a method used by the United States Geological Survey to analyze gaging station data so as to provide a means for determining the magnitude and frequency of momentary peak discharges at any place on any stream in a region.

The analysis provides two sets of data. The first depicts, by curves, the relationship between magnitude of annual floods, expressed as a ratio to the mean annual flood, and their recurrence interval. The second, expressed as a formula, relates the mean annual flood to drainage area and other significant basin characteristics. A frequency curve may be defined for any place in the region by use of these data.

The drainage basin characteristics used in the mathematical multiple correlations to determine mean annual flood are drainage area, area of lakes and ponds, runoff, precipitation, elevation, and geographic location. These factors are used in various combinations for different areas in the northwest. For example, drainage area, area of lakes and ponds, runoff, and geographic location are used to define the mean annual flood in western Washington. The standard errors of the various multiple correlations show that a reliable value for a mean flood can be determined by the methods discussed.

PETER B. BOYER (U. S. Army Engineers, 210 Custom House, Portland 9, Ore.) *Regional Flood Frequency Study, Portland District.* The logarithms of the annual peak discharges are assumed to be distributed normally. The geometric mean and the standard deviation of the observed annual extremes were computed for 110 runoff stations, having 17 to 65 years of record, and adjusted to long-term base when the correlation coefficient was equal to or greater than 0.70. The area was divided into five regions and for each region a mean-area curve was prepared. The adjusted values of the standard deviations were entered on a map. The geometric mean of the annual floods for any area is read from the regional mean-area curve, and the standard deviation is obtained from the examination of the adjacent values on the map. These two statistical measures provide the means for constructing a cumulative flood frequency curve for the project area desired.

T. NEIL DAVIS (Geophysical Institute, University of Alaska, College, Alaska) *Sand Flows and Surface Collapses Associated with the Koyukuk Basin, Alaska Earthquake of April 7, 1958.* The field epicenter of the Koyukuk Basin, Alaska, earthquake of April 7, 1958, was located in a near-level arrested sand dune area underlain by stream deposits from the Koyukuk River. Extensive fracturing occurred in the sand dune surface as well as in the frozen surfaces of nearby lakes and streams. Associated with the fracturing of the dune surface were many surface flowages of sand and water originating in the stream-deposited layer below the arrested dunes. Several of the flows covered areas in excess of one-quarter square mile leaving deposits of silty sand to several feet in thickness. Surface collapses resulting in conical pits up to 120 feet in diameter occurred near these flowages.

FRED W. DECKER AND HERBERT KERSHAW, JR. (Atmospheric Science Branch, Oregon State College, Corvallis, Ore.) *Radar Observations of Precipitation in Western Oregon.* Weather radar observations during the winter of 1958–1959 at Oregon State College revealed precipitation patterns within 80 nautical miles of Corvallis. A composite 3 cm, 35 kw peak, 3° beam radar (APR/21) provided PPI scope data which are recorded by means of single-frame movie camera techniques, one frame each 9 sec. Time compression then results from movie projection at normal speeds. Examples presented show convective show-

ers, widespread warm frontal precipitation, band precipitation with a front, and the change of intensity of a frontal rain curtain advancing to the Cascade Mountains.

The newly installed CPS-9 weather radar (3 cm, 225 kw peak, 1° beam) on the summit of Marys Peak (el. 4100 ft) provides film records at one frame per 18 sec. Time compression movies show the thunderstorms of October 18, 1959, east of the Cascades in Oregon and the cold front of November 2–3, 1959, approaching from 250 miles northwestward over the Pacific and passing inland over the Cascades.

Richard H. Fleming (Department of Oceanography, University of Washington, Seattle, Wash.) *Oceanographic Survey of the Eastern Chukchi Sea.* This intensive survey of the waters adjacent to Northwestern Alaska was made under the sponsorship of the Atomic Energy Commission as a part of Project Chariot of Operation Plowshare. It was a part of a comprehensive program, on both land and sea, to establish the qualitative and quantitative ecology of the area and to procure the basic information necessary to evaluate the possible effects of the proposed underground nuclear explosions. A variety of oceanographic observations were obtained in this remote and virtually unknown area. Preliminary results of the survey are presented.

D. W. Hendricks and C. C. Warnick (Department of Civil Engineering, University of Idaho, Moscow, Idaho) *New Techniques for Studying Canal Seepage in the Field and Laboratory.* New approaches followed by the Engineering Experiment Station, University of Idaho, in developing a quantitative analytical approach for the evaluation of seepage through earth canals utilizes measurement of the porous-media flow characteristics, principally hydraulic conductivity of the porous media and boundary conditions. Two instruments for measuring hydraulic conductivity, whose development is currently being extended beyond the applications of the original inventors, include the piezometer tube with cavity and the air permeameter.

The use of the piezometer method involves recognition of boundary conditions of the particular problem and application of an appropriate geometric function for the respective corresponding boundary conditions. The geometric function for the simplest flowing case may be evaluated by using a three-dimensional electrical analog involving a source and two sinks. Once these geometric functions are worked out for some of the more simple cases, they may be used with existing field data to evaluate hydraulic conductivity.

In many instances it is found that piezometers placed in the soil below a canal show no piezometric rise of water and remain dry. Also auger holes placed adjacent to these same canals do not show any water for quite some distince below the canal water surface; this is contrary to what [illegible] analytical treatment based upon conventio[illegible] theory would indicate. These observations ha[illegible] also been noted by others. This problem [illegible] studied analytically in accordance with Darc[illegible] law and the phenomena explained as being d[illegible] to unsaturated seepage flow. A plaster of Pa[illegible] Hele-Shaw model was adapted to demonstra[illegible] qualitatively the phenomenon of unsaturated fl[illegible] below a canal. The gravity force was believed [illegible] predominate over any capillary forces in t[illegible] porous media observed. It is believed that in the[illegible] unsaturated flow situations the porous media (so[illegible] of the surface zone of the canal controls the see[illegible] age rate.

In those instances where seepage is regulated [illegible] the surface zone a measurement of hydraulic co[illegible] ductivity of that zone suffices. The instrume[illegible] best adapted for this measurement is the a[illegible] permeameter which measures air permeability [illegible] the canal wetted perimeter when the canal [illegible] empty of water. The air permeability may be co[illegible] verted to intrinsic permeability, which may [illegible] turn be converted to hydraulic conductivity. O[illegible] of the problems remaining in applying this devi[illegible] is the variation of results with moisture content [illegible] the soil; this is currently being investigated in r[illegible] search for a Master's thesis. The air meter [illegible] simple in construction and can be operated easil[illegible] and rapidly; the authors have performed over [illegible] tests in a morning.

V. P. Hessler and Eugene Wescott (Geo[illegible] physical Institute, University of Alaska, Colleg[illegible] Alaska) *Earth-Current and Magnetic Activity [illegible] College, Alaska.* Earth currents were recorde[illegible] continuously at College, Alaska, during the epoc[illegible] 1956–1958. Curves are presented showing yearly[illegible] equinoctial, and solstitial averages of diurnal vari[illegible] ation. Relative earth-current and magnetic activ[illegible] ity is discussed. Correlation coefficients for severa[illegible] months between earth-current amplitude scalin[illegible] and magnetic *A* figures for College are presented

Robert E. Jones (Department of Physics, Lin[illegible] field College, McMinnville, Ore.) *Low-Frequenc[illegible] Satellite Radio Propagation Studies of the Uppe[illegible] Atmosphere.* The Linfield Research Institute re[illegible] cently completed a study of certain characteristic[illegible] of the ionosphere by analysis of radio transmis[illegible] sions from the IGY satellite 1958δ_2 (Sputnik III[illegible] at 20 and 40 Mc/s. Geographical locus of the sub[illegible] satellite point when received, direction of arriva[illegible] frequency variations, and fading rates are amon[illegible] the signal characteristics contributing to the stud[illegible] of the ion-density profile and distribution of th[illegible] *F* region. The work was supported by a Nationa[illegible] Science foundation grant under the IGY program

D. W. Kuehl (U. S. Weather Bureau, Portland[illegible] Ore.) *Comments on the Preparation of Precipita[illegible] tion Variables in Water Supply Forecasting.* Th[illegible] mechanics of the more common methods used i[illegible]

Water Supply Forecasting to combine individual precipitation station or snow course records into an index of moisture in a basin is discussed with reference to the effect of the data variance. Arbitrary methods, such as (1) averaging the data, (2) averaging the per cent of normal, and (3) multiplying by coefficients which are based on the magnitude of the normals, are analyzed to show how the relative variances of the individual data affect the importance of the variable in the forecast relationship. The mechanics are illustrated by a hypothetical example and are substantiated by theoretical considerations. Statistical weighting is examined to show how it provides for differing variances, but it is not given unqualified recommendation. Hydrologists are cautioned to examine the variance of the data prior to deciding on the combining method so that each observation is weighted in the desired manner consistent with hydrologic considerations such as elevation, area of influence, and excellence of the data.

Edward R. LaChapelle (Department of Meteorology and Climatology, University of Washington, Seattle, Wash.) *Post-IGY Glacier Research on Mount Olympus.* Continuation of the IGY glaciological program on the Blue Glacier is discussed for the field season of 1959. An important part of the 1959 program was a continued examination of the sources of energy for melt of a summer snow surface, and the results of this examination are summarized. In addition, preliminary results are given for a similar study over a bare ice surface. Certain aspects of the radiation balance and absorption characteristics of melting snow are also presented.

William P. Lowry (Office of the State Forester, Salem, Ore.) *Standardizing Field Estimates of Evaporative Soil Moisture Loss Rate.* A brief review is given of the relationships proposed in the literature linking evaporative moisture loss rate with soil moisture content. The author concludes that, under field conditions, special cases of a single basic process have yielded apparently contradictory results. A standardization technique intended to overcome these difficulties is presented, along with results which apparently support the theory.

Mark F. Meier (U. S. Geological Survey, Tacoma, Wash.) *The Outbreak of a Glacier-Dammed Lake.* Lakes may be formed by the sporadic advance or steady-state flow of a glacier across a stream channel. An ice dam is unique in that it flows, floats, and melts, permitting occasional or periodic dumping of the lake. Catastrophic floods may be involved; releases of 8,000,000 acre-feet of water at a rate of 2,000,000 ft^3/sec have been recorded. The typical shape of the outbreak hydrograph indicates that the size of opening varies with the rate of flow of water, suggesting that melting due to percolating water causes the release of lake water.

A typical example is Lake George near Anchorage, Alaska, which is dammed by the 5-mile-wide Knik Glacier. About 1,600,000 acre-feet of water is released yearly in a flood which endangers transportation arteries. Simple calculation shows that the heat periodically available in Lake George is more than sufficient to melt a release opening at the proper rate to cause the yearly outbreak.

Charles W. Thomas (Department of Meteorology and Climatology, University of Washington, Seattle, Wash.) *Late Pleistocene and Recent Limits of the Ross Ice Shelf.* Investigation of ocean bottom cores in polar areas has shown that strata lacking in skeletal remains of organisms indicate cold conditions during which a snow cover on sea ice insulated the transfer of short-wave radiation from atmosphere to sea water. The presence of organic sedimentation, on the other hand, is indicative of 'warm' periods during which solar energy was available for photosynthesis by holophytic plankton.

In this paper the examination of two cores from the south edge of the Ross Sea which have been correlated to carbon-14-dated horizons is discussed. The presence of sediments, volcanic ash, or aeolian deposition at times when perennial sea ice blanketed the region is enigmatic. Calculation of rates of penetration of sedimentary material under micrometeorological conditions of a cold environment discloses the mechanism of bottom sedimentation through sea ice with a snow cover.

The evidence of the sediments indicates that the Ross Ice Shelf did not advance materially beyond its present northerly limits during late Pleistocene and Recent times.

Geomagnetic and Solar Data

J. VIRGINIA LINCOLN

Central Radio Propagation Laboratory
National Bureau of Standards
Boulder, Colorado

INTERNATIONAL DATA ON MAGNETIC DISTURBANCES

This report continues the series which has ppeared regularly in this JOURNAL since volume 4, (3), 295 (1949). Please refer to that first eport for an explanation of the data given, and o *59*, (3), 423 (1954) for the definition of *Ap*.

Note: Additional and final 'Geomagnetic and Solar Data' appears in due course in the following nternational publications: *Quarterly Bulletin on Solar Activity*, International Astronomical Union, c/o Eidgen. Steinwarte, Zurich, Switzerland; *AGA Bulletins, Geomagnetic Indices K and C*, by J. Bartels, A. Romaña, and J. Veldkamp, nternational Union of Geodesy and Geophysics, Association of Geomagnetism and Aeronomy, c/o V. Laursen, Meteorologisk Institut, Charlottenlund, Denmark.

PART 1: SUDDEN COMMENCEMENTS AND SOLAR-FLARE EFFECTS, FIRST AND SECOND QUARTERS, 1959

Preliminary Report of Sudden Commencements S. c.'s given by five or more stations are in talics. Times given are mean values obtained rom normal magnetograms.

Sudden commencements followed by a magnetic storm or a period of storminess (s.s.c.)

1959 January *01d 11h 22m:* thirty-eight (ssc: 21; si: 16; sfe: Od).—*05d 01h 36m*: sixty-five (ssc: 43; si: 18; b: 1; bs: 2; sfe: Od).—05d 10h 29m: Sw Cm.—*09d 14h 59m:* forty-eight (ssc: 40; si: 2; bp: 2; bps: 2; pt: 2)—*12d 11h 24m:* Te AA Mc Lr Bi Tn Pi (si: Tu).—16d 06h 24m: Me Fr.—*16d 09h 27m:* forty-two (ssc: 39; si: 2; sfe: Es).—*25d 08h 59m:* sixty (ssc: 59; si: 1).—*25d 11h 24m:* Mb On Ka Ky Tu.—*26d 03h 22m:* twenty-five (ssc: 16; si: 8; bs: 1).—27d 09h 14m: Ba Mc (si: CF; sfe: Le).—29d 07h 04m: Me Vi (si: Tu).

1959 February 04d 05h 50m: Sw AA.—*11d 03h 18m:* sixty-six (ssc: 51; si: 15).—*11d 07h 56m:* fifty-five (ssc: 47; si: 8).—*14d 11h 42m:* fifty-one (ssc: 39; si: 10; bps: 2).—15d 23h 50m: Vl Hu.—*16d 06h 49m:* IK Ci On MB Mc Bi Va Br Pi (si: CF Tk Ak Ta Lr PM).—*22d 00h 46m:* sixty-two (ssc: 51; si: 10; sfe: Si).—*24d 23h 19m:* forty (ssc: 20; si: 10; bs: 3; sfe: Mb? Ka? Ky? Te MB Ap Tw).—25d 01h 26m: Sw Qu? Ta.—*25d 02h 15m:* thirteen (ssc: 11; si: 2).—25d 11h 57m: Bi El (si: Lr).—27d 10h 45m: Sw Ci.

1959 March *22d 22h 28m:* forty-one (ssc: 22; si: 18; bs: 1).—*25d 01h 39m:* Tk SM Qu Hu Tn (si: Cm CF Lu Hr).—*25d 12h 04m:* fifteen (ssc: 12; si: 2; sfe: Od).—*26d 08h 42m:* seventy-one (ssc: 70; si: 1).

1959 April *09d 18h 28m:* sixty-seven (ssc: 62; si: 3; bps: 1; sfe: Pi).—*10d 08h 01m:* twenty-five (ssc: 16; si: 9).—11d 10h 07m: Ba Mc (si: Bi).—*23d 10h 36m:* sixty-nine.—30d 12h 50m: Hl Sw Od (si: Pi; pt: El).

1959 May 04d 20h 21m: fifty-four.—*07d 21h 51m:* thirteen (ssc: 12; si: 1).—08d 03h 53m: Ag AA Mc.—*11d 23h 28m:* forty-eight (ssc: 43; si: 5).—*15d 07h 03m:* twenty-two (ssc: 19; si: 3).—*24d 05h 40m:* sixty-seven (ssc: 66; si: 1).—*24d 20h 27m:* twenty (ssc: 14; si: 6).

1959 June *09d 00h 16m:* forty (ssc: 22; si: 18).—*11d 09h 09m:* fifty-five (ssc: 53; si: 2).—17d 14h 44m: Hl Cm (sfe: Le).—22d 16h 51m: Ta Bi (si: Lg).—*23d 13h 16m:* Le Es Hl Wn? Wi Ma Pr Fu (si: Hr).—27d 06h 51m: Ci SM (si: Hr).—27d 11h 19m: Wn? Ma Pr Fu.—*29d 07h 28m:* forty-nine (ssc: 48; si: 1).—*30d 08h 01m:* twenty-nine (ssc: 26; si: 3).

Sudden impulses found in the magnetograms (s.i.)

1959 January *03d 05h 37m:* Ir AA Ba Lu El Hr.—03d 12h 04m: Sw Tl (sfe: Od).—05d 03h 17m: CF Ba Mc.—05d 07h 09m: Ta Mc Bi.—09d 17h 00m: Es Db CF.—*09d 23h 26m:* Wn

Vl Lg El (ssc: Ks Mc; bs: IK; bp: SM; bps: CF Tl).—10d 03h 32m: Ss Pi.—10d 05h 50m: Si Vi: (ssc: PB).—*11d 19h 22m:* Tu MB AA Mc Lu? (ssc: Te Ba Lr Hr?; pg: Bi).—12d 13h 28m: MB (ssc: Db).—13d 18h 24m: Cm Mc (ssc: Lg).—*14d 06h 06m:* thirty-eight (si: 20; ssc: 15; bps: 1; pt: 2).—*14d 06h 17m:* Ta MB Ba Pi (sfe: Bi).—18d 12h 15m: Tl (ssc: Le).—*22d 07h 04m:* twenty-five (si: 14; ssc: 8; bs: 2; sfe: Od).—*23d 12h 40m:* Wi Cm CF Aq Mc Hr (ssc: Hl Db Va).—23d 13h 19m: Wi CF (ssc: Es Va).—*24d 05h 58m:* Do Es Vl Ha Db CF Hr (sfe: Aq Tk).—*26d 16h 41m:* eleven (si: 10; sfe: Te).—*27d 13m 29h:* Wi CF MB Ba Bi Va. (ssc: Hl).—*29d 21h 26m:* thirty-three (si: 32; ssc: 1).—*30d 09h 01m:* AA Bi El Tn Va Pi (ssc: Qu Ta Ba Mc Lr).

1959 February 06d 12h 57m: Ma CF MB (pt: Ta).—08d 12h 27m: Pi Hr (sfe: Hu).—*08d 18h 21m:* thirty (si: 21; ssc: 6; sfe: Es Od Tw).—09d 10h 05m: AA (sfe: Mc?)—*10d 23h 16m:* Lg Tl Lu Hr (sfe: Te).—12d 09h 03m: Mo Hl Cm CF (pg: MB?).—15d 04h 38m: Mc Bi (ssc: Qu).—15d 06h 00m: Mo Wi (ssc: AA; sfe: MB?).—*16d 07h 42m:* twenty-two (si: 13; ssc: 4; pt. 4; pg: 1).—16d 12h 20m. CF Ta MB (ssc: Hl).—16d 12h 54m: CF Ta.—*16d 17h 34m* nineteen (si: 16; ssc: 1; bps: 1; sfe: Va).—*16d: 18h 45m:* Es Hl Wn Ma Db Pr CF (bs: Vl; bps: Cm Eb; pt: On).—22d 07h 45m: Db (ssc: Sw).—*22d 10h 57m:* eighteen (si: 11; ssc: 6; sfe: Te).—*22d 17h 08m:* Ma CF Fr MB Pi (ssc: Db).—*23d 11h 55m:* Ma Qu Hr (sfe: MB; b: Pi?; bs: Mc).—*25d 02h 33m:* CF Mb Ka Ss Ky AA? Bi (ssc: On El Va Pi To).—25d 03h 47m: CF AA? Bi Pi (ssc: Ks).—*25d 06h 55m:* Wn Pr CF Lg (ssc: Pi).—25d 08h 04m: Qu Pi (pg: Cm).—*25d 17h 00m:* Wn Sw Ma Db CF (bps: Vl Qu).

1959 March 02d 07h 20m: CF (pt: MB).—*02d 08h 24m:* twenty-one (si: 20; ssc: 1).—03d 02h 01m: Fr (pt: MB).—04d 11h 02m: Ba (sfe: Mc?).—*07d 09h 48m:* Lu Hr (ssc: Cm; bs: Ks; sfe: Fr).—*12d 05h 43m:* Ma CF AA Ba? (ssc: Sw; pt: Tr; sfe: Db).—*18d 22h 26m:* Mb Ka Ss Ky Tn Pi (b: Vl Su; pt: CF Te Lr).—*18d 22h 36m:* Lu Tn Hr (b: Qu El; bp: Tf).—18d 22h 51m: Ba AA? Tn Pi (bs: Bi).—*23d 17h 29m:* Ma Ta Ba Mc Lu Pi Hr (pg: Bi; sfe: MB?).—25d 02h 15m: CF Mc (bs: Ba).—25d 23h 10m: Mo Te MB Pi.—*25d 14h 17m:* eighteen (si: 10; ssc: 8).—26d 21h 38m: Es MB.—27d 08h 32m: Vi Te.—27d 11h 58m: Mo Od (ssc: Mc).—*27d 15h 56m:* Sw Wn Cm Ma Pr CF (bps: Lu Hr).—28d 02h 22m: Pi Hr.—28d 18h 07m: Es CF (ssc: Hl).—28d 22h 30m: CF (pt: Cm).—28d 22h 47m: SF (pt: Cm).

1959 April 06d 16h 55m: MB Pi.—*07d 03h 22m:* SM MB Bi Pi (ssc: Sr; sfe; Db Od).—09d 04h 22m: Qu (ssc: AA).—10d 02h 28m: Sr SM (ssc: Ir Vi; bs: Te).—10d 09h 00m: Si MB (pg: Cm).—11d 18h 03m: Pi (ssc: Sr).—11d 20h 22m: Mo Sw Od (ssc: Tr).—12d 00h 49m: To (ssc: Gu).—12d 01h 24m Ka Ky.—*23d 19h 36m:* Es Wn Vl Cm Ma CF Lg Tl (bs: Mo; pt: Aq Eb; pg: IK).—*23d 20h 06m:* Ma Db CF (pt: Cm Aq; pg: IK).—23d 20h 28m: Ma CF (pt: Aq; pg: IK).—*23d 21h 09m:* Mo Es Ma Db CF IK Fr SF (pt: Cm).—24d 06h 54m: CF Ba (pg: Cm).—24d 07h 05m: CF Ba.—24d 07h 47m: CF Qu Ba Bi.—24d 10h 01m: Mo Vl CF Ba.—26d 01h 08m: Ir (sfe: Tk).—29d 10h 30m: Vi (ssc: Te).—*29d 12h 33m:* nineteen (si: 12; ssc: 7).—30d 15h 59m: Es Ha Db CF.—30d 18h 58m: Fr (bp: Tf).—30d 19h 35m: Fr Te.

1959 May 03d 20h 51m: Ba Pi.—04d 08h 27m: AA? BA.—*05d 11h 06m:* seventeen (si: 14: ssc: 2: sfe: Su).—05d 11h 59m: Es Vl Ma CF.—08d 14h 10m: CF (sfe: Es).—*08d 16h 36m:* thirty-four (si: 32; ssc: 1; sfe: Hl).—08d 16h 57m: Lg Ba.—*08d 22h 47m:* Sr Cm (bs: Mo; bp: Vi Tu; sfe: Mb Ka Ky).—11d 14h 52m: Cm CF (ssc: Co Am).—11d 20h 02m: Tr So.—12d 00h 27m: Db To (bs: Mo; pg: Ba).—*12d 15h 17m:* CF Mb Ka Ky Qu Ba (bs: Mo Te).—*12d 15h 37m:* eleven.—*12d 16h 58m:* ten.—18d 07h 12m: Te Mc Pi.—24d 17h 24m: Es MB Ba (sfe: Te).—24d 21h 27m: CF Ks Ba.—24d 21h 45m: Sr IK.—*25d 04h 40m:* CF Mb Ka Ky Qu Te Ba.—29d 23h 54m: Lg (ssc. Sr; sfe: Db?).—*30d 14h 12m:* forty-seven (si: 29; ssc: 15; bs: 2; sfe: Hl).—*31d 07h 36m:* Sw AA? Pi (bs: Od; pt: Kv; sfe: El Tn).—*31d 11h 25m:* Sr Mb Ka Ky (ssc: Hl; sfe: Su).

1959 June *03d 23h 13m:* thirty-three (si: 20; ssc: 11; bs: 2).—04d 08h 31m: Lr Bi (sfe: El).—07d 21h 27m: Lg Tl.—10d 09h 37m: Db CF Bi (sfe: IK).—10d 23h 17m: Es Ma Lg.—15d 06h 26m: Ma CF Tl (pt: Wn Ta; sfe: Db).—19d 09h 57m: Es Db.—22d 17h 04m: Lg (ssc: Db).—*22d 21h 01m:* Pr Lg Ba Mc Lr Pi.—*27d 13h 48m:* thirty-three (si: 20; ssc: 12; sfe: Hl).—

27d 15h 25m: Mb Ka.—27d 17h 20m: MB El?—29d 08h 33m: Vi Am (bps: To).—30d 11h 51m: Gu To.

Preliminary Report on Solar-flare Effects (s.f.e.)

Effects confirmed by ionospheric or solar observations are in *italics*.

1959 January 01d 08h 55m–09h 05m: Lr.–*03d 11h 46m–12h 12m:* Es? Aq Eb? Bi (si: Lu Hr).—*04d 03h 07m:* Mb On Ka Ky Wa.—04d 14h 13m: Fr.—12d 15h 39m–16h 00m: Hu Va Pi (si: Te).—12d 21h 08m: Te.—*14d 14h 06m–14h 40m:* Le Es Wn Mc Lr Hu (bp: Vl MB).—14d 21h 00m: Fr.—18d 14h 28m: Te.—*19d 08h 52m–09h 02m:* Es.—*19d 10h 59m–11h 06m:* Es.—*19d 11h 53m–12h 04m:* Es.—20d 13h 56m: Fr.—21d 17h 02m: Fr Hu Pi (si: Tu?).—*22d 11h 27m:* Wi.—*25d 14h 13m–14h 29m:* Es.—*26d 08h 17m–08h 25m:* Es.—*27d 09h 31m–09h 44m:* Es.—27d 12h 06m: Hu.—*27d 14h 25m:* Hu.—*27d 15h 51m:* Hu.—*28d 19h 20m:* Hu.

1959 February *01d 04h 20m–04h 44m:* Mb On Ka Ss Ky Qu Gn.—02d 18h 20m: Fr.—*03d 11h 20m–11h 24m:* Es.—05d 19h 11m: Te.—05d 21h 46m: Te.—08d 13h 43m–14h 32m: Le.—09d 14h 10m: Le.—*09d 16h 03m–16h 21m:* Es.—09d 16h 19m: Le.—*09d 16h 39m–17h 10m:* Le Hu.—10d 08h 25m: Hr.—*10d 12h 12m:* Wn Wi Vl (b: Mc).—10d 18h 24m: Fr (si: Tu).—*14d 05h 05m:* Qu.—*15d 16h 32m–17h 01m:* Le Hu.—16d 14h 19m: Te.—18d 00h 58m: Ap.—*18d 05h 03m–05h 22m:* Mb On Ka PM Gn To.—20d 13h 29m: Fr (si: Te).—20d 14h 50m: Hu.—21d 11h 00m: MB (si: Cm).—22d 19h 40m: Te.—26d 12h 43m: MB (si: CF).

1959 March 02d 19h 55m: Te.—03d 19h 27m: Te Pi.—05d 15h 27m–16h 20m: Le.—07d 09h 47m: IK Qu El (si: Ba; bs: To).—07d 11h 05m: Fr.—10d 10h 20m: IK.—*11d 11h 30m–11h 40m:* Es Wi.—11d 18h 12m: Fr Pi (bs: Ag).—13d 03h 27m: Db (pt: Lr).—*16d 00h 50m:* Mb Ka Ss Ky PM?—16d 03h 57m: Mb Ka PM.—*16d 09h 15m:* Hr (si: AA).—17d 17h 32m–18h 15m: Le Od Fr MB Hu Pi (b: Tk Bi Tn; bp: Ir Tf AK; pt: Lr).—18d 15h 39m–16h 04m: Le.—*19d 10h 58m–11h 40m:* Le Es.—19d 14h 29m–15h 30m: Le.—*20d 13h 40m:* Wi.—21d 09h 08m–10h 20m: Le.—21d 13h 15m–14h 15m: Le Es.—22d 07h 17m: Db.—*22d 13h 39m–13h 55m:* Le Es Wn Wi Vl Hr (si: Pi).—*23d 13h 33m–13h 42m:* Es.—24d 07h 08m: Db (si: Sw).—*24d 10h 03m–10h 35m:* Le Wn Wi Es Cm Ma? CF Aq Eb? Ta MB? Mc? Lr El Hr (si: Mo; b: Sw SF; bs: Od; bp: Db; ssc: Ba).—24d 10h 50m: El.—24d 20h 22m: Te.—26d 12h 49m–13h 27m: Le (pg: Cm).—26d 15h 17m–16h 15m: Le.—29d 19h 50m: Te (b: Db).—31d 00h 42m–00h 48m: Gu.

1959 April 01d 14h 05m: Od.—02d 07h 56m: Od.—03d 07h 21m. Db.—*05d 23h 21m:* Mb Ka Ky Ho To Am (ssc: Sr Gu Ap; bs: Vi).—06d 11h 19m: Od MB.—07d 14h 00m: Le.—*07d 14h 43m–15h 12m:* Es.—*08d 09h 15m–09h 45m:* Le Es Hl Wn Wi Vl Cm Ha Ma Fu CF Su Lg Aq Tk Eb Tl Ks Qu Ta MB Lr El Tn Gn Hr (ssc: Mo Kv Od Ak; si: Ir SM Ba Mc Bi; b: Sw; bs: SF).—08d 18h 28m: Pi.—*09d 16h 47m–16h 56m:* Le Es Wi Cm Hu.—10d 14h 17m: Te (si: Sw).—10d 14h 25m: Te.—12d 09h 43m–09h 52m: Od Lg IK Fr MB El (si: Hl Ba Mc Pi Hr?).—*12d 11h 10m:* Le Wi Ta? MB Lr (si: Ba Bi).—12d 11h 33m: Le.—12d 13h 12m: Fr.—*13d 08h 34m:* Hr.—*14d 12h 20m–12h 25m:* Le Wi Cm Ta?—14d 12h 40m: Db.—14d 21h 31m: Te.—*15d 08h 33m–08h 57m:* Le Wn? (si: Hr).—18d 10h 39m: Od Su Fr MB? (si: Hl).—*22d 11h 16m–12h 30m:* Le Es.—*27d 08h 55m–09h 02m:* Wn Wi Cm Ma? Fu Od Lr Hr (si: Ba Mc).—28d 08h 59m: Od Ks.—29d 13h 50m: Te.

1959 May 02d 08h 38m–08h 43m: SM.—02d 20h 29m: Te.—*03d 03h 23m:* Gn (ssc: Sr).—03d 12h 48m: Tk Ik MB? (si: Pi).—04d 04h 00m–04h 06m: Gu.—*05d 06h 23m–06h 55m:* Le Es.—05d 08h 09m: El.—05d 10h 46m: El.—05d 14h 11m: El.—05d 17h 39m–18h 15m: Le.—05d 21h 08m: Hu.—06d 04h 30m: Od.—06d 09h 10m–09h 45m: Le Fu Lr.—06d 10h 12m–10h 48m: Le Lr.—06d 11h 55m: Od.—06d 13h 28m–14h 10m: Le.—07d 12h 04m: Su (si: Bi).—*08d 14h 21m–15h 05m:* Le Es.—*08d 22h 47m:* Mb Ka Ky (si: Sr Cm; bs: Mo; bp: Vi Tu).—*09d 17h 15m:* Hu.—10d 15h 45m: MB.—*11d 20h 17m:* Hu.—11d 21h 49m: Te.—*13d 05h 12m:* Mb Ka Ss Ky.—*13d 15h 52m:* Hu.—15d 11h 00m: El.—15d 13h 27m: El Hu Va Pi (b: 2; bs: 7; bp: 1; bps: 3).—16d 09h 50m–10h 12m: Es.—*17d 05h 24m:* Wi Mb Tk Ka Ky Ta Lr PM Gn To (ssc: Ba; si: Mo Ir IK).—*17d 07h 05m–07h 09m:* Es Wi Mb Ka Ky Lr (si: IK Bi).—*18d 04h 04m:* Mb Ka Ky (si: To; bs: Ag).—*18d 13h 30m:* Hu.—20d 15h 10m: Hu (pt: Ss).—24d 16h 35m: Te.—*27d 17h 50m:* Hu.—30d 09h 09m: Od.—31d 08h 59m: El.—31d 11h 16m: Db IK Qu Te MB AA? Ba? Bi El Tn (ssc: Cm Kv SF; si: Tk Eb Ta Mc

Lr Hr; bs: Mo; bps: Od).—31d 19h 00m: Hu.

1959 June *01d 14h 18m:* Hu.—*02d 18h 15m–19h 26m:* Es Hu.—04d 10h 31m–11h 24m: El.—*05d 09h 25m–09h 45m:* Le Es.—07d 13h 52m: Le.—*09d 16h 34m–18h 45m:* Le Es Hu.—*10d 17h 40m–17h 51m:* Es Hu.—*11d 06h 06m–06h 40m:* Le Mb Ka Ky Lr.—*12d 16h 31m:* Hu.—*13d 03h 58m:* Mb Ka.—15d 09h 41m: Vl Sm.—15d 10h 50m–11h 48m: Le.—*15d 14h 03m:* Wn? Fr (b: Hu).—*15d 16h 23m–16h 54m:* Le Wn Hu.—*16d 06h 23m–07h 00m:* Le Es Wn Wi Vl Cm Ma? Pr Fu Mb Aq IK Ka Ss Ky Lr El Tn Gn Hr To (si: Eb Ba Bi).—16d 10h 10m: Lr.—18d 11h 22m: Ks.—*18d 11h 39m–13h 10m:* Le Es Wn? Wi Vl Cm Ha Ma Fu Su Aq Eb Ta Lr Tn (ssc: SF; si: Pr CF Lg IK Tl MB Ba Bi El Hr).—19d 12h 38m–13h 30m: Le.—*20d 10h 20m–10h 23m:* Es.—22d 10h 22m–11h 00m: Le.—29d 01h 50m–02h 20m: Gu.—30d 09h 45m–10h 01m. Gu.

PART 2. Kp, Ap, Ci, AND SELECTED DAYS, FOURTH QUARTER, 1959

TABLE 1. Geomagnetic planetary three-hour-range indices *Kp*, preliminary magnetic character-figures *C* average amplitudes *Ap* (unit 2γ), and final selected days, October to December, 1959.

	October 1959								
E	1	2	3	4	5	6	7	8	Sum
1	4o	5+	6o	6−	4o	4o	4o	5−	38−
2	3−	6−	5o	4o	2o	2+	2+	2−	26−
3	1o	3−	4o	3o	3+	6−	7−	7−	33o
4	5o	7o	5+	5−	6−	3o	4+	3+	38+
5	5−	4+	3o	3−	3+	4+	6o	6−	34o
6	6−	6−	5+	5+	5−	5o	5+	4+	41+
7	3+	4−	3−	3+	3−	1+	2+	4o	23+
8	3o	3−	2−	3−	1+	2−	1o	1−	15−
9	3−	1+	2−	2−	1−	1o	3−	0+	12o
10	1o	1o	1o	1o	1−	2+	1+	1−	9o
11	1o	0o	1o	0+	0o	0o	2−	1+	5+
12	1o	0o	0+	0+	2−	2+	3+	3−	12−
13	1o	1−	1+	1+	1+	1+	1−	1−	8+
14	2−	2−	2o	3+	4−	2+	3+	3o	21o
15	3o	3+	2+	3o	3o	3−	3+	3+	24o
16	2−	1o	1−	0+	0+	1o	2o	1−	8−
17	1o	2−	3−	4+	4−	3o	4−	4−	24−
18	5−	4+	5−	5+	4+	5−	4−	4+	36o
19	4−	4o	2+	3+	2−	1+	3o	3+	23−
20	4−	2o	3o	2o	1+	0+	0+	0+	13o
21	0+	1−	1−	1o	1+	3−	1+	3−	11−
22	3+	4−	3+	3+	3+	4+	3−	3−	27−
23	4−	3−	3−	3+	2−	0+	0+	0o	15−
24	0o	1−	2o	2−	2+	2o	2−	2o	12+
25	3o	5−	4−	4+	4−	3o	2+	4−	28+
26	4−	4−	4o	4o	5o	4+	3o	3+	31o
27	2+	3+	4−	3o	2+	2+	1o	1o	19o
28	1−	1−	2+	2−	1o	0+	0+	0o	7o
29	0+	1+	1+	1o	2−	1−	0+	3+	10o
30	5+	4o	3−	2+	3+	3−	4o	6−	30o
31	4+	3o	3+	5o	4+	5o	5o	6−	36−

	November 1959								
	1	2	3	4	5	6	7	8	Sum
	4−	5o	6+	5+	5+	4−	4−	4−	37−
	5o	6−	6+	5o	6−	6−	6+	6−	45+
	6−	5−	5−	5o	5−	6−	5o	5−	40o
	2o	3−	5−	4+	5o	5−	6o	4+	34−
	5−	5o	5o	4o	4o	3−	3o	2−	31−
	4+	4o	4−	4+	3+	2+	3o	4+	29+
	1+	4−	3−	1o	1+	2+	4−	2+	18+
	1+	4−	3−	3+	3+	2+	3−	1+	21−
	1−	2o	0o	1+	2o	3−	4−	3o	15+
	3o	2+	2o	2+	3−	1+	2o	3+	19o
	2+	2−	1−	2−	1o	1−	1+	2−	11o
	2o	2+	1−	1+	1o	2−	3−	2+	14o
	2+	2−	2o	3−	3+	3−	3−	4−	21o
	4+	4−	4o	5−	5−	4o	4−	3o	32o
	3−	2−	2−	1o	1−	1−	0o	1o	9+
	1−	0+	2−	1+	2+	3+	3−	3−	15o
	2+	4+	2+	3+	3+	1−	0+	1−	17+
	2−	2+	2+	2+	3o	3o	5−	2−	21o
	2o	3−	4−	3+	3o	2+	1−	1+	19o
	3o	2−	1+	1+	0o	0o	0+	1−	8+
	1o	2+	2o	3+	4+	4o	3o	3o	23o
	3+	4o	3+	4−	3+	2+	3+	2+	26−
	5+	6−	5+	5o	4+	3+	4+	2o	35+
	3−	2o	2−	1+	3−	2o	2−	1+	15+
	2+	1+	2o	3−	3+	2o	1+	3o	18o
	2+	2o	3+	4o	3o	2−	2−	3+	21+
	4−	2+	3o	2o	2o	2o	3−	5−	22+
	6o	8o	7+	7−	4+	4−	4o	4o	44o
	4−	3−	2−	4o	3+	3o	3−	2−	23−
	3−	2+	5+	6−	5+	6o	4o	5−	36o

	December 1959								
E	1	2	3	4	5	6	7	8	Sum
1	5o	4+	4+	5−	4+	3+	3o	2−	31−
2	3+	4+	4+	5o	4o	4+	4o	4o	33+
3	5o	5−	5o	5+	5+	6−	4o	5+	40+
4	3+	4o	3−	3−	2o	2−	2+	2+	21o
5	0o	0o	4o	5−	6+	7−	8−	6+	36−
6	3o	4+	3+	3+	3o	2o	3o	2+	24+
7	3o	3−	1−	0+	2−	2−	1−	1+	12o
8	1+	2o	2−	1o	1−	3−	2+	2o	14−
9	1+	1+	3−	3−	3o	2o	1−	2o	16−
10	2+	2−	2−	1−	0+	1+	2+	1+	12−
11	0+	2o	2−	2o	1+	2+	1−	2−	12o
12	2+	4+	3−	3o	3−	2o	3o	4o	24o
13	4o	3+	2+	2−	1o	2+	3o	5+	23o
14	5−	4+	5+	5o	5−	5+	5−	3o	37o
15	3+	4+	4+	4o	3+	3+	4o	4+	31o
16	3+	2+	3o	3+	4−	4o	2+	3o	25o
17	3o	1+	3−	3−	2o	1−	1+	2−	15+
18	2o	2−	3o	3−	4−	2o	1+	2o	18+
19	2+	3−	3+	4−	4o	3−	2o	1o	22−
20	2+	2o	1+	2−	1+	2o	2−	2−	14o
21	1+	1+	1+	1−	1−	0+	1o	1o	8−
22	2−	0+	0+	0+	1o	2+	2o	3o	11o
23	3−	3−	4−	3−	3−	6o	4+	5−	29+
24	4o	1+	4o	4o	3+	1+	2−	2o	22−
25	2o	3o	2o	3−	2−	2−	2+	1+	17−
26	3−	4−	3+	4+	4+	4−	4o	5−	31−
27	5−	5−	4o	6−	4+	5−	4o	4+	36+
28	5o	5−	4+	5−	5+	5+	5−	3o	37o
29	4o	4o	4o	4−	4−	3−	1o	2o	25o
30	2−	3o	3o	4−	4−	3o	3−	1o	22−
31	2−	2−	3−	2o	1o	1o	2+	1+	14−

	Preliminary *C* 1959			Average amplitude *Ap*		
	Oct.	Nov.	Dec.	Oct.	Nov.	Dec.
1	1.3	1.3	1.1	44	43	28
2	1.0	1.6	1.2	23	69	**30**
3	1.5	1.4	1.5	46	48	**50**
4	1.3	1.3	0.7	51	36	12
5	1.3	1.1	1.7	37	28	68
6	1.5	1.1	0.9	53	23	16
7	0.9	0.7	0.3	15	11	6
8	0.3	0.6	0.3	8	13	7
9	0.3	0.7	0.3	6	9	8
10	0.2	0.6	0.2	4	10	6
11	0.2	0.1	0.2	3	5	6
12	0.4	0.2	1.0	7	7	16
13	0.2	0.8	1.1	4	12	18
14	0.8	1.2	1.4	13	28	40
15	1.0	0.1	1.1	15	5	26
16	0.1	0.5	1.0	4	8	17
17	1.0	0.5	0.3	17	12	8
18	1.2	0.9	0.5	36	14	10
19	0.9	0.5	0.8	15	11	14
20	0.4	0.1	0.3	8	4	6
21	0.4	1.0	0.1	6	16	4
22	1.2	1.0	0.4	19	17	6
23	0.5	1.4	1.3	10	40	28
24	0.3	0.2	0.9	6	8	15
25	1.2	0.6	0.4	22	10	8
26	1.2	0.7	1.2	26	13	26
27	0.7	0.8	1.4	11	15	38
28	0.0	1.7	1.4	4	82	40
29	0.2	0.8	0.9	6	15	18
30	1.3	1.4	0.8	28	43	14
31	1.5		0.4	38		7

TABLE 1. (Concluded)—Final Magnetically Selected Days, October to December 1959

Month	Five quiet days					Ten quiet days										Five disturbed days				
1959																				
October	10	11	13	16	28	9	10	11	12	13	16	21	24	28	29	1	3	4	6	31
November	11	12	15	20	24	7	9	10	11	12	15	16	20	24	25	1	2	3	28	30
December	7	10	11	21	22	7	8	9	10	11	17	20	21	22	31	3	5	14	27	28

TABLE 2. Monthly Mean Values of *Ci*, *Cp*, and *Ap*, October to December 1959

Index	October 1959	November 1959	December 1959
Mean *Ci*.....	0.78	0.83	0.81
Mean *Cp*.....	0.77	0.87	0.83
Mean *Ap*	19	22	19

COMMITTEE ON CHARACTERIZATION OF MAGNETIC DISTURBANCES

J. Bartels, *Chairman*
University
Göttingen, Germany

J. VELDKAMP
Kon. Nederlandsch Meteorologisch Instituut
De Bilt, Holland

PRINCIPAL MAGNETIC STORMS

(Advance knowledge of the character of the records at some observatories as regards disturbances)

Observatory (Observer-in-Charge)	Greenwich date	Storm-time: GMT of begin.	Storm-time: GMT of ending[1]	Sudden commencement: Type[2]	Sudden commencement: Amplitudes[3] D	Sudden commencement: Amplitudes[3] H	Sudden commencement: Amplitudes[3] Z	C-figure, degree of activity[4]	Maximal activity on K-scale 0 to 9: Gr. day	Maximal activity on K-scale 0 to 9: Gr. 3-hr. period	Maximal activity on K-scale 0 to 9: K-index	Ranges: D	Ranges: H	Ranges: Z
(1)	(2)	(3)	(4)	(5)	(6)	(7)	(8)	(9)	(10)	(11)	(12)	(13)	(14)	(15)
	1959	*h m*	*d h*		′	γ	γ					′	γ	γ
College	Oct. 3	07 ..	4 22	.....	....	....	....	ms	3	3,6	7	334	1800	1420
(C. J. Beers)	Oct. 5	01 ..	7 01	.....	....	....	....	ms	6	2	7	152	1500	800
	Oct. 31	08 45	1 22	.....	....	....	....	ms	31	4,5	7	248	1580	940
									1	3,4	7			
	Nov. 2	02 ..	4 01	.....	....	....	....	ms	2	3,4,5,6	7	319	1850	980
									3	3,6	7			
	Nov. 4	04 48	5 22	.....	....	....	....	ms	4	4,5	7	268	1450	1090
									5	3,4	7			
	Nov.27	23 50	29 01	s.c.*	+53	+98	+88	ms	28	4	7	157	1640	860
	Nov.30	06 ..	1 23	.....	....	....	....	ms	30	5,6	7	331	1350	1200
									1	3,4	7			
	Dec. 2	04 ..	3 23	.....	....	....	....	ms	2	4,5	7	324	1520	870
									3	5	7			
	Dec. 5	07 01	6 06	s.c.*	?	+203	−26	s	5	6	8	357	1980	1290
	Dec. 13	17 ..	15 02	.....	....	....	....	ms	14	3,4	7	248	1530	830
	Dec. 26	05 ..	29 04	.....	....	....	....	ms	26	4	7	259	1550	940
Sitka	*1959*													
(M. L. Cleven)	Oct. 1	04 00	1 17	.....	....	....	....	ms	1	4	7	110	820	530
	Oct. 3	06 30	7 12	.....	....	....	....	s	4	5	8	140	1500	820
									6	4				
	Oct. 25	03 00	26 21	.....	....	....	....	ms	25	4	7	60	620	570
									26	5				
	Oct. 31	09 00	5 19	.....	....	....	....	s	31	4	8	140	1180	760
									1	3,5				
	Nov.14	07 00	14 21	.....	....	....	....	ms	14	4,5	6	35	430	290
	Nov.21	10 00	21 17	.....	....	....	....	ms	21	5,6	6	50	255	470
	Nov.23	00 45	23 16	.....	....	....	....	ms	23	3,4	7	100	710	510
	Nov.27	23 51	28 19	s.c.*	−9	−16	+7	s	28	2,4	8	125	1830	800
	Nov.30	07 00	1 21	.....	....	....	....	s	30	4,5	8	125	1100	720
	Dec. 2	04 30	3 23	.....	....	....	....	ms	3	3,4,5	7	120	770	640
	Dec. 5	07 00	6 03	s.c.	+4	+10	−3	s	5	5	9	160	1160	870
	Dec. 14	03 30	14 21	.....	....	....	....	ms	14	3,4	7	150	660	670
	Dec. 26	11 00	28 21	.....	....	....	....	ms	27	4	7	90	640	530
Witteveen	*1959*													
(D. v. Sabben)	Oct. 3	15 00	5 05	.....	....	....	....	ms	3	8	7	45	245	140
	Oct. 5	14 00	6 24	.....	....	....	....	ms	5	7,8	6	45	200	120
									6	6,7				
	Oct. 17	09 00	19 12	.....	....	....	....	m	18	6,8	5	30	140	60
	Oct. 29	23 49	31 24	s.c.*	−3	+45	0	ms	30	8	6	50	225	135
									31	7,8	6			
	Nov. 1	03 00	3 24	.....	....	....	....	ms	2	7	7	55	210	120
	Nov. 4	06 00	5 15	.....	....	....	....	ms	4	7	7	45	210	90
	Nov.23	00 00	23 22	.....	....	....	....	ms	23	7	6	35	210	85
	Nov.27	23 51	28 24	s.c.*	−6	+85	0	ms	28	2	7	40	300	110
	Nov.30	05 00	30 24	.....	....	....	....	ms	30	6	6	40	155	120
	Dec. 2	04 00	3 24	.....	....	....	....	ms	3	6	7	45	175	105
	Dec. 5	06 59	5 24	s.c.*	+4	+9	0	ms	5	6,7	7	65	260	235
	Dec. 13	20 00	14 21	.....	....	....	....	ms	14	6,7	6	35	160	70

[1]Approximate time of ending of storm construed as the time of cessation of reasonably marked disturbance movements in the traces; more specifically, when the K-index measure diminished to 2 or less for a reasonable period.

[2]s.c. = sudden commencement; s.c.* = small initial impulse followed by main impulse (the amplitude in this case is that of the *main impulse only*, neglecting the initial brief pulse); ... = gradual commencement.

[3]Signs of amplitudes of D and Z taken algebraically; D reckoned positive if towards the east and Z reckoned positive if vertically downward.

[4]Storm described by three degrees of activity: *m* for moderate (when K-index as great as 5); *ms* for moderately severe (when K = 6 or 7); *s* for severe (when K = 8 or 9).

PRINCIPAL MAGNETIC STORMS—Continued

Observatory (Observer-in-Charge)	Green-wich date	Storm-time GMT of begin.	Storm-time GMT of ending[1]	Sudden commencement Type[2]	Sudden commencement Amplitudes[3] D	H	Z	C-figure, degree of activity[4]	Maximal activity on K-scale 0 to 9 Gr. day	Gr. 3-hr. period	K-index	Ranges D	H	Z
(1)	(2)	(2)	(4)	(5)	(6)	(7)	(8)	(9)	(10)	(11)	(12)	(13)	(14)	(15)
	1959	*h m*	*d h*		′	γ	γ					′	γ	γ
Witteveen	Dec. 23	15 25	24 02	s.c.	−2	+38	0	ms	23	6	6	35	150	65
—Continued	Dec. 26	10 00	29 13	.....	....	....	....	ms	26	8	6	30	175	80
(D. v. Sabben)														
Fredericksburg	*1959*													
	Oct. 1	05 ..	2 12	.....	....	....	....	ms	2	3	6	26	102	95
(R.E.Gebhardt)	Oct. 3	17 ..	7 15	.....	....	....	....	ms	4	2	7	42	151	170
	Oct. 17	05 ..	19 12	.....	....	....	....	m	18	1	5	20	120	62
	Oct. 29	23 47	3 23	s.c.*	+2*	+39*	−6*	ms	2	3	6	31	182	116
	Nov. 4	05 ..	5 16	.....	....	....	....	m	4	8	5	22	105	76
									5	1,2,3				
	Nov.22	18 ..	23 21	.....	....	....	....	m	23	2,4	5	20	93	85
	Nov.27	23 51	29 00	s.c.*	+6	+73	−11	ms	28	2,3	7	45	235	274
	Nov.30	06 ..	4 12	.....	....	....	....	ms	30	4	6	30	165	82
	Dec. 5	06 59	6 12	s.c.*	−2*	+10	−2	ms	5	7	6	27	224	96
	Dec. 13	17 ..	16 17	.....	....	....	....	m	14	5	5	19	132	72
	Dec. 23	15 25	24 14	s.c.	+5	+8	−3	m	23	6	5	19	112	44
	Dec. 25	11 ..	29 14	.....	....	....	....	m	26	4	5	28	138	44
									27	4,6,8	5			
									28	1,5	5			
Tucson	*1959*													
(R. L. Viets)	Oct. 3	04 ..	7 07	.....	....	....	....	ms	4	2,3	6	19	150	53
									6	2	6			
	Oct. 29	23 47	1 17	s.c.	....	+36	+1	ms	30	1	6	17	161	37
									31	4	6			
									1	3	6			
	Nov. 2	06 47	3 24					ms	2	3,5	6	14	145	33
	Nov. 4	04 50	5 16	.....	....	....	....	m	4	5,7	5	12	134	32
	Nov.27	23 51	28 19	s.c.*	−3	+47	+2	ms	28	2,3	7	27	263	45
	Nov.30	05 48	1 16	.....	....	....	....	ms	30	3,4	6	17	114	44
	Dec. 2	04 ..	3 23	.....	....	....	....	ms	3	4	6	14	135	33
	Dec. 5	06 59	6 11	s.c.	−1	+23	+1	ms	5	5,6	6	16	204	48
	Dec. 13	16 ..	16 17	.....	....	....	....	m	14	3,4,5,6	5	14	107	38
	Dec. 23	15 25	24 02	s.c.*	4	15	....	m	23	6	5	16	78	34
	Dec. 26	02 ..	29 13	.....	....	....	....	m	26	4	5	14	121	35
									27	4,8	5			
									28	4,5,6	5			
San Juan	*1959*													
(M. Vazquez)	Nov.27	23 51	28 19	s.c.	−1	+32	−12	ms	28	2	7	13	190	28
	Dec. 5	06 59	6 11	s.c.	+1	+12	−4	ms	5	5,6,8	6	12	210	40
Honolulu	*1959*													
(G.E.Haraden)	Oct. 29	23 48	30 09	s.c.*	+1	+35	+19	m	29	8	5			
									30	1				
	Nov.27	23 51	28 24	s.c.*	+2	+32	+23	s	28	2	8	3	290	27
	Dec. 5	06 59	6 24	s.c.	+0	+22	+12	m	5	3,5,6,7	5	4	85	30
Instituto	Oct. 1	04 32	1 22	.....	....	....	....	m	1	5,6,7	5	9	223	80
Geofísico de	Oct. 4	03 35	4 20	.....	....	....	....	m	4	1,2,5,6,7	5	6	279	46
Huancayo,	Oct. 5	12 00	6 20	.....	....	....	....	ms	5	7	6	10	332	70
Peru, (A.	Oct. 17	06 25	19 04	.....	....	....	....	ms	18	5,6	6	11	404	65
Giesecke and	Oct. 22	00 50	22 18	.....	....	....	....	ms	22	6	6	11	245	31
M. Casaverde)	Oct. 26	06 41	26 21	.....	....	....	....	ms	26	6,7	6	5	205	30
	Oct. 29	23 47	31 04	s.c.	+1	+53	+13	ms	30	5	6	8	315	45
	Oct. 31	07 00	1 20	.....	....	....	....	ms	31	6,7	6	8	222	47
	Nov. 2	06 46	3 21	.....	....	....	....	ms	2	5,6,7	6	11	310	42

PRINCIPAL MAGNETIC STORMS—Continued

Observatory (Observer-in-Charge)	Greenwich date	Storm-time GMT of begin.	Storm-time GMT of ending[1]	Sudden commencement Type[2]	Sudden commencement Amplitudes[3] D	H	Z	C-figure, degree of activity[4]	Maximal activity on K-scale 0 to 9 Gr. day	Gr. 3-hr. period	K-index	Ranges D	H	Z
(1)	(2)	(3)	(4)	(5)	(6)	(7)	(8)	(9)	(10)	(11)	(12)	(13)	(14)	(15)
Institute Geofísico de Huancayo, Peru —Continued	*1959*	*h m*	*d h*		′	γ	γ					′	γ	γ
	Nov.14	00 14	14 20	.....	....	....	....	ms	14	5,6	6	8	270	35
	Nov.23	00 20	23 19	.....	....	....	....	ms	23	6	6	8	230	51
	Nov.27	23 51	28 19	s.c.	−1	+67	+12	ms	28	2,4	6	12	388	47
	Nov.30	05 45	1 20	.....	....	....	....	ms	30	5,6	7	15	340	60
	Dec. 2	04 10	3 23	.....	....	....	....	ms	3	6	6	12	271	62
	Dec. 5	06 59	6 19	s.c.	0	+34	+5	s	5	7	8	18	462	63
	Dec. 13	11 30	14 20	.....	....	....	....	ms	14	5,6	6	9	214	32
	Dec. 23	10 50	23 20	.....	....	....	....	ms	23	5,6,7	6	9	328	47
	Dec. 26	11 32	28 23	.....	....	....	....	ms	27	5	7	13	331	63
Binza (J. Bodson)	*1959*													
	Oct. 29	23 50	31 24	s.c.	−1	+42	−1	m	30	1	...	9	214	43
	Nov.27	23 50	28 24	s.c.	−1	+63	−3	m	28	4	...	8	147	30
	Dec. 5	07 02	6 15	s.c.	−2		0	m	5	7	...	13	328	32
Port Moresby (J. A. Brooks)	Nov.27	23 51	28 19	s.c.	−2	+31	+25	ms	28	2,4	7	13	253	117
	Dec. 5	06 59	6 14	s.c.	+1	+47	+43	m	5	5,7	6	9	171	84
Elizabethville/ Karavia (A. Alexander)	1959	No principal storms October–December 1959												
Apia (R. H. Orr)	*1959*													
	Oct. 1	20 ..	3 03	.....	....	....	....	m	2	2,3	5	5	173	26
	Oct. 3	07 18	7 10	.....	....	....	....	m	3	7		6	151	38
									5	2	5			
	Oct. 29	23 47	7 06	s.c.	+1	+38	−15	ms	30	1	6	20	246	30
	Nov.21	05 ..	24 05	.....	....	....	....	m	23	5	5	8	165	25
	Nov.27	23 51	29 02	s.c.*	+0	+38	−19	s	28	2	8	11	280	43
	Nov.30	02 47	5 00	s.c.	+1	+8	−5	m	30	4	5	10	134	32
	Dec. 5	06 59	7 05	s.c.	+1	+33	−14	ms	5	6	6	12	156	21
	Dec. 13	15 40	17 06	.....	....	....	....	m	14	3	5	9	146	18
Hermanus (A. M. van Wijk)	*1959*													
	Oct. 1	00 ..	2 12	.....	....	....	....	m	1	4	5	20	126	68
									2	2,3	5			
	Oct. 3	06 ..	4 14	.....	....	....	....	ms	3	8	6	28	107	103
	Oct. 5	12 ..	6 22	.....	....	....	....	ms	5	7	6	24	101	96
	Oct. 17	03 ..	19 14	.....	....	....	....	m	17	4	5	28	123	90
									18	3,4	5			
	Oct. 29	23 48	3 22	s.c.	+2	+37	+32	ms	31	8	6	31	171	127
									2	7	6			
	Nov. 4	04 ..	6 22	.....	....	....	....	m	4	7	5	27	91	129
	Nov.18	17 ..	18 20	Bay	....	....	....	m	18	7	5	9	50	52
	Nov.21	11 37	23 22	s.c.	+1	+5	+8	m	21	5	5	30	125	94
									23	7	5			
	Nov.27	23 52	28 22	s.c.*	+4*	+52	+37	ms	28	4	7	21	205	155
	Nov.30	05 ..	1 14	.....	....	....	....	ms	30	5,6	6	31	153	146
	Dec. 3	03 ..	4 13	.....	....	....	....	m	3	4,5,6,8	5	31	121	89
	Dec. 5	06 59	6 17	s.c.*	−4*	+35	+14	ms	5	5,6,7,8	6	49	238	206
	Dec. 13	17 ..	14 21	.....	....	....	....	m	14	6,7	5	26	94	84
	Dec. 23	15 25	24 00	s.c.*	+2*	+16*	+12	ms	23	6	6	15	54	100
	Dec. 26	01 ..	29 14	.....	....	....	....	m	27	4,5	5	23	108	80
									28	1,4,5	5			

PRINCIPAL MAGNETIC STORMS—Concluded

Observatory (Observer-in-Charge)	Greenwich date	Storm-time: GMT of begin.	Storm-time: GMT of ending[1]	Sudden commencement: ..... Type[2]	Sudden commencement: Amplitudes[3] D	H	Z	C-figure, degree of activity[4]	Maximal activity on K-scale 0 to 9: Gr. day	Gr. 3-hr. period	K-index	Ranges D	H	Z
(1)	(2)	(3)	(4)	(5)	(6)	(7)	(8)	(9)	(10)	(11)	(12)	(13)	(14)	(15)
Gnangara	*1959*	*h m*	*d h*		′	γ	γ					′	γ	γ
(P. M. McGregor)	Oct. 5	12 03	7 02	s.c.	−1	+3	−6	m						
		(No record 0127–0853 6th.)												
	Oct. 17	03 09	19 06	s.c.	−1	0	−1	m	18	1,4,6	5	22	91	142
	Oct. 29	23 48	4 00	s.c.*	−6*	+20*	−15*	ms	31	4	6	21	142	158
									1	5				
									2	5,7				
									3	7				
		(No record 0313–0813 1st, 0127–0853 6th, 0223–0742 9th.)												
	Nov.13	11 ..	15 02	.....	....	....	....	m	14	1,5,6	5	17	76	100
	Nov.27	23 51	28 16	s.c.	x	x	x	ms	28	1,2,4	7	30	188	202
	Nov.30	05 ..	4 12	.....	....	....	....	ms	30	5,6	6			
									3	6,8				
	Dec. 5	07 00	6 24	s.c.	+5	+58	+40	ms	5	7	7	31	169	200
	Dec. 13	17 ..	14 19	.....	....	....	....	ms	13	8	6	20	113	160
	Dec. 26	17 ..	29 17	.....	....	....	....	ms	28	6	6	19	145	121
		(No record 2354–0629 29th.)												
Toolangi	*1959*													
(J. Cleary)	Oct. 1	04 25	2 12	.....	....	....	....	m	1	4,5	5	21	105	66
									2	2	5			
	Oct. 3	07 28	4 15	.....	....	....	....	m	3	6,7	5	20	143	70
									4	1,3,5	5			
	Oct. 5	12 02	7 15	.....	....	....	....	ms	6	4	6	24	156	81
	Oct. 17	06 22	18 20	.....	....	....	....	m	18	3,4	5	19	115	42
	Oct. 29	23 47	5 16	s.c.	x	23	x		31	4	6	29	179	88
									1	5	6			
									2	5	6			
	Nov.27	23 50	28 22	(Not Recorded)				ms	28	1,2,3,4	6	35	225	140
	Nov.30	02 47	4 18	s.c.	+1	−4	0	ms	3	4	6	25	140	55
	Dec. 5	07 00	6 14	s.c.	+2	+90	+10	ms	5	5,6,7	6	30	230	95
	Dec. 22	14 23	.. ..	s.c.	....	−5	....	m	23	3	5	10	85	45
	Dec. 23	15 24	24 15	s.c.*	+1*	+18	+4	m	23	6	5	12	75	50
	Dec. 26	01 47	29 13	.....	....	....	....	ms	27	4	6	30	160	55
Amberley	*1959*													
(A. L. Cullington)	Oct. 29	23 47	6 04	s.c.*	−2	+36	+6	m	31	4,5	5	24	204	68
	Nov.27	23 53	29 08	s.c.*	−8	+16	+40	ms	28	2,3,4	6	35	350	244
	Dec. 5	07 00	6 16	s.c.	+2	+71	−11	ms	5	7	6	30	291	140

PROVISIONAL SUNSPOT-NUMBERS FOR OCTOBER TO DECEMBER 1959

(Dependent on observations at Zurich observatory and its stations at Locarno and Arosa)

Day	October	November	December
1	54	124	142
2	72	121	150
3	81	97	171
4	97	93	190
5	115	74	126
6	128	74	147
7	130	114	136
8	115	122	129
9	103	127	94
10	91	131	70
11	78	144	82
12	81	151	71
13	70	149	59
14	102	134	88
15	96	123	123
16	116	109	113
17	107	72	107
18	116	56	111
19	84	59	114
20	99	65	110
21	111	70	103
22	129	110	121
23	135	131	106
24	143	147	108
25	137	149	110
26	126	149	95
27	112	145	132
28	110	117	114
29	115	123	135
30	117	135	127
31	130		153
Means.....	106.5	113.8	117.3
No. days....	31	30	31

Mean for quarter: 112.5 (92 days)

M. WALDMEIER

SWISS FEDERAL OBSERVATORY
Zurich, Switzerland

FREDERICKSBURG THREE-HOUR-RANGE INDICES *K* FOR OCTOBER TO DECEMBER 1959

[$K9 = 500\gamma$; Scale-Values of Variometers in γ/mm: $D = 2.70$; $H = 2.50$; $Z = 2.95$]

Gr. Day	October 1959 Values *K*	Sum	November 1959 Values *K*	Sum	December 1959 Values *K*	Sum
1	3565 3334	32	3455 5223	29	4444 4321	26
2	2554 1232	24	4364 5444	34	3445 4443	31
3	1242 2346	24	5445 3433	31	4455 4334	32
4	4765 5343	37	1333 4445	27	3433 2120	18
5	4323 3334	25	5554 3222	28	0034 5565	28
6	5555 3343	33	4444 3124	26	2533 2232	22
7	4432 2234	24	0320 1232	13	3200 1111	09
8	3313 1111	14	1333 2221	17	2210 0322	12
9	3121 1020	10	1200 2132	11	0132 3202	13
10	1100 1101	05	2211 2122	13	1110 0120	06
11	1010 0011	04	2111 1112	10	0221 1211	10
12	0000 2233	10	1101 1222	10	2522 2233	21
13	1011 1111	07	1122 3333	18	4222 2234	21
14	1223 4232	19	3334 4332	25	3334 5442	28
15	2322 3233	20	2211 1001	08	3443 2234	25
16	2000 0221	07	0010 3322	11	3333 3312	21
17	1223 4333	21	1413 3000	12	2032 2011	11
18	5344 4434	31	1222 3332	18	1043 3122	16
19	4423 2123	21	1133 3111	14	1243 2210	15
20	3231 2110	13	3111 0000	06	2202 1111	10
21	1211 2223	14	0213 3233	17	1210 1010	06
22	3344 2323	24	3422 3233	22	0000 1112	05
23	3223 2000	12	4545 4330	28	2232 2544	24
24	0112 2222	12	3111 2011	10	4134 3022	19
25	2434 4324	26	2123 2111	13	2223 1110	12
26	3344 4333	27	1244 3223	21	3435 4234	28
27	2333 2111	16	3231 2125	19	4435 4535	33
28	1132 1000	08	5775 5323	37	5434 5432	30
29	0211 1004	09	2224 2221	17	4433 3212	22
30	5432 3244	27	2156 5534	31	1344 4220	20
31	3245 4435	30			1132 0120	10

ROBERT E. GEBHARDT
Observer-in-Charge

FREDERICKSBURG MAGNETIC OBSERVATORY
Corbin, Virginia

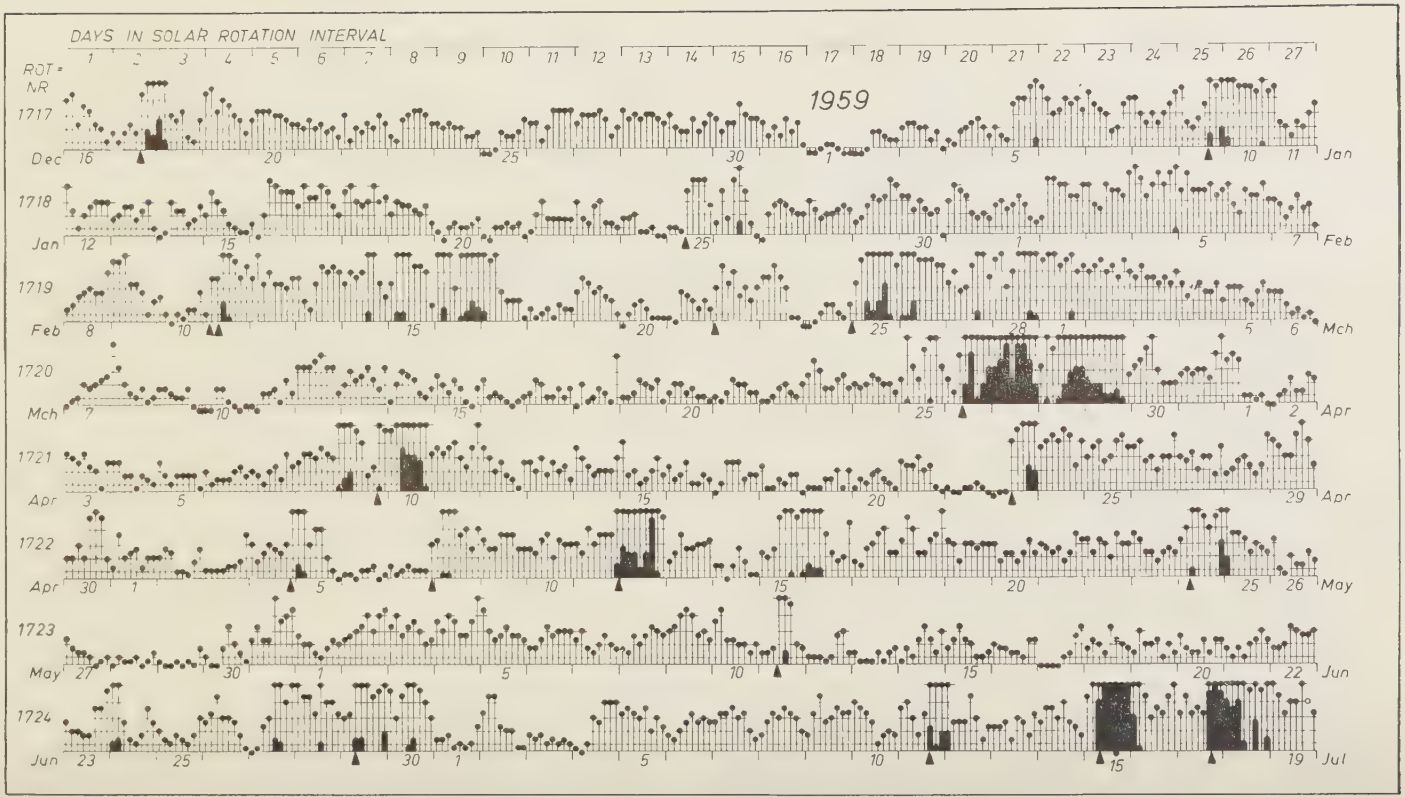
DAYS IN SOLAR ROTATION INTERVAL
1 2 3 4 5 6 7 8 9 10 11 12 13 14 15 16 17 18 19 20 21 22 23 24 25 26 27
ROT = NR
1959
1717
Dec 16 20 25 30 1 5 10 11 Jan
1718
Jan 12 15 20 25 30 1 5 7 Feb
1719
Feb 8 10 15 20 25 28 1 5 6 Mch
1720
Mch 7 10 15 20 25 30 1 2 Apr
1721
Apr 3 5 10 15 20 25 29 Apr
1722
Apr 30 1 5 10 15 20 25 26 May
1723
May 27 30 1 5 10 15 20 22 Jun
1724
Jun 23 25 30 1 5 10 15 19 Jul

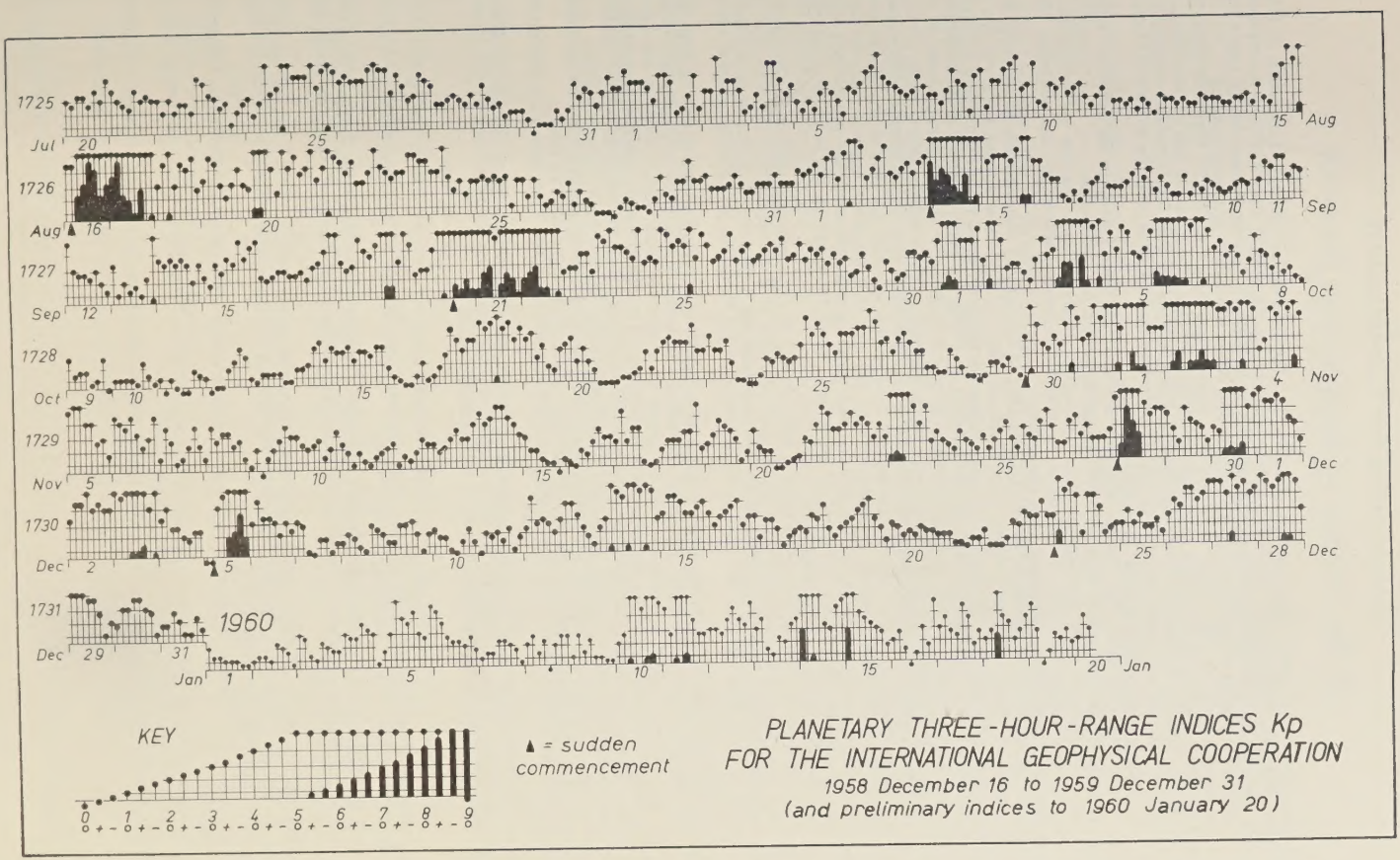
1725
Jul 20 25 31 1 5 10 15 Aug
1726
Aug 16 20 25 31 1 5 10 11 Sep
1727
Sep 12 15 21 25 30 1 5 8 Oct
1728
Oct 9 10 15 20 25 30 1 4 Nov
1729
Nov 5 10 15 20 25 30 1 Dec
1730
Dec 2 5 10 15 20 25 28 Dec
1731
Dec 29 31 1960 Jan 1 5 10 15 20 Jan
KEY
0 1 2 3 4 5 6 7 8 9
▲ = sudden commencement
PLANETARY THREE-HOUR-RANGE INDICES Kp
FOR THE INTERNATIONAL GEOPHYSICAL COOPERATION
1958 December 16 to 1959 December 31
(and preliminary indices to 1960 January 20)

Information for Contributors

to the *Journal of Geophysical Research*

Manuscripts—Send manuscripts to J. A. Peoples, Jr., Department of Geology, University of Kansa Lawrence, Kansas. Manuscripts, including proof copies of figures, should be submitted in triplicate t expedite review and publication. Manuscripts should be in English, typewritten on heavy paper on or side of page only, double spaced (including abstracts and references), with generous margins.

Ample space should be allowed for mathematical expressions, which should be typed or very plain written by hand. Particular attention should be given to legibility of subscripts and superscripts and t differentiation between capital and lower case letters. Unusual symbols and cumbersome notations shoul be avoided. Fractional exponents should be used in preference to root signs, and the solidus (/) should b used for fractions wherever its use will save vertical space.

Authors are urged to have their papers critically reviewed by their associates for scientific validity manner of presentation and use of English before submitting them for publication.

Abstracts—An abstract must accompany each manuscript. It should be a concise but comprehensiv condensation of the essential parts of the paper, suitable for separate publication, and adequate for th preparation of general indexes to geophysical literature.

References and footnotes—References should be indicated in the text by the insertion in brackets of th author's name and the year of publication, thus: [*Trelease*, 1951]. If the author's name is part of the text only the year is bracketed. If there are two or more references citing different papers published in the sam year by the same author, distinguish them by the letters a, b, c after the year. At the end of the paper, lis all references alphabetically by the authors' names. Include in each entry the following: name of senio author, followed by his initials; names of junior authors, each preceded by his initials; title of paper (or book) title of publication or journal; volume number; inclusive page numbers; year of publication. Abbreviation of journals follow the style used in *Chemical Abstracts*. If in doubt, give the full title of the publication o journal. When a book is cited, add the publisher's name, the city of publication, and the total number o pages. Reference to specific pages may be made in the text if appropriate. Acknowledge unpublished report and private communications in the text, not as references. Avoid footnotes to the text; use parentheti sentences instead of footnotes if possible.

Tables and figures—Material suitable to tabular form should be arranged as a table and may be type written on a separate page, Tables must be numbered according to their sequence in the text, and eac table should have a title. Column headings should be short and self-explanatory; more complete explana tion may be given in footnotes to the table. Authors should avoid repeating in the text material which i given in tables or figures.

Figures should be prepared with the column width of this Journal in mind (a scale of two to four time that of the published figure is usually adequate). Lettering and symbols should be large enough to stan reduction and remain legible. Captions should be typed on a separate page, not lettered in the figures Necessary legends or lettering in the figures should be executed to meet competent drafting standards, no typewritten. If the author cannot arrange for suitable lettering, he may send the drawings with the letterin lightly penciled in or shown on a proof copy, and the lettering will be done at the editorial office.

Line drawings should be in India ink on white paper or tracing cloth. Coordinate paper should be avoided but, if used, it must be blue-lined and the coordinate lines which are to show must be inked.

Photographs are acceptable only if they have good intensity and contrast. They should be unmounted glossy prints.

Figures should be identified by numbering lightly in pencil, and 'top' of each figure should be indicated

Acknowledgments—Acknowledgments should be made only for significant contributions by the author' professional associates. A brief closing statement will usually suffice.

References

American Chemical Society, *List of periodicals abstracted by Chemical Abstracts*, Chemical Abstract Service, Ohio State Univ., Columbus, 314 pp., 1956.

American Institute of Physics, *Style Manual*, American Institute of Physics, New York, 28 pp., 1951

American Mathematical Society, A manual for authors of mathematical papers, *Bull. Am. Math. Soc.* 49, no. 3, pt. 2, 1–16, 1943.

Emberger, M. R., and M. R. Hall, *Scientific writing*, Harcourt, Brace and Co., New York, 469 pp., 1955

Taft K. B., J. F. McDermott, and D. O. Jensen, *The technique of composition*, 3rd ed., Farrar and Rinehart, New York, 628 pp. 1941.

Trelease, S. F., *The Scientific paper—how to prepare it, how to write it*, Williams and Wilkins Co., Baltimore 175 pp., 1951.

U. S. Geological Survey, *Suggestions to authors of the reports of the United States Geological Survey*, 5th ed U. S. Govt. Printing Office, Washington, 255 pp., 1958.

William Byrd Press, *Mathematics in type*, Richmond, 58 pp., 1954.

Contents

(*Continued from back cover*)

(Journal of Geophysical Research, Vol. 65, No. 4, April 1960)

Contents

(*Continued inside back cover*)